Harmonics in large offshore wind farms

Kocewiak, Lukasz Hubert

Publication date:
2012

Document Version
Publisher's PDF, also known as Version of record

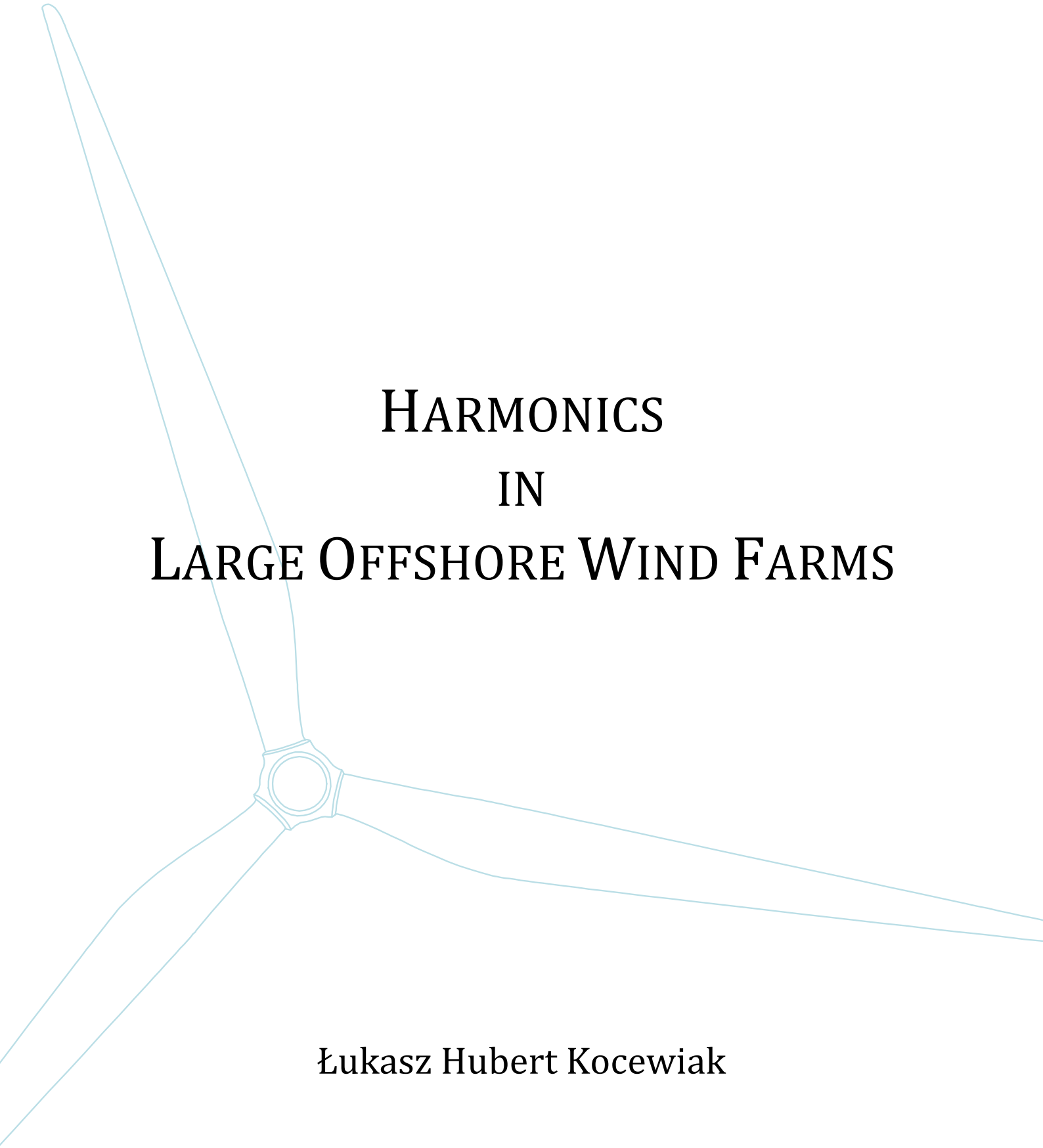

HARMONICS IN LARGE OFFSHORE WIND FARMS

Łukasz Hubert Kocewiak

Harmonics in Large Offshore Wind Farms

by

Łukasz Hubert Kocewiak

Dissertation submitted to the Faculty of
Engineering, Science and Medicine at
Aalborg University in partial fulfilment of
the requirements for the degree of Doctor
of Philosophy in Electrical Engineering

Public defence date:
February 2, 2012
Assessment committee:
Professor Neville R. Watson, University of Canterbury, New Zealand
Professor Frede Blaabjerg, Aalborg University, Denmark
Section manager, PhD Paul Thøgersen, KK-Electronic, Denmark

Department of Energy Technology
Aalborg University, Denmark
March 2012

PhD Thesis
Harmonics in Large Offshore Wind Farms

lukasz@kocewiak.eu
http://lukasz.kocewiak.eu/

Printed in Denmark

ISBN 978-87-92846-04-4

Aalborg University
Department of Energy Technology
Pontoppidanstræde 101
DK-9220 Aalborg East, Denmark.
http://www.et.aau.dk/

...to my family

PREFACE

This dissertation was submitted to the Faculty of Engineering, Science and Medicine at Aalborg University in partial fulfilment of the requirements for the PhD degree in Electrical Engineering. The research was conducted in the Department of Energy Technology at Aalborg University as well as in the Renewables Grid Analysis Department in DONG Energy. The project was industry-oriented which created a unique opportunity to carry out research gathering benefits from both the industry the academia.

The project has been followed by Prof. Claus Leth Bak who is with Department of Energy Technology, Aalborg University and Dr. Jesper Hjerrild who is with Renewables Grid Analysis Department, DONG Energy. DONG Energy has solely funded the research leading to this thesis 'Harmonics in Large Offshore Wind Farms'. The financial and technical support from the company were vital for the research.

Within the confines of the research project three months at the beginning of 2011 were spent in the EPE Centre hosted at the University of Canterbury under Prof. Neville Watson's supervision. The university has a strong theoretical background and experience in harmonic analysis that accelerated research focused on theoretical analysis of harmonic phenomena in wind turbines.

The author had also a unique opportunity to introduce the most interesting research findings during the PhD course entitled 'Harmonics in Power Electronics and Power Systems' carried out at Aalborg University. The lectures were conducted also by Dr. Lucian Asiminoaei from Danfoss Drives and Dr. Wojciech Wiechowski from WTW Power Solutions.

The dissertation comprises of 6 chapters. Corresponding literature reference list is presented at the end of each chapter. A list of the publications, written in relation to this research project is presented at the end of the thesis. Literature references are shown as [$i.j$] where i is the number of the chapter and j is the number of the literature position. References to figures and tables are shown as Figure $i.j$ or Table $i.j$ and references to equations are shown as Eq. $i.j$ where similarly i is the chapter number and j indicates the figure, table or equation.

ACKNOWLEDGEMENTS

I would like to express my thanks to my supervisors, Prof. Claus Leth Bak from Aalborg University and Dr. Jesper Hjerrild from DONG Energy for all their support and help in the project development. The feedback from the academia as well as from the industry was especially fruitful in order to create a good cooperation between both units, which is reflected in this report.

Special thanks also to all the people in the EPE Centre hosted at the University of Canterbury in New Zealand for their kindness and hospitality. I would like to thank especially Prof. Neville Watson and Prof. Alan Wood for their significant contribution to the research and numerous professional discussions.

Furthermore, I would like to express my appreciation and gratefully acknowledge the contribution of Dr. Iván Aristi Arana from DONG Energy for the cooperation during measurement campaigns at Avedøre Holme and Gunfleet Sands. Without good planning and cooperation, the measurement campaigns would not be finished with such a big success.

My grateful thanks go to all colleagues at DONG Energy for their help and encouragement they have given in these three years. Special thanks to Ole Holmstrøm and Dr. Troels Stybe Sørensen for introducing me to various commercial and technical aspects of offshore projects. It is worth mentioning that the knowledge sharing within the Grid Analysis department significantly contributed to the project development.

I also owe special thanks to all academic and administrative stuff in the Institute of Energy Technology at Aalborg University. Without their tremendous help on the scientific as well as organisational field, the project would not be finalised without any delays and with a sufficient scientific contribution.

Last but not least, I would like to thank my patient wife, Patrycja Skłodowska-Kocewiak as well as the rest of my family and my friends for their support and understanding. Research is a long and complex process which sometimes requires more time and sacrifice than actually expected.

Łukasz Hubert Kocewiak
March 2012, Skærbæk, Fredericia

ABSTRACT

The number of wind turbines with full converters in the MW range used in large offshore wind farms is rapidly increasing. They are connected through a widespread MV cable network with practicably no consumption and connected to the transmission system by long HV cables. This represents new challenges to the industry in relation to understanding the nature, propagation and effects of harmonics. Recently, the wind power sector is rapidly developing. This creates new challenges to the industry, and therefore more and more research projects, including harmonic analyses especially focused on wind power applications, are conducted and that is why the project was initiated and successfully developed. Also experience from the past regarding offshore projects developed in the company and various harmonic aspects causes a need to carry out extensive harmonic research.

The research project was initiated by the industry and carried out in cooperation with academia. In order to organize the project development process, the research development framework was suggested based on rationalistic tradition approach in order to provide knowledge and better understanding of different aspects (e.g. measurements, data processing, data analysis, modelling, and models application) in harmonic studies. Based on the framework, also the structure of the report was organized. This allows the reader to go through all of the stages in project development starting from measurements, through data processing and analysis, and finally ending up on modelling and models application. Different aspects of validation in time domain, frequency domain, and by application of statistical methods are mentioned in relation to respective problems.

Measurements constitute a core part in industry-oriented research. Due to this fact, the research project owes its uniqueness and contributes new insight to the academia. It is proven that an analysis of such systems as large offshore wind farms considers many aspects related to extended and accurate models, complex measurement campaigns and of course appropriate and more suitable data processing methods. Before any of the above aspects could be seriously taken into consideration, a reliable and robust measurement system is needed. This is achieved by carefully designing the hardware and the software layers of the measurement system.

It is explained in the report that it is of great importance to know the nature of generated harmonics in large offshore wind farms in order to apply the most suitable

data processing technique. Time-frequency analysis based on multiresolution wavelet transform is used in order to perform time-frequency domain analysis helpful to distinguish harmonic origin and observe short-term variation. Non-parametric spectrum estimation is successfully applied to interpolated signals adjusted according to the varying power system frequency. Different data processing techniques are presented and applied depending on the signal (i.e. stationary or non-stationary) or harmonic nature (i.e. spline resampling or direct spectrum estimation). Based on an in-depth investigation of measurements, it is observed that certain harmonic components generated by the grid-side converter in the wind turbine are affected by two driven frequencies, i.e. the power system fundamental frequency and the carrier signal fundamental frequency. Therefore, harmonic assessment made by major part of commercial power quality meters is to some extent inappropriate, and their measurements interpretation can be misleading.

Different statistical tools were used in order to analyse the origin and nature of various harmonic components. A comprehensive comparison of harmonic voltages and currents based on probability distribution estimation and appropriate statistics calculation (mean, variance, probability density function, etc.) is applied. Such approach gives a better overview and comparison of harmonic components variation and occurrence frequency.

Several frequency domain methods of describing wind farms comprising of various components such as wind turbines, transformers, cables, etc. are shown and compared. It is explained that large offshore wind farms can introduce additional unwanted resonances within the low frequency range. This can significantly affect overall system stability. Therefore, the analysis and design optimization of large offshore wind farms are more complex than smaller onshore wind farms.

Nowadays, wind turbines are complex devices equipped with the newest technologies. Therefore, also harmonic analysis of such devices is not a straightforward task. Harmonic studies, due to the complexity of the wind turbine structure, can be focused on several parts such as control strategy, modulation technique, converter structure, and hardware implementation.

Various control strategies are taken into consideration and their impact on possible harmonic emission and overall system stability. An analysis is performed mainly in the frequency domain. One analyses how particular components in the control structure (e.g. filters, controllers, etc.) can affect the control and its harmonic rejection capability. The influence of control strategies on overall wind farm stability is also deeply investigated. Appropriate stability indices are suggested and applied in several study cases.

Carefully modelled and aggregated large wind farms in frequency domain together with the wind turbines frequency response give a good overview about large offshore wind

farm behaviour for different frequencies. Such approach is successfully used in studies of real-life existing wind farms.

Since harmonics in wind turbines and wind farms are characterized by different origin and nature, comparison of them may be problematic. Therefore, sometimes selective validation of particular frequency components is more suitable. It was observed that comparison of results in frequency domain and time domain, as well as application of statistical methods, is the core part of results understanding.

Based on presented studies, we see that large offshore wind farms, in comparison to typical onshore wind farms, can affect more unwanted resonance scenarios. Unwanted resonances can cause overall wind farm stability and performance (e.g. unwanted harmonic excitation and amplification). Therefore, it is of great importance to carefully analyse wind farms, especially large offshore wind farms, also from a harmonic perspective.

This industrial PhD project is focused on investigating the best possible way to perform various harmonic studies of offshore wind farms including some conditions not taken into consideration before. Application of new methods and widening the range of models contributes to achieve the necessary higher reliability of offshore wind farms as large power generation units in electrical power systems.

RESUMÉ

Antallet af vindmøller med frekvensomformer til nominel effekt i MW-klassen, der anvendes til store havmølleparker, er stærkt stigende. De er tilsluttet et udbredt og forgrenet mellemspændingskabelnet stort set uden egetforbrug og er tilsluttet transmissionsnettet ved hjælp af lange højspændingskabler. Det stiller vindmølleindustrien og netselskaberne over for nye udfordringer i forhold til at forstå harmoniske svingningers karakter, udbredelse og virkning. Vindmøllebranchen udvikler sig hastigt. Det stiller branchen over for nye udfordringer, hvilket har medført gennemførelse af flere og flere forskningsprojekter, der omhandler analyse af harmoniske svingninger med særligt fokus på vindenergi, og det er grunden til, at dette projekt blev påbegyndt og gennemført med et positivt resultat. Virksomhedens erfaring fra tidligere havmølleprojekter i forbindelse med forskellige harmoniske aspekter har medført et behov for at udføre omfattende undersøgelser af harmoniske svingninger.

Forskningsprojektet blev til på branchens foranledning, og blev gennemført i et samarbejde med institut for Energiteknik, Aalborg Universitet. I forbindelse med planlægningen af projektforløbet blev rammerne for projektet lagt ud fra en traditionel rationalistisk tilgang for at kunne levere viden og en dybere forståelse for forskellige aspekter (f.eks. målinger, databehandling, dataanalyse, modellering, modelanvendelse) i studier af harmoniske svingninger. På baggrund af disse rammer, blev rapportens opbygning fastlagt. Læseren kan dermed følge alle projektforløbets stadier startende med målinger, databehandling og –analyse og sluttende med modellering og modelanvendelse. Forskellige aspekter af tidsdomænevalidering, frekvensdomæne og af brugen af statistiske metoder nævnes i forbindelse med specifikke problemer.

Målinger udgør en vigtig del af industriel forskning. Derfor er dette projekt unikt samtidig med, at det tilfører den akademiske verden vigtig praksis-orienteret indsigt og vice versa. Det er bevist, at analyse af systemer som store havmølleparker indebærer mange aspekter, der omhandler udvidede og mere præcise modeller, komplekse målekampagner og selvfølgelig bedre og mere anvendelige databehandlingsmodeller. Før de ovennævnte aspekter kan behandles, er det nødvendigt at have et pålideligt og robust målesystem til rådighed. Dette opnås gennem grundigt design af målesystemets hardware- og softwarelag.

I rapporten forklares det, at det er meget vigtigt at kende typen af de harmoniske svingninger, der genereres i store havmølleparker for at kunne anvende de rigtige

databehandlingsteknikker. Tids-/frekvensanalyse baseret på multiresolution wavelettransformation bruges til at udføre tids-/frekvensdomæneanalyser, som kan bidrage til at definere de harmoniske svingningers oprindelse og observere korttidsvariationer. Ikke-parametrisk spektralanalyse anvendes på interpolerede signaler tilpasset de varierende elsystemfrekvenser. Forskellige databehandlingsteknikker er præsenteret og anvendt afhængig af signalet (dvs. om det er stationært eller ikke-stationært) eller typen af harmoniske svingninger (dvs. spline resampling eller direkte spektralanalyse). På baggrund af grundig analyse af målinger ses det, at visse harmoniske komponenter, der dannes på netsiden af omformeren i vindmøllen påvirkes af to faste frekvenser, dvs. af elsystemets grundfrekvens og basisbærefrekvenssignalet. Derfor er målinger af harmoniske svingninger udført primært med kommercielle spændingskvalitetsmålere i nogen grad utilstrækkelige, og den efterfølgende vurdering af resultaterne kan derfor være misvisende.

Forskellige statistiske værktøjer er anvendt til at analysere oprindelsen og karakteren af forskellige harmoniske komponenter. En omfattende sammenligning af harmoniske spændinger og strømme baseret på en vurdering af den sandsynlige fordeling samt passende statistiske beregninger (f.eks. middel, varians, sandsynlig tæthedsfunktion mv.) anvendes. En sådan tilgang giver et bedre overblik og en bedre sammenligning af harmoniske komponenters variationer og forekomst.

Flere frekvensdomænemetoder til beskrivelse af vindmølleparker bestående af flere komponenter såsom vindmøller, transformere, kabler mv. beskrives og sammenlignes. Det forklares, at store havmølleparker kan producere yderligere uønskede resonanser i lavfrekvensområdet. Dette kan have en betydelig indflydelse på systemets generelle stabilitet. Derfor er analyse og designoptimering af store havmølleparker mere komplekst end analyse og designoptimering af små landmølleparker.

I dag er vindmøller komplekse anlæg udstyret med den nyeste teknologi. Derfor er analyse af harmoniske svingninger i sådanne anlæg ikke så ligetil. På grund af vindmøllernes kompleksitet kan man ved studier af harmoniske svingninger fokusere på flere forskellige aspekter såsom reguleringsstrategi, moduleringsteknik, omformerdesign og hardwareimplementering.

Forskellige reguleringsstrategier er blevet overvejet sammen med deres indflydelse på dannelsen af harmoniske svingninger og generel systemstabilitet. Analyser er hovedsaglig udført i frekvensdomænet. En analyse går ud på at finde ud af, hvordan forskellige komponenter i reguleringskonceptet (f.eks. filtre, kontrolenheder mv.) kan påvirke styringen og dens evne til at udkompensere harmoniske svingninger. Reguleringsstrategiernes indflydelse på mølleparkens generelle stabilitet er ligeledes blevet grundigt undersøgt. Egnede stabilitetsindeks er foreslået og anvendt i flere konkrete cases.

Omhyggeligt modelerede ækvivalenter af store vindmølleparker i frekvensdomænet sammen med møllernes frekvensrespons giver et godt overblik over, hvordan store

havmølleparker reagerer ved forskellige frekvenser. En sådan tilgang har vist gode resultater i forbindelse med studier af eksisterende mølleparker.

Da harmoniske svingninger i vindmøller og vindmølleparker har forskellig oprindelse og er af forskellige typer, kan det være problematisk at sammenligne dem. Derfor er selektiv validering af specifikke frekvenskomponenter til tider mere anvendelig. Det blev observeret, at sammenligning af resultater i frekvensdomænet og tidsdomænet og anvendelse af statistiske metoder er nøglen til forståelse af resultaterne.

På baggrund af de præsenterede studier kan det ses, at store havmølleparker sammenlignet med typiske landmølleparker kan generere flere uønskede resonansscenarier. Uønskede resonanser kan påvirke mølleparkens generelle stabilitet og ydelse (f.eks. kan harmonisk resonans anslåsog forstærkes). Derfor er det meget vigtigt at analysere mølleparker grundigt, især store havmølleparker, også ud fra et harmonisk perspektiv.

Denne erhvervsPhD fokuserer på at finde frem til de bedst mulige metoder til at gennemføre forskellige harmoniske studier af havmølleparker, herunder en række forhold som ikke før er blevet overvejet. Anvendelse af nye metoder og en udvidelse af rækken af modeller bidrager til at opnå den højere rådighed, der er nødvendig på havmøllerparker, hvis de skal fungere som store kraftværker i det elektriske system.

TABLE OF CONTENTS

Chapter 1
INTRODUCTION

The wind power sector is rapidly developing. This creates new challenges to the industry. Therefore, more and more research projects, including harmonic analyses especially focused on wind power applications, are conducted. This chapter briefly presents nowadays trends as well as a historical background of both wind power and the development of harmonic analyses. At the end of the chapter, based on the brief introduction to the wind power and harmonic analysis, the project hypothesis is put forward.

1.1 NOWADAYS WIND POWER INDUSTRY

1.1.1 NOWADAYS OFFSHORE WIND FARMS

The number of wind turbines with converters used in large offshore wind farms is increasing (see Figure 1.1). They are mainly connected through a widespread MV subsea cable network and long HV cables to the transmission system. At the same time, the interest in the power quality of wind farms has increased as renewable energy sources become more important to face the global environmental challenges. The new technology which is less tolerant to voltage quality disturbances as well as the widespread use of power electronic converters contribute to the relevance of the power quality [1.1].

Figure 1.1 Gunfleet Sands Offshore Wind Farm where measurements within the project were carried out (www.kocewiak.eu).

Therefore, it is of major importance to provide power quality analysis guidelines and assess the possible impact that wind farms have on the power quality of a specific grid. Furthermore, from the distribution system operator's and the transmission system operator's perspective it is of great importance to supply adequate power quality to consumers. Therefore, wind farms should fulfil power quality requirements. For the wind farm developer an optimal assessment means a cost-effective design fulfilling the requirements [1.2].

The interest in the power quality of wind farms has increased as renewable energy sources become more important to face the global environmental challenges, and the power industry grows with the trend of embedded and dispersed generation. The new technology which is less tolerant to voltage quality disturbances as well as the widespread use of power electronic converters contribute to the relevance of the power quality . It is of major importance to assess the possible impact that wind farms have on the power system also from a power quality perspective. Additionally, from both the power system (i.e. distribution or transmission) operator's as well as developer's perspective, it is important to fulfil various power quality requirements (e.g. harmonic emission). Therefore, wind farms should be designed with special care, taking many aspects into consideration. Some of them, including frequency domain, will be taken into account in this report.

The process of the power quality assessment must be carried out not only on a wind turbine manufacturer level but also on a wind farm developer level. Thus, additional wind turbine analyses for specific applications (i.e. wind farm layout, characteristics of an external network) are needed. Due to this fact and extensive analyses based on real-life measurements, advanced data processing and multidomain modelling were performed and compared with data provided by manufacturers.

1.1.2 FULL-SCALE WIND TURBINES

Nowadays, variable-speed wind turbines are grid-friendly machines in most power quality respects. The power electronic devices with advanced semiconductor technology and advanced control methods that are used in wind turbines for transferring power from the generator to the grid can meet the most demanding grid requirements seen today [1.3]. However, there are issues with regard to the power quality, voltage stability, transmission losses and reliability that need to be addressed and improved [1.4], [1.5] in order to exploit the potential and advantages that large offshore wind farms have. Such issues are obviously important elements in the efforts to reach renewable energy targets while maintaining a reliable and robust power system [1.6].

The report concerns full-scale back-to-back converter wind turbines which are, and are going to be, widely applied in already developed and future DONG Energy's wind farms. It is a variable-speed wind turbine utilizing full scale frequency converters. The frequency converter system comprises two AC/DC converters and a DC-link decoupling the variable-frequency generator and the grid frequency. There is a transformer to step up the voltage installed in each wind turbine. The wind turbine transformer is connected with a vacuum circuit breaker to the MV network.

The tendency in the industry shows that instead of using a partially rated converter such as in a doubly fed induction generator, fully rated converters can be applied to control active and reactive power injection into the system. The power converted from wind energy to electrical energy can be injected by the power converter from any kind of rotating generator (i.e. an induction generator or a synchronous generator excited by any suitable means such as permanent magnets or conventional or superconducting field windings). In general, the AC frequency that is developed at the stator terminals of the generator is directly proportional to the speed of the rotation of the rotor. The voltage at the generator terminals also varies as a function of speed, depending on the particular type of generator and the flux level. Such schemes are used with renewable energy systems and give the widest range of speed control but at the expense of a converter. It should be rated to cope with the full generator output power [1.7].

Such a power conversion scheme is presented in Figure 1.2. The rapid power electronic development contributes to the use of fully rated converter systems and will probably replace the partially rated converters and doubly fed induction generators. Current trends show that permanent magnet machines become more attractive in wind power applications. It is due to its efficiency, since no magnetizing or field current is necessary to provide the magnetic field, and it also allows introducing new generator topologies applicable in specific conditions. The permanent magnet generator size is smaller than the synchronous wound field and asynchronous squirrel cage induction generators, and it does not need an external power supply source to support excitation [1.8].

It is worth emphasizing that the price of permanent magnets is of great uncertainty because they are made from limited sources as rare earth metals.

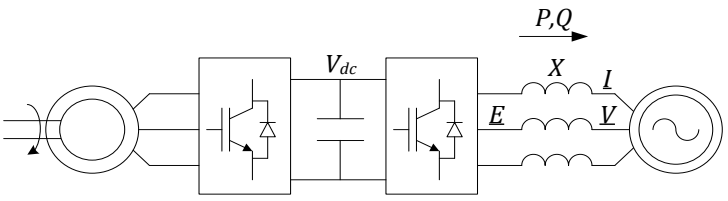

Figure 1.2 Full rated power converter connected to the grid.

The full scale converter system allows full control of active and reactive power. Although few control schemes are possible, the generator-side converter is normally operated to control the generator torque loading while the grid-side converter is controlled to maintain constant voltage on the DC-link and control the power output. Both converters are normally current-controlled to achieve their control objectives. However, it should be emphasized that the pulse-width modulated converters can adjust the phase and magnitude of the injected phase voltage. Different aspects of the grid converter control will be shown later.

1.1.3 GRID-SIDE INVERTER

As mentioned, the grid converter is normally controlled to transfer power to maintain a constant voltage on the DC-link capacitor. If the charge of the capacitor decreases, the control loop will decrease the power transfer to increase the voltage and vice versa. It should be realized that the grid inverter is also able to control the reactive power supplied to the system which becomes very important to satisfy contemporary grid codes.

Assuming that the system voltage $\underline{V} = V_a + j0$ acts along the real axis, that the voltage injected by the converter is $\underline{E} = E_a + jE_b$ and that the current injected into the system is $\underline{I} = I_a + jI_b$ (see Figure 1.2), the current through the reactance is given by [1.9]

$$\underline{I} = I_a + jI_b = \frac{\underline{E} - \underline{V}}{jX} = \frac{E_b}{X} - j\frac{(E_a - V_a)}{X} \tag{4.1}$$

that is

$$I_a = \frac{E_b}{X} \tag{4.2}$$

and

$$I_b = -\frac{(E_a - V_a)}{X} \tag{4.3}$$

while the apparent power injection into the system is

$$\underline{S} = 3V_a\underline{I}^* = 3V_aI_a - j3V_aI_b = 3\frac{V_aE_b}{X} + j3\frac{V_a(E_a - V_a)}{X} \quad 4.4$$

now components E_a and E_b can be expressed in terms of magnitude E and phase angle δ

$$E_a = E\cos(\delta) \quad 4.5$$

$$E_b = E\sin(\delta) \quad 4.6$$

substituting into Eq. 4.4 gives

$$\underline{S} = 3\frac{V_aE\sin(\delta)}{X} + j3\frac{V_a(E\cos(\delta) - V_a)}{X} \quad 4.7$$

Generally, it can be assumed that δ is small and for small δ sin function can be considered as linear, and cos function can be assumed equal to 1. Therefore, Eq. 4.7 becomes

$$\underline{S} \approx 3V_a\frac{E}{X}\delta + j3V_a\frac{(E - V_a)}{X} \quad 4.8$$

Eq. 4.8 demonstrates how real power can be controlled by the phase angle δ of the grid-connected converter voltage $\underline{E}$ and reactive power by the magnitude of $\underline{E}$. Although there is some cross-coupling between the terms, this can be taken into consideration in the control structure.

1.2 HISTORICAL BACKGROUND

The first well-documented appearance of harmonics in relation to mathematics and science is from ancient Greece. The science which pursued the investigation of multiple and epimoric (ratios of the form [n+1]:n) ratios in music was concerned with the mathematical 'fitting-together' (harmonia) of the constituent notes and intervals of music [1.10].

Harmonics were described by Claudius Ptolemy who related musical harmonies to the properties of mathematical proportions derived from the production of sounds themselves. Ptolemy argued for basing musical intervals on mathematical ratios, in agreement with the followers of Pythagoras, backed up by empirical observation. Ptolemy wrote about how musical notes could be translated into mathematical equations and vice versa [1.11].

Those harmonies he considered to be distributed in all aspects of the physical universe. In particular, they were there in the phenomena of the planets and the human soul [1.12].

Nowadays, harmonic analysis is the branch of mathematics that studies the representation of functions or signals as the superposition of basic waves.

It investigates and generalizes the notions of Fourier series and Fourier transforms, mathematical tools significantly useful in different areas of engineering. The basic waves are called harmonics, but the name harmonic in this context is generalized beyond its original meaning of integer frequency multiples.

It can be said that nowadays harmonic analysis reaches back to a French mathematician and physicist, Joseph Fourier, who originally defined the Fourier series for real-valued functions of real arguments and used the sine and cosine functions as the basis set for the decomposition. Fourier series could be used only for analysis of periodic functions.

Many different approaches of defining and understanding the concept of Fourier series have been developed since that time. All are consistent with one another, but each of which emphasizes different aspects of the topic simultaneously extending significantly the basic concept of harmonic analysis. Some of the more powerful and elegant approaches, based on mathematical ideas and tools not available at the time Fourier extended his original work, are successful in harmonic analysis at present.

Many other Fourier-related transforms (e.g. Laplace transform, Fourier transform, short-time Fourier transform, wavelet transform) have since been defined, extending the initial idea to other applications. This general area of inquiry is now called by physicists and engineers harmonic analysis.

1.3 SHORT STORY ABOUT RESEARCH

Harmonics were always of special concern in power system studies. In the past the power system comprised mainly passive components with relatively linear operating range as well as synchronous generators. Harmonic analysis of such systems is state-of-the art right now. Nowadays modern power systems include more and more power electronic components than in the past. The most significant power electronic components are different types of flexible alternating current transmission system (FACTS) devices, such as static synchronous compensator (STATCOM) or static VAR compensator (SVC). Also renewable energy sources (e.g. wind turbines, photo voltaic installations, tidal steam generators) as well as high-voltage, direct current (HVDC) electric power transmission systems are becoming more popular. Power electronic equipment in modern power systems is obviously a source of additional harmonic components not seen previously. On the other hand, the application of advanced and fast control in grid-connected power converters introduces possibility of control higher than the fundamental frequency components. Appropriately used power electronics can definitely improve the quality of power.

To show how harmonics are becoming more and more important in electrical engineering and power system studies, a popular electrical engineering database was investigated. Institute of Electrical and Electronics Engineers (IEEE) is considered by many as the biggest professional association gathering electrical and electronics engineers from many fields. The association has an extended digital library comprising

more than 3 million technical and scientific documents. Unfortunately, access to the documents, if not open for all interested parties and therefore knowledge sharing, is limited especially for small research units all around the world.

Analyses of such a database from a harmonic and wind power research perspective can provide a good overview of how advancement of technology in both areas has developed in the space of the years. At the beginning, let us see how publications regarding harmonics have appeared.

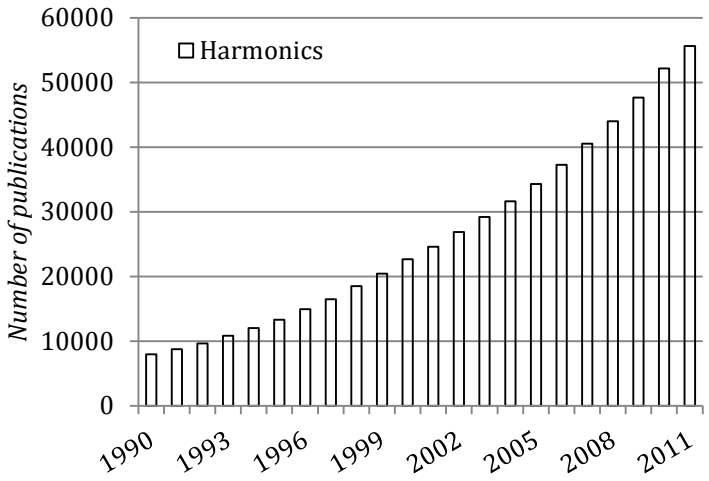

Figure 1.3 Total number of publications concerning harmonics.

The first paper regarding harmonics in the IEEE database is from 1899, but the most significant development within the area of harmonics started in late 80ies. In Figure 1.3 one can see that the interest of harmonics is still increasing. Up until now, there are more than 55000 of publications only about harmonics. Obviously, harmonic analyses can be applied in many fields of electrical engineering. Let us additionally see how in the same period the interest in wind turbines and wind farms development has increased.

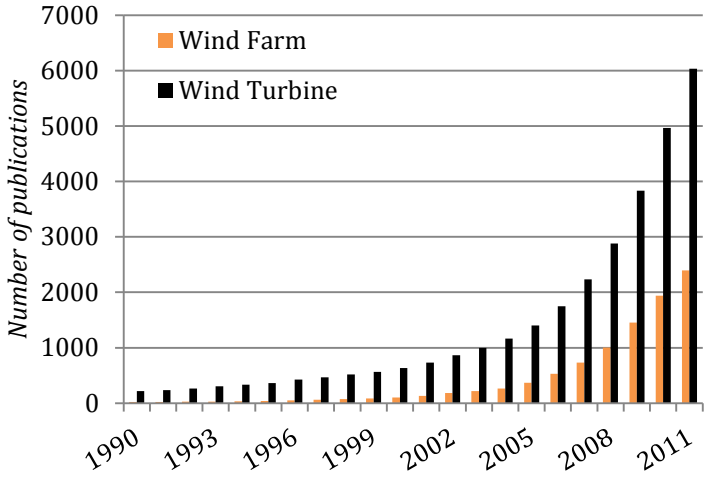

Figure 1.4 Total number of publications about wind turbines and wind farms.

In case of research associated with harmonics, the tendency is rather linear, but regarding both wind turbines and wind farms, there is an exponential growth of interest directly reflected in the number of publications. This tendency can be easily seen in Figure 1.4. This general interest in wind power can also be easily seen in the increasing number of commercial projects. Therefore, harmonics analyses in this particular field of electrical engineering seem to be important also from a market tendencies perspective.

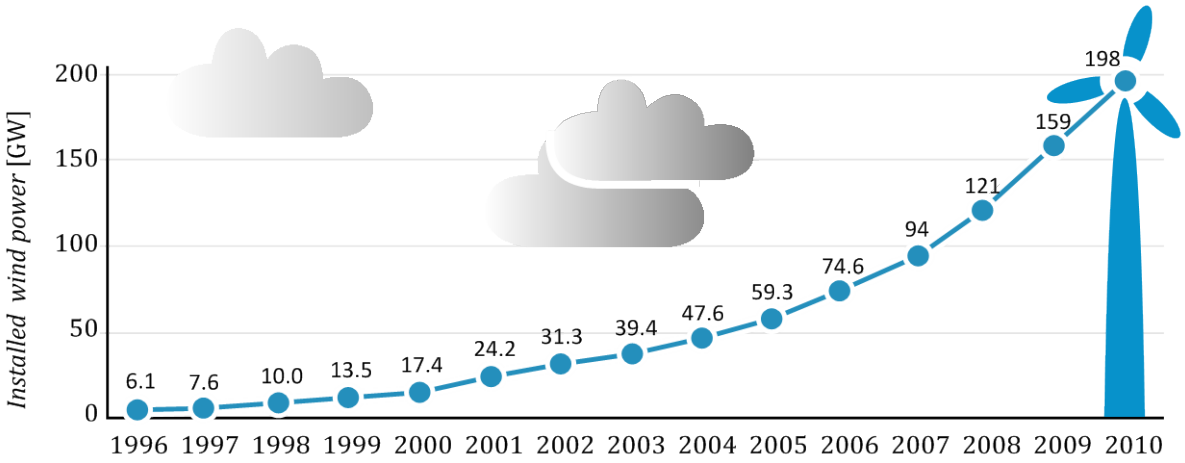

Figure 1.5 Existing world capacity of wind power.

Figure 1.5 shows that the increasing interest of wind power technology is correlated with the increasing world capacity of wind power [1.13]. It can be concluded that this tendency will be increasing within the next few years. Therefore, new research projects are required to extend knowledge and experience in the area of renewable energy sources. This also implies an increasing interest of harmonic research within this area of power industry.

As it can be seen also in Figure 1.4, wind turbine studies are more popular than wind farms. It seems to be a natural way of research. Although it also indicates that there is much less experience with wind farm analysis as a whole system comprising many wind turbines and other components. The first observed publication in the IEEE database regarding wind turbines is from 1958, but regarding wind farms it is much later (1982). Even less experience is gained in offshore wind power solutions. This field is new (first mention in 2000) in comparison with onshore installations. Anyway, nowadays knowledge sharing capability and technology development allow deriving knowledge from other fields and continuous improvement.

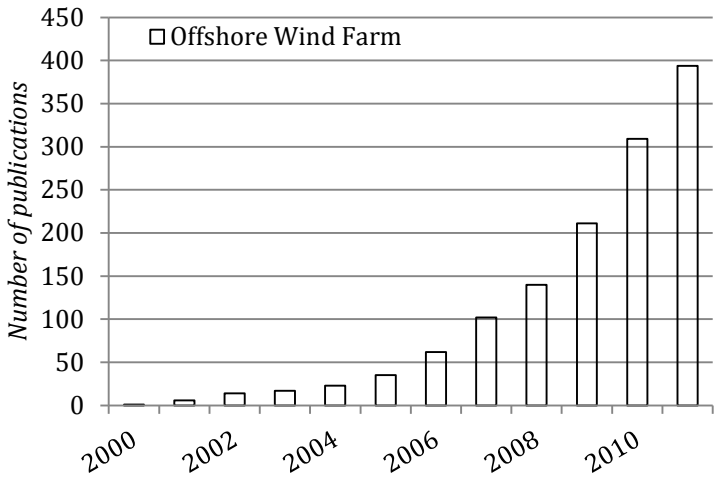

Figure 1.6 Number of publications regarding strictly offshore wind farms.

In Figure 1.6, we can see an even clearer tendency of exponential growth of interest and research within the field of offshore wind farms.

1.4 PROJECT HYPOTHESIS

The project was initiated in order to provide in-depth knowledge of all relevant aspects related to harmonics in offshore wind farms including:

- The voltage source converter as harmonic sources
- Modelling and analysis of wind turbines and wind farm network elements in relation to harmonics (i.e. the frequency range from DC to 5kHz) in time and frequency domain
- Modelling of wind turbine converters and other wind turbine components in time and frequency domain
- Interaction of offshore wind farms with AC transmission system (other harmonic sources, controllers, etc)
- Additional interactions with VSC and CSC converters within the same wind farm
- Dynamic phenomena, harmonic instability, etc.
- Operation of VSC with harmonic resonances near its characteristic frequency
- Engineering standards and power quality standards.

Based on those assumptions, a project hypothesis was defined. Is it possible to model offshore wind farms equipped with many voltage source converter wind turbines and connected to the power systems in time and frequency domain in a consistent way to analyse possible harmonic generation, harmonic resonances and power system impedance variation due to overall system changes?

1.5 SUMMARY

Even if a large part of harmonic studies is nowadays state-of-the-art, there are still many issues to investigate and improve. This is especially associated with the application of harmonic analyses in wind turbines and wind farms. Frequency domain analyses associated with eigenfrequencies are even more important in large offshore wind farms.

The project hypothesis was specified in this chapter in order to clearly specify the scope of the project. It is assumed that the project is focused on the development of various analysis methods and tools which can be successfully used in future commercial wind farm projects development. Additionally, extensive knowledge regarding harmonic phenomenon in wind farms was achieved.

1.6 REFERENCES

[1.1] F. Blaabjerg and Z. Chen, *Power Electronics for Modern Wind Turbines*, 1st ed. Morgan & Claypool, 2006.

[1.2] Ł. Kocewiak, J. Hjerrild, and C. L. Bak, "Harmonic analysis of offshore wind farms with full converter wind turbines," in *Proc. 7th International Workshop on Large Scale Integration of Wind Power and on Transmission Networks for Offshore Wind Farms*, 14-15 October 2009, pp. 539-544.

[1.3] V. Akhmatov, J. Nygaard Nielsen, J. Thisted, E. Grøndahl, P. Egedal, M. Nørtoft Frydensbjerg, and K. Høj Jensen, "Siemens Windpower 3.6 MW Wind Turbines for Large Offshore Windfarms," in *Proc. 7th International Workshop on Large Scale Integration of Wind Power and on Transmission Networks for Offshore Wind Farms*, 26-27 May 2008, pp. 494-497.

[1.4] V. Akhmatov, "Experience with voltage control from large offshore windfarms: the Danish case," *Wind Energy*, vol. 12, no. 7, pp. 692-711, 2009.

[1.5] I. Arana, Ł. Kocewiak, J. Holbøll, C. L. Bak, A. H. Nielsen, A. Jensen, J. Hjerrild, and T. Sørensen, "How to improve the design of the electrical system in future wind power plants," in *Proc. Nordic Wind Power Conference*, Bornholm, 2009.

[1.6] A. Baggini, *Handbook of Power Quality*. Wiley and Sons, 2008.

[1.7] R. Jones, P. B. Brogan, E. Grondahl, and H. Stiesdal, "Power Converters," U.S. Patent 7 372 174 B2, May 13, 2008.

[1.8] P. Maibach, A. Faulstich, M. Eichler, and S. Dewar, "Full-Scale Medium-Voltage Converters for Wind Power Generators up to 7 MVA," ABB Switzerland Ltd., 2006.

[1.9] J. Machowski, J. W. Bialek, and J. R. Bumby, *Power System Dynamics - Stability and Control*. John Wiley and Sons, 2008.

[1.10] D. Creese, *Monochord in Ancient Greek Harmonic Science*. Cambridge University Press, 2010.

[1.11] J. Solomon, *Ptolemy Harmonics: Translation and Commentary*. Brill Academic Publishers, 1999.

[1.12] A. Barker, *Scientific Method in Ptolemy's Harmonics*. Cambridge University Press, 2001.

[1.13] J. L. Sawin and E. Martinot, "Renewables 2011 Global Status Report," Renewable Energy Policy Network for the 21st Century, Annual Report, 2011.

[1.14] P. Brogan and R. Yacamini, "Stability of selective harmonic active filters," in *International Conference on Power Electronics and Variable Speed Drives*, 2000, pp. 416-421.

Chapter 2
RESEARCH APPROACH

The research project was initiated by the industry and carried out in cooperation with the academia which is described in this chapter. Also an introduction to harmonics in power systems and wind farms is presented. The research development framework is suggested based on rationalistic tradition approach in order to provide knowledge and better understanding of different aspects (e.g. measurements, data processing, data analysis, modelling, and models application) in harmonic studies. Some issues related with knowledge sharing in order to better utilize the project findings are also mentioned.

2.1 INDUSTRIAL ORIENTED RESEARCH

In modern industrial and academic research and development units the design of a new product is not an isolated activity. The term product can be understood broadly, starting from commercial products that can be sold on the market and ending with methods, tools, procedures or standards that are assumed to be used internally in order to accelerate other products' development process, usually commercial products are financially beneficial. Product design is part of a more comprehensive process called the product innovation process. In short, product innovation is the development of a new business activity relating to a new product.

A research and development project is characterized by exploring new, immature technologies. Often, a positive business case for the implementation cannot be established. Normally, the project is undertaken to discover or establish facts and principles. The project will increase the knowledge and experience within a certain area; and the project may eventually develop and mature this knowledge/technology for deployment in the business units.

Since harmonic distortion of voltages and currents can have negative effects on power system components, the necessity of performing harmonic studies is justified. DONG Energy is one of Europe's leading wind power generators and has developed strong wind energy capabilities. The company has more than 19 years of experience in

constructing and operating offshore wind farms. Needless to say, the knowledge of power quality in wind farms as well other electrical and non-electrical aspects increases after every new wind project is commissioned.

It must be emphasized that every new project creates new challenges and sometimes unpredictable phenomena. Due to this fact, a need to extend and intense research area in the wind industry is seen and in many cases strongly desired. New research activities simultaneously with commercial wind projects are born and an unavoidable symbiosis starts between the industry, commercial and research and development units. This shows that research projects are not artificial marvels, but stems from the industry and cannot exist without appropriate cooperation between industrial and academic units.

The main expected project findings are the following:

- Appropriate flexible measurement equipment and techniques dedicated to measure harmonics in offshore wind farms as well to properly assess the power quality level.
- Advanced data processing algorithms suitable for different signals measured in wind farms and for harmonics characterized by different origin and nature.
- New models and modelling techniques. The main approach is a model-based investigation. It is necessary to derive power system component models that have such high complexity to sufficiently describe the system behaviour in time and especially in frequency domain.
- Large offshore wind farms connected to the transmission system demonstrate complex behaviour in analysis scenarios. Impedance characteristic variation during system changes will be observed and compared to measurement sets.
- Various analysis methods appropriate for harmonic studies. Sometimes offshore wind farms with many degrees of freedom cannot be taken into consideration from a deterministic point of view. Different probabilistic aspects of harmonic emission will be taken into account.
- Unwanted resonances preventing methods. Mitigation of power system harmonics is necessary to eliminate such characteristic for power system behaviour. Precautionary and corrective solutions will be shown.
- Different validation methods applicable for different models, simulations results and measurement data.

2.2 INTRODUCTION TO HARMONICS

Ideally, an electrical power system in every certain point should show a perfectly sinusoidal voltage signal. However, due to many reasons, utilities often find it hard to preserve such desirable conditions. The deviation of the voltage and current waveforms from sinusoidal is described in terms of the waveform distortion, often expressed as harmonic distortion.

Harmonics cause distortions of the voltage and current waveforms, which have adverse effects on electrical components in wind farms. The increased use of nonlinear equipment such as power electronic and electronic devices has caused harmonics to become more common and the need of extended harmonic analysis has become more desired.

Harmonics emission and propagation are one of the major power quality concerns [2.1]. Harmonics are created when nonlinear loads draw nonsinusoidal current from a sinusoidal voltage source or are generated on purpose by active components. The estimation of harmonics from nonlinear loads is the first step in a harmonic analysis and this may not be straightforward. More subtle analysis methods become more important in systems with nonlinearities.

Harmonic distortion is caused by nonlinear devices in the power system where the driven frequency is the fundamental component. A nonlinear device is one in which the current is not proportional to the applied voltage. While the applied voltage is perfectly sinusoidal, the resulting current is distorted. Nonlinear loads, like adjustable speed drives, solid-state heating controls, electronic ballasts for fluorescent lighting, switched-mode power supplies in computers, static UPS systems, electronic and medical test equipment, rectifiers, filters, and other power electronic devices cause harmonics appearance in power systems [2.2].

It is also worth emphasizing that nowadays power electronic devices (e.g. grid-side converter in wind turbines, STATCOMS, SVCS, HVDCS), which can be identified as active components, can be driven by other frequency than the power system fundamental component. Therefore, the injected current can also contain harmonics even if the harmonic current is not as a consequence of nonlinear load with applied sinusoidal voltage. Sometimes simply sinusoidal voltage components generated by active components (e.g. voltage source converters) can be of different frequency than the power system fundamental driven frequency.

According to [2.3], characteristic harmonic exists when the analysed three-phase electrical system is considered to be balanced, the voltages and currents waveforms have identical shape and current and voltage are separated by exactly $\pm 1/3$ of the fundamental period. In such case, zero sequence harmonics are for orders $n = 3m$ where $m = 1, 2, 3, \dots$, positive sequence harmonics are for orders $n = 3m - 2$ and negative sequence harmonics are for orders $n = 3m - 1$.

A typical device with a driven frequency other than fundamental component in the power system is the voltage source converter with pulse width modulation. If such a converter is a grid-connected device, the frequency components generated by it are dependent on both the power system fundamental component (i.e. modulated signal) and the carrier signal fundamental component (i.e. modulating signal). In this particular case, harmonic components generated by the voltage source converter can be integer multiple of grid frequency, carrier frequency or a mixture of both of them.

Therefore, in power systems where there is more than one driven frequency it is not straightforward to identify harmonic components and their origin. In fact, the occurrence of only integer multiple frequencies of the power system fundamental frequency is the trivial case where a single sinusoid interacts with itself or its own harmonics. This situation was popular in the past when power systems comprised only passive components and synchronously rotating generators. Nowadays, broadly used in modern power systems, advanced power electronics contains also its own driven frequencies (not always equal or multiple integer of the power system frequency) which can affect generation of harmonic components of frequencies constituting a mixture of different driven frequencies.

Harmonic currents and voltages have a detrimental effect on utility and end-user equipment. They cause overheating of transformers, power cables, and motors; inadvertent tripping of relays; and incorrect measurement of voltage and current by meters. Harmonic voltages cause increased iron losses in transformers. Harmonics cause motors to experience rotor heating and pulsating or reduced torque [2.4].

2.2.1 HARMONICS IN WIND FARMS

A wind turbine with an induction generator directly connected to the electrical system is not expected to cause any significant harmonic distortions during normal operation. However, commonly applied wind turbines with power electronic converters must be checked for harmonics. Although variable-speed wind turbines are grid-friendly machines in most power quality respects, harmonics generated by the grid power converters may be of concern in networks, where harmonic resonance conditions may exist [2.5]. Performing a detailed and accurate harmonic analysis in a real-life power system is a quite complicated issue, involving advanced models for all system components, including the consumer loads, which present the greatest uncertainties. The harmonic current emission of wind turbines with power electronics is given in standards regarding power quality measurements and assessment. Limits for harmonic emissions are often given only for harmonic currents, not for harmonic voltages. Thus, harmonic voltages must be calculated from the harmonic current emission of the wind turbine while the frequency dependent short circuit impedance may vary. Considering that the grid impedance varies with frequency, where the utilities often cannot give the frequency dependency of the grid impedances, makes

calculations difficult [2.6]. Another aspect is related with harmonic background distortions which are also of great uncertainty [2.7].

Harmonic emission is recognized as a power quality concern for modern variable-speed wind turbines. For this reason, relevant standards (e.g. IEC 61400-21) require the measurement of harmonics and their inclusion in the power quality certificates of wind turbines, and grid interconnection assessment procedures always comprise provisions for their control. Understanding the harmonic behaviour of wind turbines is essential in order to analyse their effect on a grid to which they are connected. Wind turbines with power electronic converters are potential sources of harmonic distortion, and therefore knowledge of their harmonic current emissions is needed to predict wind farm behaviour and to design reliable wind farms [2.8]. The emission of harmonic currents during the continuous operation in steady state of a wind turbine with a power electronic converter must be stated according to the standards.

The usage of renewable energy sources has resulted in the use of many varied power converters topologies. These inverters are available in single-phase such as photo voltaic units and in three-phase units commonly used in wind turbines, and their output may be very clean sinusoids with near unity power factor or may contain various characteristic and non-characteristic harmonics and power factors that may cause unacceptable power quality on the electric utility grid or interfere with its controls or relays.

Wind turbine generators with a power electronic interface significantly contribute to overall harmonic emission in nowadays large offshore wind farms. The harmonic contribution at the point of common coupling of a wind farm consisting of multiple wind turbine generators results from the harmonic generation of all individual wind turbines [2.9]. Harmonics can be distinguished between characteristic harmonics and non-characteristic harmonics from power electronic equipment perspective, where the phase angle is randomly distributed among different wind turbines.

If the loads and transmission and distribution systems are balanced only characteristic harmonics exist. These are of zero sequence for orders $n = 3m$, $(m = 1,2,3 \ldots)$, of positive sequence for the $n = 3m - 2$ orders, and of negative sequence for the $n = 3m - 1$ orders. However, asymmetries always exist, causing non-characteristic harmonics in the system [2.3].

The harmonic emission of wind turbines with an integrated power electronic interface can be categorized in characteristic and non-characteristic harmonics. The characteristic harmonic emissions are determined by the converter topology and the switching pattern applied. For instance, a typical configuration found nowadays in wind turbine generators is a two-level, three-phase voltage source converter with sinusoidal pulse-width modulation. The modulation frequency ratio m_f is defined as the switching frequency divided by the power system fundamental frequency. When

m_f is sufficiently large, the predominant characteristic harmonics for this configuration will occur at orders $2m_f \pm 1$, and next lowercontent harmonics at orders $m_f \pm 2$, $3m_f \pm 2$, $4m_f \pm 1$, etc. [2.10], [2.11]. In a wind power plant, these harmonics show a certain degree of correlation among the different wind turbines and are determined by the modulation technique.

Non-characteristic harmonics are not related to the converter topology, but are determined by the operating point and control scenario of the individual converter. Therefore, these are weakly correlated or even completely uncorrelated between different wind turbine generators [2.12].

A significant number of power converter topologies and control methods introduced by the industry gives extended variation of harmonic emission depending on the applied solutions. These inverters may act as current sources attached to the electric utility or as voltage sources tied to the electric utility through series impedance, usually an inductor, to limit the current between the inverter and the electric utility grid. Power electronic converters (AC/DC, DC/AC) are the main factor responsible for voltage and current harmonic generation in electrical networks. These converters are also now frequently employed in wind turbines, so that harmonic distortion can affect wind farm components. On the other hand, wind turbine converter's control can be adjusted to limit harmonic current flow. It is known that a DC/AC converter can be considered, at the supply-bus side, as a generator of harmonic currents, injected from the converter terminals to the network. These harmonic currents cause harmonic voltage drops along the line impedance distorting the voltage. The extent of distortion is related to the distorting load power and the short-circuit power of the equivalent network, so that even small power distorting loads can affect significantly the bus voltage if the line short-circuit power is low [2.13].

2.2.2 RESONANCES IN WIND FARMS

System resonant conditions are the most important factors taken into consideration during harmonic analysis and have direct influence to system harmonic levels. The resonance effect occurs when inductive reactance and capacitive reactance are equal in absolute value. Parallel resonance is high impedance to the flow of harmonic current, and series resonance is low impedance to the flow of harmonic current. When resonant conditions are not a problem, the system has the capability to absorb significant amounts of harmonic currents. But in case of offshore wind farm connected by long AC cables to the transmission network, resonance problems become significant [2.14]. Therefore, it is important to be able to analyse the system frequency dependent characteristics and to avoid system resonance problems with harmonic excitation and propagation in power systems with high degree of wind power penetration [2.15], [2.3].

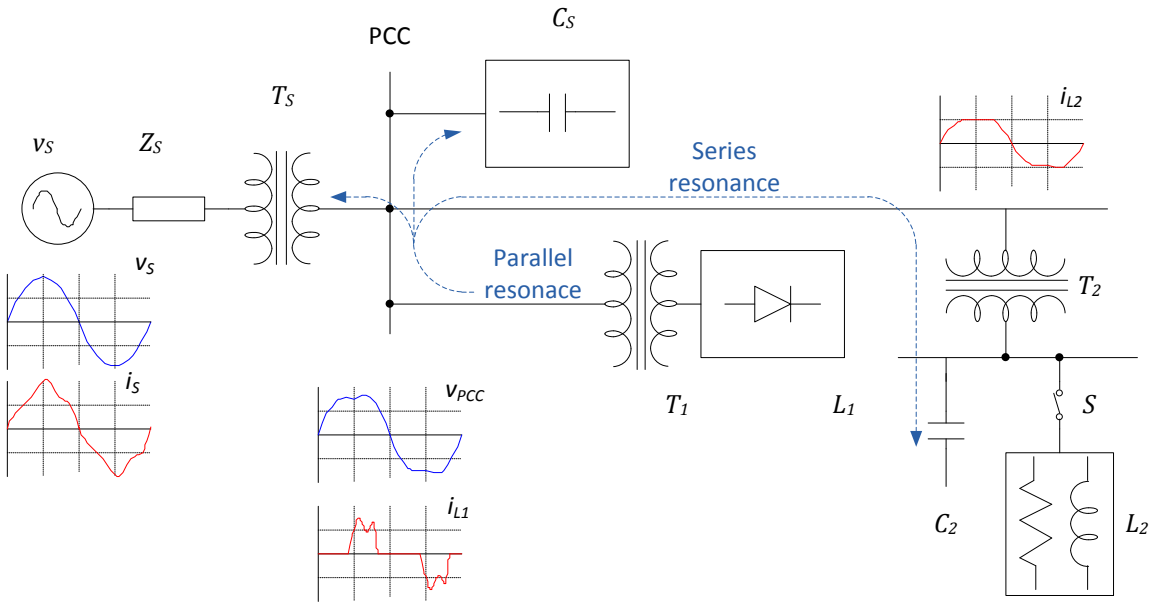

Figure 2.7 Possible resonance scenarios in power systems.

Parallel resonance occurs when parallel connected system inductive reactance with capacitive reactance are equal at some frequency. If the combination of capacitor banks and the system inductance such as in transformers result in a parallel resonance for certain harmonics generated by the nonlinear load (see Figure 2.7), that harmonic current will excite the tank circuit, thereby causing an amplified current to oscillate between the energy storage in the inductance and the energy storage in the capacitance [2.16]. This high oscillating current can cause significant voltage distortion in the system [2.17].

Series resonance is a result of the series combination of cables, capacitor banks and line or transformer inductances. At a particular frequency these two reactances are equal in magnitude but opposite in sign. Series resonance presents a low impedance path to harmonic currents. This is a low impedance trap circuit to the resonance frequencies [2.18]. Series resonance can result in high-voltage distortion levels between the inductance and the capacitor in the series circuit. An example of a series circuit is a load centre transformer with capacitors connected to its secondary side. This appears as a series circuit when viewed from the transformer primary side [2.19] as presented in Figure 2.7.

2.2.3 Effect of Harmonics on Wind Farms

Clearly defined previously, harmonic sources must be interpreted in terms of their effects on the system. Due to common harmonic presence in wind farms each element of offshore wind farms must be examined for its sensitivity to harmonics. It gives allowable harmonic levels examination for every certain component. The main effects of voltage and current harmonics within wind farms are:

- Reduction in the efficiency of the generation and transmission of electric energy within a wind farm.
- Possibility of amplification of harmonic levels resulting from series and parallel resonances.
- Thermal stress of electrical components with consequent shortening of their useful life or damage.
- Malfunctioning of offshore wind farm components and protection systems.

Among the possible external effects of harmonics are an excessive audible noise, degradation in communication systems performance, and harmonic-induced voltages and currents [2.20].

2.2.4 HARMONICS IN STANDARDS

The IEC standard for harmonics [2.21] regarding harmonics and interharmonics measurements and instrumentation for power supply systems uses the following notation for the Fourier series

$$f(t) = c_0 + \sum_{m=1}^{\infty} c_m \sin\left(\frac{m}{N}\omega_o t + \varphi_m\right) \qquad 2.1$$

where $\omega_o = 2\pi f_o$ is the angular frequency of the fundamental, c_m is the amplitude of the component with frequency $f_m = \frac{m}{N} f_o$, N is the number of fundamental periods within the window width, c_0 id the DC component, m is the order of the spectral line.

According to the IEC 61000-4-7 [2.21] and IEC 61000-4-30 [2.22] standards, the Fourier series must be obtained over a rectangular window with a length equal to 10 cycles in a 50 Hz system. The length of this basic window is about 200 ms. The window length is not exactly 200 ms as the frequency always differs somewhat from the nominal frequency. Therefore more correct term used in the IEC documents is 10-cycle window.

The use of a rectangular window requires that the measurement window is synchronized with the actual power system frequency, hence the use of a 10-cycle window instead of a window of exactly 200 ms. The IEC standard requires that 10 cycles correspond with an integer number of samples within 0.03%. To ensure synchronism between the measurement window and the power system frequency, most harmonic analysers use a phase-locked loop generating a sampling frequency that is an integer multiple of the actual power system frequency. A synchronization error leads to cross-talk (spectral leakage) between the different harmonic frequencies. The 50 Hz component is by far the dominating component in most cases so that the main concern is the cross-talk from the 50 Hz component to higher order components. Of course it is worth mentioning that other frequency components will also suffer due to the spectral leakage.

The result of applying the discrete Fourier transform to the basic window is a spectrum of 5-Hz spacing between frequency components. The spectrum thus contains both harmonics and interharmonics with certain accuracy.

Another IEC 61400-21 standard [2.23] concerning measurements and power quality assessment in wind turbines assumes measurements of 10-minute harmonic current generated by a wind turbine for frequencies up to 50 times the fundamental frequency of the grid [2.24], [2.25].

2.3 RATIONALISTIC TRADITION

There is a close correlation between the western culture approach of organized science and rationalistic tradition. The tradition of rationalism and logical empiricism can be tracked back at least to Plato. This tradition has been the inspiration of western science and technology. Especially in hard sciences (i.e. natural, physical, and computing sciences), that explain the operation of deterministic mechanisms whose principles can be described by means of formal systems, this tradition has introduces a great influence.

Based on rationalistic tradition the basic concept of research is focused on deriving formulations of systematic rules that can be used to draw logical conclusions. In western philosophy this approach can be seen as a drive to come up with more systematic and precise formulations of what constitute valid reasoning. Therefore, thinking and reasoning are the most natural ways of research and development [2.26].

In nowadays science, obviously, there must be a certain degree of adherence to the scientific methods having their roots in the rationalistic tradition. The scientific method can be described as involving the following operations [2.27]:

(a) observation of a phenomenon that, henceforth, is taken as a problem to be explained,
(b) proposition of an exemplary hypothesis in the form of a deterministic system that can generate a phenomenon isomorphic with the one observed,
(c) proposition of a computed state or process in the system specified by the hypothesis as a predicted phenomenon to be observed,
(d) observation of the predicted phenomenon.

According to the presented approach, the first step is to characterize the phenomenon in terms of identifiable objects with well-defined properties based on observations. The next step is to find general rules which apply to the phenomenon in terms of those objects and their properties. And later apply specified rules to the phenomenon of concern, drawing conclusions and generic characteristic of the phenomenon.

It is worth emphasizing that rationalistic tradition not only constitutes a mainstream of both either pure or applied science but also underlies as a paradigm of what it means

to think. Therefore, for people of science and technology this approach seems to be appropriate and self-evident way of serious thinking.

Based on rationalistic tradition also the research and development framework of the project was proposed. The framework assumes that all possible models and conclusions can be derived from measurements which were performed at the beginning of the studies. Furthermore, the predictions obtained from models are at the end compared with observations, and thus, the research framework is represented as a cycle.

2.4 Project Development Framework

Comprehensive scientific tools from wide area of the engineering world were used during the wind turbine analysis. In nowadays wind farms it has been observed that a satisfactory analysis (i.e. harmonic analysis, transient analysis, load flow analysis) becomes a complex process. It requires extended measurement campaigns, advanced data analysis techniques as well as detailed modelling of wind farm components in order to assess different phenomenon as accurately as possible. Additionally, the development of appropriate, well-defined and strict analysis methods is crucial. And of course, the whole analysis would not be reliable if not advanced validation techniques.

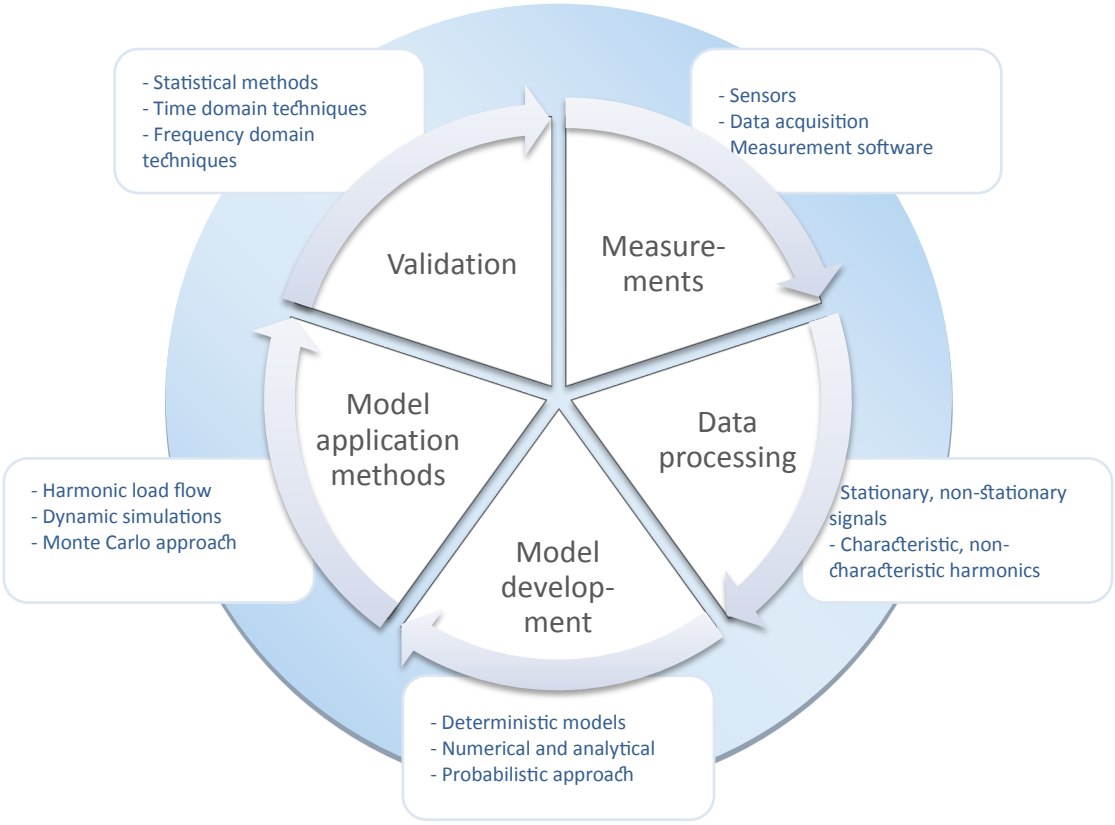

Figure 2.8 Project development framework.

Each stage of the analysis process has to be carried out with an appropriate care. Possible errors in results obtained from each of stages can significantly affect other stages. That is why it is crucial to spend sufficient amount of time on development of each of stages (i.e. measurements, data processing, modelling, analysis, and validation).

Since the project was developed based on the framework, also the report is organized in the same way. That is why at the beginning the measurement system development process as well as measurement campaigns are presented. Afterwards, an extended data processing and data analysis using various sophisticated techniques are presented. And finally, model development in time domain, frequency domain and harmonic domain together with their application are extensively described.

2.4.1 MEASUREMENTS

Accurate measurements are essential in many fields of science, and all measurements are approximations of real-world existing systems. In order to observe the system of interest without any misleading disturbances, a great deal of effort must be taken to make measurements as accurate as possible.

The measurement system was developed taking into consideration its application and environmental conditions. In places where access is limited (i.e. offshore wind farm) due to weather conditions and significant operational costs, reliable and trustful measurement systems are especially important. Reliable long-term measurement systems for harmonic analysis consisting of optimized hardware and software layers were applied. The appropriate configuration and optimisation of the measurement system decided of successful progress of measurements.

An appropriate measurement system was developed for harmonic measurement purposes. Such systems must be extremely robust and reliable due to the fact that harmonic measurements are often long-term processes. Measurement software must be developed with special care to provide uninterruptable data logging. Also data acquisition devices as well as sensors must be chosen carefully for predefined frequency band and electromagnetic environment in wind turbines. In offshore wind farms appropriate timestamp synchronization between measurement units is also an important issue.

2.4.2 DATA PROCESSING

Having data with reduced aliasing and noise level, appropriate measurement data processing techniques are required to estimate harmonic components in logged waveforms. Due to the power system frequency variation, resampling is needed to obtain the properly estimated spectrum. Different harmonic estimation techniques are needed depending on origin and nature of analysed components. Measurements

and data processing according to guidelines stated in commonly known standards are sometimes inappropriate for particular applications.

An analysis of such systems as wind turbines or wind farms considers many aspects related to extended and accurate models, complex measurement campaigns and of course appropriate and more suitable data processing methods. It must be emphasized that there is no possibility to develop and validate accurate and extended models without appropriate processed measurements. This became a crucial issue, especially if small changes in model development process are applied and signal processing begins to play a significant role.

Measured electrical signals such as voltage and current waveforms can be classified into two cases: stationary and non-stationary signals. The signal processing methods introduced in this report are for stationary and non-stationary signals. Methods based on stationarity assumptions are applied in measurements for steady-state operation of the wind turbine and methods applicable for non-stationary signals are applied in wind turbine transient operations (i.e. wind turbine shutdown, wind turbine start-up).

2.4.3 MODEL DEVELOPMENT

In order to develop a model of the full-scale converter, appropriate measurement data processing and analysis are required. The main concern of the investigation constitutes the grid-side converter, since it directly affects the harmonic generation as well as harmonic background mitigation.

Different models are required depending on application. Time domain models appear to be needed for grid interaction studies such as harmonic compensation of distorted network. Various frequency domain models are essential in stability assessment and resonance studies. And harmonic domain models find a broad application in load-flow simulations.

2.4.4 MODEL APPLICATION METHODS

In order to properly assess harmonic emission or investigate stability in frequency domain in offshore wind farms, different analysis methods are required. Beginning from a typical harmonic load flow simulation, through short dynamical simulation and ending up with probabilistic harmonic assessment using the Monte Carlo approach. For each method, different models need to be used. This shows that modelling is a complex and time-consuming process.

2.4.5 VALIDATION

Each of the harmonic analysis methods gives certain results, which are expected to be comparable with measurement data. Sometimes this is not a straightforward task, and due to this fact, appropriate in time and frequency domain validation techniques

are required and used. Sometimes statistical approach is used, especially for large datasets. It is also common practice to compare results from different models and later also with measurements.

2.5 KNOWLEDGE SHARING

Why share knowledge is an important question, because sharing knowledge is essential to the functioning of every social system. It is also a potential collective dilemma, because there are obvious and fairly general reasons why people may not share knowledge, even when the benefits (to potential receivers) are considerable. Sharing knowledge takes time and can sometimes undermine the source's competitive position. Further, it is obvious that not everyone in every situation is willing to share their knowledge. It must be performed voluntarily, intentionally and without the expectation of any external rewards, therefore it is costly which implies a limited willingness to share knowledge within an institution/company.

People live in complex and confusing times. More and more information is available at every human being fingerprints than ever before, yet it is too easy to get lost in the forest of data. At the same time, people accumulate so much information and are told to be knowledge workers and create knowledge culture. This means that the information needs to be more available to more people than at any time in the past. On an individual level, there is a need to create and refine information but not keep it to ourselves. On an organizational level, the knowledge sharing framework must be put in place to allow people to provide and find information quickly and easily without duplicating data. It should be possible to finish work faster, smarter, and with less effort, if information is provided according to appropriate procedures and to a suitable knowledge framework. In theory, it sounds very nice and optimistic, but in practice difficulties appear when knowledge culture becomes actuality.

People must assimilate the need to provide knowledge and to be willing to do this. Nowadays, too many people hoard knowledge in the hope that information represents power. While this is true for some critical data, such as lottery winning numbers for the next week, it is not usually true of the type of information found floating around research and business units especially within the same company. The challenge of changing individual attitudes to knowledge sharing is not easy and will not happen overnight [2.28].

Nowadays, the global society is oriented towards new knowledge production and sharing. More and more new research projects are developed in different areas of human being activities, while increasing work efficiency, comfort and safety. This means that the information needs to be more available to more people than at any time in the past. On an individual level, there is a necessity to create knowledge and distribute it, among others. On an organization level, the knowledge sharing framework must be applied to allow quick and easy knowledge sharing among people. Using well-

specified knowledge frameworks and appropriate knowledge sharing procedures, it should be possible to increase human work efficiency and accelerate knowledge culture growth.

Unfortunately, there is an attitude that knowledge can give power, position in the society and even money. Therefore, knowledge sharing even in scientific world is still affected by many constraints and probably will be as long as people do not change in the way of thinking. In science, access to knowledge is supposed to be open and therefore accelerate research progress. Unfortunately, the most important scientific databases have restricted access and charge an additional fee even if the author does not get any financial benefits from that.

2.5.1 PATENTS

Knowledge and development are key words in academia as well as industrial units, but up until now special efforts to protect the knowledge which is possess in companies are made. Knowledge is protected by patents, and this work is now being systematized. The objective is to protect the company knowledge, but also to ensure higher earnings.

Many companies' ambition and also DONG Energy's is to incorporate the patent work as a natural part of the research and development work in the company. In this way, it can be ensured that it will benefit fully from the value creation of what the development work brings.

Patents have been criticized as a restraint of trade which means the enforceability of contractual restrictions on freedom to conduct business. Particularly for conferring a negative right, whereas negative rights permit or oblige inaction, upon a patent owner, permitting them to exclude competitors from using or exploiting the invention, even if the competitor subsequently develops the same invention independently. Simply saying, in many cases it is impossible to develop and launch an idea to the business by a research centre with limited financial and potential resources.

From my research project perspective, it would be better to publish discoveries as scientific papers giving other possibility to learn and eventually further develop the ideas. Of course, it must be underlined that the project is not expected to produce a commercial product. As mentioned previously, the final outcomes of the project are model development procedures as well as analysis techniques supported by many delicate indirect solutions. Sharing this knowledge can be internally beneficial for commercial projects development within the company as well as externally helpful to strengthen cooperation with partners. Appropriate and purposeful knowledge sharing with partner companies creates a palette of opportunities to associate work as well as common goals; not only taken into consideration business projects aimed at giving money to commercial products such as wind farms.

2.5.2 PAPERS

Papers are more appropriate to improve knowledge sharing internally in the company but also outside, while at the same time strengthening the cooperation link between the company and other partners. Scholarship entrenched in an idea for transmitting knowledge via scientific or popular papers. When it is finished, it can be described as a static, one-dimensional paper, normally in PDF format. By appropriate knowledge sharing approach, the paper can no longer be treated as a static document. In the digital world papers can become living and breathing works by, for instance, linking to data sets, other relevant papers, other sources of information. But this needs to change the way of thinking about scholarly publishing, about knowledge sharing.

The idea is to start thinking of papers as containers of knowledge which do not like to be situated at the bottom of a drawer covered by many-year surface of forgiveness dust. And here networked knowledge solutions mentioned previously become an interesting alternative. They make the content legally and technically accessible. Where patents lock the knowledge presented in them, scientific and popular papers are characterized by open access. And by this term, one means its free availability on the public internet.

2.6 EXPECTED OUTCOME OF PROJECT

The industrial PhD project entitled "Harmonics in Large Offshore Wind Farms" had a well-defined background at the beginning. Of course, as in the case of many and probably all research projects, it is difficult to predict, especially at the very beginning, the final outcome. Behind harmonics analysis many, many various problem treatments can be specified. In Figure 2.8 the main project diversification can be found. Each level is expected to produce new knowledge about a defined area and is connected to the rest which simply means that even a small mistake in the analysis can affect the overall result.

Measurement data analysis methods are helpful to process noised signals with harmonics, and interharmonics and needed to be developed. In order to develop the methods, appropriate and reliable measurement data are needed. How to perform measurement and how to configure measurement equipment is another aspect of this long chain which consists of complex harmonic studies.

Well-developed and extended in time and frequency domain models of offshore wind farms connected to the power system directed to analyse possible resonances and power system impedance variation due to transmission system changes can only be developed based on the whole system behaviour premises obtained from appropriately processed measurement data.

Methods to analyse and predict unwanted resonances and complex nonlinear behaviour, due to small distortions in the whole power system modelled from

a nonlinear point of view [2.29], can be only validated by using appropriate techniques defined for a certain specific approach which was deeply analysed within the project.

One of objectives of the PhD project is to make generic model of various components in the wind farm power grid in the frequency range of interest for harmonic analyses of power grids. The following components will be included:

- Developing a voltage source converter simulation model as harmonic sources,
- Developing models of other wind farm network elements in relation to harmonics (i.e. the frequency range from DC to 5kHz) and dynamical behaviour,
- Developing the models of power grid element when needed.

Another desired outcome is to propose measurement approach, measurement data processing methods and validation techniques constituting a solid substrate for models and analysis methods development. The results of the PhD project should eventually provide proposals for new standards related to harmonics in offshore wind farms.

2.7 SUMMARY

A strong advantage of this project is that the project is industry-oriented. This creates a unique opportunity to carry out research gathering benefits from the industry (e.g. measurements, real-life study cases, etc.) as well as the academia (e.g. strong theoretical background, the newest trends in research, etc.).

Problems associated with harmonic generation and propagation in large offshore wind farms were briefly described in this chapter. Possible resonance scenarios affected by wind farm passive components are emphasized in case of large offshore wind farms. Various standards dealing with harmonic measurements and assessment are described and commented.

Also the philosophical approach of the research based on rationalistic tradition is shown. The research approach is compared to the proposed research and development framework. The framework is developed based on the experience gained during the project which was focused on real-life systems. Therefore, measurements, like in the rationalistic tradition, constitute an important part of the project and have significant contribution. Additionally, data processing, model development, model application methods, and validation are included in the framework and are equally important.

At the end of the chapter, few important aspects regarding knowledge sharing are put forward. It is observed that currently the idea of knowledge sharing is rapidly

developing, but still, there are many limitations affecting the general research progress. Few of the most important limitations are patents of undeveloped technologies, knowledge sharing culture, and limited access to databases.

2.8 REFERENCES

[2.1] D. D. Sabin, D. L. Brooks, and A. Sundaram, "Indices for assessing harmonic distortion from power quality measurements: definition and benchmark data," *IEEE Transactions on Power Delivery*, vol. 14, no. 2, pp. 489-496, Apr. 1999.

[2.2] B. W. Kennedy, *Power Quality Primer*. New York: McGraw-Hill, 2000.

[2.3] N. R. Watson and J. Arrillaga, *Power System Harmonics*. Wiley and Sons, 2003.

[2.4] A. Kusko, *Power Quality in Electrical Systems*. Blacklick: McGraw-Hill, 2007.

[2.5] C. H. Chien and R. W. G. Bucknall, "Theoretical Aspects of the Harmonic Performance of Subsea AC Transmission Systems for Offshore Power Generation Schemes," in *Proc. Generation Transmission and Distribution*, 2006, pp. 599-609.

[2.6] T. Ackerman, *Wind Power in Power Systems*. Wiley and Sons, 2005.

[2.7] Ł. H. Kocewiak, C. L. Bak, and J. Hjerrild, "Harmonic Generation and Mitingation by Full-Scale Converter Wind Turbines: Measurements and Simulation," in *International Workshop on Large-Scale Integration of Wind Power and on Transmission Networks for Offshore Wind Power Plants*, Aarhus, 2011, pp. 136-143.

[2.8] G. M. Masters, *Renewable and Efficient Electric Power Systems*. New York: John Wiley and Sons, 2004.

[2.9] G. J. Wakileh, *Systems Harmonics: Fundamentals, Analysis, and Filter Design*. Springer, 2001.

[2.10] N. Mohan, T. M. Undeland, and W. P. Robbins, *Power electronics: Converters, Applications, and Design*, 3rd ed. New York: Wiley and Sons, 2003.

[2.11] D. G. Holmes and T. A. Lipo, *Pulse Width Modulation for Power Converters: Principles and Practice*. IEEE Press, 2003.

[2.12] J. Verboomen, R. L. Hendriks, Y. Lu, and R. Voelzk, "Summation of Non-Characteristic Harmonics in Wind Parks," in *Proc. Nordic Wind Power Conference*, Bornholm, 2009.

[2.13] D. Fabiani and G. C. Montanari, "The effect of voltage distortion on ageing acceleration of insulation systems under partial discharge activity," *Electrical Insulation Magazine, IEEE* , vol. 17, no. 3, pp. 24-33, May 2001.

[2.14] S. Rahimi, W. Wiechowski, J. Ostergaard, and A. H. Nielsen, "Identification of problems when using long high voltage AC cable in transmission system II: Resonance and harmonic resonance," in *Transmission and Distribution Conference and Exposition*, Chicago, 2008, pp. 1-8.

[2.15] F. C. De La Rosa, *Harmonics and power systems*. CRC Press, 2006.

[2.16] L. Colla, S. Lauria, and F. M. Gatta, "Temporary overvoltages due to harmonic resonance in long EHV cables," in *International Conference on Power Systems Transients*, Lyon, 2007.

[2.17] G. J. Wakileh, *Power Systems Harmonics: Fundamentals, Analysis, and Filter Design*. Springer, 2001.

[2.18] Y. Cui and W. Xu, "Harmonic resonance mode analysis using real symmetrical nodal matrices," *IEEE Transactions on Power Delivery*, vol. 22, no. 3, pp. 1989-1990, Jul. 2007.

[2.19] N. R. Watson, A. R. Wood, J. Arrillaga, and B. C. Smith, *Power system harmonic analysis*. John Wiley and Sons, 1997.

[2.20] W. Wiechowski and P. B. Eriksen, "Selected studies on offshore wind farm cable connections – challenges and experience of the Danish TSO," in *Proc. Power and Energy Society General Meeting – Conversion and Delivery of Electrical Energy in the 21st Century*, July 2008, pp. 1-8.

[2.21] "Electromagnetic Compatibility (EMC) – Part 4–7: Testing and Measurement Techniques – General Guide on Harmonics and Interharmonics Measurements and Instrumentation, for Power Supply Systems and Equipment Connected Thereto," IEC 61000-4-7, August 2002.

[2.22] "Testing and measurement techniques – Power quality measurement methods," IEC 61000-4-30, 2008.

[2.23] "Wind Turbine Generator Systems – Measurement and Assessment of Power Quality Characteristics of Grid Connected Wind Turbines," IEC 61400-21, 2008.

[2.24] A. Morales, X. Robe, and M. J. C, "Assessment of Wind Power Quality: Implementation of IEC61400-21 Procedures," in *International Conference on Renewable Energy and Power Quality*, Zaragoza, 2005, pp. 1-7.

[2.25] H. Emanuel, M. Schellschmidt, S. Wachtel, and S. Adloff, "Power quality measurements of wind energy converters with full-scale converter according to IEC 61400-21," in *International Conference on Electrical Power Quality and Utilisation*, Lodz, 2009, pp. 1-7.

[2.26] T. Winograd and F. Flores, *Understanding computers and cognition: a new foundation for design*. Addison-Wesley Professional, 1987.

[2.27] H. R. Maturana, *Biology of Language: The Epistemology of Reality*. New York: Academic Press, 1978.

[2.28] T. Casciaro and M. S. Lobo, "Competent Jerks, Lovable Fools, and the Formation of Social Networks," *Harvard Business Review*, vol. 83, no. 6, pp. 1-9, Jun. 2005.

[2.29] Y. Kuznetsov, *Elements of Applied Bifurcation Theory*, 2nd ed. New York: Springer-Verlag, 1998.

Chapter 3
MEASUREMENTS

Measurements constitute an extremely important part of industry-oriented research projects. Therefore, it is of great importance to develop an appropriate measurement system for specific applications and to carry out well planned measurement campaigns. This chapter describes how the measurement system, comprising the software and hardware layer, was developed for harmonic measurement purposes. Additionally, measurement campaigns scheduled exclusively for the research project purposes are described including measurement points, wind farm description and measurement goals.

3.1 MEASUREMENT UNCERTAINTIES

All measurement set-ups had to face some error due to systematic (bias) and random (noise) error sources. By appropriate calibration of sensors and data acquisition boards and synchronization boards the systematic error can be significantly reduced. Specially designed EMC-proof boxes used during measurements were equipped with fans in order to keep constant ambient temperature by continuous forced air cooling. If the ambient temperature differs from the calibration temperature by more than ± 5 °C the results can be disturbed and it is recommended to recalibrate the data acquisition board. The data acquisition board input impedance is very high (1 MΩ as presented in Figure 3.10), therefore energy drawn from sensors (loading error) can be neglected [3.1], [3.2].

3.1.1 MEASUREMENT ERRORS

Precision and accuracy are terms used to describe systems and methods that estimate, measure, or predict. The method provides a measured value, which is wanted to be as close to the true value as possible. Precision and accuracy are ways of describing the error that can exist between these two values [3.3], [3.4].

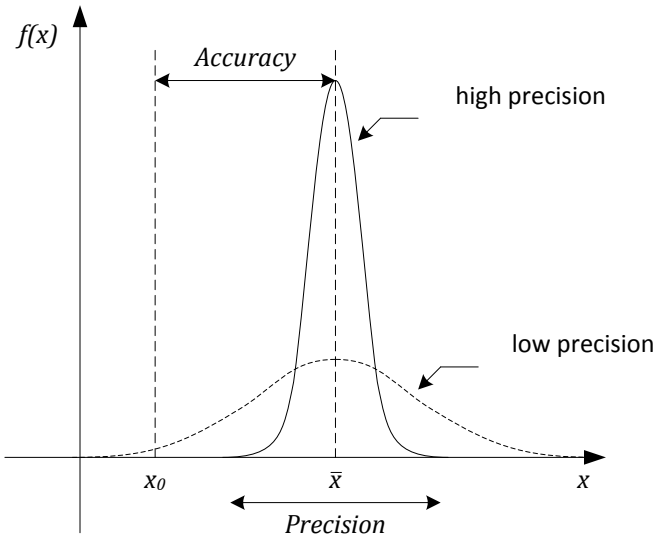

Figure 3.9 Accuracy indicates proximity of measurement results to the true value, precision to the repeatability or reproducibility of the measurement.

Poor precision results from random errors while poor accuracy results from systematic errors and is usually dependent on how the measurement equipment is calibrated. While random errors occur instantaneously, in the course of the measurements, the actual values of systematic errors are predetermined before the measurements get started. Therefore it is of great importance to be certain about possible systematic errors before measurement process is started in order to compensate errors and improve the accuracy. Random errors have to be attributed to small fluctuations of estimated values which affect the measuring process and prove to be uncontrollable. According to experience, the random errors of stationary experimental set-ups may be considered, at least in reasonable approximation, to follow a normal probability distribution. Due to fact that it is not a straight forward task to understand these phenomena in detail, some guidance in the central limit theorem of statistics [3.5] can be found. According to this, loosely stated, the superposition of sufficiently many similar random perturbations tends to a normal distribution [3.6].

A random variable is said to be normally distributed with parameters μ and σ^2, and can be written $X \sim \mathcal{N}(\mu, \sigma^2)$, if its probability density function is [3.7]

$$f(x) = \frac{1}{\sqrt{2\pi\sigma}} e^{-(x-\mu)^2/2\sigma^2}, -\infty < x < \infty \qquad 3.1$$

Precision of the measurement is expressed by quoting standard deviation, or signal-to-noise ratio.

The standard deviation can be described as the root mean square deviation of the measurements $x_1, x_2, \dots, x_N$. It proves to be a useful way to characterise the reliability of the measurements. The standard deviation can be estimated in the following way

$$s_x = \sqrt{\frac{1}{N-1}\sum_{i=1}^{N}(x_i - \bar{x})^2} \tag{3.2}$$

where $\bar{x}$ is the mean value as the best estimator following expressed

$$\bar{x} = \frac{1}{N}\sum_{i=1}^{N} x_i \tag{3.3}$$

Signal-to-noise ratio [3.8] is defined as the power ratio between a signal and the background noise

$$SNR = \frac{P_{signal}}{P_{noise}} \tag{3.4}$$

$$\begin{aligned} SNR_{dB} &= 10\log_{10}\left(\frac{P_{signal}}{P_{noise}}\right) = 10\log_{10}\left(\frac{A_{signal}}{A_{noise}}\right)^2 \\ &= 20\log_{10}\left(\frac{A_{signal}}{A_{noise}}\right) \end{aligned} \tag{3.5}$$

Before signal as meaningful information is logged it is also recommended to measure input noise level in order to assess the measurement precision [3.9].

From measurements it can be seen that signal-to-noise ratio which is defined by Eq. 3.5 is significant for higher frequencies. Some estimated signal-to-noise ratios around certain frequencies (i.e. carrier groups) in wind turbine measurements are presented in Table 3.1.

Table 3.1 Estimated signal-to-noise ratios around carrier groups in measured output voltage of the grid-side converter.

Carrier group	Frequency [Hz]	SNR value [dB]
1	2500	55
2	5000	48
3	7500	48
4	1000	39
5	12500	32

This shows that the analysis of frequency components above 8 kHz can provide inaccurate results. This also indicates that sample rate above 16 kS/s/ch is not necessary for long-term harmonic measurements. Please note that in practice the noise level in the estimated spectrum is also strongly dependent on the window length of the analysed signal.

3.1.2 ELECTROMAGNETIC INTERFERENCE DURING MEASUREMENTS

If during measurements the transfer of electromagnetic energy from source (emitter) equipment, which in a wind turbine is the main power circuit, through a coupling path to a receptor (receiver), which is the measurement equipment, an EMI occurs.

The most likely scenario for incompatibility occurs when a relatively high power circuit (i.e. power converter) is located near a very sensitive receptor (e.g. sensors, cables, measuring head unit) [3.10], [3.11]. Switch-mode high power density converters commonly used nowadays in wind turbines are potential generators of EMI due to the switching action of the converter The switching action generates a spectrum of the switching frequency and its harmonics. The main noise sources of switching frequency harmonics are the switched currents and the commutating diode. This noise is a combination of the switching frequency and its associated rise time (approximately 100 ns) and turn on spikes caused by the diode recovery current. This recovery current spike occurs at the end of a diode conduction cycle when reverse voltage is just applied by the transistor [3.10].

Different types of noise can affect the overall measurement process. The first type, known as differential mode noise, is propagated out one wire and other wire carries noise exactly equal and opposite. Differential mode noise amplitudes are usually minimal above 2 MHz because line-to-line or line-to-ground capacitance and wiring inductance tend to filter this type noise [3.10]. The other type of conducted noise, common mode noise, travels in the same direction in both wires and returns through the ground. Common mode noise, requires a different type filter. Common mode filters are usually common mode chokes. Such choke relies on the magnetic properties of ferrite cores to absorb common mode noise and were used during measurements as presented in Figure 3.10 [3.12].

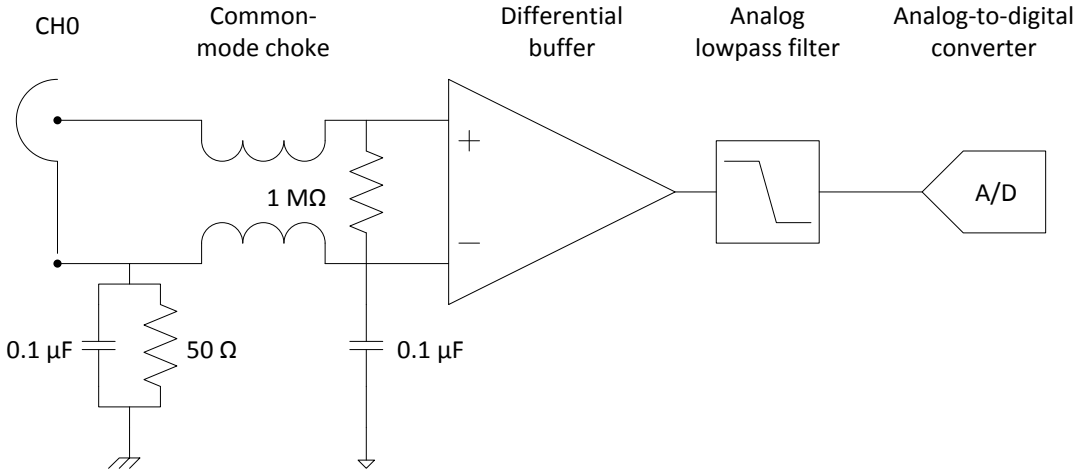

Figure 3.10 National Instruments 4472 data acquisition board analog block diagram.

Time-frequency representation of measured continuous-time signals achieved using continuous wavelet transform is presented in Figure 3.11. In order to analyse measured

signal which statistics vary in time and exhibits some oscillations non-orthogonal complex Morlet mother wavelet base was used. The theory behind wavelet transform will be described later in the part about measurement data analysis. Figure 3.11 shows how different frequency components affects measured open circuit channel from the 4472 data acquisition board working inside the wind turbine. It can be seen that within the first period (0-0.14 s) the wind turbine is producing and frequency components around 2.5 kHz and 5 kHz generated by the modulator of the grid-side converter can be easily observed. Later the wind turbine is stopped and only harmonics affected by the external network can be measured.

The channel was measured by SI-9001 voltage differential probe which full scale range is ± 7 V and input voltage differential range is ± 700 V. As it can be seen from Figure 3.11 the measured noise is less than 1 % of the sensor full scale range and does not affect measurements significantly. Still it has to be emphasized that the interference is much higher when the power electronic equipment of the main power circuit in the wind turbine is in operation. Normally open circuit measurements performed in laboratory conditions are very close to Gaussian distribution (not including crosstalk between adjacent channels). Additionally it has to be emphasized that the crosstalk for adjacent channels is lower than -80 dB and the idle channel noise for applied sample rate (44.1 kS/s) is -94 $\mathrm{dBV_{max}}$.

The width of a wavelet function is defined here as the e-folding time of the wavelet amplitude and for Morlet wavelet basis function is equal to $\sqrt{2}s$, where s is a wavelet scale. The black line in Figure 3.11 indicates cone of influence, region of the wavelet spectrum in which edge effects became important as the e-folding time for each at each scale [3.13].

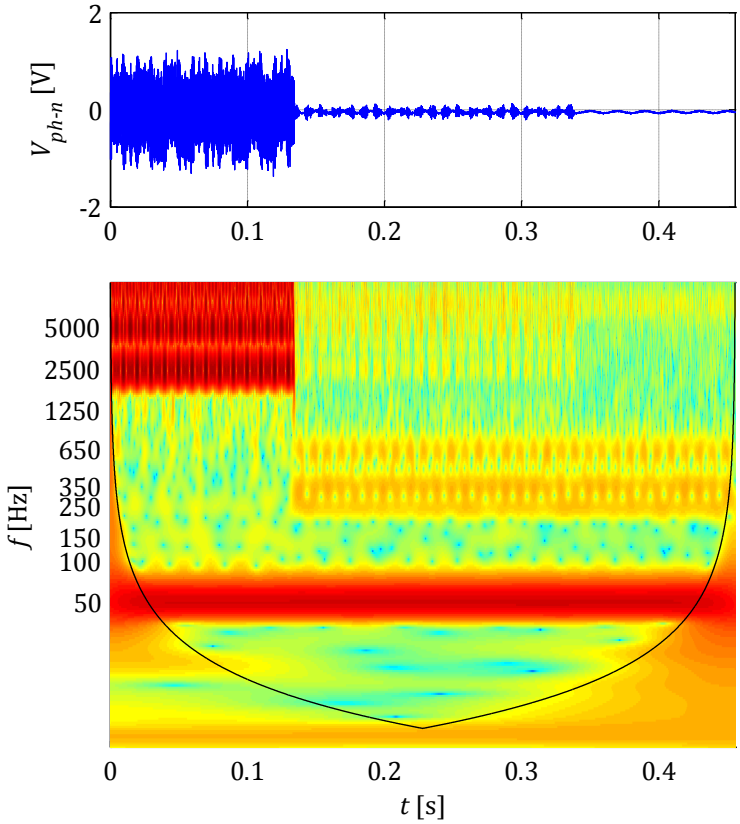

Figure 3.11 Continuous wavelet transform showing electromagnetic interference in the wind turbine.

3.2 Measurement System Description

In order to perform appropriate harmonic measurements a measurement system was developed taking into consideration measurement campaign's goals. Extensive measurement campaigns were carried out to provide trustful and representative data for harmonic analysis purposes. The measurement system was optimized in order to meet challenging requirements of measurement in rough offshore environment. The optimization process was focused on both hardware and software layer of the measurement setup. An illustrative description of the developed measurement system is presented in Figure 3.25 and more detailed description is in Figure 3.26.

3.2.1 Software Layer

One of the most important parts in harmonic measurement process is measurement software, developed and optimized for the respective applications. It must be emphasized that there is no possibility to develop and validate accurate analysis methods for harmonic emission assessment without appropriate electrical quantities measuring and later processing of data. This is a crucial issue nowadays in large offshore wind farms, characterized by an extended and complex structure. In such

systems measurement software must be carefully developed, and it begins to play a significant role.

Developed software for long-term harmonic measurements has to meet certain requirements in order to provide reliable and trustworthy measurement system. More complex data logging structure is introduced in long-term logging. Additional buffer represented by linear data structure and appropriate design pattern are used to secure long-term data acquisition without any interruptions and user interference.

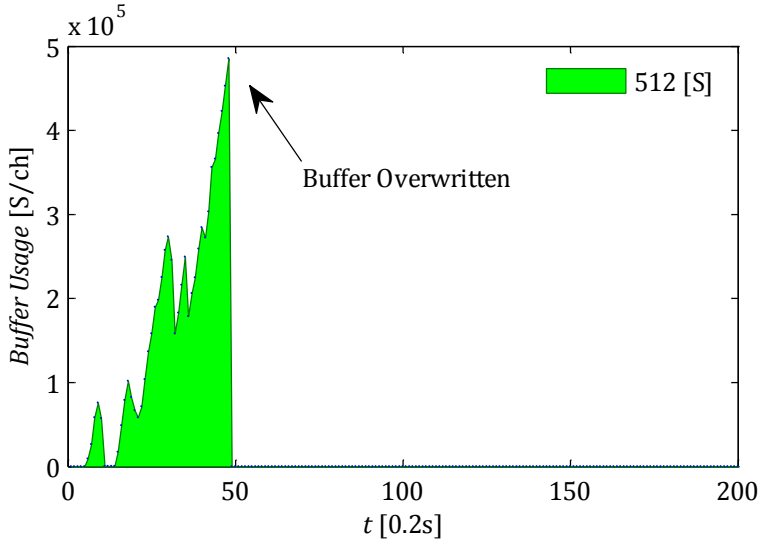

Figure 3.12 The requested sample is no longer available, because of buffer overrun.

The most typical problem in high-speed logging, when the use of measurement system processing capabilities reaches its limits, is buffer overflow. And if attempted to read samples that are no longer available, this can only mean that the single, fixed-size, circular buffer is overrun. It is a good habit to monitor the buffer during a continuous acquisition, to ensure the data is not overwritten. There is a need to apply some adjustments, if the value continuously increases during the acquisition as can be seen in Figure 3.12. Of course, buffer monitoring also takes some measurement system resources which can be directly used for data logging purposes, so only the measurement software development seems to be a reasonable solution. Please note that scale 0.2s used on the abscissa (i.e. horizontal axis) in Figure 3.12 donates the step size (interval) between neighbouring samples. For instance, if there are 200 samples in the presented results the total duration is 40 seconds (i.e. $0.2\text{s} \times 200 = 40\text{s}$).

By introducing an additional circular buffer used in the producer-consumer design pattern represented by a linear data structure such as first-in-first-out queue, it is possible to reduce user-defined buffer usage to which are copied samples directly from the data acquisition board buffer. This sample manipulation significantly increases the measurement system reliability.

Data is acquired with relatively small sampling rate which means the measurement unit is not overloaded during data acquisition and logging. For long-term measurement

purposes data must be saved in separated files every certain period to improve management of the large amount of data. In order to improve this process data acquisition and data logging have to be separated on the software level and asynchronously executed. This can be successfully implemented based on producer-consumer pattern.

3.2.1.1 DATA COMPACTION

The primary factors which affect reliable long-term streaming to disk (e.g. continuous acquisition of many channels) in a PC-based data acquisition system are disk I/O bandwidth, central processing unit (CPU) bandwidth, and bus bandwidth. Assuming the developed measurement system has sufficient bandwidth for both the disk I/O as well as the bus, data compaction can provide significant performance gains for high-speed streaming to disk applications.

Data compaction significantly reduces storage device footprint, therefore by reducing it, data transfer can affect streaming-to-disk performance. If measurement data compaction is performed on a hardware level, no additional CPU resources are needed and can be successfully applied for long-term logging purposes. If data compaction is performed on a software level, data logging requires CPU bandwidth while hard drive footprint optimization. During data logging it is recommended to save raw data directly acquired by the data acquisition device without any data processing at this stage. If one can store appropriate sensors scaling information then only raw data will be stored. Right now many commercial applications can do so by an appropriate user application interface. Streaming the raw data to a file generally speeds up the measurement application and reduces the disk footprint of data files.

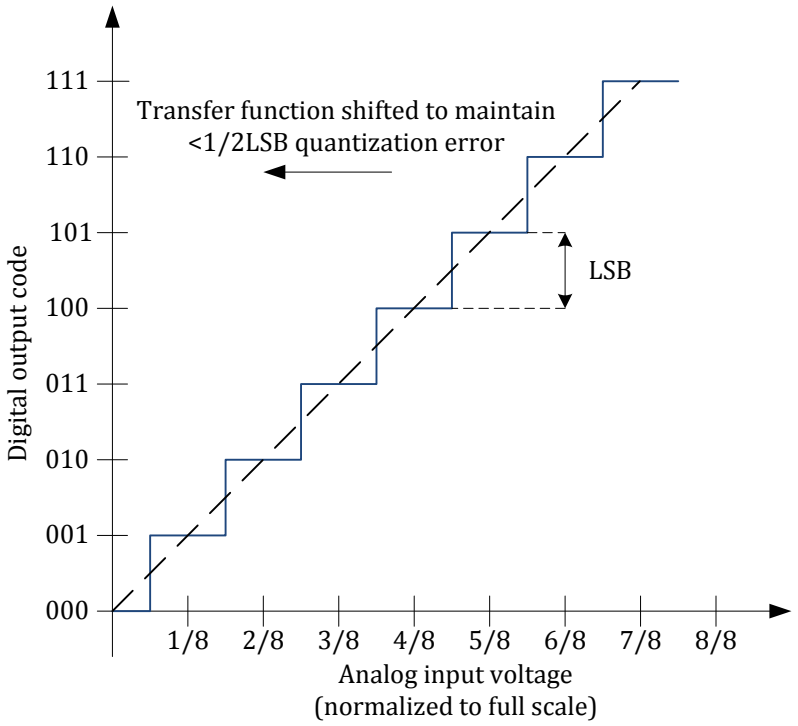

Figure 3.13 Analog-to-digital converter with 3-bit resolution and with - 1/2 LSB offset.

Data acquisition device developers improve all the time dedicated drivers in order to optimize usage of all of the above significant factors such as bus, CPU, and I/O bandwidths. If during data acquisition and logging process still some resources are available data compaction is strongly recommended. The simplest data compaction could be performed by removing bits at the end of samples out and the resulting samples are packed into memory. It is of great importance to know the analog-to-digital converter resolution in order to estimate how many least significant bits (LSBs) can be discarded in order not to lose any information, in other words use lossless data compression. LSB is defined as the minimum increment of the voltage that an analog-to-digital converter can represent as a digital output. Hence, LSB varies with the operating input voltage range of the analog-to-digital converter. Figure 3.13 illustrates the resolution for a 3 bit analog-to-digital converter and graphical representation of LSB. Sometimes a sensor operating range does not cover the whole range of data acquisition device acceptable input voltages. In this case the lossless compression is even more efficient. In this situation, the number of bits M_S needed to digitally represent the signal without any losses can be expressed in the following way

$$M_S = \left\lceil \log_2 \left(\frac{E_s}{Q} \right) \right\rceil \tag{3.6}$$

where Q is the analog-to-digital converter resolution which can be expressed as

$$Q = \frac{E_{DAQ}}{N} \tag{3.7}$$

$$E_s = V_{S_{Hi}} - V_{S_{Low}}$$
$$E_{DAQ} = V_{DAQ_{Hi}} - V_{DAQ_{Low}}$$
$$N = 2^{M_{DAQ}}$$

where E_s is the full scale voltage range of the sensor, E_{DAQ} is the full scale voltage range of the analog-to-digital converter, $V_{S_{Hi}}$, and $V_{DAQ_{Hi}}$ are respectively the upper extremes of the sensor and the analog-to-digital converter operating ranges, $V_{S_{Low}}$ and $V_{DAQ_{Low}}$ are respectivley the lower extremes of the sensor and the analog-to-digital converter operating ranges, N is the number of voltage intervals, and M_{DAQ} is the analog-to-digital converter resolution in bits. The resolution of the converter Q indicates the number of discrete values it can produce over the range of analog values and is equal to LSB voltage.

For example, a data acquisition device with 24-bit resolution (e.g. PXI-4472) is taken into consideration and a 32-bit sample size is returned, e.g. unsigned integer or signed integer. If the full scale range of the input signal acceptable by the data acquisition device is ± 10 V and the sensor full scale range output voltage is ± 2.5 V, the number of bits $M_s = 22$. This means that 10 bits are unused. Discarding those bits reduces the required disk space by 31.25 %.

Please note that in some cases data was acquired for four weeks with sample rate of 44.1 kS/s/s and 20 analog inputs. Let us assume that no data compaction is applied so each of samples acquired by 24-bit analog-to-digital converter should be represented by 32-bit signed integer (I32). Thus it is easy to calculate that such a period of data logging will require 3974.4 GB storage place.

In some cases, no data is lost because the samples already contain unused bits. During data acquisition, two types of compression can be used: lossless packing, and lossy LSB removal. Lossless packing will take off unused bits (i.e. the 8 most significant bits (MSBs) that are discarded because the analog-to-digital converter resolution from the example above is only 24 bits). Lossy LSB removal does the same, and then removes the lower bits as well. This becomes very useful if the sensor accuracy is much smaller than LSB. Assuming the sensor has 1 % accuracy which means that measuring values with analog-to-digital converter LSB less than 25 mV are of great uncertainty, and the analog-to-digital converter performance with LSB of 1.2 µV is definitely not fully used.

Lossless packing removes unused bits from samples. No information carrying bits is lost, and the resolution is kept. Lossy compression removes unused bits from samples. Then, if necessary, also lower bits from the samples as specified are removed. This compression type limits resolution to the specified sample size.

3.2.1.2 ASYNCHRONOUS STRUCTURE

The master-slave pattern is generally useful when two or more processes are expected to run continuously but at different rates. The master-slave design pattern supports fault tolerance, parallel computation and computational accuracy. A master component

distributes work to identical slave components and computes a final result from the results these slaves return [3.14].

The producer-consumer problem is a classic example of a multi-process synchronization problem (e.g. data acquisition and data logging in measurements). The problem describes two processes, the producer and the consumer, which share a common, fixed-size buffer. The producer's task is to provide a data item, put it into the buffer and start again. At the same time the consumer is consuming the data, removing it from the buffer, one data item at a time. The problem is to make sure that the producer will not try to add data into the buffer if it is full and that the consumer will not try to remove data from an empty buffer. One of the more common patterns in threaded programming is based on the problem described above, videlicet the producer-consumer pattern. The idea is to process data asynchronously by partitioning requests among different groups of the thread. The producer is a thread that generates requests (or data) to be processed. The consumer is a thread that takes those requests (or data) and acts upon them. This pattern provides a clean separation that allows for better thread design and makes development and debugging easier [3.15]. The producer-consumer pattern is really just a subclass of the master-slave pattern where the main communication between the loops is via queue. Using queues rather than global variable to pass data provides a buffering effect, but if the data writer occasionally produces data faster than the reader can process it, data will not be lost [3.16].

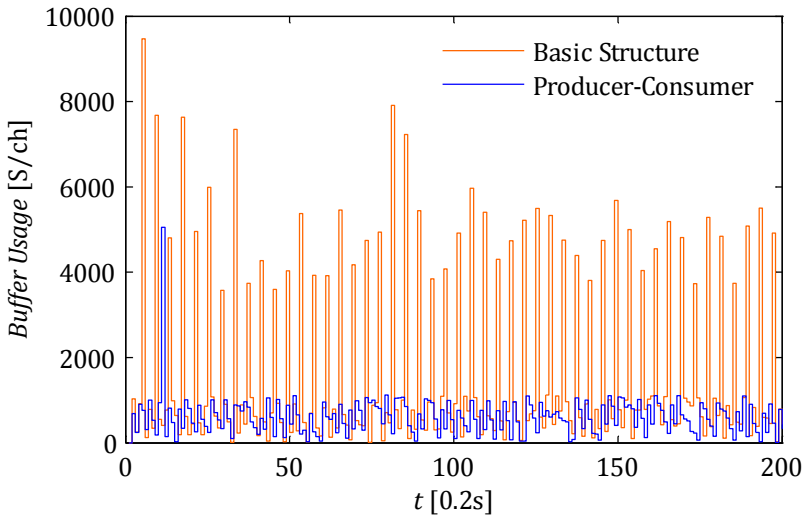

Figure 3.14 Basic measurement software compared with producer-consumer application.

The producer-consumer design pattern is geared towards enhanced data sharing between multiple loops running at different rates. The producer-consumer pattern is used to decouple processes that produce and consume data at different rates (see Figure 3.15). This can be easily observed in real-time applications such as data acquisition and logging. Data acquisition is strictly dependent on sample rate and cannot afford any significant delays. However data logging rate is dependent on I/O

bandwidth which can be affected by many factors which will be shown later. The producer-consumer pattern's parallel loops are broken down into two categories; those that produce data and those that consume the data produced. Data queues are used to communicate data between loops in the producer-consumer design pattern. These queues offer the advantage of data buffering between producer and consumer loops.

In described application, the producer loop acquires data from a data acquisition device and passes it to a queue. At the same time, the consumer loop reads data from the queue and writes it to a hard disk. During the whole process, the queue is handled as a block of allocated PC memory. This memory block is utilized as a temporary storage first-in-first-out (FIFO) for data passing between two loops. In most programming languages, sharing memory between multiple processes requires significant overhead programming. This makes the application of this structure impossible for short high-speed data streaming applications, but is very helpful in case of long-term harmonic measurements, thus improving the reliability and robustness of the overall measurement software.

Figure 3.15 Producer-consumer pattern for asynchronous partitioning requests among different threads.

In a FIFO data structure, the first element added to the queue will be the first one to be removed. This is equivalent to the requirement that whenever an element is added, all elements that were added must be removed before the new element can be invoked. A queue is an example of a linear data structure [3.17].

The comparison between measurement software with and without additional buffer is show in Figure 3.14. The additional buffer also assures that all of the acquired samples would be saved providing continuous and robust long-term data logging.

3.2.1.3 OTHER ASPECTS

Many aspects during measurement system development process should be taken into consideration. This covers optimization on both hardware as well as software level. In order to provide reliable measurement system for harmonic analysis purposes it is of great importance to optimize it for this specific application.

Deterministic versus non-deterministic

A program is deterministic on a given input if every memory location is updated with the same sequence of values in every execution. The program always behaves the same way. Two different memory locations may be updated in different orders, but each location always sees the same sequence of updates. A determinacy race [3.18] occurs when two logically parallel instructions access the same memory location and at least

one of the instructions performs the same memory allocation and at least one of the instructions performs a write. A program execution with no determinacy races means that the program is deterministic on that input. The program always behaves the same on that input, no matter how it is scheduled and executed [3.19].

Windows OS does not allow, due to its non-deterministic nature, to really optimize applications especially for measurement purposes or set the priority of a measurement application. Since the Windows environment is non-deterministic, the time to execute the same code will differ every time it is executed. These properties can be controlled in a Real-Time OS where the determinism can be forced (the code will execute in the same amount of time every time). A Real-Time OS is designed to run applications with very precise timing and a high degree of reliability [3.20]. Within the confines of harmonic measurements described here, measurement system designed for Windows will be taken into consideration.

File pre-allocation

File pre-allocation is another logging optimization possibility. One can specify the file size ahead of time to pre-allocate. This might gain enough performance to get over the hump. File size pre-allocation specifies a size in samples to be used to pre-allocate space on drive. Pre-allocation can improve file I/O performance, especially in situations where multiple files are being written to the disk. If the finite number of samples to be acquired is specified, it is easy to pre-allocate the file based on the number of samples configured to acquire. Unfortunately, in case of continuous logging, this value must be specified based on user expectations, but it still offers significant flexibility and performance increase. Please note that harmonic measurements are expected to be a long-term process (e.g. weeks or even months) which requires acquisition of large amount of data. Due to this fact acquired data is saved in many files with fixed size which allows specifying exactly the size of pre-allocated file.

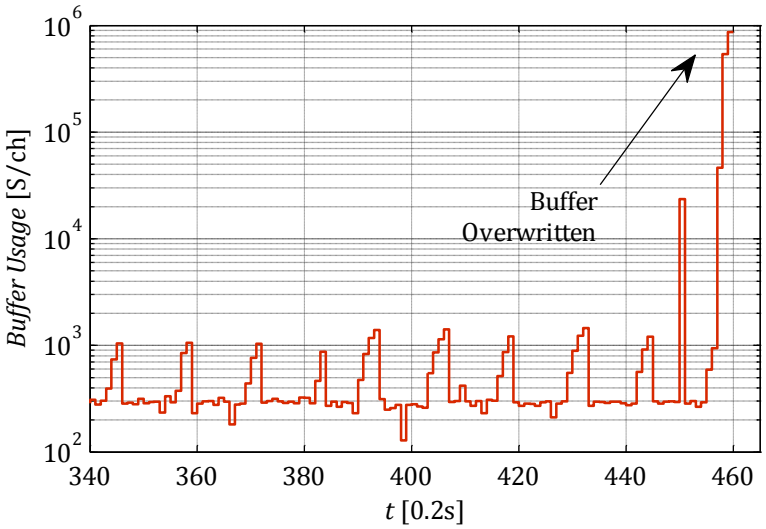

Figure 3.16 Buffer overflow after the pre-allocated file size is exceeded.

Figure 3.16 illustrates the importance of the file size pre-allocation. It can easily be seen that the number of samples in the buffer is being kept roughly constant with a value slightly less than $1 \cdot 10^3$ s and when the pre-allocated file size was exceeded, the samples in the buffer were overwritten by the data acquisition card. The number of samples in the buffer gets higher than defined buffer size, which in this case is $1 \cdot 10^6$ s.

Non-buffered I/O

This feature would bypass application memory (user's buffer) and write to the disk directly from kernel memory (user-kernel shared buffer), which results in lower CPU usage and higher streaming performance (assuming the drive is physically capable of writing this much data). Direct I/O is an unbuffered [3.21] form of I/O. The user is requesting direct data transfer between the disk and the user-defined, sector aligned, user-kernel shared buffer for reads and writes. This bypasses additional buffering of data between the kernel memory and the application memory, and reduces the CPU overhead associated with I/O by eliminating the data copy between the kernel buffer and the user's buffer. This also prevents that space in the buffer cache being taken up, that might be better used for something else. The direct I/O feature can provide significant performance gains for data acquisition applications. The CPU cost of direct I/O is about the same as a raw disk transfer. For sequential I/O to very large files, using direct I/O with large transfer sizes can provide the same speed as buffered I/O with much less CPU overhead.

With a disabled system caching, an application must fulfil certain requirements. In these circumstances, user-defined within the application local buffer is the only file buffer that exists for write access. Because of physical disk layout, file system storage layout, and system-level file pointer position tracking, this write operation will fail, unless the buffer meets certain alignment criteria. File access size specified as a number of bytes must be an integer multiple of the volume sector size and file access buffer addresses for read and write operations should be sector-aligned, which means aligned on addresses in memory that are integer multiples of the volume sector size.

Specifying the size, in samples, in which data will be written to disk can significantly improve the overall performance of the measurement system designed for logging large amount of data. The size must be evenly divisible by the volume sector size of the drive, in bytes, or cluster size (i.e. the smallest drive allocation unit) [3.21]. In order to improve logging performance, one can seek the most optimum settings for a particular hardware configuration. The sector size is typically 512 bytes, so a good practice is to start with 512 and work up from this value by increments of 512. Table 3.2 shows approximate buffer sized dependent on assumed sample rate. The influence of this parameter will be discussed more broadly later.

In order to start data streaming, the user specifies the size of the buffer. Using very large buffers may result in diminished system performance due to excessive reading and writing between memory and the hard disk. Reducing the size of the buffer or adding

more memory to the system can reduce the severity of these problems. Before starting a transfer of data from the data acquisition card to the PC, the driver needs to allocate a buffer to hold the data and lock the buffer into the PC's physical memory.

Table 3.2 Recommended by National Instruments [3.22] approximate buffer size in samples per channel dependent on sampling rate.

Sample Rate [S/s]	Buffer Size [kS]
0–100	1
100–10,000	10
10,000–1,000,000	100
>1,000,000	1000

The buffer size adjusted before measurements is allocated for data acquisition and is independent of the size of the data acquisition card's onboard buffer. The specified buffer will be a user-kernel shared, page-locked buffer allocated by the driver. Data are streamed directly from that user-kernel buffer to disk. If data are read and processed, the data are additionally taken from the buffer and copied (and scaled) into the user's application buffer. That is why data processing, i.e. data scaling, filtering, single tone detection, is not recommended during data logging and can significantly decrease the performance or even interrupt measurements. In case of data logging only, the user-mode buffering of data is bypassed, therefore overall measurement system overhead is reduced (like CPU utilization and memory bandwidth) by eliminating the data copy between the kernel buffer and the user's buffer. User-kernel shared buffer is characterized by low latency and high throughput.

Synchronous and asynchronous I/O

Supporting asynchronous write to disk, or overlapped I/O can improve data logging process. Overlapped I/O allows multiple threads to write to the file and at the same time optimize write to file speeds. In synchronous file I/O, a thread starts an I/O operation and immediately enters a wait state until the I/O request is completed. During file I/O operation in the synchronous I/O mode the thread execution is installed awaiting completion of the I/O operation instead of performing processing. This significantly decreases the system performance, and thus an asynchronous I/O has been introduced. A thread performing asynchronous file I/O sends an I/O request to the kernel by calling an appropriate function. If the request is accepted by the kernel, the calling thread continues processing another job until the kernel signals to the thread that the I/O operation is complete. It then interrupts its current job and processes the data from the I/O operation as necessary [3.21].

Asynchronous I/O allows a thread to request I/O operations and continue performing other computational tasks until the previously requested I/O operations have been completed. This makes for greater parallelism in completing computational tasks as

opposed to the purely sequential model in which a thread must wait for an I/O operation to proceed before it proceeds with other activities.

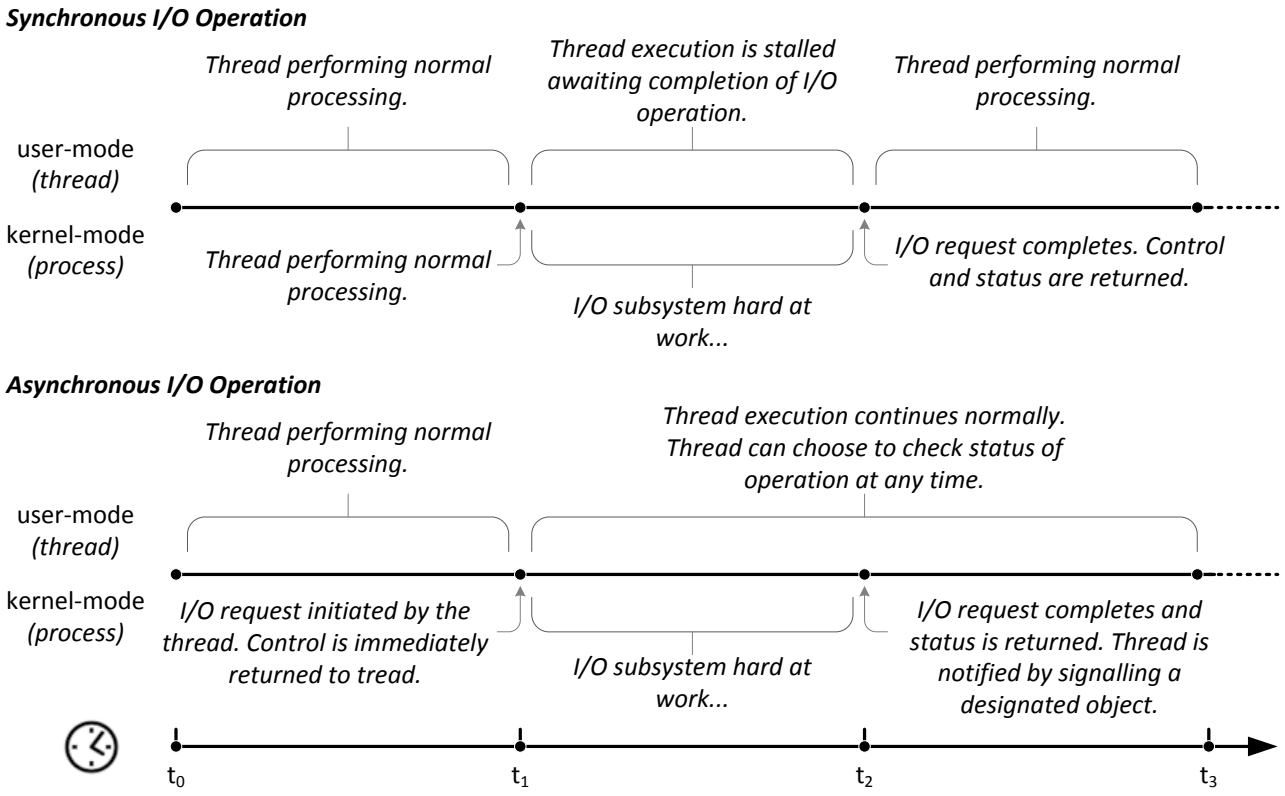

Figure 3.17 Activities of synchronous and asynchronous I/O operations.

Figure 3.17 graphically illustrates the sequence of activities that occurs when performing synchronous and asynchronous I/O operations. As it can be seen from the illustration, the thread using asynchronous I/O can continue performing computational activity in parallel with the servicing of the I/O request it has initiated. This results in higher performance and higher net throughput for the system. Note that the default I/O mechanism is the synchronous model [3.23].

In situations where an I/O request is expected to take a large amount of time, such as long-term measurements, asynchronous I/O is generally a good way to optimize processing efficiency. However, for relatively fast I/O operations, the overhead of processing kernel I/O requests and kernel signals may make asynchronous I/O less beneficial, particularly if many fast I/O operations need to be made. In this case, synchronous I/O would be better. Asynchronous data transfer requires page-locked host memory which cannot be reallocated by the operating system.

3.2.2 HARDWARE LAYER

3.2.2.1 SENSORS

Some of the power quality disturbances of interest such as harmonics and transients require the measurement of significantly higher frequencies than commonly used for measurement purposes of electrical quantities close to the grid frequency. For those

frequencies the accuracy of the instrument transformers can no longer be taken for granted. For some measurements special equipment such as differential voltage sensors, Hall-effect based current sensors and Rogowski coils is being used.

Precisely selected sensors were used for harmonic measurement purposes. It was expected to carry out measurements with sample rate of 44.1 kS/s/ch which requires sensors with a flat bandwidth (± 3 dB) at least up to 22.05 MHz. Since the frequency band of interest in case of harmonic measurements is relatively low most of the probes available in the market (e.g. differential voltage sensors, Rogowski coils) are suitable. Of course such frequency range of interest creates also problems with electromagnetic interference. It was expected to have higher frequency components than the Nyquist frequency therefore additional anti-aliasing filtering was crucial. In order to deal with the electromagnetic interference, EMC-proof boxes were used as well as sophisticated shielding solutions.

Current measurements

In order to measure currents Powertek CWT3LF and CWT30LF flexible Rogowki coils were used with 0.055 Hz - 3 MHz minimum bandwidth. The cable from sensor to integrator is a fixed-length double screened RG58 type which is suitable to be used in harsh wind turbine electromagnetic environment. The cable is relatively long (8 m) and cable parasitic capacitance is compensated to achieve flat performance within the bandwidth. Please note that there is an extremely limited space in wind turbines and thus wind turbine main power circuit components are situated on different levels (relatively far from each other). Also the integrator, to which the Rogowski coil is connected, by its low-pass filter nature is suitable to attenuate electromagnetic interference.

Voltage measurements

Additionally SI-9001 differential voltage sensors with bandwidth of DC-25 MHz were used and capacitive MV voltage sensors installed as "dead-end" T-connectors with bandwidth of 1 Hz-1 MHz.

A standard MV T-connector is installed to the MV network as a "dead-end" and the phase-to-earth voltage is measured using an end-plug. Since the capacitive end-plug is not normally used for precision measurements, an amplifier for precision measurements with high frequency response developed by DELTA has been used [3.24].

The MV voltage probes and amplifiers were calibrated in the high voltage laboratory at DTU. The corresponding gains and offsets of each voltage probe-set were found using the variable frequency voltage amplifier. The high voltage amplifier used at DTU is TREK P0621P and a Tektronix P6015A High Voltage Probe.

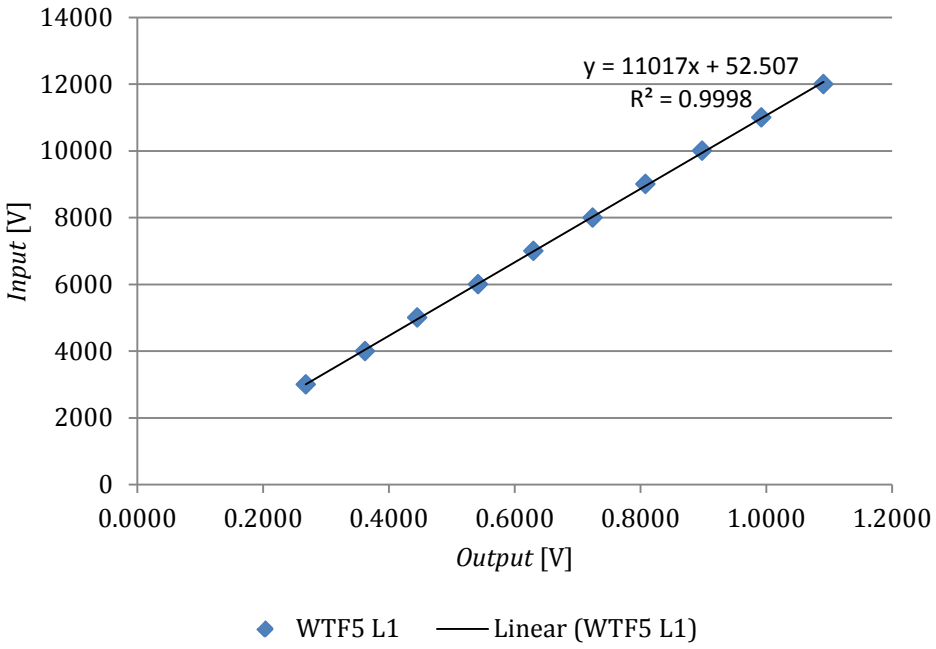

Figure 3.18 Input-output characteristic from one of the voltage probes.

Some of the results from the calibration are shown in Figure 3.18; here it is possible to see that the sensor has a linear characteristic from 3 kV to 12 kV. Once the main values of the linear characteristic are known, appropriate scaling factors were programmed in the software to be used during the measurement campaigns. Please note that the coefficient of determination is almost equal to 1.

Additionally frequency dependent characteristic of the capacitive voltage sensor together with dedicated amplifier was obtained. Please note that it is difficult on lab scale to obtain full range of possible frequencies and harmonic amplitudes. It was decided that frequency range up to 3 kHz should be enough within the most significant observable harmonic components in wind farms. As it can be seen from Figure 3.19 the T-connector has constant gain within a wide frequency range. Only for low frequencies there are insignificant differences and therefore the coefficient of determination is not close to 1.

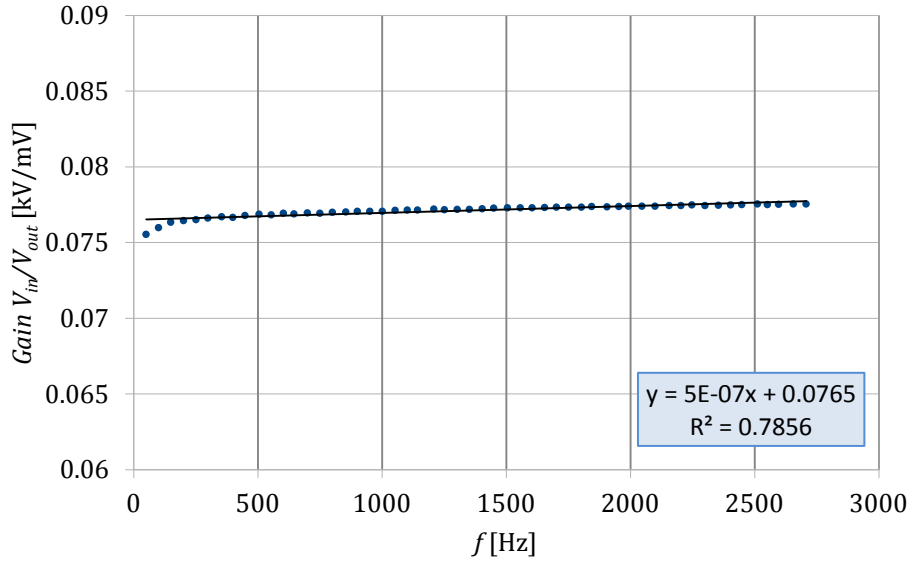

Figure 3.19 Capacitive voltage sensor frequency dependent characteristic.

Since the offshore wind farms have particular operating conditions and environmental constraints, special attention should be placed when selecting additional equipment to be installed offshore as measurement equipment. In order to avoid problems in the field measurements (e.g. electromagnetic interference, relatively high humidity, transportation, reliable built and casing), industrial solutions were used. For example the LV voltage probes installed in the wind turbines were fitted to the terminals of the switchboard and DC/AC converter though fuses and banana plugs. The MV voltage probes were built with standard cables and cable connections.

3.2.2.2 SYNCHRONIZATION

Another very important aspect of measurement system configuration for long-term harmonic measurements in wind farms is a reference timestamp. Especially in case of offshore measurements where data logging is carried out simultaneously in different locations.

The measurement system was prepared for simultaneous measurements in few different places with synchronization according to the global positioning system (GPS) timestamp. Measurement software for is designed to start according to a digital trigger synchronized which is specified by user GPS timestamp as is shown in Figure 3.20. This allows starting measurement almost in the same time. There are of course some accuracy considerations which will be described later. It must be underlined that the synchronization accuracy of this measurement method is limited to the stability of the sample clock timebase which can randomly drift in time. Due to fact that measurements for harmonic studies are normally carried out at least within few weeks, the synchronization process must be repeated periodically.

When the measurement process starts, an initial time reference is defined, data points can be later referenced using the time period of the data acquisition device sample

clock. However, if this clock is not aligned with a GPS time reference anymore, the accuracy of the timestamp data degrades over time as the clock skews. Every oscillator introduces drifts according to a random walk pattern.

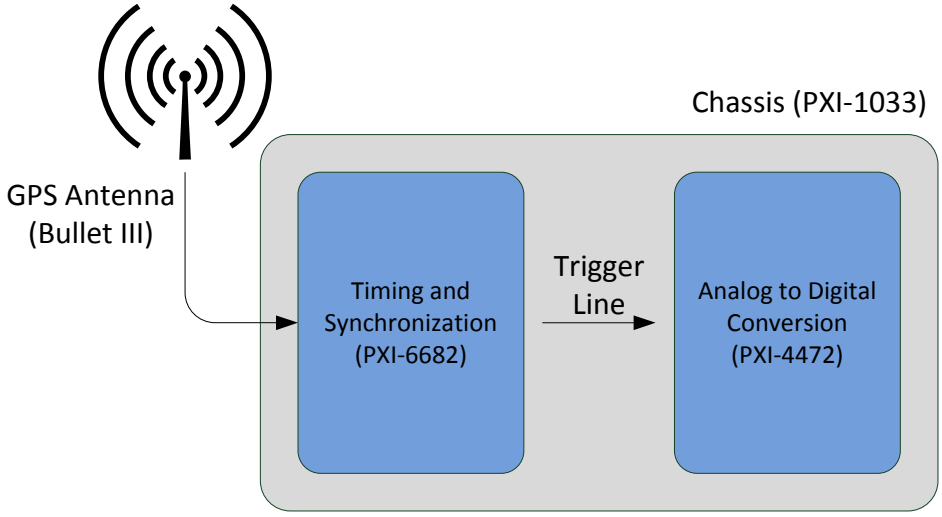

Figure 3.20 Trigger according to specified timestamp synchronized with GPS.

Suppose the master clock timebase of a data acquisition device has a stability of 25 ppm (e.g. PXI-4472), which is quite popular value nowadays for data acquisition devices in the industry, the worst case scenario of timestamp accuracy after one minute of continuous measurement will be the following: $25 \cdot 10^{-6}$ drift error $\times$ 60 seconds per minute = $15 \cdot 10^{-4}$ drift error seconds per minute.

So in the worst case scenario, the timestamps will be inaccurate by a factor of 1.5 ms per minute. By continuously aligning data every minute from the data acquisition device with a GPS-derived clock, it will be ensured that the accuracy of the timestamps over long acquisition periods will be within acceptable range for harmonic measurements. Even if the oscillator will drift the timestamp of measured data will be every certain defined period aligned according to the GPS time stamp. Of course the worst case scenario is described above and normally an oscillator would drift in time according to random walk pattern.

The accuracy of the timestamps is a function of the accuracy of the hardware and the GPS satellites. Though the atomic clock on the GPS satellites is accurate to 10^{-13} seconds, the accuracy of the time signals they send for civilian use is only guaranteed to be within $\pm$170 ns of UTC [3.25]. If the propagation delays in the measurement chassis are within this limit and assumed to be constant, the time accuracy of the acquired data should be within $\pm$170 ns of UTC.

Used for offshore measurement purposes, receivers provide a 1 pps on-time pulse. The GPS receiver is limited to using SPS the uncertainty is defined by the top row in Table 3.3. It shows that there is a 50 % probability that a given on-time pulse from GPS will be

within ±115 ns of UTC. The 1σ uncertainty of GPS (~68 % probability) is ±170 ns, and the 2σ uncertainty (95 %) is ±340 ns [3.26], [3.25].

Table 3.3 Timing uncertainty of GPS in One-Way Mode.

Service	Uncertainty (ns) 50th percentile	Uncertainty (ns) 1σ	Uncertainty (ns) 2σ
SPS	±115	±170	±340
PPS	±68	±100	±200

To achieve uncertainties presented in Table 3.3 one has to calibrate the receiver and antenna delays, and estimate synchronization errors. The antenna providing reliable performance in harsh radio frequency jamming environments was connected to the receiver and mounted outdoors where it had clear, unobstructed view of the sky. This condition can be easily satisfied in large offshore wind farms situated far from natural barriers and effects such as multipath propagation [3.27] due to the signal reflection, and high dilution of precision when detected satellites are close together in the sky, can be neglected. Positional accuracy was improved due to the fact that the wind turbines and the substation at Gunfleet Sands offshore wind farm are situated far from each other and naturally are far from multipath reflectors (see Figure 3.21) [3.28].

Figure 3.21 GPS antenna mounted at the top of the Gunfleet Sands offshore substation.

In order to synchronize accurate transient measurements, digital hardware trigger was used based on absolute GPS timestamp obtained from a timing and synchronization board with temperature-compensated crystal oscillator (TCXO) characterized by onboard high-stability 10 MHz reference (±1 ppm) guaranteed over the operating

temperature range. The GPS receiver on the PXI-6682 used as a part of the measurement equipment used for software tests can power an active GPS antenna and receive and process the radio frequency signals (1.575 GHz) from satellites. It generates a very precise pulse-per-second (PPS) signal that the board uses to achieve sub-microsecond synchronization. Therefore, one can use the timing and synchronization board to synchronize spatially located measurement systems, as long as GPS satellites are visible to the antenna from those locations. This configuration can provide the trigger accuracy of 100-200 ns.

It is important to mention that in all location data was acquired using the same data acquisition boards with the same sampling rate, so phenomena such as filter delay does not affect the synchronization effectiveness. Also RG59/U coaxial cables with the same length of 30 m were used to connect the active GPS antenna with the timing and synchronization board, which means the propagation delays were the same.

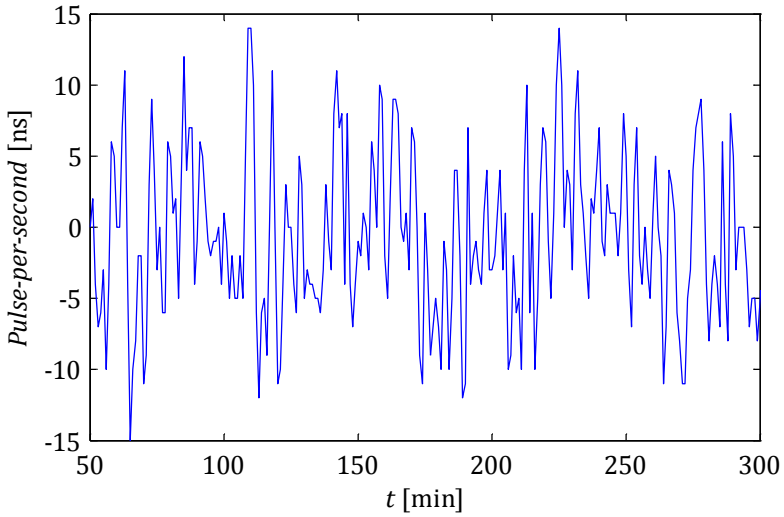

Figure 3.22 Sub-microsecond synchronization of the timing and synchronization board to the GPS timestamp.

Pulse-per-second signal accuracy measured during measurement campaign at Gunfleet Sands offshore wind farm is shown in Figure 3.22. The accuracy is even better than provided by the manufacturer (15 ns, 1σ).

3.2.2.3 DATA ACQUISITION DEVICES

According to Whittaker–Nyquist–Kotelnikov–Shannon [3.29], [3.30], [3.31], [3.32] sampling theorem a bandlimited signal can be fully reconstructed from its samples, provided that the sampling rate exceeds twice the maximum frequency in the bandlimited signal. This minimum sampling frequency is called the Nyquist rate. It means if the continuous-time signal $x(t)$ is sampled at rate of $f_s = 1/T_s > 2f$, the discrete signal is expressed as $x[n] = x(nT_s)$ for all integer n, then the signal $x(t)$ can be completely reconstructed from these samples [3.33].

The signal $x(t)$ can be fully reconstructed from acquired samples with minimum sampling frequency equal to Nyquist rate $x[n] = x(nT_s)$ by application of the Whittaker–Shannon interpolation formula [3.34]

$$x(t) = \sum_{n=-\infty}^{\infty} x[n] \cdot \mathrm{sinc}\left(\frac{t - nT_s}{T_s}\right) \tag{3.8}$$

where $\mathrm{sinc}(\xi)$ is normalized to obtain zero crossing at nonzero integer values

$$\mathrm{sinc}(\xi) = \frac{\sin(\pi\xi)}{\pi\xi} \tag{3.9}$$

Theoretically interpolation formula can be implemented as a low-pass filter, whose impulse response is $\mathrm{sinc}(t/T_S)$ and whose input is a Dirac comb in form

$$\sum_{n=-\infty}^{\infty} x(nT_s)\delta(t - nT_s) \tag{3.10}$$

In that case the interpolation formula can be expressed as convolution of Dirac comb (infinite impulse train) with a sinc function

$$x(t) = \left(\sum_{n=-\infty}^{\infty} x(nT_s)\delta(t - nT_s)\right) * \mathrm{sinc}\left(\frac{t}{T_s}\right) \tag{3.11}$$

This is equivalent to filtering the impulse train with an ideal (brick-wall) low-pass filter. For practical applications a windowed sinc filter is often used instead. Windowing and truncating a sinc filter kernel in order to use it on any practical real world data set destroys its ideal properties.

Anti-aliasing is needed to prevent frequency components above the Nyquist frequency f_N (half the sampling frequency) that might be sampled by analog-digital converters from showing up at low-frequency components. This is a standard part of any digital measurement device (see Figure 3.23).

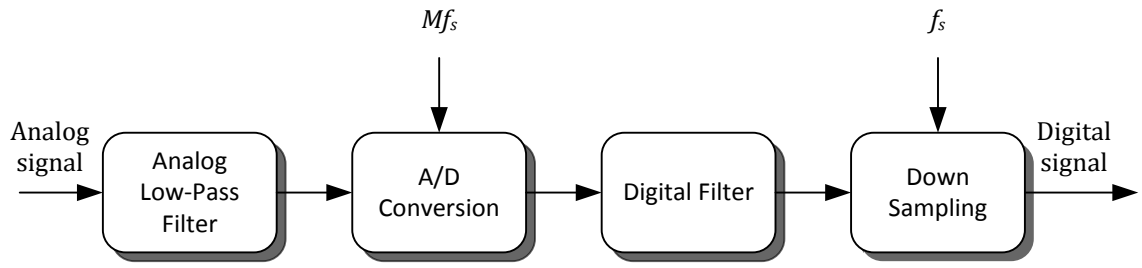

Figure 3.23 Analog to digital conversion in data acquisition cards using oversampling.

The first step with any harmonic measurement is to remove unwanted frequency components. When an analog signal is sampled with a sample frequency f_s, the highest

frequency component that is present in the digital signal should be lower than half the sample frequency

$$f_N = \frac{1}{2} f_s \tag{3.12}$$

If the analog signal contains frequency components higher than the Nyquist frequency, these will appear as lower frequency components in the digital signal due to aliasing phenomena. In other words it is the undesirable effect of the digitizer modulating out-of-band components into Nyquist bandwidth. The greatest danger of aliasing is that it cannot be determined if whether aliasing occurred by looking at the analog-to-digital converter output. If an input signal contains several frequency components or harmonics, some of those components might be represented correctly while others contain aliased artefacts. To prevent high-frequency components from affecting the measured spectrum, an anti-aliasing filter is used. The anti-aliasing filter is an analog low-pass filter that is placed before the analog–digital conversion, as shown in Figure 3.23.

One of the results of using a high-order filter is the introduction of time delay and phase errors. A decreasing phase angle is not a problem by itself. What matters is the difference in time delay for different frequencies. During measurements carried out in analysed wind farms dynamic signal acquisition cards, two-pole low-pass Butterworth filter were used. This solution minimizes phase errors as well as delays and improves data acquisition performance. Butterworth filter has a smooth response over all frequencies and a monotonic decrease from the specified cut-off frequency [3.35].

Each analog-to-digital converter in dynamic signal acquisition devices uses a conversion method known as delta-sigma modulation. Within sampling rate of interest which is 44.1 kS/s/ch each of analog-to-digital converters actually samples its input signal with 128 times higher sampling rate simultaneously improving anti-aliasing filtering. Close to maximum data acquisition board sample rate $64 f_s$ oversampling is applied, due to this fact lower sample rate was used in order to improve data acquisition performance.

Low-pass filtering to eliminates components above the Nyquist frequency either before or during the digitization process can guarantee that digitized data set is free of aliased components. Dynamic signal acquisition devices employ both digital and analog low-pass filters to achieve this protection. The delta-sigma analog-to-digital converters on the data acquisition boards include an oversampled architecture and sharp digital filters which cut-off frequencies that track the sampling rate. Even if the digital filter eliminates almost all out-of-band frequencies, it is still susceptible to aliasing from certain narrow frequency bands which are related with multiplied sampling rates due to oversampling, dependent on assumed sampling rate.

This can be improved by applying low-pass analog filter which removes high-frequency components in the analog signal path before they reach the analog-to-digital converter.

This filtering addresses the possibility of high-frequency aliasing from the narrow bands that are not covered by the digital filter. Described above anti-aliasing filtering approach can be seen in Figure 3.23.

During measurements carried out on the wind farm's dynamic signal acquisition cards with two-pole low-pass Butterworth filter were used. Let us consider more in details the anti-aliasing filtering phenomena used in the data acquisition cards. Generally the input and output variables of a linear, time-invariant, causal filter can be characterized either in the time-domain through the convolution integral given by

$$y(t) = \int_0^t h(t-\tau)x(t)d\tau \tag{3.13}$$

or, equivalently, in the frequency domain through the transfer function

$$H(s) = \frac{Y(s)}{X(s)} = \frac{\sum_{i=0}^{N} b_i s^i}{1 + \sum_{i=0}^{N} a_i s^i} \tag{3.14}$$

where $H(s)$ is the Laplace transform of the impulse response $h(t)$ and $X(s)$, $Y(s)$ are the Laplace transforms of the input signal $x(t)$ and the output or the filtered signal $y(t)$. $X(s)$ and $Y(s)$ are polynomials in $s = \sigma + j\omega$ and the overall transfer function $H(s)$ is a real rational function of s with real coefficients. For a stable transfer function $H(s)$ is reduced to $H(j\omega)$ on the $j\omega$-axis, which is the continuous-time Fourier transform of the impulse response $h(t)$ which in general is complex and can be expressed in terms of real function

$$H(\omega) = |H(\omega)|e^{j\Phi(\omega)} \tag{3.15}$$

where $H(\omega)$ is the magnitude and $\Phi(\omega)$ is the phase.

Taking into consideration Nth-order Butterworth filter one can describe it in terms of energy spectra (squared magnitude) which has form

$$|H(\omega)|^2 = \frac{1}{1 + (\omega/\omega_c)^{2N}} \tag{3.16}$$

where ω_c is -3 dB cutoff frequency. The Butterworth approximation of an ideal low-pass filter has only poles (i.e. no finite zeros) and yields a maximally flat response around zero and infinity. This approximation is also called maximum flat magnitude. This feature becomes extremely important in case of harmonic measurements where each frequency within the bandpass has to be filtered in the same way [3.36].

3.2.2.4 OTHER ASPECTS

Storage devices

The most popular storage device is a hard disk drive (HDD). The mechanical nature of HDDs introduces certain performance compromises. The HDD access time is determined

by the sum of following time delays: spin-up time, seek time, rotational delay, and transfer time. Spin-up time is the time required to accelerate the disk to operating speed. Seek time is the time for the read-and-write heads mounted on an access arm to reach the desired disk track. Rotational latency is the time required for the addressed area to rotate into a position where it is accessible by read-and-write heads. Transfer time is the time during which data is actually read or written to the drive.

The manipulation of sequential data depends upon the rotational speed of the platters and the data recording density. Data transfer rate depends on the track location, so it will be higher for data on the outer tracks (where there are more data sectors) and lower toward the inner tracks (where there are fewer data sectors). Transfer rate can be also influenced by file system fragmentation and the layout of the files as well. Since HDDs are equipped in mechanical component such as arms, headers, and rotating plates, spin-up time, seek time, rotational latency and data transfer time read/write delays are introduced. The main way to decrease access time is to increase rotational speed, thus reducing rotational delay, increase the number of plates and sectors density on tracks, thus reducing transfer time. HDDs can be successfully used for sequential write purposes during continuous logging of measurement tasks. Unfortunately, more efficient solutions such as redundant array of independent disks (RAID), solid state drives (SSDs), and buffered HDDs are needed for high-speed logging purposes.

Nowadays, non-volatile storage devices such as SSDs have become more popular. In comparison to HDDs, it has no moving parts such as the motor, disks and heads of a hard drive. Thus, it eliminates spin-up time, seek time and rotational latency while delivering sustained high-speed data transfers. The SSD is also highly rugged, standing up to shock and vibration while performing in a broad range of temperatures. These performance features make it well suited to a broad range of measurement applications. In regard to SSDs, there is no need to consider seek time, as file system fragmentation is no longer an issue.

Another interesting solution that might be taken into consideration is a Hybrid-HDD. Any data written to the hybrid drive is written to the buffer, therefore there is no risk of data loss in case of power failure, since the buffer's flash memory is non-volatile. This feature became a crucial factor in case of transient measurements where power during switching operation is usually supplied from external sources such as diesel generators or UPSs. In other words, a Hybrid-HDD is a mechanical drive equipped with non-volatile NAND flash used as a buffer. It is automatically used by the drive to store data for quicker access and also any data written to the hybrid drive is written to the buffer which significantly improves such parameters as seek time and rotational latency. It was observed that, in case of high-speed logging, the first few milliseconds are the most important when the buffer is exposed to be overwritten. In theory, Hybrid-HDD solution offers the best of HDDs and SSDs, the overall capacity of HDDs and the performance of SSDs and simultaneously reduces the risk of buffer problems.

For the developed measurement software the Hybrid-HDD was used for relatively high sample rate and many channels as well as external HDDs for long-term measurements with relatively small sample rate and limited number of simultaneously acquired channels. For higher sample rates Hybrid-HDD solution was used due to the improved reliability and transfer rate in comparison to conventional HDDs. Also due to the fact that SSD technology is not reliable if continuous sequential logging is taken into account. It has been observed by National Instruments engineers from RAID & Servers that the transfer can immediately decrease for a short while to an unaccepted value and therefore interrupt the whole measurement process [3.37]. This feature plays a crucial role in case of single buffering used for transient measurements.

As mentioned above, also the type of drive used to store data can play a very important role during data logging. Two different types of drives were used: a drive with a hybrid technology that comprises: built inside 500 GB of HDD, 4 GB of SSD and 32 MB of double-data-rate (DDR3) synchronous dynamic RAM (SDRAM) fused together to significantly improve overall performance and a conventional HDD.

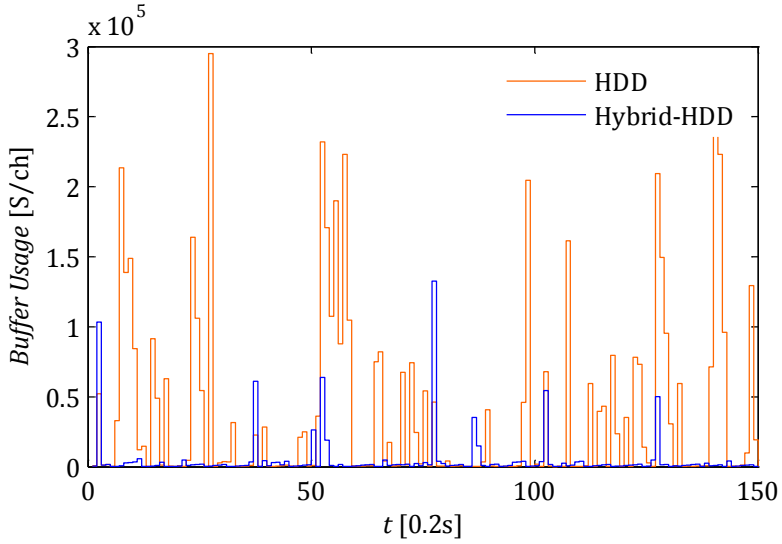

Figure 3.24 Comparison between a HDD and a Hybrid-HDD used for high-speed logging.

During tests one observed that the Hybrid-HDD can perform 3 times better than the conventional HDD. Exemplary results can be seen in Figure 3.24 which presents buffer fill during data logging with the following parameters: 2048 s of file write size, 1 MS/ch of buffer size, 900 MS of pre-allocated file size, and 2.5 MS/s/ch of sampling rate.

Internal bus

When considering the technical merits of different buses, bandwidth and latency are two of the most important bus characteristics. Bandwidth measures the rate at which data are sent across the bus. Latency measures the delay in data transmission across the bus.

Nowadays, USB, PCI Express, and Ethernet/LAN have gained attention as attractive communication options for instrument control. The most promising option seems to be

the PCI solution. The main difference between PCI and PCI Express performance is that PCI Express is a higher bandwidth bus and gives dedicated bandwidth to each device. From all of the buses commonly used for measurement instrumentation, only PCI Express offers dedicated bandwidth to each peripheral on the bus. This creates new opportunities in terms of high-speed multichannel data acquisition.

PXI Express provided by existing on the market measurement solutions, built on PCI Express technology, offers dedicated bandwidth per instrument. PCI Express, available in x1, x4, x8, and x16 links, provides 250 MB/s of throughput per lane with very low latency. The x1 and x4 options are most common for instrument-class hardware and provide 250 MB/s and 1 GB/s of dedicated throughput, respectively [3.38]. Therefore it was decided to use measurement system based on PCI Express technology.

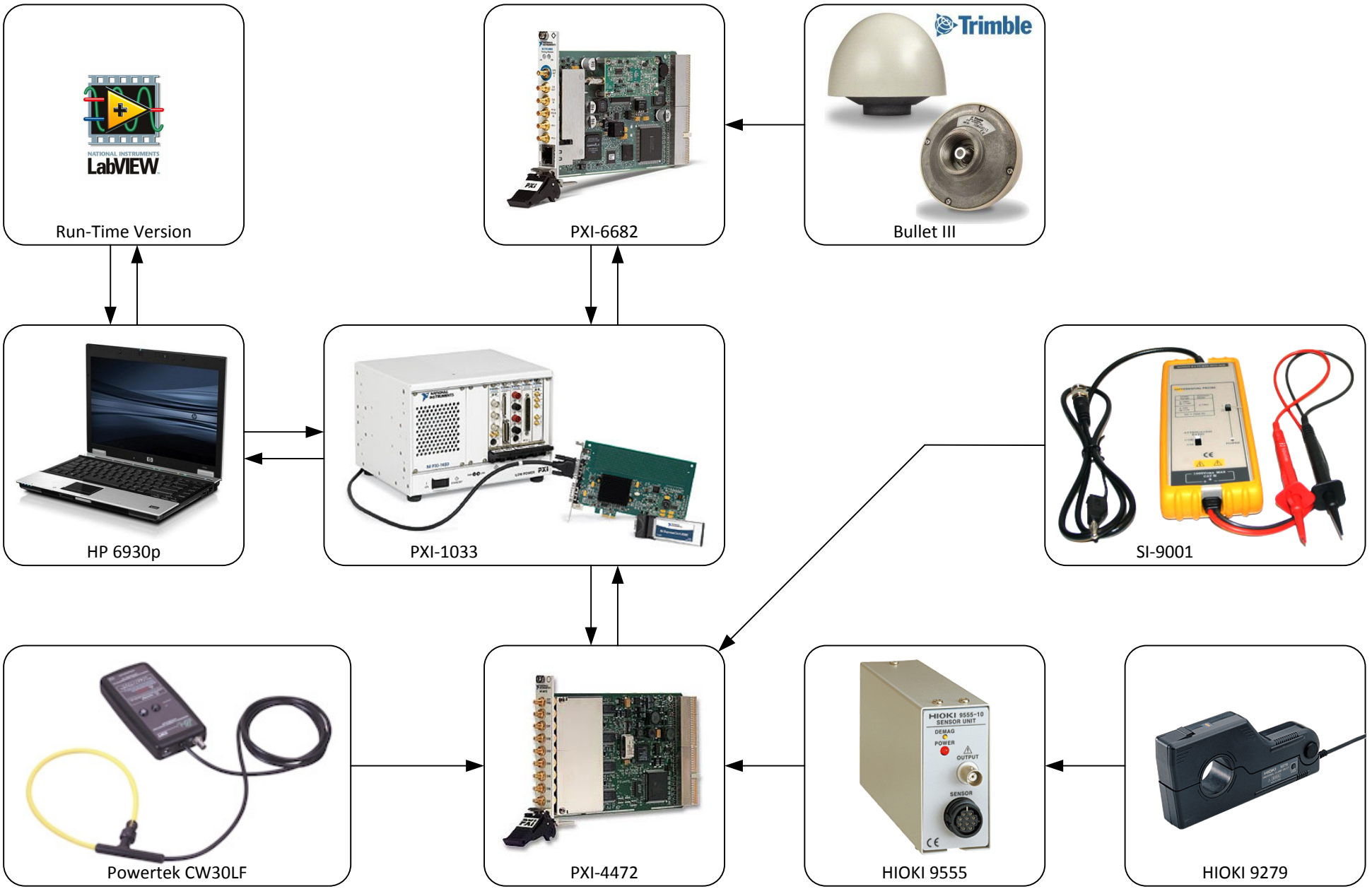

Figure 3.25 Measurement set-up illustrative drawing.

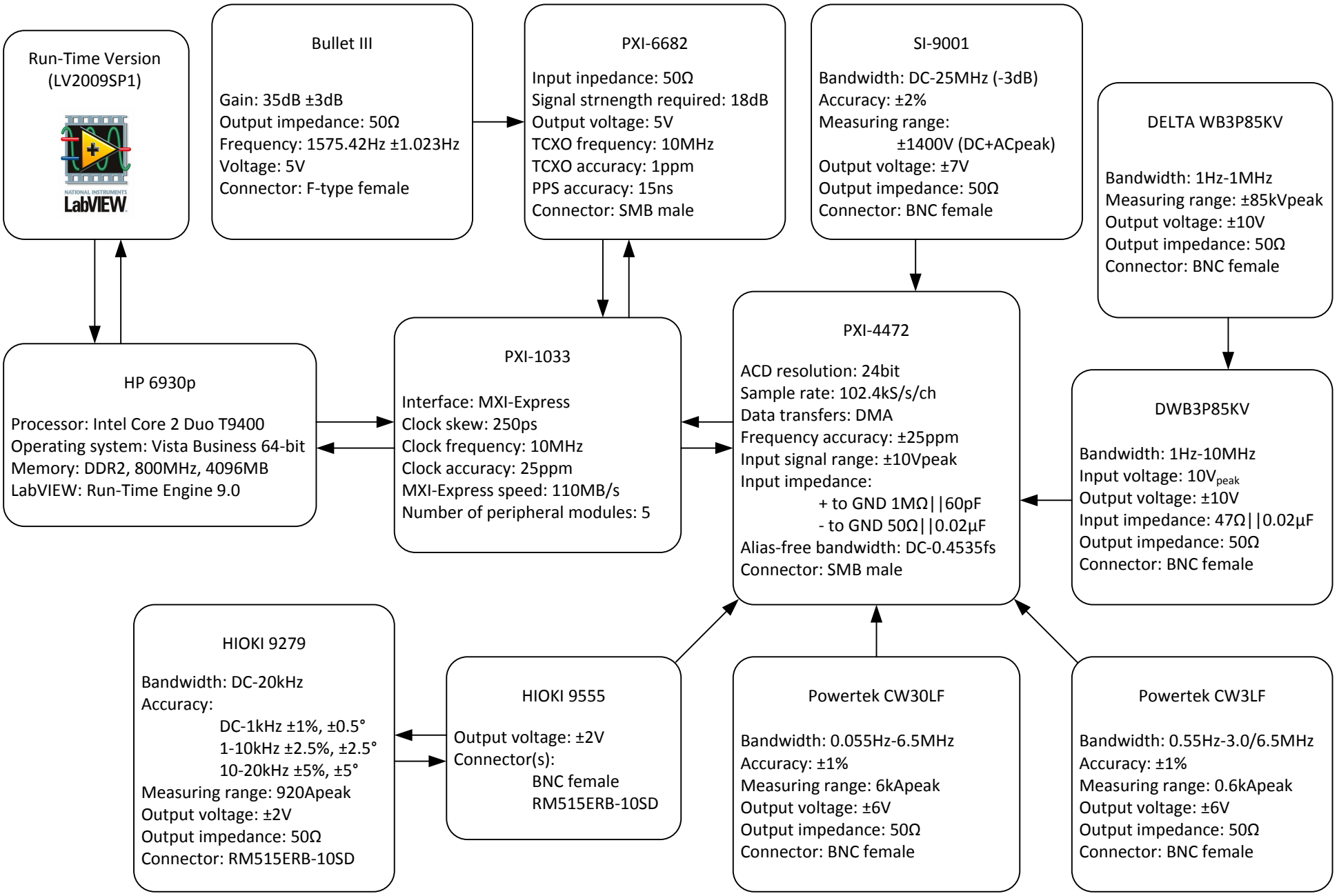

Figure 3.26 Measurement set-up detailed description.

3.3 BURBO BANK

In order to investigate harmonic emission of offshore wind farms, measurement campaigns have been conducted. In harmonic analysis Burbo Bank Offshore Wind Farm was taken into consideration as an example [3.39], where measuring systems were installed and used for simultaneous measurement at different locations within the wind farm.

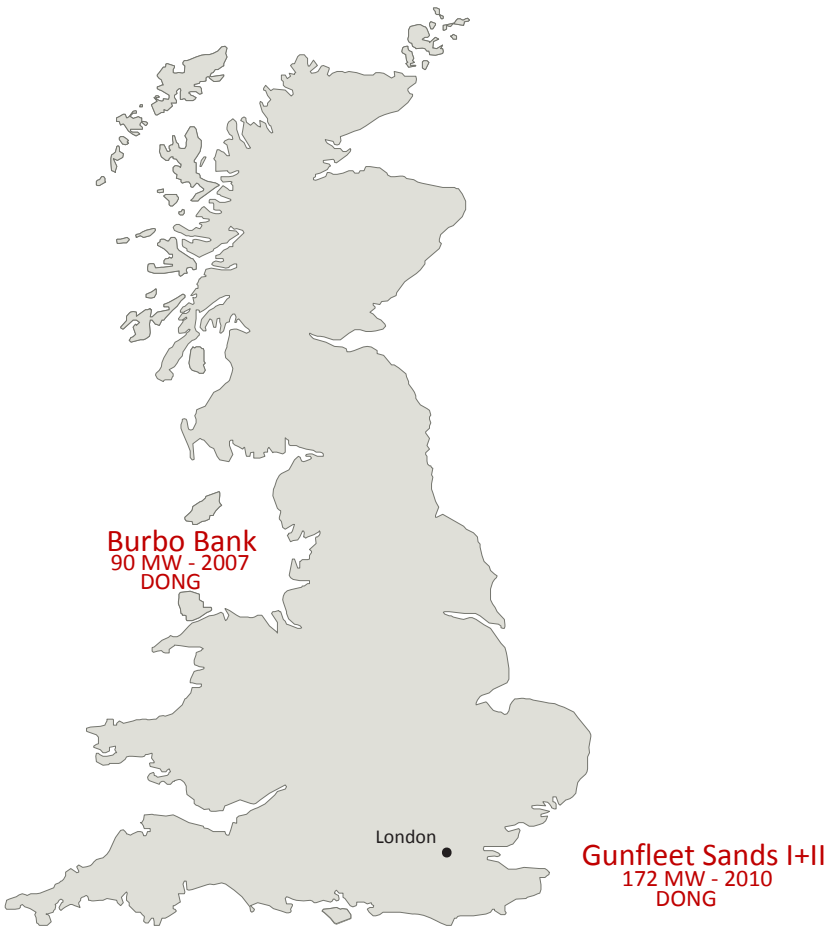

Figure 3.27 Burbo Bank and Gunfleet Sands offshore wind farms location.

3.3.1 MEASUREMENT GOALS

The measurement campaign was organized before this project was initiated and therefore the results were not focused on harmonic analysis shown within the research project. Anyway the data acquisition and logging approach was comparable with the measurement system presented in this report thus measurement data can be also used for harmonic analysis purposes. The measurements were carried out with a PC equipped with National Instruments data acquisition card and controlled by software developed in LabVIEW. Voltage and currents were sampled at 44.1 kHz, using NI PCI-4472 8-channel dynamic signal acquisition board. The dynamic signal acquisition board has an analog filter to remove any signal components beyond the range of the analog-to-digital

converter. However, in order to cut frequency components above half programmed sampling rate digital anti-aliasing filters are implemented [3.40].

3.3.2 WIND FARM DESCRIPTION

Burbo Bank wind farm is located on Burbo Flats in Liverpool Bay (see Figure 3.27 and Figure 3.28). At its closest point, the site is approximately 6.4 km from the Selfton coastline and 7.2 km from North Wirral. The wind farm consists of 25 SWT-3.6-107 variable speed wind turbines [3.41], each with rated capacity of 3.6 MW. Burbo Bank is therefore capable of providing a maximum output of 90 MW of electricity. The wind turbine has a fully rated IGBT-based power electronic converter.

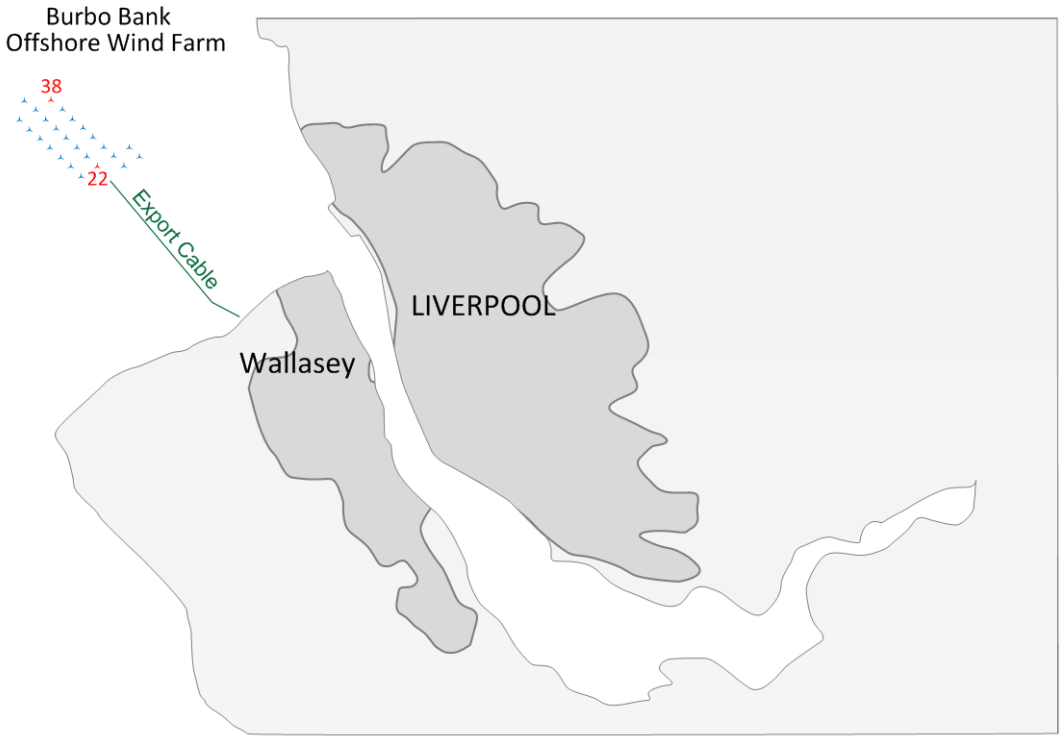

Figure 3.28 Burbo Bank offshore wind farm location.

The wind turbines are arranged in three radial connected directly to shore. Three 33 kV radials go back to the shore-based substation adjacent to the SP Manweb BSP substation and they are located near the consumption centre. 9, 8 and 8 wind turbines are connected to each radial. The substation consists of the wind park transformer, a capacitor bank and earthing transformer which is also used for substation supplies. Please note that due to the fact that Burbo Bank does not have offshore substation it is different slightly from the newest offshore wind farms.

Burbo Bank wind farm is connected to SP Manweb's Network which is designed to operate substations in interconnected groups with standard transformer and cable sizes. In order to limit effects of distortion of the system voltage waveform, the harmonic content of any connected load complies with the limits set out in Engineering

Recommendation G4/5 [3.42]. The 132 kV and 33 kV networks comprise sections of underground cable or overhead lines or combinations of each. The offshore wind farm is connected to the 132 kV Wallasey Circuit 1.

3.3.3 MEASUREMENT POINTS

The measurements were carried out in November and December 2007 as well as January and February 2008. Electrical quantities were logged form different locations simultaneously at that time. The measurement system was installed from both sides of the wind turbine transformer in wind turbine 38 and wind turbine 22, which are emphasized in Figure 3.28. Please note that both wind turbines are connected to the substation by the same radial. It is worth emphasizing that wind turbine 38 is situated at the beginning of the radial and wind turbine 22 at the end of the radial (i.e. the closest to the substation). Measurements at the onshore substation (MV and HV side) were performed at the same time. Due to limited number of data acquisition units and sensors it was sometimes impossible to perform measurements simultaneously in each of the aforementioned locations. Due to this fact the measurement period used in data analysis is much shorter than from other wind farms.

3.4 AVEDØRE HOLME

For measurement purposes National Instruments instrumentation was used. The test equipment used in Avedøre Holme consisted a PXI-1033 chassis which three PXI-4472 dynamic signal acquisition boards with second-order low-pass anti-aliasing filter [3.43] applied in case of harmonic measurements. The chassis was connected to a portable computer via ExpressCard laptop host. Used MXI-Express remote controller achieves up to 110 MB/s sustained throughput. The measurement PC units used for measurements comprised Intel Core 2 Duo T9400 @ 2.53 GHz CPU, 4 GB @ 800 MHz RAM, Windows Vista Enterprise operating system and Seagate ST95005620AS Hybrid-HDD and additional external HDDs.

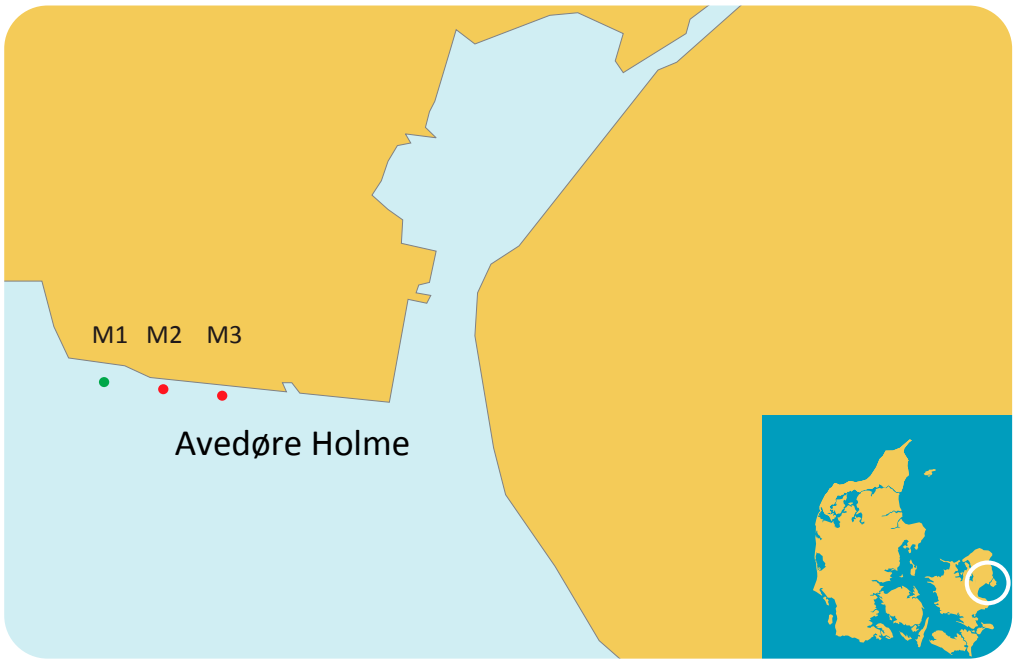

Figure 3.29 Avedøre Holme offshore wind farm location.

3.4.1 MEASUREMENT GOALS

Wind turbine is one of the most important components in wind farms which can contribute to harmonic generation and mitigation. Therefore it was decided to investigate the wind turbine more in details. It was decided to perform measurements in a small wind farm which is directly connected to the distribution system. In such a configuration the wind turbine operation is less affected by other wind turbines and wind farm internal electrical network. This allows observing the wind turbine interaction with the grid depending on different external network configuration and background distortions. The measurements were performed only inside the wind turbine number 3 (M3 in Figure 3.29). The purpose of the measurement campaign was to acquire all electrical quantities related to the wind turbine power converter steady-state operation.

Based on the measurements it was possible to observe the wind turbine operation from harmonic perspective and its interaction with the external network. The measurements were useful to analyse different harmonic phenomena existing in the wind turbine. Based on results from measurement data analysis it was possible to develop appropriate wind turbine models.

3.4.2 WIND FARM DESCRIPTION

Avedøre Holme offshore wind farm in the south of Copenhagen is a shared project between DONG Energy and Hvidovre Vindmøllelaug A/S. The three wind turbines are located less than 10 metres from shore in a water depth of 0.5-2 metres. A location so

close to shore and easy accessibility to the offshore wind turbines via a footbridge is the basic idea behind the project. This gives DONG Energy a unique opportunity to test and try out new wind turbine concepts, before they are implemented in large scale in offshore wind farms.

It was mentioned that the wind farm comprises of three wind turbines but actually during measurements carried out in July and August 2010 there were only two installed. Only M2 and M3, as presented in Figure 3.29, were installed and operating.

3.4.3 MEASUREMENT POINTS

In the wind turbine number 3 (M3 from Figure 3.29) of Avedøre Holme the LV voltage probes were installed in the auxiliary switchboard, DC/AC grid-side converter and DC-link of the wind turbine. The LV current probes were installed on the output terminals of the DC/AC convert, DC-link and LV side of the wind turbine transformer. The MV voltage and current probes in the wind turbine were installed in the wind turbine transformer side of the vacuum circuit breaker.

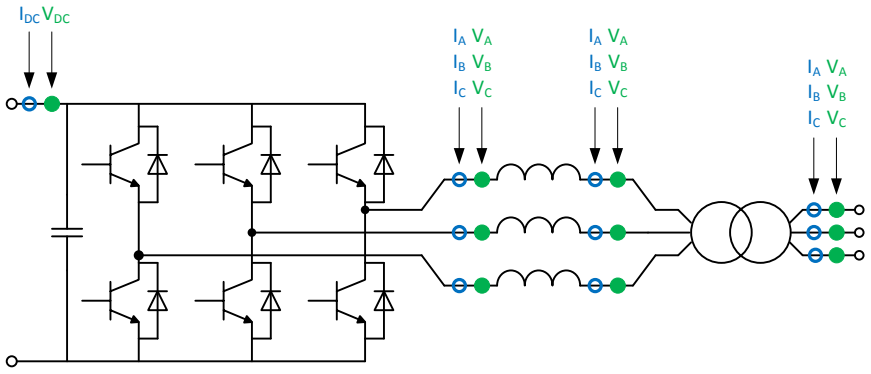

Figure 3.30 Measurement points installed in the wind turbine.

Figure 3.30 shows where the measurement points were located in the wind turbine main power circuit. In order to observe fully the wind turbine behaviour from harmonic emission and propagation perspective different measurement system was installed in almost all possible locations. Please note that the shunt filter of the wind turbine converter is not shown in the drawing.

3.5 GUNFLEET SANDS

After measurements in Avedøre Holme it was decided to carry out measurements in a large offshore wind farm. For the research project purposes Gunfleet Sands was chosen. The same measurement equipment was used as earlier [3.44]. Due to the fact that electrical quantities were acquired from different locations synchronization process was performed based on GPS timestamp. Previously synchronization was not needed due to the fact that in one wind turbine all data acquisition boards were installed in the same chassis and common reference clock was taken for all data acquisition devices.

In the case of Gunfleet Sands measurements three identical measurement unit were installed in various locations. Additionally to the previous measurement hardware configuration PXI-6682 timing and synchronization board with Trimble Bullet III GPS antenna was used to read GPS timestamp and synchronize the measurements at three different locations. Each of PXI-4472 dynamic signal acquisition boars were situated in separated PXI-1033 chassis. Previously the data acquisition device was installed in the synchronization slot (i.e. Slot 2) and in case of Gunfleet Sands the timing and synchronization board was installed there instead [3.2].

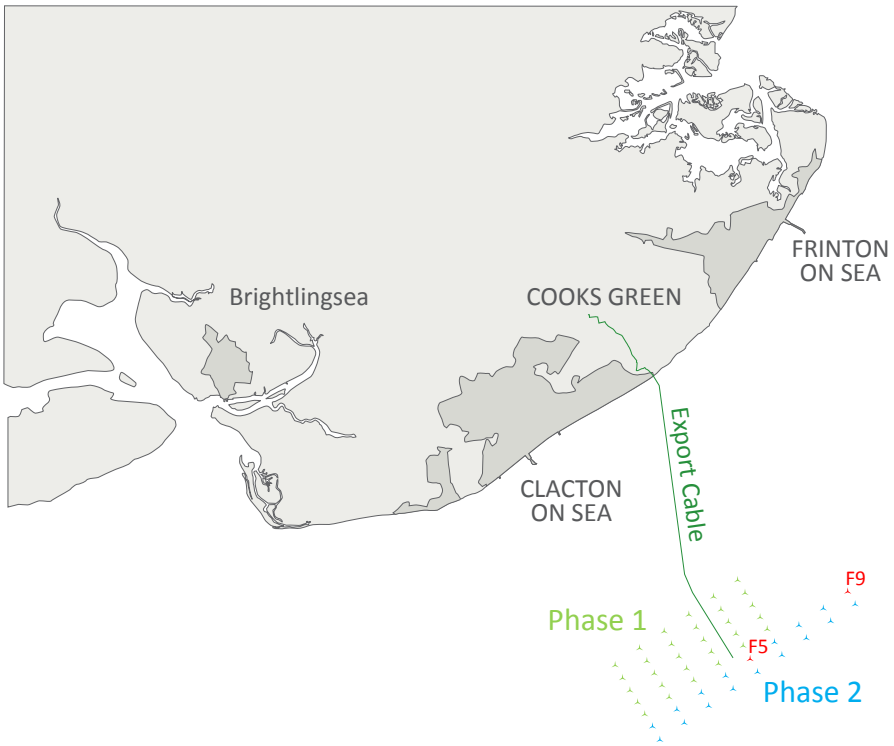

Figure 3.31 Gunfleet Sands offshore wind farm location.

3.5.1 MEASUREMENT GOALS

As mentioned before, the measurement system was designed to measure the harmonic emission in offshore wind farms. The measuring process was planned and adjusted for the project purposes (i.e. harmonic analysis). To record the harmonic emission of a single wind turbine the measurement system was installed at the LV and MV side of the wind turbine transformer in Gunfleet Sands. To record the harmonic emission of a group of wind turbines the measurement system was installed in the substation of Gunfleet Sands. In both instances the measurement system was left recording continuously for more than three weeks. As it was mentioned earlier the measurement equipment was installed in three different locations. This allows tracking possible harmonic emission and propagation within the whole wind farm.

3.5.2 WIND FARM DESCRIPTION

Gunfleet Sands wind farm is located on the east cost of the UK (see Figure 3.27 and Figure 3.31) and consists of two phases, one with 30 wind turbines (Phase 1) and another with 18 turbines (Phase 2). Each of the phases is indicated in Figure 3.31 and the measurements were carried out in Gunfleet Sands II. The wind turbines are connected to radials by 33 kV submarine cables. Each pair of radial is then connected to the platform by one root cable. Two park transformers (120 MVA, 132/33 kV) are placed in the centre of the wind farm in the offshore substation. Each root cable is connected in the substation to a MV busbar via a vacuum circuit breaker. From the substation the electricity is transmitted to shore via a 8.5 km long submarine cable which comes ashore at Holland Haven and connects to the Clacton substation at Cooks Green [3.44].

3.5.3 MEASUREMENT POINTS

The measuring locations within the collection grid of Gunfleet Sands were the transformer platform, the first turbine of radial (F5) and the last turbine of radial (F9). The wind turbines location is presented in Figure 3.31. In both of the wind turbines, the LV voltage and current probes were installed in the auxiliary switchboard. The MV voltage and current probes in the wind turbines were installed in the transformer side of the vacuum circuit breaker; while in the substation the voltage and current probes were installed in the cable side of the vacuum circuit breaker of the radial.

3.6 SUMMARY

Harmonic analysis in large offshore wind farms represents new challenges to the industry in relation to understanding the nature, propagation, effects and appropriate assessment of harmonics [3.45]. An analysis of such systems considers many aspects related to extended and accurate models, complex measurement campaigns and of course appropriate and more suitable data processing methods. Before any of the above aspects can seriously be taken into consideration, a reliable and robust measurement system is needed. This can be achieved by careful designing taking into consideration both the hardware and the software layers as it was explained above.

Appropriate understanding of harmonics behaviour in wind farms requires extended measurement campaigns carried out in rough offshore environments. In places where access is limited due to weather conditions and significant operational costs, robust and reliable measurement systems are especially important. Reliable long-term measurement systems consisting of optimized hardware and software layers are absolutely needed.

At the end several measurement campaigns carried out especially for harmonic studies are described. The measurement campaigns were carefully planned and scheduled in order to acquire and log sufficient amount of representative data. Measurement goals in

case of each campaign are described and further usage of measurement data is explained.

3.7 REFERENCES

[3.1] National Instruments Corporation. (2008, Aug.) NI Dynamic Signal Acquisition.

[3.2] National Instruments, "NI 4472 User Manual," National Instruments Manual, 2001.

[3.3] J. R. Taylor, *An Introduction to Error Analysis: The Study of Uncertainties in Physical Measurements*, 2nd ed. University Science Books, 1997.

[3.4] S. W. Smith, *The Scientist and Engineer's Guide to Digital Signal Processing*, 2nd ed. San Diego, California: California Technical Publishing, 1999.

[3.5] Y. V. Prokhorov and V. Statulevičius, *Limit Theorems of Probability Theory*. Berlin: Springer, 2000.

[3.6] M. Grabe, *Measurement Uncertainties in Science and Technology*. Springer, 2005.

[3.7] R. M. Sheldon, *Introduction to Probability and Statistics for Engineers and Scientists*, 3rd ed. Elsevier Academic Press, 2004.

[3.8] L. M. Surhone, M. T. Timpledon, and S. F. Marseken, *Signal-to-noise Ratio: Signal (electronics), Noise (telecommunications), Bandwidth (signal processing), Amplitude, Decibel, Standard deviation, Signal to Noise Ratio (image processing)*. Betascript Publishing, 2010.

[3.9] M. Drosg, *Dealing with Uncertainties: A Guide to Error Analysis*, 2nd ed. Berlin: Springer-Verlag, 2009.

[3.10] T. L. Clark, M. B. McCollum, D. H. Trout, and K. Javor, *Marshall Space Flight Center Electromagnetic Compatibility Design and Interference Control Handbook*. Alabama: National Aeronautics and Space Administration, 1995.

[3.11] R. P. Clayton, *Introduction to Electromagnetic Compatibility*, 2nd ed. New Jersey: John Wiley & Sons, 2006.

[3.12] R. Lai, Y. Maillet, F. Wang, S. Wang, R. Burgos, and D. Boroyevich, "An Integrated EMI Choke for Differential-Mode and Common-Mode Noise Suppression," *IEEE Transactions on Power Electronics*, vol. 25, no. 3, pp. 539-544, Mar. 2010.

[3.13] C. Torrence and G. P. Compo, "A Practical Guide to Wavelet Analysis," *Bulletin of the American Meteorological Society*, vol. 79, pp. 61-78, 1998.

[3.14] F. Buschmann, R. Meunier, H. Rohnert, P. Sommerlad, and M. Stal, *Pattern-Oriented Software Architecture: A System Of Patterns*. West Sussex, England: John Wiley & Sons, 1996.

[3.15] S. Oaks and H. Wong, *Java Threads*. O'Reilly, 2004.

[3.16] E. Gamma, R. Helm, R. Johnson, and J. M. Vlissides, *Design Patterns: Elements of Reusable Object-Oriented Software*. Canada: Addison-Wesley, 1995.

[3.17] S. K. Chang, *Data Structures and Algorithms*. World Scientific Publishing Company, 2003.

[3.18] C. E. Leiserson. (2009) Nondeterministic Programming. MIT OpenCourseWare.

[3.19] I. Gilvarry, "IA-32 Features and Flexibility for Next-Generation Industrial Control," *Intel Technology Journal*, vol. 13, no. 1, pp. 146-159, Mar. 2009.

[3.20] J. S. Wilson, S. Ball, C. Huddleston, E. Ramsden, and D. Ibrahim, *Test and Measurement: Know It All*. Elsevier, 2008.

[3.21] Microsoft Corporation. (2010, Feb.) I/O Concepts. [Online]. http://msdn.microsoft.com/en-us/library/aa365199(v=VS.85).aspx

[3.22] National Instruments. Knowledge Base . [Online]. http://www.ni.com/kb/

[3.23] R. Nagar, *Windows NT File System Internals: A Developer's Guide*, 1st ed. O'Reilly Media, 1997.

[3.24] F. Blaabjerg and Z. Chen, *Power Electronics for Modern Wind Turbines*, 1st ed. Morgan & Claypool, 2006.

[3.25] Department of Defense, *Global Positioning System Standard Positioning Service Signal Specification*, 4th ed. USA, September 2008.

[3.26] J. G. Webster, *The Measurement, Instrumentation and Sensors Handbook*. New York: Springer-Verlag, 2000.

[3.27] N. Kamarudin and Z. Mat Amin, "Multipath Error Detection Using Different GPS Receiver's Antenna," in *3rd FIG (International Federation of Surveyors) Regional Conference*, Jakarta, 2004, pp. 1-11.

[3.28] B. Ramakrishna Rao, A. D. Sarma, and Y. Ravi Kumar, "Technique to reduce

multipath GPS signals," *Current Science*, vol. 90, no. 2, pp. 207-211, Jan. 2006.

[3.29] E. T. Whittaker, "On the Functions Which are Represented by the Expansions of the Interpolation Theory," *Proceedings of the Royal Society of Edinburgh*, vol. 35, pp. 181-194, 1915.

[3.30] H. Nyquist, "Certain topics in telegraph transmission theory," *Trans. AIEE*, vol. 47, pp. 617-644, Apr. 1928.

[3.31] V. A. Kotelnikov, "On the carrying capacity of the ether and wire in telecommunications," in *All-Union Conference on Questions of Communication*, Moscow, Russia, 1933.

[3.32] C. E. Shannon, "Communication in the presence of noise," *Proceedings of the Institute of Radio Engineers*, vol. 37, no. 1, pp. 10-21, Jan. 1949.

[3.33] R. J. Marks, *Handbook of Fourier Analysis & Its Applications*. Oxford University Press, 2009.

[3.34] G. F. Franklin, J. D. Powell, and M. L. Workman, *Digital control of dynamic systems*, 3rd ed. Prentice-Hall, 2006.

[3.35] E. Lai, *Practical Digital Signal Processing for Engineers and Technicians*. Elsevier, 2003.

[3.36] C. Gasquet and P. Witomski, *Fourier analysis and applications: filtering, numerical computation, wavelets*, 1st ed. New York: Springer-Verlag, 1999.

[3.37] A. Mierau. (2010, Sep.) Save high sampling rate data . [Online]. http://forums.ni.com

[3.38] National Instruments. Developer Zone. [Online]. http://zone.ni.com/dzhp/app/main

[3.39] S. Scheibye. DONG Energy Homepage. [Online]. www.dongenergy.com/SiteCollectionDocuments/NEW Corporate/Burbo/BurboBankLeaflet.pdf

[3.40] L. S. Christensen, M. J. Ulletved, P. Sørensen, T. Sørensen, T. Olsen, and H. K. Nielsen, "GPS Synchronized high voltage measuring system," in *Nordic Wind Power Conference*, Roskilde, 2007, pp. 1-6.

[3.41] V. Akhmatov, J. Nygaard Nielsen, J. Thisted, E. Grøndahl, P. Egedal, M. Nørtoft Frydensbjerg, and K. Høj Jensen, "Siemens Wind Power 3.6 MW Wind Turbines for Large Offshore Wind Farms," in *Proc. 7th International Workshop on Large*

Scale Integration of Wind Power and on Transmission Networks for Offshore Wind Farms, 26-27 May 2008, pp. 494-497.

[3.42] Engineering Group, "Planning levels for harmonic voltage distortion and connection of non-linear equipment to transmission and distribution networks in the UK," The Electricity Association Engineering Recommendations G5/4-1, 2001.

[3.43] Ł. H. Kocewiak, J. Hjerrild, and C. Leth Bak, "The Impact of Harmonics Calculation Methods on Power Quality Assessment in Wind Farms," in *International Conference on Harmonics and Quality of Power*, Bergamo, 26-29 September 2010, pp. 1-9.

[3.44] Ł. H. Kocewiak, I. Arana Aristi, J. Holbøll, C. L. Bak, and J. Hjerrild, "Development and Design of a Flexible Measurement System for Offshore Wind Farm Applications," in *10th International Workshop on Large-Scale Integration of Wind Power into Power Systems as well as on Transmission Networks for Offshore Wind Power Plants*, Aarhus, 2011.

[3.45] Ł. H. Kocewiak, C. L. Bak, and J. Hjerrild, "Harmonic Aspects of Offshore Wind Farms," in *Danish PhD Seminar on Detailed Modelling and Validation of Electrical Components and Systems*, Fredericia, 2010, pp. 40-45.

Chapter 4
DATA ANALYSIS

While appropriate measurements are performed, there is a necessity to perform appropriate data processing and data analysis. At the beginning of this chapter, various data processing techniques applied on the measurement are described. Techniques vary depending on expected outcome approach as well as the nature of an analysed signal. Afterwards, processed data are analysed by application of sophisticated statistical methods. Observations and conclusions from data analysis allow better understanding the nature and origin of various harmonic components as well as constituting a solid basis in model development.

4.1 SPECTRAL ANALYSIS

Nowadays wind turbines equipped in back-to-back converters can meet the most demanding grid requirements seen today [4.1]. However, increasing density of renewable dispersed sources of electricity with power electronic interface creates issues with regard to the power quality that need to be addressed and improved [4.2], [4.3] in order to exploit the potential and advantages that large offshore wind farms introduce. Power quality is an important element in the effort to reach renewable energy targets in modern power systems while maintaining a stable and robust power system [4.4].

Analysis of such systems as large offshore wind farms considers many aspects related to extended and accurate models, complex measurement campaigns and of course appropriate and more suitable data processing methods. It must be emphasized that there is no possibility to develop and validate accurate and extended models for harmonic studies without appropriate processed measurements. This became a crucial issue especially if small changes in harmonic model development process are applied and signal processing begins to play a significant role.

4.1.1 SPECTRUM ESTIMATION

Different methods of calculating harmonics in measurements obtained from offshore wind farms are shown in this section. Appropriate data processing methods are suggested for harmonics with different origin and nature (e.g. harmonics affected by modulation or control of grid-connected converter). Enhancements of discrete Fourier transform application in order to reduce measurement data processing errors are proposed and compared with classical methods. Comparison of signal processing methods for harmonic studies is presented and application, dependent on harmonics origin and nature recommended. Certain aspects related to magnitude and phase calculation in stationary measurement data are analysed and described.

Measured electrical signals can be classified into two cases: stationary and non-stationary signals. The signal processing methods introduced for harmonic studies are for stationary signals and performed on measurements from steady-state operation of wind farms. A signal is stationary when the statistics (e.g. mean value, variance, probability density function, etc.) of the signal are independent of time (or are statistical time invariant). However, strictly stationary signals as well as steady-state operation do not exist in real-life wind farms and power systems: Both small and large statistical changes occur in the signal parameters. The presence of small and relatively slow statistical changes is addressed through so-called block-based methods typically applied in harmonic assessment. The signal is assumed stationary over a short duration of time (or window), a block of data; the signal features (or characteristics or attributes) are estimated over this window. Afterwards the window is shifted in analysed time-series and the calculations are repeated for a new block of data. The resulting estimated features, such as mean value, variation, frequency, RMS value or harmonic magnitude and phase, become a function of time depending on the location of the window. This is a commonly applied technique in harmonic analysis [4.5].

It can be difficult in some cases to judge whether a signal is stationary or non-stationary. To mathematically prove the stationarity requires the knowledge of the probability density function of the signal and is therefore not a straightforward task. Stationarity or a more broad type, wide-sense stationarity, where a signal is statistically invariant to the time difference of the signal is however a property that is implicitly assumed with all the signal-processing tools for harmonic studies discussed in this section. Under this assumption the statistical properties of a signal are the same over any window.

Non-model-based methods (or nonparametric methods) to decompose the signal into components and transform into a different domain where the signal characteristics can be easily extracted are taken into account in this analysis. One of the main disadvantages of these methods is a relatively low frequency resolution, which is dependent on the length of the signal being processed. For harmonic purposes it has been assumed that signals with 51.2 ks/s/ch and 10-cycle window will

be used [4.6]. This allows extracting high-order harmonics generated by switching power electronic equipment and decomposing signal with sufficient accuracy.

Analysing the sampled voltage or current waveforms offers quantitative descriptions of power quality. For harmonic studies they are the most dominant harmonic components and their associated magnitudes and phases as well as quantitative indices (e.g. total harmonic distortion, signal-to-noise ratio, and statistics) related mainly with stationary signals and application of appropriate transforms (e.g. fast Fourier transform) for harmonic studies.

If the measurement data (or block of the data) are stationary, frequency-domain decomposition of the data is often desirable. A standard and commonly preferred method is the discrete Fourier transform which provides discrete spectrum from discrete time series or its fast algorithm, the fast Fourier transform [4.5].

4.1.1.1 WIND TURBINE SPECTRUM

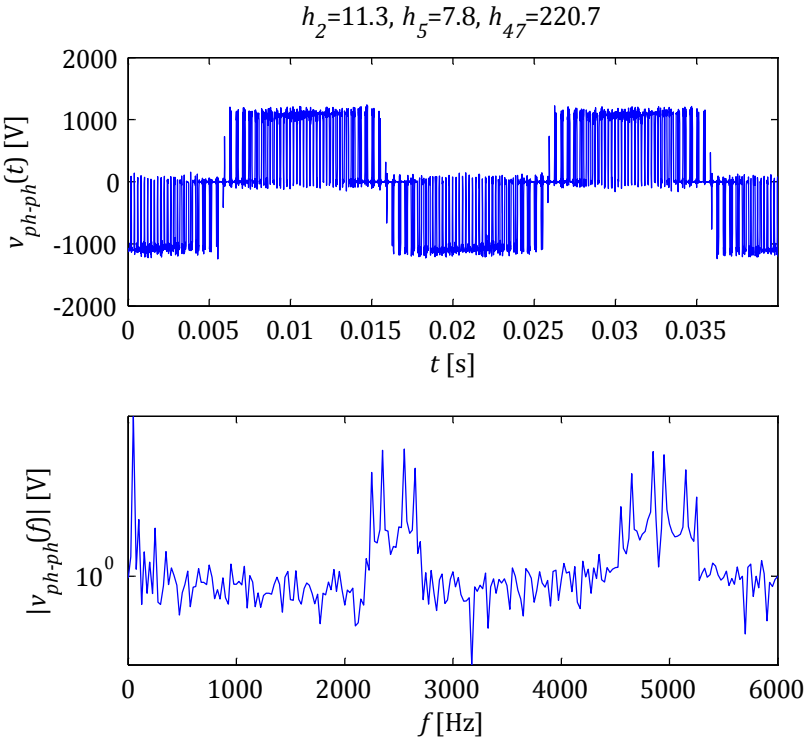

Figure 4.32 Voltage waveform seen form grid-side converter AC terminals and its spectral analysis (sample rate: 102.4 kS/s/ch).

Two cases, measurements during full wind turbine production and really close to wind turbine shutdown condition due to lack of sufficient wind speed were taken into account during this analysis. The most significant voltage harmonic components seen from the grid-side converter AC terminals during low production are the 2nd, the 5th and the carrier group harmonics as presented in Figure 4.32 while in the current waveform the 7th can also be easily seen (Figure 4.33). During full production the phase-to-phase voltage waveform looks similar. The 2nd harmonic ($V_{h_2} = 14$ V) and the 7th

harmonic as well as carrier group harmonics ($V_{h_{47}} = 236.6$ V) are slightly higher. A certain dependency on power production can be seen. Relation between wind turbine power output and selected harmonic components magnitude will be explained later based on statistical analysis.

Systematic error during measurements was small as it can be seen from mean value estimation $\hat{\mu} = 0.35$ which consists 0.025 % of the differential voltage sensor full-scale range. In Figure 4.32 one can also see that the analysed period could be considered as a steady-state operation of the grid-side converter. Due to complex dynamic behaviour of power converters it is difficult to discuss about steady-state operation. This affects some uncertainties during post-processing but it is assumed if the wide-sense stationarity condition is satisfied, fast Fourier transform which is a discrete representation of Fourier transform can be applied and the results can be trustful.

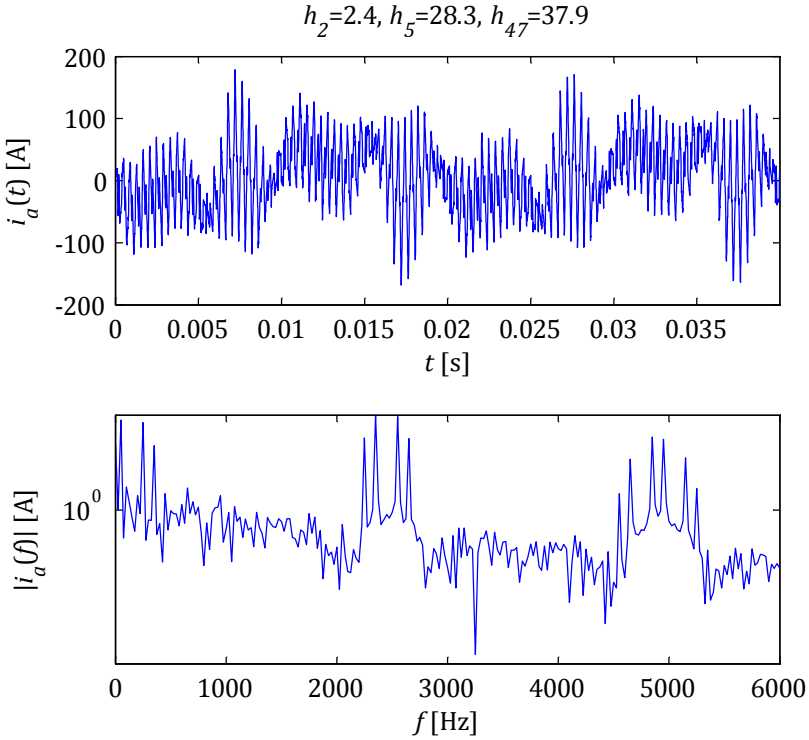

Figure 4.33 Current waveform measurements and its spectrum at the grid-side converter AC terminals (sample rate: 102.4 kS/s/ch).

Wide-sense stationarity of a random process only requires that its mean value μ and variance σ^2 do not vary with respect to time. Different aspects of wide-sense stationarity assessment are described later in the chapter.

4.1.1.2 DATA PROCESSING ALGORITHM

Various techniques of spectrum estimation from measured signals have been developed. They can be mainly divided into non-parametric and parametric (model-based) techniques [4.7]. In general all techniques based on Fourier analysis (harmonic analysis) are non-parametric (e.g. wavelet transform, short-time Fourier transform).

Many common integral transforms used in signal processing have their discrete counterparts. For example, for the Fourier transform the counterpart is the discrete Fourier transform. Such discrete transforms can be successfully used in obtaining spectrum estimate from measurement data [4.8], [4.9].

These methods are commonly applied in the field of electrical engineering and even one can say that the fast Fourier transform is a daily bread for electrical engineers. Of course application of non-parametric techniques has some constraints, i.e. the resulting signal in discrete frequency domain is strongly dependent on the input signal and the engineer's responsibility to select or adjust (e.g. filter, detrend, apply window, specify length, resample) input signal to obtain interpretable results from physical perspective.

In data processing for harmonic analysis purposes one can specify a few important stages. These are, assuming that data acquisition process is performed properly, input data preparation before transformation to discrete frequency domain, spectral analysis by application of appropriate either parametric or non-parametric technique, output data selection and scaling. Please note that data processing can be performed online or offline. One of the biggest disadvantages of online data processing is that the data processing cannot be undone or repeated. Most of commercial power quality meters are working in this way therefore possible data processing error estimation is problematic. For research purposes it is much better is to deal with offline processing because different scenarios of data processing can be applied and afterwards compared.

In harmonic analysis in large offshore wind farms data processing algorithm was applied offline, which its overall structure is presented in Figure 4.34. All measurement data were acquired and logged previously and are loaded via producer-consumer queued structure. Such structure allows data loading independently on data processing. In research it is difficult to assess what exactly is expected to measure therefore raw voltage and current waveforms were measured. That is also why no additional filtering is introduced in data processing. Only the signal is resampled in order to keep constant number of samples per cycle which is 1024 S/c. Such signal is processed using fast Fourier transform and scaled depending on the analysed signal length. Afterwards transformed complex signal is expressed in terms of magnitude and phase. Additionally the phase angle is locked to the fundamental frequency voltage of the first electrical phase.

Different variations of presented data processing scenario can be applied. For example, depending on frequency components of interest the signal can be resampled or not, also different resampling methods can be applied. The same is with harmonic components phase angles, i.e. not always should be referred to the fundamental frequency.

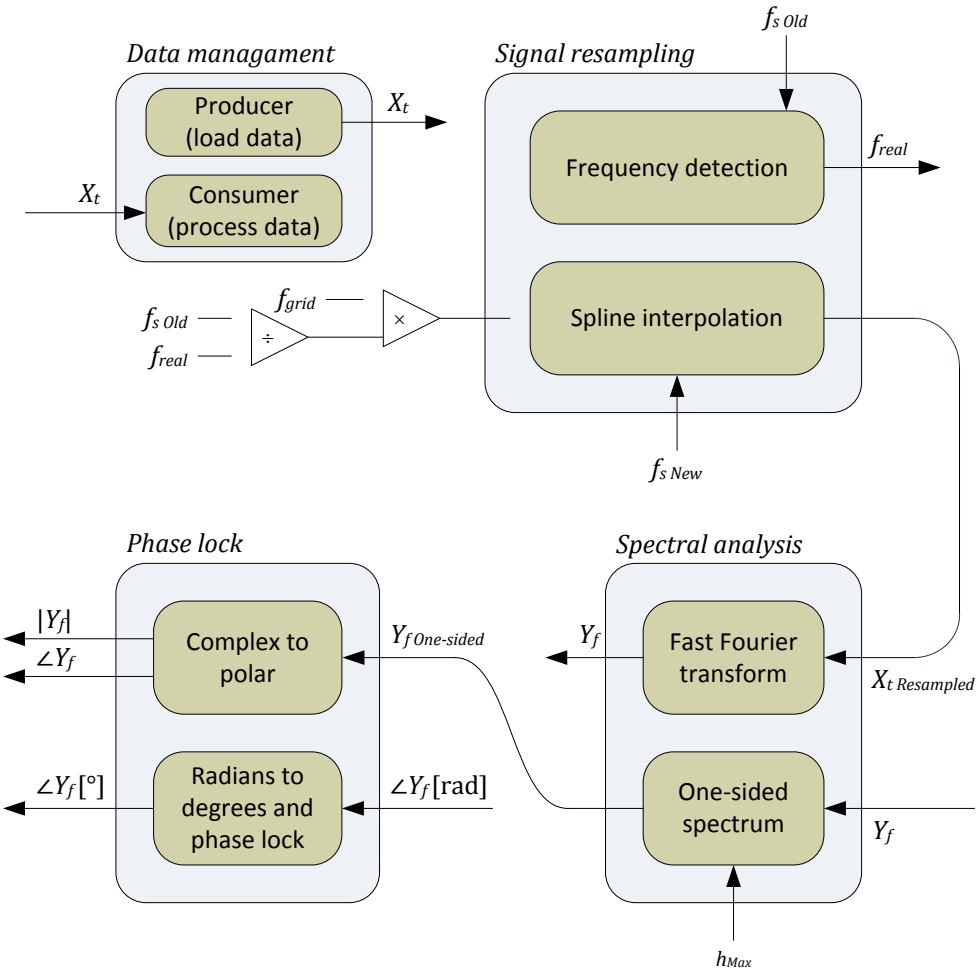

Figure 4.34 Block diagram of data processing algorithm.

Maintaining the power system fundamental frequency close to its nominal value is a natural consequence of maintaining the balance between generation and consumption. Due to this fact the variations in the frequency of the voltage are the first power quality disturbance which violate stationary assumption and has an influence on characteristic harmonics behaviour and nature.

One potentially can transform a non-stationary time series into a stationary time series by removing any trend or slow variation from the time series. There might be also some benefits by slicing the time series into approximately stationary sections and separately analyse each section as it is also recommended in mentioned previously standards.

Resampling consists an important issue since it cannot be said that measurement data are stationary in nature. Changing the sampling rate of the signal improves the precision of calculated harmonics linked with the power grid frequency. This process helps to minimize spectral leakage of frequencies which are exact multiplication of an integer number and the mains frequency.

During resampling one of most important parts is signal single tone detection. This can be done from the Hanning weighted spectrum [4.10], [4.11]. Of course everything

can be done with stationarity assumptions. That is why small blocks of data are used during signal processing. The changes of the power frequency during 10 cycles which consists the block, can be neglected which also is checked applying stationarity test if a time series is mean and variance stationary with 95% of confidence interval.

Another issue is that the disturbances in their higher frequency range are typically not linked to the power system frequency but are due to the grid-side converter built that operate at a certain switching frequency which tends to produce power converter characteristic harmonics which are dependent on power system fundamental frequency and carrier signal fundamental frequency. This limits a need to resample measured signals according to the main period. Furthermore, resampling can even give wrong results and guide to misinterpretation of calculated data and as a consequence develop inappropriate models for high-frequency components in wind turbines and wind farms.

The discrete Fourier transform provides discrete spectrum from a time series. If the time series is limited the estimated spectrum is represented by finite orthogonal basis of complex vectors. The finite number of complex vectors is manifested as a loss of detail (resolution) in the discrete Fourier transform. From all possible frequencies in the signal only those which coincide with the basis will project onto a single basis vector; all other frequencies will exhibit non zero projections on the entire basis set. This is called spectral leakage.

Discrete Fourier transform [4.12] takes the sequence of N complex numbers $x_0, \dots, x_{N-1}$ transforms into another sequence of N complex numbers

$$X_k = \frac{1}{N}\sum_{n=1}^{N-1} x_n e^{-j2\pi\frac{k}{N}n} \qquad 4.1$$

where the orthogonal basis u_k of complex vectors is

$$u_k = \left[e^{j2\pi\frac{k}{N}n} | n = 0, 1, \dots, N-1\right]^T \qquad 4.2$$

A natural and intuitive approach of understanding leakage is that signals with frequencies other than those of the basis set are not periodic in the observation window. Therefore periodic extension of a frequency component in the window which is not proportional to the frequency component natural period will affect discontinuities at the boundaries of the observation window. The discontinuities are responsible for spectral contribution (or leakage) over the entire basis set [4.13].

4.1.1.3 FUNDAMENTAL FREQUENCY ESTIMATION

There are various single tone estimation methods available in data processing. Also National Instruments provided a fast way of obtaining magnitude and phase estimate of harmonic components of interest. Figure 4.35 shows a brief description of the applied algorithm. The fundamental frequency estimation is a crucial issue in harmonic data

processing because further data processing is completely dependent on this value (i.e. real fundamental frequency).

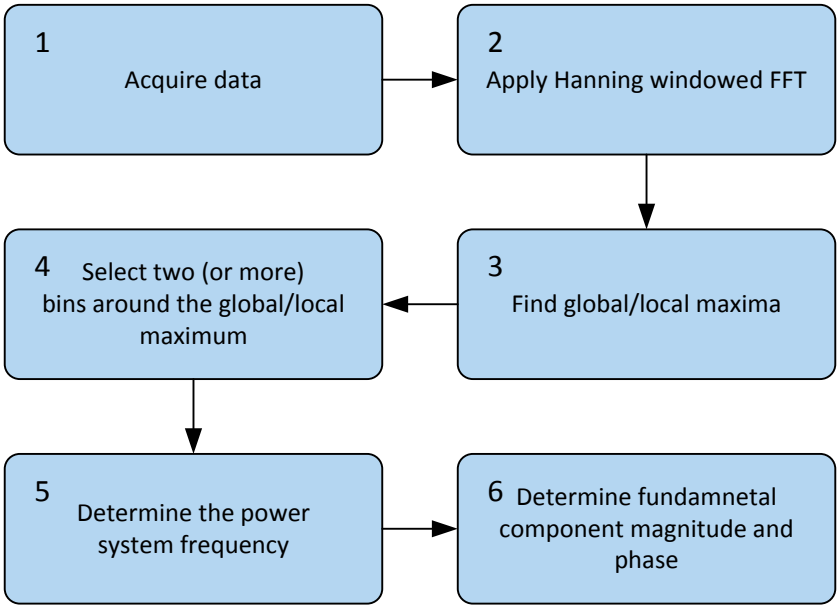

Figure 4.35 Single tone detection algorithm based on Hanning weighted spectrum [4.14].

Single tone information is extracted from Hanning weighted spectrum. Later three dominant bins from the complex spectrum are taken into account. If the bin with index i_{n-1} is bigger than i_{n+1} the following algorithm is applied

$$G(n+1) < G(n-1) \tag{4.3}$$

$$i_o = \frac{\frac{G(n)}{G(n-1)-2}}{\frac{G(n)}{G(n-1)+1}} + i_n \tag{4.4}$$

Otherwise the index i_o of estimated tone is estimated in the following way

$$G(n+1) > G(n-1) \tag{4.5}$$

$$i_o = \frac{\frac{2-G(n)}{G(n+1)}}{\frac{G(n)}{G(n+1)+1}} + i_n \tag{4.6}$$

where i_n is the index (frequency bin number) of the highest bin, $G(n)$ is the highest bin and $G(n-1)$, $G(n+1)$ are left-side and right-side neighbouring bins respectively [4.14]. The fundamental frequency f_o can be calculated in the following way

$$f_o = f_s \frac{i_o}{N} \tag{4.7}$$

where f_S is the sample rate [4.15].

4.1.1.4 OVERSAMPLING DATA

When using a rectangular window, it is important to synchronize the measurement window accurately with the power system frequency to achieve integer multiple of periods in analysed time series (i.e. window period is and integer multiple of analysed frequency component natural period). For example, if the power system frequency is 50.2 Hz whereas the window size is 200 ms, the fundamental frequency spectral line of the discrete Fourier transform is no longer projected (represented) by one complex vector in the orthogonal basis but spanned over the whole basis. One can even say that the power system frequency in the estimated spectrum becomes an interharmonic with spectral leakage as a consequence. Therefore appropriate data should be prepared before the projection into frequency domain.

In order to limit possible data processing errors the signal should be adjusted before spectral analysis. Power system frequency variation can be limited by application of various interpolation methods. It is strongly recommended to always oversample the analysed signal. In this particular case acquired waveforms with sample rate of 44.1 kS/s/ch are oversampled up to 51.2 kS/s/ch. According to this procedure 1024 samples per cycle is obtained, which is an integer power of 2 and can be used to apply fast Fourier transform. Please note that for 10-cycle data blocks discrete Fourier transform should be applied.

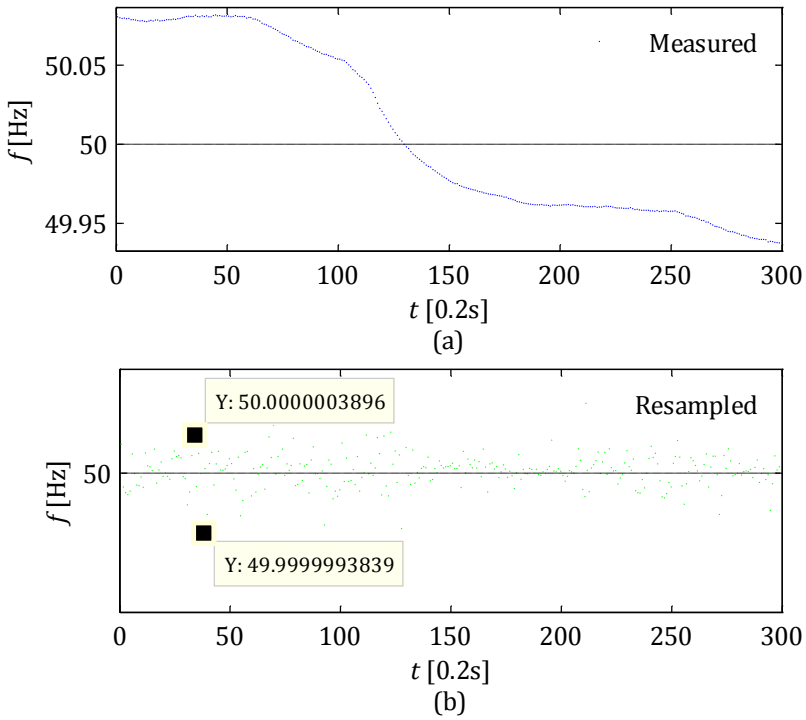

Figure 4.36 Single tone frequency. (a) Measured power system frequency variation. (b) Frequency variation after resampling (spline interpolation).

Oversampling of each 10-cycle data blocks before spectrum estimation significantly limits fundamental frequency variation over analysed window and therefore the stationarity assumption is strengthened for frequency component of interest (i.e. linked with the fundamental frequency). As it can be seen in Figure 4.36 resampling with high precision definitely improves signal quality. The figure presents analysed one minute of acquired voltage waveform and each point is an estimated fundamental frequency over 10-cycle rectangular window. The discrepancy as a difference between two measured values, given in Figure 4.36(b), is acceptably small and the sample standard deviation is $4.3548 \cdot 10^{-6}$. Please note that scale 0.2s used on abscissa (i.e. horizontal axis) in Figure 4.36 denotes the step size between neighbouring samples. If there are 300 samples in presented results (as in Figure 4.36) the total duration is 1 minute (i.e. $0.2\text{s} \times 300 = 60\text{s}$).

It can be seen that both factors such as main tone detection algorithm as well as interpolation algorithm are crucial in appropriate harmonic magnitude and phase estimation. Various interpolation techniques can give different results. The most sophisticated unfortunately are usually the most time consuming. Therefore taking into consideration enormous amount of data to process from few months of multipoint measurements also the interpolation should be optimized and agreement between acceptable accuracy and calculation speed should be found.

Roughly speaking, during interpolation process new samples between existing samples are computed. Different methods were used in data processing such as nearest (coerce) method, linear method, spline method, cubic method, and finite impulse response filter method [4.16]. The nearest method finds the point nearest to x_i in an X array and then assigns the corresponding y value in an interpolated Y to y_i. The linear method interpolates y_i on the line which connects the two points (x_j , x_{j+1}) when the corresponding location x_i of interpolated value y_i which is located between the two points in an X array. The spline method known also as cubic spline method is almost always the most suitable solution. Within the method the third-order polynomial for each interval between two adjacent points in X (x_j, x_{j+1}) is derived. The polynomials have to meet the following conditions: the first and second derivatives at x_j and x_{j+1} are continuous, the polynomials pass all the specified data points, the second derivatives at the beginning and end are zero. The cubic Hermitian spline method is the piecewise cubic Hermitian interpolation. This method is similar to cubic spline interpolation and derives a third-order polynomial but in Hermitian form for each interval (x_j, x_{j+1}) and ensures only the first derivatives of the interpolation polynomials are continuous. Compared to the cubic spline method, the cubic Hermitian method is characterized by better local property. The cubic Hermite interpolation method guarantees that the first derivative of the interpolant is continuous and sets the derivative at the endpoints in order to preserve the original shape and monotonicity of the data [4.15]. Also interpolation based on finite impulse response filter

is popular [4.17], [4.18]. This method provides excellent results also for frequency analysis, although it is more intensive computationally [4.15].

Table 4.4 Comparison of different interpolation algorithms computation times.

Order	Interpolation method	Computation time [ms]	Marker
1	Linear	110	×
2	Coerce	70	✳
3	Cubic spline	130	•
4	Hermitian spline	430	+
5	FIR filter	290	★

Table 4.4 shows the computation time of data interpolation with different algorithms. In each of the cases the presented time is measured for resampling of 10 cycles of measured data. It can be seen that the simplest algorithms exhibit less computation burden. On the other hand in many cases simple algorithms cannot give satisfactory interpolation results and thus affect the harmonic calculation results. Figure 4.37 shows how different interpolation techniques affect harmonic magnitude estimation from measurements carried out at the LV side of the wind turbine transformer. It can be seen that the coerce method is affected the worst while other algorithms give comparable results.

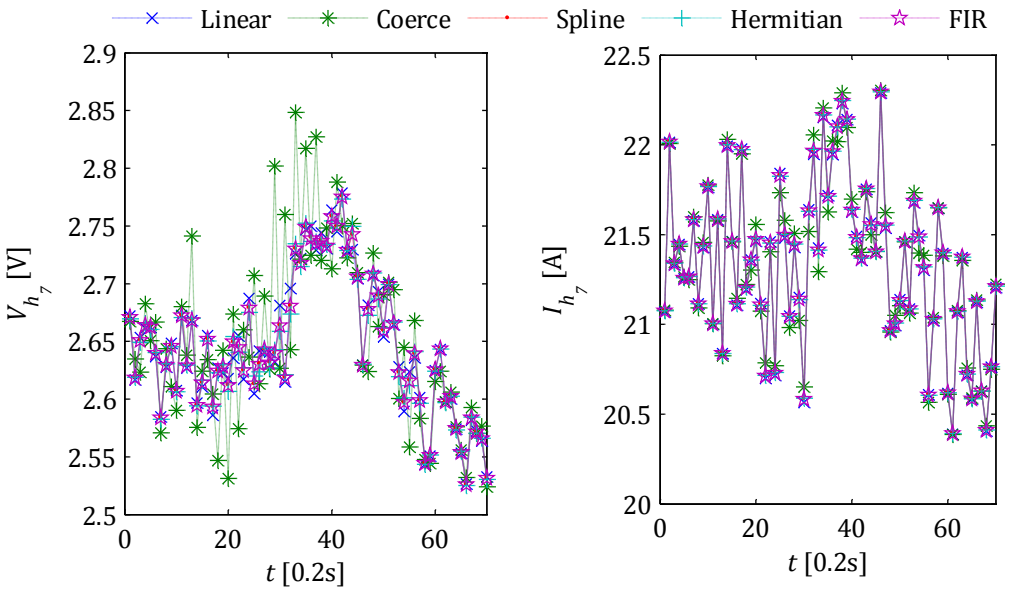

Figure 4.37 Different interpolation techniques used in oversampling of waveforms measured at LV side of the wind turbine transformer.

It was observed that in case of more distorted waveforms (e.g. gird-side converter output voltage) interpolation method choice plays a crucial role. In Figure 4.38 one can see that also linear interpolation and cubic Hermitian spline interpolation do not give satisfactory results. Therefore the most suitable for harmonic components estimation appear to be cubic spline interpolation as well as finite impulse response filter

interpolation. Since the spline method (as presented in Table 4.4) is less time consuming, this method was used in further data processing. The selected measurement period was selected when the power system frequency were varying below 50 Hz or above 50 Hz.

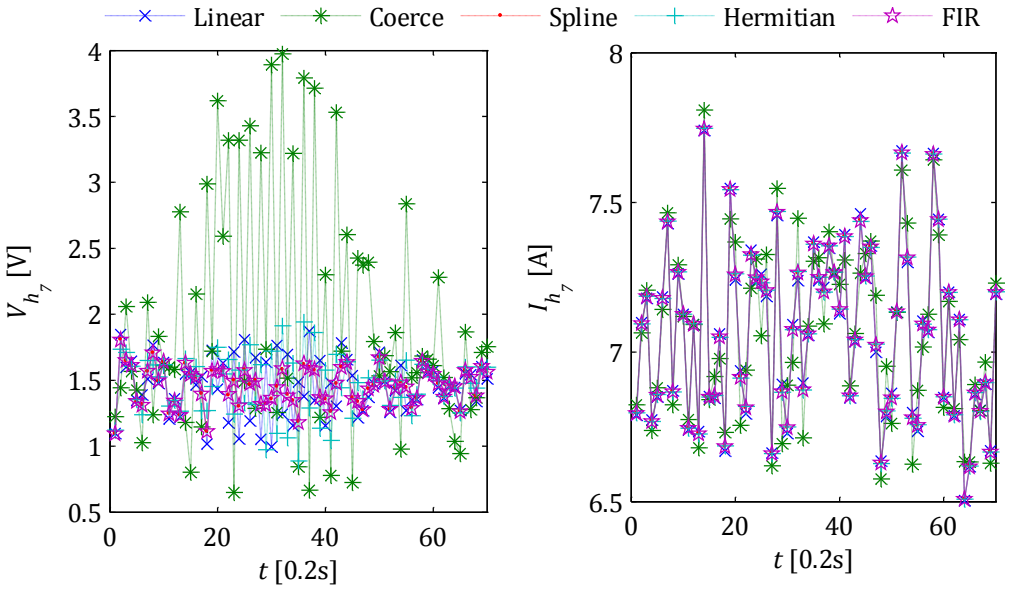

Figure 4.38 Different interpolation techniques used in oversampling of waveforms measured at the grid-side converter AC terminals.

4.1.1.5 MAGNITUDE ESTIMATION

It was decided to choose one minute of 44.1 kS/s/ch sampled measurement data. The criterion of choosing was to observe significant frequency variation during one minute of measurements. As it can be seen in Figure 4.36, at the beginning of measurements the frequency is higher than expected and goes through 50 Hz value to finally be lower than expected value.

Measurements are obtained using National Instruments 4472 dynamic signal acquisition board with oversampling-based anti-aliasing filtering described previously. Processed signals are resampled to 51.2 kS/s, what gives 1024 samples per analysed cycle. Every certain analysed block constitutes 10 cycles calculated according to the sample rate.

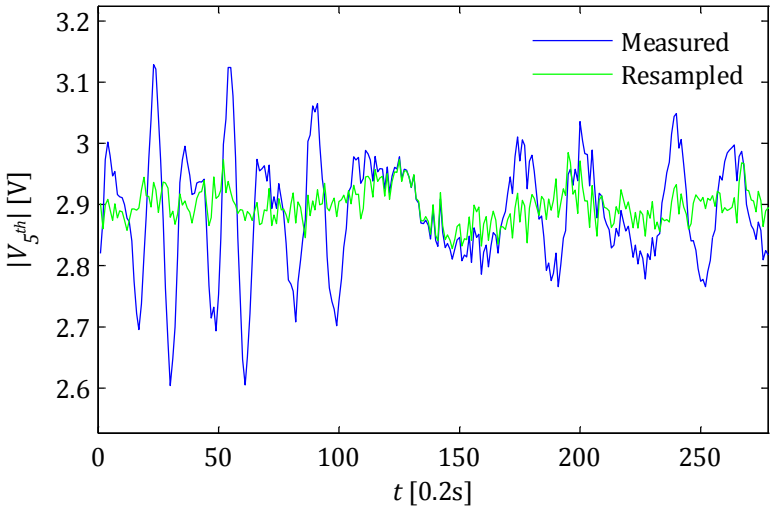

Figure 4.39 Comparison between voltage harmonics calculated from measured and resampled signals.

Firstly the 5th voltage harmonic was taken into account during signal processing. In Figure 4.39 one can see that the processing precision of resampled data is much higher. The sample standard deviations for measured and resampled signal are 0.0935 and 0.0294 respectively. Results are comparable only when measured signal main frequency component is close to the theoretical value. Otherwise if the frequency variation increases, the precision decreases.

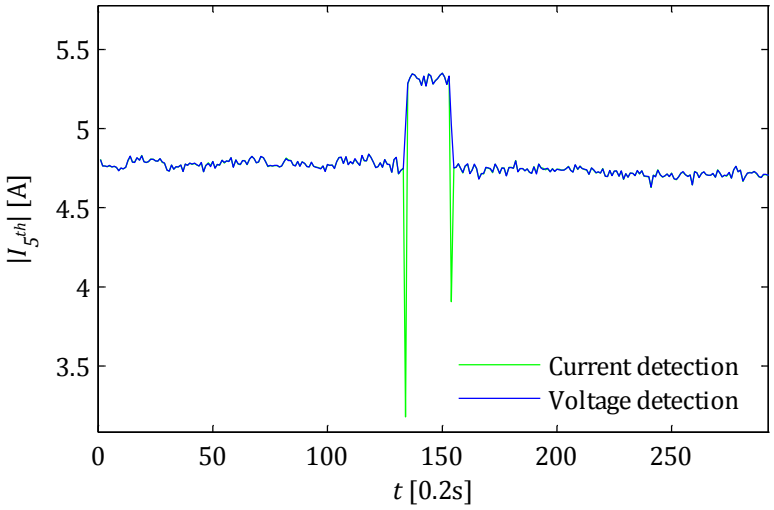

Figure 4.40 Current harmonic calculated based on voltage or current frequency detection.

Another step of the analysis is to compare harmonic current calculation results. It was observed that it is better to detect voltage frequency for both voltage and current processing from the same phase. This is mainly due to fact that generally voltage waveform has a smaller total harmonic distortion level than a current waveform. This can be clearly seen when certain current harmonic level changes rapidly, for instance due to changes in wind turbine power production. During such kind of changes frequency detection algorithm calculates less accurate which implies additional

processing errors. In Figure 4.40 one can see how current frequency detection during 5th current harmonic level changes affects measurement data processing results.

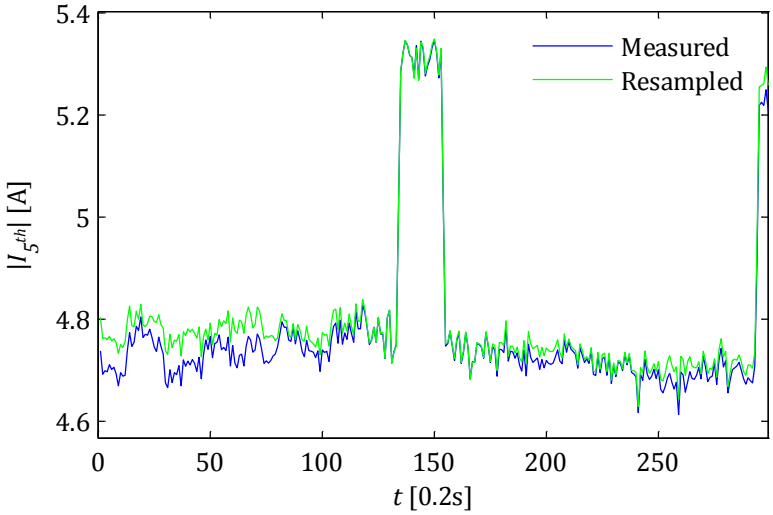

Figure 4.41 Harmonic current calculated from measured and resampled data.

Current calculation also exhibits errors in harmonic assessment due to power grid frequency variation. In Figure 4.41 the highest errors can be seen at the beginning of processed one-minute current waveform where the grid frequency is around 50.08 Hz. This is mainly because of spectral leakage observable during the Fourier transform. In other words due to limited number of complex vectors in the orthogonal basis some of the frequency components are spanned along the whole discrete Hilbert space.

It has to be emphasized that dependent on grid codes different frequency variation is allowable. As an example the Polish grid code entitled the Transmission Grid Traffic and Maintenance Instruction [4.19] it is stated that the minimum acceptable frequency is higher than 47.5 Hz and maximum is 51.5 Hz what indicates that frequency variation can be even higher than in the analysed case and can produce less accurate results without resampling.

Due to this fact (i.e. significant power system fundamental frequency variation) characteristic harmonics generated by power electronic equipment are not any longer harmonics from power system perspective because the power frequency varies to balance production and loading. While frequency components are generated by power converter modulator which is with constant carrier frequency in most cases which obviously is not aligned with the varying power grid frequency. According to IEC standard [4.20] the harmonic frequency is an integer multiple of the power supply (fundamental) frequency

$$f_n = nf_o \tag{4.8}$$

and in this case is considered as an interharmonic. There are actually some methods to synchronize the carrier signal frequency of pulse-width modulated converters in power systems [4.21]. Therefore distinguishing high-frequency components generated by converter pulse width modulation, i.e. the carrier frequencies and sideband frequencies around carrier frequencies, between harmonics and interharmonics can be misleading.

In case of pulse width modulation harmonic components are dependent on both power system fundamental frequency f_o and carrier signal fundamental frequency f_c. Being more specific baseband harmonic components are dependent on the power system fundamental frequency, carrier harmonic component only on the carrier signal fundamental frequency, and sideband harmonic components are dependent on both of them. The nature of the generated harmonic components is the same, independently on frequency ratio $m_f = f_c/f_o$. Carrier and sideband harmonic components are integer multiple of the power system fundamental frequency only if the frequency ratio is an integer number. Please note that this is a trivial case and rare in real-life power systems where fundamental frequency varies. All frequencies generated by converter modulator frequency components can be still called harmonics but driven by two independent fundamental frequencies (i.e. power system fundamental and carrier fundamental). Note that naturally sampled pulse width modulation does not affect low-frequency components except the desired fundamental which is synchronized with the power system frequency by phase-locked loop [4.22].

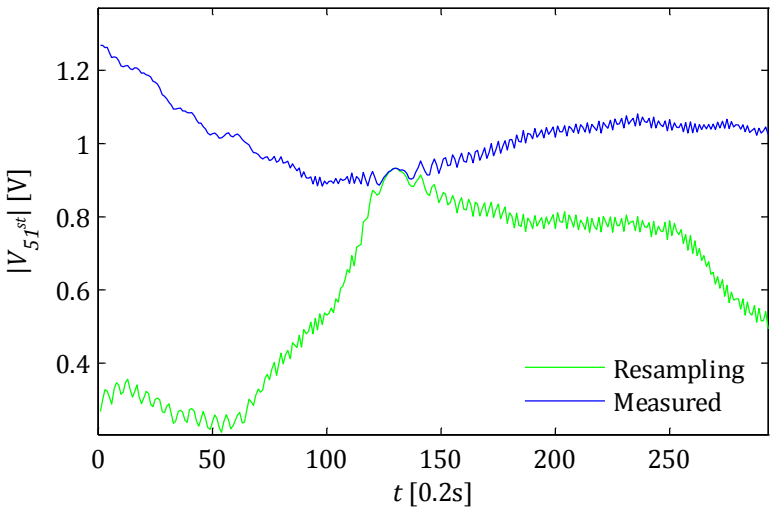

Figure 4.42 Sideband frequency around carrier frequency calculated from measured and resampled signals.

As it was mentioned previously, not always in wind turbine grid converters carrier signal frequency is adjusted according to the power system frequency variation. This shows that resampling can contribute to processing errors due to the spectral leakage which is significant for high-frequency components. It emphasizes a need to choose appropriate calculation technique dependent on frequency components origin

in measured waveforms. Figure 4.42 shows significant errors if the grid frequency variation is high. It can be seen if the measured frequency goes close to the nominal the errors can be neglected and obviously both calculation methods give comparable results. Please note that the frequency variation for this particular period is presented in Figure 4.36.

Earlier it was mentioned that actually sideband harmonic components are dependent on both power system fundamental frequency and carrier signal fundamental frequency. Therefore it is expected that also spectral leakage can occur for waveforms not resampled. This is of course true but sideband harmonic components frequency variation is so small they can be omitted for 10-cycle windows. Analytical description of harmonic components generated by three-phase voltage source converters with pulse width modulation will be shown later and this problem also explained.

The question is how to check if certain frequency components are actually linked only with the power system fundamental frequency or also driven by other fundamental frequencies. This can be checked by analysing sufficiently long (i.e. includes data measured for various power system fundamental frequencies) time series. Therefore once again long-term measurements are required to observe signal tendencies and statistical properties.

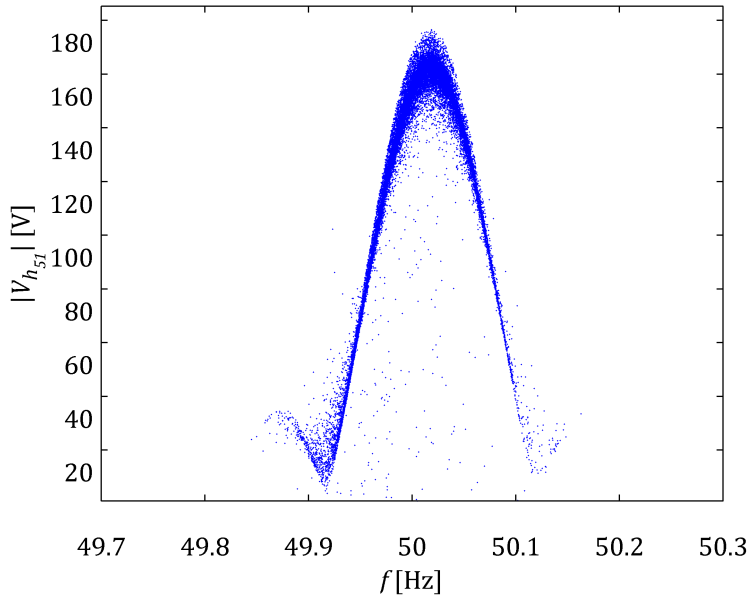

Figure 4.43 Sideband harmonic component calculated from resampled data displayed versus the power system frequency.

If a certain frequency component is not an integer multiple of the power system frequency shapes similar to presented using scatterplot in Figure 4.43 can be observed. It can be seen that some regularities are exhibited due to spectral leakage. The scatterplot showing sideband harmonic component generated by the modulator in grid converters in nowadays wind turbines consists of data from more than three days of measurements. This indicates that resampling or adjustment of sampling rate

during measurement process can provide inappropriate results for frequencies not synchronized with the power frequency and finally can blurry harmonic assessment.

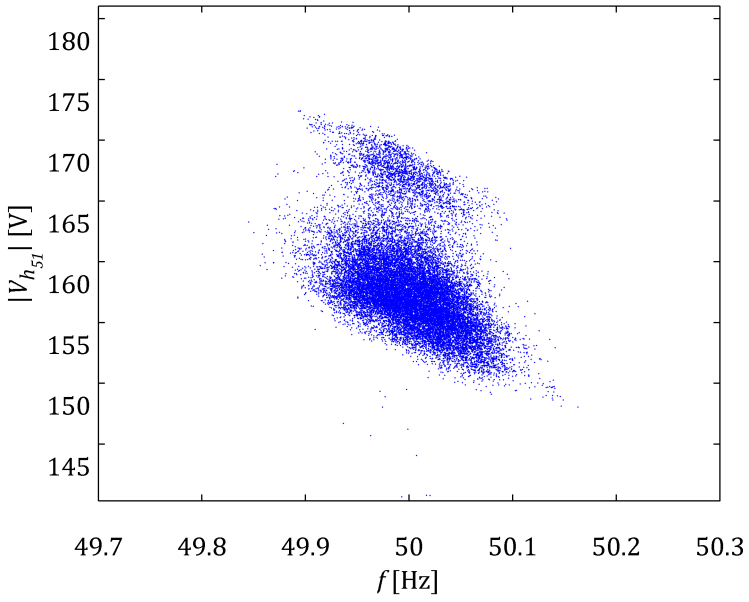

Figure 4.44 Sideband harmonic component calculated directly from measured data displayed versus the power system frequency.

If the scatterplot shows random dependence between a harmonic and the power system frequency it can be assumed that there was no deterministic influence in the calculation algorithm during measurement data processing. Fairly normal distributed observations in Figure 4.44 give an overview of the measurement and processing precision.

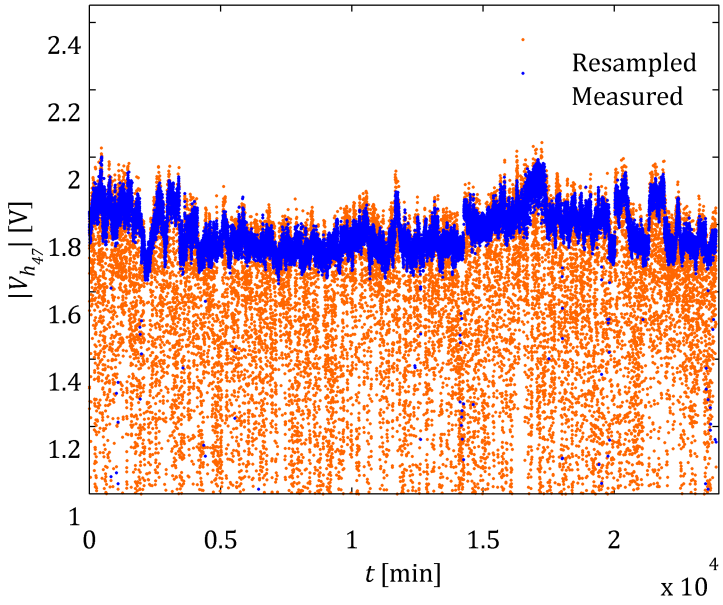

Figure 4.45 Sideband harmonic magnitude estimation for directly measured data or resampled according to the fundamental frequency.

Very important aspect in measurement data analysis is what kind of data analysis techniques are applied. As mentioned at the beginning different aspects of measured signal nature need to be taken into consideration. Different techniques are used for non-stationary signals (e.g. continuous and discrete wavelet transforms with non-orthogonal basis), different for stationary signals (e.g. discrete and fast Fourier transforms). Of course it is impossible to find stationary signals in real-life wind power systems. There are always different parameters that may vary. One of the most important is the power system frequency which plays a significant role in success of non-parametric spectrum estimation methods (i.e. discrete and fast Fourier transform). One has to be aware, that practically, during spectrum estimation only finite-length segments of infinitive signals are analysed and energy from real spectrum can leak to other frequency components in estimated spectrum. This of course affects data processing errors and one has to know how to interpret processing results using non-parametric analysis methods. According to IEC standards [4.6], [4.23], [4.24] a rectangular widow is recommended for measured signal spectrum estimation using discrete Fourier transform. Therefore spectral leakage is caused by the frequency response of the rectangular window and its Fourier transform, the sinc function, has oscillation of periodic width. If there is no integer number of cycles of a certain frequency component of interest within analysed window, numerical calculations will exhibit more significant spectral leakage.

Spectrum bins calculated from discrete Fourier transform are distant from each other of half of the sampling frequency divided by length of one-sided spectrum (i.e. half of the window length). Wavelengths of such bins are divisors of the applied rectangular window length. In order to reduce signal processing errors, a natural way is to resample measured signal in order achieve harmonic signals of interest to be represented exactly by one bin from discrete Fourier transform (i.e. there is an integer number of periods of analysed frequency components within the whole window). Good practice is to resample data to get 1024 S/c and later take a window of 10 cycles to analyse. If the cycle of interest is $T = 0.02$ s, resampled data with 51.2 kS/c sample rate allows obtaining discrete Fourier transform bins with 5 Hz resolution. Resampling becomes to play a crucial role if f_o varies significantly, especially during analysis of higher frequency components.

Resampling can be successfully applied during data processing if one assume that all frequency components of interest are linked with the power system frequency f_o (i.e. frequency components are integer multiple of f_o). Based on presented measurement data one can conclude that in the analysed grid-side converter the switching frequency f_c is fixed (i.e. fixed-frequency modulation). If the carrier fundamental component is constant during wind turbine operation, respampling contributes to significant processing errors which cannot be accepted. That is why it is of great importance to know the nature of analysed frequency components in order to apply appropriate data processing techniques and estimate spectrum as accurate

as it can be possible. Figure 4.43 shows sideband voltage harmonic (h_{51}) estimation laden with significant processing errors affected by spectral leakage. The same harmonics are presented also in Figure 4.44 where are correctly calculated without resampling since sideband harmonics due to fixed carrier frequency f_c are not linked directly with the power system frequency f_o.

In case of double-edge naturally sampled pulse-width modulation and asymmetrically regular sampled pulse-width modulation all odd sideband harmonics are eliminated in the first carrier harmonic group. This means that significant sideband harmonics in this carrier group will occur at frequencies of $\omega_c t \pm 2\omega_o t$, $\omega_c t \pm 4\omega_o t$. And for the second carrier group, the significant sideband harmonics will occur at $2\omega_c t \pm \omega_o t$, $2\omega_c \pm 5\omega_o t$, $2\omega_c t \pm 7\omega_o t$. All triplen sideband harmonics (e.g. $2\omega_c t \pm 3\omega_o t$, etc.) are cancelled between legs because the phase angles of these harmonics rotated by multiples of 2π for all phase legs (i.e. common mode signals). It can be seen that sideband harmonics vary with the fundamental f_o, even if the carrier fundamental f_c is fixed. This is due to fact that the switching function S is dependent on command signal frequency, amplitude, and phase as well as carrier signal. This creates certain problems in frequency component identification as actual harmonics (according to definition used in power system studies). According to the definition of a harmonic of a wave is a component frequency of the signal that is an integer multiple of the fundamental frequency f_o. That is why in real life power converter systems with pulse-width modulation it might be confusing to talk about harmonics generated by the switching function since the power system frequency varies.

Talking about sideband harmonics is a simplification for theoretical investigation (i.e. $f_c = nf_o, n \in \mathbb{N}$). Later it will be shown based on double Fourier approach, that actually sideband frequency components can be called harmonics but for a system with two drive fundamental frequencies. First considered frequency is the power system fundamental frequency and second is the carrier signal fundamental frequency. Such frequency component can still be theoretically derived by Fourier decomposition and from harmonic analysis perspective are simply harmonics.

Another interesting aspect is that even if the switching frequency f_c is fixed in the analysed system the sideband harmonics vary with the power system frequency f_o. Unfortunately they are not anymore integer multiples of f_o. This creates additional problems during measurement data processing. Resampling definitely will bring unacceptable numerical errors due to the nature of discrete Fourier transform as well as analysis without resampling is inappropriate since sideband harmonics' frequency varies. One way to deal with this problem is to estimate power system frequency f_o and resample data for separated sideband harmonics since there is no common integer multiple. Another approach is to estimate processing error for different calculation methods and apply the most acceptable. Assume that the power system frequency f_0 variation within certain measurement period is $\Delta f_o \pm 0.2$ Hz. Since sideband harmonics are not anymore linked with the power system frequency f_o, the variation of even

sideband harmonics generated by double-edge naturally and asymmetrical regular sampled pulse-width modulation for the first odd carrier group $m = 1$ is $\omega_c t \pm n2\pi(f_o + \Delta f_o)t$, where $n = 2, 4$. If one will take sufficiently narrow rectangular window (e.g. 10 c), the spectrum estimation errors are negligible since spectrum resolution will be 5 Hz and the frequency variation only 0.2 Hz. Therefore no significant energy leakage from actual frequency component will be seen in other discrete Fourier transform bins situated ± 5 Hz.

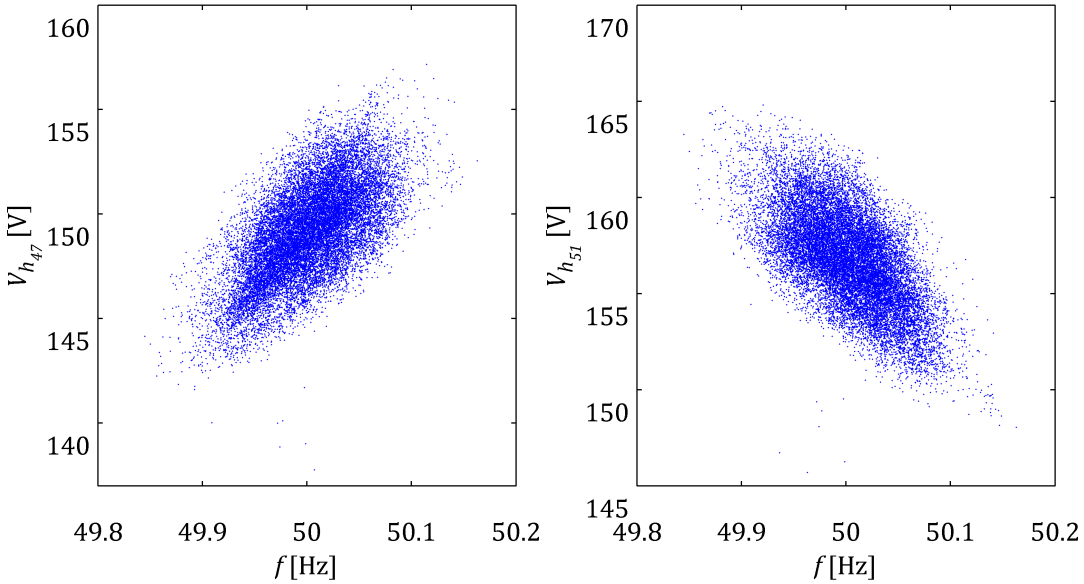

Figure 4.46 Sideband harmonic components magnitude variation depending on power system frequency.

Figure 4.46 shows how the estimated magnitude of sideband harmonic components can vary in real life systems depending on power system frequency variation. Sideband harmonic components presented in the figure are from the first carrier group, thus $\omega_c t \pm 2\omega_o t$ is valid. Please note that the scatterplot was obtained by separation of one class from the whole population using sophisticated statistical methods which will be described later. Normally (i.e. without sub-population separation) the scatterplot should look like in Figure 4.44. The dependency shown in Figure 4.46 indicates that the magnitude of $\omega_c t - 2\omega_o t$ is increasing with the power system frequency while $\omega_c t + 2\omega_o t$ is decreasing. Spectral leakage should affect magnitude decrement for both lower and higher frequencies than the theoretical one. This cannot be seen directly in the figure because due to asymmetrically regular sampled pulse-width modulation which will be explained later based on double Fourier approach. Anyway spectral leakage of course affect uncertainty of analysed data.

4.1.1.6 PHASE ANGLE ESTIMATION

From discrete Fourier transform also phase information can be obtained. This can be used in order to analyse harmonic origin, nature and propagation in wind farms. It also can help distinguish between characteristic and non-characteristic harmonics.

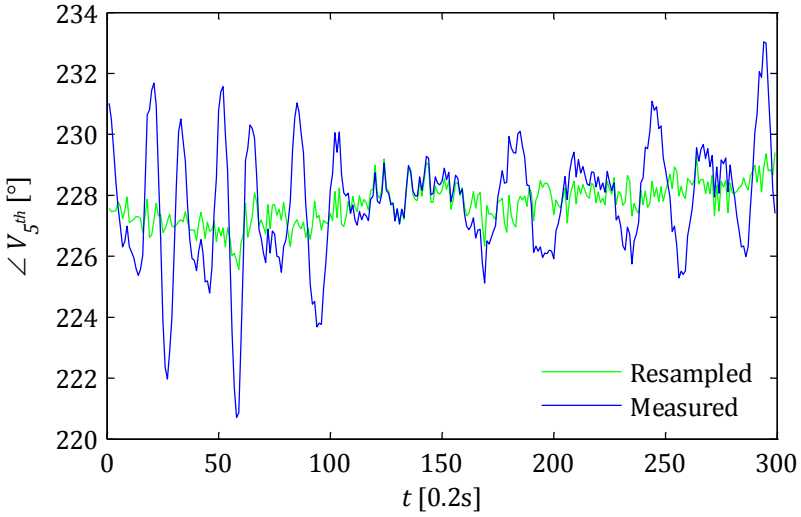

Figure 4.47 Harmonic phase obtained using different signal processing approaches.

Previously observed conclusions regarding 5th voltage harmonic magnitude calculation methods can be seen also for the harmonic phase presented in Figure 4.47 where the 5th harmonic phase angle calculated form resampled data has smaller sample standard deviation ($s_x = 0.6656$) than calculated directly from measured data ($s_x = 1.9264$). The phase angles are phase locked to the first harmonic of the first-phase voltage waveform in order to find non-parametric methods physical meaning. To compare Figure 4.48 presents data obtained directly from discrete Fourier transform.

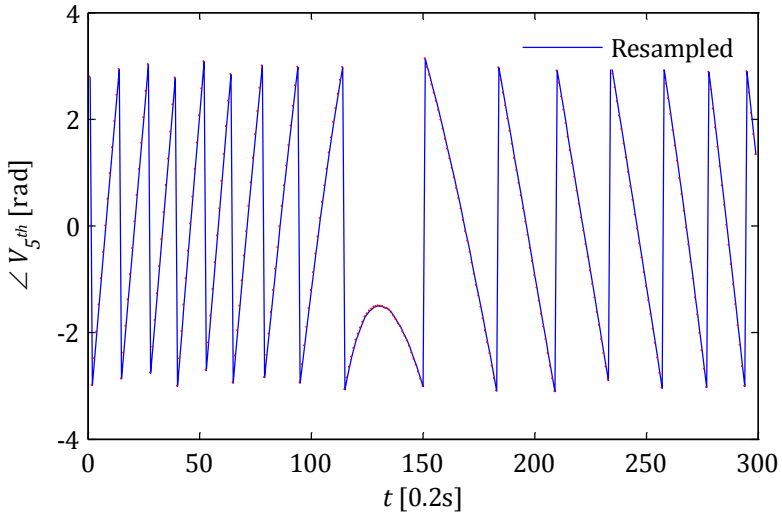

Figure 4.48 Phase angle information obtained from analysis in the frequency domain.

From Figure 4.48 one can see that the phase shift of the 5th harmonic angle varies depending if the power system frequency is higher or lower than the theoretical. Theoretically if no power system frequency variation would be observed the 5th harmonic angle should be constant (i.e. the same phase shift in reference to the rectangular window).

If certain frequency components of interest are not linked with the power system fundamental frequency f_0, problems also appear with phase angle calculations. Normally all harmonic phase angle have to be referred (phase locked) to a certain absolute value in order to clarify physical interpretation of results. A good practice is to lock phases of all harmonics to the voltage phase of the first electrical phase in three phase systems. Unfortunately if, in this particular case, sideband frequency components in carrier groups are not linked with the power system frequency, phase lock causes wrong and impossible to interpret results. As it was mentioned previously in harmonic magnitude estimation resampling plays a crucial role in order to avoid unwanted harmonic energy distribution between more than one bins of estimated spectrum. In case of harmonic phase calculation resampling is not so significant. Despite different data pre-processing techniques before application of discrete Fourier transform, phase would not be changed. It is simply dependent on rectangular window shift in time domain. Due to resampling according the fundamental frequency the wavelength of frequency components not linked to the fundamental f_0 will vary in time. This can produce phase calculation errors which can appear significant as the frequency increases.

To show differences in phase calculation between phase-locked sideband harmonics to the fundamental and without phase lock, a certain measurement period where f_0 significantly varies is taken. Fundamental component frequency variation is shown in Figure 4.49. Frequency detection in this case is carried out for 2-cycle (0.04s) rectangular window. In order to calculate the fundamental frequency single tone information is extracted from Hanning weighted spectrum. From the spectrum three significant bins are extracted. From the given three dominant bins exact frequency is calculated according to aforementioned formula.

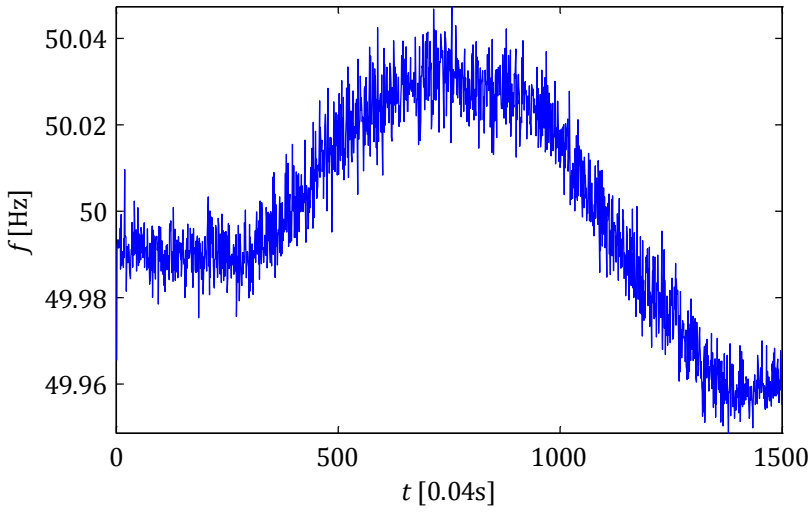

Figure 4.49 Power system frequency variation in one minute of measurements.

As it can be seen in Figure 4.50, the calculated harmonic angle is slightly dependent on the power system frequency. Due to the fact f_0 varies the phase calculated from

discrete Fourier transform is different for every calculated window. The rectangular window length is assumed to be $10T$, where T it the theoretical period equal to 0.02s. With the assumption that the switching frequency is fixed $f_c = 2450$ Hz and the fundamental frequency variation is within $\Delta f_0 = \{49.95 \leq f_0 \leq 50.05\}$, sideband harmonics vary (double-edge naturally and asymmetrical regular sampled pulse-width modulation in three-phase converters) according to the following relation $mf_c \pm n\Delta f_0$ where n is even for odd m and n is odd for even m. Taking into consideration $f_c - 2f_0$ as an example one has $\Delta f_{2350} = \{2349.9 \leq f_{2350} \leq 2350.1\}$. If the window size is fixed and f_{2350} is not phase-locked the maximum phase calculation error is 2%.

Of course this is the worst case and normally the frequency would not change instantly as it can be observed in Figure 4.51. It can be also seen that the calculated angle is monotonically increasing. The angle variation is only affected by f_0 variation according to $mf_c \pm nf_0$. This means that the carrier frequency is slightly higher than integer multiple of theoretical fundamental frequency $f_0 = 50$ Hz. Constant average angle increments of 12^o imply the same spectral leakage and also fixed carrier frequency.

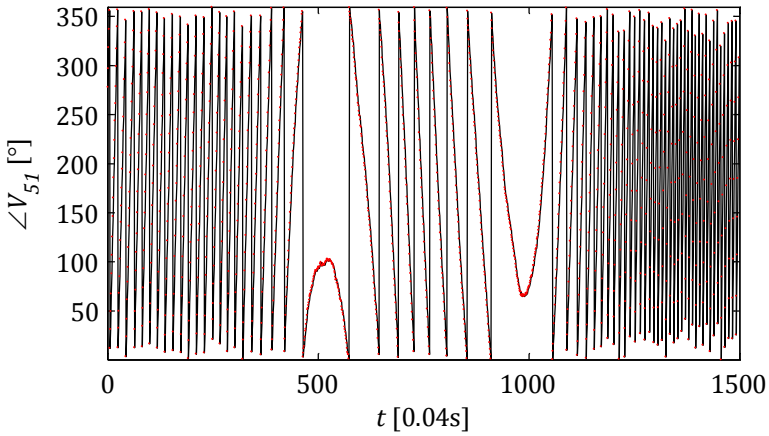

Figure 4.50 Sideband harmonic phase angle estimation using algorithm with phase lock.

If the calculated angles of sideband frequency components from the first carrier group are phase-locked with the varying fundamental power system frequency f_0, significant calculation error may appear as shown in Figure 4.50. Different angle increments as well as periodical monotonic increase and decrease are dependent on f_0. Due to the fact that f_c is fixed, phases between the fundamental component and sideband frequency components are not correlated.

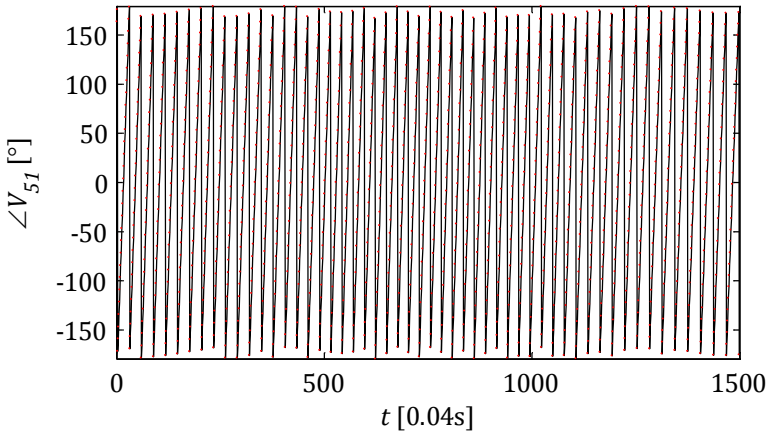

Figure 4.51 Sideband harmonic component phase angle estimated without phase lock.

Another issue is that common averaging practices can be catastrophic in case of high-order (i.e. above the converter bandwidth) harmonics phase calculation. Those harmonics rotate much faster in comparison to baseband harmonics and even small window length variation (or window is not a multiple of high-order harmonics wavelength) can cause significant changes in angle calculation, as seen in Figure 4.50 and Figure 4.51. Averaging of such harmonic angles can bring unacceptable errors as presented in Figure 4.53. Thus in some studies [4.25] related with harmonic angle estimation of sideband harmonic components it is assumed that the angle is uniform distributed or fixed.

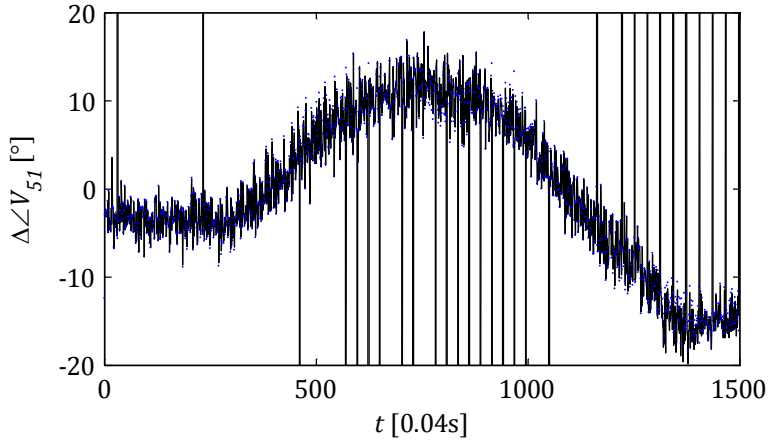

Figure 4.52 Phase angle estimation error affected by resampling.

As it was mentioned earlier resampling can affect also phase angle estimation. Figure 4.52 shows difference in phase estimation of not resampled and resampled waveforms. It can be easily seen that actually the difference is correlated with the power system frequency variation (compare with Figure 4.49). Due to resampling the power system frequency f_o variation affects of phase shift in the rectangular window of frequency components not linked with f_o. The phase angle in degrees error is just simply $180 \cdot 2\pi\Delta f_o/\pi$.

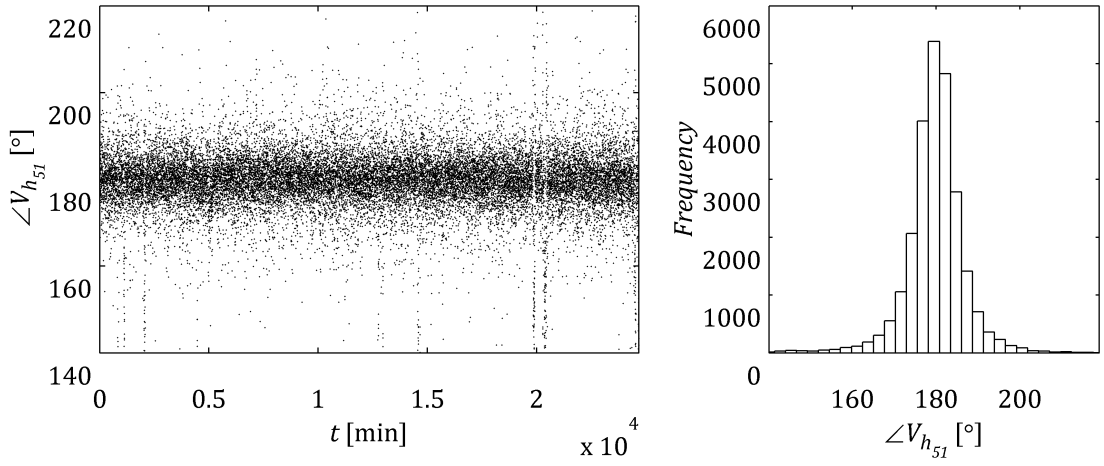

Figure 4.53 Wrong sideband harmonic phase estimation.

Precise phase angle estimation is very important because it allows observing how harmonic components are related to the fundamental one. Since the grid-connected voltage source converter can generate any harmonic (i.e. any amplitude and angle) phase angle analysis become more important. It cannot be no longer just assumed that, for instance, the 2nd harmonic is always of negative sequence.

Of course for low order harmonics data processing errors caused by spectral leakage are negligible and harmonic components magnitude estimation results are comparable for both resampled and not resampled waveforms. Similar situation is also for phase angle estimation. Appropriate data processing is more important for frequencies of higher order where even small variation of the power system fundamental component can affect significant changes. Nowadays more and more power electronic equipment with relatively high switching frequency is installed in modern power systems therefore also harmonics of high order are more and more important to consider.

Most of power electronic devices are modulated by pulse width and also that is why it is important to consider harmonics generated by systems with two driven frequencies. Unfortunately switching frequencies are not the same in different wind turbines therefore many frequency components are expected in future power systems which are not necessarily integer multiples of the power system fundamental frequency. Sometimes even if the switching frequency is expected to be the same the carrier signal either can be locked with the power system frequency or not [4.21] which causes different spectrum at the grid-side converter AC terminals.

4.1.1.7 COMMERCIAL POWER QUALITY METERS

The use of a rectangular window requires that the measurement window is synchronized with the actual power system frequency, hence the use of a 10-cycle window instead of a window of exactly 200 ms. The IEC standard requires that 10 cycles correspond with an integer number of samples within 0.03%. To ensure synchronism between the measurement window and the power system frequency, most

power quality meters use a phase-locked loop generating a sampling frequency that is an integer multiple of the actual power system frequency. One of the commonly used in the company power quality meters is Elspec G4500 which provides full functionality regarding measurements of power quality. An exemplary connection of such measurement equipment in there phase system is presented in Figure 4.54 [4.26].

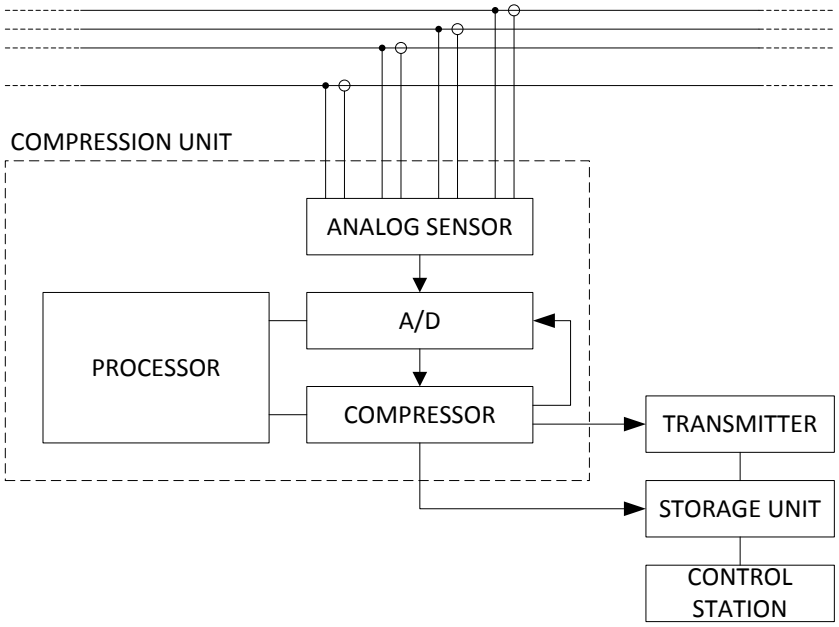

Figure 4.54 Exemplary connection of Elspec equipment in wind turbines.

Before power quality indices are calculated by the Elspec equipment, acquired data is processed. Processing stage comprises of fundamental frequency detection, sample rate adjustment according to the detected frequency, and Fourier decomposition applied. The approach of sample rate adjustment is to adjust the finite orthogonal Hilbert basis in order to express each of frequency components in the Fourier space only by one vector from the Hilbert basis. The whole data acquisition, processing and logging process is briefly presented in Figure 4.55.

A synchronization (i.e. sample rate adjustment according to the fundamental frequency) error leads to cross-talk between different harmonic frequencies. The 50 Hz component is by far the dominating component in most cases so that the main concern is the cross-talk from the 50 Hz component to higher order components. From the other side, resampling process can affect frequency components which are not integer multiple of the fundamental frequency.

This phenomenon can be easily seen in the spectrum of pulse width modulated voltage source converters with fixed frequency ratio. Since generated output voltage of the wind turbine is a function of the fundamental frequency (f_o) and the carrier frequency (f_c), results obtained by the Elspec system are incorrect to some extent. The magnitudes of Fourier transform harmonic components are the more inaccurate the higher significant is the fundamental variation. Even if the result of applying

the discrete Fourier transform to the basic window is a spectrum with 5-Hz spacing between frequency components and the spectrum thus contains both harmonics and interharmonics, the results can be sometimes significantly inaccurate.

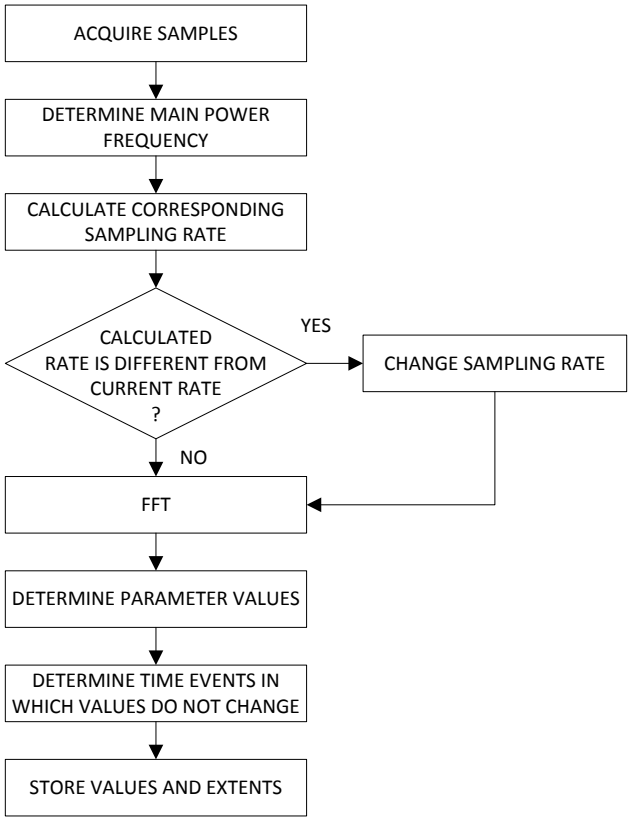

Figure 4.55 Data processing algorithm used by Elspec equipment.

As a good example of this is one of the most significant sideband harmonic components from the first carrier group. Exemplary results of measurements form the LV side of the wind turbine transformer can be seen in Figure 4.56. As it was mentioned previously the wind turbine frequency ratio is $m_f = 49$ and the analyzed sideband harmonic component is of frequency $f_c + 2f_o$. Three scatter plots present the same harmonic component measured during the same period using different data acquisition devices and processing techniques.

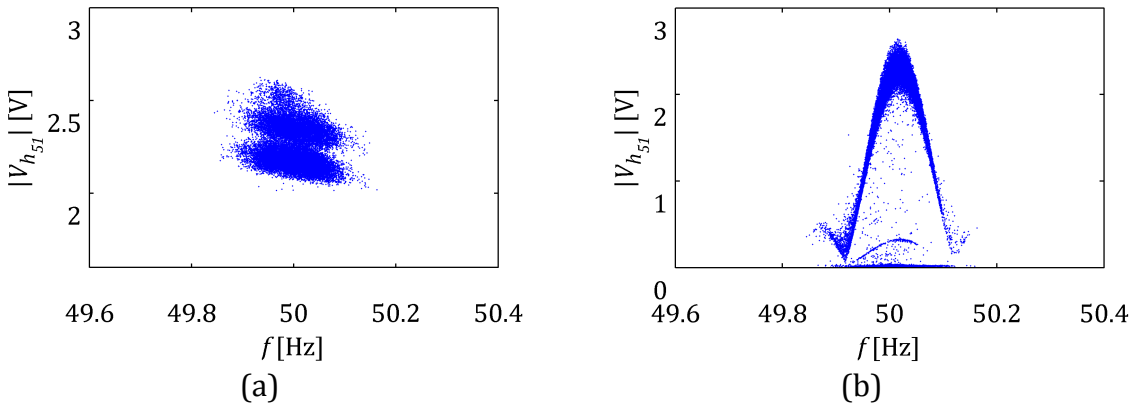

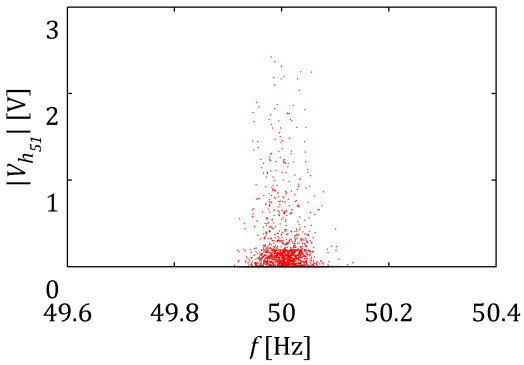

(c)

Figure 4.56 Sideband harmonic component affected by different processing techniques: (a) sideband harmonic calculated in post-processing from resampled signal, (b) sideband harmonic calculated in post-processing from original signal, (c) sideband harmonic calculated on-line by power quality meter.

Data processing results presented in Figure 4.56 show how easily inappropriately applied processing techniques can provide wrong results. Results from Figure 4.56(a) show sideband harmonic component measured using results obtained from the measurement campaign with direct Fourier decomposition (i.e. without sample rate adjustment). From Figure 4.56(b) presents the same data but resampled and later discrete Fourier transform is applied, Figure 4.56(c) describe sideband harmonic component magnitude obtained by the Elspec measurement system.

It can be observed that results using various processing approach provide different results. Due to the fact that the frequency of sideband harmonic components generated by modulation with constant carrier frequency does not vary significantly and Fourier decomposition without earlier sample rate adjustment gives the most appropriate results. This is presented in Figure 4.56(a) and only small magnitude variation affected by nonlinear relation between the modulation index (M) and the sideband harmonic components as well as measurement and data processing (i.e. small spectral leakage) errors. Completely different and unacceptable results are seen in Figure 4.56(b) where analysed waveform is resampled. One can observe that due to significant spectral leakage the estimated magnitude sometimes can be even equal to zero. Therefore sometimes power quality meters can provide values significantly affected by processing errors. This behaviour is present in the scatter plot from Elspec measurements (Figure 4.56(c)). It is important to emphasize that the algorithm in the power quality meter applies lossy compression which also determines estimated magnitudes. Estimated harmonic components are assumed to be insignificant and not saved (i.e. set to zero) if the magnitude is lower than a certain threshold which is defined based on measured waveform distortion and maximum allowed database storage capacity per month. Such limitations provides scatter plots as in Figure 4.56(c) which is similar to Figure 4.56(b) but modified due to averaging and magnitudes below the threshold artificially set to zero.

4.1.2 MULTIRESOLUTION ANALYSIS

According to the uncertainty principle in context of harmonic analysis, one cannot at the same time localize the value of a function and its Fourier transform [4.27]. From signal processing perspective it can be expressed as the product of the time domain resolution and the frequency resolution is constant, and it is not possible to obtain high resolution at both the time domain and frequency domain at the same time. Wavelet transform due to its multiresolution approach can capture the short duration, high frequency and the long duration, low frequency information by changing the location and scaling of the mother wavelet, which is the window function in wavelet transform.

Let $\psi(t) \in L^2(\mathbb{R})$ will be a time-limited mother wavelet function. To ensure that the wavelet transforms at each scale s are directly comparable to each other and to the transforms of other time series, the wavelet function at each scale s is normalized to have unit energy [4.28].

$$\int_{-\infty}^{\infty} \psi(t)dt = 0 \tag{4.9}$$

$$\|\psi(t)\|^2 = \int_{-\infty}^{\infty} \psi(t)\psi^*(t)dt = 1 \tag{4.10}$$

Now let us define a mother wavelet orthonormal basis

$$\left\{\psi_{s,u}(t) = \frac{1}{\sqrt{s}}\psi\left(\frac{t-u}{s}\right)\right\}\Big|_{u\in\mathbb{R},s\in\mathbb{R}+} \tag{4.11}$$

where u is the translating parameter and s is dilation (scaling) parameter. The continuous wavelet transform is the coefficient of the basis $\psi_{u,s}(t)$

$$\begin{aligned} Wf(s,u) = \langle f(t), \psi_{s,u}\rangle &= \int_{-\infty}^{\infty} f(t)\psi_{s,u}^*(t)dt \\ &= \int_{-\infty}^{\infty} f(t)\frac{1}{\sqrt{s}}\psi\left(\frac{t-u}{s}\right)dt \end{aligned} \tag{4.12}$$

Using wavelet transform from Eq. 4.12 one can map one-dimensional signal $f(t)$ to two-dimensional coefficients $Wf(s,u)$. This allows performing multiresolution time-frequency analysis [4.29].

In contrast to Fourier transform, the continuous wavelet transform is capable of constructing a time-frequency representation. This allows tracking changes in the frequency spectrum of a waveform of interest. One of the good examples in harmonic analysis in wind farms is a sudden change of system state such as wind turbine shutdown, and wind turbine start-up, capacitor bank switched on or off.

In order to investigate wind turbine dynamic behaviour, a wind turbine shut-down event was investigated. This allows observing how the wind turbine responds

to the external network which introduces significantly distorted voltage. Figure 4.57 shows that the grid-side converter is oriented to provide smooth voltage waveform. During wind turbine operation the converter mitigates harmonic voltage distortions caused by the external network. Voltage distortions when the wind turbine is off are affected by the external network and can be seen at the grid-side converter AC terminals. During transition period of the wind turbine shutdown frequency components generated by the generator-side converter can be seen as well. It should be underlined that the applied time-frequency analysis can clearly show changes of the spectrum in time.

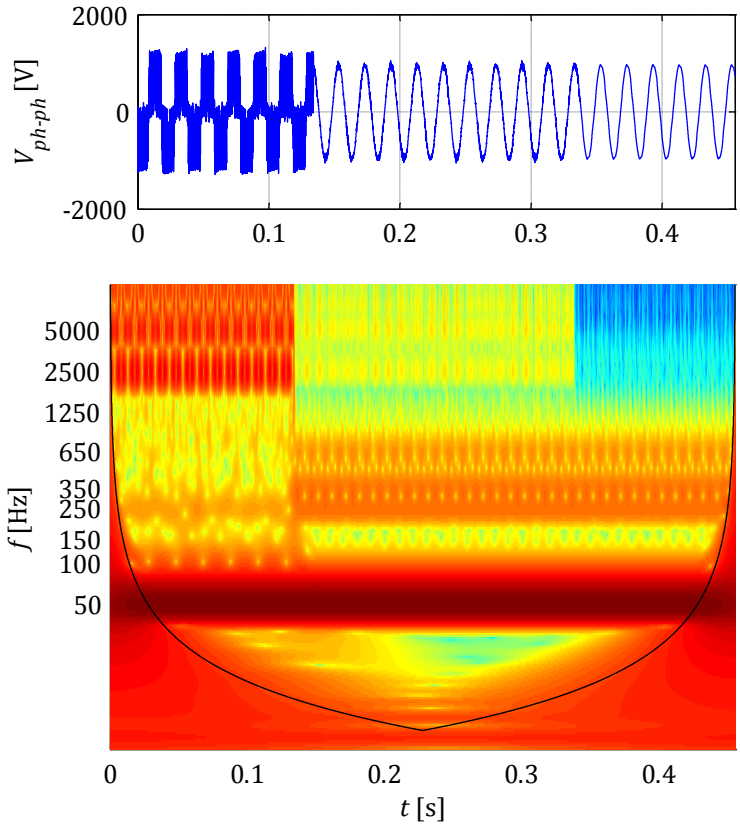

Figure 4.57 Time-frequency analysis of wind turbine shutdown obtained from measurements of the grid-side converter.

Time-frequency representation of measured continuous-time signals achieved using continuous wavelet transform with discrete coefficients is presented in Figure 4.57. In order to analyse measured signal which statistics vary in time and exhibits some oscillations non-orthogonal complex Morlet mother wavelet basis [4.30] was used. It can be seen that within the first period (0-0.14 s) the wind turbine is producing and frequency components around 2.5 and 5 kH generated by the modulator of the grid-side converter can be easily observed. Later the wind turbine is stopped and only harmonics caused by the external network can be measured.

The channel was measured by SI-9001 voltage differential probe which full scale range is ± 7 V and input voltage differential range is ± 700 V. The measured noise is less than 1 % of the sensor full scale range and does not affect measurements significantly. Still it has to be emphasized that the observed interference was much higher when the power electronic equipment of the main power circuit in the wind turbine was in operation. Normally open circuit measurements performed in laboratory conditions were very close to Gaussian distribution. Additionally it has to be emphasized that the crosstalk for adjacent channels is lower than -80 dB and the idle channel noise for applied sample rate (44.1 kS/s) is -94 dBV_{max}.

Frequency components affected by the grid-side converter obscure generated by the generator-side converter components during normal operation. The transition period (i.e. between 0.14-0.34 s) exhibits to certain extent also the generator-side converter behaviour. The switching frequency of the generator side-converter is 1250 Hz which means that the frequency ratio $m_f = f_c/f_o$ is equal to 25. In case of generator-side converter as well as grid-side converter both frequency ratios are multiple integer values (i.e. fixed switching frequencies). In such case phenomena such as cross-modulation [4.12] and associated interharmonic generation should not be an issue.

The width of a wavelet function is defined here as the e-folding time of the wavelet amplitude and for the Morlet wavelet basis function is equal to $\sqrt{2}s$, where s is a wavelet scale. The black line in Figure 4.57 indicates a cone of influence, region of the wavelet spectrum in which edge effects became important as the e-folding time for each at each scale [4.28].

Based on time-frequency analysis of the wind turbine shutdown operation one can see that the wind turbine actually operates independently of background distortion. This feature is characteristic for the newest technologies and trends in wind turbine development process. One can say that the wind turbine is transparent to harmonics introduced by the network which is reflected in additional control improvements in the fast current control loop of the grid-side converter. Independently on wind turbine location the voltage output is unchanged with high quality within the baseband range of harmonic components.

4.1.3 SUMMARY OF SPECTRAL ANALYSIS

An analysis of detailed measurement data processing focused on harmonic analysis was presented. Different harmonic calculation methods were analysed and compared. It was shown that the resampling of voltage and current waveforms and application of stated in IEC standards harmonic calculation guides can significantly improve data series processing precision and accuracy.

It was observed that the different origin and nature of the frequency components in a wind turbine measurements output spectrum can affect appropriate harmonic

calculation method choice. A quantitative analysis was carried out in order to distinguish between frequency components synchronized with the power system frequency and dependent also on carrier signal fundamental frequency.

Different data processing techniques were presented and applied depending on signal (i.e. stationary or non-stationary) or harmonic nature (i.e. spline resampling or direct spectrum estimation). It was observed that certain harmonic components generated by the grid-side converter in the wind turbine are not only linked with the power system fundamental frequency but also with the carrier signal fundamental frequency. Therefore, harmonic assessment by major part of commercial power quality meters is inappropriate and affects misleading measurement interpretation.

4.2 STATISTICAL ANALYSIS

4.2.1 INTRODUCTION

As it was described earlier in harmonic analysis, measurements play a crucial role. It is of course important to define appropriate measurement setup which can provide trustful measurements. But another equally important aspect is related to the duration of measurements. In order to observe all possible harmonic levels in the measured system long-term measurements are needed. Right now the question is, how long it should be, when one can be sure that the measurements can represent the overall system behaviour from harmonic perspective. In case of wind turbines the answer seems to be quite obvious.

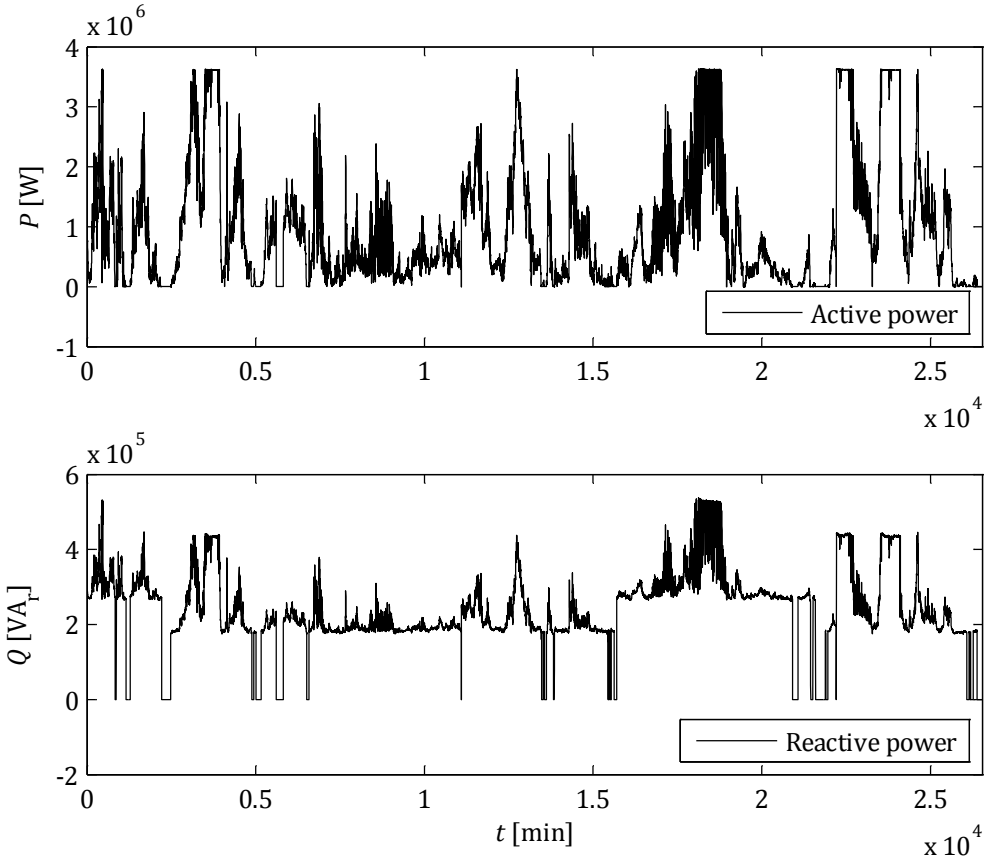

Figure 4.58 Active and reactive power of the wind turbine during one month of measurements measured at the LV side of the wind turbine transformer.

It is important to measure all possible wind turbine operating stages. If measurements can cover all possible power production levels (see Figure 4.58), all possible harmonic phenomena should be covered. In practice one month of measurements is enough to record all possible production levels. Typical wind turbine power curve from measurements is shown in Figure 4.59.

Intuitive is the statement that it is much easier to track characteristic harmonics caused by the converter structure (i.e. modulator and network bridge) instead of non-characteristic harmonics which are dependent on wind turbine operation including interaction with the external network (i.e. plant changes and background distortions).

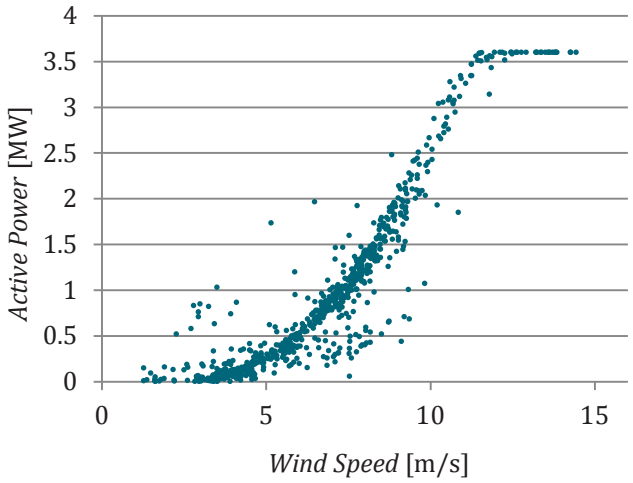

Figure 4.59 Wind turbine power curve obtained from measurements.

It is important to emphasize that logging all possible levels of harmonic components affected by background distortions is difficult due to the complexity of the external network. That is why it is crucial to distinguish during harmonic assessment between harmonic components generated by the wind turbine and caused by the grid. This can be done using sophisticated data processing and data analysis techniques which can reveal the true behaviour of analysed wind turbines.

4.2.2 CENTRAL LIMIT THEOREM

In general, the central limit theorem in probability theory states conditions under which the mean of a sufficiently large number of independent random variables are approximately normally distributed. It must be emphasized that considered random variables should be with finite mean and variance [4.31].

Let random sample (e.g. harmonic components) $\{X_1, X_2, \dots, X_n\}$ of size n is a sequence of independent and identically distributed random variables with expected value $\mathrm{E}[X_i] = \mu$ and variance $\mathrm{Var}[X_i] = \sigma^2$. Now let average sample of these random variables is

$$S_n = \frac{1}{n}(X_1 + X_2 + \cdots + X_n) = \frac{1}{n}\sum_{i=1}^{n} X_i \qquad 4.13$$

Then according to the Lindeberg-Lévy central limit theorem as n approaches infinity the asymptotic distribution of S_n is normal with mean μ and variance $1/n\,\sigma^2$ [4.32]. Formal formula is the following ($\xrightarrow{D}$ donates convergence in distribution)

$$\sqrt{n}(S_n - \mu) = \sqrt{n}\left(\frac{1}{n}\sum_{i=1}^{n} X_i - \mu\right) \xrightarrow{D} \mathcal{N}(0, \sigma^2) \qquad 4.14$$

It is worth emphasizing that the true strength of the theorem is that S_n approaches normality regardless of the shapes of the distributions of individual X_i's. That is also why it is expected to observe normally distributed harmonic components from measurements due to the fact that the estimated harmonic components based on measurements and data processing are an average value within the analysed window.

Normally averaging is affected by an application of Fourier transform on time-varying harmonic components and later averaging within certain period which is necessary in long-term harmonic measurements. In IEC 61000-4-7 and IEC 61000-4-30 standards about harmonics measurements and power quality measurements respectively [4.23], [4.6] it is recommended to apply Fourier transform on 10-cycle rectangular window. High frequency components can change significantly their magnitude within this period and averaging is unavoidable and at first glance can provide misleading estimation. Therefore it is quite natural that high-order harmonics (e.g. sideband harmonics) will tend to be more normally distributed than low-order harmonics.

On the other hand if one considers sufficiently large number of samples (and their sample averages) the asymptotic distribution is expected to be the same normal distribution if averaged random variables are independent and identically distributed. One can note that as long as signal stationarity is assumed in analysis the asymptotic distribution should be the same for all observations. General definition of a stochastic process stationarity is that its joint probability distribution does not change when shifted in time or space. Consequently this means that parameters such as the mean and variance, if they exist, also do not change over time or position [4.33].

4.2.3 STATIONARITY TEST

Stochastic process is considered as stationarity if its joint probability distribution does not change when shifted in time or space. Consequently this means that parameters such as the mean and variance, if they exist, also do not change over time or position.

If $\{X_t\}$ is a weakly stationary time series, than the vector of random variables $(x_1, \dots, x_n)$ and time shifted vector $(x_{1+\tau}, \dots, x_{n+\tau})$ have the same mean vectors and covariance matrices for every integer τ and positive integer n. A strictly stationary sequence one in which the joint distributions of these two vectors (and not just the means and covariances) are the same. A weaker form of stationarity, which is mentioned above, is commonly employed in data processing and is known as wide-sense stationarity. Wide-sense stationarity random processes only require that 1st $\mathrm{E}[(X_t - \mathrm{E}[X_t])^1] = \mathrm{E}[(X_t - \mu)^1] = \mu_1 = 0$ and 2nd $\mathrm{E}[(X_t - \mu)^2] = \mu_2 = \sigma^2$ moments do not vary with respect to time. Please note that any strictly stationary process which has a mean and a covariance is also a wide-sense stationary process [4.34]. One of method of checking if analysed time series is a wide-sense stationary stochastic

process is by application of reverse arrangement test [4.35]. Such procedure is easy to implement and useful for detecting underlying trend in random data records.

The sample mean and unbiased estimator of the variance of a population from a sample can be calculated in the following way

$$m = \bar{x} = \hat{\mu} = \frac{1}{n}\sum_{i=1}^{n} x_i \tag{4.15}$$

$$s^2 = \hat{\sigma}^2 = \frac{1}{n-1}\sum_{i=1}^{n} (x_i - \bar{x})^2 \tag{4.16}$$

Consider a sequence of n observations of a random variable X, where observations are denoted by $x_i, i = 1, \dots, n$. And now, count number of times that $x_i > x_j$ for $i < j$. Each such inequality is called reverse arrangement. The total number of reverse arrangements is denoted by S.

$$S = \sum_{i=1}^{n-1} S_i \tag{4.17}$$

$$S_i = \sum_{j=i+1}^{n} h_{ij} \tag{4.18}$$

where

$$h_{ij} = \begin{cases} 1 & \text{if} \quad x_i > x_j \\ 0 & \text{if} \quad x_i \leq x_j \end{cases} \tag{4.19}$$

What is important in this particular application, if a sequence of n observations is independent observations of the same random variable X, then the number of reserve arrangements is a random variable S, with a mean value μ and variance σ^2 expressed in the following way [4.36]

$$\mu_S = \frac{n(n-1)}{4} \tag{4.20}$$

$$\sigma_S^2 = \frac{2n^3 + 3n^2 - 5n}{72} = \frac{n(2n+5)(n-1)}{72} \tag{4.21}$$

Now let it be hypothesized that the observations are independent observations of a random variable X, where there is no trend. The acceptance region for this hypothesis within $\alpha = 0.05$ level of significance is

$$\left[S_{n,1-\alpha/2} < S \leq S_{n,\alpha/2}\right] \tag{4.22}$$

The stationarity test is performed on a univariate time series by testing the inversion number. The time series X_t is divided into n nonoverlapping subsequences, where data of each subsequence can be considered as independent. The mean value of each subsequence forms a time series $\mu_1,\ \mu_2, \dots, \mu_n$ and the standard deviation value of each subsequence forms a time series $\sigma_1,\ \sigma_2, \dots, \sigma_n$. The sum S_μ and S_σ of inversion number is computed for the time series $\mu_1,\ \mu_2, \dots, \mu_n$ and $\sigma_1,\ \sigma_2, \dots, \sigma_n$ respectively. If X_t is stationary, the statistical values ε_μ and ε_σ satisfy the normal distribution with a mean value of 0 and a standard deviation value of 1.

$$\varepsilon_\mu = \frac{S_\mu + 0.5 - \mu_S}{\sigma_S} \tag{4.23}$$

$$\varepsilon_\sigma = \frac{S_\sigma + 0.5 - \mu_S}{\sigma_S} \tag{4.24}$$

If $\varepsilon_\mu < \mathcal{N}_{\alpha/2}(0,1)$ and $\varepsilon_\sigma < \mathcal{N}_{\alpha/2}(0,1)$ the time series is wide-sense stationary within α level of significance.

By removing any trend or slow variation from the time series using resampling, non-stationary data blocks can be transformed to stationary. Sometimes even if resampling is applied the stationarity test may not be passed. This is due to fact that there are also frequency components not synchronized with the grid frequency which show higher variation after resampling. Normally in voltage and current waveforms comprise more integer multiple frequencies of the nominal one and resampling should improve the analysed data series. Also if one is aware which frequency components in analysed data series are directly linked with the main tone (e.g. power system fundamental frequency) appropriate filtering can be applied and stationarity test only performed on filtered and improved by resampling data series. Stationarity test results are compared in Table 4.5. It can be seen that frequency variation after resampling exists only for sideband frequencies of the carrier signal and is smaller but on a certain level. Therefore the number of passed test is smaller for resampled data series within 99% confidence interval. This would require separating baseband harmonic, since they are associated with the power system fundamental component, and sideband harmonics, since they are mainly affected by the carried signal fundamental frequency. Later in this report it will be shown how zero-phase infinite impulse response filters can be used for such analysis. Applying non-casual [4.37] filters such as the zero-phase digital filter can improve stationarity test for resampled (baseband harmonic analysis) and not-resampled (sideband harmonic analysis) time series. Unfortunately such approach is time consuming because the filter should be tuned depending on the converter switching frequency therefore can be beneficial for pure academic research but not necessarily in practical applications.

Table 4.5 Stationarity test results for different confidence intervals.

	Number of tests	Passed	Failed	Confidence interval
Resampled data	299	251	48	95 %
	299	286	13	99 %
Measured data	299	173	126	95 %
	299	299	0	99 %

4.2.4 SIDEBAND HARMONIC COMPONENTS

Sideband harmonics generated by the wind turbine grid-side converter are affected by the modulation. The frequency of sideband harmonic components is above the converter control bandwidth. Therefore sideband harmonic components are considered to be characteristic harmonics from power electronics perspective. Please note that the frequency of carrier group harmonic components is dependent on two variables: power system fundamental frequency and carrier signal fundamental frequency. If the modulation ratio $m_f = f_c/f_o$, where f_o is the power system fundamental frequency and f_c is the carrier signal fundamental frequency, is not an integer number sideband harmonic components frequency is not an integer multiple of the power system frequency [4.21]. Thus such harmonic component cannot be considered as harmonics from power system studies point of view. Please note that they are still harmonic components from harmonic analysis perspective because they can be theoretically explained by application of Fourier series which will be shown later.

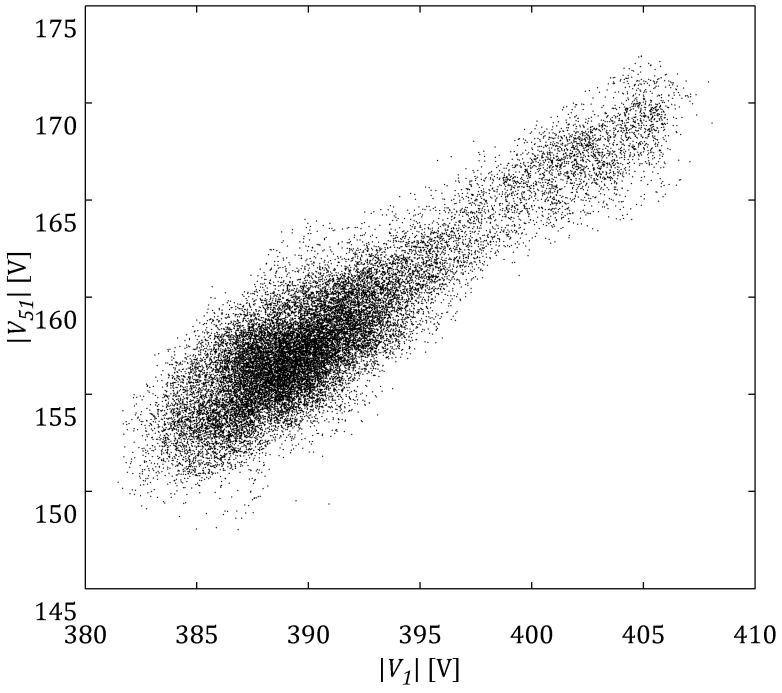

Figure 4.60 Dependency between fundamental harmonic and sideband harmonic component.

It is important to mention that sideband harmonic components are dependent on the modulation index M of the fundamental component in the command signal (see Figure 4.60) as well as amplitude M_h of injected harmonic components into the command signal. Both relationships are nonlinear and are strongly dependent on nonlinear nature of Bessel functions of the first kind. In Figure 4.60 it is difficult to observe this nonlinear relationship because the modulation index M is varying only within a small range. Of course the magnitude of sideband harmonic components is proportional to the DC-link voltage. Besides the factors mentioned above sideband harmonic component can be affected by the modulation ratio m_f. This is only observable in case of regularly sampled pulse-width modulation which is actually observed in measurements. Asymmetrically regular sampled pulse-width modulation is exhibited by skewed (asymmetrical) pairs of sideband harmonic components around carrier fundamental frequency and its integer multiples [4.38].

Assuming a harmonic component is dependent on voltage fundamental harmonic, it is not surprising that the harmonic component is only a little dependent on power production. In grid-connected wind turbines not only the fundamental voltage amplitude affects the active power level but also the angle and the grid voltage level as it was presented previously. Of course it is not possible to provide active power control only by changing the angle. Therefore grid-side converter voltage has to be increased if more active power is expected to be pushed to the grid.

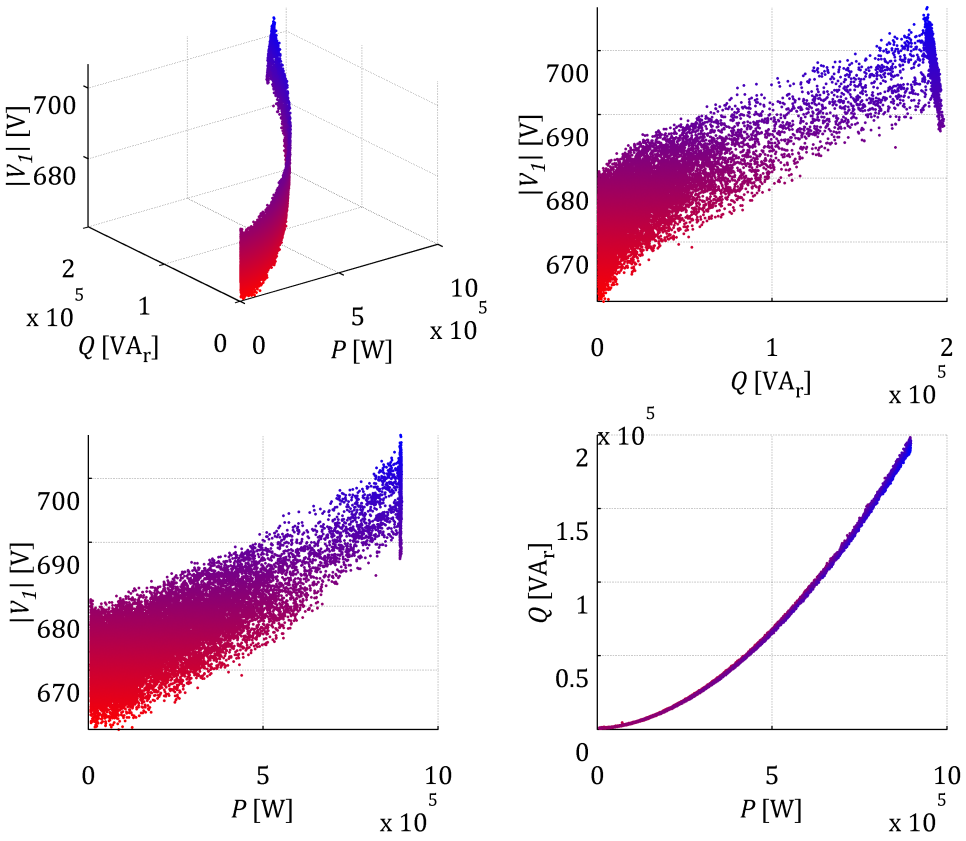

Figure 4.61 Voltage fundamental component variation depending on active and reactive power production measured at the converter AC terminals.

Based on Figure 4.61 one can see that there is quite scattered linear relation between both active and reactive power and the voltage fundamental component. This also explains why sideband harmonic components are also dependent on active and reactive power, and not only on the output voltage. It is worth mentioning that for this particular wind turbine the reactive power control was set to keep constant power factor at the wind turbine transformer HV side. That is why there is an obvious dependency between active and reactive power associated with increment of reactive power losses compensation with increasing active power production.

From Figure 4.61 it can be seen that different power production can be achieved for the same fundamental voltage magnitude. This is affected by possible grid-side converter voltage angle shift in relation to the grid voltage. That is also why scatter plots of both active and reactive power are significantly dispersed. It allows thinking about random harmonic generation for different power production levels.

On the other hand it is worth (even if presented in Figure 4.60 dependency is more obvious for the converter voltage) to deal with active power in harmonic analysis because this is commonly taken approach in standards and power system studies. In standards regarding measurements and assessment of power quality in grid-connected wind turbines [4.24] it is recommended to specify harmonic current levels for specific power production levels. The harmonic current is provided as an average value. This approach excludes information about the worst case scenario and probability of observations. Therefore statistical methods can be helpful to provide better description and understanding of harmonic phenomena in measured wind turbine.

Knowing that the measured dataset contains representative data (i.e. contains all possible power levels) one can investigate dependence of harmonic component on wind turbine output power. A scatter plot can suggest various kinds of correlations between these two variables. It can be seen that harmonic component in Figure 4.62 is systematically incremented and decremented depending on active power production, let us call it an independent variable and is plotted along the horizontal axis. The sideband harmonic component is a dependent variable and is plotted along the vertical axis. For small active power brackets there is no clear dependency between the harmonic and active power and therefore stochastic modelling is reasonable.

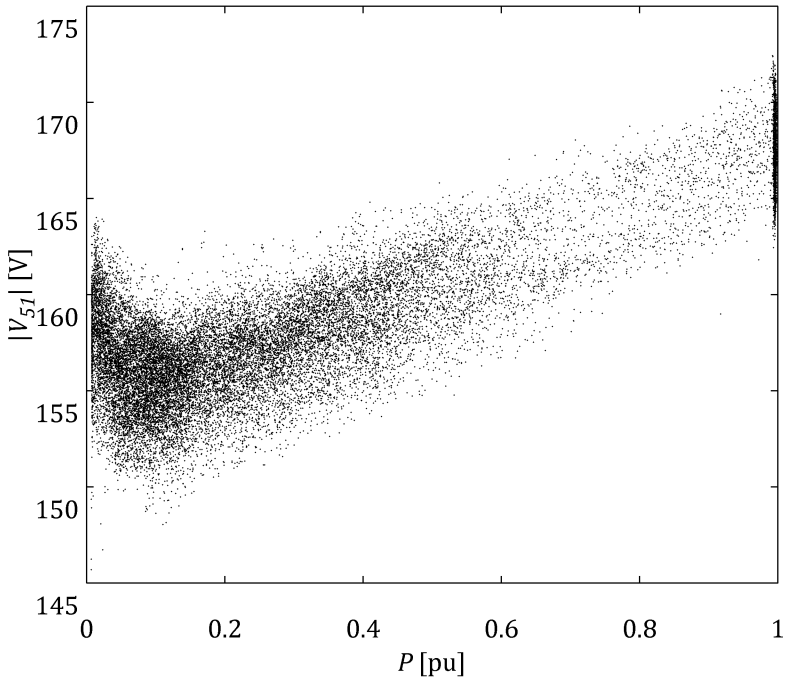

Figure 4.62 Sideband harmonic component dependency on wind turbine power production.

From Figure 4.62 it can be seen that within different output power levels the dependent variable behaves differently. One can specify three separated datasets of the sideband harmonic components assigned to different power range. This constitutes a premise that measured harmonic components, which can be considered as an independent random variable, can be random samples from different probability distributions.

Based on the presented above results it can be concluded that sideband harmonic components are only slightly dependent on power production and within limited active power ranges are independent random variables from different probability spaces.

4.2.4.1 HISTOGRAM ANALYSIS

Histogram analysis is one of the first steps in quantitative statistical analysis of harmonic components. It is used to roughly assess the probability density function of a given dataset by depicting the frequencies of observations occurring in certain ranges of values. In practice histogram is nothing else than graphical representation of analysed data showing visual impression of its distribution.

According to central limit theorem the mean of sufficiently large number of identically distributed independent random variables, each with finite mean and variance, will be approximately normally distributed (i.e. there is a normal asymptotic distribution). A consequence of central limit theorem is that if measurements averaged for a particular quantity, the distribution of obtained average values tends to be normal. Furthermore, if a measured and processed variable is actually a combination of several uncorrelated variables with random error of any distribution, the measurements

introduce a random error that also tend to be normally distributed as the number of these variables increases.

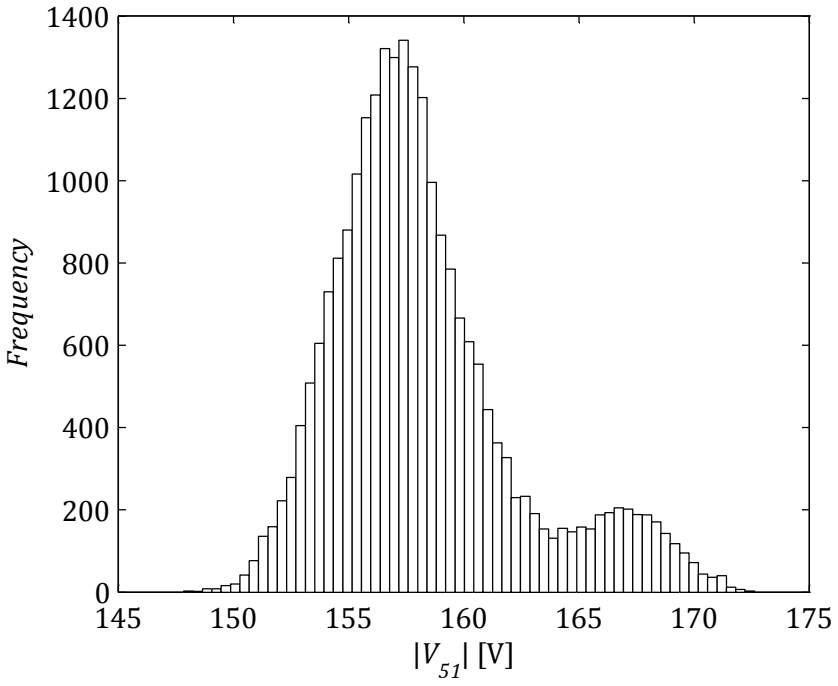

Figure 4.63 Distribution of sideband harmonic components generated by the grid-side converter.

In Figure 4.63 shows that the sideband harmonics generated by the grid-side converter modulator are multimodal data sets (i.e. statistical distribution is with multiple peaks). It can be seen that distributions are a mixture of at least two different unimodal normal distributions. The harmonics are distributed within relatively small range (i.e. small standard deviation) which can be due to uncertainties affected by measurement system and calculation method precision as well random nature of harmonic generation by the grid-side converter. As it was shown earlier the harmonic magnitude is correlated with active power production of the wind turbine. Therefore one can say that different distributions are due to changes in the modulation index.

A distribution with many modes indicates a mixture distribution [4.39], i.e. considered population contains a set of subpopulations. Mixture densities can be used to model a statistical population (e.g. harmonic magnitudes) with subpopulations (e.g. harmonic magnitudes dependent on power production). Mixture distributions can be described by weighted set of probability density functions. Consider a finite set of probability density functions $p_1, \dots, p_n$ and weights $w_1, \dots, w_n$ and the mixture distribution can be represented

$$f(x) = \sum_{i=1}^{n} w_i p_i(x) \qquad 4.25$$

and for Gaussian parametric families $p_i \sim \mathcal{N}(\mu_i, \sigma_i)$

$$f(x|\mu_1, \ldots, \mu_n, \sigma_1, \ldots, \sigma_n) = \sum_{i=1}^{n} w_i p_i(x|\mu_i, \sigma_i) \tag{4.26}$$

Since f is a density function, it must be nonnegative and integrate to one as well. Thus

$$\begin{aligned} 1 &= \int_{-\infty}^{\infty} f(x|\mu_1, \ldots, \mu_n, \sigma_1, \ldots, \sigma_n)\, dx \\ &= \int_{-\infty}^{\infty} \sum_{i=1}^{n} w_i p_i(x|\mu_i, \sigma_i)\, dx \\ &= \sum_{i=1}^{n} w_i \int_{-\infty}^{\infty} \sum_{i=1}^{n} w_i p_i(x|\mu_i, \sigma_i)\, dx = \sum_{i=1}^{n} w_i \end{aligned} \tag{4.27}$$

so that $w_i \geq 0$ and $\sum w_i = 1$ [4.40]. This can be extended from univariate to any dimensional multivariate distributions.

Gaussian mixture models are formed by combining multivariate normal density components. Each cluster corresponds to one of the bivariate (in this case fundamental voltage magnitude and sideband voltage magnitude) normal components in the mixture distribution. Gaussian mixture models are often used for data clustering that allows separating harmonic components depending on a particular parameter. Such separation (clustering) can be done by application of expectation maximization algorithm [4.40]. Gaussian mixture modelling based on expectation maximization uses an iterative algorithm that converges to a local optimum.

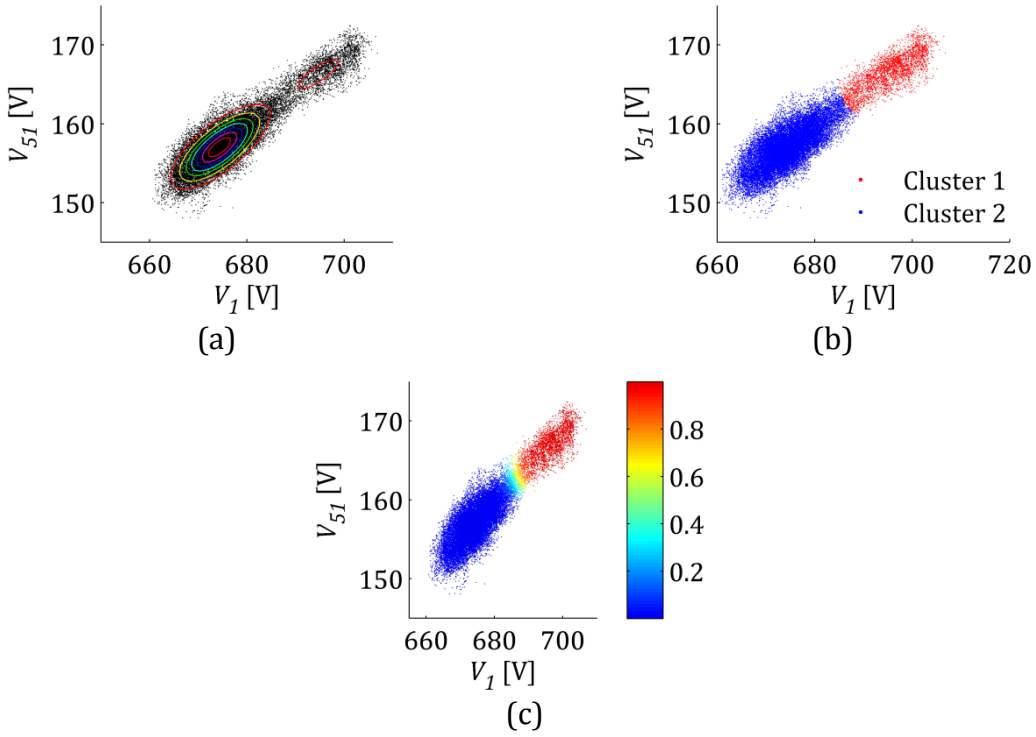

Figure 4.64 Gaussian mixture model of a sideband harmonic components (a) estimated probability density contours for the two-component mixture distribution (b) partition the data into clusters (c) points assigned to clusters based on the estimated posterior probability.

From Figure 4.60 and Figure 4.63 it can be seen that there at least two sub-populations in the analysed dataset. One of possible methods of sub-populations separation from entire population is a mixture model approach. Figure 4.64 presents nicely how two clusters of sideband harmonics are dependent on fundamental voltage.

4.2.4.2 KERNEL SMOOTHING

Kernel density estimation is a nonparametric technique for probability density function estimation. Knowledge about probability distribution of analysed harmonics can be extensively used in comparison of the same frequency components from different data sets (e.g. different wind turbines, measurement points in a wind farm) as well as can be applied in modelling of harmonic sources. Additionally description of harmonics from its probability distribution perspective provides better overview about harmonic phenomena and power quality.

A good example where probability distribution estimation can be beneficial is harmonic emission assessment of a wind turbine. It is described in IEC 61400-21 standard [4.24] concerning measurements and power quality assessment in wind turbines. The standard predicts measurements of 10-minute harmonic current generated by a wind turbine for frequencies up to 50 times the fundamental frequency of the grid [4.41], [4.42]. It has to be emphasized that the most popular standard concerning measurements and power quality assessment of grid-connected wind turbines refers only to current harmonic components.

Furthermore harmonic components description by means of probability distribution gives a better overview about power quality. It is quite natural to say that one (e.g. average magnitude) value cannot provide satisfactory description about overall behaviour of a certain harmonic component. The values of the individual current harmonic components and the total harmonic current distortion are specified in tables in percentage of the fundamental component and for operation of the wind turbine within different active power levels (i.e. 0, 10, 20, …, 100 % of Pn). Specified active power levels are the midpoints of bins in measurements. According to the standard it is also recommended that the wind turbine during measurements should operate with reactive power as close as possible to zero.

Nonparametric probability density function estimation by kernel smoothing can be viewed as a generalization of histogram density estimation with improved statistical properties. It is very useful when one has to deal with limited number of observation. In general the goal of density estimation is to take a finite sample of data and to make inferences about the underlying probability density function everywhere, including where no data are observed. This approach allows predicting possible harmonic component occurrence in analysed system. In kernel density estimation, the contribution of each data point is smoothed out from a single point into a region of space surrounding it. Aggregating the individually smoothed contributions gives an overall picture of the structure of the data and its density function. Based

on the following example it is shown that this approach leads to a reasonable estimate of the underlying density function.

Let $(x_1, x_2, \ldots, x_n)$ be samples drawn from some distribution with an unknown probability density function f. There is possibility to estimate the shape of the probability density function by application of kernel smoothing. Kernel density estimator of f is [4.43]

$$\hat{f} = \frac{1}{n}\sum_{i=1}^{n} K_h(x - x_i) = \frac{1}{nh}\sum_{i=1}^{n} K\left(\frac{x - x_i}{h}\right) \qquad 4.28$$

where $K(\cdot)$ is the kernel, weighting function used in non-parametric estimation, $h > 0$ is the smoothing parameter. Normally for non-parametric estimation of probability density function of harmonic components a normal (Gaussian) kernel function is used. This is affected by normally distributed asymptotic distribution according the central limit theorem.

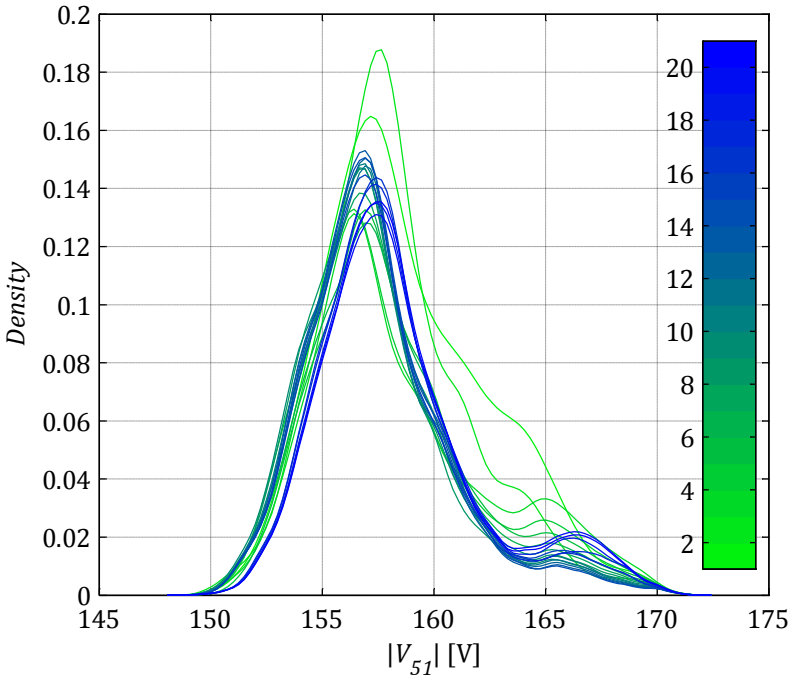

Figure 4.65 Non-parametric estimation of probability density function using kernel smoothing.

In Figure 4.65 it is possible to observe how non-parametric estimation of probability density function is dependent on number of observations. Another aspect of estimation is associated with a problem if actually measured observations of harmonic components are representative dataset. In the figure one can see that the estimation does not change significantly the probability density function. In this particular case the initial dataset size of the 51st sideband harmonic components is equal to 1190 observations. The initial dataset does not contain representative data to estimate the probability distribution,

but if the length of analysed harmonic series is more than 10 times bigger (i.e. 11900 observations and more), the estimation gives comparable results.

This practical approach can be used to observe if analysed dataset actually contains representative data for statistical analysis purposes. If the estimation of probability density function does not change significantly, one can assume that the dataset is appropriate for further statistical analysis.

4.2.4.3 PARAMETRIC ESTIMATION

Based on scatter plot from Figure 4.62 some dependency of estimated sideband harmonic component magnitude can be seen. It also can be observed that depending on wind turbine production levels the harmonic component dataset can be roughly divided into three subsets. This allows specifying separated unimodal distributions from multimodal distribution presented in Figure 4.63. Such separation allows estimating different probability distributions from which observations are taken. Please note that according to the central limit theorem one expects to observe different (i.e. by means of mean and variance) normally distributed random variables.

In order to specify appropriate active power ranges a series of goodness-of-fit hypothesis tests are performed. This allows, by means of sophisticated statistical methods, verifying conclusions derived from the first glance of Figure 4.62. It is expected to estimate normal distributions and therefore both two-sample as well as single sample goodness-of-fit hypothesis test can be carried out.

In case of two-sample goodness-of-fit tests (e.g. Kolmogorov-Smirnov, Ansari-Bradley) the null hypothesis H_0 states that two independent random samples, X_1 and X_2, are drawn from the same underlying continuous population. Taking into consideration single sample goodness-of-fit hypothesis test (e.g. Lilliefors', Chi-square, Jarque-Bera) the null hypothesis considers normal distributed population and states that a random variable X is normally distributed with unspecified mean and standard deviation. In some cases (e.g. single sample Kolmogorov-Smirnov goodness-of-fit hypothesis test) it is possible to test null hypothesis if a random variable X is distributed according to a standard normal distribution $X \sim \mathcal{N}(0,1)$.

Each of the tests has its own advantages and disadvantages depending on application. Based on nonparametric (i.e. distribution free) Kolmogorov–Smirnov test a statistic is calculated which quantifies a distance between the empirical distribution function of the sample and the cumulative distribution function of the reference distribution, or between the empirical distribution functions in case of two-sample test. The empirical distribution function F_n for n independent and identically distributed observations X_i can be defined in the following way [4.44]

$$F_n(x) = \frac{1}{n}\sum_{i=1}^{n} I_{X_i \leq x} \qquad 4.29$$

where $I_{X_i \leq x}$ is the indicator function

$$I_{X_i \leq x} = \begin{cases} 1 & \text{if} \quad X_i \leq x \\ 0 & \text{if} \quad X_i > x \end{cases} \tag{4.30}$$

Two-sample Kolmogorov–Smirnov statistic is calculated as follows

$$D_{n,n'} = \sup_x \left| F_{1,n}(x) - F_{2,n'}(x) \right| \tag{4.31}$$

where $F_{1,n}$ and $F_{2,n'}$ are empirical distribution functions of the first and the second sample respectively. If K_α is the Kolmogorov distribution the null hypothesis H_0 is rejected at specified significance level α if

$$\sqrt{\frac{nn'}{n+n'}} D_{n,n'} > K_\alpha \tag{4.32}$$

In practice, the statistic requires relatively large number of data to properly reject the null hypothesis. Please note that the two-sample test checks whether the two data samples come from the same distribution. It does not need to be normal distribution. The Kolmogorov–Smirnov test tends to be more sensitive near the centre of the distribution than at the tails.

An interesting alternative to the Kolmogorov–Smirnov test is the chi-square χ^2 test. The test is performed by grouping the data into k bins (classes), calculating the observed and expected counts for those bins, and computing the chi-square test statistic for each i-th bin.

$$X^2 = \sum_{i=1}^{k} \frac{(O_i - E_i)^2}{E_i} \tag{4.33}$$

where O_i is the observed counts (frequency) and E_i is the expected counts (frequency) for bin i. X^2 statistic asymptotically approaches χ^2 distribution. The statistic is therefore a measure of the deviation of a sample from expectation. The expected frequency is calculated by

$$E_i = N\big(F(x_u) - F(x_l)\big) \tag{4.34}$$

where F is the cumulative distribution function for the tested distribution (in this particular case normal distribution is considered), x_u is the upper limit for class i (i.e. limits for bin i), $x_l$is the lower limit for class i, and N is the sample size.

The chi-square goodness-of-fit test is applied to binned data. However, the value of the chi-square test statistic is dependent on how the data is binned. Another disadvantage of the chi-square test is that the statistic has an approximate chi-square distribution when the counts are sufficiently large. This surely justifies a need of long-

term harmonic measurements. Due to harmonics nature and its tendencies to vary in time it is of great importance to provide representative set of observations.

Another approach is presented in Jarque–Bera goodness-of-fit test [4.45] which checks whether sample data have the skewness and kurtosis matching a normal distribution. The Jarque-Bera statistic is calculated in the following way

$$JB = \frac{n}{6}\left(g_1^2 + \frac{(b_2 - 3)^2}{4}\right) \tag{4.35}$$

where n is the sample size, g_1 is the sample skewness, and b_2 is the sample kurtosis. This test allows examining two samples from its asymmetry and peakedness of the probability distribution [4.46]. For large size n of the sample if data come from normal distribution, the test statistic has an asymptotic chi-square distribution with two degrees of freedom. Therefore the tests often use the chi-square distribution to estimate critical values for large samples.

The skewness γ_1 (third central moment divided by the cube of its standard deviation) and Pearson's kurtosis β_2 (the fourth central moment divided by fourth power of its standard deviation) are defined in the following way

$$\gamma_1 = \mathrm{E}\left[\left(\frac{X - \mu}{\sigma}\right)^3\right] = \frac{\mu_3}{\sigma^3} \tag{4.36}$$

$$\gamma_2 = \mathrm{E}\left[\left(\frac{X - \mu}{\sigma}\right)^4\right] - 3 = \frac{\mu_4}{\sigma^4} - 3 \tag{4.37}$$

and its estimation (statistics) used in the Jarque–Bera goodness-of-fit test are calculated as follows

$$g_1 = \hat{\gamma}_1 = \frac{m_3}{m_2^{3/2}} = \frac{\frac{1}{n}\sum_{i=1}^{n}(x_i - \bar{x})^3}{\left(\frac{1}{n}\sum_{i=1}^{n}(x_i - \bar{x})^2\right)^{3/2}} \tag{4.38}$$

$$g_2 = \hat{\gamma}_2 = \frac{m_4}{m_2^2} - 3 = \frac{\frac{1}{n}\sum_{i=1}^{n}(x_i - \bar{x})^4}{\left(\frac{1}{n}\sum_{i=1}^{n}(x_i - \bar{x})^2\right)^2} - 3 \tag{4.39}$$

where m_2, m_3 and m_4 are the second (i.e. the sample variance), third and the fourth sample moments about the mean (central moments), x_i is the i-th value, and $\bar{x}$ is the sample mean. The kurtosis is also known as excess kurtosis.

Despite the Jarque-Bera test the Lilliefors test is for small samples [4.47]. It uses a table of critical values computed using Monte-Carlo simulation for small sample sizes. Lilliefors test performs of the default null hypothesis that the measured sample comes from a distribution in the normal family (i.e. any mean value and any finite variance).

In contrast to the one-sample Kolmogorov-Smirnov test the Lilliefors test is a two-sided (two-tailed) goodness-of-fit test suitable when a fully-specified null distribution is unknown and its parameters must be estimated. The Lilliefors test statistic is the same as for the single sample Kolmogorov-Smirnov test.

$$D_n = \sup_x |F_n(x) - F(x)| \tag{4.40}$$

where sup{·} is the supremum (maximum) of the set of distances, $F_n(x)$ is the empirical cumulative distribution function estimated from the sample and $F(x)$ is the normal cumulative distribution function with mean and standard deviation equal to the mean and standard deviation of the sample.

Ansari-Bradley test is an alternative test to Kolmogorov-Smirnov test of the hypothesis that two independent samples come from the same distribution, against the alternative that they come from distributions that have the same median and shape but different dispersions (e.g. variances) [4.48]. It does not require the assumption that the two samples come from normal distributions. The theory behind the Ansari-Bradley test requires that the groups have equal medians. If the assumption is not satisfied the test results can be misleading. The test checks if distributions in each group are continuous and identical, the test does not depend on the distributions in each group.

Statistical tests based on specific distributional assumptions are in general more powerful than these non-parametric (i.e. not based on a specific distributional assumption) and robust (i.e. performs well under a wide range of distributional assumptions) techniques. By power, one means the ability to detect a difference when that difference actually exists. Therefore, if the distributional assumptions can be confirmed, the parametric techniques are generally preferred.

Different single sample and two-sample goodness-of-fit tests with H_0 hypothesis that either both datasets are from the same distribution or with H_0 that sideband harmonic components come from distribution in the normal family are carried out for different datasets to specify number of unimodal distributions. The two-sample Kolmogorov-Smirnov test is one of the most useful and general nonparametric methods for comparing two samples, as it is sensitive to differences in both location and shape of the empirical cumulative distribution functions of the two samples.

Different tests were performed in order to define output power levels and separate unimodal distribution from the multimodal distribution shown in Figure 4.63. The tests are briefly described above and various differences indicated. Each of the tests is focused on different features of probability distribution (e.g. average, deviation, asymmetry, peakedness) which can provide better overview of fit. The tests return the logical value 1 if they reject the null hypothesis at the 5% significance level, and 0 if they cannot reject the null hypothesis H_0.

Table 4.6 Results of different goodness-of-fit tests in case of sideband harmonics generated if the wind turbine has high output power.

Power Output *P*	**Goodness-of-fit test**				
	Two-sample Kolmogorov-Smirnov	Two-sample Ansari-Bradley	Chi-square	Lilliefors'	Jarque-Bera
$> 0.55P_n$	1	1	1	1	1
$> 0.75P_n$	0	0	1	1	1
$> 0.86P_n$	0	0	0	0	1
$> 0.87P_n$	0	0	0	0	0
$> 0.90P_n$	0	0	0	0	0
$> 0.92P_n$	0	0	0	0	0
$> 0.93P_n$	0	0	1	0	1
$> 0.95P_n$	0	1	1	1	1

Table 4.6 presents test results for different output power levels. It can be seen that separated dataset fits normal distribution for active power level in range $P \in (0.87P_n, P_n)$. Based on … the sideband harmonic components are generated during approximately full power production. This means that the harmonic variation is affected by wind speed variation and associated with it pitching. Blade pitch refers to turning the angle of attack of the wind turbine blades. Standard modern turbines all pitch the blades in high winds which affects sideband harmonic components fluctuation.

Based on different goodness-of-fit tests described above a parametric estimation of probability distribution was done. Generally speaking parametric methods make more assumptions than non-parametric methods (e.g. kernel smoothing). If those extra assumptions are correct, parametric methods can produce more accurate and precise estimates and more suitable stochastic model (i.e. harmonics description). In this particular case this allows comparing different harmonics of the same waveform and, even more, different harmonic measurements from different locations and wind farms.

In Figure 4.66 one can see that it is possible to fit Gaussian curve to the sideband harmonic component distribution measured during high production ($P > 0.87P_n$). Also one can see that cumulative distribution functions are almost identical (i.e. it is assumed that the null hypothesis cannot be rejected within assumed confidence interval). Measured empirical cumulative distribution function is calculated based on Eq. 4.29 directly from estimated harmonic magnitude. However estimated empirical cumulative distribution function is calculated from generated random sample synthesized from Mersenne twister [4.49] which is a pseudorandom number generator. The random sample is normally distributed and normal distribution parameter describing the location of the peak (i.e. mean μ) and the measure of the width of the distribution (i.e. variance σ^2) are estimated. The mean value estimator is provided based

on maximum likelihood estimates as in Eq. 4.15 and the variance estimation is given by minimum variance unbiased estimator as in Eq. 4.16.

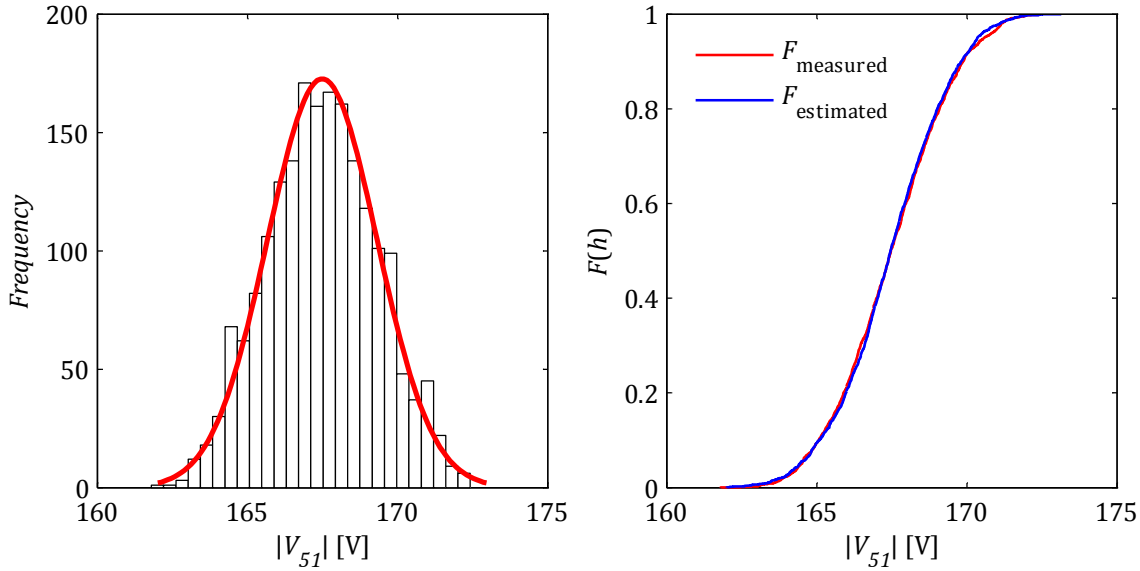

Figure 4.66 Gaussian curve fitting and empirical cumulative distribution function of sideband harmonic generated during high production.

The fitted curve in Figure 4.66 is bell-shaped Gaussian function which is a probability density function of the normal distribution

$$f(x|\mu,\sigma) = \frac{1}{\sigma\sqrt{2\pi}} e^{-\frac{(x-\mu)^2}{2\sigma^2}} \tag{4.41}$$

where parameter μ is the mean and σ^2 is the variance. Please note that he distribution with $\mu = 0$ and $\sigma^2 = 1$ is called the standard normal distribution. For this particular dataset sample mean $\bar{x}$ is equal to 167.3191, sample variance s^2 is equal to 3.6199, sample skewness g_1 is equal to -0.0791, and sample kurtosis g_2 is equal to -0.2005. In case of normal distribution skewness and kurtosis are equal to 0 and 0 respectively. Mean value is any real-valued number ($\mu \in \mathbb{R}$) and variance is any positive real-valued number ($\sigma^2 > 0$).

The next step would be to separate sideband harmonic components from the dataset and determine possible normal distributions. Based on Figure 4.62 for different active power levels during wind turbine production can be seen. The analysis based on different goodness-of-fit tests should point out a power range within sideband harmonic components are drawn from the same distribution and according to central limit theorem an asymptotic probability distribution of the sample average is normal distribution.

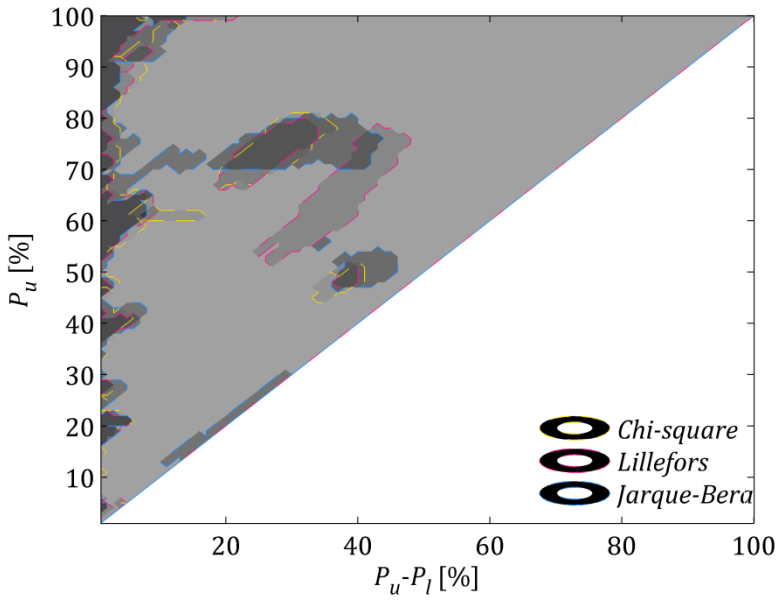

Figure 4.67 Different goodness-of-fit tests results depending on power production levels.

A series of goodness-of-fit test was carried out for different production levels. In Figure 4.67 one can see the results of the tests. Dark grey indicates where the tests were passed, i.e. the null hypothesis that the analysed sample is normally distributed cannot be rejected. Common areas indicate power production ranges (lower threshold P_l and upper threshold P_u). Based on the test results stochastic model of the sideband harmonic components can be built.

The ordinate (i.e. vertical axis) in Figure 4.67 indicates the upper power threshold P_u in percent of nominal power P_n while the abscissa (i.e. horizontal axis) indicates the range (i.e $P_u - P_l$), where P_l is the lower power treshold. For example, the parametric probability distribution estimation presented in Figure 4.66 was done for $P_u = 100\ \%$ of P_n and $P_u - P_l = 13\ \%$ of P_n presented in Figure 4.67. From the same figure it can be also seen that actually the estimation could be carried out successfully also for $P_l \in (0.87, 0.92)$ of P_n as also indicated in Table 4.6. It was decided to use $P_l = 0.87P_n$ (i.e. $P_u - P_l = 13\ \%$) because it provides the widest bracket and the sample kurtosis is the closest to 0 (i.e. theoretical kurtosis for normal distribution).

Only single-sample parametric tests (i.e. chi-square, Lillefors', and Jarque-Bera) are taken into consideration in Figure 4.67. It was observed that if the null hypothesis cannot be rejected by using parametric test, the non-parametric tests (i.e. Kolmogorov-Smirnov and Ansari-Bradley) will most probably give the same results. As it was mentioned earlier parametric methods make more assumptions than non-parametric methods that do not rely on data belonging to any particular distribution.

It can be concluded from Figure 4.67 that two additional datasets can be selected from measurements. Active power brackets and goodness-of-fit results are presented in Table 4.7. It can be seen that right now almost the whole range of possible active

power production is covered by models. Models can provide the mean value which can be considered as the most frequent sideband harmonic magnitude for particular production levels. Also variance provides important information of how far harmonic components are spread out from each other.

Table 4.7 Results of different goodness-of-fit tests in case of sideband harmonics generated if the wind turbine has average and low output power.

Power Output *P*	**Goodness-of-fit test**				
	Two-sample Kolmogorov-Smirnov	Two-sample Ansari-Bradley	Chi-square	Lilliefors'	Jarque-Bera
$0.12P_n < P < 0.53$	0	0	0	0	0
$0.51P_n < P < 0.81$	0	0	0	0	0

The results of probability distribution estimation are presented in Figure 4.68. One can see that it is possible to fit the Gaussian curve to the histogram. Also empirical cumulative distribution functions of measured sideband harmonic components as well as generated based on estimated Gaussian function parameters show a good match between observations and model. For this particular dataset which represents harmonic components during average production sample mean $\bar{x}$ is equal to 161.471, sample variance s^2 is equal to 5.2394, sample skewness g_1 is equal to 0.0659, and kurtosis g_2 is equal to -0.0963. Comparing the model of sideband harmonic components for high production it can be seen that this model (i.e. average production) is characterized by lower sample mean and higher dispersion from the average value.

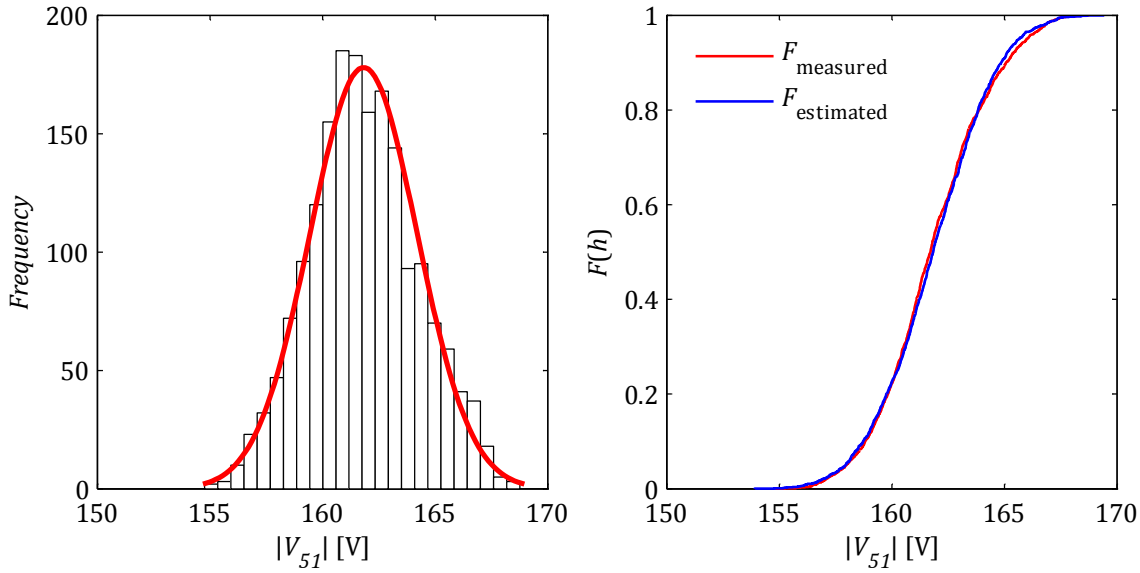

Figure 4.68 Gaussian curve fitting and empirical cumulative distribution function of sideband harmonic generated during average production.

From Figure 4.68 it can be seen that two bars close to the mean value are slightly higher than expected based on Gaussian curve fitting. This can be corrected by tuning power levels according to the results from Figure 4.67 and comparison of sample skewness and sample kurtosis. The closest values to 0 should give better results. It was not done since all goodness-of-fit test are passed and it was assumed to cover as broader active power bracket as possible.

Figure 4.69 shows sample skewness changes depending, on wind turbine active power brackets variation. Additionally another transparent surface (a horizontal plane) is presented at $z = 0$ to indicate where sample skewness is equal to 0. As it was mentioned earlier, it is expected in probability distribution estimation that the sample skewness (i.e. no asymmetry) should be as close to zero as possible. Theoretical skewness of normal probability distribution is equal to 0 the same as kurtosis. From the figure one can see that the sample skweness is high if broad dataset is chosen (i.e. $P_u \cong P_n$ and $P_u - P_l \cong P_n$). This strong asymmetry can be seen also from the histogram in Figure 4.63 and non-parametric probability density function estimation presented in Figure 4.65.

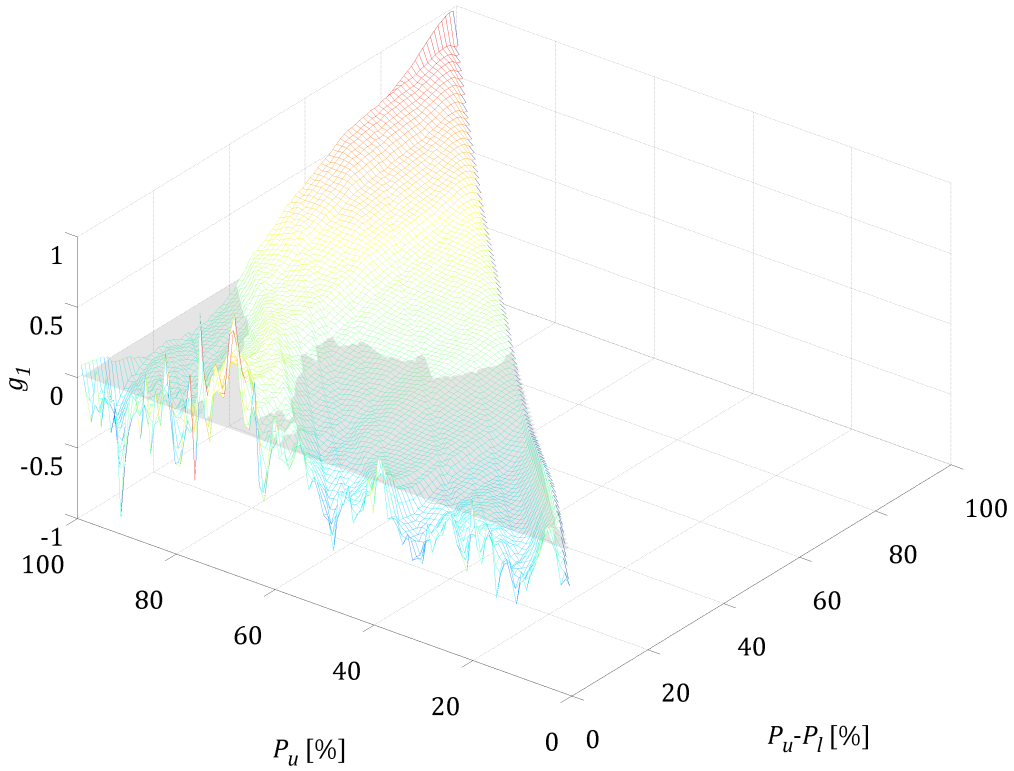

Figure 4.69 Sample kurtosis variation of the sideband harmonic component depending on active power levels in percent of nominal power.

The last dataset of interest is related to low producing wind turbines. The results of normal probability distribution parametric estimation are presented in Figure 4.70. Thanks to goodness-of-fit tests the probability distribution estimation is much easier and actually can be applied in case of any harmonic component of interest.

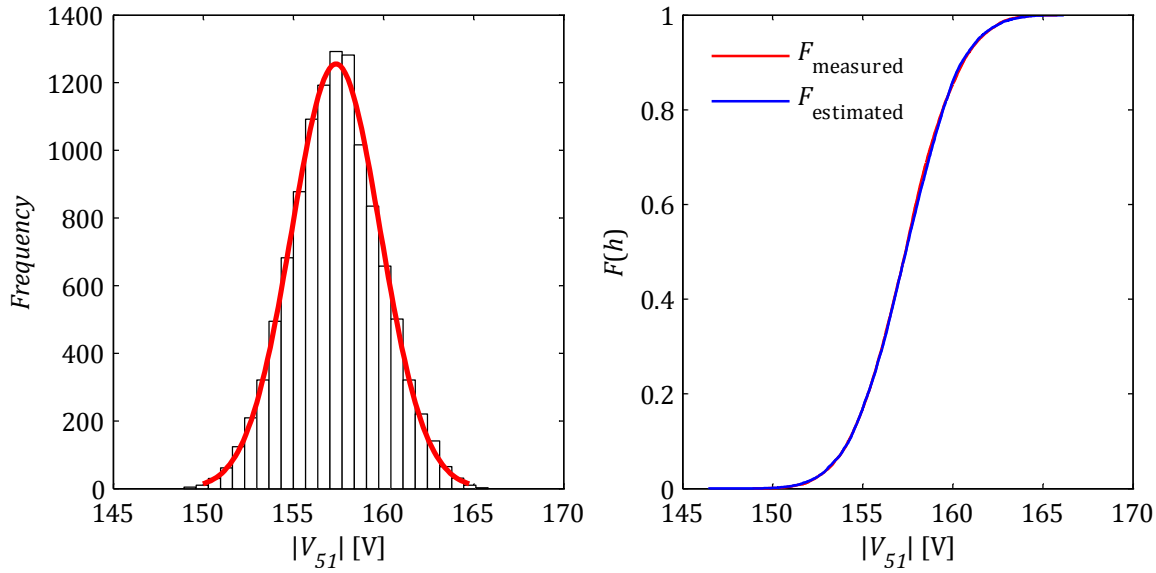

Figure 4.70 Gaussian curve fitting and empirical cumulative distribution function of sideband harmonic generated during low production.

For this particular dataset which represents harmonic components during low production sample mean $\bar{x}$ is equal to 157.1147, sample variance s^2 is equal to 5.8451, sample skewness g_1 is equal to -0.0191, and sample kurtosis g_2 is equal to -0.0756. Comparing the model of sideband harmonic components for average production and low production it can be seen that both models are characterized by comparable variance which much higher than in case of high production. A conclusion can be derived that during high production lower sideband harmonic components variation is seen.

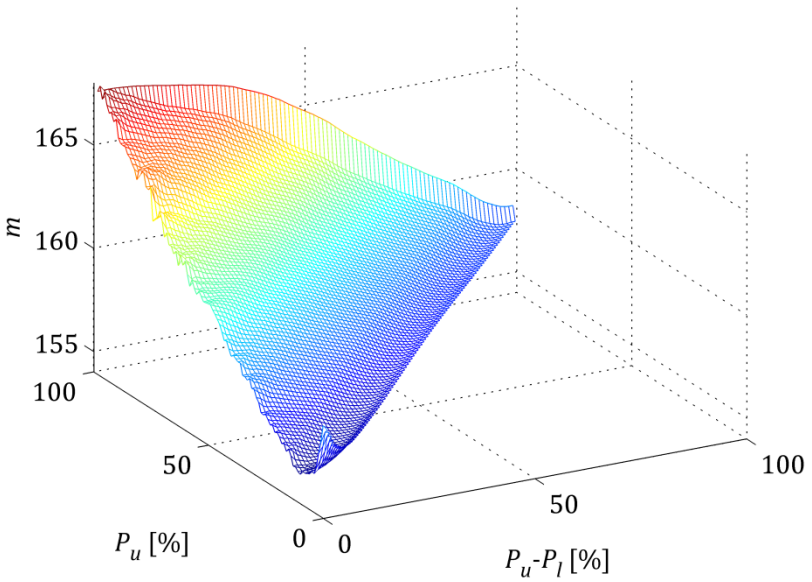

Figure 4.71 Sample mean variation of the voltage sideband harmonic component depending on active power levels in percent of nominal power.

At the end of the voltage sideband harmonic statistical analysis it is also interesting to focus on the sample mean value. Figure 4.71 presents sample mean variation of the voltage sideband harmonic component depending on active power levels (upper threshold P_u and lower threshold P_l) in percent of nominal power P_n. One can see that the harmonic average magnitude strongly varies with the wind turbine active power output. This is also presented in Figure 4.62 where the magnitude is increasing simultaneously with active power. Only for low power production the magnitude is slightly decreasing as also is seen in Figure 4.71. For $P_u = P_n$ the sample mean value is significantly higher due to the fact that for full power production sideband harmonic components are differently distributed (see multimodal distribution in Figure 4.63).

As it can be seen from Figure 4.67 different smaller datasets can be selected but they are not of interest within this analysis because the number of observations is relatively small. In other words harmonic components do not appear frequently (i.e. small value on the horizontal axis) in the measurements and are not considered of significant importance. It is also important to emphasize that for small number of observation goodness-of-fit test can provide misleading results because it might be problematic to reach asymptotic distribution of the statistics associated with the tests.

Regarding the current side-band harmonic components the analysis is expected to give similar results. Based on measurement data analysis it was shown that the sideband harmonic current is exclusively caused by the wind turbine. It is also observed that the harmonic impedance of the system does not vary significantly for frequencies within the sideband harmonic components.

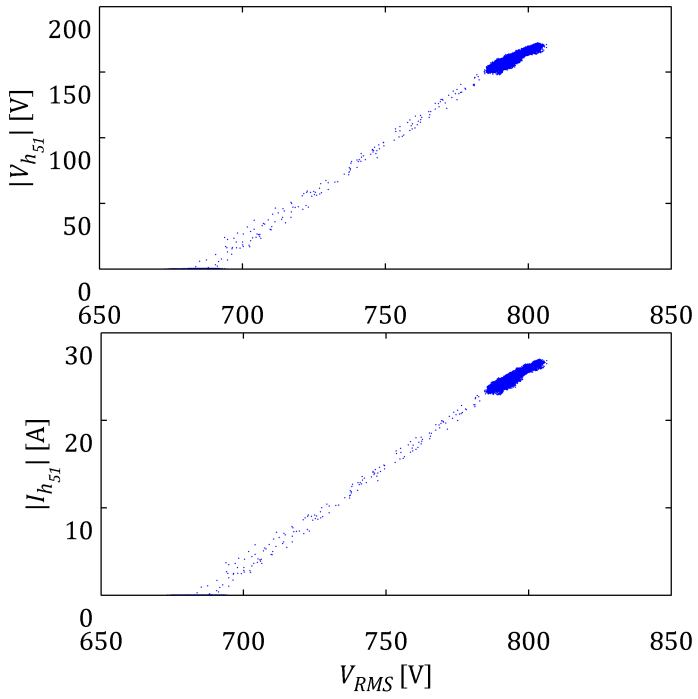

Figure 4.72 Sideband harmonic voltage and current measured at the converter AC terminals.

In order to distinguish if sideband harmonic components are generated directly by the voltage source converter or to some extend are also affected by the harmonic background a quantitative analysis is carried out. As it can be seen from Figure 4.72 the phase-to-phase RMS voltage is around 690 V when the wind turbine converter is turned off. If the voltage is around 790 V the grid-side converter is in operation.

Please note that there is a contribution of all harmonic components in calculation of RMS value. This is simply a numerical integration over the fundamental period. Therefore if the converter is operating sideband harmonic components significantly affects the voltage RMS value. The value of the RMS voltage measured and the grid-side converter AC terminals also varies depending on modulation index which is expected to be higher in case of full production.

From Figure 4.72 it can be seen that there is no sideband harmonic distortions h_{51} present in the grid voltage when the converter is turned off. Thus the harmonic current flow during production in this case is only affected by the grid-side converter. Moreover sideband harmonic components are considered to be characteristic harmonics from a power electronics perspective, i.e. are affected by topology, modulation of the grid-side converter. Such harmonic components are not influenced by internal converter control method as well as external conditions of the grid.

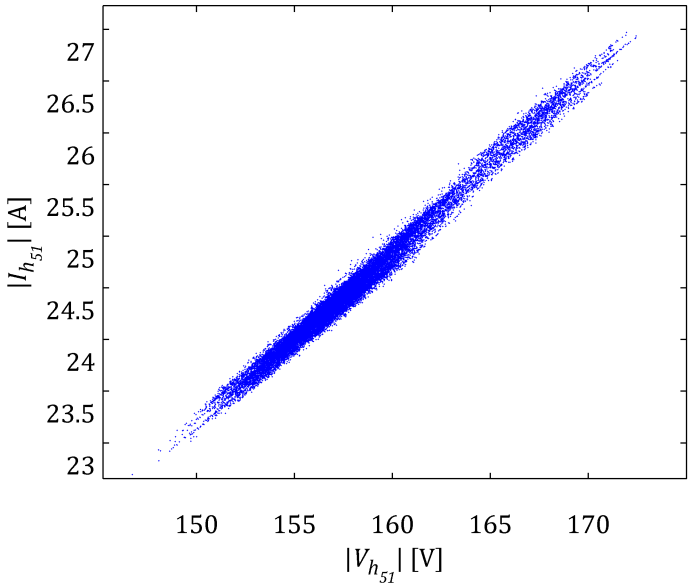

Figure 4.73 Linear dependence between harmonic voltage and current measured and the grid-side converter AC terminals.

Based on measurement results presented in Figure 4.73 one can conclude that current flow if the sideband harmonic component, is not affected by grid distortions and by changes in the plant frequency response for this particular frequency. This means that the current is strongly correlated with the grid-side converter voltage. Changes in the gird frequency dependent impedance are not so significant because the converter filter constitutes a low impedance path for sideband harmonic

components. Therefore the sideband harmonic current flowing through the wind turbine transformer is small and strongly dependent on grid frequency dependent impedance.

In order to indicate how both harmonic components are correlated a correlation coefficient can be defined. The correlation coefficient between two random variables X and Y with expected values μ_X and μ_Y and standard deviations σ_X and σ_Y is defined as

$$\rho_{X,Y} = \operatorname{corr}(X,Y) = \frac{\operatorname{cov}(X,Y)}{\sigma_X \sigma_Y} = \frac{\mathrm{E}[(X-\mu_X)(Y-\mu_Y)]}{\sigma_X \sigma_Y} \tag{4.42}$$

where cov means covariance and corr means Pearson's correlation. It is worth to emphasize that Pearson's correlation is sensitive only to a linear relationship between two variables. The sample correlation coefficient is written

$$r_{xy} = \frac{\sum_{i=1}^{n}(x_i-\bar{x})(y_i-\bar{y})}{(n-1)s_x s_y} = \frac{\sum_{i=1}^{n}(x_i-\bar{x})(y_i-\bar{y})}{\sqrt{\sum_{i=1}^{n}(x_i-\bar{x})^2 \sum_{i=1}^{n}(y_i-\bar{y})^2}} \tag{4.43}$$

where n is the number of observation of random variables X and Y written as x_i and y_i, $i = 1, 2, \dots, n$.

The sample correlation coefficient r is equal to 0.9935 and sample coefficient of determination r^2 is equal to 0.9871. Therefore it is expected that the same statistical analysis introduced for the sideband harmonic voltage should give the same results in case of the sideband harmonic current. Please note that all baseband and sideband harmonic components are expressed as an RMS value.

Summing up, it was possible to separate three datasets from measurements with observations from three different probability distributions. Unimodal distribution separation was done based on central limit theorem assumption, i.e. it is expected to obtain asymptotic normal distribution of observations in each of separated datasets. Non-parametric and parametric probability distribution estimation was done. The results of parametric estimation can be seen in Table 4.8.

Table 4.8 Stochastic models parameters of the sideband harmonic component dependent on output power.

Power Output *P*	**Parameters**				
	Sample mean $(m, \bar{x})$	Sample standard deviation (s)	Sample variance (s^2)	Sample skewness (g_1)	Sample kurtosis (g_2)
$0.12P_n < P < 0.53$	157.1147	2.4177	5.8451	-0.0191	-0.0756
$0.51P_n < P < 0.81$	161.471	2.289	5.2394	0.0659	-0.0963
$P > 0.92P_n$	167.3191	1.9026	3.6199	-0.0791	-0.2005

It was possible to model sideband harmonic components almost for the full active power range. This approach is useful taking into consideration power quality

measurements described in standards where it is expected to record harmonics for different power levels. Instead of one value (e.g. average, min, max) estimated probability distribution (i.e. developed stochastic model) can give a better overview about possible harmonic levels.

It was mentioned that sideband harmonic components are affected by the modulation technique. Of course the wind turbine output power in voltage source converters is affected by the output voltage. Analysis of sideband harmonic components can be performed based on either output power or output voltage depending on preferences, approach, and measurements.

It is also worth emphasizing that in this particular case there was no specified reactive power control since the analysed wind farm comprises only of two wind turbines. In this case both active and reactive powers are strongly correlated (see Figure 4.74). Therefore analysis of either active power or reactive power influence on sideband harmonic components provides comparable results.

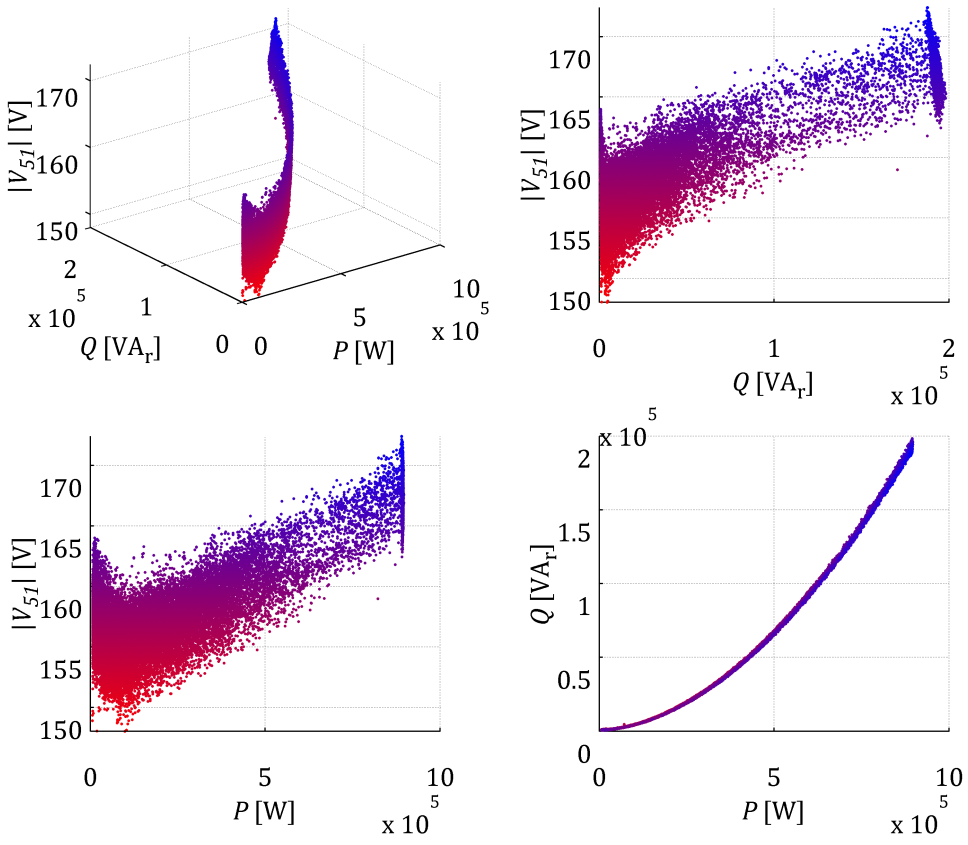

Figure 4.74 Sideband harmonic component dependence on active and reactive power.

Analysis of sideband harmonic angles is quite problematic directly from measurements because they are not linked with the power system fundamental component. The phase angle can significantly vary in the rectangular window when the signal is resampled during data processing. Also if no resampling is applied depending on the power system

fundamental frequency variation still a small variation in the angle is observed. This is due to the fact that sideband harmonic components are affected by two driving frequencies (i.e. power system fundamental component and carrier signal fundamental component). The angle of sideband harmonic components can be inappropriately estimated due to this fact. Results can lead to misleading conclusions that the angle is uniformly distributed. In some studies [4.50] such conclusion can be seen. In other chapter a deterministic approach of sideband harmonic components will be shown and also nature of their angles explained.

4.2.5 HARMONIC CONTENT IN THE DC-LINK CIRCUIT

In order to investigate how the harmonic content in the DC-link circuit of the full-scale back-to-back converter can affect harmonic spectrum observed at the ac terminals of the grid-side converter both voltage and current at the dc terminals of the network bridge were measured. As described earlier, measurement from both sides of the grid side converter were carried out simultaneously.

It was observed that there is an insignificant influence of the generator-side converter on the grid-side converter and thus the grid. Please note that in order to reduce the harmonic currents in the DC-link circuit inductors are used [4.51]. Therefore the grid is even less affected by the AC network from the generator side. Based on measurement data analysis it can be said that the DC-link circuit provides an effective decoupling between the wind turbine generator and the grid.

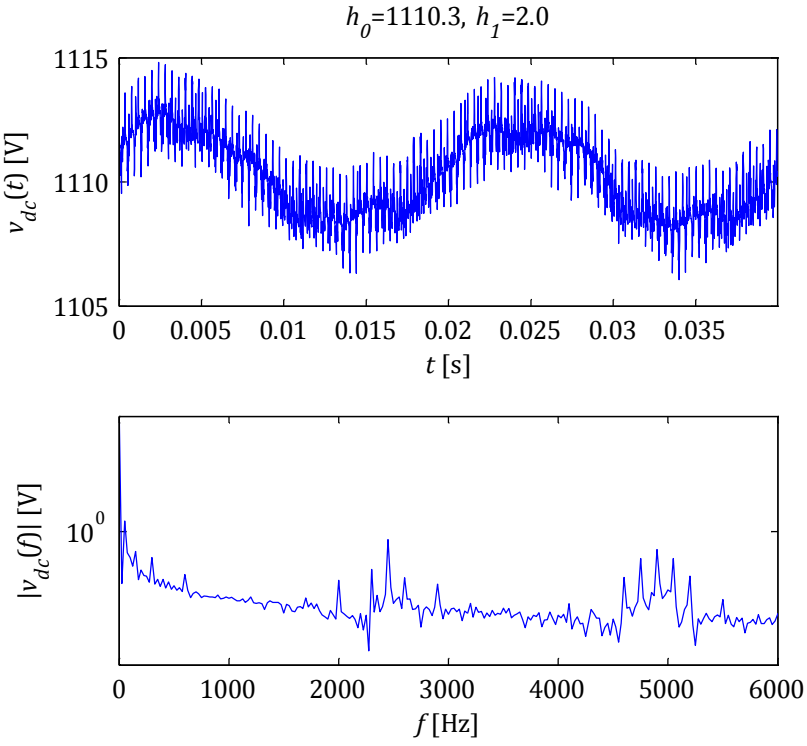

Figure 4.75 DC-link voltage waveform and its spectrum estimation.

However, some harmonic content in DC-link measurement can be seen. The most significant voltage harmonic is the 1st harmonic (h_1) as it can be seen in Figure 4.75. This harmonic is affected by the grid voltage unbalanced conditions. Some other harmonics can be seen in the estimated spectrum but they are almost at the same level as noise. It was also observed that the amplitude of h_1 is higher for wind turbine lower production as presented in Figure 4.76. For lower production the difference between the 3rd phase and other phases is more significant (see Figure 4.77).

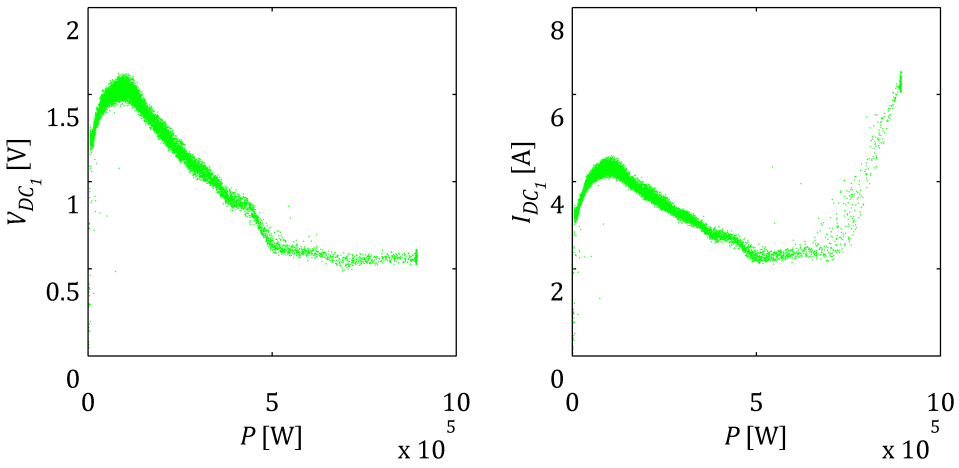

Figure 4.76 DC-link harmonic dependence on the wind turbine output power.

The difference of the fundamental component between phases is presented in Figure 4.77. It can be seen that the 1st harmonic in the DC-link voltage has the highest magnitude when the 1st and the 2nd phase amplitudes are equal and only the 3rd differs. Please note that for all harmonic components the RMS value is presented. The difference between phases is presented in relation to the equivalent three-phase voltage [4.52].

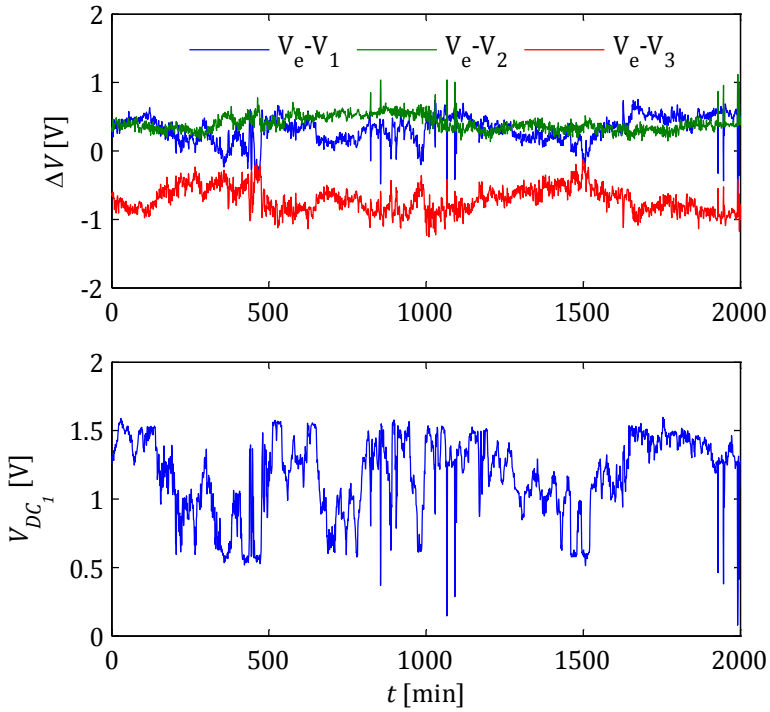

Figure 4.77 Unbalanced fundamental voltage component and the harmonic content variation.

Referring to the equivalent three-phase voltage allows comparing different phases independently in the grid voltage amplitude variation. The equivalent three-phase voltage was calculated in the following way

$$V_e = \sqrt{\frac{V_1^2 + V_2^2 + V_3^2}{3}} \tag{4.44}$$

where $V_j, j = 1, 2, 3$ is the voltage RMS value of each phase.

Another significant harmonic component measured in the DC-link is the network bridge natural frequency [4.53] which is 6 times higher than the grid voltage ($6\omega_o$). The harmonic component (h_6) is clearly seen in current measurements presented in Figure 4.78.

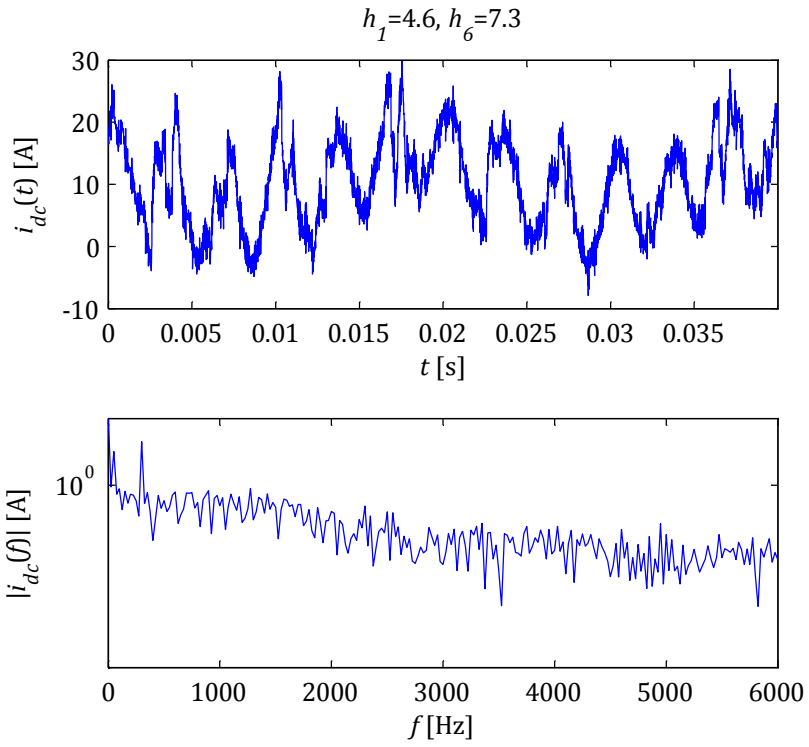

Figure 4.78 DC-link current waveform and its spectrum estimation.

Later in this report it will be shown how the harmonic content in the DC-link circuit can affect harmonic emission by the grid-side converter to the grid. The phenomenon will be analytically explained based on double Fourier series approach.

4.2.6 BASEBAND HARMONIC COMPONENTS

In contrast to sideband harmonic components which are well determined by the modulation technique, baseband harmonics are affected by different and many factors. One of the most crucial is the harmonic background distortion which is always present to certain extent during wind turbine operation. Also power network frequency dependent impedance can more significantly vary for lower frequencies.

Therefore prediction and analysis of baseband harmonic components is more time consuming and complex. Not infrequently it is difficult or even impossible to gather information about harmonic background and frequency dependent characteristic of the system to which the wind turbine is connected. In such cases harmonic analysis and assessment results is of great uncertainty and can provide misleading conclusions. It is also worth to emphasize that various wind turbines can differently interact with the plant changes and background distortions. Such variety implies significant difficulties in deterministic modelling of wind turbines and consequently wind farms.

In such case statistical methods became very helpful. They provide better overview of harmonic phenomena in the analysed system and allow extracting the most important harmonic information. This allows to consider the most important

and significant harmonic aspects during deterministic modelling either in time domain or in frequency domain.

Nowadays in standards concerning power quality measurements and assessment [4.24] different grid conditions are specified (e.g. total harmonic distortion less than 5%, grid frequency within $\pm 1\%$ of the nominal frequency). Unfortunately still harmonic evaluation can be problematic which will be shown in this part. Such variation in conditions can affect data acquisition (e.g. power quality meter sample rate adjusted according to power system frequency variation) and data processing (e.g. non-parametric spectrum estimation and possible spectral leakage).

It was decided to focus only on the most significant (i.e. the highest either voltage or current estimated magnitude) baseband harmonic measured at the converter AC terminals. Measurements at the voltage source converter terminals seem to be the most appropriate. In theory it is assumed that the converter provides distorted voltage and the distorted current flow is an effect of converter and network distorted voltages.

4.2.6.1 BASEBAND HARMONICS ABSENT IN THE BACKGROUND

At the beginning of the analysis a baseband harmonic was chosen which was not detected in the background distortions. In other words is only generated by the converter and flowing current is dependent on voltage at the AC terminals and grid impedance for this particular frequency.

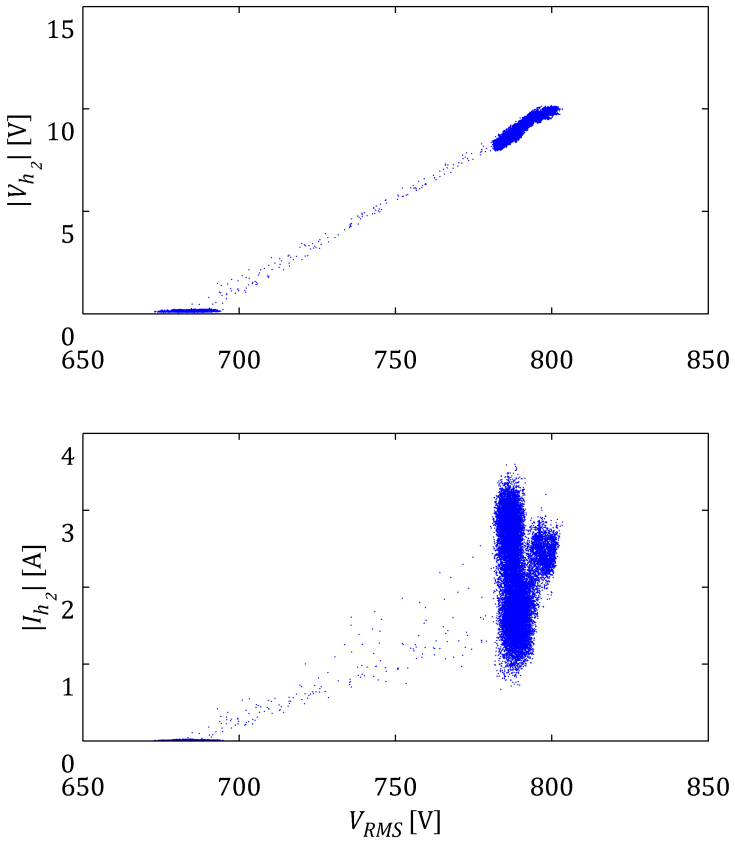

Figure 4.79 Baseband harmonic voltage and current measured at the converter AC terminals.

The 2nd harmonic, which is only generated by the converter, is presented in Figure 4.79. It is relatively easy to distinguish that this particular baseband harmonic component is generated directly by the voltage source converter and is not affected by the harmonic background. Voltage harmonic values assigned for the phase-to-phase RMS voltage around 690 V are measured when the wind turbine is not producing and are equal to 0. On the other hand, when the wind turbine converter is turned on, the grid voltage is around 790 V and significant voltage distortion of 10V can be seen.

Due to the fact that this harmonic does not exist in the background distortions the harmonic current is flowing from the wind turbine into the grid and its value is mainly affected be the plant impedance. Please note that the voltage variation is small in comparison to current variation. In contrast to the sideband harmonic component analysed before (see Figure 4.72) the baseband harmonic current varies significantly during wind turbine production. Therefore the dependence between measured harmonic voltage and current (see Figure 4.80) is not any longer linear (as it was in case of the sideband harmonic component presented in Figure 4.73).

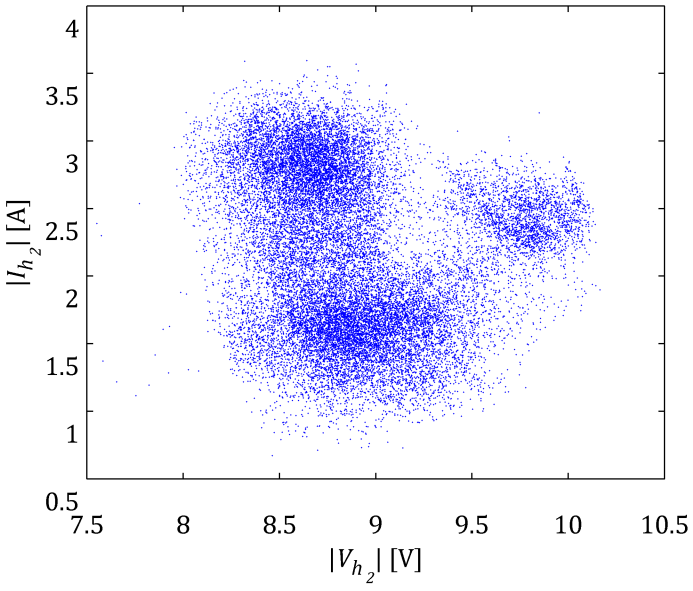

Figure 4.80 Dependence between baseband harmonic voltage and current.

It is worth emphasizing that the measured current amplitude is close to the sensor accuracy. This is another aspect which makes it difficult to analyse harmonics. For current measurements Rogowski current transducers with a small coil loop were used. This allowed situating converter power cables centrally inside that loop and thus improve measurements accuracy. High random errors in current measurements can be seen in Figure 4.80 where the scatter plot tends to be normally distributed around at least three points. These points indicate possible frequency dependent impedance changes in the system. Anyway, obvious lack of linear dependency between baseband harmonic current and voltage can be seen.

Please note that also possible zero sequence currents at the LV side of the wind turbine power circuit can affect overall harmonic current measurements. Since only the phase-to-phase voltage is considered in the analysis it is assumed that the 2nd harmonic is of negative sequence. In case of the harmonic current both either negative or zero sequence components can be measured.

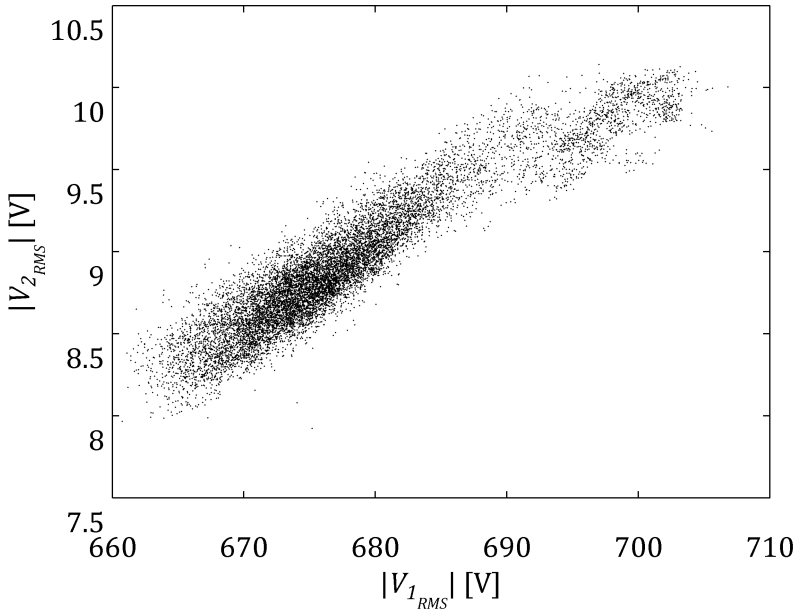

Figure 4.81 Dependency between fundamental harmonic and baseband harmonic component.

As it is expected the 2nd harmonic is also almost linearly (see Figure 4.81) dependent on the fundamental voltage. The sample Pearson's correlation coefficient is equal $r = 0.9323$ which indicates strong correlation between both variables. Previously it was shown that this particular baseband harmonic component is not present in the background which means that is only generated by the wind turbine. Therefore might be considered as a power converter characteristic harmonic, which is not affected by the grid conditions.

Also in Figure 4.82 it is possible to see that the estimated probability density function indicates multimodal probability distribution with at least local peaks. A series of estimated curves also proves that the 2nd harmonic is described by a representative dataset at least for lower magnitudes, i.e. applicable statistical analysis can be performed. It is easy to see that the estimated density function has similar shape to the 51st harmonic component non-parametric estimation of probability density function (see Figure 4.65). Therefore there are strong premises that both voltage harmonic components have the same origin and nature. Both of them are only affected by the grid-side converter of the wind turbine.

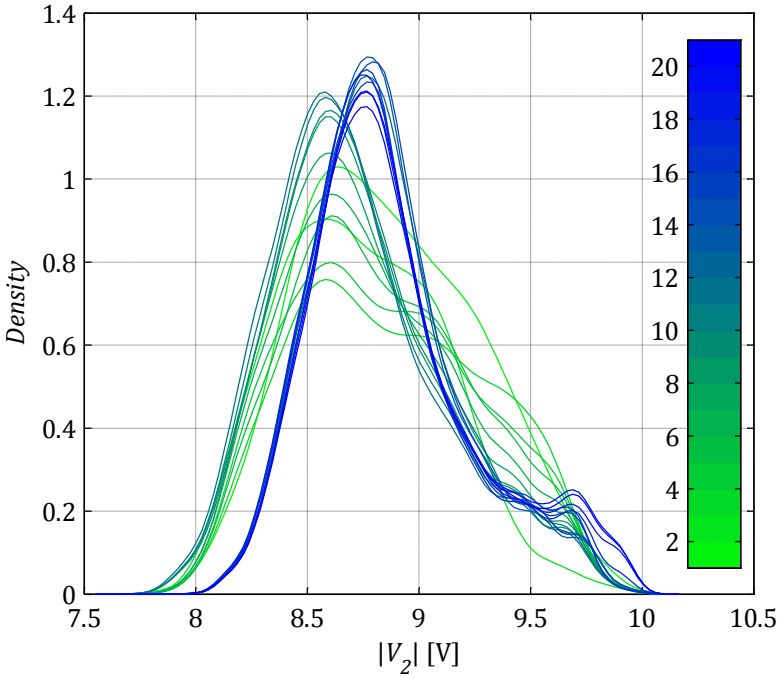

Figure 4.82 Nonparametric estimation of probability density function.

If one would analyse how the 2nd harmonic is dependent on power production as presented in Figure 4.83, it can be observed that the harmonic is almost independent on power production. Marginal linear dependency can be observed, but on the other hand 2nd harmonic voltage can be at almost any observed level within 50% of overall production.

Figure 4.82 shows that the multimodal distribution does not reach its final shape even for so many number of observations (i.e. 26541 one-minute average observations). This can be easily seen on case of higher estimated magnitude. Therefore there are some premises that statistical analysis would not give satisfactory results. In general it is expected that measurement period of harmonic components generated only by the converter should be shorter in comparison to harmonic components affected also by the background distortions. This can be easily seen regarding sideband harmonic components. Unfortunately in case of the 2nd harmonic the period is also insufficient. Comparing Figure 4.65 and Figure 4.82 the conclusion is that non-parametric probability density function estimation of the harmonic component provides relatively close results for even small datasets where the baseband harmonic component probability density function estimation varies significantly depending of observation number.

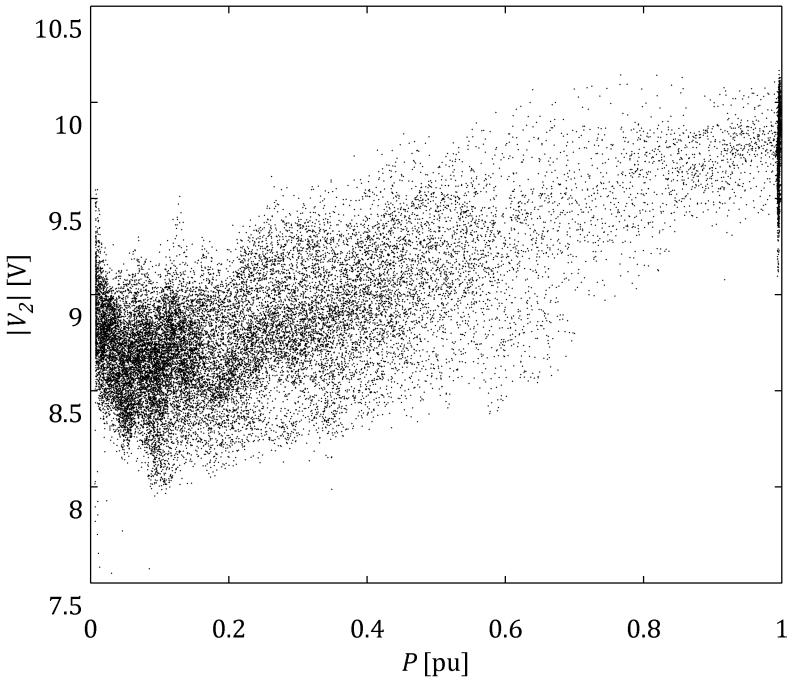

Figure 4.83 Baseband harmonic dependence on active power production.

The correlation coefficient between the active power production and 2nd voltage harmonic amplitude is $r = 0.7786$. This value seems to be quite high but for statistical analysis in social science. In electrical engineering more accurate values are expected. According to the central limit theorem normally distributed harmonic observations are expected to be found in the analysed dataset.

It is not surprising that harmonic generation is only a little dependent on active power production. In a few places [4.54], [4.55], and [4.25] it is clearly presented that the most significant harmonics measured in wind farms are not dependent on both active and reactive power production. In this section, based on both baseband and sideband harmonic components it can be seen the dependency is marginal.

There were not so many studies regarding stochastic nature of harmonic components because it is difficult and not straight forward task. First of all there is a necessity to acquire enormous amount of data and later process it. Only research projects directly connected with the industry can afford to carry out extensive measurement campaigns. Also in few publications [4.54], [4.56], [4.55], [4.25] one can see normal distribution fitting approach to measured harmonic components. This also proves expected observation based on the central limit theorem. In a few places [4.56] where measurement period was not long enough quite bad fitting is presented and results can provide misleading interpretation.

It is possible to specify appropriate power production levels to model stochastically also the 2nd harmonic. This can be done in the same way as it was performed in case of the sideband harmonic component. According to various non-parametric as well

as parametric goodness-of-fit tests appropriate active power brackets were specified and are presented in Table 4.9.

Table 4.9 Stochastic models parameters of the baseband harmonic component dependent on output power.

Power Output *P*	**Parameters**				
	Sample mean $(m, \bar{x})$	Sample standard deviation (s)	Sample variance (s^2)	Sample skewness (g_1)	Sample kurtosis (g_2)
$0.00 < P < 0.27P_n$	8.6844	0.2472	0.0611	-0.0197	-0.0054
$0.53 < P < 0.61P_n$	9.1738	0.3077	0.0947	-0.1590	-0.2396
$0.68 < P < 0.85P_n$	9.5485	0.2408	0.0580	-0.2532	-0.0308
$0.88 < P < 0.95P_n$	9.7115	0.1562	0.0244	-0.2722	0.3888

Even if all goodness-of-fit test gave a positive outcome (i.e. the null hypothesis cannot be rejected within assumed significance level $\alpha = 0.05$) the probability density function estimation gives rather pure results for higher active power levels. This is mainly affected by lack of observations of the 2nd harmonic during wind turbine high production. As presented in Figure 4.82, for higher estimated magnitudes of the baseband harmonic there is no representative dataset.

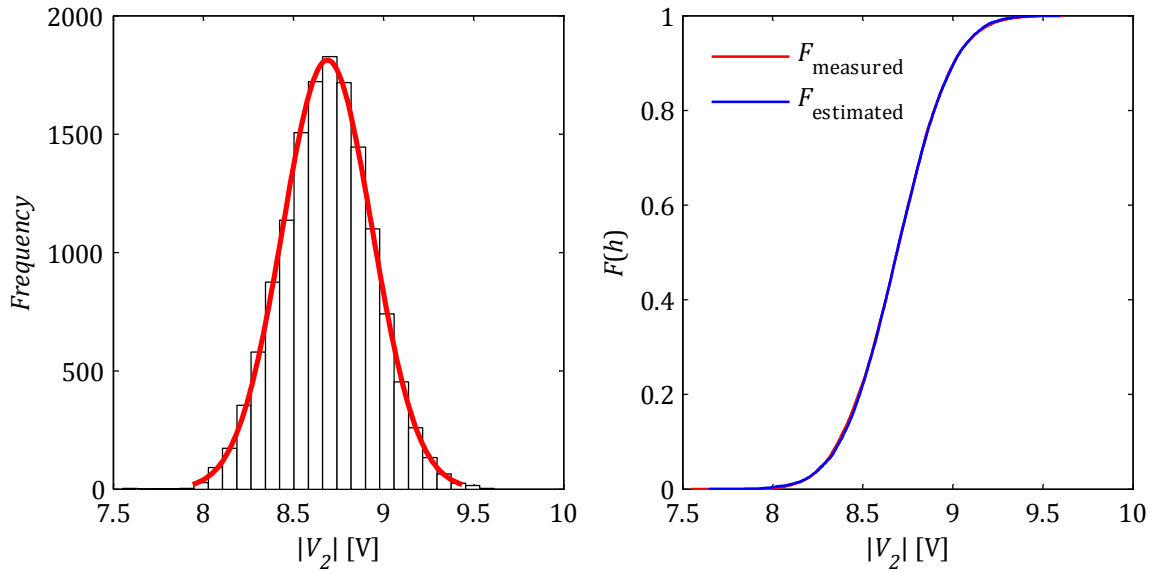

Figure 4.84 Gaussian curve fitting and empirical cumulative distribution function of baseband harmonic generated during low production.

Anyway for the first active power production bracket (i.e. $0.00 < P < 0.27P_n$) the number of observations is sufficient and normal probability density function estimation can be carried out successfully. Empirical cumulative distribution function as well as normal distribution fitting is presented in Figure 4.84. It is worth emphasizing that for all estimated probability density functions sample standard deviation

and sample variance are small. Therefore the 2nd baseband voltage harmonic can be modelled deterministically as a sample mean value.

Previously it was mentioned that 2nd harmonic current measurements are affected by measurement system uncertainty and the estimated magnitude is insignificant in comparison to other harmonics, thus the harmonic current is not going to be investigated.

Since the 2nd baseband harmonic is of low frequency and also generated only by the converter it is interesting to investigate its phase angles. This allows observing how the 2nd baseband harmonic is related to the fundamental component. In theory one expects to observe 2nd harmonic as a negative sequence component. Earlier it was mentioned that the 2nd harmonic is purely generated by the voltage source converter. Of course for low order harmonics data processing errors caused by spectral leakage are negligible and harmonic components magnitude estimation results are comparable for both resampled and not resampled waveforms.

Different situation is for phase angle estimation and the estimation is much more precise if analysed waveforms are not resampled. In Figure 4.85 one can see estimated phase angle of the 2nd harmonic for all three phases. It can be seen that actually the angle replacement for all three phases indicates negative sequence components. Thus one can say that the grid-side converter generates mainly negative sequence 2nd harmonic.

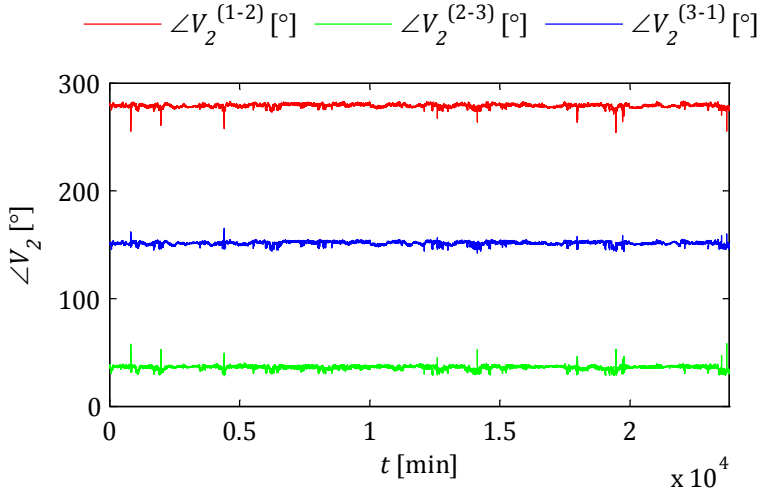

Figure 4.85 Estimated phase angle of the 2nd harmonic for all three phases.

Since the 2nd harmonic is of negative sequence it is expected to observe harmonic current for this particular frequency from the primary side of the wind turbine transformer. The wind turbine transformer is with Dyn11 configuration and can be considered as an open circuit for zero sequence harmonic components but not for negative sequence components. Please note that the analysed 2nd harmonic

is calculated from line-to-line voltages (i.e. potential difference between two lines of different phases) and therefore no zero sequence components are present.

Taking into consideration phase voltages (potential difference between phase and ground) of the converter additional common-mode voltage is introduced. Since the 2nd harmonic is generated by the converter it is not surprising that common-mode voltage can be observed also for this particular frequency. Taking into consideration only line voltages the 2nd harmonic can be considered as balanced (within the measurement equipment accuracy and precision). In case of phase voltages zero sequence components also can be distinguished. Table 4.10 presents line and phase voltages calculated using discrete Fourier transform from measured voltage waveforms.

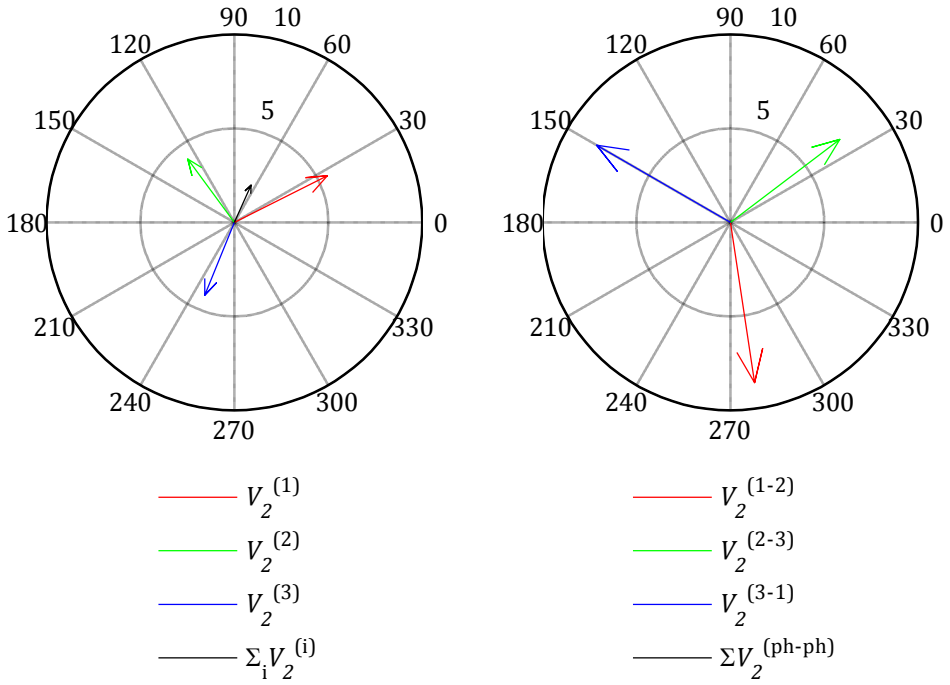

Figure 4.86 Vector graphs of phase and line converter voltages.

Observation of common-mode 2nd harmonic voltage is shown in Figure 4.86 where the sum of all phase voltages is not equal to 0, while the sum of all line voltages is actually equal to 0. This observation proves that looking into modern systems from classical definition of harmonics can confuse. According to [4.12] characteristic harmonics exist when analysed three-phase electrical system is considered to be balanced, the voltages and currents waveforms have identical shape and current and voltage are separated by exactly $\pm 1/3$ of the fundamental period. In such case zero sequence harmonics are for orders $n = 3m$ where $m = 1, 2, 3, \ldots$, positive sequence harmonics are for orders $n = 3m - 2$ and negative sequence harmonics are for orders $n = 3m - 1$. According to the classical definition the 2nd harmonic should be a negative

sequence component. It should be emphasized that power converter are capable to generate harmonics of any frequency and of any phase angle.

Unbalanced situation in converter harmonic voltages can be affected due to floating DC-link neutral point. In some converters, especially in two-level, the DC-link circuit neutral point can be floating in reference to the load neutral point. This can cause unbalanced current flow. Therefore it is not surprising that grid-connected converters can generate not only zero sequence 3rd harmonic component as well as not only negative sequence 2nd harmonic component.

Table 4.10 Phase and line voltages (magnitude and phase) calculated form measurements for the 2nd harmonic.

Magnitude $\lvert\cdot\rvert$ [V]	**Value (RMS)**	**Phase $\angle$ [°]**	**Value**
$\left\lvert V_{h_2}^{(1-2)}\right\rvert$	8.62	$\angle V_{h_2}^{(1-2)}$	278.60
$\left\lvert V_{h_2}^{(2-3)}\right\rvert$	7.31	$\angle V_{h_2}^{(2-3)}$	37.11
$\left\lvert V_{h_2}^{(3-1)}\right\rvert$	8.22	$\angle V_{h_2}^{(3-1)}$	149.97
$\left\lvert V_{h_2}^{(1)}\right\rvert$	5.54	$\angle V_{h_2}^{(1)}$	26.59
$\left\lvert V_{h_2}^{(2)}\right\rvert$	4.20	$\angle V_{h_2}^{(2)}$	126.38
$\left\lvert V_{h_2}^{(3)}\right\rvert$	4.18	$\angle V_{h_2}^{(3)}$	247.86

The analysis presented above primary is devoted to harmonic components generated by the three-phase converter. Estimated harmonic components were generally expressed in terms of line-to-line (phase-to-phase) voltages. These harmonic components are expressed in so-called differential mode since they are the relative voltage difference between two points of the load. Also performing measurements focus on phase-to-phase voltage of the grid-side converter is more convenient since it is difficult to refer to the DC-link neutral point which sometimes can be floating in reference to the load neutral point. However, obviously there are components which can be only seen in phase (phase-to-ground) voltages. These are called common mode voltages.

It has been shown that in some cases common mode voltages can affect current flow through motor bearings [4.38]. In industrial applications, such voltage and associated with it current can cause malfunctions of computers and control equipment. In motor drives and electrical networks, common-mode current even has the potential to cause unwanted tripping of ground fault relays or even physical damage [4.57].

4.2.6.2 BASEBAND HARMONICS PRESENT IN THE BACKGROUND

In order to distinguish which harmonics are generated directly by the voltage source converter and which are simple the harmonic background measured at the AC terminals

of the power converter, a quantitative analysis is carried out. As it can be seen from Figure 4.87 the phase-to-phase RMS voltage is around 690 V when the wind turbine converter is turned off. If the voltage is around 790 V the grid-side converter is in operation. Figure 4.87 shows that voltage harmonic level h_5 is very low when the converter is in operation. This proves that the control harmonic rejection of the power converter is satisfactory and it keeps as low as possible voltage harmonic distortion even if the background voltage is distorted. From Figure 4.87 it also is seen that the background voltage distortions are normally high as it is presented by the scatter plots when the RMS voltage is around 690 V. When the grid-side converter is in operation the distorted background voltage affects harmonic current flow. In order to reduce voltage background harmonic distortions, the converter needs to adjust the command signal depending on harmonic voltage distortions by cancelation of oscillations in the control frame. That is why the measured voltage waveform to some extent is free of baseband harmonics affected by the grid even if there harmonic current is still flowing.

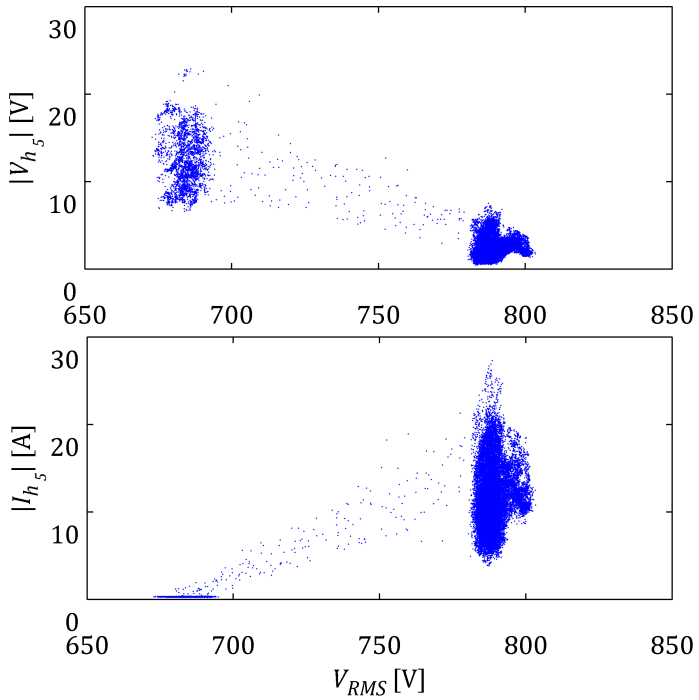

Figure 4.87 Baseband harmonic voltage and current measured at the converter AC terminals when the wind turbine is in operation and is shutdown.

It was shown that the 2nd baseband harmonic is purely generated by the grid-connected converter. Another more complex example of baseband harmonics is related with existing in the background harmonics. The most significant are non-triplen odd harmonics such as 5th, 7th, 11th and 13th. These are also observed in measurements and the most interesting from analysis perspective. In case of such harmonic

components it is of great importance to have an overview of existing distortions in the grid and how the grid-connected converter interacts with it.

There are many various control techniques dealing with robust operation of the grid-side converter if the grid voltage is distorted. Some techniques are focused on voltage quality improvement while others are focused on current quality improvement. Grid-connected converters with implemented harmonic current compensation can act as active filters but it is not required by wind farms developers and transmission system operators.

Harmonic control is also, to some extent, dependent on wind turbine application. If the wind turbine is separately connected to the network (e.g. at the distribution level) harmonic compensation may be required to improve the quality of current. On the other hand if the wind turbine is one of many wind turbines in large offshore wind farms harmonic compensation is not so crucial. It is even less important if the offshore wind farm is connected via HVDC transmission system. In that case the number of potential nonlinear loads within such system is significantly limited and it is better to focus on voltage quality within the wind farm internal AC network.

The first step of such baseband harmonic analysis is to carry out measurements of background distortions. At this point a question of how long the measurements should be carried out is quite obvious. Unfortunately it is difficult to answer in a simply way. Harmonic distortions are dependent on many aspects in the external network (e.g. variation of nonlinear loads, changes in the short circuit impedance, etc.). Of course by application of statistical methods (e.g. kernel smoothing) it is possible at least to assess if number of observation is sufficient for further analysis.

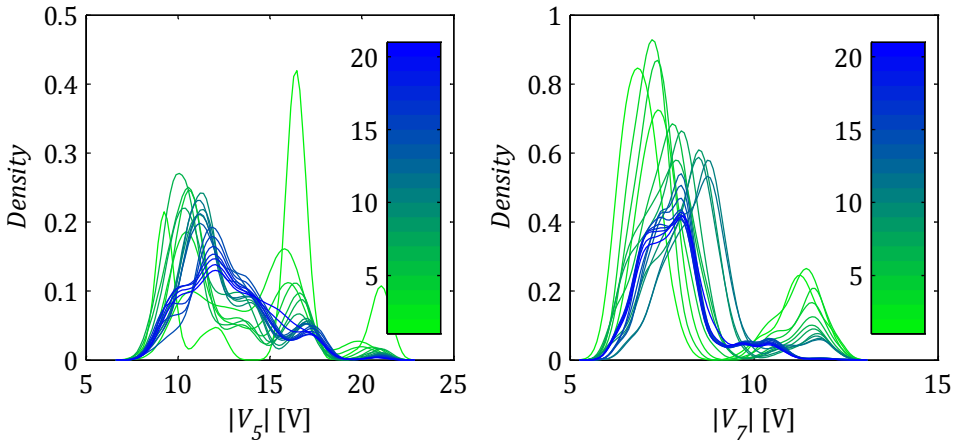

Figure 4.88 Probability density function estimation of background harmonics.

From Figure 4.88 one can see that it is complicated to measure background harmonics. This case is even more complicated in existing wind power systems. Measurements of harmonic background should be carried out when a certain wind farm is disconnected. This can be done only in case of some grid tests or maintenance which

is not so frequent in commercial projects. Therefore to avoid unwanted losses in terms of money it is much better to carry out measurements of background distortions before wind farm starts commercial operation. Please note that even a wind farm not producing but connected at the point of common coupling, can significantly change impedance at that point and thus also expected harmonic distortion.

It can be seen from Figure 4.89 that the grid-side converter control system is robust and no significant influence from the background can be observed. Therefore harmonic measurements when the wind turbine is producing can give an overview about its behaviour. Anyway knowledge about the background distortion is needed. To see how the wind turbine interacts with the distorted network it is required to carry out measurements of voltage harmonics in a voltage source converter from its AC terminals. Harmonic current for the same frequencies will be affected by many factors such as background distortions and possible impedance variation. Please note that here only control structure without harmonic current compensation is taken into consideration.

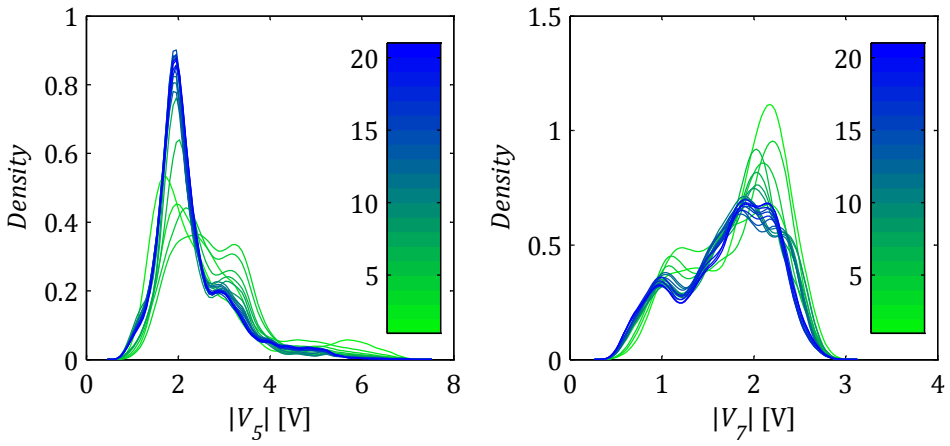

Figure 4.89 Baseband voltage harmonics measured during wind turbine operation.

In general it is difficult to estimate what a sufficient period of measurements is in order to acquire representative dataset. This is strongly dependent on external network configuration. In measurements presented in Figure 4.88 the harmonic background was measured with energized wind turbine main power circuit. This allows to see how the wind turbine sees the distortions if is connected to the grid. Not always such measurements can be carried out.

Knowing that harmonic current in case of power converter non-characteristic harmonics (e.g. 5^{th}, 7^{th}, 11^{th}, etc.) is also affected by the harmonic background one can conclude that also harmonic voltage will change at the wind turbine output terminals. Therefore it is much complicated to analyse power converter non-characteristic harmonics. Harmonic current measured during wind turbine production is presented in Figure 4.90.

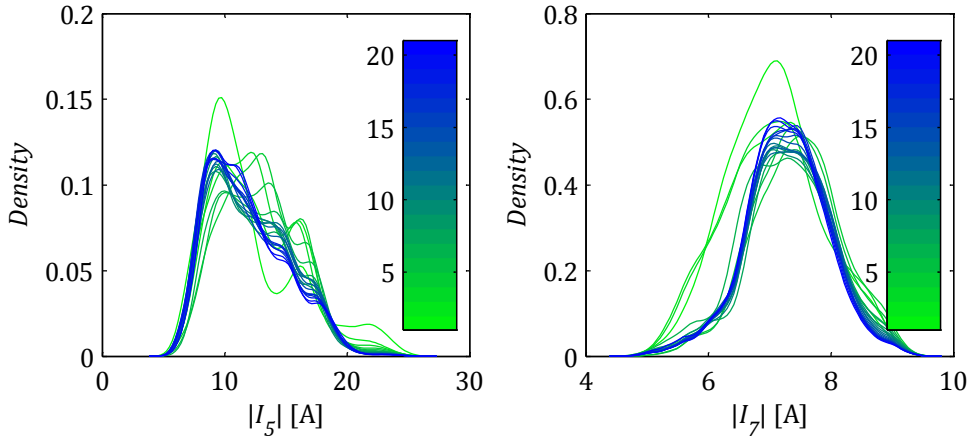

Figure 4.90 Non-parametric probability density function estimation of baseband current harmonic components.

In this particular case measured harmonic background distortions are seen at the HV side of the wind turbine transformer, assuming that when the wind turbine grid-side converter is off there is no low frequency current flowing in the wind turbine power circuit (e.g. wind turbine transformer, shunt filter, main reactor). In that case the current is dependent on at least two independent random variables, i.e. grid-side converter harmonic voltage and grid harmonic background. Please note that there is always some degree of correlation between both harmonic voltages because the converter control cannot provide ideal attenuation for all frequencies. And thus those baseband harmonic components are not any longer dependent on the fundamental voltage, in contrast to the 2nd and all sideband harmonic components.

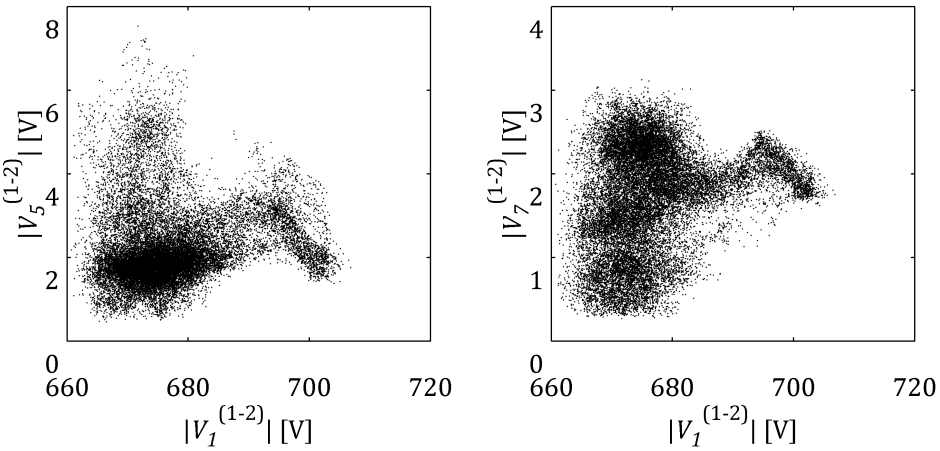

Figure 4.91 Baseband voltage harmonics dependence on the fundamental voltage component.

Figure 4.91 shows that seen previously linear dependency between the fundamental voltage component and power converter characteristic harmonics (i.e. 2nd and 51st) is not valid for baseband harmonics affected by the grid (i.e. 5th and 7th). In such case the harmonics are not purely generated by the converter therefore deterministic analysis of such harmonic components is difficult (even if not possible) and requires extended modelling with high accuracy. Therefore statistical analysis can be helpful.

Based on measurement data it can be concluded that baseband voltage harmonics are strongly affected by the grid. Therefore their dependence on either active or reactive power is minor (see Figure 4.92). This dependence is even less significant if harmonic measurements are carried out in other places than at the grid-side converter AC terminals. In case where harmonic generation is dependent on many properties the statistical approach of harmonic description becomes even more important. Unfortunately in such analysis more extended measurements are required thus long-term offshore measurements were carried out.

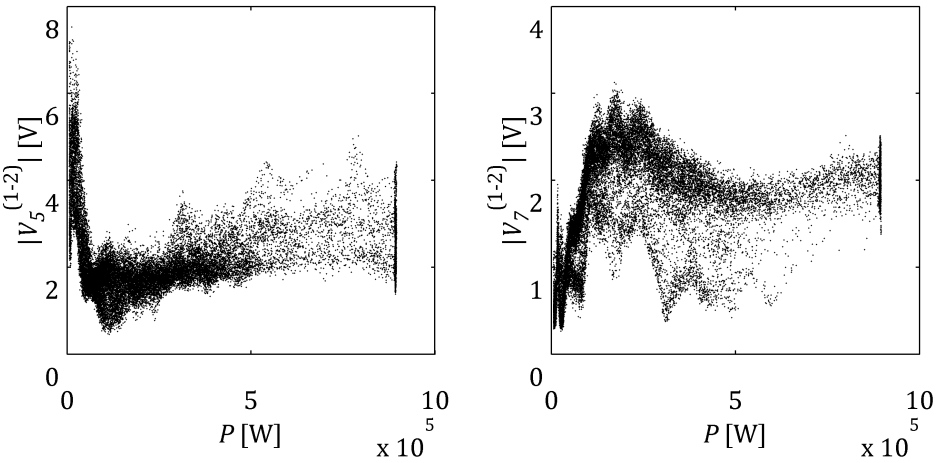

Figure 4.92 Voltage harmonics seen from converter terminals dependence on active power.

Based on probability density function estimation presented in Figure 4.65 and Figure 4.82 even if the same measurement period is considered it is more difficult to get representative dataset for lower frequencies. Quite natural is the statement that high frequency components (e.g. sideband harmonic components) variation can be seen for shorter measurement periods and also in spectrum estimation averaged magnitudes are calculated for higher number of periods. Please note that the entire time 10-cycle rectangular window is considered in calculations and for the 2nd harmonic there will be only 20 cycles while for the 51st there are 510 cycles. Therefore according to the central limit theorem the asymptotic normal distribution is achieved if number of observations reaches infinity. That is also why it was not possible to model stochastically the 2nd harmonic for wind turbine high production while in case of the 51st harmonic component it was not an issue.

Sometimes it is convenient to show harmonics using the box plot. It is a useful way of graphically depicting measured harmonic components through their five-number summaries [4.58]: the sample minimum, the lower quartile (Q1), the median (Q2), the upper quartile (Q3), and sample maximum.

Figure 4.93 shows baseband harmonics measured at LV side of the wind turbine transformer. Harmonics are scaled in reference to nominal voltage and current. Significant 5th and 7th harmonic variation can be easily observed. On each box, the central mark is the median, the edges of the box are the 25th and 75th percentiles

(Q1 and Q3 respectively), the whiskers extend to the most extreme data points where outliers are not considered, and outliers are not plotted.

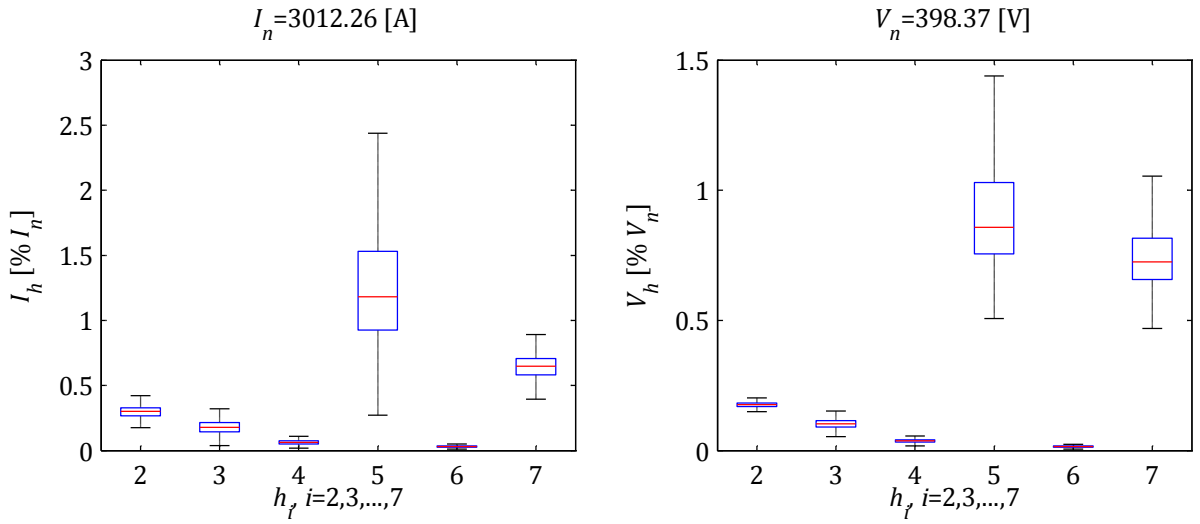

(a) (b)

Figure 4.93 Harmonic voltage and current measured at wind turbine number 3 LV terminals in Avedøre Holme.

The default whisker length w used in the box plots is of 1.5. Points are drawn as outliers if they are larger than Q3 + w(Q3 – Q1) or smaller than Q1 – w(Q3 – Q1), where Q1 and Q3 are the 25th and 75th percentiles, respectively. The default of 1.5 corresponds to approximately $\pm 2.7\sigma$ and 99.3 coverage if the data are normally distributed. The plotted whisker extends to the adjacent value, which is the most extreme data value that is not an outlier. Outliers are not shown in the analysis.

4.2.7 HARMONICS IN LARGE OFFSHORE WIND FARMS

It can be expected that background distortions should be much lower at wind turbines output terminals in large offshore wind farms. Potential distortions from various nonlinear loads such as rectifiers should not be observable. Therefore it is also expected to observe lower harmonic currents flowing internally in wind farm electrical network structures. In order to investigate the differences in harmonics presence in different wind farm systems various measurement campaigns were carried out. Detailed measurements of one wind turbine can provide good understanding of its behaviour as a harmonic source. Investigation of different harmonics measured in the wind turbine was presented above. Different harmonic components depending of their origin and nature were analysed separately. It was observed that deterministic analysis of harmonic components caused by the external network is not possible without extensive knowledge about background distortions.

Non-characteristic harmonics (from power electronics perspective) generated by the converter such as the 5th and 7th should be analysed separately for different wind farms. Therefore additional measurements in other offshore wind farms were carried out. Additionally in two offshore wind farms (i.e. Burbo Bank Offshore Wind Farm

and Gunfleet Sands Offshore Wind Farm) measurement equipment was placed from the LV side of the wind turbine transformer. This will allow comparing results from different systems. Also in case of Avedøre Holme Offshore Wind Farm voltages and currents were measured inter alia at the LV side of the wind turbine transformer. Please note that measurements in Burbo Bank were done before the project and therefore lack of representative measurements was observable.

Earlier it was mentioned that wind turbine harmonic emission can be analysed taking into consideration harmonic dependence on output power. Therefore commonly taken approach in standards is understood. It was presented that actually grid-connected converter characteristic harmonics are strongly correlated with the wind turbine voltage. And due to the fact that wind turbine active power is controlled mainly by the angle probabilistic approach of harmonic generation can be applied. In large offshore wind farms where many wind turbines are connected together via the collection grid harmonic emission is of great uncertainty. In this case it is difficult to discuss about harmonic dependency on power production. If the number of wind turbines in an offshore wind farm is sufficiently large it is expected, according to the central limit theorem, to observe normal distribution of harmonic components [4.56]. Please note that in wind farms wind turbines are considered as only significant internal source (excluding harmonics form the grid) of harmonic components during continuous normal operation (i.e. fault free operation excluding wind turbine start-up and shutdown and other switching operations).

Figure 4.94 shows that sideband harmonic components are not dependent on both active and reactive power based on measurements from Gunfleet Sands. This approach was shown earlier in case of Burbo Bank [4.54]. Therefore it can be said that statistical analysis of harmonics in large offshore wind farms is even more needed. Earlier it was shown that baseband harmonics are even less dependent on power production therefore at the substation level the same conclusion is not surprising.

Figure 4.94 Sideband harmonic voltage at the substation dependence on radial output power.

In general it is expected that if there are many wind turbines connected to the same node their carrier group harmonics should cancel each other. This of course is truth if carrier signal phase shift in reference to synchronized command signal in different wind turbines is random and if the sum of phase angles in all wind turbines is asymptotically equal to 0. Due to this fact it is expected to observe low distortions at the substation level regarding sideband harmonic components.

Figure 4.95 shows that actually sideband harmonic components are insignificant in the wind farm internal network. This is caused by appropriately tuned wind turbine filters and also random cancellation of carrier group harmonic components in parallel-connected wind turbines. Appropriate control of carrier signals phase shift between parallel-connected converters or wind turbines can significantly limit carrier group harmonic component and in theory additional filters are not needed [4.59], [4.60]. Such operation scenario can be applied locally between only few connected devices. Therefore in large offshore wind farms this harmonic control method can be implemented in small groups of neighbouring wind turbines. On the other hand if the offshore wind farm contains sufficiently enough power generation units it can be assumed that such harmonic components will cancel each other. Carrier group harmonic cancellation aspects will be also shown later from deterministic point of view by application of double Fourier series approach.

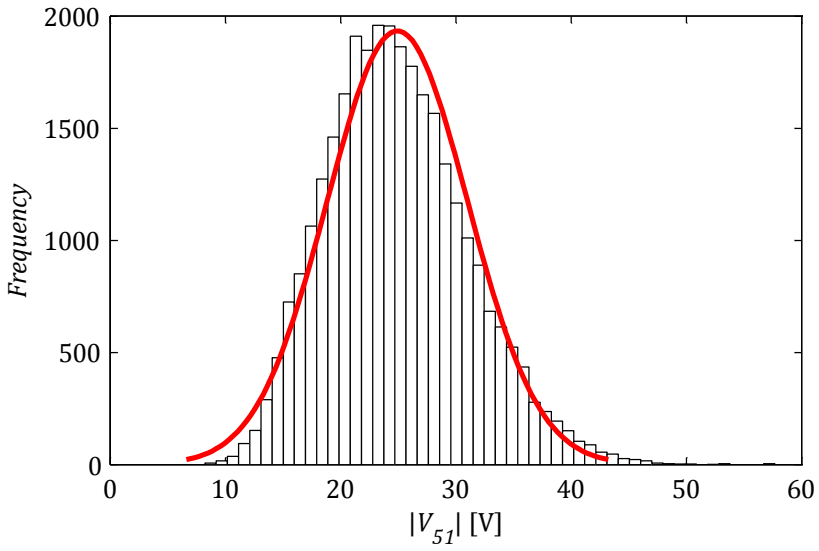

Figure 4.95 Fairly normal distribution of sideband harmonic component measured at the substation level.

Based on Figure 4.95 please note that the central limit theorem gives only an asymptotic distribution. As an approximation for a finite number of observations, it provides a reasonable approximation only close to the peak of the normal distribution; it requires a very large number of observations to stretch into the tails. Therefore one can conclude that the observed distribution of measured harmonics can be for instance log-normal as suggested in [4.54].

In the IEC standard [4.24] about measurements and assessment of power quality it is stated that it is up to the wind turbine supplier to define the wind turbine terminals to be at the LV or HV side of the transformer. Normally power quality measurements are performed at the LV because it is more convenient. It is assumed that changing the transformer from one output voltage to another is not expected to cause the wind turbine to behave differently with respect to power quality. Please note that usually Dyn type transformers are used to separate zero sequence components between the wind turbine power circuit and the wind farm collection grid.

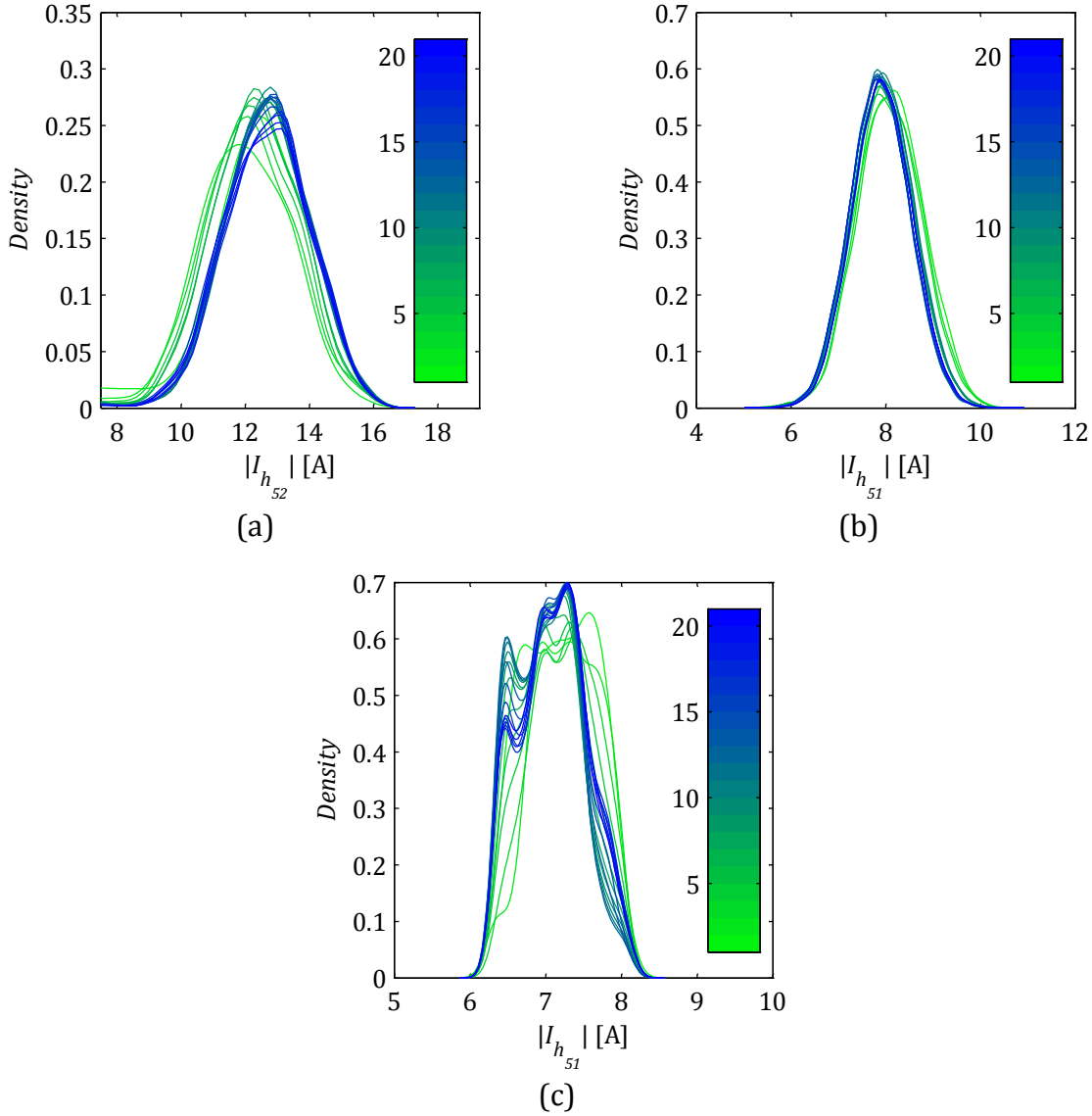

Figure 4.96 Sideband harmonic current components measured at LV side of the wind turbine (a) Burbo Bank wind turbine 38 (b) Gunfleet Sands 2 wind turbine 9 (c) Avedøre Holme wind turbine 3.

The main part of carrier group harmonic current flows through wind turbines filters. The rest of the sideband harmonic current flows from the wind turbine and is strongly affected by frequency dependent external network impedance. In large offshore wind farms it is expected that there are no significant changes in the impedance. Please note that the impedance seen from the wind turbine can vary depending on number of wind turbines connected to the grid but such changes are rather gradual. In Figure 4.96 one can see that measured sideband harmonic current tends to be normally distributed in measurements from large offshore wind farms (i.e. Burbo Bank, Gunfleet Sands) and its nature is specified even by small datasets. In contrast in Avedøre Holme, which is small offshore wind farm, sideband harmonic current is significantly affected by external network impedance variation. Please note that the same current measured at the grid-side converter AC terminals tends to be normally distributed and the sample correlation coefficient r was equal to 0.9935 (see Figure 4.73). In case of sideband

harmonic current and voltage measured at the LV side of the wind turbine transformer the sample correlation coefficient is equal only to 0.3794.

Table 4.11 Sideband harmonic current component values measured at wind turbine transformer LV terminals in different offshore wind farms.

Offshore wind farm	Wind turbine	Number of samples	Min value [A]	Max value [A]	Sample mean [A]	Sample standard deviation [A]
Avedøre Holme	03	23805	5.87	8.57	7.09	0.54
Gunfleet Sands 2	09	58701	5.02	10.92	7.93	0.68
Burbo Bank	38	4320	0.11	17.30	13.04	1.73

Additionally Table 4.11 shows that sideband harmonic current measured at both Avedøre Holme and Gunfleet Sands has comparable statistical values. The current at Burbo Bank varies more significant because the wind turbine was turned on and shutdown many times during measurements. Also the number of observations in case of Burbo Bank measurements is small but even if the dataset is so small (only 4320 minutes) it is clearly seen in Figure 4.96a that the current tends to be normally distributed.

Based on measurement (see Figure 4.96) one can see that wind turbines have different switching frequencies. It can be said as long as the modulation ratio m_f is roughly the same the harmonic components affected by the modulation technique should be comparable (i.e. comparable values of Bessel function of the first kind). Later this issue will be described more in details based on double Fourier series approach.

In case of Gunfleet Sands and Avedøre Holme the carrier signal frequency is an odd harmonic. The approach of using odd frequency ratios m_f is in relation to widely applied harmonic standards. Integer odd harmonics are more preferable than integer even harmonics. This is because the allowable emissions exported into the supply network can be higher for integer odd harmonics than for integer even harmonics [4.21].

Regarding baseband harmonics it was observed that the harmonic current measured at the LV side of the wind turbine transformer was strongly dependent on harmonic background. At first glance it can be concluded that in large offshore wind farms such high current flowing into the wind turbine should not be present. Statistical analysis of measurements from offshore wind farms also can show it.

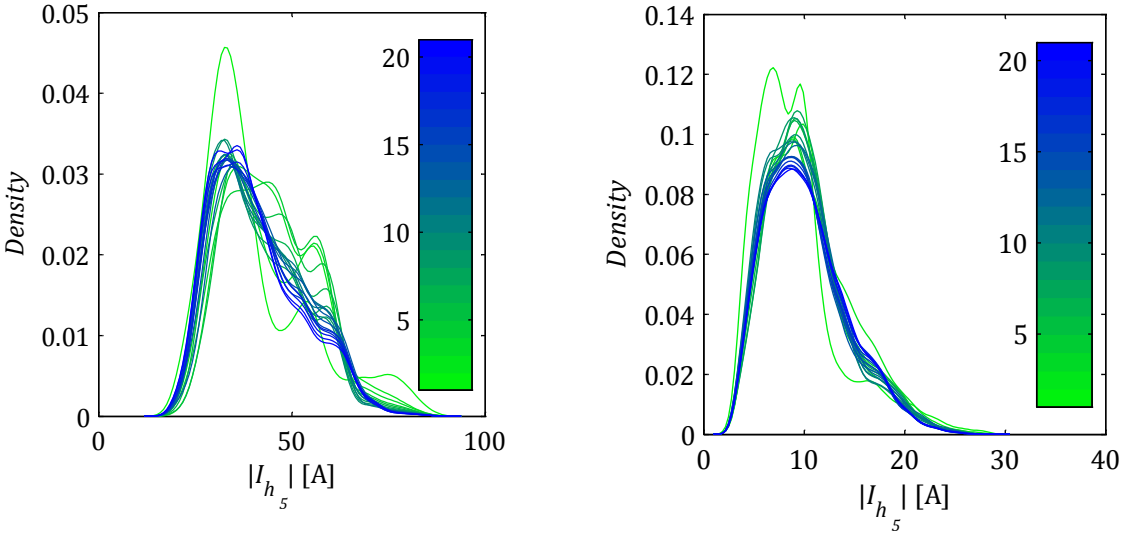

(a) (b)

Figure 4.97 Baseband harmonic measured in the wind turbine at LV side
(a) Avedøre Holme, (b) Gunfleet Sands.

From Figure 4.97 one can see that the current flow into the wind turbine at Gunfleet Sands is much lower (around four times) than measured at Avedøre Holme. It is due to the fact the background distortions seen from the wind turbine in Gunfleet Sands is also much lower. Please note that currents for one phase are provided as RMS value.

It also can be seen that the probability density function estimation from Figure 4.97 looks similar to Rayleigh distribution. Such distribution arises in the case of random complex numbers (e.g. obtained from Fourier transform) whose real and imaginary components are independently and identically distributed Gaussian $X \sim \mathcal{N}(0, \sigma^2)$ and $Y \sim \mathcal{N}(0, \sigma^2)$. In that case, the absolute value of the complex number is Rayleigh-distributed $R \sim \text{Rayleigh}(\sigma)$ where $= \sqrt{X^2 + Y^2}$ [4.56]. In this case even if the real part tends to be normally distributed unfortunately the imaginary does not in the measurements.

In Avedøre Holme harmonic analysis showed that, to some extent, harmonic emission is dependent on power production. This would mean that no harmonic current is expected when the wind turbine is not producing. In case of large offshore wind farm this assumption is not any longer valid. In large offshore wind farms with extended internal cable network wind turbines operate to compensate reactive power. Therefore sometimes even if one particular wind farm does not (or small amount) produce active power it still can produce reactive power. As described earlier, reactive power is controlled by voltage amplitude and harmonic voltage generation by wind turbines is correlated with the fundamental component. Thus extensive harmonic current flow can be measured even if the wind turbine active power production is limited.

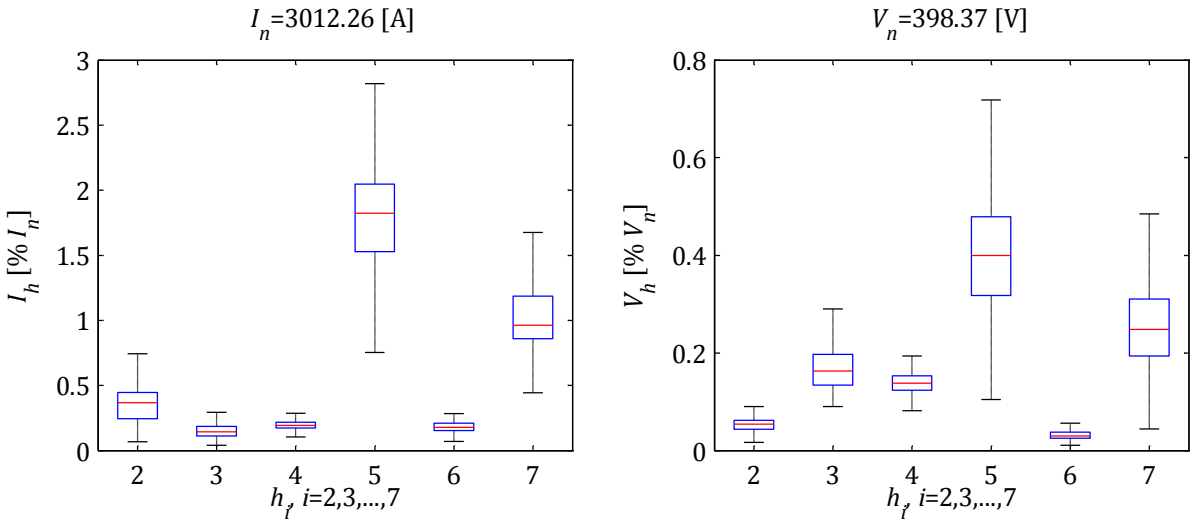

Figure 4.98 Harmonic voltage and current measured at wind turbine 38 LV terminals in Burbo Bank.

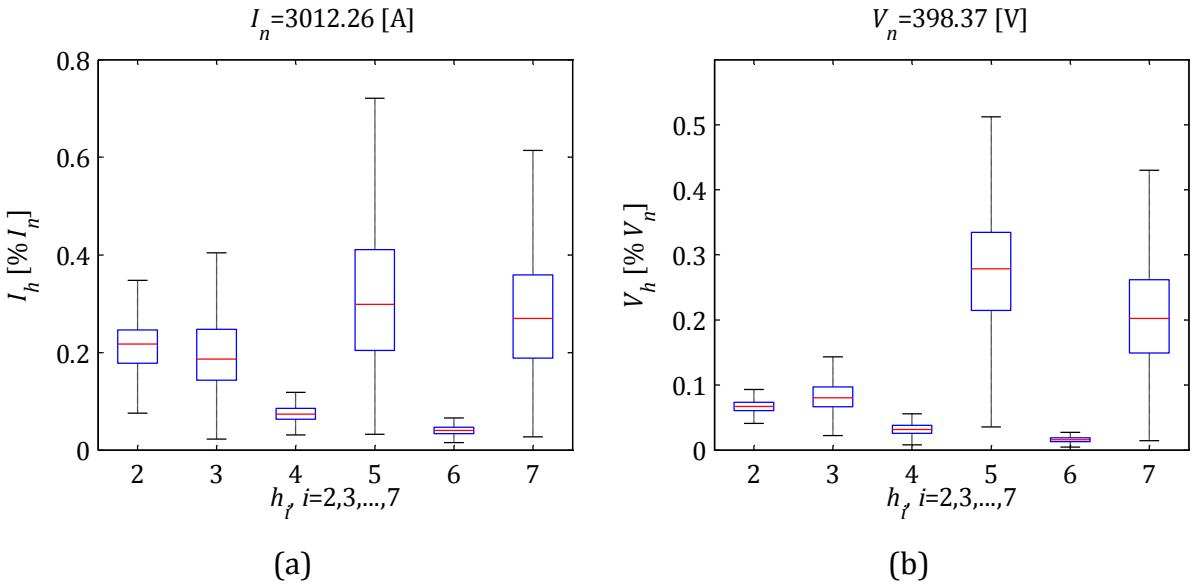

Figure 4.99 Harmonic voltage and current measured at wind turbine F9 LV terminals in Gunfleet Sands.

Harmonic current and voltage measured at each individual wind turbines comprising a small piece of large offshore wind farms are presented in Figure 4.98 and Figure 4.99. It can be seen that Burbo Bank the harmonic emission is much higher in comparison to Gunfleet Sands. The same situation exists with measurements carried out at the substation level as presented in Figure 4.100 and Figure 4.101. Please note that both offshore wind farms are approximately within the same distance from shore which is relatively small in comparison to new ongoing offshore projects. However Burbo Bank is situated near the consumption centre which can cause additional harmonic distortions. Another important factor that affects the harmonic content in Burbo Bank is the capacitor bank for reactive power compensation which was in service during measurements and could cause possible resonances.

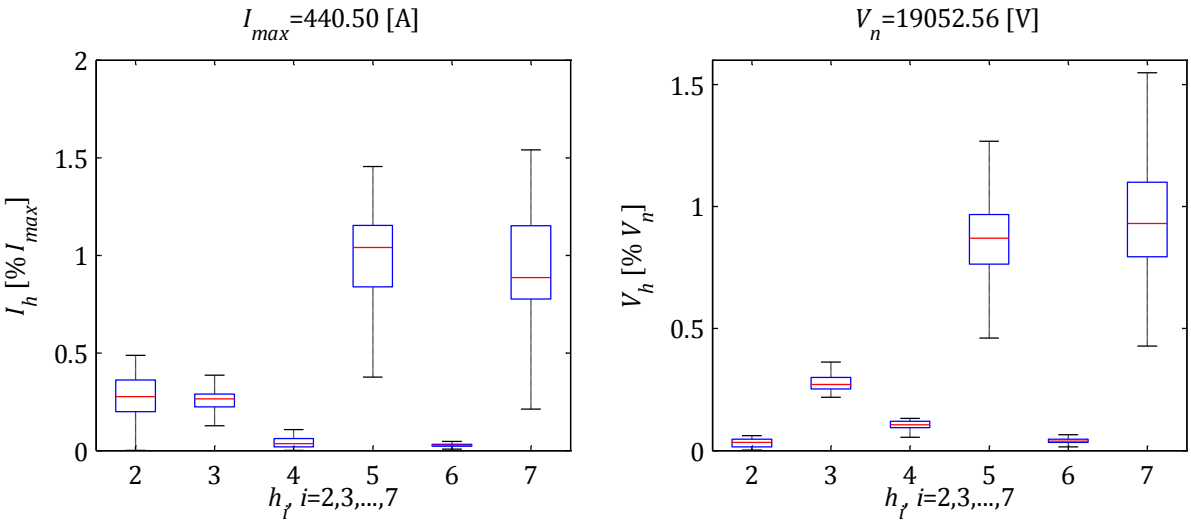

(a) (b)

Figure 4.100 Harmonic voltage and current measured at substation MV level in Burbo Bank.

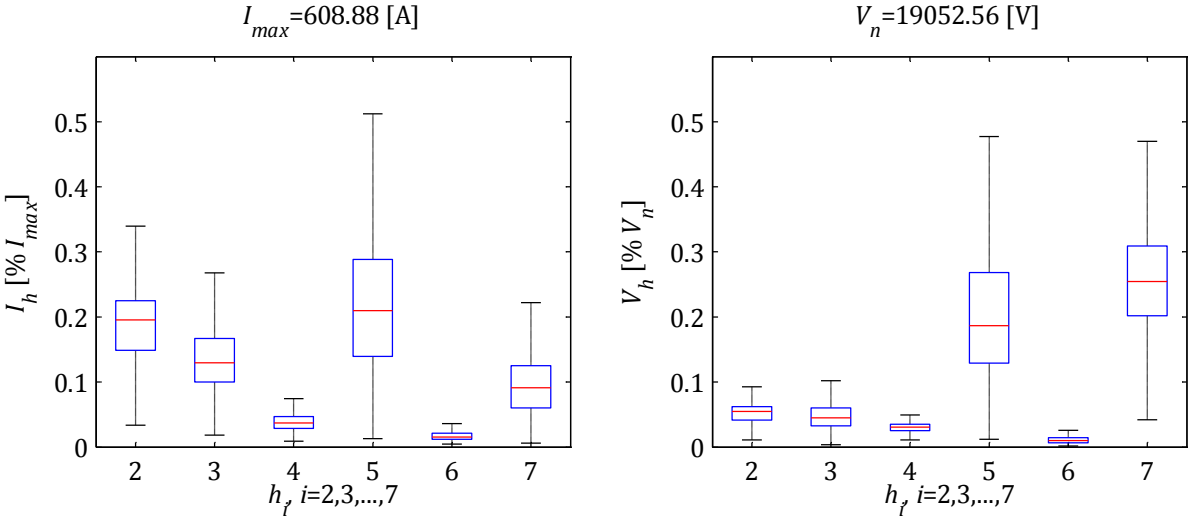

(a) (b)

Figure 4.101 Harmonic voltage and current measured at substation MV level in Gunfleet Sands.

4.2.8 SUMMARY OF STATISTICAL ANALYSIS

A comprehensive comparison of voltage and current harmonics based on probability distribution estimation and appropriate statistics calculation (e.g. mean, variance, probability density function, etc.) was presented. The results are clearly compared using solid statistical techniques and are extensively discussed. All similarities and differences are described and explained in detail.

Nonparametric probability density function estimation based on kernel smoothing for different number of observations is presented. It provides an overview if a certain harmonic distribution tends to vary depending of the dataset size. If above certain length of the measured harmonic dataset, there are no significant changes in the estimated probability density function, one can assume that the measurements

were performed long enough. Thus, analysis of the dataset would provide a good overview of the analysed system from a harmonic perspective.

Nowadays, sideband harmonic components are not emphasized enough. Baseband harmonic are nowadays mainly of interest based on traditional power system harmonic studies. However, more and more power electronic converters are installed in modern power systems. They are mainly generating harmonics due to pulse-width modulation. Such harmonic components are affected by two driven frequencies (i.e. power system fundamental frequency and carrier signal fundamental frequency). Therefore, such harmonic components can be not integer multiple of the power system fundamental frequency. Please note that wind turbines provided by different manufacturers can introduce different modulation techniques and thus different harmonic spectrum. Such diversity can affect different harmonic phenomena at higher frequency levels (e.g. the presence of frequencies below the power system fundamental in a DC-link circuit).

Actually, in separated modern power systems (e.g. offshore wind farms with internal AC network connected to the grid through a HVDC solution) with many grid-connected converters, sideband harmonic components can be more important, since baseband components' emission is limited.

An advantage of industry-oriented research is associated with dealing with real-life existing electrical systems such as wind turbines, onshore as well offshore wind farms. This creates a unique opportunity applying developed on academic level knowledge and technology directly in commercial projects. On the other hand, it helps solve real-life system problems based on academic knowledge. However, the application of methods and tools used in academia or other files of science into wind farms requires additional research and possible improvements. It is obvious that during academic research some aspects which simply exist in real existing systems might not be taken into consideration.

In order to find a good match between academic findings and their successful application in the industry appropriate validation methods should be applied. This is always strongly associated with extensive filed measurements. In order to get a good overview of harmonic phenomena in large offshore wind farms, long-term measurements need to be carried out. It is known that harmonic components can vary in time depending on different states of the system. Therefore, it is not a straightforward task to obtain form measurements' trustful information about analysed system behaviour. And here statistical tools can really be helpful to describe measured datasets and to compare different datasets (i.e. measured harmonic components) between each other (e.g. different harmonic components, different measurement points, different wind farms).

Statistical analysis allows specifying if measured period provides representative data of harmonic behaviour in the system. Nonparametric probability density function estimation based on kernel smoothing for different number of observations provides

an overview if a distribution tends to vary depending of the dataset size. If above certain length of the measured harmonic dataset, there are no significant changes in the estimated probability density function, one can assume the measurements were performed long enough. Thus, analysis of the dataset would provide a good overview of an analysed system from a harmonic perspective.

The probabilistic approach of harmonic analysis in wind farms gives supplementary information in relation to harmonic assessment recommended in standards. Except for one average value within certain power production levels, stochastic modelling also provides information about the probability of the occurrence of certain harmonic amplitudes and angles. In the standard about power quality measurements and assessment in wind turbines it is specified to measure and evaluate different harmonic levels depending on active power production. That is why it is also worth using active power to stochastically model harmonic components.

Apart from the standard, even if harmonic components generation is only a little correlated with actual active power production, it is worth developing stochastic models of different harmonic components depending on active power production. It can be seen based on measurements (see Figure 4.58) that not so often there are immediate changes in active and reactive power during wind turbine continuous normal operation. Therefore, averaging of harmonic components (due to fast Fourier transform and grouping) between measurements during full and limited production is rare in data processing. Please note that fundamental voltage amplitude is slightly correlated with active power production and strongly correlated with power converter characteristic harmonic generation. That is why distribution as presented in Figure 4.63 is not surprising. Anyway, for a sufficiently long measurement period it is expected to observe asymptotic normal distribution.

It was shown that wind turbine modelling as a harmonic current source according to measurements based on IEC standard about wind turbine power quality assessment and measurements can provide misleading understanding about wind turbine harmonic behaviour. Since most nowadays wind turbines are equipped with voltage source converters, it is better to think about converters as a harmonic voltage source. Unfortunately, harmonic voltage measured at the LV side of the wind turbine transformer is a consequence of current flowing from the grid into the wind turbine (in case of control focused on voltage quality at the grid-side converter AC terminals). Therefore, a harmonic model of wind turbines should be provided by manufacturers having extensive knowledge about their grid-side converter build (e.g. control method, modulation, possible harmonic compensation) or at least harmonic should be developed based on measurement at the ac side of the wind turbine network bridge.

Within the confines of the research project another smaller project was supervised. The issue was to evaluate possible harmonic emission at the point of common coupling

based on the Monte Carlo approach [4.54]. Within the studies it was observed that the probabilistic approach of harmonic emission in large offshore wind farms can provide a better estimation of the harmonic distortion at the point of common coupling compared to the deterministic analysis because the harmonic current magnitudes and angles are in fact described by a probability density function rather than a fixed value. Unfortunately, it was also observed that such analysis can provide satisfactory results if the external network stochastic model is known. Normally data provided by transmission system operators to wind farm developers are rather laconic. Another important aspect that must be taken into consideration is non-linear components detailed modelling. In the studies the wind turbine harmonic current model was assumed. Unfortunately, it was observed based on Avedøre Holme measurements that current emission of the wind turbine is strongly dependent on possible background distortions. Summarizing the method has great potential if the problems stated above would be solved.

4.3 SUMMARY

It was observed in this chapter that data processing plays a crucial role in overall harmonic emission evaluation. It was presented that it is of great importance to know the nature of generated harmonics in large offshore wind farms in order to apply the most suitable data processing technique. Multiresolution analysis was used in order to perform time-frequency domain analysis helpful to distinguish harmonic origin (e.g. harmonics generated by the grid-side converter or affected by the background). A non-parametric spectrum estimation was performed on interpolated signals according to detected single tone and was performed on signals without significant data processing. It was observed that cubic spline interpolation gives the most satisfactory results taking into consideration processing errors and calculation burden.

According to IEC standards, it is recommended to adjust sample rate of power quality meters according to varying power system frequency. Therefore, based on measurement results, sideband harmonic component are inappropriately estimated. One can simply conclude that for research purposes, it is better not to use commercial power quality meters and develop dedicated measurements system instead.

A bunch of different statistical tools were used in order to analyse the origin and nature of various harmonic components by sophisticated statistical analysis. It was observed that one can distinguish few different types of harmonics in measurements, i.e. DC-link harmonic content, sideband harmonic, baseband harmonic not affected by the grid, and baseband harmonic strongly affected by the grid.

DC-link harmonics are affected by slightly unbalanced voltages in the measured wind turbine and by the nature of the network bridge. Sideband harmonics are negligible dependent on the external network (i.e. short circuit impedance variation and background distortions) and contain a sufficient number of periods within the

analysed window. Therefore, it is relatively easy to analyse them and observe normal distribution according to the central limit theorem. Baseband harmonics not affected by the grid (i.e. purely generated by the converter) are also easy to analyse. However, baseband harmonics strongly affected by the grid are difficult to be analysed because the external network usually is of great uncertainty.

Baseband harmonics present in the background distortions can significantly affect the harmonic current flowing in the wind turbine. This current is of the main concern in wind turbine power quality measurement and assessment based on IEC standards. Therefore, modelling based on IEC test reports can be significantly inappropriate. It was also observed that actually power quality assessment of wind turbines should be adapted depending on assumed control strategy (e.g. with and without harmonic compensation).

On the other hand, it was observed that in large offshore wind farms harmonic content in the background does not affect significantly harmonic current flow at the wind turbine level. This additionally confirms that modelling wind turbines in large offshore wind farms cannot be performed based on current measurements of a wind turbine connected to the distribution network. Needless to say, an appropriate and trustful harmonic study requires cooperation with distribution and transmission system operators.

4.4 REFERENCES

[4.1] V. Akhmatov, J. Nygaard Nielsen, J. Thisted, E. Grøndahl, P. Egedal, M. Nørtoft Frydensbjerg, and K. Høj Jensen, "Siemens Windpower 3.6 MW Wind Turbines for Large Offshore Windfarms," in *Proc. 7th International Workshop on Large Scale Integration of Wind Power and on Transmission Networks for Offshore Wind Farms*, 26-27 May 2008, pp. 494-497.

[4.2] V. Akhmatov, "Experience with voltage control from large offshore windfarms: the Danish case," *Wind Energy*, vol. 12, no. 7, pp. 692-711, 2009.

[4.3] I. Arana, Ł. Kocewiak, J. Holbøll, C. L. Bak, A. H. Nielsen, A. Jensen, J. Hjerrild, and T. Sørensen, "How to improve the design of the electrical system in future wind power plants," in *Proc. Nordic Wind Power Conference*, Bornholm, 2009.

[4.4] A. Baggini, *Handbook of Power Quality*. Wiley and Sons, 2008.

[4.5] M. H. Bollen and I. Gu, *Signal Processing of Power Quality Disturbances*. Wiley-IEEE Press, 2006.

[4.6] "Electromagnetic compatibility (EMC) - Part 4-30: Testing and measurement techniques - Power quality measurement methods," International Electrotechnical Commission Standard IEC 61000-4-30, 2008.

[4.7] P. M. Djuric and P. M. Kay, "Spectrum Estimation and Modeling," in *Digital Signal Processing Handbook*. CRC Press, 1999, ch. 14.

[4.8] G. F. Franklin, J. D. Powell, and M. L. Workman, *Digital control of dynamic systems*, 3rd ed. Prentice-Hall, 2006.

[4.9] S. W. Smith, *The Scientist and Engineer's Guide to Digital Signal Processing*, 2nd ed. San Diego, California: California Technical Publishing, 1999.

[4.10] National Instruments, "LabVIEW Analysis Concepts," National Instruments Manual, 2004.

[4.11] T. Rikitake, R. Satō, and Y. Hagiwara, *Applied Mathematics for Earth Scientists*. Japan: Springer, 1987.

[4.12] N. R. Watson and J. Arrillaga, *Power System Harmonics*. Wiley and Sons, 2003.

[4.13] F. J. Harris, "On the use of windows for harmonic analysis with the discrete Fourier transform," in *Proceedings of the IEEE*, 1978, pp. 51-83.

[4.14] Y. Rao and M. Cerna, "System and method for estimating one or more tones in an input signal," Patent 6775629, Aug. 10, 2004.

[4.15] National Instruments, "LabVIEW 2011 Help," National Instruments Manual, 2011.

[4.16] S. C. Chapra and R. Canale, *Numerical Methods for Engineers: With Software and Programming Applications*, 6th ed. McGraw-Hill Science, 2009.

[4.17] R. A. Losada, "Digital Filters with MATLAB," The Mathworks, 2008.

[4.18] R. W. Schafer and L. R. Rabiner, "A digital signal processing approach to interpolation," *Proceedings of the IEEE*, vol. 61, no. 6, pp. 692-702, Jun. 1973.

[4.19] PSE-Operator S.A., "Transmission Grid Traffic and Maintenance Instruction," 2006.

[4.20] "Electromagnetic Compatibility (EMC) – Part 4–7: Testing and Measurement Techniques – General Guide on Harmonics and Interharmonics Measurements and Instrumentation, for Power Supply Systems and Equipment Connected Thereto," IEC 61000-4-7, August 2002.

[4.21] R. Jones, R. V. Fulcher, and E. A. Lewis, "Control Methods for Pulse Width Modulation (PWM)," Patent US 2008/00622728 A1, Mar. 13, 2008.

[4.22] M. Odavic, M. Sumner, P. Zanchetta, and J. C. Clare, "A Theoretical Analysis of the Harmonic Content of PWM Waveforms for Multiple-Frequency Modulators," *IEEE Transactions on Power Electronics*, vol. 25, no. 1, pp. 131-141, 2010.

[4.23] "Electromagnetic Compatibility (EMC) - Part 4–7: Testing and Measurement Techniques – General Guide on Harmonics and Interharmonics Measurements and Instrumentation, for Power Supply Systems and Equipment Connected Thereto," International Electrotechnical Commission Standard IEC 61000-4-7, 2002.

[4.24] "Wind turbines - Part 21: Measurement and assessment of power quality characteristics of grid connected wind turbines," International Electrotechnical Commission Standard IEC 61400-21, 2008.

[4.25] S. T. Tentzerakis, N. Paraskevopoulou, S. A. Papathanassiou, and P. Papadopoulos, "Measurement of wind farm harmonic emissions," in *Proc. IEEE Power Electronics Specialists Conference*, 15-19 June 2008, pp. 1769-1775.

[4.26] P. Nisenblat, A. M. Broshi, and O. Efrati, "Methods of compressing values of a monitored electrical power signal," U.S. Patent 7,415,370 B2, Aug. 19, 2008.

[4.27] C. Gasquet and P. Witomski, *Fourier analysis and applications: filtering, numerical computation, wavelets*, 1st ed. New York: Springer-Verlag, 1999.

[4.28] C. Torrence and G. P. Compo, "A Practical Guide to Wavelet Analysis," *Bulletin of the American Meteorological Society*, vol. 79, pp. 61-78, 1998.

[4.29] C. L. Liu, "A Tutorial of the Wavelet Transform," National Taiwan University Tutorial, 2010.

[4.30] Y. Meyer, *Wavelets and Operators, Volume 1*. New York, United States of America: Cambridge University Press, 1995.

[4.31] J. A. Rice, *Mathematical statistics and data analysis*, 3rd ed. Duxbury Press, 2007.

[4.32] P. Billingsley, *Probability and Measure*, 3rd ed. John Wiley and Sons, 1995.

[4.33] P. J. Brockwell and R. A. Davis, *Introduction to Time Series and Forecasting*. New York: Springer-Verlag, 2002.

[4.34] M. B. Priestley, *Spectral Analysis and Time Series*. Academic Press, 1981.

[4.35] J. S. Bendat and A. G. Piersol, *Preview Random Data: Analysis and Measurement Procedures*, 4th ed. New Jersey: John Wiley & Sons, 2010.

[4.36] T. Chau, D. Chau, M. Casas, G. Berall, and D. J. Kenny, "Investigating the stationarity of paediatric aspiration signals," *Transactions on Neural Systems and Rehabilitation Engineering*, vol. 13, no. 1, pp. 99-105, Mar. 2005.

[4.37] J. O. Smith, *Introduction to Digital Filters with Audio Applications*. W3K Publishing, 2007.

[4.38] D. G. Holmes and T. A. Lipo, *Pulse Width Modulation for Power Converters: Principles and Practice*. IEEE Press, 2003.

[4.39] S. Frühwirth-Schnatter, *Finite Mixture and Markov Switching Models*. Springer, 2006.

[4.40] A. P. Dempster, N. M. Laird, and D. B. Rubin, "Maximum likelihood from incomplete data wia the EM algorithm," *Journal of the Royal Statistical Society*, vol. 39, no. 1, pp. 1-22, 1977.

[4.41] A. Morales, X. Robe, and M. J. C, "Assessment of Wind Power Quality: Implementation of IEC61400-21 Procedures," in *International Conference on Renewable Energy and Power Quality*, Zaragoza, 2005, pp. 1-7.

[4.42] H. Emanuel, M. Schellschmidt, S. Wachtel, and S. Adloff, "Power quality measurements of wind energy converters with full-scale converter according to IEC 61400-21," in *International Conference on Electrical Power Quality and Utilisation*, Lodz, 2009, pp. 1-7.

[4.43] A. W. Bowman and A. Azzalini, *Applied Smoothing Techniques for Data Analysis*. New York: Oxford University Press, 1997.

[4.44] R. M. Feldman and C. Valdez-Flores, *Applied Probability and Stochastic Processes*, 2nd ed. Springer, 2010.

[4.45] A. Bera and C. Jarque, "Efficient tests for normality, heteroskedasticity and serial independence of regression residuals: Monte Carlo evidence," *Economics Letter*, vol. 7, p. 313–318, 1981.

[4.46] G. Brys, M. Hubert, and A. Struyf, "A robustification of the Jarque-Bera test of normality," in *Computational Statistics*, Prague, 2004, pp. 753-760.

[4.47] H. Lilliefors, "On the Kolmogorov-Smirnov test for normality with mean and variance unknown," *Journal of the American Statistical Association*, no. 62, pp.

399-402, 1967.

[4.48] M. Hollander and D. A. Wolfe, *Nonparametric Statistical Methods*, 2nd ed. New York, United States of America: John Wiley & Sons, 1999.

[4.49] M. Matsumoto and T. Nishimura, "Mersenne twister: a 623-dimensionally equidistributed uniform pseudo-random number generator," *ACM Transactions on Modeling and Computer Simulation*, vol. 8, no. 1, pp. 3-30, 1998.

[4.50] S. Tentzerakis, S. Papathanassiou, P. Papadopoulos, D. Foussekis, and P. Vionis, "Evaluation of Wind Farm Harmonic Emissions," in *Proc. European Wind Energy Conference*, Milan, 2007.

[4.51] Alstom, "ALSPA MV3000 DC Link Inductors," ALSTOM Power Conversion Instruction Sheet, 1999.

[4.52] P. Salmerón, R. S. Herrera, A. Pérez, and J. Prieto, "Distortion and Unbalance Assessing Indices Using Commercial Analysers," in *International Conference on Renewable Energies and Power Quality*, Zaragoza, 2005.

[4.53] M. H. Rashid, *Power Electronics Handbook*, 2nd ed. San Diego, California, United States of America: Elsevier, 2007.

[4.54] C. F. Jensen, C. L. Bak, Ł. Kocewiak, J. Hjerrild, and K. K. Berthelsen, "Probabilistic Aspects of Harmonic Emission of Large Offshore Wind Farms," in *International Workshop on Large-Scale Integration of Wind Power into Power Systems as well as on Transmission Networks for Offshore Wind Power Plants*, Aarhus, 2011, pp. 699-703.

[4.55] S. T. Tentzerakis and S. A. Papathanassiou, "An Investigation of the Harmonic Emissions of Wind Turbines," *IEEE Trans. Energy Conversion*, vol. 22, pp. 150-158, Mar. 2007.

[4.56] L. Sainz, J. J. Mesas, R. Teodorescu, and P. Rodriguez, "Deterministic and Stochastic Study of Wind Farm Harmonic Currents," *IEEE Transactions on Energy Conversion*, vol. 25, no. 4, pp. 1071-1080, Dec. 2010.

[4.57] S. Wei, N. Zargari, B. Wu, and S. Rizzo, "Comparison and mitigation of common mode voltage in power converter topologies," in *Industry Applications Conference*, Toronto, 2004, pp. 1852-1857.

[4.58] D. C. Hoaglin, F. Mosteller, and J. W. Tukey, *Understanding robust and exploratory data analysis*. John Wiley and Sons, 1983.

[4.59] J. Birk and B. Andresen, "Parallel-connected converters for optimum reliability and grid performance in the Gamesa G10X 4.5 MW wind turbine," in *European Wind Energy Conference*, Brussels, 2008.

[4.60] R. Jones, R. V. Fulcher, and H. Stiesdal, "Control methods for the synchronization and phase shift of the pulse width modulation (PWM) strategy of power converters.," Patent US 2008/0284252 A1, Nov. 20, 2008.

Chapter 5
WIND FARM MODELLING

Wind turbine and wind farm model development is a complex process comprising different wind farm components modelling in various domains such as time, frequency, and harmonic depending on approach and application. This chapter is dedicated to wind farm frequency domain description including various aggregation techniques as well as deep wind turbine modelling taking special care of the grid-side converter. Numerical and analytical models are compared with measurement data.

5.1 WIND FARM AGGREGATION TECHNIQUES

Many wind farm aggregation techniques are developed depending on application. Some aggregated models were presented in [5.1] for grid disturbances studies, or to represent a collective behaviour in [5.2] for large power systems simulations, as well as represent the whole power system seen from wind turbine AC terminal [5.3].

This section provides some guidelines for the representation of the wind farm system used in models intended for low frequency stability analysis within the grid-side converter control bandwidth of wind turbines. The guidelines presented are solely based on the experiences gained on earlier DONG Energy projects and based on continuous cooperation with different wind turbine manufacturers. Therefore it is not guaranteed that these guidelines apply on every analysed wind power system. Some limitations caused by different aggregation techniques will be emphasized based on the obtained results and compared.

The model of aggregated collection grid and the external network can later be used for wind turbine stability assessment purposes for every specific analysed system. The analysis is carried out in the frequency domain taking into consideration different wind farm internal network as well external network configurations. The gain, vector gain and phase margins are normally presented and evaluated in order to assess stability of wind farms with particular wind turbine converter control method. The analysis should be performed within the control system bandwidth which normally

(depending on analysed control) is not higher than Nyquist frequency of sampled command signal.

In order to accurately express the whole analysed wind power system there is a necessity to model each of wind farm components as well as the external network. From DONG Energy's experience the external network model is normally provided by either the transmission system operator or the distribution system operator. This is done based on extensive knowledge about the system which in many cases is not available for both wind farm developer as well as wind turbine manufacturer. Therefore really close cooperation between all three parties (i.e. transmission system operator distribution network operator, wind farm developer, and wind turbine manufacturer) is needed. Normally the model of external network for frequency domain studies is in form of frequency response of the network seen from wind farm connection point. Due to the fact that it is difficult (or even impossible) to describe the whole system by means of one frequency dependent characteristic and thus different study cases are taken into consideration. In industrial cases sometimes also impedance plots as performance loci (i.e. areas presented in the complex plane for different frequencies) are used.

All internal components of the analysed wind farm can be modelled based on details provided by manufacturers. Unfortunately in many cases such data are insufficient for detailed modelling. However usually detailed models do not contribute significantly into the results for frequency range of interest specified for harmonic studies. There are many well developed low-frequency models of wind farm components such as transformers, reactors, cables which are broadly described in [5.4], [5.5], [5.6]. Description of models is not going to be presented in this report because no scientific contribution was provided within the confines of this project.

During wind farm aggregation process it was observed that some simplifications in skin effect modelling can be obtained based on the identities of the Bessel function of the first kind. Therefore it was possible to obtain a closed form solution of frequency dependent impedance of round conductors. This is of course a minor part of cable modelling but it was decided to put it here because it might be helpful in other research projects concerning, for instance, only in underground cable modelling.

5.1.1 IMPEDANCE OF ROUND CONDUCTORS

Please note that cable modelling is a complex process and still there is a place for research within this area. Different high-frequency modelling approaches should be taken in case of single-phase underground cables [5.7] and for three-phase submarine cables where such phenomena as proximity effect is more significant [5.8]. Different effects in advanced modelling such as skin effect, proximity effect, earth return path impedance, etc.

It was decided to include some aspects of skin effect modelling into the report because the author provided a few simplifications and the closed form solution which was not seen earlier (Eq. 5.6). The internal impedance (i.e. resistance and contribution to reactance from magnetic flux inside the wire) of cable conductors is affected by non-uniform current distribution. This phenomenon is often called skin effect. According to [5.9] the internal impedance per unit length [Ω/m] of conductors with circular cross section can be expressed

$$Z_i = -\frac{TJ_0(Tr_0)}{2\pi r_0 \sigma J_0'(Tr_0)} \tag{5.1}$$

where $T^2 = -j\omega\mu\sigma$, r_0 is the wire radius in [m] and $\omega = 2\pi f$ is the angular frequency in [rad/s], μ is permeability in [H/m], and σ is conductivity in [S/m]. To interpret Eq. 5.1 for any frequency of interest, it is useful to break the zero order Bessel function of the first kind J_0 for complex arguments $\xi \in \mathbb{C}$ into real and imaginary parts in the following way

$$\mathrm{Ber}(\xi) + j\mathrm{Bei}(\xi) = J_0\left(j^{-\frac{1}{2}}\xi\right)$$

$$\mathrm{Ber}'(\xi) + j\mathrm{Bei}'(z) = \frac{d}{d\xi}\left(\mathrm{Ber}(\xi) + j\mathrm{Bei}(\xi)\right) = j^{-\frac{1}{2}}J_0'\left(j^{-\frac{1}{2}}\xi\right)$$

Then Eq. 5.1 can be written

$$Z_i = R_i + j\omega L_i = \frac{jR_s}{\sqrt{2}\pi r_0}\left[\frac{\mathrm{Ber}(q) + j\mathrm{Bei}(q)}{\mathrm{Ber}'(q) + j\mathrm{Bei}'(q)}\right]$$

where

$$R_s = \frac{1}{\sigma\delta} = \sqrt{\frac{\pi f\mu}{\sigma}}, q = \frac{\sqrt{2}r_0}{\delta}.$$

and δ in [m] is called the depth of penetration or skin depth and is expresses in the following way

$$\delta = \frac{1}{\sqrt{\pi f\mu\sigma}}.$$

And now the real and imaginary part of the conductor internal impedance

$$\mathrm{Re}\{Z_i\} = R_i = \frac{R_s}{\sqrt{2}\pi r_0}\left[\frac{\mathrm{Ber}(q)\mathrm{Bei}'(q) - \mathrm{Bei}(q)\mathrm{Ber}'(q)}{\left(\mathrm{Ber}'(q)\right)^2 + \left(\mathrm{Bei}'(q)\right)^2}\right] \tag{5.2}$$

$$\mathrm{Im}\{Z_i\} = \omega L_i = \frac{R_s}{\sqrt{2}\pi r_0}\left[\frac{\mathrm{Ber}(q)\mathrm{Ber}'(q) + \mathrm{Bei}(q)\mathrm{Bei}'(q)}{\left(\mathrm{Ber}'(q)\right)^2 + \left(\mathrm{Bei}'(q)\right)^2}\right] \tag{5.3}$$

Eq. 5.2 and Eq. 5.3 are the expressions for resistance and internal reactance of a round conductor at any frequency in terms of parameter q.

Knowing that for any integer and non-integer parameter $\alpha \in \mathbb{R}$ and $n \in \mathbb{R}$

$$J_n'(\alpha\xi) = \frac{\alpha}{2}[J_{n-1}(\alpha\xi) - J_{n+1}(\alpha\xi)] \tag{5.4}$$

$$J_n^{(i)}(\alpha\xi) = \frac{\alpha}{2}\left[J_{n-1}^{(i-1)}(\alpha\xi) - J_{n+1}^{(i-1)}(\alpha\xi)\right]$$

Eq. 5.1 can be expressed in terms of frequency dependent parameter $Q = r_0 T$

$$Z_i(Q) = -\frac{TJ_0(Q)}{\pi r_0 \sigma[J_{-1}(Q) - J_1(Q)]}$$

Applying the following identity

$$J_{-n}(\xi) = (-1)^n J_n(\xi). \tag{5.5}$$

one can finally obtain

$$Z_i(Q) = \frac{TJ_0(Q)}{2\pi r_0 \sigma J_1(Q)} \tag{5.6}$$

According to [5.10] and [5.5] the Bessel function of the first kind can be approximated by an infinite series

$$\mathrm{Ber}(q) = 1 - \frac{q^4}{2^2 4^2} + \frac{q^8}{2^2 4^3 6^2 8^2} - \cdots, \tag{5.7}$$

$$\mathrm{Bei}(q) = \frac{q^2}{2^2} - \frac{q^6}{2^2 4^2 6^2} + \frac{q^{10}}{2^2 4^3 6^2 8^2 10^2} - \cdots. \tag{5.8}$$

In practical calculations the use of infinite series is not convenient. Also truncation errors provide significant inaccuracy. Derived analytical solution from Eq. 5.6 provides exact values of resistance and inductance for any frequency of interest. The solution allows avoiding numerical calculation of Bessel function derivative. The identity from Eq. 5.5 uses even and odd properties of Bessel function of the first kind and the identity from Eq. 5.4 which states that the derivative of any order n of Bessel function of the first kind is related with Bessel functions of order $n \pm 1$. Application of identities provides a closed-from generic solution of impedance in cable with circular cross section which is easy to implement and free of truncation errors.

The above presented analytical investigation of skin effect was implemented and compared. An exemplary frequency dependent impedance of aluminium conductor in power cables ($r_0 = 0.0087$ m, $\mu_0 = 4\pi \cdot 10^{-7}$ H/m, $\mu_R = 1.000022$, $\sigma = 3.5461 \cdot 10^7$ S/m) was calculated. The results of calculation of the internal inductance L_i and resistance R_i, performed for trunked approximation of Bessel function of the first

kind up to three terms and for generic analytical closed-form solution, are shown in Figure 5.1.

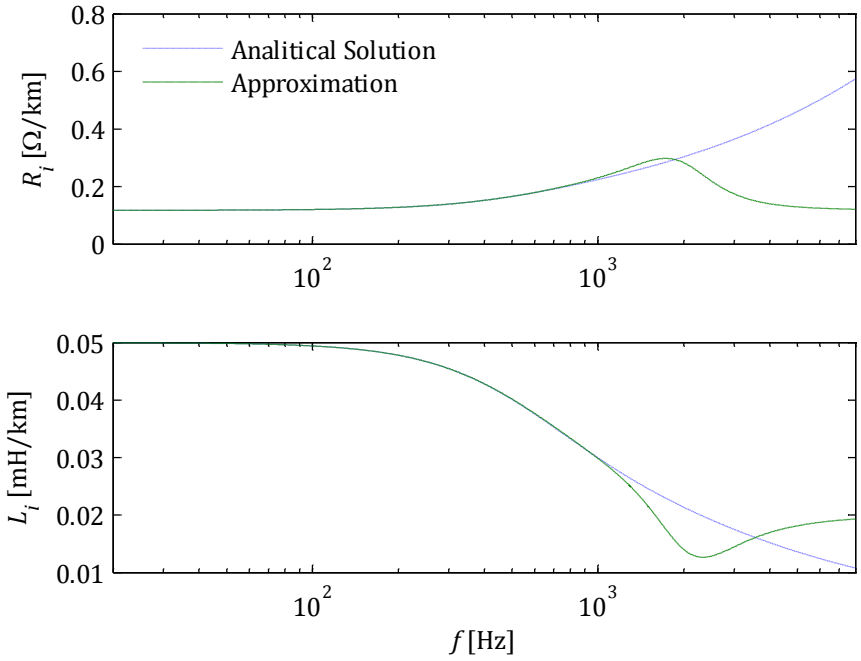

Figure 5.1 Internal resistance and inductance per unit calculated from trunked approximation of the Bessel function of the first kind and from analytical closed-form solution.

As seen from Figure 5.1 the results from approximation significantly vary within frequencies of interest for harmonic analysis which is assumed to be up to 5 kHz. Of course approximations with higher number of terms will give more accurate results. Based on this example one can see that the impedance within the range below 1000 Hz gives in both cases satisfactory results. Therefore the way of calculating internal impedance for application such as baseband harmonic components assessment of tuning converter controllers does not affect significantly the final outcome.

As an alternative approach to the presented analytical calculations is often a simple approximation by means of correction factors used by different power companies. Exemplary correction factors used by National Grid Company (NGC) in the UK and Électricité de France (EDF) are presented below [5.4]

Company	Voltage level	Harmonic order	Resistance
NGC	132 kV	$h \geq 2.35$	$R_1\left(0.187 + 0.532\sqrt{h}\right)$
EDF	150 kV, 90 kV	$h \geq 2$	$R_1\left(0.187 + 0.532\sqrt{h}\right)$

5.1.2 MV COLLECTION GRID AGGREGATION

The wind farm MV collector system consists of a certain number of radials (M), where a certain number of wind turbines (N) are connected as presented in schematic diagram

in Figure 5.2. In order to simplify the system for different studies, an aggregation of the MV network should be lumped by one single equivalent (e.g. T-model, Π-model or equivalent Π-model [5.4]) circuit, connecting wind turbines with the HV transmission system. The choice of MV cable models is dependent on many aspects described before such as cable length, assumed accuracy, and calculation burden. Different wind farm internal network aggregation methods have been presented [5.2], [5.1]since wind farms were an issue in modern power system. Aggregation procedure is dependent on model application (e.g. load flow calculations, stability assessment).

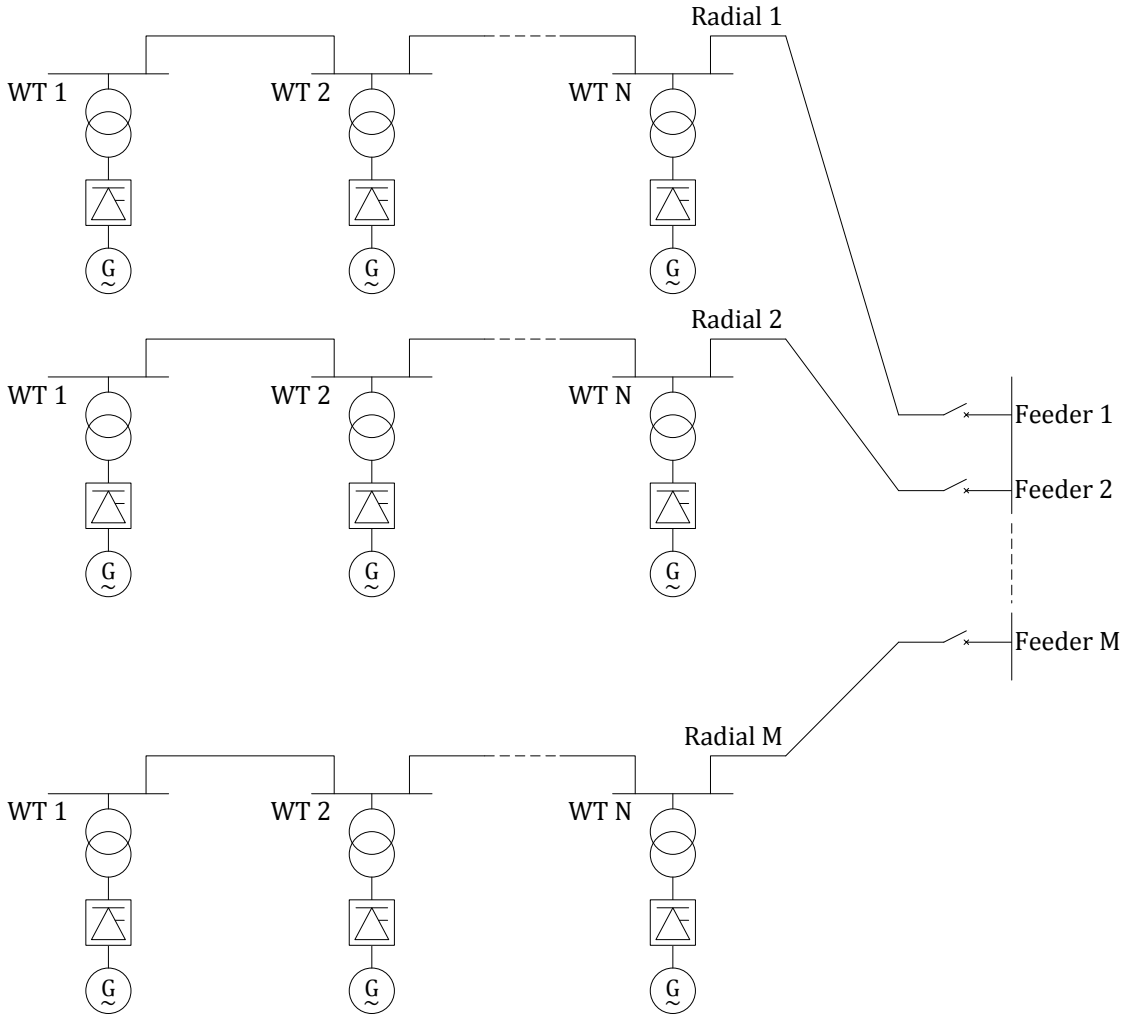

Figure 5.2 Typical MV cable collector system of wind farms.

As it can be seen in Figure 5.2, wind turbines are distributed over each radial and therefore each cable in the MV radial is not transporting the same amount of current from the wind turbines. This difference should be taken into account in the MV radial equivalent circuit calculation. Because the length between wind various wind turbines as well as type of cables can vary, the aggregation procedure is more complex and results from various aggregation techniques may be different. However it is possible to calculate impedance Z_{eq_m} for the m-th MV radial. Z_{eq_m} is the equivalent

impedance for the m-th radial, which takes into account the placement of the wind turbines on the radial and consequently the current distribution in the radial.

5.1.2.1 AGGREGATION BASED ON VOLTAGE DROP

For stability assessment studies such as presented in [5.11], the most appropriate aggregation method is based on voltage drop assumptions. Wind turbine stability study concerns grid-side converter control frequency response and its interaction with the system impedance seen from the converter AC terminals. Nowadays normally control methods are based on fast current control loop to which current measurements are fed and voltage reference is obtained. From this perspective the input value of the plant (i.e. wind farm system aggregated impedance) is voltage from the controller and current is an output value. The transfer function of the plant is simply an admittance obtained from aggregation.

Radial equivalent impedance

Let us consider the system presented in Figure 5.2. The system comprises M radials with N_m wind turbines connected to the m-th radial. Under the assumption that the current injection from every single wind turbine is the same, the current at every radial can be expressed as

$$I_m = \sum_{n_m=1}^{N_m} I_{n_m}, m = 1,2, \dots, M \tag{5.9}$$

where m is the respective radial number and I_{n_m} is the current generated from the n-th wind turbine in the m-th radial. The equivalent impedance Z_{eq_m} of respective radials can be obtained

$$I_m Z_{eq_m} = \sum_{n_m=1}^{N_m} n_m \frac{I_m}{N_m} Z_{n_m} = \frac{1}{N_m} \sum_{n_m=1}^{N_m} n_m I_m Z_{n_m}$$

and therefore

$$Z_{eq_m} = \sum_{n_m=1}^{N_m} \frac{n_m}{N_m} Z_{n_m} = \frac{1}{N_m} \sum_{n_m=1}^{N_m} n_m Z_{n_m} \tag{5.10}$$

and Z_{n_m} is the cable impedance between n-th and $(n+1)$-th wind turbine situated in the m-th radial.

Overall aggregated impedance

The different radials can be reduced to one equivalent by parallel connection of the different radials impedances Z_{eq_m} and the MV collector system equivalent impedance can be calculated

$$Z_{MV} = \frac{1}{\sum_{m=1}^{M} \frac{1}{Z_{eq_m}}} \tag{5.11}$$

Capacitance calculation

The capacitance of the different MV radials is simply added together because they only vary with voltage and the voltage can be regarded as uniform in the MV collector system

$$C_{MV} = \sum_{n_1=1}^{N_1} C_{n_1} + \sum_{n_2=1}^{N_2} C_{n_2} + \cdots + \sum_{n_M=1}^{N_M} C_{n_M} \tag{5.12}$$

where C_{n_m} is the cable shunt capacitance between n-th and $(n+1)$-th wind turbine situated in the m-the radial.

5.1.2.2 FULL WIND FARM AGGREGATION BASED ON POWER LOSSES

This approach is commonly used in case of load-flow studies as well as electromechanical (RMS) stability and successfully was applied in many real-life wind farm projects.

Radial equivalent impedance

Let us again consider the system presented in Figure 5.2. The system comprises M radials with N_m wind turbines connected to every m-th radial. Under the assumption that the current injection from every single wind turbine is the same (e.g. full power production), the total current at the point of common coupling can be expressed as

$$I_{PCC} = I_{total} = \sum_{m=1}^{M} \sum_{n_m=1}^{N_m} I_{n_m} \tag{5.13}$$

where m is the respective radial number and I_{n_m} is the current generated from the n-th wind turbine in the m-th radial. The equivalent impedance Z_{eq_m} of respective radials can be obtained

$$I_{total}^2 Z_{eq_m} = \sum_{n_m=1}^{N_m} \left(n_m \frac{I_{PCC}}{N_{total}} \right)^2 Z_{n_m}$$

$$Z_{eq_m} = \sum_{n_m=1}^{N_m} \left(\frac{n_m}{N_{total}} \right)^2 Z_{n_m} = \frac{1}{N_{total}^2} \sum_{n_m=1}^{N_m} n_m^2 Z_{n_m} \tag{5.14}$$

and Z_{n_m} is the cable impedance between n-th and $(n+1)$-th wind turbine situated in the m-th radial. The total number of wind turbines in the whole analysed wind farm is N_{total}.

Overall aggregated impedance

The different radials can be reduced to one equivalent impedance by sum of impedances from different radials which can be expressed in the following way

$$Z_{MV} = \left(\frac{N_1}{\sum_{m=1}^{M} N_m}\right)^2 Z_{eq_1} + \left(\frac{N_2}{\sum_{m=1}^{M} N_m}\right)^2 Z_{eq_2} + \cdots + \left(\frac{N_M}{\sum_{m=1}^{M} N_m}\right)^2 Z_{eq_M} \quad 5.15$$

Capacitance calculation

The same as in case of MV network aggregation based on voltage drop the capacitance of the different MV radials is simply added together because they only vary with voltage and the voltage can be regarded as uniform in the MV collector system.

$$C_{MV} = \sum_{n_1=1}^{N_1} C_{n_1} + \sum_{n_2=1}^{N_2} C_{n_2} + \cdots + \sum_{n_M=1}^{N_M} C_{n_M} \quad 5.16$$

where C_{n_m} is the cable shunt capacitance between n-th and (n + 1)-th wind turbine situated in the m-the radial.

5.1.2.3 RADIAL AGGREGATION BASED ON POWER LOSSES

Another approach based on power losses similar to presented above is to aggregate separately each of radials within analysed wind farm and later consider equivalent impedances as parallel connected to the same point of common coupling. The aggregation outcome will of course give slightly different impedance values.

Radial equivalent impedance

Once again let us consider the system presented in Figure 5.2. The system comprises M radials with N_m wind turbines connected to every m-th radial. Under the assumption that the current injection from every single wind turbine is the same, the total current of each radial (not at the point of common coupling as before) can be expressed as

$$I_{m_{total}} = \sum_{n_m=1}^{N_m} I_{n_m}, m = 1,2, \dots, M \quad 5.17$$

where m is the respective radial number and I_{n_m} is the current generated from the n-th wind turbine in the m-th radial. The equivalent impedance Z_{eq_m} of respective radials can be obtained

$$I_{m_{total}}^2 Z_{eq_m} = \sum_{n_m=1}^{N_m} \left(n_m \frac{I_{m_{total}}}{N_{m_{total}}}\right)^2 Z_{n_m}$$

$$Z_{eq_m} = \sum_{n_m=1}^{N_m} \left(\frac{n_m}{N_{m_{total}}} \right)^2 Z_{n_m} = \frac{1}{N_{m_{total}}^2} \sum_{n_m=1}^{N_m} n_m^2 Z_{n_m} \qquad 5.18$$

and Z_{n_m} is the cable impedance between n-th and $(n+1)$-th wind turbine situated in the m-th radial. This time $N_{m_{total}}$ is the total number of wind turbines connected within m-th radial.

Overall aggregated impedance

And now different radials can be reduced to one equivalent by parallel connection of the different radials impedances. Finally the MV collector system equivalent impedance can be calculated

$$Z_{MV} = \frac{1}{\sum_{m=1}^{M} \frac{1}{Z_{eq_m}}} \qquad 5.19$$

Capacitance calculation

Once again as in all previous cases the capacitance of all MV radials is simply added together because it only vary with voltage and the voltage can be regarded as uniform in the MV collector system.

$$C_{MV} = \sum_{n_1=1}^{N_1} C_{n_1} + \sum_{n_2=1}^{N_2} C_{n_2} + \cdots + \sum_{n_M=1}^{N_M} C_{n_M} = \sum_{m=1}^{M} \sum_{n_m=1}^{N_m} C_{n_m} \qquad 5.20$$

where C_{n_m} is the cable shunt capacitance between n-th and $(n+1)$-th wind turbine situated in the m-the radial.

5.1.3 KARNICE WIND FARM NETWORK AGGREGATION

The presented above internal MV network aggregation methods as well as different models now can be applied to real-life wind farms. This approach can be successfully applied for stability studies for different frequencies in onshore as well as offshore wind farms. Slightly different approach can be assumed in case of load flow calculations [5.3].

Figure 5.3 Horns Rev 2 and Karnice wind farms location.

5.1.3.1 KARNICE WIND FARM DESCRIPTION

The onshore wind farm is located in Karnice Commune in the north-western part of Poland, just 5 kilometres from the Baltic Sea. The wind farm went into operation in early 2010 and consists of 13 Siemens wind turbines each with a capacity of 2.3 MW. The wind farm is expected to produce 90,000 MWh every year, corresponding to the power consumption of 45,000 households. DONG Energy is the sole owner of the wind farm. The primary use of the area is agriculture. DONG Energy is already operator of the nearby Lake Ostrowo Wind Farm, a wind farm with a total capacity of 31 MW and was commissioned in 2007, and the nearby Karcino Wind Farm, a wind farm with a total capacity of 50 MW and was commissioned at the same time as the Karnice Wind Farm (see Figure 5.4).

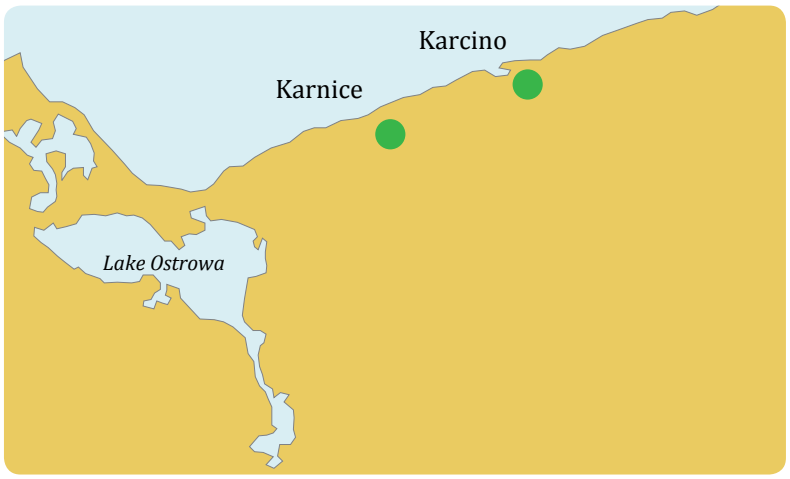

Figure 5.4 Location of Karnice Wind Farm and Karcino Wind Farm.

The Karnice wind farm (see Figure 5.3) comprises of 13 SWT-2.3-93 wind turbines with a capacity of 2.3 MW each. The farm is connected to the 110 kV Trzebiatów–Niechorze line through a 110/20 kV transformer with a capacity of 31.5 MVA located in the wind farm area. Therefore, the farm's point of connection to the National Power System (NPS) is the 110 kV bus system. The turbines are connected to 20 kV Main Supply Point (MSP) Skrobotowo switching station with three cable lines. The connections between particular turbines as well as the turbines and the MSP are made of XRUHAKXS 12/20 kV 120 and 240 mm² cables. The overall structure of the wind farm is presented in Figure 5.5. The wind turbines (SWT-2.3-90) organized in the MV internal network of 20 kV voltage level four feeders. The layout is almost symmetrical which significantly simplifies calculations.

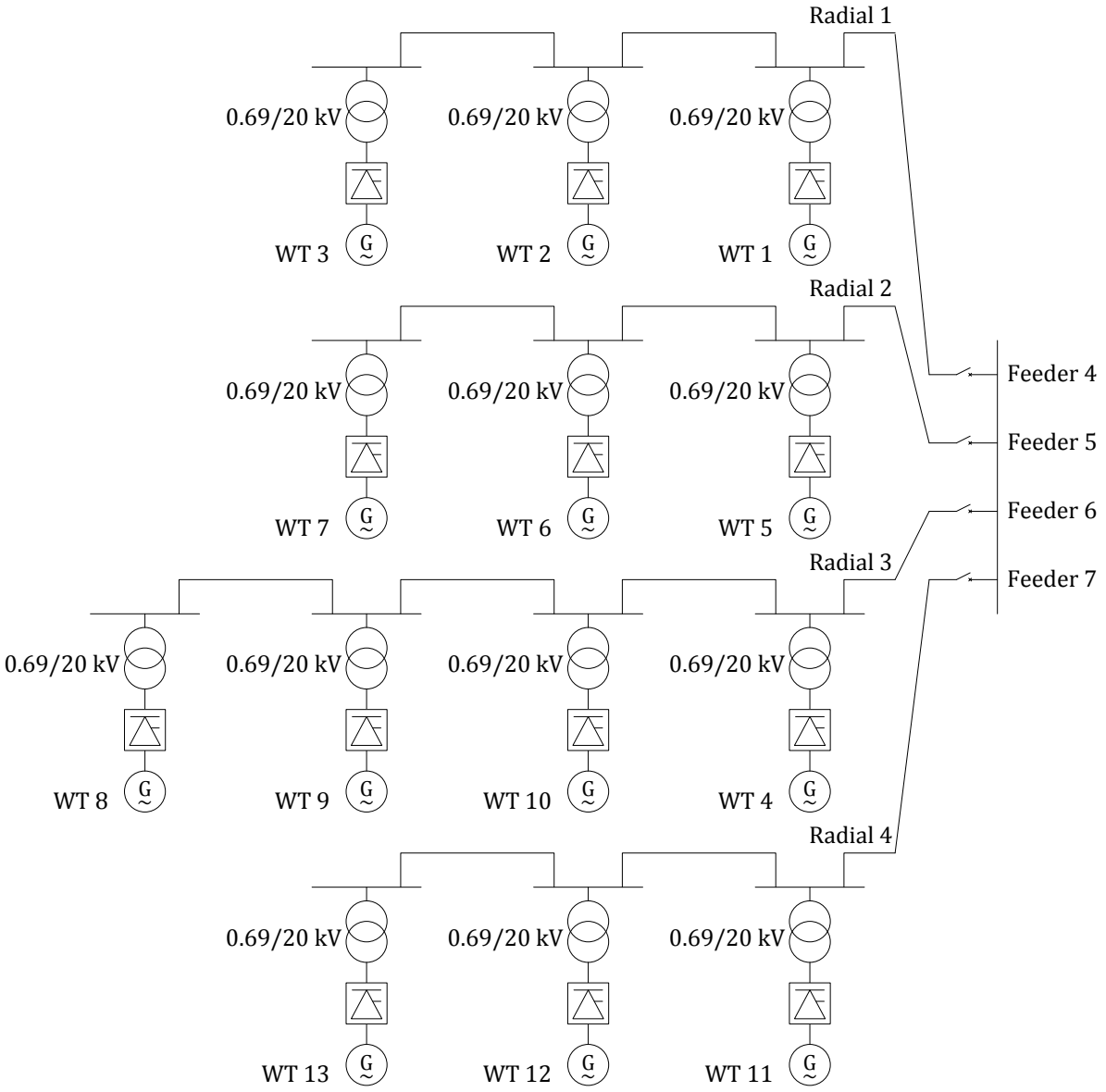

Figure 5.5 Karnice Wind Farm layout.

5.1.3.2 MV COLLECTION NETWORK AGGREGATION

Three different aggregation techniques of internal MV cable network are now implemented for this real-life wind farm. Karnice Wind Farm is taken as an example, with its simplified electrical layout as presented in Figure 5.5. The collection grid is not so widespread and the structure is relatively symmetrical which allow easily perform calculations and compare result from different aggregation methods.

Aggregation based on voltage drop

The equivalent impedance of respective radials is presented in the following way

$$Z_{eq_4} = \frac{1}{3}\left(Z_{3_4} + 2Z_{2_4} + 3Z_{1_4}\right) = 0.6295 + j0.3816\ [\Omega]$$

$$Z_{eq_5} = \frac{1}{3}\left(Z_{7_5} + 2Z_{6_5} + 3Z_{5_5}\right) = 0.0809 + j0.0683\ [\Omega]$$

$$Z_{eq_6} = \frac{1}{4}\left(Z_{8_6} + 2Z_{9_6} + 3Z_{10_6} + 4Z_{4_6}\right) = 0.7188 + j0.4495\ [\Omega]$$

$$Z_{eq_7} = \frac{1}{3}\left(Z_{13_7} + 2Z_{12_7} + 3Z_{11_7}\right) = 0.9776 + j0.6116\ [\Omega]$$

And the total equivalent impedance is equal to

$$Z_{MV} = \frac{1}{\frac{1}{Z_{eq_4}} + \frac{1}{Z_{eq_5}} + \frac{1}{Z_{eq_6}} + \frac{1}{Z_{eq_7}}} = 0.0615 + j0.0479\ [\Omega]$$

The capacitance is obtained by simple summation of cable shunt capacitances as in Eq. 5.12

$$C_{MV} = 5.4058\ [\mu F]$$

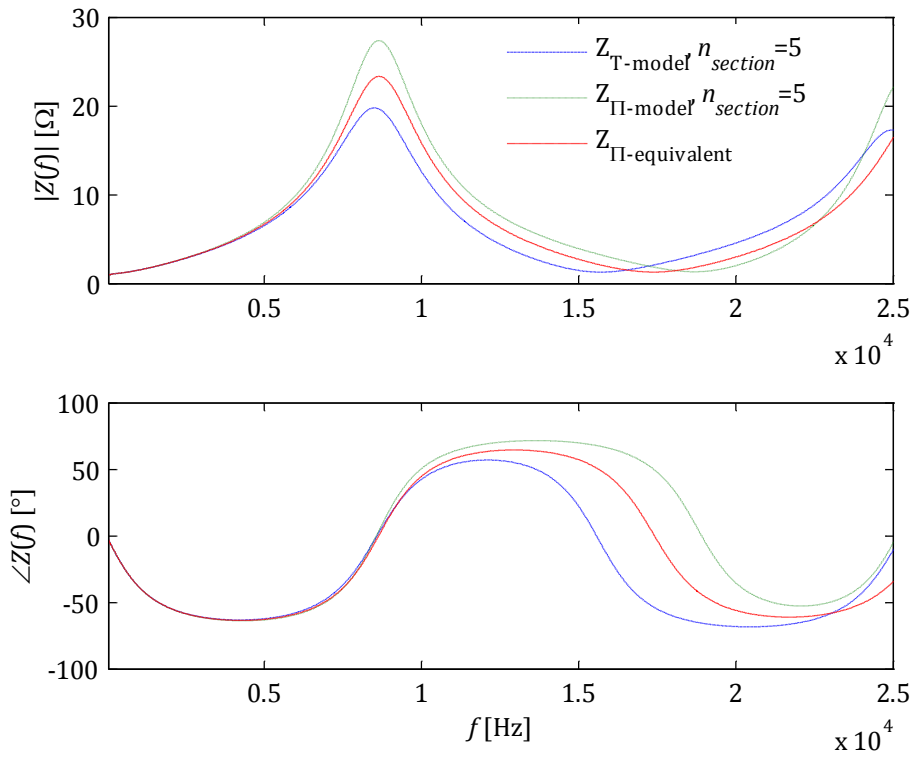

Figure 5.6 Frequency characteristics of MV cable impedance aggregated based on voltage drop for different cable models.

Based on Figure 5.6 one can see that there is no significant difference between different models within the frequency range of interest (i.e. 50-1950 Hz). Skin effect is taken into consideration based on EDF correction factor assumptions regarding underground and submarine cables. The MV cable impedance is connected to a unity resistive load. To compare results from different aggregation methods simple cable T-models were

used however for stability assessment purposes (later in the chapter) it was decided to use Π-equivalent models.

Collection grid aggregation based on power losses

The equivalent impedance of respective radials is presented in the following way

$$Z_{eq_4} = \left(\frac{1}{13}\right)^2 Z_{3_4} + \left(\frac{2}{13}\right)^2 Z_{2_4} + \left(\frac{3}{13}\right)^2 Z_{1_4}$$

$$Z_{eq_5} = \left(\frac{1}{13}\right)^2 Z_{7_5} + \left(\frac{2}{13}\right)^2 Z_{6_5} + \left(\frac{3}{13}\right)^2 Z_{5_5}$$

$$Z_{eq_6} = \left(\frac{1}{13}\right)^2 Z_{8_6} + \left(\frac{2}{13}\right)^2 Z_{9_6} + \left(\frac{3}{13}\right)^2 Z_{10_6} + \left(\frac{4}{13}\right)^2 Z_{4_6}$$

$$Z_{eq_7} = \left(\frac{1}{13}\right)^2 Z_{13_7} + \left(\frac{2}{13}\right)^2 Z_{12_7} + \left(\frac{3}{13}\right)^2 Z_{11_7}$$

And the total equivalent impedance is equal to

$$Z_{MV} = Z_{eq_4} + Z_{eq_5} + Z_{eq_6} + Z_{eq_7} = 0.141 + j0.0904\ [\Omega]$$

The capacitance is obtained by simple summation of cable shunt capacitances

$$C_{MV} = 5.4058\ [\mu F]$$

Radial aggregation based on power losses

The equivalent impedance of respective radials is presented in the following way

$$Z_{eq_4} = \left(\frac{1}{3}\right)^2 Z_{3_4} + \left(\frac{2}{3}\right)^2 Z_{2_4} + \left(\frac{3}{3}\right)^2 Z_{1_4}$$

$$Z_{eq_5} = \left(\frac{1}{3}\right)^2 Z_{7_5} + \left(\frac{2}{3}\right)^2 Z_{6_5} + \left(\frac{3}{3}\right)^2 Z_{5_5}$$

$$Z_{eq_6} = \left(\frac{1}{4}\right)^2 Z_{8_6} + \left(\frac{2}{4}\right)^2 Z_{9_6} + \left(\frac{3}{4}\right)^2 Z_{10_6} + \left(\frac{4}{4}\right)^2 Z_{4_6}$$

$$Z_{eq_7} = \left(\frac{1}{3}\right)^2 Z_{13_7} + \left(\frac{2}{3}\right)^2 Z_{12_7} + \left(\frac{3}{3}\right)^2 Z_{11_7}$$

And the total equivalent impedance is equal to

$$Z_{MV} = \frac{1}{\frac{1}{Z_{eq_4}} + \frac{1}{Z_{eq_5}} + \frac{1}{Z_{eq_6}} + \frac{1}{Z_{eq_7}}} = 0.0341 + j0.0321\ [\Omega]$$

The capacitance is obtained by simple summation of cable shunt capacitances

$$C_{MV} = 5.4058\ [\mu F]$$

5.1.3.3 TOTAL KARNICE WIND FARM AGGREGATION

Wind farm aggregation is done based on single line diagram and the aggregated impedance is seen from the grid-side converter AC terminals towards the grid. The aggregation can be successfully used for stability analysis and assessment purposes. Basically such study investigates the wind turbine current controller interaction with the external network. Due to this fact there is a need to represent the wind farm as a single line diagram. The system description is obtained by means of the network frequency characteristic based on the wind farm single phase equivalent circuit. The stability analysis is carried out in frequency domain. Therefore frequency response of all components either based on measurements or theoretical assumptions is needed. Please note that the system simplification to single line diagram used to analyse interaction between the wind turbine converter and the plant (i.e. wind turbine main power circuit, wind farm internal network, and external network.) can be assumed only if there is no coupling in the grid-side converter control structure. This assumption will be described later in more details.

Analysed system description

The single-line diagram of the analysed system is presented in Figure 5.7. As it can be seen the whole system comprises of the external network, park transformer, shunt reactor, internal MV cable network, wind turbine transformer, shunt turbine filter, and main reactor.

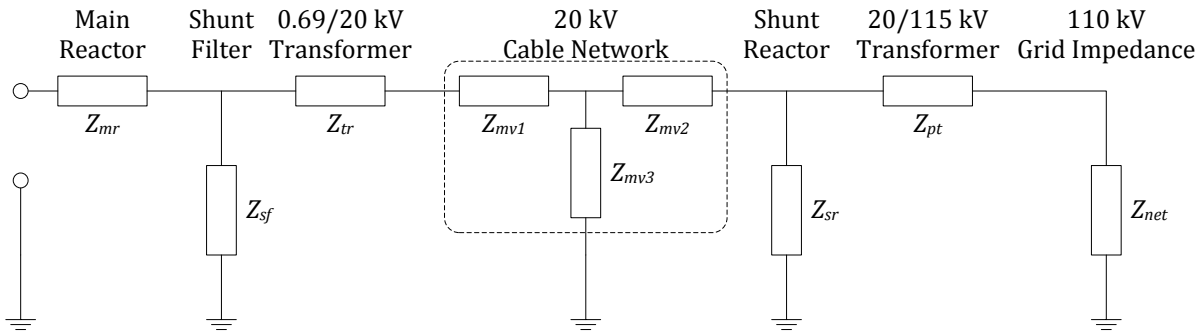

Figure 5.7 Single phase equivalent circuit of Karnice Wind Farm.

The grid impedance is assumed basis of detailed harmonic analysis of impedance seen from the connection point of Karnice Wind Farm prepared by Institute of Power Engineering, Gdansk (www.ien.gda.pl). The aim of the impedance calculations was to identify resonance points at the 110 kV power busbar of Skrobotowo substation. Calculations were carried out for different network configurations. Different cable modelling possibilities were taken into account but finally T-model for MV cable was applied in order to simplify analytical calculations. The skin effect of the MV cables is considered based on EDF correction factors.

All partial impedances have been scaled to wind turbine transformer LV side voltage level. The wind turbine transformer impedance, the converter output filter impedance and the main reactor impedance are scaled taking into consideration how many turbines are in operation. The shunt reactor L_{sr} (see Figure 5.7) is connected only in case of no and low load conditions. The purpose of the shunt reactor is to compensate the capacitance of cables when the wind farm production is low and power factor at the 110 kV connection point may not fall within the range required by connection conditions. It is assumed that park transformer is connected to the grid. There is only a short bus or line connection of few metres, which is ignored in calculations. Calculations were carried out for a different number of turbines in operation. Maximum number of turbines taken into consideration is 13 and minimum is 1 turbine.

Equivalent impedance calculation

The equivalent impedance of the analysed system can be obtained in the following way

$$Z_{eq} = Z_{mr} + \frac{1}{\frac{1}{Z_{sf}} + \frac{1}{Z_{tr} + Z_{mv1} + \frac{1}{\frac{1}{Z_{mv3}} + \frac{1}{Z_{mv2} + \frac{1}{\frac{1}{Z_{sr}} + \frac{1}{Z_{pt} + Z_{net}}}}}}}$$

Assuming circuit linearity (i.e. constant R, L, and C values for each of wind farm components) the equivalent impedance Z_{eq} was calculated for each frequency of interest. The frequency range of interest is between 50 Hz and 1950 Hz and is influenced by the current controller bandwidth. Please note that the maximum converter control bandwidth is limited by the command signal sampling frequency and therefore cannot be higher that the Nyquist frequency. Please also note that the grid-side converter current controller can introduce high harmonic rejection for frequencies lower than Nyquist frequency and also significantly affect the bandwidth.

Please note that it is considered that the wind turbines are connected in parallel in the aggregation process. Therefore components from the wind turbine main power circuit (i.e. main reactor Z_{mr}, shunt filter Z_{sf}, wind turbine transformer Z_{tr}) are scaled depending on number of wind turbines in operation.

Aggregation results

Based on results presented in Figure 5.8, Figure 5.9, and Figure 5.10 one can see how the system impedance can change depending on number of wind turbines in operation. It should be emphasized that this effect can be more significant in case of large offshore wind farms such as Horns Rev 2 or Walney I where many more wind turbines are installed. This aspect creates also a need to introduce more subtle stability analysis in case of large offshore wind farms equipped with many wind turbines, widespread internal cable network, and connected by long HVAC cables.

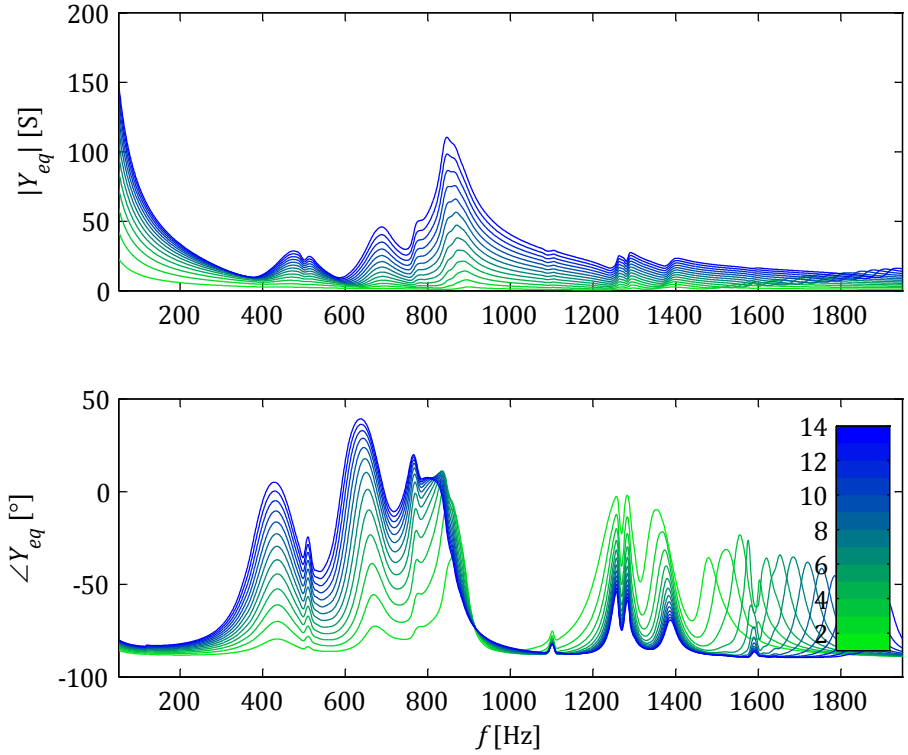

Figure 5.8 Karnice Wind Farm admittance seen from converter terminals and dependent on number of wind turbines in operation.

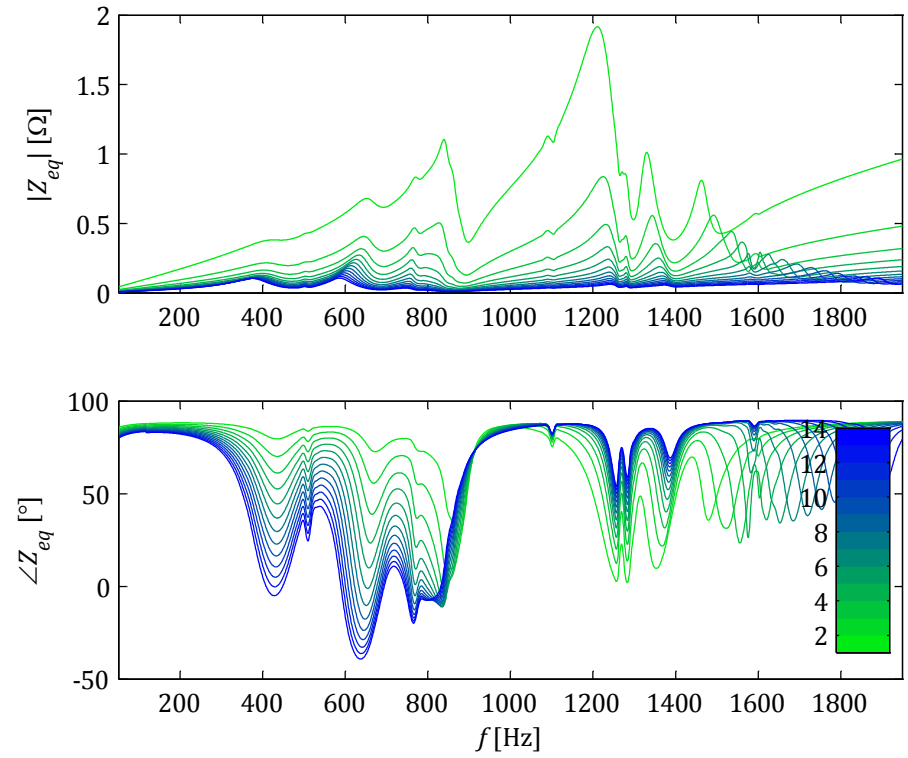

Figure 5.9 Karnice Wind Farm impedance seen from converter terminals and dependent on number of wind turbines in operation.

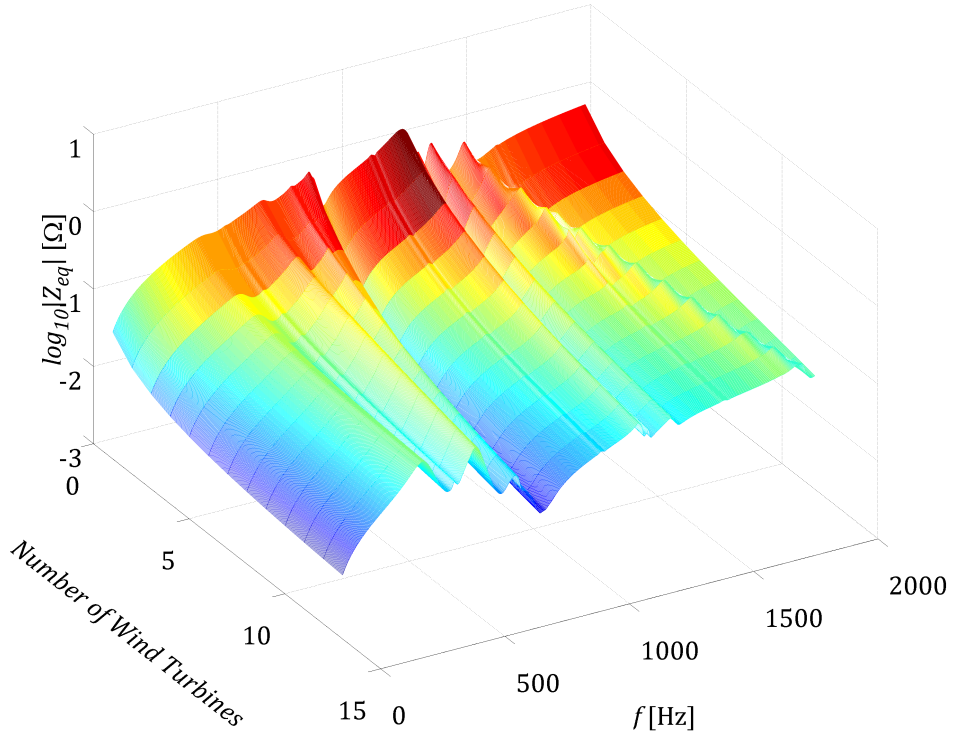

Figure 5.10 Three dimensional plot of Karnice Wind Farm impedance dependent on number of wind turbines in operation.

The results presented in Figure 5.8, Figure 5.9, and Figure 5.10 are obtained with the following system configuration:

- Basic external network configuration supplied from ENEA Szczecin,
- Shunt reactor is not connected,
- Skin effect correction factor is included - $R_1\left(0.187 + 0.532\sqrt{h}\right)\Big|_{h\geq 2.35}$,
- MV network is modelled using T-model.

Of course this aggregation approach has many limitations caused by sometimes rough and inappropriate assumptions. One of those is a linearity assumption. This can be improved by use of frequency responses obtained from measurements. Also sensitivity analysis of modelled components can provide some important information about overall system behaviour. As an example in Figure 5.11 and Figure 5.12 it can be easily seen that actually different MV cable network aggregation results, even if different, do not significantly affect overall system frequency response. Thanks to sensitivity analysis one can conclude which actually system parameters are more important and can affect the system stability. As it can be seen from the figures in this particular case the MV network equivalent impedance affects insignificantly the system and only slightly can affect stability margins. Of course in case of large offshore wind farms where internal structure is more extended this parameter can be more seriously taken into consideration.

Comparing Figure 5.11 and Figure 5.12 together one can see that when only one wind turbine is connected to the system the impedances from different aggregation techniques does not affect significantly the overall frequency response. But in case of all wind turbines in operation the modelling approach becomes more important for higher frequencies. Based on experience, instability problems are more expected for lower frequencies (i.e. below 1000 Hz).

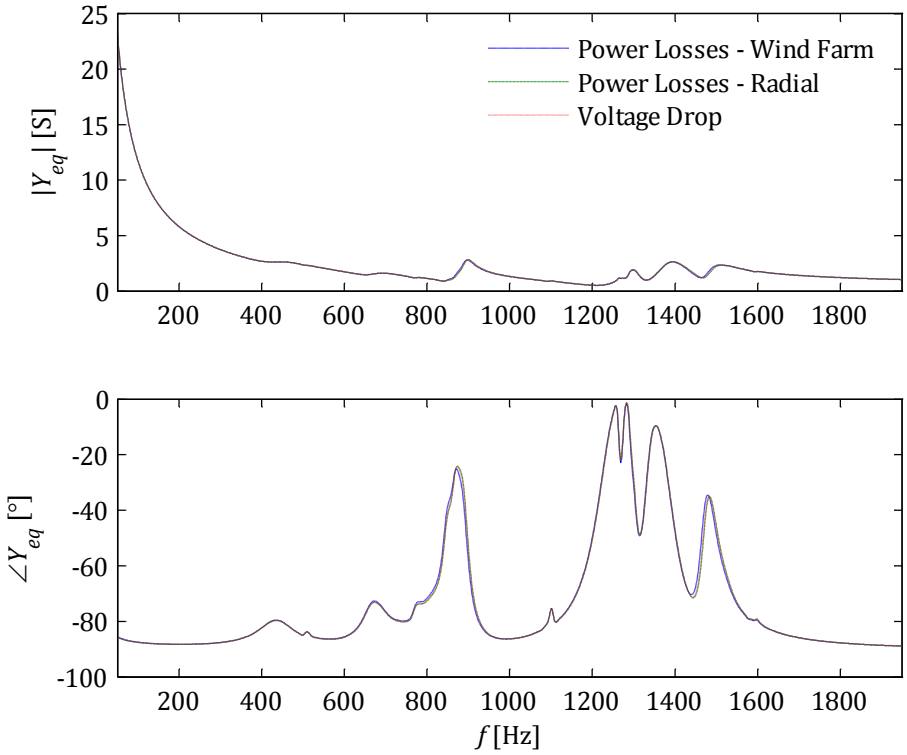

Figure 5.11 System admittance dependent on different internal network aggregation techniques (Case: 1 wind turbine in operation, no skin effect, 1 section of T-model, basic network configuration).

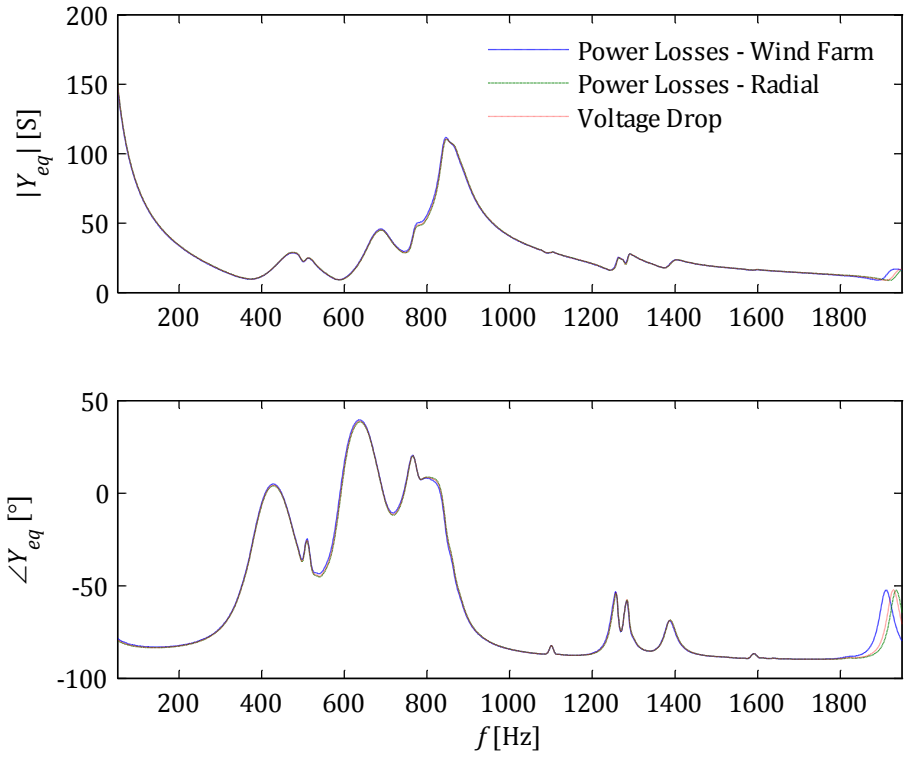

Figure 5.12 System admittance dependent on different internal network aggregation techniques (Case: 13 wind turbines in operation, no skin effect, 1 section of T-model, basic network configuration).

5.1.3.4 NUMERICAL VALIDATION

In order to validate analytical approach results obtained in Matlab 2011b, a model in DIGSILENT Power Factory 14.1.2 was developed and investigated. The version of the software should be emphasized because the modelling approach of wind farm components, especially in case of Power Factory, can vary between versions. As an example different line modelling approach can be found in Power Factory 14.1 and earlier. In version 14.1 operating temperature of cables is taken into consideration which can affect impedance calculation.

Model description

The model is presented in Figure 5.14. Frequency sweep function is used in calculations of network impedances in order to identify series and parallel resonances in the network as well as compare results obtained from Matlab (i.e. analytical model).

The first approach is to vary number of wind turbines (only the converter is switched on and off) in service and calculate the frequency sweep of system impedance seen from converter AC terminals. It has to be emphasized that depending on which converter model is chosen the results may significantly vary. In Figure 5.13 one can see how the wind turbine was modelled in DIGSILENT Power Factory. In order to model the grid-side converter the PWM Converter model (.ElmVscmono) was used. This model allows easy changing between either ideal voltage source or ideal current source by changing of parameter ictrltp.

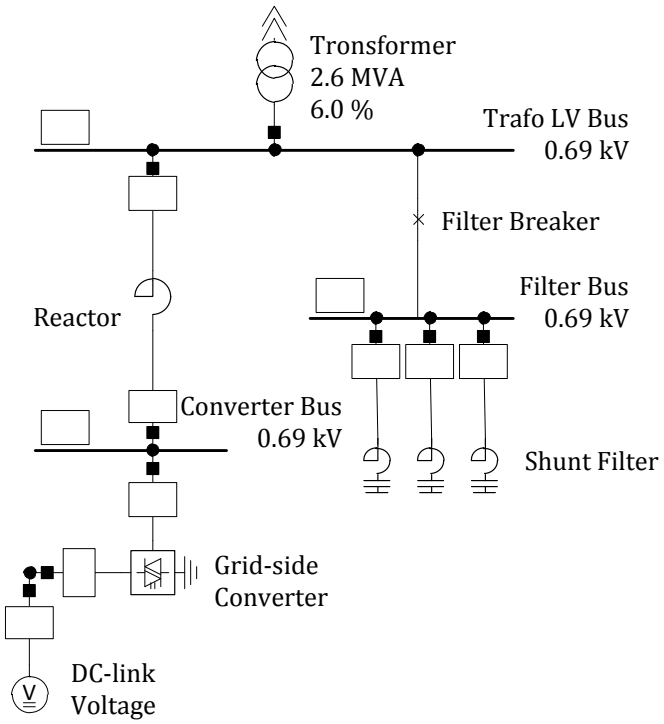

Figure 5.13 Wind turbine model implemented in Power Factory.

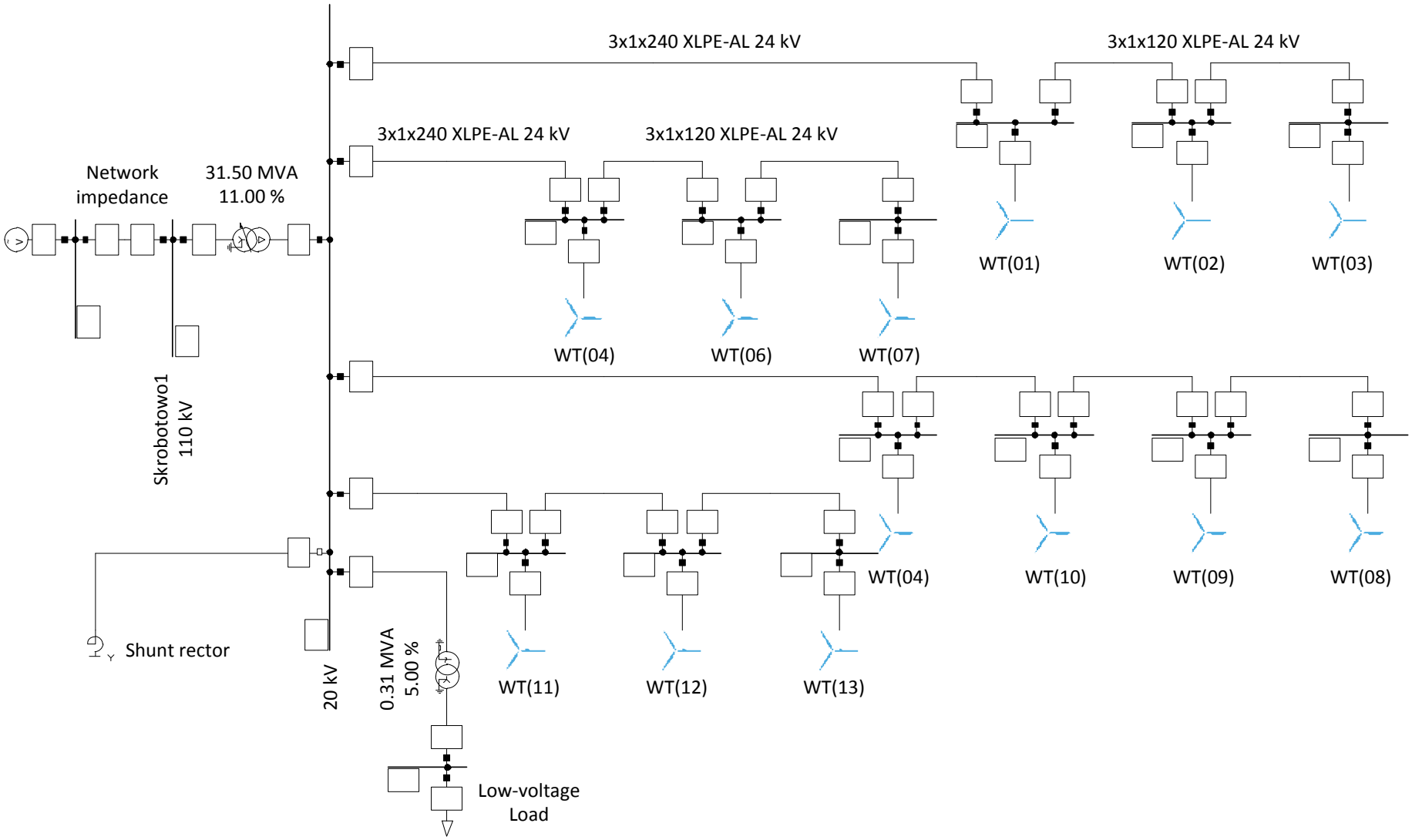

Figure 5.14 Model from Power Factory of Karnice Wind Farm.

Results from numerical calculations

It was decided to observe how different wind turbine grid-side converter modelling (e.g. ideal voltage source, ideal current source) can affect the impedance seen by other grid-side converters. It was observed that as long the converter is modelled as an ideal current source there is no difference in frequency sweep if the converter is connected to the network or not. Please note that the wind turbine main power circuit is still energized. In general it was observed that modelling wind turbines as ideal current sources can be inappropriate at least in case of impedance frequency sweep and can provide misleading results.

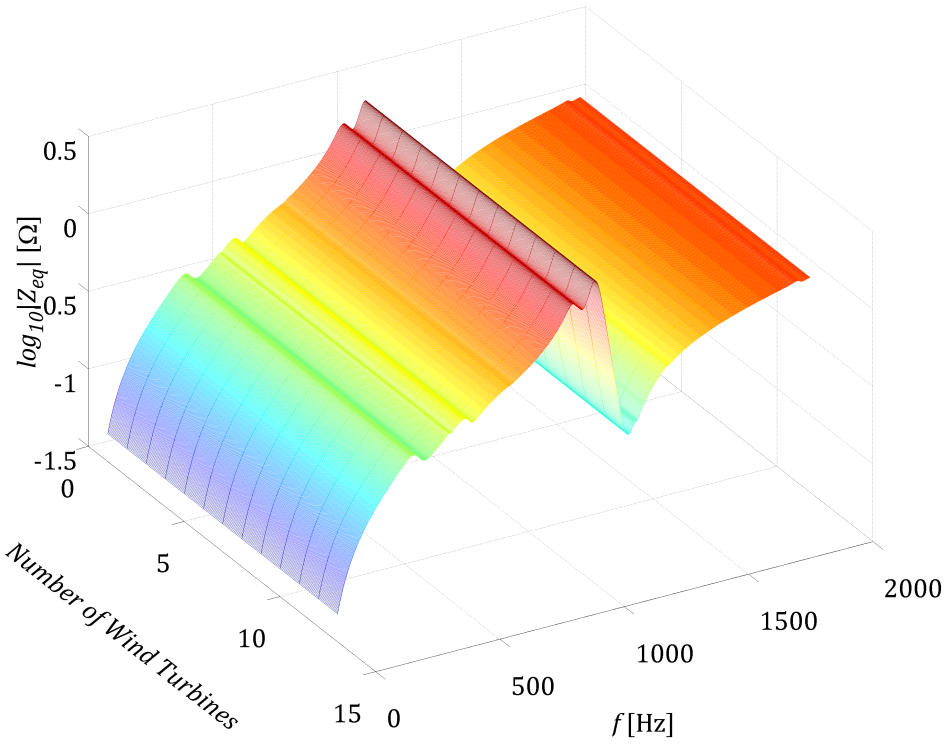

Figure 5.15 Karnice Wind Farm impedance dependent on number of wind turbines in operation obtained from Power Factory by using ideal current source model.

As it can be seen from Figure 5.15 there are no changes in the impedance due to the fact the current source is defined as Norton equivalent model with sufficiently large impedance that can be treated as ideal current source. Due to this fact there is no difference in system impedance if wind turbines are out of service or connected to the network. Due to significant limitations of current source application it was decided to perform numerical calculations using ideal voltage source.

In case of ideal voltage source changes in impedance depending on number of wind turbines in operation can be easily seen from Figure 5.16 and Figure 5.17. Unfortunately the results differ from results presented in Figure 5.9 and Figure 5.10. This is caused by consideration of different approaches in both numerical and analytical calculations. The impedance magnitude level is comparable but resonance scenarios are different.

This is mainly due to the fact that an ideal voltage source is effectively a short-circuit and therefore makes a short-circuit between converter AC terminals of wind turbines which are in operation.

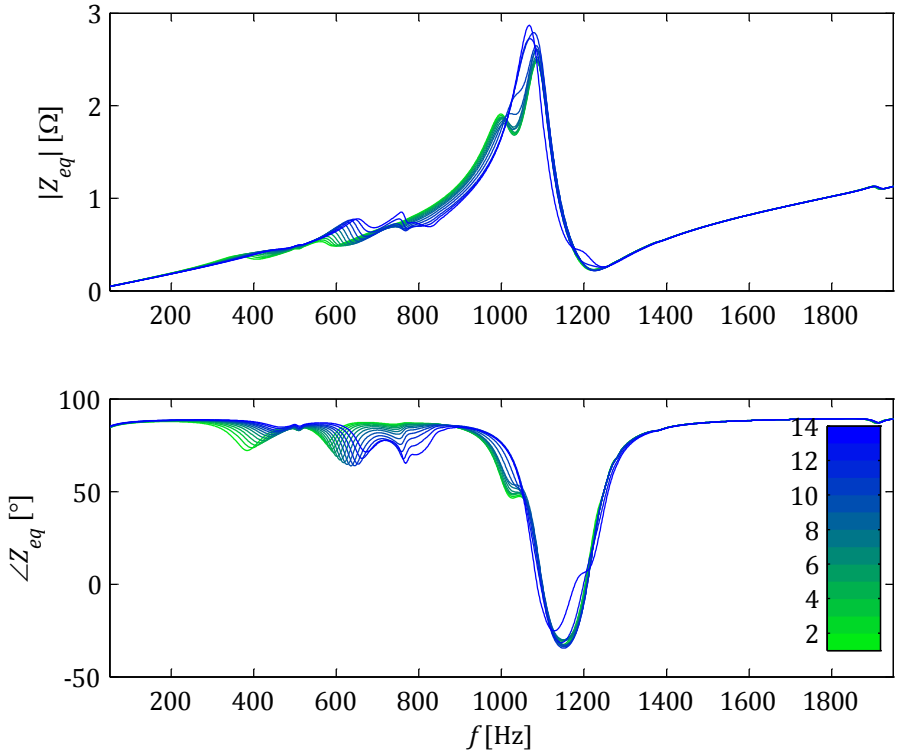

Figure 5.16 Impedance plot obtained from Power Factory for ideal voltage source.

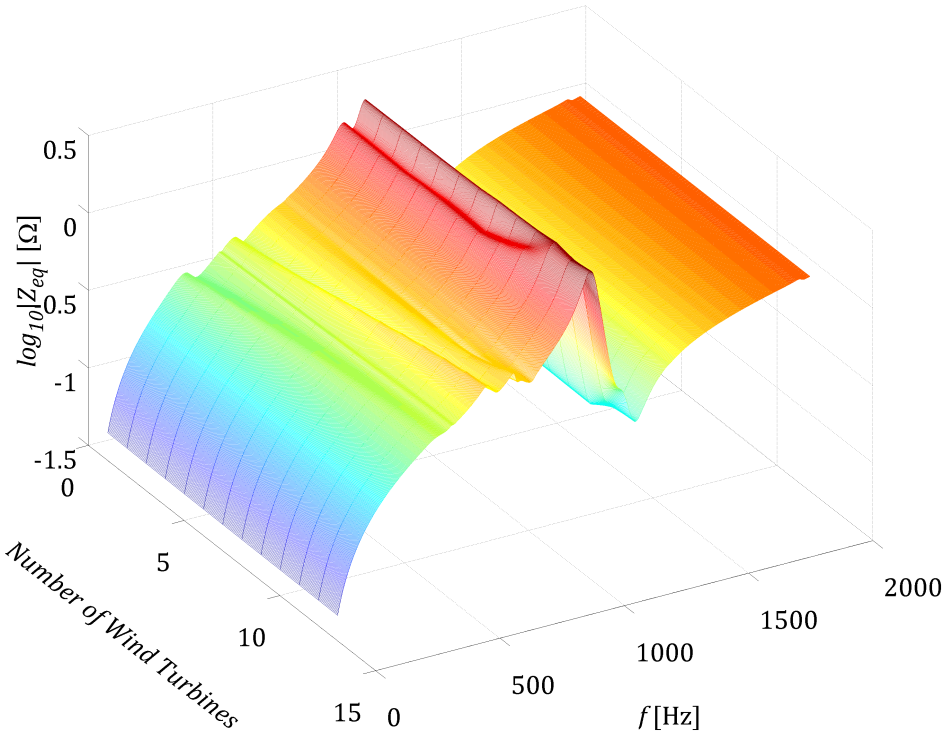

Figure 5.17 Karnice Wind Farm impedance dependent on number of wind turbines in operation obtained from Power Factory by using ideal voltage source model.

Due to the short-circuit behaviour of ideal voltage sources the frequency sweep for all wind turbines connected to the network gives impedance equal to 0 for all analysed frequencies. This case is therefore not presented in results. It was observed that impedance calculated at AC terminals of the converter which is connected to the grid is equal to 0 due to short circuit. It is also worth emphasizing that the case when ideal current sources are used is equal to results when all ideal voltage sources are disconnected from the network.

In Figure 5.16 and Figure 5.17 the impedance plot is taken from the AC terminal of the grid-side converter in the wind turbine number 13. This is done in this way due to the fact that wind turbines are connected to the grid starting from wind turbine number 1. Calculating impedance in the last wind turbine allows avoiding short circuit during all calculations (i.e. iterations).

Due to the fact that in real life wind farms which are characterized by unsymmetrical internal structure, the impedance seen from different wind turbines terminals also differs. A question which has to be put forward is if the difference in impedances is significant and should be taken into consideration during the aggregation procedure. Based on theoretical analysis (in Matlab) it is assumed that each of the wind turbines is expected to be connected to the same system. This assumption can provide some incorrect results. Fortunately DIgSILENT Power Factory allows investigating the impedance seen from the grid-side converter of each wind turbine independently and observing expected differences.

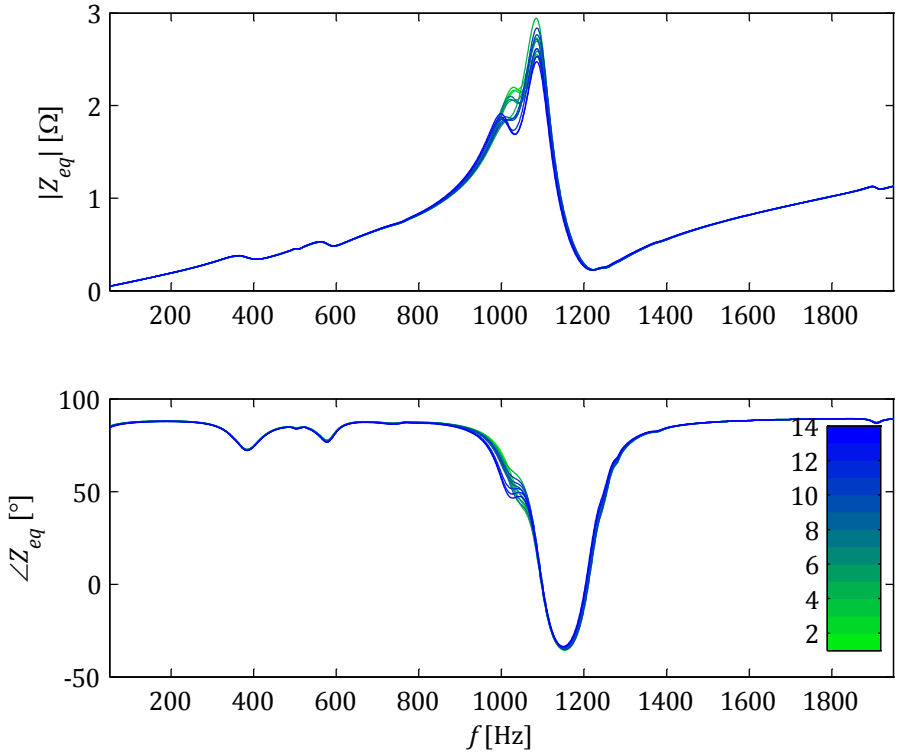

Figure 5.18 Impedance seen from each of the wind turbines.

Figure 5.18 shows that actually the impedance in the case of Karnice Wind Farm does not change significantly depending from which grid-side converter AC terminal the system is seen. Of course the results can be different for every particular wind farm under consideration. Changes in impedance plots will be more significant if the internal MV cable network is strongly unsymmetrical (i.e. different number of wind turbines connected to each of radials, different radial cable lengths). In general one can conclude that the assumption in the theoretical model should not provide inaccurate and misleading results but for every study case it should be validated based on numerical impedance frequency sweep. Of course knowledge about limitations is strongly needed and interpretation of results is in the researcher's hands.

As it was shown above the results significantly are affected by applied models of the grid-side converter. It can be seen that both approaches either ideal voltage source or ideal current source give results different from expected in the theoretical investigation based on using of different MV network aggregation techniques. The impedance in case of ideal current source does not change if the converter is connected to the grid or is out of service. However, ideal voltage source affects short circuit of grid-side converter AC terminals and common grounding point and therefore does not only show the impedance of the network seen from the terminals.

Thus, the aggregation results from wind farm model with an ideal voltage sources cannot be used if someone would like to express the whole wind farm as one equivalent wind turbine connected to one equivalent impedance. However this approach can

be used if one would like to investigate stability of one particular wind turbine connected to a bigger wind power system and analyse how the wind turbine behave depending on number of wind turbines producing in the analysed wind farm. Please note that the grid side converter also introduces internal impedance which is dependent on the control method. Ideally it can be said that for frequencies other than controlled (e.g. the fundamental component, compensated harmonics) the impedance should be equal to 0 (i.e. ideal harmonic rejection) therefore modelling grid-side converters as an ideal voltage source is understood.

The purpose of MV cable network aggregation and calculation of equivalent impedance is to investigate how hypothetically connected converter can be affected by an external network and overall system impedance [5.11]. This can show how the grid-side converter current control can respond within its control bandwidth and if the analysed system (including external network, internal cable network and wind turbines) is stable. Therefore there is a need to calculate the impedance seen from the converter AC terminals but without its interference in the results. In order to achieve this goal the impedance was calculated still from the AC terminals but this time with disconnected converters. Of course one needs to observe changes in the system impedance caused by the number of wind turbines in operation. This can be successfully investigated by connecting converter terminals together depending on number of wind turbines in service (i.e. short circuit between terminals of interest).

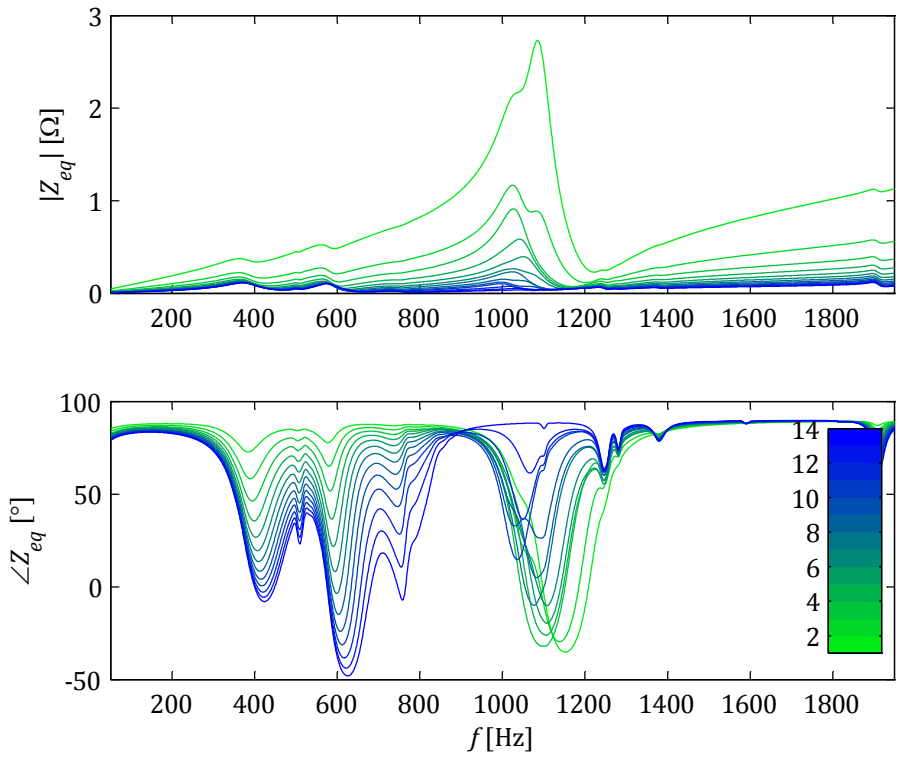

Figure 5.19 Frequency sweep taken from grid converter terminals in case of short circuit between terminals.

The impedance plot seen from different wind turbine terminals for the same number of wind turbines in operation can slightly differ. As long as one can say that the radial length is similar and number of wind turbines connected to each of the radials is close to each other, there is no significant difference in the equivalent impedance if the same number of wind turbines is connected either within the same radial or from different sites of analysed wind farm. More important is the size of the wind farm (i.e. number of wind turbines, internal cable network size), how the wind farm is connected to the network (i.e. long or short HVAC cable) and the characteristic of the external network.

Another interesting aspect regarding obtained results is about definition of wind turbine in operation. Based on analytical approach when the wind turbine is not in operation all components inside the wind turbine such as wind turbine transformer, shunt filter, main reactor and the converter do not affect the equivalent impedance of analysed system. But is actually in real life applications this assumption correct? The extensive measurement campaign at Avedøre Holme showed that not in all cases can one accept this assumption. If the wind turbine shutdown is affected by low wind speed only the grid-side converter stops its normal operation in order to reduce switching losses. The main power circuit is still energized and the DC-link voltage is kept on constant level by charging the capacitor. This is done in order to allow the wind turbine fast start if the wind speed would be sufficient to produce. On the other hand a full scale converter of the wind turbine due to its back-to-back nature can operate as a rectifier. In this particular case all wind turbine passive components can still affect the impedance seen from another wind turbine in operation. Results of aggregation based on this assumption are shown in Figure 5.19 and actually in most of cases are closer to reality than results from the analytical investigation. Please note that it is of common practice to disconnect the shunt filter in the wind turbine main power circuit in order to avoid unwanted current flow when the wind turbine is not producing.

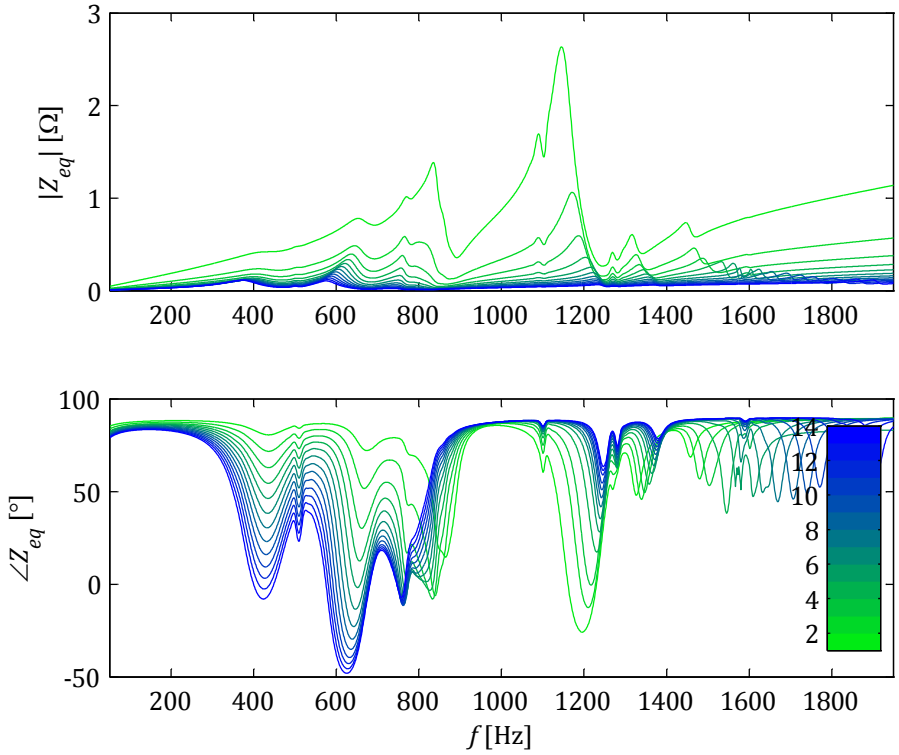

Figure 5.20 Impedance of aggregated system obtained from Power Factory based on analytical assumptions.

The impedance presented in Figure 5.20 is obtained from numerical simulations in Power Factory based on the same assumptions as in the analytical approach. One can see sufficiently good agreement between both analytical as well as numerical aggregation. Good agreement can be seen by comparing Figure 5.9 and Figure 5.20. This also indicates that wind power system can be successfully aggregated to equivalent impedance using commercial tools which allow saving some time during development of commercial wind farm projects.

5.1.4 Comparison between Horns Rev 2 and Karnice

Horns Rev 2 is able to produce 209 MW of power and thereby it was the largest offshore wind farm in the world at the time when it was built and this analysis was performed. The wind farm is connected to the transmission network by the longest, 100 km HVAC cable in Denmark (see Figure 5.3). The system with large shunt capacitance and reactor inductance may result in problems not normally observed in smaller onshore wind farms. In comparison Karnice Wind Farm has a total capacity of 30 MW and the cable length between the last wind turbine and the point of common coupling is 2.5 km. Both analysed (i.e. Horns Rev 2 and Karnice) wind farms are equipped with SWT-2.3-93, which is a variable speed with a full-scale converter wind turbine.

The wind farms are characterized by completely different internal structures. The most significant difference is the number of installed wind turbine generators. The change

of harmonic impedance depending on different number of wind turbines in operation is presented in this section. Nowadays, offshore wind farms are mainly connected through a widespread MV submarine cable network and long HV power cables which can be clearly seen in Horns Rev 2. A completely different scenario is observable in Karnice Wind Farm where the internal MV cable structure is much smaller and no HVAC underground cable is used to connect to the external distribution network [5.12].

5.1.4.1 HORNS REV 2 DESCRIPTION

Horns Rev 2 contains 91 SWP wind turbines. The grid connection of Horns Rev 2 Offshore Wind Farm is arranged through a 100 km HVAC cable connecting the offshore transformer substation with a 165/400 kV transformer in the 400 kV substation at Endrup in the transmission system.

Horns Rev 2 is constructed and operated by DONG Energy. The wind farm is located off the west coast of Denmark, 30 km from the coast line near Esbjerg. The wind farm is situated in a shallow water area with water depths of 9-17 m and average wind speed is less than 10 m/s. The connection to land consists of three main parts: a transformer platform, a subsea cable and a land cable. The total length of the cable is above 100 km. A 42 km long 165 kV 3x630 mm² submarine cable is jointed with a 2.3 km land cable at station Blåbjerg. The cable is produced by Nexans. The submarine cable is a three phase cable where the three conductors are placed in a common metallic sheath. The insulation consists of an 18 mm layer of cross-linked non-polar thermoplastic polyethylene (XLPE). The 2.3 km land cable is jointed with another 55.4 km land cable to reach the Endrup 400/150 kV substation. Both land cables are of the same type – three single-phase conductor aluminium cables and were produced by ABB. The voltage rating is 165 kV, and the cross section of the conductor is 1200 mm². The dielectric used in the cable is XLPE, and the thickness of this layer is 17 mm.

Three 170 kV shunt reactors are used to compensate for the reactive power produced by the cables. Two reactors are installed at station Endrup: 40 MVAr and 80 MVAr. Between the 2.3 km and 55.4 km land cable at station Blåbjerg an additional 80 MVAr reactor is installed.

The Horns Rev 2 external network harmonic model was used on the basis of Energinet.dk's technical analyses and simulations using, among other tools, the DIGSILENT PowerFactory simulation software. A model of the entire electrical power network was used, with exact representation of all 400 kV, 150 kV and 132 kV power lines. The aggregated 60 kV distribution network models, main power plants, aggregated onshore wind power generation units, central heating plants and loads are connected to the 60 kV. Presented here studies on Horns Rev 2 cable connection concerning harmonic network impedance were performed using this full network model [5.13].

5.1.4.2 *RESULTS COMPARISON*

Aggregated models of Karnice Wind Farm as well as Horns Rev 2 were obtained in the same way. Wind turbines used in both wind farms are identical, i.e. contain the same power converters (including reactors and capacitive filters) and wind turbine transformers. This creates an ideal opportunity to compare both wind farms. The external networks are different, as previously described, but they can be treated as representative networks to which offshore and onshore wind farms can be connected. This issue even emphasizes the differences in impact and interaction between wind farms and external network.

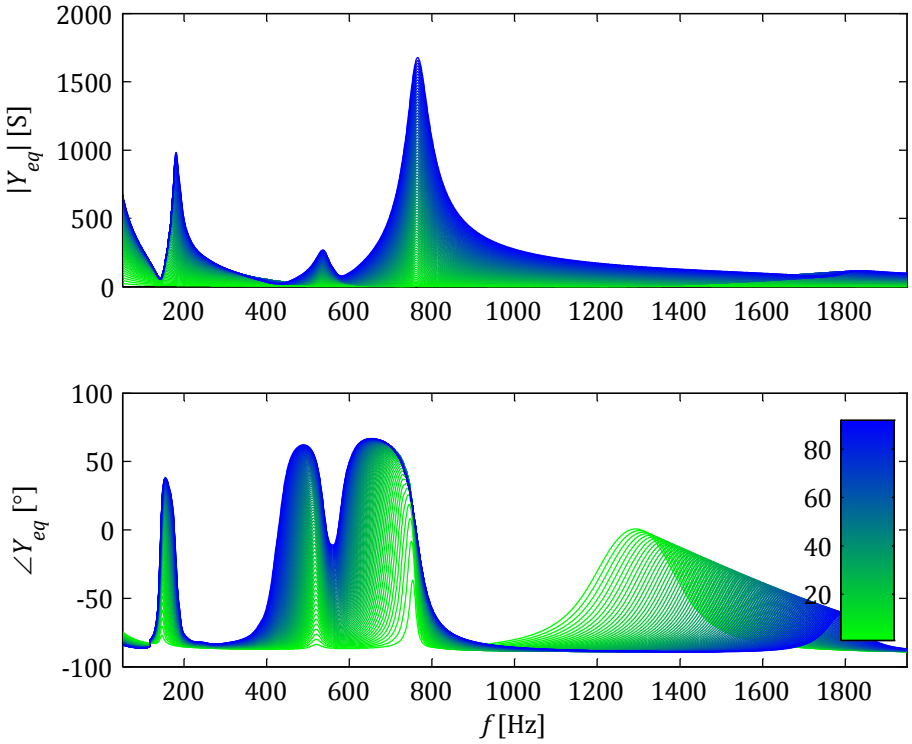

Figure 5.21 Horns Rev 2 admittance seen from converter terminals and dependent on number of wind turbines in operation.

As it was observed earlier, the analysis shows that the system admittance seen from the converter terminals significantly changes when the number of turbines in operation varies. This is presented in case of Karnice Wind Farm in Figure 5.8 and for Horns Rev 2 in Figure 5.21. The impedances are presented in Figure 5.9 and Figure 5.22, describing Karnice and Horns Rev 2 respectively. The highest admittance and significant resonance peaks of the whole system seen from the power converter AC terminals are observed in case of all wind turbines in operation. Obviously this situation is relatively frequent and can happen during normal operation. From Figure 5.8 and Figure 5.21 one can conclude that the admittance rapidly increases when the number of turbines in service also increases. This occurs if wind farms contain many power generation units which is common in case of large offshore wind farms. Horns Rev 2 is equipped with 91 units

but in the nearest future much bigger wind farms are planned to be erected. This emphasized a need for such kind of system studies.

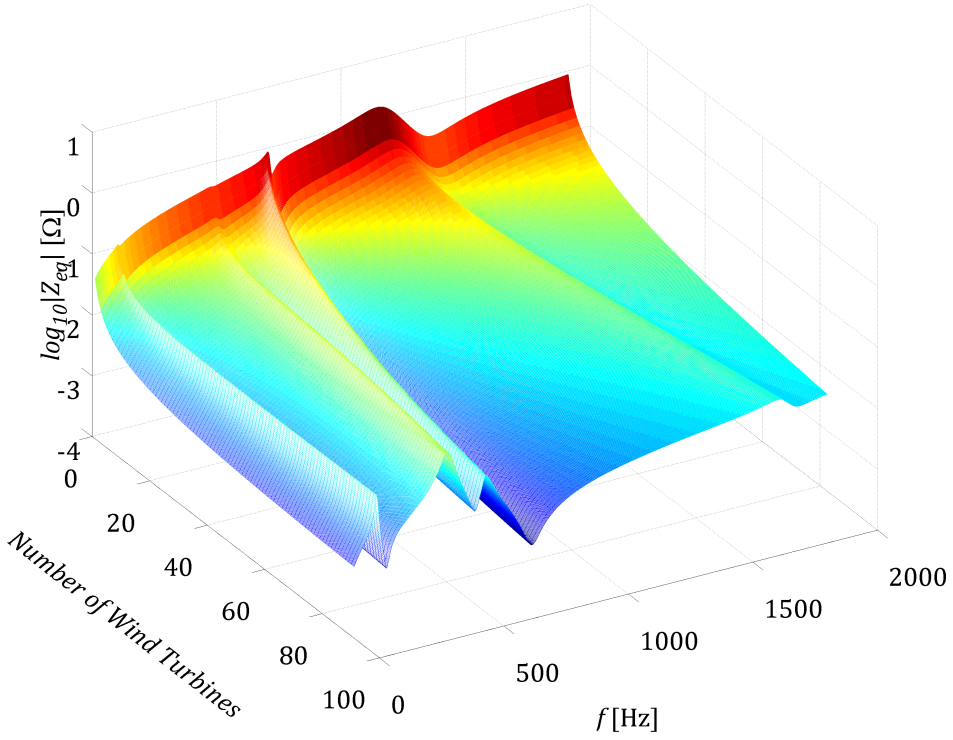

Figure 5.22 Three dimensional plot of Horns Rev 2 impedance dependent on number of wind turbines in operation.

Another aspect to take into consideration is the variation of resonant points. Changes in the overall system impedance cause changes to resonant peaks. This becomes a crucial thing in harmonic studies reliability. It indicates a necessity to take into account different system configurations, not only capacitor banks, shunt reactors or external network but even number of turbines in operation [5.3]. This is of course the worst case in case of wind farms with significantly irregular internal structure.

Normally, large wind farms are connected to the transmission network which typically characterizes smaller equivalent impedance in comparison to the distribution network. This affects smaller voltage variations at the connection point [5.14]. Due to the tendency to construct large wind farms, the connection will be to strong grids characterized by small short circuit impedance.

Both wind farms evaluation exhibits small differences when only few wind turbines are in operation. Typical series resonance points around 800 Hz and strongly dumped close to 500 Hz are characteristic for both systems. But it can be seen that for higher number of turbines connected to the network, additional resonance points appear within low-order harmonic area. This creates significant disturbance in the system considering harmonic emission assessment. For example series resonance in Horns

Rev 2 around 200 Hz seen in Figure 5.21 is due to the wind farm transformer series reactance and HV cables shunt capacitance. It is obvious that the harmonic resonance seen from power converter AC terminals cannot be present in the harmonic impedance of Karnice Wind Farm which does not contain any long HVAC power cable connections.

5.1.5 Summary of wind farm aggregation

As it can be seen based on the above example, the procedure of equivalent impedance calculation is relatively straightforward and can be applied to any wind farm. Approaches appropriate for stability assessment purposes and load flow calculations are presented. Different aggregation techniques provide different results, but it was observed that the differences do not significantly affect an overall system description in the frequency domain.

Based on numerical calculations, it was shown that different aggregation approaches can provide various results. It is of great importance to know how the frequency characteristic of any aggregated wind farm is going to be used. It was presented that different calculation approaches must be used if one would like to aggregate both wind turbines into one equivalent wind turbine and an electrical system to which it is connected. It was also described that another calculation approach is needed if one would like to investigate how one wind turbine can behave when is connected to the whole system with a varying number of wind turbines in operation. Please note that the converter impedance was not taken into consideration. This can be easily done by taking the controller transfer function. It was mentioned that in theory the converter control should not affect higher frequencies (if not intended). and therefore the impedance can sometimes simply be omitted.

It was observed that large offshore wind farms can introduce additional unwanted resonances within a low frequency range. This can significantly affect the overall system stability. Therefore, analysis and design optimization of large offshore wind farms are more complex than smaller onshore wind farms. In the case of the Horns Rev 2 analysis, it was observed that the capacitance of long HVAC export cable and series inductance of the wind farm transformer creates unwanted and significant series resonance. Such situation is of concern in most of the erected large offshore wind farms.

5.2 Wind Turbine Models

5.2.1 Harmonic modulator model

Based on measurement data it was observed that the wind turbine modulator constitutes state-of-the-art technology commonly seen on nowadays industrial solutions. The two-level voltage source converter with parallel connected sharing reactors [5.15] IGBT units is one of typical solutions in high power density [5.16] wind turbines with grid side converters operating at the low voltage level (e.g. 690 V).

5.2.1.1 CHARACTERISTIC HARMONICS

According to [5.4] characteristic harmonics exist when analysed three-phase electrical system is considered to be balanced, the voltages and currents waveforms have identical shape and current and voltage are separated by exactly $\pm 1/3$ of the fundamental period. In such case zero sequence harmonics are for orders $n = 3m$ where $m = 1, 2, 3, \dots$, positive sequence harmonics are for orders $n = 3m - 2$ and negative sequence harmonics are for orders $n = 3m - 1$.

On the other hand [5.17] considers characteristic harmonics as inherent to the pulse-width modulation operating principle. They are defined as harmonics that are generated by the converter without any additional distortion in the system. The same approach is taken for example in [5.18] where non-characteristic harmonics are analysed. Therefore knowledge about characteristic harmonics is extremely beneficial for designing filters and assessing the degree of distortion other wind farm components may experience.

According to [5.18] the harmonic emissions of a device with an integrated power electronic interface can be categorized into characteristic and non-characteristic harmonics. The characteristic harmonic emissions are determined by the converter topology and the switching pattern applied. For instance, a typical configuration found in wind turbines is a two-level, three-phase voltage-source converter with sinusoidal pulse-width modulation. Non-characteristic harmonics are not related to the converter topology and applied modulation techniques, but are determined by the operating point of the individual converter and external network conditions to which is connected. Therefore, they can be weakly correlated or even completely uncorrelated between different wind turbines.

Let us consider modulator based on carrier-based pulse-width modulation with fixed carrier signal frequency. In this case in real-life systems, due to the fact that the power system frequency may vary, the frequency ratio can be a non-integer value. In nowadays power electronic solutions the carrier frequency tends to be kept constant and the fundamental frequency varies in the power system. Therefore harmonic components (e.g. sideband harmonic components) generated by the grid-side converter cannot be any longer an integer multiple of the power system frequency and cannot be considered as harmonics from classical approach of harmonic studies in power systems, saying nothing of being considered as either characteristic or non-characteristic.

It has to be emphasized that the frequency of sideband harmonic components is dependent on both power system frequency and carrier frequency. Some solutions on how to adjust the carrier frequency to the fundamental frequency in order to avoid non-integer frequency ratios can be found in [5.19], but it is not commonly applied. Frequency synchronization between carrier signal and command signal can be inconvenient, because it affects significant carrier group harmonic components

frequency variation, especially for high m_f. This can cause difficulties in filtering process as well decrease robustness of the converter connected to different networks (i.e. different frequency variation).

5.2.1.2 *Analytical approach based on Double Fourier series*

Based on Fourier series theory any time-varying 2π-periodic function $f(t)$ can be expressed as a summation of harmonic components, set of functions consisting an orthonormal basis for the Hilbert space $L^2([-\pi,\pi])$ of square-integrable functions of $[-\pi,\pi]$ [5.20], [5.21]

$$f(t) = \frac{a_0}{2} + \sum_{m=1}^{\infty} [a_m \cos(m\omega t) + b_m \sin(m\omega t)] \tag{5.21}$$

where

$$a_m = \frac{1}{\pi}\int_{-\pi}^{\pi} f(t)\cos(m\omega t)\, d\omega t\,, \qquad m = 0, 1, \dots, \infty \tag{5.22}$$

$$b_m = \frac{1}{\pi}\int_{-\pi}^{\pi} f(t)\sin(m\omega t)\, d\omega t\,, \qquad m = 1, 2, \dots, \infty \tag{5.23}$$

Let us take into consideration a periodic function $f(x,y)$ which varies depending on two time variables

$$x(t) = \omega_c t + \theta_c \tag{5.24}$$

$$y(t) = \omega_o t + \theta_o \tag{5.25}$$

Eq. 5.21 can be expressed using $f(x,y)$ periodic function [5.22]

$$\begin{aligned} f(x,y) = \frac{A_{00}}{2} &+ \sum_{n=1}^{\infty} [A_{0n}\cos(ny) + B_{0n}\sin(ny)] \\ &+ \sum_{m=1}^{\infty} [A_{m0}\cos(mx) + B_{m0}\sin(mx)] \\ &+ \sum_{m=1}^{\infty}\sum_{\substack{n=-\infty \\ n\neq 0}}^{\infty} [A_{mn}\cos(mx+ny) + B_{mn}\sin(mx+ny)] \end{aligned} \tag{5.26}$$

where coefficients are defined in the following way

$$A_{mn} = \frac{1}{2\pi^2}\iint_{-\pi}^{\pi} f(x,y)\cos(mx+ny)\, dxdy, \qquad \begin{matrix} m = 1, 2, \dots, \infty \\ n = 1, 2, \dots, \infty \end{matrix} \tag{5.27}$$

$$B_{mn} = \frac{1}{2\pi^2} \iint_{-\pi}^{\pi} f(x,y) \sin(mx + ny)\, dxdy, \qquad \begin{matrix} m = 1, 2, \dots, \infty \\ n = 1, 2, \dots, \infty \end{matrix} \tag{5.28}$$

And finally Eq. 5.26 can be expressed in terms of time by substituting Eq. 5.25 and Eq. 5.24

$$\begin{aligned} f(t) = \frac{A_{00}}{2} &+ \sum_{n=1}^{\infty} [A_{0n} \cos(n[\omega_o t + \theta_o]) + B_{0n} \sin(n[\omega_o t + \theta_o])] \\ &+ \sum_{m=1}^{\infty} [A_{m0} \cos(m[\omega_c t + \theta_c]) + B_{m0} \sin(m[\omega_c t + \theta_c])] \\ &+ \sum_{m=1}^{\infty} \sum_{\substack{n=-\infty \\ n\neq 0}}^{\infty} \begin{bmatrix} A_{mn} \cos(m[\omega_c t + \theta_c] + n[\omega_o t + \theta_o]) \\ +B_{mn} \sin(m[\omega_c t + \theta_c] + n[\omega_o t + \theta_o]) \end{bmatrix} \end{aligned} \tag{5.29}$$

Eq. 5.29 allows describing harmonic spectrum generated by carrier-based modulation techniques. The first line defines the DC component, the fundamental component ($n = 1$) and baseband harmonic components which are integer multiples of the fundamental component. The second line defines carrier harmonic components as integer multiples of the carrier frequency. The third line defines sideband harmonic components displaced from the carrier harmonic components by integer multiples of the fundamental frequency component.

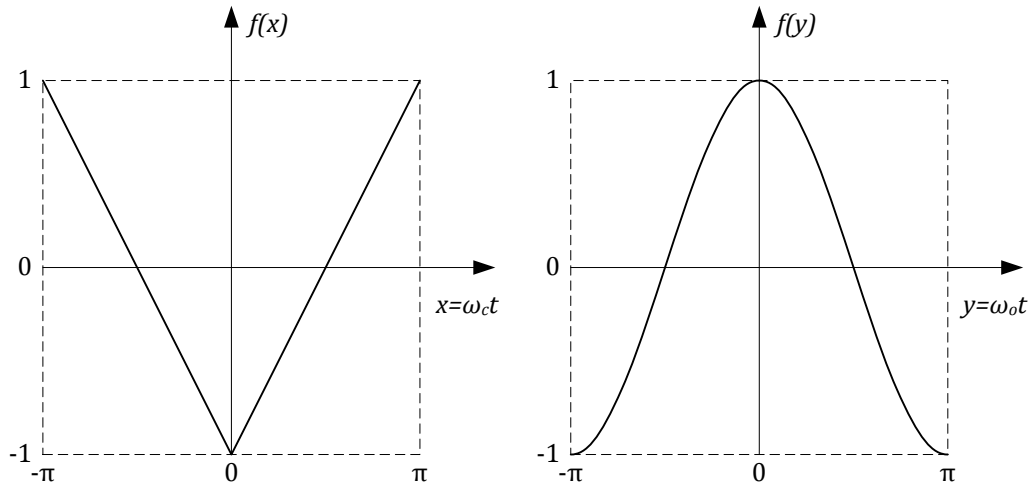

Figure 5.23 Triangle carrier and sine command functions in double-edge naturally sampled pulse-width modulation.

Eq. 5.27and 5.28 can be also expressed in complex Hilbert space L^2 in the following form [5.20]

$$\underline{C}_{mn} = A_{mn} + jB_{mn} = \frac{1}{2\pi^2} \iint_{-\pi}^{\pi} f(x,y) e^{j(mx+ny)}\, dxdy \tag{5.30}$$

In Eq. 5.30 $\left|\underline{C}_{mn}\right|$ defines the magnitude of the $(m\omega_c + n\omega_o)^{th}$ harmonic component of the switched waveform $f(x, y)$ created during a certain modulation process. Such an approach for the analytical description of various modulation techniques was investigated in [5.23], [5.24], [5.25], [5.26], [5.27], [5.28], [5.29]. In order to define $f(x, y)$ in case of double-edge naturally sampled modulation process it is first necessary to define the carrier and the command functions in terms of the time-dependent variables x and y shown in Figure 5.23. Based on the waveforms in the figure, the carrier waveform is defined by

$$f(x) = \begin{cases} -1 - \dfrac{2x}{\pi}, & x \in \langle -\pi, 0) \\ -1 + \dfrac{2x}{\pi}, & x \in \langle 0, \pi) \end{cases} \tag{5.31}$$

while the command waveform is defined by

$$f(y) = M\cos(y) \tag{5.32}$$

In multi-leg converters the phase leg switches between 0 and V_{DC} voltage rails. The phase leg switches from 0 to V_{DC} when the command waveforms is greater than the carrier waveform. It is also possible to assume that the phase leg switches from $-V_{DC}/2$ to $V_{DC}/2$ to obtain output voltage in reference to the DC-link neutral (zero) point v_{az} (see Figure 5.28), but this approach complicates the mathematics. Combining Eq. 5.31 and Eq. 5.32 the following expression of $f(x, y)$ can be achieved for $x \in \langle -\pi, 0)$

$$f(x,y) = V_{DC} \;\Rightarrow\; M\cos(y) \geq -1 - \frac{2x}{\pi} \;\Leftrightarrow\; x \geq -\frac{\pi}{2}(1 + M\cos(y)) \tag{5.33}$$

$$f(x,y) = 0 \;\Rightarrow\; M\cos(y) < -1 - \frac{2x}{\pi} \;\Leftrightarrow\; x < -\frac{\pi}{2}(1 + M\cos(y)) \tag{5.34}$$

and for $x \in \langle 0, \pi)$

$$f(x,y) = V_{DC} \;\Rightarrow\; M\cos(y) \geq -1 + \frac{2x}{\pi} \;\Leftrightarrow\; x \leq \frac{\pi}{2}(1 + M\cos(y)) \tag{5.35}$$

$$f(x,y) = 0 \;\Rightarrow\; M\cos(y) < -1 + \frac{2x}{\pi} \;\Leftrightarrow\; x > \frac{\pi}{2}(1 + M\cos(y)) \tag{5.36}$$

From Eq. 5.33 and Eq. 5.35 a unit cell of $f[x(t), y(t)]$ which identifies contours within the function $f(t)$ is constant for cyclic variations of $x(t)$ and $y(t)$, as presented in Figure 5.24. Within the contour $f(t)$ (i.e. dashed area) is constant and assumes the value V_{DC}.

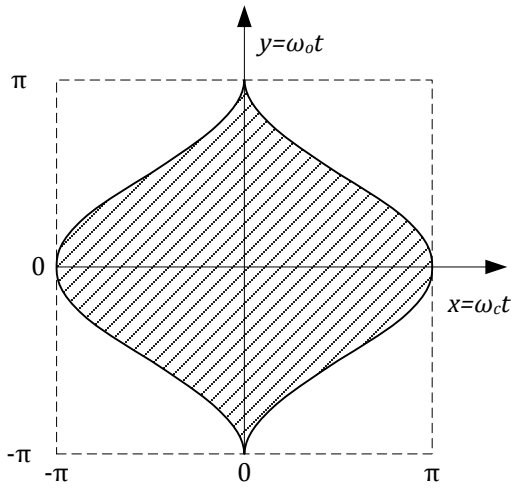

Figure 5.24 Unit cell for double-edge naturally sampled pulse-width modulation with $M = 1$.

Now based on Eq. 5.33 and Eq. 5.35 as well as Figure 5.24 one can define integration limits for the complex Fourier coefficient from Eq. 5.30

$$x \in \left[-\frac{\pi}{2}(1 + M\cos(y)), \frac{\pi}{2}(1 + M\cos(y))\right] \tag{5.37}$$

$$y \in [-\pi, \pi] \tag{5.38}$$

and Eq. 5.30 can be expressed for this particular conditions in the following way

$$\underline{C}_{mn} = A_{mn} + jB_{mn} = \frac{1}{2\pi^2}\int_{-\pi}^{\pi}\int_{-\frac{\pi}{2}(1+M\cos(y))}^{\frac{\pi}{2}(1+M\cos(y))} V_{DC}e^{j(mx+ny)}\,dxdy \tag{5.39}$$

which can be evaluated taking possible values of m and n into consideration. This approach allows evaluating separately DC offset, fundamental harmonic, baseband harmonics, sideband harmonics as well as carrier harmonics. Eq. 5.39 analytically describes converter output voltage $v_{an}(t)$ measured between the phase leg and the DC-link negative bus. The phase leg switched output voltage measured with respect to DC-link midpoint z is the same as the output voltage measured with respect to the negative rail n of the DC-link., but with $-V_{DC}/2$ offset. It is convenient to define $f[x, y]$ with respect to the negative rail n, instead of the DC-link midpoint z, it simplifies mathematics of the solution (this approach is also taken in [5.30]). It is also possible to define other integration limits by describing y as a function of x, but this makes mathematics more complex.

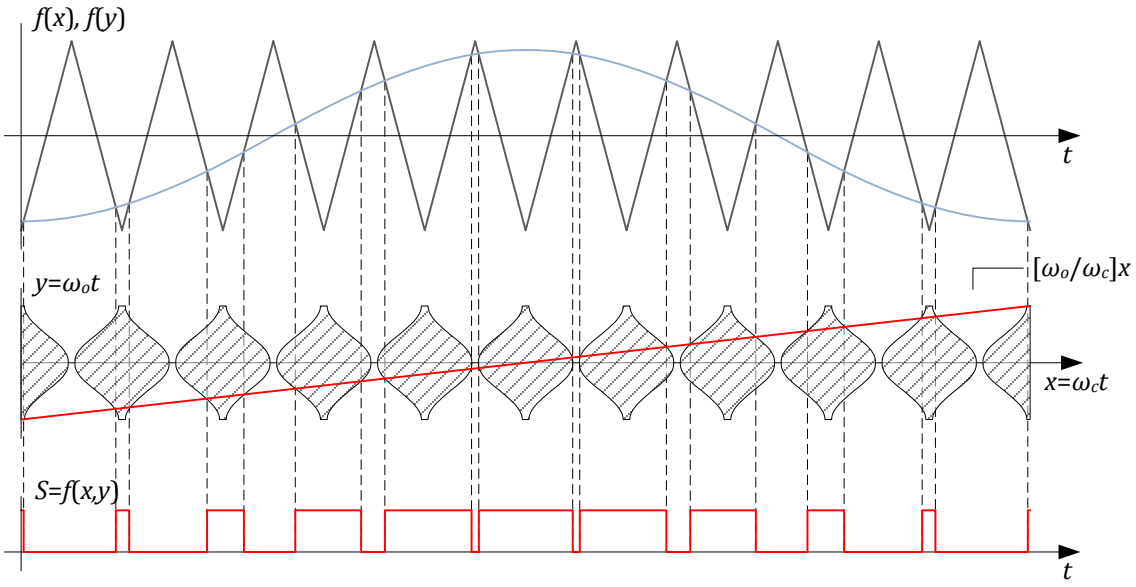

Figure 5.25 Double-edge naturally sampled pulse-width modulation within linear operation range ($M = 0.9, m_f = 10$).

Based on Eq. 5.39 one can achieve analytical solution separated frequency components generated by the two-level converter with double-edge naturally sampled pulse-width modulation [5.30].

– DC offset ($m = 0, n = 0$)

$$\underline{C}_{00} = A_{00} + jB_{00} = V_{DC} \tag{5.40}$$

– Baseband harmonics ($m = 0, n > 0$)

$$\underline{C}_{0n} = A_{0n} + jB_{0n}|_{n=1} = M\frac{V_{DC}}{2} \tag{5.41}$$

Double-edge naturally sampled pulse-width modulation produces only fundamental harmonic defined by modulation index M and DC-link voltage V_{DC} within the baseband harmonics range.

– Carrier harmonics ($m > 0, n = 0$)

$$\underline{C}_{m0} = A_{m0} + jB_{m0} = \frac{2V_{DC}}{m\pi}J_0\left(m\frac{\pi}{2}M\right)\sin\left(m\frac{\pi}{2}\right) \tag{5.42}$$

– Sideband harmonics ($m > 0, n \neq 0$)

$$\underline{C}_{mn} = A_{mn} + jB_{mn} = \frac{2V_{DC}}{m\pi}J_n\left(m\frac{\pi}{2}M\right)\sin\left([m+n]\frac{\pi}{2}\right) \tag{5.43}$$

Eq. 5.43 describes sideband harmonics generated by the modulation and caused by both the command and the carrier waveform. Please note that n can be negative as well positive which simply means that sideband harmonic component are distributed above

and below the carrier harmonics. The complete solution for the double-edge naturally sampled pulse-width modulation can be achieved by substituting results of the DC-link component in Eq. 5.40, baseband harmonic component from Eq. 5.41, carrier harmonic components from Eq. 5.42, and sideband harmonic components described in Eq. 5.43 into double Fourier series Eq. 5.29, which gives the time varying phase leg output voltage $v_{an}(t)$

$$\begin{aligned} f(t) = \frac{V_{DC}}{2} + M\frac{V_{DC}}{2}\cos(\omega_o t + \theta_o) \\ + \frac{2V_{DC}}{\pi}\sum_{m=1}^{\infty}\left[\frac{1}{m}J_0\left(m\frac{\pi}{2}M\right)\sin\left(m\frac{\pi}{2}\right)\cos(m[\omega_c t + \theta_c])\right] \\ + \frac{2V_{DC}}{\pi}\sum_{m=1}^{\infty}\sum_{\substack{n=-\infty \\ n\neq 0}}^{\infty}\left[\begin{array}{l}\frac{1}{m}J_n\left(m\frac{\pi}{2}M\right)\sin\left([m+n]\frac{\pi}{2}\right) \\ \times\cos(m[\omega_c t + \theta_c] + n[\omega_o t + \theta_o])\end{array}\right] \end{aligned} \quad 5.44$$

Figure 5.26 and Figure 5.27 present analytically calculated harmonic components for one phase leg of two-level inverter with double-edge natural sampled pulse-width modulation. The results are presented in time and frequency domain with reference to the DC-link midpoint z.

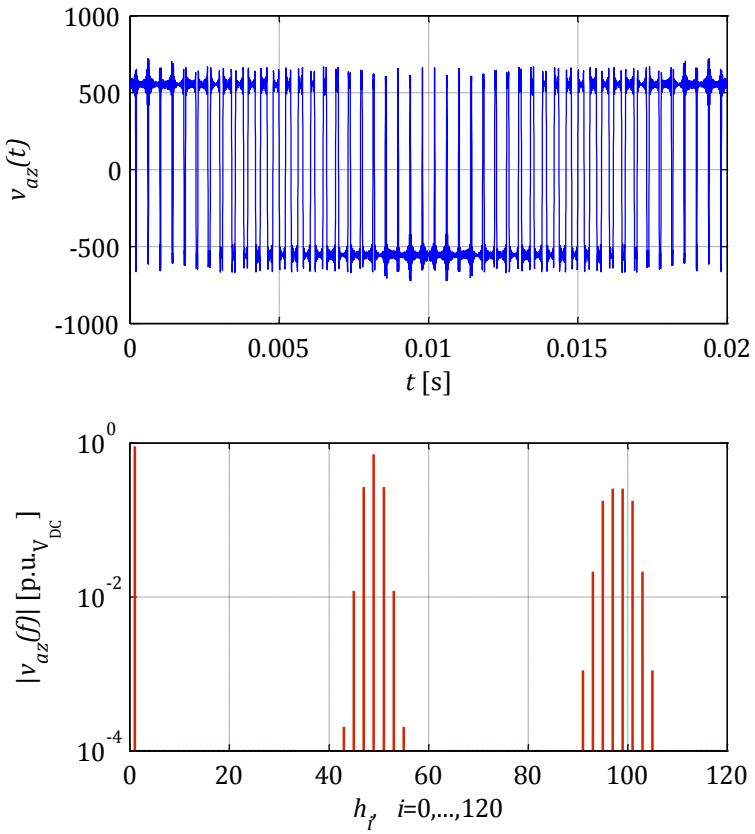

Figure 5.26 Theoretical waveform and spectrum of one leg with double-edge naturally sampled pulse-width modulation ($M = 0.9, m_f = f_c/f_o = 49$).

Harmonic spectrum presented in Figure 5.26 is normalized according to the DC-link voltage V_{DC}. Therefore it is easier comparing results from different converters with different modulation strategies. Characteristic in the voltage spectrum of double-edge natural sampled pulse-width modulation presented in Figure 5.26 is that there are no harmonic components within baseband except the first one. Calculation results presented in the figure are for the conditions of carrier ratio $m_f = 49$ and modulation index $M = 0.9$.

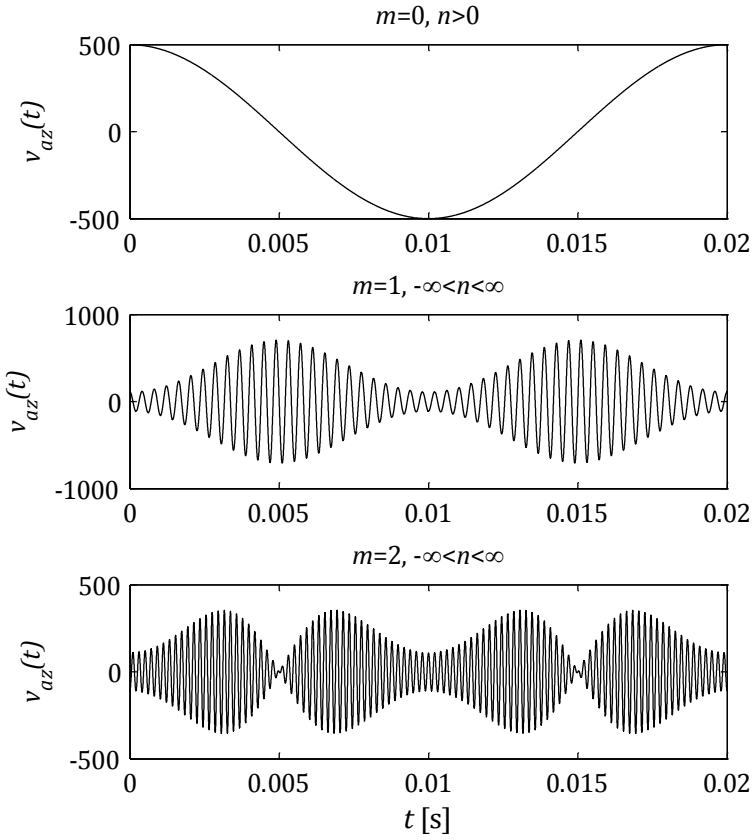

Figure 5.27 Baseband harmonics and harmonic carrier group presented in time domain.

The most significant feature of natural sampled pulse-width modulation with triangular carrier signal is that all odd sideband harmonic components around odd multiples of the carrier fundamental component, and all even sideband harmonic components are around even multiples of the carrier fundamental component are eliminated. This is caused by the $\sin[(m+n)\,\pi/2]$ expression contained in Eq. 5.44. Simply saying, if $m+n$ is an odd number the harmonic component is not eliminated.

Figure 5.28 presents a schematic diagram of two-level voltage source converter. The two-level voltage source converter is composed of three identical half-bridge converters (phase legs). The converter from Figure 5.28 is called two-level voltage source converter because each of its AC-side terminals can assume two voltage levels, either $-V_{DC}/2$ or $V_{DC}/2$. The DC sides of half-bridge converters are connected in parallel

with a common DC-side voltage source. Each of AC-side terminals of half-bridge converters is associated with one phase of the three-phase voltage source converter, thus term phase leg is commonly used. The two-level voltage source converter can provide a bidirectional power flow either from the DC-side voltage source to the three-phase AC system or in opposite direction [5.31].

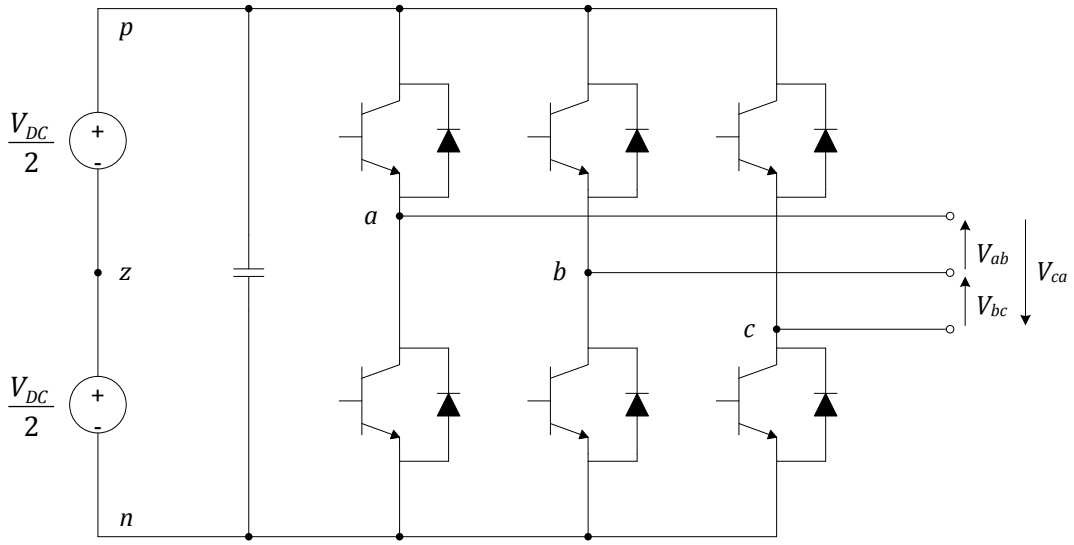

Figure 5.28 Schematic diagram of three-phase two-level voltage source converter.

The fundamental modulation concepts of three-phase inverters remain the same as of single-phase inverters. In the case of three-phase voltage source converter, the sine pulse-width modulation process requires three sinusoidal references (command signals) displaced by 120° with unity gain.

$$v_{az}^{*}(t) = \frac{2V_o}{V_{DC}}\cos(\omega_o t) = M\cos(\omega_o t) \tag{5.45}$$

$$v_{bz}^{*}(t) = \frac{2V_o}{V_{DC}}\cos\left(\omega_o t - \frac{2\pi}{3}\right) = M\cos\left(\omega_o t - \frac{2\pi}{3}\right) \tag{5.46}$$

$$v_{cz}^{*}(t) = \frac{2V_o}{V_{DC}}\cos\left(\omega_o t + \frac{2\pi}{3}\right) = M\cos\left(\omega_o t + \frac{2\pi}{3}\right) \tag{5.47}$$

where V_o is the power converter output voltage, $M = 2V_o/V_{DC}$ is the modulation index. Sometimes in different publications can be found the expression $M = V_o/V_{DC}$. In this analysis it is assumed that DC-link voltage is the voltage measured between positive and negative DC busbars. This is due to the fact that sometimes the DC-link midpoint is not defined. Also in different datasheets DC-link voltage nominal value used to be provided in reference to voltage between positive p and negative n rails of the DC-link circuit. Due to this fact it is also commonly seen to talk about voltage between phase legs of the converter. Three-phase $l - l$ (line-to-line) fundamental command signals are given by differences between phase leg command signals

$$v_{ab}^{*}(t) = v_{az}^{*}(t) - v_{bz}^{*}(t) = M\sqrt{3}\cos\left(\omega_o t + \frac{\pi}{6}\right) \tag{5.48}$$

$$v_{bc}^{*}(t) = v_{bz}^{*}(t) - v_{cz}^{*}(t) = M\sqrt{3}\cos\left(\omega_o t - \frac{\pi}{2}\right) \tag{5.49}$$

$$v_{ca}^{*}(t) = v_{cz}^{*}(t) - v_{az}^{*}(t) = M\sqrt{3}\cos\left(\omega_o t + \frac{5\pi}{6}\right) \tag{5.50}$$

In order to analytically describe each of phase voltages of the three-phase two-level voltage source converter the phases should be displaced by electrical 120°. The analytical calculation of harmonics generated by three-phase two-level voltage source converter with double-edge naturally sampled pulse-width modulation can be directly obtained from Eq. 5.44 by setting the displacement angle $\theta_{3ph} = [0, -2\pi/3\,, 2\pi/3]$ for phase a, b and c respectively

$$\begin{aligned} v_{az}(t) &= M\frac{V_{DC}}{2}\cos(\omega_o t) \\ &+ \frac{2V_{DC}}{\pi}\sum_{m=1}^{\infty}\sum_{n=-\infty}^{\infty}\left[\begin{array}{c}\frac{1}{m}J_n\left(m\frac{\pi}{2}M\right)\sin\left([m+n]\frac{\pi}{2}\right)\\ \times\cos(m[\omega_c t+\theta_c]+n[\omega_o t+\theta_o])\end{array}\right] \end{aligned} \tag{5.51}$$

$$\begin{aligned} v_{bz}(t) &= M\frac{V_{DC}}{2}\cos\left(\omega_o t - \frac{2\pi}{3}\right) \\ &+ \frac{2V_{DC}}{\pi}\sum_{m=1}^{\infty}\sum_{n=-\infty}^{\infty}\left[\begin{array}{c}\frac{1}{m}J_n\left(m\frac{\pi}{2}M\right)\sin\left([m+n]\frac{\pi}{2}\right)\\ \times\cos\left(m[\omega_c t+\theta_c]+n\left[\omega_o t+\theta_o-\frac{2\pi}{3}\right]\right)\end{array}\right] \end{aligned} \tag{5.52}$$

$$\begin{aligned} v_{cz}(t) &= M\frac{V_{DC}}{2}\cos\left(\omega_o t + \frac{2\pi}{3}\right) \\ &+ \frac{2V_{DC}}{\pi}\sum_{m=1}^{\infty}\sum_{n=-\infty}^{\infty}\left[\begin{array}{c}\frac{1}{m}J_n\left(m\frac{\pi}{2}M\right)\sin\left([m+n]\frac{\pi}{2}\right)\\ \times\cos\left(m[\omega_c t+\theta_c]+n\left[\omega_o t+\theta_o+\frac{2\pi}{3}\right]\right)\end{array}\right] \end{aligned} \tag{5.53}$$

Subtracting the phase leg analytical solutions from Eq. 5.51, Eq. 5.52, and Eq. 5.53 the phase-to-phase voltage is obtained as following

$$\begin{aligned} &v_{ab}(t) = v_{az}(t) - v_{bz}(t) \\ &= M\frac{V_{DC}}{2}\left[\cos(\omega_o t+\theta_o) - \cos\left(\omega_o t+\theta_o-\frac{2\pi}{3}\right)\right] \\ &+ \frac{2V_{DC}}{\pi}\sum_{m=1}^{\infty}\sum_{n=-\infty}^{\infty}\left[\begin{array}{c}\frac{1}{m}J_n\left(m\frac{\pi}{2}M\right)\sin\left([m+n]\frac{\pi}{2}\right)\\ \times\left\{\begin{array}{c}\cos(m[\omega_c t+\theta_c]+n[\omega_o t+\theta_o])\\ -\cos\left(m[\omega_c t+\theta_c]+n\left[\omega_o t+\theta_o-\frac{2\pi}{3}\right]\right)\end{array}\right\}\end{array}\right] \end{aligned} \tag{5.54}$$

In order to simplify Eq. 5.54 some trigonometric identities can be used

$$\cos(\xi_1) - \cos(\xi_2) = -2\sin\left(\frac{\xi_1 + \xi_2}{2}\right)\sin\left(\frac{\xi_1 - \xi_2}{2}\right) \tag{5.55}$$

After using the identity from Eq. 5.55 and some manipulation Eq. 5.54 can be expressed as

$$\begin{aligned} & v_{ab}(t) \\ & = M\frac{V_{DC}}{2}\left[-\sqrt{3}\sin\left(\omega_o t + \theta_o - \frac{\pi}{3}\right)\right] \\ & + \frac{4V_{DC}}{\pi}\sum_{m=1}^{\infty}\sum_{n=-\infty}^{\infty}\left\{\begin{array}{c}\frac{1}{m}J_n\left(m\frac{\pi}{2}M\right)\sin\left([m+n]\frac{\pi}{2}\right) \\ \times\left[-\sin\left(m[\omega_c t + \theta_c] + n\left[\omega_o t + \theta_o - \frac{\pi}{3}\right]\right)\sin\left(n\frac{\pi}{3}\right)\right]\end{array}\right\} \end{aligned} \tag{5.56}$$

Using trigonometric functions symmetry identities $\sin(-\xi) = -\sin(\xi)$, $\cos(-\xi) = \cos(\xi)$ and co-function identities $\sin(\pi/2 - \xi) = \cos(\xi)$, $\cos(\pi/2 - \xi) = \sin(\xi)$ Eq. 5.56 can be finally modified to

$$\begin{aligned} & v_{ab}(t) \\ & = M\frac{V_{DC}}{2}\sqrt{3}\cos\left(\omega_o t + \theta_o + \frac{\pi}{6}\right) \\ & + \frac{4V_{DC}}{\pi}\sum_{m=1}^{\infty}\sum_{n=-\infty}^{\infty}\left\{\begin{array}{c}\frac{1}{m}J_n\left(m\frac{\pi}{2}M\right)\sin\left([m+n]\frac{\pi}{2}\right)\sin\left(n\frac{\pi}{3}\right) \\ \times\cos\left(\frac{\pi}{2} + m[\omega_c t + \theta_c] + n\left[\omega_o t + \theta_o - \frac{\pi}{3}\right]\right)\end{array}\right\} \end{aligned} \tag{5.57}$$

Figure 5.29 and Figure 5.30 present analytically calculated harmonic components for phase-to-phase output voltage of three-phase two-level voltage source converter with double-edge naturally sampled pulse-width modulation. The results are presented in time and frequency domain in Figure 5.29. According to Eq. 5.57 all triplen sideband harmonics are cancelled. This is caused by the $\sin(n\pi/3)$ term which eliminates all harmonics when n is a multiple of 3. This can be interpreted that all harmonics which are multiples of 3 are common mode (zero-sequence) and are cancelled on an $l - l$ basis.

Such analytical description constitutes a basis to explain harmonic generation by the wind turbine. It can be seen that harmonic spectrum presented in Figure 5.29 is comparable with measurements of the grid-side converter. Of course additional conditions such as harmonic content in the command signal as well as sampling of the command signal should be taken into consideration in order to better understand harmonic phenomenon present in the analysed system. Both aspects will be described later in this chapter.

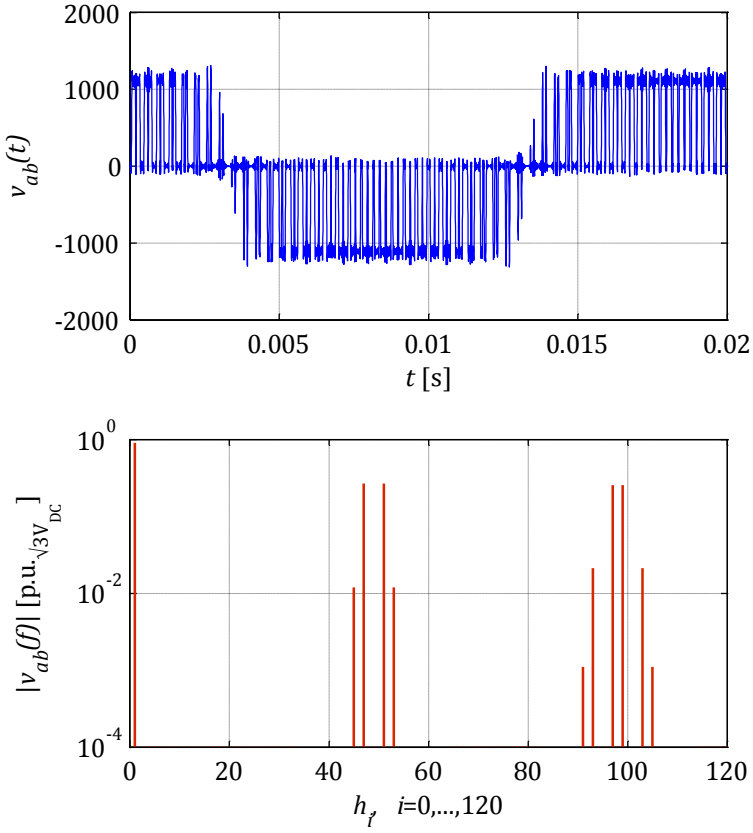

Figure 5.29 Harmonic components of phase-to-phase output voltage ($M = 0.9, m_f = 49$).

Similarly like in case of phase-leg voltages, all sideband harmonics for which term $\sin([m+n]\,\pi/2)$ from Eq. 5.57 is equal to 0 are cancelled (i.e. even the combination $m \pm n$) in phase-to-phase output voltage. Saying in other words, all odd sideband harmonics in carrier groups of odd carrier fundamental multiples and all even sideband harmonics in carrier groups of even carrier fundamental multiples are cancelled in double-edge naturally sampled pulse-width modulation. Additionally it is worth emphasizing that carrier harmonics are also cancelled, since they are the same (common mode harmonics) for all phase legs as it can be seen in Figure 5.29.

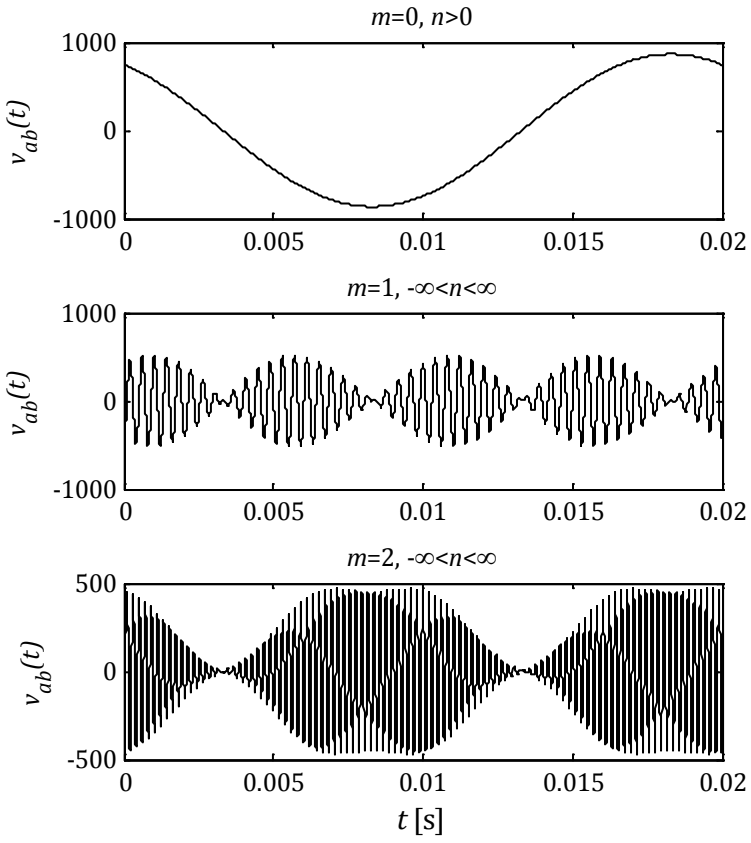

Figure 5.30 Baseband harmonic and harmonics from first two carrier groups presented in time domain.

The most significant sideband harmonics from the first carrier group are at frequencies of $\omega_c t \pm 2\omega_o t$, $\omega_c t \pm 4\omega_o t$ and from the second carrier group are at frequencies of $2\omega_c t \pm \omega_o t$, $2\omega_c t \pm 5\omega_o t$, and $2\omega_c t \pm 7\omega_o t$. Sideband harmonic components at frequency of $2\omega_c t \pm 3\omega_o t$ in the second carrier group are cancelled due to the term $\sin(n\pi/3)$.

5.2.1.3 PARALLEL-CONNECTED WIND TURBINES

From Eq. 5.57 one can see that all harmonic angles are analytically defined. Only θ_c and θ_o phase angles can be freely defined in double-edge naturally sampled pulse-width modulation. This opportunity can be beneficial for instance in harmonic cancellation process. Changes of θ_o in three-phase grid-connected voltage source converter is associated with output power changes therefore cannot be freely adjusted.

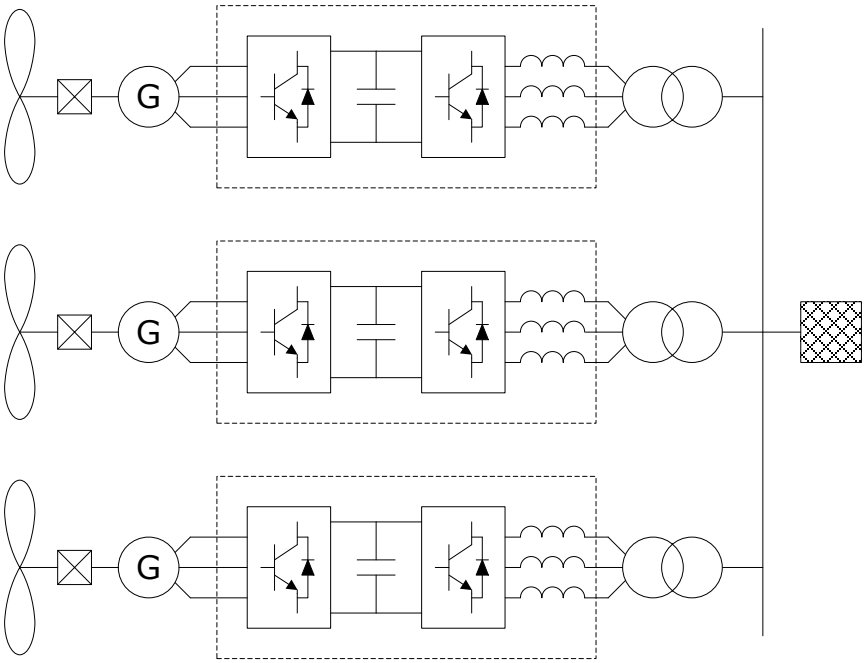

Figure 5.31 Wind turbines equipped with full-scale back-to-back converters and connected to the grid.

Appropriate adjustment of grid-connected wind turbines operating in parallel in wind farm clusters (see Figure 5.31) with pulse-width modulation strategy can reduce harmonic content generated by the modulator according to Eq. 5.57. The full-scale power converter presented in Figure 5.31 typically includes a generator bridge, which in normal operation operates as an active rectifier to supply power to a DC-link circuit. The generator-side converter can have any suitable topology based on half-bridge converters fully controlled and regulated using pulse-width modulation. The DC output of the generator bridge to the DC terminals of a network bridge though the DC-link circuit. The grid-side converter normally operates and is also considered within the analysis as an inverter. The network bridge can have a topology as presented in Figure 5.28 fully controlled using the pulse-width modulation strategy. The AC output voltage of the grid-side converter is filtered and supplied to the fixed frequency supply network via a step-up transformer.

If two or more power converters are connected to the power grid, the overall harmonic voltage distortion may exceed required limits defined for the point of common coupling. Such scenario can be typical in case of large offshore wind warms where a plurality of wind turbines might be connected to the grid through a parallel connection. The pulse-width modulation strategy used in grid-side converters typically operates at a given fixed switching frequency. The mixing between the nominally fixed frequency of the power grid and the switching frequency of the double-edge naturally sampled pulse-width modulation causes harmonics in the output voltage of the three-phase network bridge according to formula in Eq. 5.57 [5.15].

Appropriate control method of the grid-side converter that uses a plurality of parallel connected converters can be used to interface the power grid [5.32], [5.33]. As it can be

seen from Eq. 5.57 carrier group harmonic angles are determined by the fundamental frequency component phase angle θ_o as well as carrier signal phase angle θ_c. Well adjusted carrier signal phase in different parallel connected wind turbines can affect partial or even complete harmonic cancelation [5.34]. Assuming that wind turbines in a particular offshore wind farm operate in clusters, each cluster can be considered as a separated network and harmonics due to pulse-width modulation strategy generated in other clusters can be neglected [5.35].

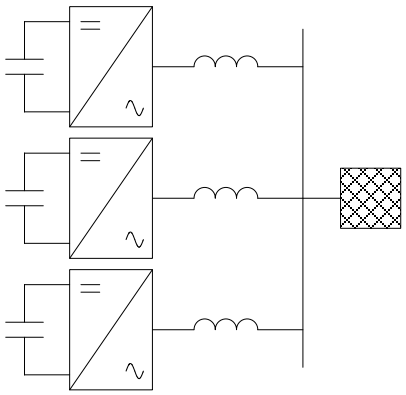

Figure 5.32 Simplified single line diagram of parallel connected wind turbines.

Figure 5.32 shows a simplified single-phase equivalent circuit of parallel-connected wind turbines within the same cluster in a particular offshore wind farm. Since wind turbines with full-scale back-to-back converter are taken into consideration, only the network bridge is of the main concern. Earlier it was presented based on measurement data that the harmonic content in the DC-link circuit has insignificant contribution to harmonic generation by the wind turbine. Normally in wind farm electrical networks wind turbines are connected via Δ-Y step-up transformer. Due to this fact all common-mode signals are cancelled between phases as it is described by Eq. 5.57.

Taking into consideration that the resistive part of the main reactor as well as the wind turbine transformer is negligible in comparison to the inductive part, the impedance between power converter AC terminals and the common connection point is simplified to pure inductance (see Figure 5.32). In this particular case the phase current flowing from each wind turbine lags the voltage by $\pi/2$. The magnitude if proportional to the inductance L, is according to Eq. 5.58

$$i(t) = \frac{1}{L}\int v(t)\,dt = \frac{1}{L}\int A\cos(\omega t + \theta)\,dt = \frac{A}{\omega L}\cos\left(\frac{\pi}{2} - [\omega t + \theta]\right) \qquad 5.58$$

In order to clearly show possible harmonic cancellation of parallel-connected grid-side converters, few significant system simplifications are needed. Of course such simplifications would not affect the idea of carrier signal phase shift adjustment. It can be assumed that all of the wind turbines are connected through the same impedance to the same node. If one assumes that the point of connection is shorten (i.e. the external

network short circuit impedance for frequencies around sideband harmonic components is equal to 0), the current can be expressed in the following way

$$\begin{aligned} i_a(t) &= \frac{1}{L}\int v_{az}(t)\,dt \\ &= \frac{M}{\omega_o L}\frac{V_{DC}}{2}\cos\left(\frac{\pi}{2} - [\omega_o t + \theta_o]\right) \\ &+ \frac{2V_{DC}}{\pi L}\sum_{m=1}^{\infty}\sum_{n=-\infty}^{\infty}\left\{\begin{array}{c}\frac{1}{[m\omega_c + n\omega_o]}\frac{1}{m}J_n\left(m\frac{\pi}{2}M\right)\sin\left([m+n]\frac{\pi}{2}\right) \\ \times\cos\left(\frac{\pi}{2} - m[\omega_c t + \theta_c] - n[\omega_o t + \theta_o]\right)\end{array}\right\} \end{aligned} \quad 5.59$$

All possible harmonic cancellations due to the application of Δ-Y transformers as well as introduction of additional filters are not taken into consideration in this analysis. If all carrier signals are in phase (i.e. $\theta_c = 0°$) the total current flowing from three wind turbines presented in Figure 5.32 is summed up and equal to

$$\begin{aligned} & i_{total}(t) \\ &= \frac{3M}{\omega_o L}\frac{V_{DC}}{2}\cos\left(\frac{\pi}{2} - [\omega_o t + \theta_o]\right) \\ &+ \frac{6V_{DC}}{\pi L}\sum_{m=1}^{\infty}\sum_{n=-\infty}^{\infty}\left\{\begin{array}{c}\frac{1}{m[m\omega_c + n\omega_o]}J_n\left(m\frac{\pi}{2}M\right)\sin\left([m+n]\frac{\pi}{2}\right) \\ \times\cos\left(\frac{\pi}{2} - m\omega_c t - n[\omega_o t + \theta_o]\right)\end{array}\right\} \end{aligned} \quad 5.60$$

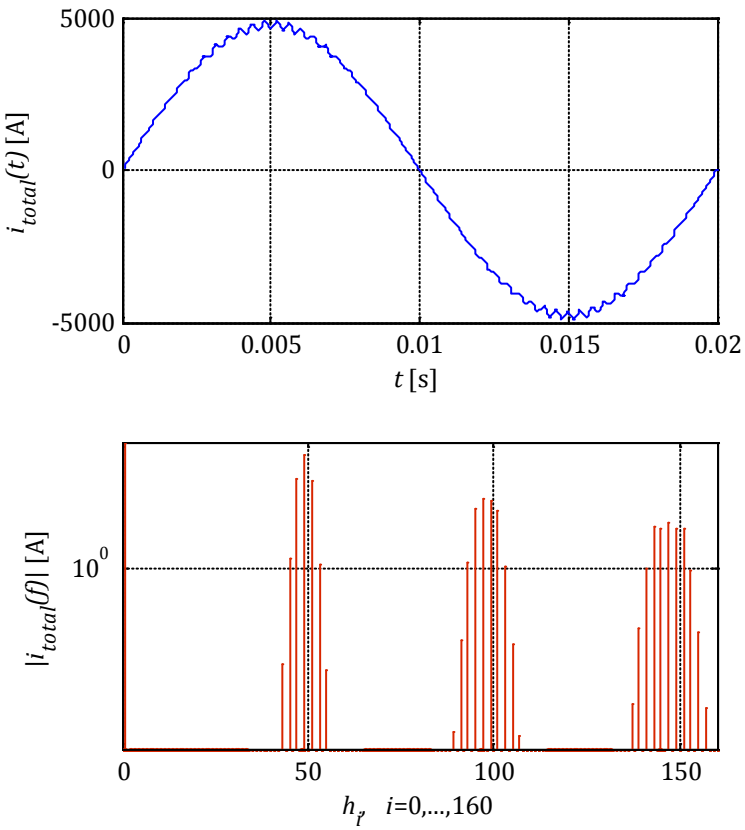

Figure 5.33 Total current generated by three parallel-connected wind turbines with ideally synchronized carrier signals.

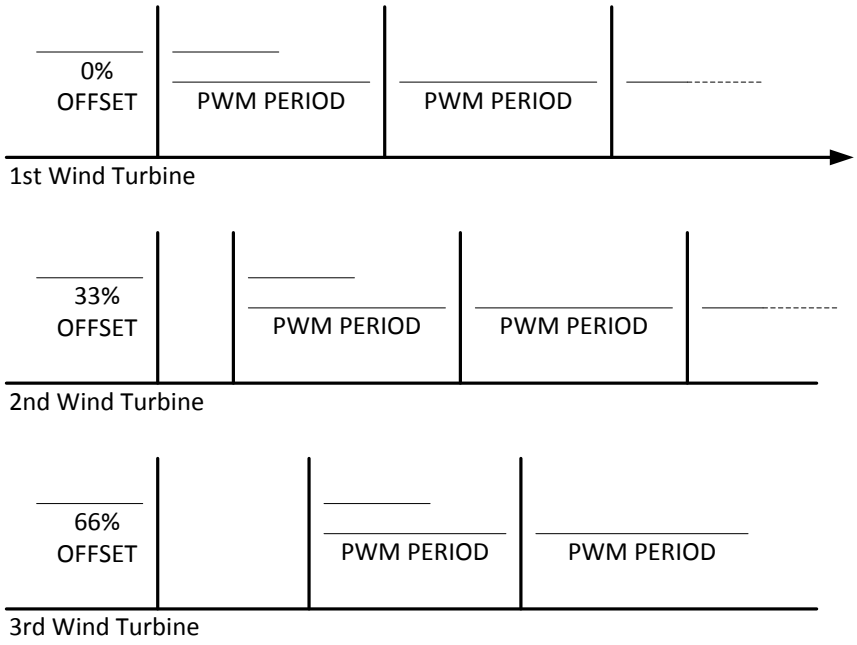

Figure 5.34 Carrier signal phase angle offset in three de-synchronized wind turbines.

Although additive harmonic components from carrier groups can be reduced by the change of phase of the carrier signals for particulars wind turbines. If θ_c is equal

to 0°, 120°, and 240° for wind turbine 1, 2, and 3 respectively (see Figure 5.34), the total current is expressed in the following way

$$\begin{aligned} & i_{total}(t) \\ & = \frac{3M}{\omega_o L}\frac{V_{DC}}{2}\cos\left(\frac{\pi}{2} - [\omega_o t + \theta_o]\right) \\ & + \frac{2V_{DC}}{\pi L}\sum_{m=1}^{\infty}\sum_{n=-\infty}^{\infty}\left\{\begin{array}{l} \dfrac{1}{m[m\omega_c + n\omega_o]}J_n\left(m\dfrac{\pi}{2}M\right)\sin\left([m+n]\dfrac{\pi}{2}\right) \\ \times\left[\begin{array}{c} \cos\left(\dfrac{\pi}{2} - m\omega_c t - n[\omega_o t + \theta_o]\right) \\ +\cos\left(\dfrac{\pi}{2} - m\left[\omega_c t + \dfrac{2\pi}{3}\right] - n[\omega_o t + \theta_o]\right) \\ +\cos\left(\dfrac{\pi}{2} - m\left[\omega_c t + \dfrac{4\pi}{3}\right] - n[\omega_o t + \theta_o]\right) \end{array}\right] \end{array}\right\} \end{aligned} \tag{5.61}$$

After some rearrangements and application of the following trigonometric identity

$$\cos(\xi_1 \pm \xi_2) = \cos(\xi_1)\cos(\xi_2) \mp \sin(\xi_1)\sin(\xi_2) \tag{5.62}$$

Eq. 5.61 can be expressed

$$\begin{aligned} & i_{total}(t) \\ & = \frac{3M}{\omega_o L}\frac{V_{DC}}{2}\cos\left(\frac{\pi}{2} - [\omega_o t + \theta_o]\right) \\ & + \frac{2V_{DC}}{\pi L}\sum_{m=1}^{\infty}\sum_{n=-\infty}^{\infty}\left\{\begin{array}{l} \dfrac{1}{m[m\omega_c + n\omega_o]}J_n\left(m\dfrac{\pi}{2}M\right)\sin\left([m+n]\dfrac{\pi}{2}\right) \\ \times\left[\begin{array}{c} \cos\left(\dfrac{\pi}{2} - n[\omega_o t + \theta_o]\right)\cos(-m[\omega_c t + 0]) \\ +\sin\left(\dfrac{\pi}{2} - n[\omega_o t + \theta_o]\right)\sin(-m[\omega_c t + 0]) \\ +\cos\left(\dfrac{\pi}{2} - n[\omega_o t + \theta_o]\right)\cos\left(-m\left[\omega_c t + \dfrac{2\pi}{3}\right]\right) \\ +\sin\left(\dfrac{\pi}{2} - n[\omega_o t + \theta_o]\right)\sin\left(-m\left[\omega_c t + \dfrac{2\pi}{3}\right]\right) \\ +\cos\left(\dfrac{\pi}{2} - n[\omega_o t + \theta_o]\right)\cos\left(-m\left[\omega_c t + \dfrac{4\pi}{3}\right]\right) \\ +\sin\left(\dfrac{\pi}{2} - n[\omega_o t + \theta_o]\right)\sin\left(-m\left[\omega_c t + \dfrac{4\pi}{3}\right]\right) \end{array}\right] \end{array}\right\} \end{aligned} \tag{5.63}$$

After rearrangement Eq. 5.63 can be simplified to

$$
\begin{aligned}
&i_{total}(t)\\
&=\frac{3M}{\omega_o L}\frac{V_{DC}}{2}\cos\left(\frac{\pi}{2}-[\omega_o t+\theta_o]\right)\\
&+\frac{2V_{DC}}{\pi L}\sum_{m=1}^{\infty}\sum_{n=-\infty}^{\infty}\left\{\times\left[\begin{array}{l}\dfrac{1}{m[m\omega_c+n\omega_o]}J_n\left(m\dfrac{\pi}{2}M\right)\sin\left([m+n]\dfrac{\pi}{2}\right)\\ \cos\left(\dfrac{\pi}{2}-n[\omega_o t+\theta_o]\right)\left\{\begin{array}{c}\cos(-m[\omega_c t+0])\\ +\cos\left(-m\left[\omega_c t+\dfrac{2\pi}{3}\right]\right)\\ +\cos\left(-m\left[\omega_c t+\dfrac{4\pi}{3}\right]\right)\end{array}\right\}\\ +\sin\left(\dfrac{\pi}{2}-n[\omega_o t+\theta_o]\right)\left\{\begin{array}{c}\sin(-m[\omega_c t+0])\\ +\sin\left(-m\left[\omega_c t+\dfrac{2\pi}{3}\right]\right)\\ +\sin\left(-m\left[\omega_c t+\dfrac{4\pi}{3}\right]\right)\end{array}\right\}\end{array}\right]\right\}
\end{aligned}
\tag{5.64}
$$

Taking into consideration Euler's formulas from Eq. 5.65 and Eq. 5.66

$$\cos(\theta)=\mathcal{R}e\{e^{j\theta}\}=\frac{e^{j\theta}+e^{-j\theta}}{2} \tag{5.65}$$

$$\sin(\theta)=\mathcal{I}m\{e^{j\theta}\}=\frac{e^{j\theta}-e^{-j\theta}}{2j} \tag{5.66}$$

it becomes

$$
\begin{aligned}
&i_{total}(t)\\
&=\frac{3M}{\omega_o L}\frac{V_{DC}}{2}\cos\left(\frac{\pi}{2}-[\omega_o t+\theta_o]\right)\\
&+\frac{2V_{DC}}{\pi L}\sum_{m=1}^{\infty}\sum_{n=-\infty}^{\infty}\frac{1}{m[m\omega_c+n\omega_o]}J_n\left(m\frac{\pi}{2}M\right)\sin\left([m+n]\frac{\pi}{2}\right)\\
&\times\left[\begin{array}{l}\cos\left(\dfrac{\pi}{2}-n[\omega_o t+\theta_o]\right)\left\{\dfrac{1}{2}\left[\begin{array}{c}e^{jm\omega_c t}\left(e^{jm0}+e^{jm\frac{2\pi}{3}}+e^{jm\frac{4\pi}{3}}\right)\\ +e^{-jm\omega_c t}\left(e^{-jm0}+e^{-jm\frac{2\pi}{3}}+e^{-jm\frac{4\pi}{3}}\right)\end{array}\right]\right\}\\ +\sin\left(\dfrac{\pi}{2}-n[\omega_o t+\theta_o]\right)\left\{\dfrac{1}{2j}\left[\begin{array}{c}e^{-jm\omega_c t}\left(e^{-jm0}+e^{-jm\frac{2\pi}{3}}+e^{-jm\frac{4\pi}{3}}\right)\\ -e^{jm\omega_c t}\left(e^{jm0}+e^{jm\frac{2\pi}{3}}+e^{jm\frac{4\pi}{3}}\right)\end{array}\right]\right\}\end{array}\right]
\end{aligned}
\tag{5.67}
$$

Based on Eq. 5.67 all sideband harmonic components are cancelled for non-triplen values of m. If $m=3,6,9,\ldots$ angles assume integer multiple of π and due to the common-mode harmonic components no cancellation occurs.

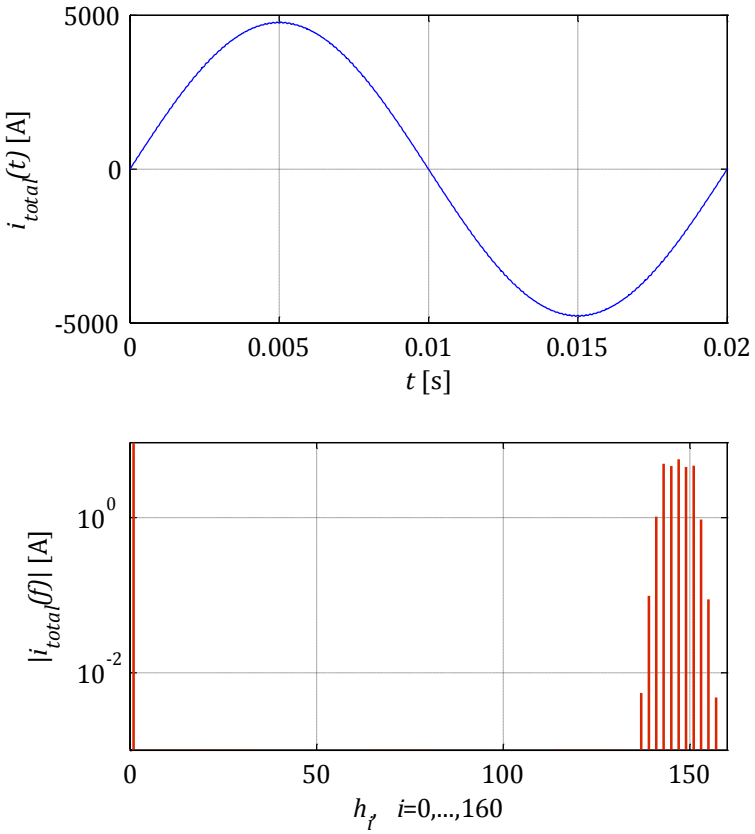

Figure 5.35 Total current generated by three parallel-connected wind turbines with ideal carrier signal phase shift.

Of course it is possible to de-synchronize any number of parallel-connected wind turbines. Some constraints are associated with increasing the number of wind turbines which are going to be present. The solution of three parallel-connected converters can be generalized to any number of wind turbines p in the following way

$$\begin{aligned} & i_{total}(t) \\ & = \frac{p}{\omega_o L} M \frac{V_{DC}}{2} \sin(\omega_o t + \theta_o) \\ & + \frac{2V_{DC}}{\pi L} \sum_{m=1}^{\infty} \sum_{n=-\infty}^{\infty} \left\{ \begin{array}{l} \dfrac{1}{m[m\omega_c + n\omega_o]} J_n\left(m\frac{\pi}{2}M\right) \sin\left([m+n]\frac{\pi}{2}\right) \\ \times \left[\begin{array}{l} \sin(n[\omega_o t + \theta_o]) \displaystyle\sum_{i=0}^{p-1} \cos\left(m\left[\omega_c t + \frac{2i\pi}{p}\right]\right) \\ -\cos(n[\omega_o t + \theta_o]) \displaystyle\sum_{i=0}^{p-1} \sin\left(m\left[\omega_c t + \frac{2i\pi}{p}\right]\right) \end{array} \right] \end{array} \right\} \end{aligned} \quad 5.68$$

And finally

$$
\begin{aligned}
&i_{total}(t) \\
&= \frac{p}{\omega_o L} M \frac{V_{DC}}{2} \sin(\omega_o t + \theta_o) \\
&+ \frac{2V_{DC}}{\pi L} \sum_{m=1}^{\infty} \sum_{n=-\infty}^{\infty} \left\{ \times \left[\begin{array}{l} \dfrac{1}{m[m\omega_c + n\omega_o]} J_n\left(m\dfrac{\pi}{2}M\right) \sin\left([m+n]\dfrac{\pi}{2}\right) \\ \dfrac{\sin(n[\omega_o t + \theta_o])}{2} \left\{ \begin{array}{l} e^{jm\omega_c t} \sum_{i=0}^{p-1} e^{jm\frac{2i\pi}{p}} \\ +e^{-jm\omega_c t} \sum_{i=0}^{p-1} e^{-jm\frac{2i\pi}{p}} \end{array} \right\} \\ -\dfrac{\cos(n[\omega_o t + \theta_o])}{2j} \left\{ \begin{array}{l} e^{jm\omega_c t} \sum_{i=0}^{p-1} e^{jm\frac{2i\pi}{p}} \\ -e^{-jm\omega_c t} \sum_{i=0}^{p-1} e^{-jm\frac{2i\pi}{p}} \end{array} \right\} \end{array} \right] \right\}
\end{aligned}
\tag{5.69}
$$

From the general solution in Eq. 5.69 it can be seen that no harmonic components cancellation occurs for carrier groups in which m is every integer multiple of the number of parallel-connected wind turbines p.

$$
\sum_{i=0}^{p-1} e^{\pm jm\frac{2i\pi}{p}} = 0, \qquad \{im \neq p : \; i, m \in \mathbb{N}_0, p \in \mathbb{N}\} \tag{5.70}
$$

$$
\sum_{i=0}^{p-1} e^{\pm jm\frac{2i\pi}{p}} = p, \qquad \{m = p : m \in \mathbb{N}_0, p \in \mathbb{N}\} \tag{5.71}
$$

With appropriate carrier signal phase adjustments according to Eq. 5.70, all carrier groups except $p = m$ can be cancelled. Figure 5.35 presents cancellation of the first and the second carrier group in three wind turbines connected in parallel. The current waveform is without the most significant harmonic components generated due to the pulse-width modulation, as in Figure 5.33.

Another interesting issue to take into consideration is that in practice, the ideal performance of the real-life parallel-connected converters may be degraded. This can be affected by many factors, such as ideal carrier signal phase angle variation because of delays in the transmission or synchronization errors [5.36]. However, even if plural grid-side converters within the same cluster are operated with less than analytically calculated phase shift, harmonic component magnitudes still can be reduced, compared to the results shown in Figure 5.33. Assuming that the phase angle variation can be introduced by a normally distributed real-valued random variable $X \sim \mathcal{N}(0, \sigma^2)$, the random variable X can be introduced into Eq. 5.69 to describe the synchronization error

$$
\begin{aligned}
&i_{total}(t)\\
&=\frac{p}{\omega_o L}M\frac{V_{DC}}{2}\sin(\omega_o t+\theta_o)\\
&+\frac{2V_{DC}}{\pi L}\sum_{m=1}^{\infty}\sum_{n=-\infty}^{\infty}\left\{\times\left[\begin{array}{l}\dfrac{1}{m[m\omega_c+n\omega_o]}J_n\left(m\dfrac{\pi}{2}M\right)\sin\left([m+n]\dfrac{\pi}{2}\right)\\ \sin(n[\omega_o t+\theta_o])\displaystyle\sum_{i=0}^{p-1}\cos\left(m\left[\omega_c t+\frac{2i\pi}{p}+X_i\right]\right)\\ -\cos(n[\omega_o t+\theta_o])\displaystyle\sum_{i=0}^{p-1}\sin\left(m\left[\omega_c t+\frac{2i\pi}{p}+X_i\right]\right)\end{array}\right]\right\}
\end{aligned}
\tag{5.72}
$$

And after using the same rearrangement as above

$$
\begin{aligned}
&i_{total}(t)\\
&=\frac{p}{\omega_o L}M\frac{V_{DC}}{2}\sin(\omega_o t+\theta_o)\\
&+\frac{2V_{DC}}{\pi L}\sum_{m=1}^{\infty}\sum_{n=-\infty}^{\infty}\left\{\times\left[\begin{array}{l}\dfrac{1}{m[m\omega_c+n\omega_o]}J_n\left(m\dfrac{\pi}{2}M\right)\sin\left([m+n]\dfrac{\pi}{2}\right)\\ \dfrac{\sin(n[\omega_o t+\theta_o])}{2}\left\{\begin{array}{l}e^{jm\omega_c t}\displaystyle\sum_{i=0}^{p-1}e^{jm\frac{2i\pi}{p}}e^{jmX_i}\\ +e^{-jm\omega_c t}\displaystyle\sum_{i=0}^{p-1}e^{-jm\frac{2i\pi}{p}}e^{-jmX_i}\end{array}\right\}\\ -\dfrac{\cos(n[\omega_o t+\theta_o])}{2j}\left\{\begin{array}{l}e^{jm\omega_c t}\displaystyle\sum_{i=0}^{p-1}e^{jm\frac{2i\pi}{p}}e^{jmX_i}\\ -e^{-jm\omega_c t}\displaystyle\sum_{i=0}^{p-1}e^{-jm\frac{2i\pi}{p}}e^{-jmX_i}\end{array}\right\}\end{array}\right]\right\}
\end{aligned}
\tag{5.73}
$$

For large p and $\sigma \ll p$ the deterministic part plays significant role

$$
\sum_{i=0}^{p-1}e^{\pm jm\frac{2i\pi}{p}}e^{\pm jmX_i}=0,\qquad \forall m\neq p: m\in\mathbb{N}_0, p\in\mathbb{N}, X\sim\mathcal{N}(0,\sigma^2) \tag{5.74}
$$

And for large p and $\sigma \gg p$ the stochastic part is more significant

$$
\sum_{i=0}^{p-1}e^{\pm jm\frac{2i\pi}{p}}e^{\pm jmX_i}=0,\qquad \forall m: m\in\mathbb{N}_0, p\in\mathbb{N}, X\sim\mathcal{N}(0,\sigma^2) \tag{5.75}
$$

If $2\pi/p \sim\sigma$, the synchronization does not play significant role in harmonic cancellation process. Synchronization error dominates over determined phase angles and harmonic generation by parallel-connected converters becomes a random process. Therefore it is reasonable to apply deterministic de-synchronization of the carrier signals of in parallel-connected wind turbines only for limited number of wind turbines within

the controlled cluster. In large offshore wind farms it is also reasonable to assume that harmonic carrier groups can cancel each other based on random nature of carrier signals phase angles θ_c. This was shown earlier based on measurement data analysis based on results from Gunfleet Sands.

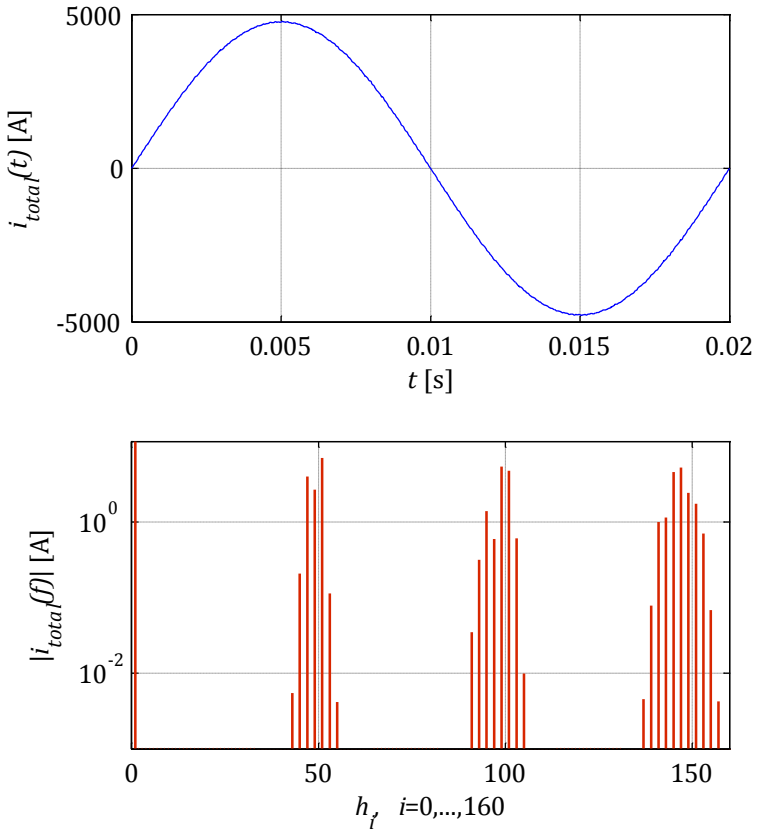

Figure 5.36 Total current generated by three parallel-connected wind turbines including random de-synchronization errors.

Figure 5.36 shows that harmonic cancellation within carrier groups is also possible to even not ideally shifted carrier signals. In this particular case it was assumed that random error is normally distributed with mean value $\mu = 0$ and standard deviation $\sigma = \pi/10$ ($X_i \sim \mathcal{N}(0,0.1\pi)$).

Appropriate adjustment of grid-connected wind turbines operating in parallel in wind farm clusters with carrier-based pulse-width modulation strategy can reduce harmonic content generated by the modulator. In some cases this can even allow omitting the shunt filter while still keeping the same high power quality level and improve the wind turbine robustness [5.37]. Good understanding based on analytical approach allows predicting harmonic generation as well as design control and modulation which can allow harmonic generation and thus overall voltage quality. Based on calculations presented in Table 5.12 one can see that an appropriate carrier signal phase angle adjustment can significantly improve power quality of connected in parallel wind turbines.

Table 5.12 Comparison of sideband harmonic cancellation depending on different phase angles between carrier signals.

Case	Number of wind turbines	Carrier signal phase angle	Total harmonic distortion
Ideal case	3	$\theta_{c_{1,2,3}} = [0°, 0°, 0°]^T$	0.23 %
Random error	3	$\theta_{c_i} = [0°, 120°, 240°]^T + X_i$ $X_i \sim \mathcal{N}(0, \pi/10)$	0.30 %
Worst case	3	$\theta_{c_{1,2,3}} = [0°, 120°, 240°]^T$	1.92 %

5.2.1.4 HARMONIC CONTENT IN THE REFERENCE SIGNAL

Existence of harmonic content in the command signal is not rare. It is expected that different control scenarios in grid-connected converters can include unwanted distortions or sometimes distortions introduced by a certain control purpose. One of good examples is common-mode third-harmonic injection in order to extend linear operation of the modulator [5.38], [5.39].

In a general way the harmonic injection into the command signal can be expressed in the following way

$$v_{az}^*(t) = M\cos(\omega_o t + \theta_o) + M_h\cos(h\omega_o t + \theta_h) \tag{5.76}$$

$$v_{bz}^*(t) = M\cos\left(\omega_o t + \theta_o - \frac{2\pi}{3}\right) + M_h\cos(h\omega_o t + \theta_h) \tag{5.77}$$

$$v_{cz}^*(t) = M\cos\left(\omega_o t + \theta_o + \frac{2\pi}{3}\right) + M_h\cos(h\omega_o t + \theta_h) \tag{5.78}$$

The theoretical harmonic solution for double-edge naturally sampled pulse-width modulation with any harmonic injection is calculated similar than previously. The integration process is slightly more complex due to introduction of additional harmonic component in the reference signal. Right now the integration limits have to be redefined taking into consideration extra harmonic signals. Therefore Eq. 5.32 has to be updated to the following form

$$f(y) = M\cos(y) + M_h\cos(hy + \theta_h) \tag{5.79}$$

where $y = \omega_o t$. The phase angle of the fundamental component in the command signal θ_o is relative and assumed to be 0 in order to simplify calculations. The harmonic angle can be any and defines positive, negative, or zero sequence harmonic content in three-phase converters.

And thus for double-edge naturally sampled pulse-width modulation with any harmonic injection the integration limits are

$$x \in \begin{bmatrix} -\frac{\pi}{2}(1 + M\cos(y) + M_h\cos(hy + \theta_h)), \\ \frac{\pi}{2}(1 + M\cos(y) + M_h\cos(hy + \theta_h)) \end{bmatrix} \quad 5.80$$

$$y \in [-\pi, \pi] \quad 5.81$$

According to the new integration limits presented above, the double Fourier series coefficients can be evaluated in the following way

$$\underline{C}_{mn} = A_{mn} + jB_{mn} = \frac{1}{2\pi^2}\int_{-\pi}^{\pi}\int_{-\frac{\pi}{2}(1+M\cos(y)+M_h\cos(hy+\theta_h))}^{\frac{\pi}{2}(1+M\cos(y)+M_h\cos(hy+\theta_h))} V_{DC}e^{j(mx+ny)}\,dxdy \quad 5.82$$

– DC offset ($m = 0, n = 0$)

$$\begin{aligned} A_{00} + jB_{00} &= \frac{1}{2\pi^2}\int_{-\pi}^{\pi}\int_{-\frac{\pi}{2}(1+M\cos(y)+M_h\cos(hy+\theta_h))}^{\frac{\pi}{2}(1+M\cos(y)+M_h\cos(hy+\theta+h))} V_{DC}e^{j(0x+0y)}\,dxdy \\ &= \frac{V_{DC}}{2\pi^2}\int_{-\pi}^{\pi}\int_{-\frac{\pi}{2}(1+M\cos(y)+M_h\cos(hy+\theta_h))}^{\frac{\pi}{2}(1+M\cos(y)+M_h\cos(hy+\theta+h))} 1\,dxdy \\ &= \frac{V_{DC}}{2\pi^2}\int_{-\pi}^{\pi} x + C\Big|_{-\frac{\pi}{2}(1+M\cos(y)-M_3\cos(3y))}^{\frac{\pi}{2}(1+M\cos(y)+M_h\cos(hy+\theta+h))} dy = \\ &= \frac{V_{DC}}{2\pi^2}\int_{-\pi}^{\pi}[\pi(1 + M\cos(y) + M_h\cos(hy + \theta_h))]\,dy = V_{DC} + j0 \end{aligned} \quad 5.83$$

– Baseband harmonics ($m = 0, n > 0$)

In order to calculate baseband, sideband, and carrier harmonics the Euler's formulas from Eq. 5.65 and Eq. 5.66 will be frequently used

$$
\begin{aligned}
A_{0n} + jB_{0n} &= \frac{V_{DC}}{2\pi^2} \int_{-\pi}^{\pi} \int_{-\frac{\pi}{2}(1+M\cos(y)+M_h\cos(hy+\theta_h))}^{\frac{\pi}{2}(1+M\cos(y)+M_h\cos(hy+\theta_h))} e^{jny}\, dxdy \\
&= \frac{V_{DC}}{2\pi^2} \int_{-\pi}^{\pi} \left[\pi(1 + M\cos(y) + M_h\cos(hy+\theta_h))e^{jny}\right] dy \\
&= \frac{V_{DC}}{2\pi} \int_{-\pi}^{\pi} \left[\begin{array}{c} e^{jny} + M\left(\dfrac{e^{jy}+e^{-jy}}{2}\right)e^{jny} \\ +M_h\left(\dfrac{e^{j(hy+\theta_h)}+e^{-j(hy+\theta_h)}}{2}\right)e^{jny} \end{array} \right] dy = \\
&= \frac{V_{DC}}{2\pi} \int_{-\pi}^{\pi} \left[\begin{array}{c} e^{jny} + M\left(\dfrac{e^{j[n+1]y}+e^{j[n-1]y}}{2}\right) \\ +M_h\left(\dfrac{e^{j[n+h]y}e^{j\theta_h}+e^{j[n-h]y}e^{-j\theta_h}}{2}\right) \end{array} \right] dy
\end{aligned}
\tag{5.84}
$$

where h is any integer number which satisfies condition $h > 1$. Note that Eq. 5.84 makes physical sense only for positive frequencies (i.e. $n > 0$), thus one can assume that

$$
\int_{-\pi}^{\pi} e^{jny}\, dy = 0, \qquad n \neq 0 \tag{5.85}
$$

Therefore any particular harmonic component added to the command signal, the baseband harmonic component magnitude is expressed as $|\underline{C}_{mn}|$ of following term

$$
\underline{C}_{0h} = A_{0h} + jB_{0h} = \frac{V_{DC}}{2\pi} \int_{-\pi}^{\pi} \frac{M_h e^{-j\theta_h}}{2}\, dy = M_h \frac{V_{DC}}{2} e^{-j\theta_h} \tag{5.86}
$$

By application of another form of Euler's formula from Eq. 5.87

$$
e^{\pm j\theta} = \cos(\theta) \pm j\sin(\theta) \tag{5.87}
$$

Depending on the phase angle of the additional harmonic content in the command signal, $\underline{C}_{0h}$ can be real or complex

$$
\underline{C}_{0h} = A_{0h} + jB_{0h} = M_h \frac{V_{DC}}{2} e^{-j\theta_h} = M_h \frac{V_{DC}}{2}\cos(\theta_h) - jM_h \frac{V_{DC}}{2}\sin(\theta_h) \tag{5.88}
$$

For all other frequency components (i.e. $n > 1$), Eq. 5.84 is equal to 0. This shows that the double-edge natural sampled pulse-width modulation with harmonic injection into the reference signal produces only fundamental harmonic defined by modulation index M and DC-link voltage V_{DC} within the baseband harmonics range and injected harmonic with magnitude dependent on M_h and V_{DC}.

Higher than fundamental frequency oscillations in the command signal are mainly caused by the control method or harmonic background measured by the grid-side

converter. It is expected that additional harmonic components in the command signal are below half of the sampling frequency (i.e. Nyquist frequency) of the signal. Typically sampling frequency of the command signal is equal to the carrier signal frequency (i.e. symmetrical regular sampled pulse-width modulation) or two times higher than the carrier signal frequency (i.e. asymmetrical regular sampled pulse-width modulation).

– Sideband harmonics ($m > 0, n \neq 0$)

$$\begin{aligned} A_{mn} + jB_{mn} &= \frac{V_{DC}}{2\pi^2} \int_{-\pi}^{\pi} \int_{-\frac{\pi}{2}(1+M\cos(y)+M_h\cos(hy+\theta_h))}^{\frac{\pi}{2}(1+M\cos(y)+M_h\cos(hy+\theta_h))} e^{j(mx+ny)}\, dxdy \\ &= \frac{V_{DC}}{j2m\pi^2} \int_{-\pi}^{\pi} e^{jny} \begin{bmatrix} e^{jm\frac{\pi}{2}(1+M\cos(y)+M_h\cos(hy+\theta_h))} \\ -e^{-jm\frac{\pi}{2}(1+M\cos(y)-M_h\cos(hy+\theta_h))} \end{bmatrix} dy \\ &= \frac{V_{DC}}{j2m\pi^2} \int_{-\pi}^{\pi} e^{jny} \begin{bmatrix} e^{jm\frac{\pi}{2}} e^{jm\frac{\pi}{2}M\cos(y)} e^{jm\frac{\pi}{2}M_h\cos(hy+\theta_h)} \\ -e^{-jm\frac{\pi}{2}} e^{-jm\frac{\pi}{2}M\cos(y)} e^{-jm\frac{\pi}{2}M_h\cos(hy+\theta_h)} \end{bmatrix} dy \end{aligned} \quad 5.89$$

At this point another Bessel function identity known as Jacobi-Anger expansion in series of Bessel coefficients has to be applied in order to simplify Eq. 5.89 [5.21]. Using Jacobi-Anger expansion from Eq. 5.90

$$e^{\pm j\xi\cos(\theta)} = J_0(\xi) + 2\sum_{k=1}^{\infty} j^{\pm k} J_k(\xi)\cos(k\theta) \quad 5.90$$

After application of the Jacobi-Anger expansion

$$\begin{aligned} &A_{mn} + jB_{mn} \\ &= \frac{V_{DC}}{j2m\pi^2} \int_{-\pi}^{\pi} \begin{bmatrix} e^{jny} e^{jm\frac{\pi}{2}} \begin{bmatrix} \left\{ J_0\left(m\frac{\pi}{2}M\right) + 2\sum_{k=1}^{\infty} j^k J_k\left(m\frac{\pi}{2}M\right)\cos(ky) \right\} \\ \times \begin{Bmatrix} J_0\left(m\frac{\pi}{2}M_h\right) \\ +2\sum_{l=1}^{\infty} j^l J_l\left(m\frac{\pi}{2}M_h\right)\cos(l[hy+\theta_h]) \end{Bmatrix} \end{bmatrix} \\ -e^{jny} e^{-jm\frac{\pi}{2}} \begin{bmatrix} \left\{ J_0\left(m\frac{\pi}{2}M\right) + 2\sum_{k=1}^{\infty} j^{-k} J_k\left(m\frac{\pi}{2}M\right)\cos(ky) \right\} \\ \times \begin{Bmatrix} J_0\left(m\frac{\pi}{2}M_h\right) \\ +2\sum_{l=1}^{\infty} j^{-l} J_l\left(m\frac{\pi}{2}M_h\right)\cos(l[hy+\theta_h]) \end{Bmatrix} \end{bmatrix} \end{bmatrix} dy \end{aligned} \quad 5.91$$

After multiplication, rearrangement, application of trigonometric identities from Eq. 5.92

$$\cos(\xi_1)\cos(\xi_2) = \frac{\cos(\xi_1 - \xi_2) + \cos(\xi_1 + \xi_2)}{2} \tag{5.92}$$

and usage of identity from Eq. 5.93

$$j^{\pm n} = \left(\sqrt{-1}\right)^{\pm n} = \left(\sqrt{e^{j\pi}}\right)^{\pm n} = e^{\pm j\frac{\pi}{2}n} \tag{5.93}$$

Eq. 5.91 is simplified to

$$\begin{aligned} &A_{mn} + jB_{mn} \\ &= \frac{V_{DC}}{j2m\pi^2} \int_{-\pi}^{\pi} 2j \left[\begin{array}{c} J_0\left(m\frac{\pi}{2}M\right) J_0\left(m\frac{\pi}{2}M_h\right) \left[\frac{e^{jm\frac{\pi}{2}} - e^{-jm\frac{\pi}{2}}}{2j}\right] e^{jny} \\ +2J_0\left(m\frac{\pi}{2}M\right) \sum_{l=1}^{\infty} J_l\left(m\frac{\pi}{2}M_h\right) \left[\begin{array}{c} \frac{e^{j(m+l)\frac{\pi}{2}} - e^{-j(m+l)\frac{\pi}{2}}}{2j} \\ \times \cos(l[hy+\theta_h])\, e^{jny} \end{array}\right] \\ +2J_0\left(m\frac{\pi}{2}M_h\right) \sum_{k=1}^{\infty} J_k\left(m\frac{\pi}{2}M\right) \left[\begin{array}{c} \frac{e^{j(m+k)\frac{\pi}{2}} - e^{-j(m+k)\frac{\pi}{2}}}{2j} \\ \times \cos(ky)\, e^{jny} \end{array}\right] \\ 4\sum_{k=1}^{\infty}\sum_{l=1}^{\infty} J_k\left(m\frac{\pi}{2}M\right) J_l\left(m\frac{\pi}{2}M_h\right) \left[\begin{array}{c} \frac{e^{j(m+k+l)\frac{\pi}{2}} - e^{-j(m+k+l)\frac{\pi}{2}}}{2j} \\ \times \cos(l[hy+\theta_h]) \\ \times \cos(ky)\, e^{jny} \end{array}\right] \end{array} \right] dy \end{aligned} \tag{5.94}$$

And can be rearranged considering Euler's formulas from Eq. 5.65 and Eq. 5.66 to

$$\begin{aligned} &A_{mn} + jB_{mn} \\ &= \frac{V_{DC}}{m\pi^2} \int_{-\pi}^{\pi} \left[\begin{array}{c} J_0\left(m\frac{\pi}{2}M\right) J_0\left(m\frac{\pi}{2}M_h\right) \sin\left(m\frac{\pi}{2}\right) e^{jny} \\ +J_0\left(m\frac{\pi}{2}M\right) \sum_{l=1}^{\infty} \left[\begin{array}{c} J_l\left(m\frac{\pi}{2}M_h\right) \sin\left([m+l]\frac{\pi}{2}\right) \\ \times \left[e^{j(n+hl)y} e^{jl\theta_h} + e^{j(n-hl)y} e^{-jl\theta_h}\right] \end{array}\right] \\ +J_0\left(m\frac{\pi}{2}M_h\right) \sum_{k=1}^{\infty} \left[\begin{array}{c} J_k\left(m\frac{\pi}{2}M\right) \sin\left([m+k]\frac{\pi}{2}\right) \\ \times \left[e^{j(n+k)y} + e^{j(n-k)y}\right] \end{array}\right] \\ \sum_{k=1}^{\infty}\sum_{l=1}^{\infty} \left[\begin{array}{c} J_k\left(m\frac{\pi}{2}M\right) J_l\left(m\frac{\pi}{2}M_h\right) \sin\left([m+k+l]\frac{\pi}{2}\right) \\ \times \left[\begin{array}{c} e^{j(n+k+hl)y} e^{jl\theta_h} + e^{j(n-k-hl)y} e^{-jl\theta_h} \\ +e^{j(n+k-hl)y} e^{-jl\theta_h} + e^{j(n-k+hl)y} e^{jl\theta_h} \end{array}\right] \end{array}\right] \end{array} \right] dy \end{aligned} \tag{5.95}$$

After integration of Eq. 5.95 the solution is as follow

$$A_{mn} + jB_{mn}$$

$$= \frac{2V_{DC}}{m\pi}\left[\begin{array}{l} J_0\left(m\frac{\pi}{2}M\right)\sum_{l=1}^{\infty} J_l\left(m\frac{\pi}{2}M_h\right)\sin\left([m+l]\frac{\pi}{2}\right)e^{jl\theta_h}\Big|_{n=-hl} \\ +J_0\left(m\frac{\pi}{2}M\right)\sum_{l=1}^{\infty} J_l\left(m\frac{\pi}{2}M_h\right)\sin\left([m+l]\frac{\pi}{2}\right)e^{-jl\theta_h}\Big|_{n=hl} \\ +J_0\left(m\frac{\pi}{2}M_h\right)\sum_{k=1}^{\infty} J_k\left(m\frac{\pi}{2}M\right)\sin\left([m+k]\frac{\pi}{2}\right)\Big|_{n=-k\,\cup\,n=k} \\ +\sum_{k=1}^{\infty}\sum_{l=1}^{\infty} J_k\left(m\frac{\pi}{2}M\right)J_l\left(m\frac{\pi}{2}M_h\right)\sin\left([m+k+l]\frac{\pi}{2}\right)e^{jl\theta_h}\Big|_{\substack{n=-(k+hl)\\ n=k-hl}} \\ +\sum_{k=1}^{\infty}\sum_{l=1}^{\infty} J_k\left(m\frac{\pi}{2}M\right)J_l\left(m\frac{\pi}{2}M_h\right)\sin\left([m+k+l]\frac{\pi}{2}\right)e^{-jl\theta_h}\Big|_{\substack{n=k+hl\\ n=-k+hl}} \end{array}\right] \quad 5.96$$

Depending on the phase angle of the additional harmonic content in the command signal, $\underline{C}_{mn}$ can be real, imaginary, or complex

$$\underline{C}_{mn} = A_{mn} + jB_{mn}$$

$$= \frac{2V_{DC}}{m\pi}\left[\begin{array}{l} J_0\left(m\frac{\pi}{2}M\right)\sum_{l=1}^{\infty} J_l\left(m\frac{\pi}{2}M_h\right)\sin\left([m+l]\frac{\pi}{2}\right)\cos(l\theta_h)\Big|_{n=-hl\,\cup\,n=hl} \\ +J_0\left(m\frac{\pi}{2}M_h\right)\sum_{k=1}^{\infty} J_k\left(m\frac{\pi}{2}M\right)\sin\left([m+k]\frac{\pi}{2}\right)\Big|_{n=-k\,\cup\,n=k} \\ +\sum_{k=1}^{\infty}\sum_{l=1}^{\infty}\left[J_k\left(m\frac{\pi}{2}M\right)J_l\left(m\frac{\pi}{2}M_h\right)\sin\left([m+k+l]\frac{\pi}{2}\right)\times\cos(l\theta_h)\right]\Big|_{\substack{n=-(k+hl)\,\cup\,n=k-hl\\ n=k+hl\,\cup\,n=-k+hl}} \end{array}\right]$$

$$+ j\frac{2V_{DC}}{m\pi}\left[\begin{array}{l} J_0\left(m\frac{\pi}{2}M\right)\sum_{l=1}^{\infty} J_l\left(m\frac{\pi}{2}M_h\right)\sin\left([m+l]\frac{\pi}{2}\right)\sin(l\theta_h)\Big|_{n=-hl} \\ -J_0\left(m\frac{\pi}{2}M\right)\sum_{l=1}^{\infty} J_l\left(m\frac{\pi}{2}M_h\right)\sin\left([m+l]\frac{\pi}{2}\right)\sin(l\theta_h)\Big|_{n=hl} \\ +\sum_{k=1}^{\infty}\sum_{l=1}^{\infty}\left[J_k\left(m\frac{\pi}{2}M\right)J_l\left(m\frac{\pi}{2}M_h\right)\sin\left([m+k+l]\frac{\pi}{2}\right)\times\sin(l\theta_h)\right]\Big|_{n=-(k+hl)\,\cup\,n=k-hl} \\ -\sum_{k=1}^{\infty}\sum_{l=1}^{\infty}\left[J_k\left(m\frac{\pi}{2}M\right)J_l\left(m\frac{\pi}{2}M_h\right)\sin\left([m+k+l]\frac{\pi}{2}\right)\times\sin(l\theta_h)\right]\Big|_{n=k+hl\,\cup\,n=-k+hl} \end{array}\right] \quad 5.97$$

– Carrier harmonics ($m > 0, n = 0$)

In case of carrier harmonics also Bessel functions of the first kind will be used. The Bessel function identity known as Jacobi-Anger expansion in the series of Bessel

coefficients will one more time will be applied [5.21]. Bessel functions are also sometimes called cylindrical harmonics [5.40]. Some examples of Bessel functions of the first kind are presented in Figure 5.37.

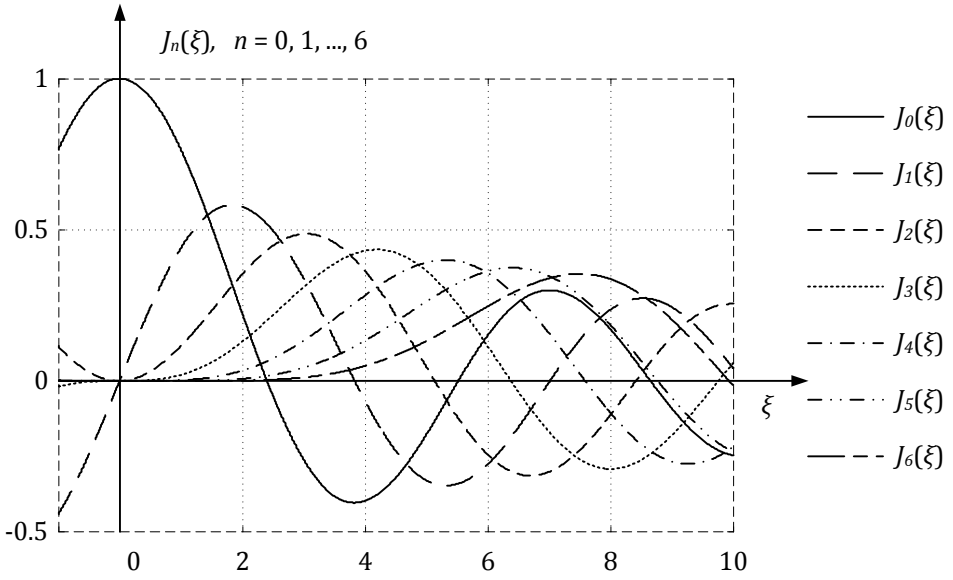

Figure 5.37 Bessel functions of the first kind.

Carrier harmonics can be calculated directly from Eq. 5.95

$$A_{m0} + jB_{m0} = \frac{V_{DC}}{m\pi^2} \int_{-\pi}^{\pi} \left[\begin{array}{c} J_0\left(m\frac{\pi}{2}M\right) J_0\left(m\frac{\pi}{2}M_h\right) \sin\left(m\frac{\pi}{2}\right) \\ +J_0\left(m\frac{\pi}{2}M\right) \sum_{l=1}^{\infty} \left[\begin{array}{c} J_l\left(m\frac{\pi}{2}M_h\right) \sin\left([m+l]\frac{\pi}{2}\right) \\ \times \left[e^{jhly} e^{jl\theta_h} + e^{-jhly} e^{-jl\theta_h}\right] \end{array} \right] \\ +J_0\left(m\frac{\pi}{2}M_h\right) \sum_{k=1}^{\infty} \left[\begin{array}{c} J_k\left(m\frac{\pi}{2}M\right) \sin\left([m+k]\frac{\pi}{2}\right) \\ \times \left[e^{jky} + e^{-jky}\right] \end{array} \right] \\ + \sum_{k=1}^{\infty} \sum_{l=1}^{\infty} \left[\begin{array}{c} J_k\left(m\frac{\pi}{2}M\right) J_l\left(m\frac{\pi}{2}M_h\right) \sin\left([m+k+l]\frac{\pi}{2}\right) \\ \times \left[\begin{array}{c} e^{j(k+hl)y} e^{jl\theta_h} + e^{-j(k+hl)y} e^{-jl\theta_h} \\ +e^{j(k-hl)y} e^{-jl\theta_h} + e^{-j(k-hl)y} e^{jl\theta_h} \end{array} \right] \end{array} \right] \end{array} \right] dy \qquad 5.98$$

and after integration and application of Euler's formulas

$$A_{m0} + jB_{m0} = \frac{2V_{DC}}{m\pi}\left[\begin{array}{c} J_0\left(m\frac{\pi}{2}M\right)J_0\left(m\frac{\pi}{2}M_h\right)\sin\left(m\frac{\pi}{2}\right) \\ +2\sum_{k=1}^{\infty}\sum_{l=1}^{\infty}\left\{\begin{array}{c} J_k\left(m\frac{\pi}{2}M\right)J_l\left(m\frac{\pi}{2}M_h\right) \\ \times \sin\left([m+k+l]\frac{\pi}{2}\right)\left[\frac{e^{jl\theta_h}+e^{-jl\theta_h}}{2}\right]\end{array}\right\}\Bigg|_{k=hl}\end{array}\right] \quad 5.99$$
$$= \frac{2V_{DC}}{m\pi}\left[\begin{array}{c} J_0\left(m\frac{\pi}{2}M\right)J_0\left(m\frac{\pi}{2}M_h\right)\sin\left(m\frac{\pi}{2}\right) \\ +2\sum_{k=1}^{\infty}\sum_{l=1}^{\infty}J_k\left(m\frac{\pi}{2}M\right)J_l\left(m\frac{\pi}{2}M_h\right)\sin\left([m+k+l]\frac{\pi}{2}\right)\cos(l\theta_h)\Big|_{k=hl}\end{array}\right]$$

The complete harmonic solution for double-edge naturally sampled pulse-width modulation of a half-bridge phase leg now can be formed by subtracting Eq. 5.82, Eq. 5.84, Eq. 5.99 and Eq. 5.97 into Eq. 5.29. Time-varying phase leg voltage $v_{az}(t)$ can be finally expressed in terms of harmonic components as below.

Eq. 5.100 is a generic solution of double-edge naturally sampled pulse-width modulation which takes into account any harmonic content injection into the command signal. The harmonic content can assume any magnitude M_h and any phase angle θ_h.

$$\begin{aligned} & v_{az}(t) \\ & = M\frac{V_{DC}}{2}\cos(\omega_o t+\theta_o) + M_h\frac{V_{DC}}{2}\left[\begin{array}{c}\cos(\theta_h)\cos(h[\omega_o t+\theta_o]) \\ -\sin(\theta_h)\sin(h[\omega_o t+\theta_o])\end{array}\right] \\ & + \sum_{m=1}^{\infty}\frac{2V_{DC}}{m\pi}\left[\begin{array}{c} J_0\left(m\frac{\pi}{2}M\right)J_0\left(m\frac{\pi}{2}M_h\right)\sin\left(m\frac{\pi}{2}\right) \\ +2\sum_{k=1}^{\infty}\sum_{l=1}^{\infty}J_k\left(m\frac{\pi}{2}M\right)J_l\left(m\frac{\pi}{2}M_h\right)\sin\left([m+k+l]\frac{\pi}{2}\right)\cos(l\theta_h)\Big|_{k=hl} \\ \times\cos(m[\omega_c t+\theta_c])\end{array}\right] \\ & + \sum_{m=1}^{\infty}\sum_{\substack{n=-\infty \\ n\neq 0}}^{\infty}\frac{2V_{DC}}{m\pi}\left[\left\{\begin{array}{c} J_0\left(m\frac{\pi}{2}M\right)\sum_{l=1}^{\infty}J_l\left(m\frac{\pi}{2}M_h\right)\sin\left([m+l]\frac{\pi}{2}\right)\cos(l\theta_h)\Big|_{|n|=hl} \\ +J_0\left(m\frac{\pi}{2}M_h\right)\sum_{k=1}^{\infty}J_k\left(m\frac{\pi}{2}M\right)\sin\left([m+k]\frac{\pi}{2}\right)\Big|_{|n|=k} \\ +\sum_{k=1}^{\infty}\sum_{l=1}^{\infty}\left[\begin{array}{c} J_k\left(m\frac{\pi}{2}M\right)J_l\left(m\frac{\pi}{2}M_h\right) \\ \times\sin\left([m+k+l]\frac{\pi}{2}\right)\cos(l\theta_h)\end{array}\right]\Bigg|_{\substack{|n|=k+hl \\ |n|=k-hl}}\end{array}\right\} \right. \\ & \left. \times\cos(m[\omega_c t+\theta_c]+n[\omega_o t+\theta_o])\right] \end{aligned} \quad 5.100$$

$$+\sum_{m=1}^{\infty}\sum_{\substack{n=-\infty\\ n\neq 0}}^{\infty}\frac{2V_{DC}}{m\pi}\left[\begin{array}{l}\left\{\begin{array}{l} J_0\left(m\frac{\pi}{2}M\right)\sum_{l=1}^{\infty}J_l\left(m\frac{\pi}{2}M_h\right)\sin\left([m+l]\frac{\pi}{2}\right)\sin(l\theta_h)\Big|_{n=-hl} \\ -J_0\left(m\frac{\pi}{2}M\right)\sum_{l=1}^{\infty}J_l\left(m\frac{\pi}{2}M_h\right)\sin\left([m+l]\frac{\pi}{2}\right)\sin(l\theta_h)\Big|_{n=hl} \\ +\sum_{k=1}^{\infty}\sum_{l=1}^{\infty}\left[\begin{array}{c} J_k\left(m\frac{\pi}{2}M\right)J_l\left(m\frac{\pi}{2}M_h\right) \\ \times\sin\left([m+k+l]\frac{\pi}{2}\right)\sin(l\theta_h)\end{array}\right]\Bigg|_{\substack{n=k-hl\\ n=-k-hl}} \\ -\sum_{k=1}^{\infty}\sum_{l=1}^{\infty}\left[\begin{array}{c} J_k\left(m\frac{\pi}{2}M\right)J_l\left(m\frac{\pi}{2}M_h\right) \\ \times\sin\left([m+k+l]\frac{\pi}{2}\right)\sin(l\theta_h)\end{array}\right]\Bigg|_{\substack{n=-k+hl\\ n=k+hl}}\end{array}\right\} \\ \times\sin(m[\omega_c t+\theta_c]+n[\omega_o t+\theta_o])\end{array}\right]$$

In the linear modulation region (i.e. $M \leq 1$), the magnitude of fundamental harmonic component varies linearly with the modulation index M. In some publications modulation index M can be also expressed as modulation ratio $m_a = V_r/V_c$, where V_r is the reference signal (also called command, control or modulating) and V_c is the carrier signal (also called triangular in case of double-edge pulse-width modulation, or modulated). The restriction for $M \leq 1$ can be relaxed if a zero sequence (common mode) signal is added to the command signals [5.41].

Introduction of zero sequence third-harmonic components reduces the peak magnitude of resulting command signals, while the fundamental harmonic components stay unchanged and DC-link voltage is utilized more efficiently [5.42].

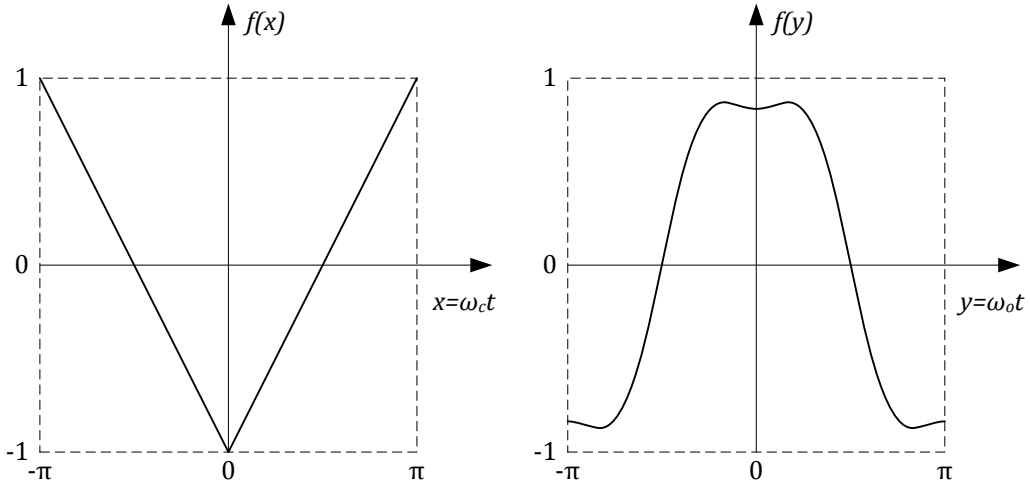

Figure 5.38 Triangle carrier signal and command signal with third harmonic injection.

The theoretical harmonic solution for double-edge naturally sampled pulse-width modulation with third-harmonic injection is calculated in a similar way to previously. The integration process is the same as for any harmonic content in the command signal

but in this case the index $h = 3$ and injected harmonic phase shift $\theta_h = \pi$. Right now the integration limits have to be redefined taking into consideration extra common mode signals.

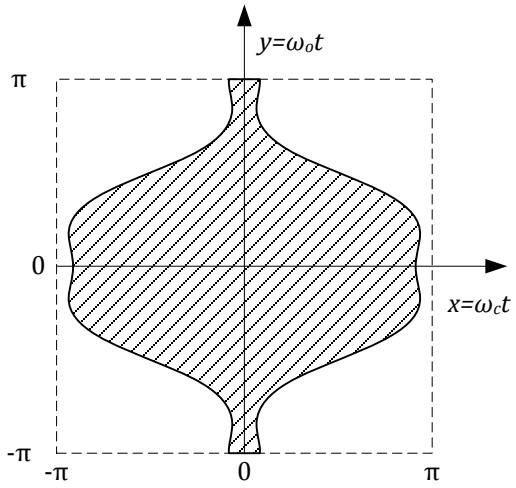

Figure 5.39 Unit cell for double-edge naturally sampled pulse-width modulation with third harmonic injection.

Due to the fact that the third-harmonic component is injected, the command signal has different shape as shown in Figure 5.38. Thus the contour shape within the unit cell of $f(t) = f[x(t), y(t)]$ is different, which is shown in Figure 5.39. Within the contour (dashed area) the function has value V_{DC}, outside the contour the function takes value of 0.

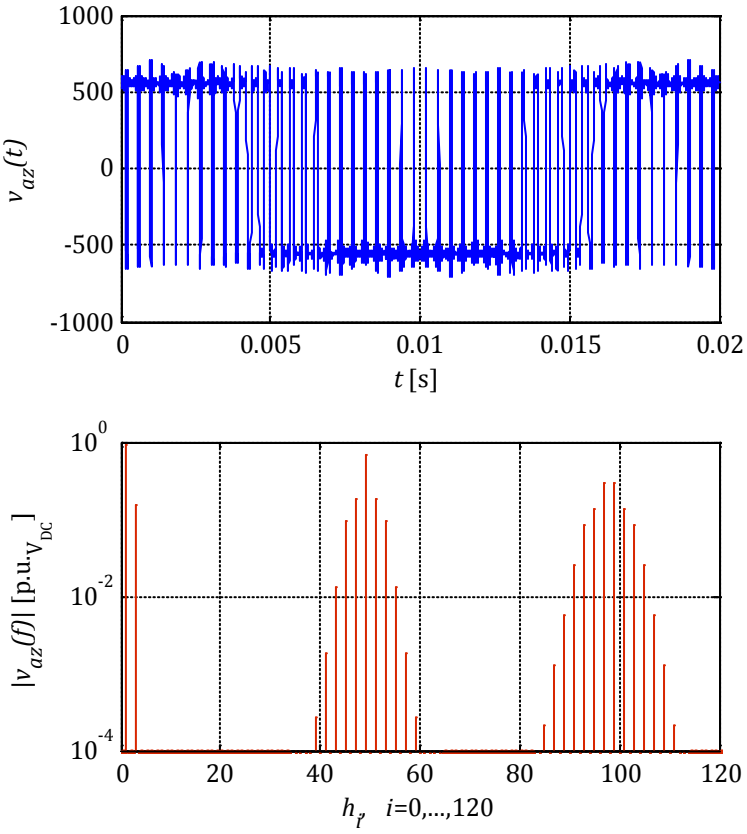

Figure 5.40 Analytical harmonic solution of half-bridge leg of double edge naturally sampled pulse-width modulation ($M = 0.9, \gamma = M/M_3 = 1/6, m_f = \omega_c/\omega_o = 49$).

Figure 5.40 and Figure 5.41 present complete harmonic solution for double-edge naturally sampled pulse-width modulation with third-harmonic component injection into the reference signal of one phase leg of a half-bridge. The results are obtained from the generic closed-form solution from Eq. 5.100. As it can be seen in addition, a significant third-harmonic baseband component is present in the grid-side converter voltage output $v_{az}(t)$. In comparison to double-edge naturally sampled pulse-width modulation with a sine reference (i.e. no additional harmonic components in the command signal), magnitudes of the first and the second carrier group harmonic components are flattened and broadly distributed (i.e. harmonic energy from the first pair around the carrier harmonic component is distributed to outer sideband pairs).

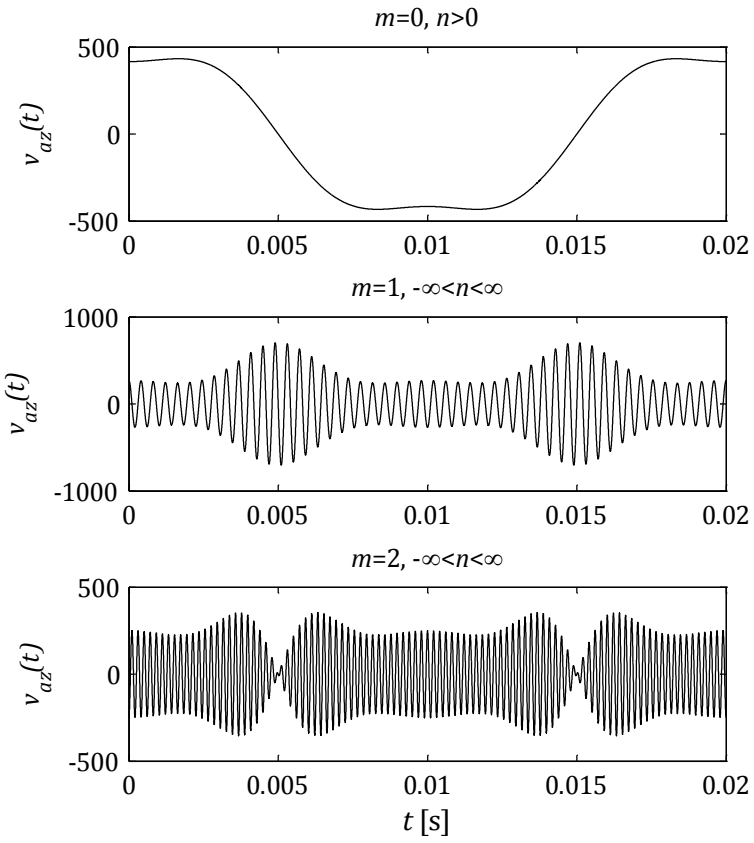

Figure 5.41 Baseband, first and second carrier group harmonic components presented in time domain.

5.2.1.5 HARMONIC CONTENT IN THE DC-LINK VOLTAGE

In equation below $|\underline{C}_{mn}|$ defines the magnitude of the $(m\omega_c + n\omega_o)^{th}$ harmonic component of the switched waveform $f(x,y)$ created during a certain modulation process.

$$\underline{C}_{mn} = A_{mn} + jB_{mn} = \frac{1}{2\pi^2}\iint_{-\pi}^{\pi} f(x,y)e^{j(mx+ny)}\,dxdy \qquad 5.101$$

Assume that DC-link voltage contains oscillations affected by the generator-side converter as well as demodulation process. For non-ideal DC-link voltage (i.e. containing harmonic components) combining Eq. 5.31 and Eq. 5.32 the following expression of $f(x,y)$ can be achieved for the first half of the carrier signal period

$$f(x,y) = V_{DC} + M_{DC}\cos(h_{DC}y) \;\Rightarrow\; M\cos(y) \geq -1 - \frac{2x}{\pi} \qquad 5.102$$

$$f(x,y) = 0 \;\Rightarrow\; M\cos(y) < -1 - \frac{2x}{\pi} \qquad 5.103$$

where $M_{DC}\cos(qy)$ is any type of harmonic of the fundamental component with magnitude M_{DC} and angular frequency $h_{DC}\omega_o$. And for the second half of the carrier signal period

$$f(x,y) = V_{DC} + M_{DC}\cos(h_{DC}y) \;\Rightarrow\; M\cos(y) \geq -1 + \frac{2x}{\pi} \tag{5.104}$$

$$f(x,y) = 0 \;\Rightarrow\; M\cos(y) < -1 + \frac{2x}{\pi} \tag{5.105}$$

and the harmonic magnitude in case of double-edge naturally sampled pulse-width modulation can be expressed for this particular conditions in the following way

$$\begin{aligned}\underline{C}_{mn} &= A_{mn} + jB_{mn} \\ &= \frac{1}{2\pi^2}\int_{-\pi}^{\pi}\int_{-\frac{\pi}{2}(1+M\cos(y))}^{\frac{\pi}{2}(1+M\cos(y))}\begin{pmatrix}V_{DC}\\ +M_{DC}\cos(h_{DC}y)\end{pmatrix}e^{j(mx+ny)}\,dxdy\end{aligned} \tag{5.106}$$

which can be evaluated taking possible values of m and n into consideration. This approach allows evaluating separately DC offset, fundamental harmonic, baseband harmonics, sideband harmonics as well as carrier harmonics.

- DC offset ($m = 0, n = 0, h_{DC} > 0$)

$$\begin{aligned}A_{00} + jB_{00} &= \frac{1}{2\pi^2}\int_{-\pi}^{\pi}\int_{-\frac{\pi}{2}(1+M\cos(y))}^{\frac{\pi}{2}(1+M\cos(y))}(V_{DC} + M_{DC}\cos(h_{DC}y))e^{j(0x+0y)}\,dxdy \\ &= \frac{V_{DC}}{2\pi^2}\int_{-\pi}^{\pi}\int_{-\frac{\pi}{2}(1+M\cos(y))}^{\frac{\pi}{2}(1+M\cos(y))}1\,dxdy \\ &\quad + \frac{M_{DC}}{2\pi^2}\int_{-\pi}^{\pi}\cos(h_{DC}y)\int_{-\frac{\pi}{2}(1+M\cos(y))}^{\frac{\pi}{2}(1+M\cos(y))}1\,dxdy \\ &= \frac{V_{DC}}{2\pi^2}\int_{-\pi}^{\pi}[\pi(1+M\cos(y))]\,dy \\ &\quad + \frac{M_{DC}}{2\pi^2}\int_{-\pi}^{\pi}[\pi\cos(h_{DC}y)\,(1+M\cos(y))]\,dy\end{aligned} \tag{5.107}$$

After integration the closed form solution can be expressed as

$$
\begin{aligned}
A_{00} + jB_{00} &= \frac{V_{DC}}{2\pi^2} \int_{-\pi}^{\pi} [\pi(1 + M\cos(y))]\, dy \\
&+ \frac{M_{DC}}{2\pi^2} \int_{-\pi}^{\pi} [\pi \cos(h_{DC}y)\,(1 + M\cos(y))]\, dy \\
&= \frac{V_{DC}}{2\pi}(y + C)\Big|_{-\pi}^{\pi} - \frac{MV_{DC}}{2\pi}(\sin(y) + D)\Big|_{-\pi}^{\pi} \\
&+ \frac{M_{DC}}{2\pi}\left(\frac{1}{h_{DC}}\sin(h_{DC}y) + E\right)\Big|_{-\pi}^{\pi} \\
&+ \frac{MM_{DC}}{2\pi}\left(\left[\frac{h_{DC}\cos(y)\sin(h_{DC}y) - \sin(y)\cos(h_{DC}y)}{h_{DC}^2 - 1}\right] + F\right)\Big|_{-\pi}^{\pi} \\
&= V_{DC}
\end{aligned}
\tag{5.108}
$$

– Baseband harmonics ($m = 0, n > 0, h_{DC} > 0$)

$$
\begin{aligned}
A_{0n} + jB_{0n} &= \frac{1}{2\pi^2} \int_{-\pi}^{\pi} \int_{-\frac{\pi}{2}(1+M\cos(y))}^{\frac{\pi}{2}(1+M\cos(y))} (V_{DC} + M_{DC}\cos(h_{DC}y))e^{jny}\, dxdy \\
&= \frac{V_{DC}}{2\pi^2} \int_{-\pi}^{\pi} \left[\pi(1 + M\cos(y))e^{jny}\right] dy \\
&+ \frac{M_{DC}}{2\pi^2} \int_{-\pi}^{\pi} \left[\pi\cos(h_{DC}y)\, e^{jny}(1 + M\cos(y))\right] dy
\end{aligned}
\tag{5.109}
$$

After rearrangement and application of Euler's formula from Eq. 5.65

$$
\begin{aligned}
A_{0n} + jB_{0n} &= \frac{V_{DC}}{2\pi} \int_{-\pi}^{\pi} \left[1 + M\left(\frac{e^{jy} + e^{-jy}}{2}\right)\right] e^{jny}\, dy \\
&+ \frac{M_{DC}}{2\pi} \int_{-\pi}^{\pi} \left(\frac{e^{jh_{DC}y} + e^{-jh_{DC}y}}{2}\right) e^{jny} \left[1 + M\left(\frac{e^{jy} + e^{-jy}}{2}\right)\right] dy \\
&= \frac{V_{DC}}{2\pi} \underbrace{\int_{-\pi}^{\pi} e^{jny}\, dy}_{0} + \frac{MV_{DC}}{2\pi} \int_{-\pi}^{\pi} \frac{e^{j[n+1]y} + e^{j[n-1]y}}{2} dy \\
&+ \frac{M_{DC}}{2\pi} \int_{-\pi}^{\pi} \frac{e^{j[n+h_{DC}]y} + e^{j[n-h_{DC}]y}}{2} dy \\
&+ \frac{MM_{DC}}{2\pi} \int_{-\pi}^{\pi} \left(\frac{e^{jh_{DC}y} + e^{-jh_{DC}y}}{2}\right)\left(\frac{e^{j[n+1]y} + e^{j[n-1]y}}{2}\right) dy
\end{aligned}
\tag{5.110}
$$

Note, that the equation above makes physical sense only for positive frequencies (i.e. $n > 0, h_{DC} > 0$), thus based on identity from Eq. 5.85 it can be simplified to

$$
\begin{aligned}
A_{0n} + jB_{0n} = {} & \frac{MV_{DC}}{4\pi} \underbrace{\int_{-\pi}^{\pi} e^{j[n+1]y}\, dy}_{0} + \frac{MV_{DC}}{4\pi} \int_{-\pi}^{\pi} e^{j[n-1]y}\, dy \\
& + \frac{M_{DC}}{4\pi} \underbrace{\int_{-\pi}^{\pi} e^{j[n+h_{DC}]y}\, dy}_{0} + \frac{M_{DC}}{4\pi} \int_{-\pi}^{\pi} e^{j[n-h_{DC}]y}\, dy \\
& + \frac{MM_{DC}}{8\pi} \underbrace{\int_{-\pi}^{\pi} e^{j[n+h_{DC}+1]y}\, dy}_{0} + \frac{MM_{DC}}{8\pi} \underbrace{\int_{-\pi}^{\pi} e^{j[n+h_{DC}-1]y}\, dy}_{0} \\
& + \frac{MM_{DC}}{8\pi} \int_{-\pi}^{\pi} e^{j[n-h_{DC}+1]y}\, dy + \frac{MM_{DC}}{8\pi} \int_{-\pi}^{\pi} e^{j[n-h_{DC}-1]y}\, dy
\end{aligned}
\tag{5.111}
$$

therefore for the first harmonic (i.e. $n = 1, h_{DC} > 1$) Eq. 5.111 has the following form

$$
A_{01} + jB_{01} = \frac{V_{DC}}{2\pi} \int_{-\pi}^{\pi} \frac{M}{2}\, dy = M\frac{V_{DC}}{2} \tag{5.112}
$$

and for the baseband harmonic components (i.e. $n > 0$ and $m = 0$) for $h_{DC} = 1$ Eq. 5.111 can be expressed as below. Please note that in the measurement of grid-side converter the 1st harmonic (i.e. $h_{DC} = 1$) can be seen in the DC-link voltage due to unbalanced conditions.

$$
A_{01} + jB_{01} = \frac{MV_{DC}}{4\pi} \int_{-\pi}^{\pi} 1\, dy + \frac{M_{DC}}{4\pi} \int_{-\pi}^{\pi} 1\, dy = M\frac{V_{DC}}{2} + \frac{M_{DC}}{2} \tag{5.113}
$$

$$
A_{02} + jB_{02} = \frac{M_{DC}}{4\pi} \int_{-\pi}^{\pi} M\, dy = M\frac{M_{DC}}{2} \tag{5.114}
$$

For all other frequency components (i.e. $\forall n = \{n \in \mathbb{N}: n \neq 1, n \neq h_{DC}, n \neq h_{DC} + 1\}$) Eq. 5.111 is equal to 0. This shows that the double-edge naturally sampled pulse-width modulation within the baseband harmonics range produces only fundamental harmonic defined by modulation index M and DC-link voltage V_{DC}, harmonic component for $n = h_{DC}$ with magnitude of M_{DC} and harmonic component for $n = h_{DC} + 1$ with magnitude defined by modulation index M and harmonic content magnitude M_{DC} in the DC-link.

– Carrier harmonics ($m > 0, n = 0, h_{DC} > 0$)

$$
\begin{aligned}
A_{m0} + jB_{m0} &= \frac{1}{2\pi^2} \int_{-\pi}^{\pi} \int_{-\frac{\pi}{2}(1+M\cos(y))}^{\frac{\pi}{2}(1+M\cos(y))} (V_{DC} + M_{DC}\cos(h_{DC}y)) e^{jmx}\, dxdy \\
&= \frac{1}{2jm\pi^2} \int_{-\pi}^{\pi} (V_{DC} + M_{DC}\cos(h_{DC}y)) \begin{bmatrix} e^{jm\frac{\pi}{2}(1+M\cos(y))} \\ -e^{-jm\frac{\pi}{2}(1+M\cos(y))} \end{bmatrix} dy \\
&= \frac{V_{DC}}{2jm\pi^2} \int_{-\pi}^{\pi} \left[e^{jm\frac{\pi}{2}(1+M\cos(y))} - e^{-jm\frac{\pi}{2}(1+M\cos(y))} \right] dy \\
&+ \frac{M_{DC}}{4jm\pi^2} \int_{-\pi}^{\pi} \left[e^{jh_{DC}y} + e^{-jh_{DC}y} \right] \begin{bmatrix} e^{jm\frac{\pi}{2}(1+M\cos(y))} \\ -e^{-jm\frac{\pi}{2}(1+M\cos(y))} \end{bmatrix} dy
\end{aligned}
\tag{5.115}
$$

Please note that from Bessel function integral relationships one can obtain the following formula [5.30], [5.43]

$$
\int_{-\pi}^{\pi} e^{\pm j\xi\cos\theta} e^{jn\theta}\, d\theta = 2\pi j^{\pm n} J_n(\xi) \tag{5.116}
$$

in a particular situation when $n = 0$, the formula becomes

$$
\int_{-\pi}^{\pi} e^{\pm j\xi\cos\theta}\, d\theta = 2\pi J_0(\xi) = 2\pi J_0(-\xi) \tag{5.117}
$$

where J_0 is the zero-order Bessel function of the first kind. Applying now the relation stated in Eq. 5.116 and Eq. 5.117 into Eq. 5.115 it becomes

$$
\begin{aligned}
&A_{m0} + jB_{m0} \\
&= \frac{V_{DC}}{2jm\pi^2} \int_{-\pi}^{\pi} \left[e^{jm\frac{\pi}{2}(1+M\cos(y))} - e^{-jm\frac{\pi}{2}(1+M\cos(y))} \right] dy \\
&+ \frac{M_{DC}}{4jm\pi^2} \int_{-\pi}^{\pi} \begin{bmatrix} e^{jm\frac{\pi}{2}(1+M\cos(y))} e^{jh_{DC}y} - e^{-jm\frac{\pi}{2}(1+M\cos(y))} e^{jh_{DC}y} \\ +e^{jm\frac{\pi}{2}(1+M\cos(y))} e^{-jh_{DC}y} - e^{-jm\frac{\pi}{2}(1+M\cos(y))} e^{-jh_{DC}y} \end{bmatrix} dy \\
&= \frac{V_{DC}}{2jm\pi^2} \left[e^{jm\frac{\pi}{2}} 2\pi J_0\left(m\frac{\pi}{2}M\right) - e^{-jm\frac{\pi}{2}} 2\pi J_0\left(-m\frac{\pi}{2}M\right) \right] \\
&+ \frac{M_{DC}}{4jm\pi^2} \begin{bmatrix} e^{jm\frac{\pi}{2}} 2\pi j^{h_{DC}} J_{h_{DC}}\left(m\frac{\pi}{2}M\right) - e^{-jm\frac{\pi}{2}} 2\pi j^{-h_{DC}} J_{h_{DC}}\left(m\frac{\pi}{2}M\right) \\ +e^{jm\frac{\pi}{2}} 2\pi j^{-h_{DC}} J_{-h_{DC}}\left(m\frac{\pi}{2}M\right) - e^{-jm\frac{\pi}{2}} 2\pi j^{h_{DC}} J_{-h_{DC}}\left(m\frac{\pi}{2}M\right) \end{bmatrix}
\end{aligned}
\tag{5.118}
$$

and knowing that J_0 is an even function (i.e. $J_0(\xi) = J_0(-\xi)$) and applying identity from Eq. 5.93

$$A_{m0} + jB_{m0} = \frac{2V_{DC}}{m\pi} J_0\left(m\frac{\pi}{2}M\right)\left[\frac{e^{jm\frac{\pi}{2}} - e^{-jm\frac{\pi}{2}}}{2j}\right] + \frac{M_{DC}}{m\pi} J_{h_{DC}}\left(m\frac{\pi}{2}M\right)\left[\frac{e^{j[m+h_{DC}]\frac{\pi}{2}} - e^{-j[m+h_{DC}]\frac{\pi}{2}}}{2j}\right] + \frac{M_{DC}}{m\pi} J_{-h_{DC}}\left(m\frac{\pi}{2}M\right)\left[\frac{e^{j[m-h_{DC}]\frac{\pi}{2}} - e^{-j[m-h_{DC}]\frac{\pi}{2}}}{2j}\right] \quad 5.119$$

knowing that $J_{-n}(\xi) = (-1)^n J_n(\xi)$ and applying the Euler's formula (Eq. 5.66) finally the closed-form solution becomes

$$A_{m0} + jB_{m0} = \frac{2V_{DC}}{m\pi} J_0\left(m\frac{\pi}{2}M\right)\sin\left(m\frac{\pi}{2}\right) + \frac{M_{DC}}{m\pi}\begin{bmatrix} J_k\left(m\frac{\pi}{2}M\right)\sin\left([m+h_{DC}]\frac{\pi}{2}\right) \\ +(-1)^{h_{DC}} J_{h_{DC}}\left(m\frac{\pi}{2}M\right)\sin\left([m-h_{DC}]\frac{\pi}{2}\right)\end{bmatrix} \quad 5.120$$

– Sideband harmonics ($m > 0, n \neq 0, h_{DC} > 0$)

$$\begin{aligned} A_{mn} + jB_{mn} &= \frac{1}{2\pi^2}\int_{-\pi}^{\pi}\int_{-\frac{\pi}{2}(1+M\cos(y))}^{\frac{\pi}{2}(1+M\cos(y))} (V_{DC} + M_{DC}\cos(h_{DC}y))e^{j(mx+ny)}\,dxdy \\ &= \frac{V_{DC}}{2jm\pi^2}\int_{-\pi}^{\pi} e^{jny}\left[e^{jm\frac{\pi}{2}(1+M\cos(y))} - e^{-jm\frac{\pi}{2}(1+M\cos(y))}\right]dy \\ &+ \frac{M_{DC}}{2jm\pi^2}\int_{-\pi}^{\pi}\cos(h_{DC}y)\,e^{jny}\begin{bmatrix} e^{jm\frac{\pi}{2}(1+M\cos(y))} \\ -e^{-jm\frac{\pi}{2}(1+M\cos(y))}\end{bmatrix}dy \\ &= \frac{V_{DC}}{2jm\pi^2}\int_{-\pi}^{\pi}\begin{bmatrix} e^{jny}e^{jm\frac{\pi}{2}}e^{jm\frac{\pi}{2}M\cos(y)} \\ -e^{jny}e^{-jm\frac{\pi}{2}}e^{-jm\frac{\pi}{2}M\cos(y)}\end{bmatrix}dy \\ &+ \frac{M_{DC}}{4jm\pi^2}\int_{-\pi}^{\pi}\begin{bmatrix} \left(e^{jh_{DC}y} + e^{-jh_{DC}y}\right)e^{jny}e^{jm\frac{\pi}{2}}e^{jm\frac{\pi}{2}M\cos(y)} \\ -\left(e^{jh_{DC}y} + e^{-jh_{DC}y}\right)e^{jny}e^{-jm\frac{\pi}{2}}e^{-jm\frac{\pi}{2}M\cos(y)}\end{bmatrix}dy \end{aligned} \quad 5.121$$

Taking into consideration the relation from Eq. 5.116, the expression above becomes

$$
\begin{aligned}
&A_{mn}+jB_{mn}\\
&=\frac{V_{DC}}{2jm\pi^2}\int_{-\pi}^{\pi}\begin{bmatrix}e^{jny}e^{jm\frac{\pi}{2}}e^{jm\frac{\pi}{2}M\cos(y)}\\-e^{jny}e^{-jm\frac{\pi}{2}}e^{-jm\frac{\pi}{2}M\cos(y)}\end{bmatrix}dy\\
&+\frac{M_{DC}}{4jm\pi^2}\int_{-\pi}^{\pi}\begin{bmatrix}e^{jm\frac{\pi}{2}}e^{jm\frac{\pi}{2}M\cos(y)}e^{j[n+h_{DC}]y}+e^{jm\frac{\pi}{2}}e^{jm\frac{\pi}{2}M\cos(y)}e^{j[n-h_{DC}]y}\\-e^{-jm\frac{\pi}{2}}e^{-jm\frac{\pi}{2}M\cos(y)}e^{j[n+h_{DC}]y}-e^{-jm\frac{\pi}{2}}e^{-jm\frac{\pi}{2}M\cos(y)}e^{j[n-h_{DC}]y}\end{bmatrix}dy\\
&=\frac{V_{DC}}{2jm\pi^2}\left[e^{jm\frac{\pi}{2}}2\pi j^{n}J_n\left(m\frac{\pi}{2}M\right)-e^{-jm\frac{\pi}{2}}2\pi j^{-n}J_n\left(m\frac{\pi}{2}M\right)\right]\\
&+\frac{M_{DC}}{4jm\pi^2}\begin{bmatrix}e^{jm\frac{\pi}{2}}2\pi j^{n+h_{DC}}J_{n+h_{DC}}\left(m\frac{\pi}{2}M\right)+e^{jm\frac{\pi}{2}}2\pi j^{n-h_{DC}}J_{n-h_{DC}}\left(m\frac{\pi}{2}M\right)\\-e^{-jm\frac{\pi}{2}}2\pi j^{-[n+h_{DC}]}J_{n+h_{DC}}\left(m\frac{\pi}{2}M\right)-e^{-jm\frac{\pi}{2}}2\pi j^{-[n-h_{DC}]}J_{n-h_{DC}}\left(m\frac{\pi}{2}M\right)\end{bmatrix}
\end{aligned}
\tag{5.122}
$$

Applying the Euler's formula (Eq. 5.66) and taking expression from Eq. 5.93 into consideration

$$
\begin{aligned}
A_{mn}+jB_{mn}&=\frac{V_{DC}}{jm\pi}J_n\left(m\frac{\pi}{2}M\right)\left[e^{jm\frac{\pi}{2}}e^{jn\frac{\pi}{2}}-e^{-jm\frac{\pi}{2}}e^{-jn\frac{\pi}{2}}\right]\\
&+\frac{M_{DC}}{2jm\pi}J_{n+h_{DC}}\left(m\frac{\pi}{2}M\right)\left[e^{jm\frac{\pi}{2}}e^{j[n+h_{DC}]\frac{\pi}{2}}-e^{-jm\frac{\pi}{2}}e^{-j[n+h_{DC}]\frac{\pi}{2}}\right]\\
&+\frac{M_{DC}}{2jm\pi}J_{n-h_{DC}}\left(m\frac{\pi}{2}M\right)\left[e^{jm\frac{\pi}{2}}e^{j[n-h_{DC}]\frac{\pi}{2}}-e^{-jm\frac{\pi}{2}}e^{-j[n-h_{DC}]\frac{\pi}{2}}\right]\\
&=\frac{V_{DC}}{jm\pi}J_n\left(m\frac{\pi}{2}M\right)\left[e^{j\frac{\pi}{2}(m+n)}-e^{-j\frac{\pi}{2}(m+n)}\right]\\
&+\frac{M_{DC}}{2jm\pi}J_{n+h_{DC}}\left(m\frac{\pi}{2}M\right)\left[e^{j[m+n+h_{DC}]\frac{\pi}{2}}-e^{-j[m+n+h_{DC}]\frac{\pi}{2}}\right]\\
&+\frac{M_{DC}}{2jm\pi}J_{n-h_{DC}}\left(m\frac{\pi}{2}M\right)\left[e^{j[m+n-h_{DC}]\frac{\pi}{2}}-e^{-j[m+n-h_{DC}]\frac{\pi}{2}}\right]\\
&=\frac{2V_{DC}}{m\pi}J_n\left(m\frac{\pi}{2}M\right)\sin\left([m+n]\frac{\pi}{2}\right)\\
&+\frac{M_{DC}}{m\pi}\begin{bmatrix}J_{n+h_{DC}}\left(m\frac{\pi}{2}M\right)\sin\left([m+n+h_{DC}]\frac{\pi}{2}\right)\\+J_{n-h_{DC}}\left(m\frac{\pi}{2}M\right)\sin\left([m+n-h_{DC}]\frac{\pi}{2}\right)\end{bmatrix}
\end{aligned}
\tag{5.123}
$$

Closed form solution of the DC content (Eq. 5.108), baseband harmonic components (Eq. 5.113), carrier harmonic components (Eq. 5.120), sideband harmonic components (Eq. 5.123) in case of harmonic generated by the voltage source converter when harmonic content is present in the DC-link voltage is presented in this section. It can be seen that the solution is an extension of the closed form solution presented for double-edge naturally sampled pulse-width modulation from Eq. 5.40, Eq. 5.41, Eq. 5.42, and Eq. 5.43.

In real life wind turbines both the DC-link harmonic content as well as the command signal harmonic content affect harmonic generation of grid-connected voltage source converters. The converter switching pattern S described by the closed-form solution

is dependent on many factors. For example, baseband harmonic components are described as follows

$$\begin{aligned} & A_{0n} + jB_{0n} \\ & = \frac{1}{2\pi^2} \int_{-\pi}^{\pi} \int_{-\frac{\pi}{2}\left(\begin{matrix}1+M\cos(y)\\ +M_h\cos(hy+\theta_h)\end{matrix}\right)}^{\frac{\pi}{2}\left(\begin{matrix}1+M\cos(y)\\ +M_h\cos(hy+\theta_h)\end{matrix}\right)} \left(\begin{matrix}V_{DC}\\ +M_{DC}\cos(h_{DC}y+\theta_{DC})\end{matrix}\right) e^{jny}\, dxdy \\ & = \frac{1}{2\pi^2} \int_{-\pi}^{\pi} \pi \left(\begin{matrix}1+M\cos(y)\\ +M_h\cos(hy+\theta_h)\end{matrix}\right)\left(\begin{matrix}V_{DC}\\ +M_{DC}\cos(h_{DC}y+\theta_{DC})\end{matrix}\right) e^{jny}\, dy \end{aligned} \quad 5.124$$

After rearrangement

$$\begin{aligned} & A_{0n} + jB_{0n} \\ & = \frac{V_{DC}}{2\pi} \underbrace{\int_{-\pi}^{\pi} e^{jny}\, dy}_{0} + \frac{MV_{DC}}{4\pi}\left[\underbrace{\int_{-\pi}^{\pi} e^{j[n+1]y}\, dy}_{0} + \int_{-\pi}^{\pi} e^{j[n-1]y}\, dy\right] \\ & + \frac{M_{DC}}{4\pi}\left[\underbrace{\int_{-\pi}^{\pi} e^{j[(n+h_{DC})y+\theta_{DC}]}\, dy}_{0} + \int_{-\pi}^{\pi} e^{j[(n-h_{DC})y-\theta_{DC}]}\, dy\right] \\ & + \frac{MM_{DC}}{8\pi}\left[\begin{matrix}\underbrace{\int_{-\pi}^{\pi} e^{j[n+h_{DC}+1]y}\, dy}_{0} + \underbrace{\int_{-\pi}^{\pi} e^{j[n+h_{DC}-1]y}\, dy}_{0} \\ \int_{-\pi}^{\pi} e^{j[n-h_{DC}+1]y}\, dy + \int_{-\pi}^{\pi} e^{j[n-h_{DC}-1]y}\, dy\end{matrix}\right] \\ & + \frac{M_hV_{DC}}{4\pi}\left[\underbrace{\int_{-\pi}^{\pi} e^{j[(n+h)y+\theta_h]}\, dy}_{0} + \int_{-\pi}^{\pi} e^{j[(n-h)y-\theta_h]}\, dy\right] \\ & + \frac{M_hM_{DC}}{8\pi}\left[\begin{matrix}\underbrace{\int_{-\pi}^{\pi} e^{j[(n+h+h_{DC})y+\theta_h+\theta_{DC}]}\, dy}_{0} + \int_{-\pi}^{\pi} e^{j[(n+h-h_{DC})y+\theta_h-\theta_{DC}]}\, dy \\ \int_{-\pi}^{\pi} e^{j[(n-h+h_{DC})y-\theta_h+\theta_{DC}]}\, dy + \int_{-\pi}^{\pi} e^{j[(n-h-h_{DC})y-\theta_h-\theta_{DC}]}\, dy\end{matrix}\right] \end{aligned} \quad 5.125$$

And the baseband harmonic components are

$$A_{0n} + jB_{0n} = \frac{MV_{DC}}{2}\Big|_{n=1} + \frac{M_{DC}}{2}e^{-j\theta_{DC}}\Big|_{h=h_{DC}} + \frac{MM_{DC}}{4}e^{-j\theta_{DC}}\Big|_{n=h_{DC}\pm 1} + \frac{M_h V_{DC}}{2}e^{-j\theta_h}\Big|_{n=h} + \frac{M_h M_{DC}}{4}e^{j(\theta_h-\theta_{DC})}\Big|_{n=h_{DC}-h} + \frac{M_h M_{DC}}{4}e^{\pm j(\theta_h\mp\theta_{DC})}\Big|_{n=h\mp h_{DC}} \quad 5.126$$

Based on analysis of measurement data it was observed that the 1st harmonic is frequently present in the DC-link voltage. It was also observed that third-harmonic is injected into the reference signal in order to extend the linear operation of the grid-side converter. This can be seen based on carrier group harmonics analysis which exhibits wider energy distribution in the spectrum. Additionally it can be seen that the modulation index is often close to unity and sometimes even higher especially in case of the wind turbine full production.

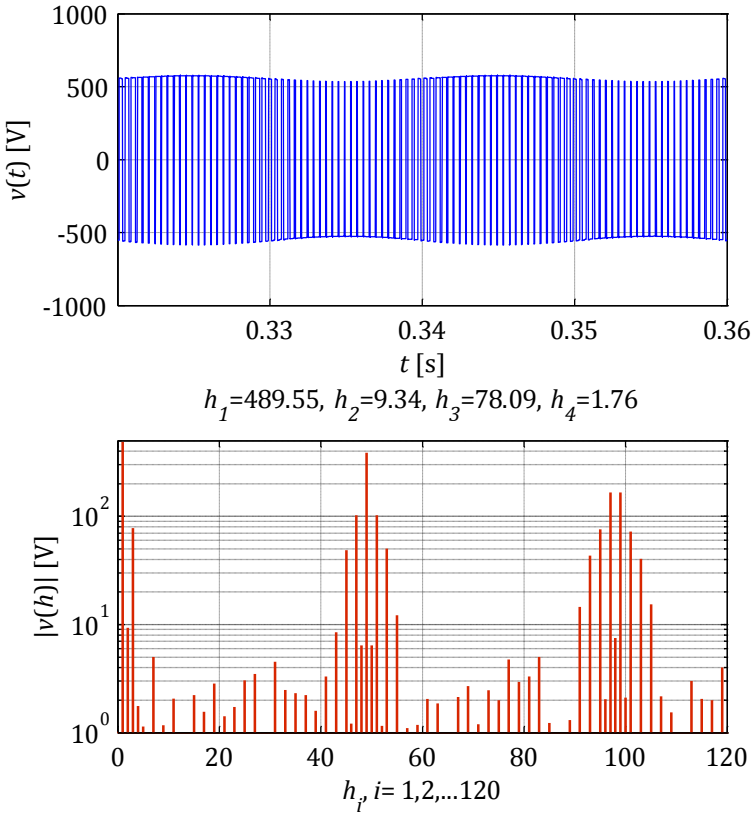

Figure 5.42 Harmonic spectrum estimated from numerical simulations of three-phase two-level voltage source converter.

In that case let us consider that $h_{DC} = 1$ and $h = 3, \theta_h = \pi$. Based on Eq. 5.126 it can be seen that this configuration causes generation of the 1st harmonic, the 2nd harmonic, the 3rd harmonic, and the 4th harmonic within the baseband harmonic range. From Figure 5.42 one can see numerical simulation results of a three-phase grid-connected converter. During simulations a certain DC-link harmonic content was assumed

(i.e. $M_{DC} = 50$ V) and third-harmonic injection into the reference signal was applied (i.e. $M_h = 0.15$) with a modulation index M equal to 0.9. Please note that the DC-link voltage was equal to 1110 V as typically seen in the measurements. As it can be seen a good agreement between the numerical model and analytical model can be found (see Table 5.13). Of course the voltage source converter model based on the switching function is the closest to the analytical description because it does not take into consideration physical properties of the network bridge. Please note that in this model it is not possible to measure the phase voltage in relation to the DC-link neutral point (i.e. there is no electrical connection between the DC-link circuit and the AC network).

Table 5.13 Comparison between numerical and analytical model.

Case	h_1	h_2	h_3	h_4
Analytical model	499.5	11.25	83.25	1.875
Numerical model (switching function)	494.7	11.07	-	-
Numerical model (ideal switches)	491.83	9.31	78.73	1.74
Numerical model (IGBTs/diodes)	489.5	9.34	78.09	1.76

5.2.1.6 ASYMMETRICALLY REGULAR SAMPLED PWM

Naturally sampled pulse-width modulation is successfully used in applications when analog modulation is used. Nowadays more and more often digital approach is used, because processors become more powerful as well as cheap. Due to the fact that naturally sampled pulse-width modulation is difficult to implement in digital signal processors, there is a need to apply sampling process in order to overcome such difficulties. Many variations of regular sampled pulse-width modulation are widely used, thanks to their simplicity to be digitally implemented. Of course such an approach introduces new aspects related to harmonic generation. Such approach was firstly introduced by Bowes [5.44] and was originally used for AC motor drives application purposes.

The sinusoidal reference signal is sampled and compared against triangular carrier waveform to control the switching process of each phase leg of the three-phase two-level converter. The sampled command must change value at positive or negative peaks of the carrier signal. This avoids instantaneous changes of the switching function S. In Figure 5.43 the command waveform changes its value at the positive carrier peak, i.e. the switching function assumes the value of 1 for the same value of the carrier signal within its one period.

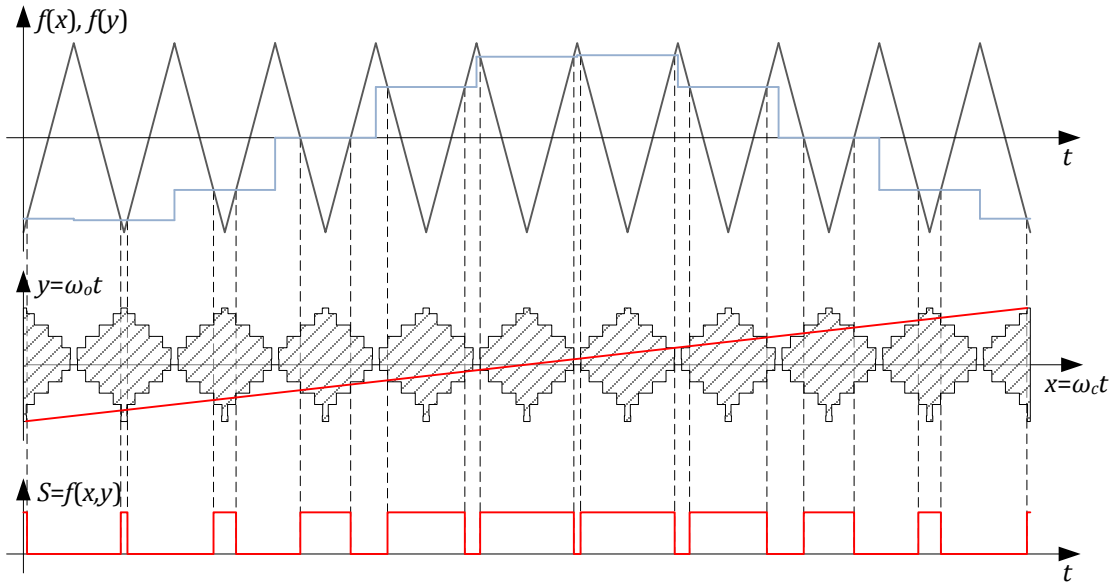

Figure 5.43 Double-edge symmetrically regular sampled pulse width modulation within linear operation range ($M = 0.9, m_f = 10$).

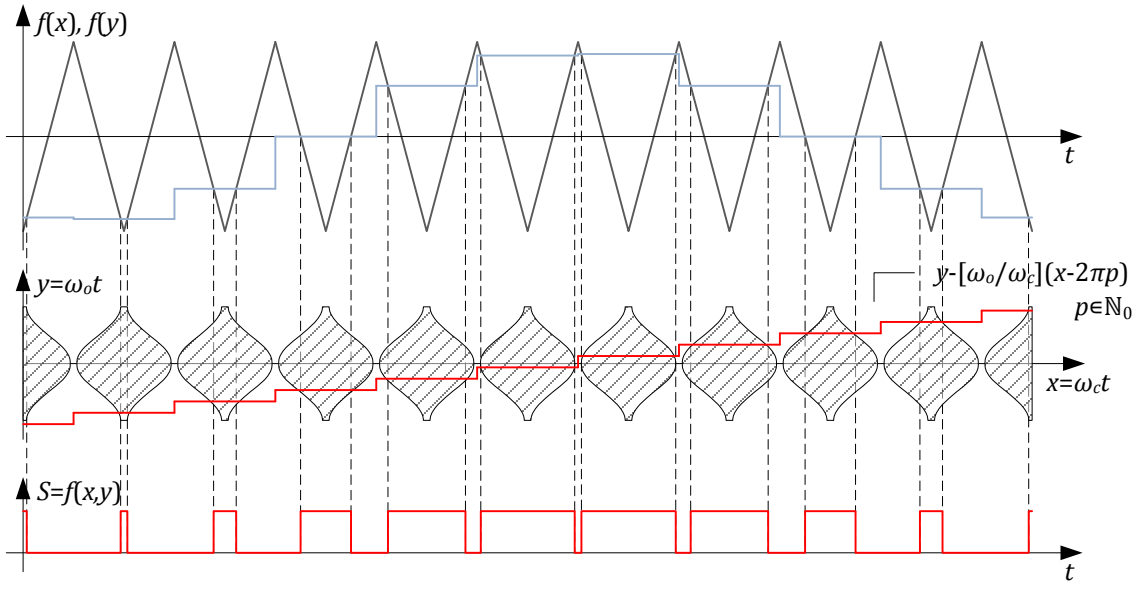

Figure 5.44 Double-edge symmetrically sampled pulse-width modulation with smooth unit cell and staircase solution trajectory ($M = 0.9, m_f = 10$).

Due to the fact that in the case of asymmetrically regular sample pulse-width modulation for triangular carrier signal, in contrast to symmetrically regular sampled, a significant harmonic cancellation occurs between phase legs. Therefore such modulation is commonly applied in three-phase inverters and is also expected based on measurements [5.30]. Figure 5.45 presents asymmetrically regular sampled pulse-width modulation of a pure sine command waveform. Additionally the switching function S is presented as an outcome of the modulation process. The switching function expresses the ideal, theoretical spectrum caused by the modulation process.

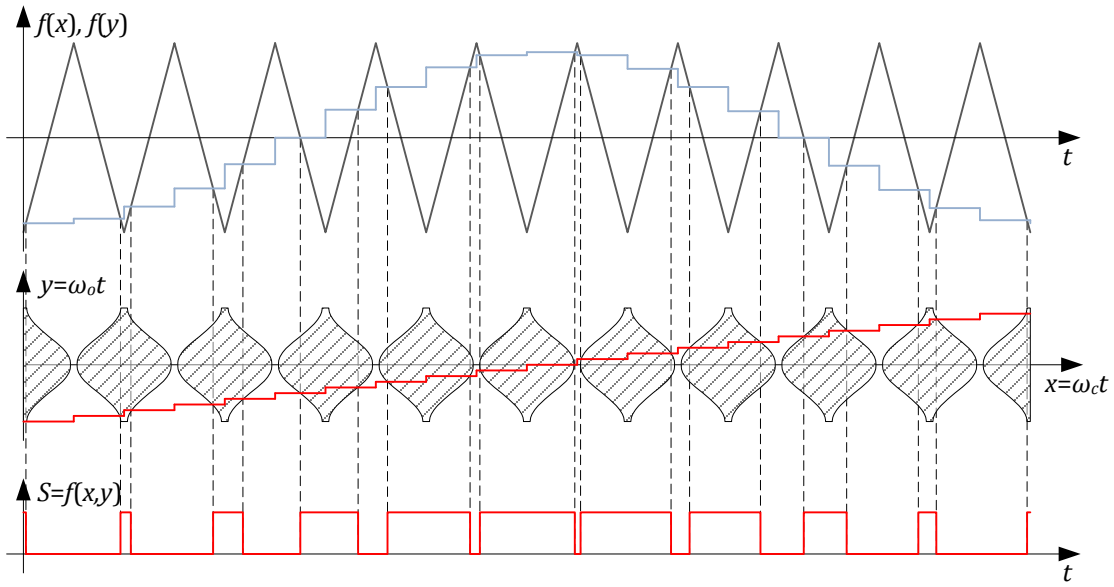

Figure 5.45 Double-edge asymmetrically sampled pulse-width modulation with smooth unit cell and staircase solution trajectory ($M = 0.9, m_f = 10$).

$$
\begin{aligned}
&v_{az}(t) \\
&= \frac{2V_{DC}}{\pi}\sum_{n=1}^{\infty}\frac{1}{\left[n\frac{\omega_o}{\omega_c}\right]}J_n\left(n\frac{\omega_o}{\omega_c}\frac{\pi}{2}M\right)\sin\left(n\frac{\pi}{2}\right)\cos(n[\omega_o t+\theta_o]) \\
&+\frac{2V_{DC}}{\pi}\sum_{m=1}^{\infty}\frac{1}{m}J_0\left(m\frac{\pi}{2}M\right)\sin\left(m\frac{\pi}{2}\right)\cos(m[\omega_c t+\theta_c]) \\
&+\frac{2V_{DC}}{\pi}\sum_{m=1}^{\infty}\sum_{\substack{n=-\infty\\ n\neq 0}}^{\infty}\frac{1}{\left[m+n\frac{\omega_o}{\omega_c}\right]}\left[\begin{matrix}J_n\left(\left[m+n\frac{\omega_o}{\omega_c}\right]\frac{\pi}{2}M\right)\sin\left([m+n]\frac{\pi}{2}\right)\\ \times\cos(m[\omega_c t+\theta_c]+n[\omega_o t+\theta_o])\end{matrix}\right]
\end{aligned}
\qquad 5.127
$$

As it can be seen from Eq. 5.127, the magnitude of harmonic components generated by double-edge asymmetrically sampled pulse-width modulation is dependent on frequency ratio $m_f = \omega_c/\omega_o$. This is generally characteristic for regular sampled pulse-width modulation, and was not seen in naturally sampled pulse-width modulation. Since the carrier fundamental frequency tends to be kept constant and the power system fundamental frequency varies, harmonic magnitude variation can occur in regular sampled modulation. Therefore harmonic components generated by grid-side converters change their magnitude depending on fundamental frequency variation. It has to be emphasized that the carrier frequency can be adjusted to the fundamental frequency [5.19] in order to avoid non-integer frequency ratios, but it is not commonly applied. Frequency synchronization between carrier signal and command signal can be inconvenient, because it causes significant carrier group harmonic components frequency variation, especially for high m_f. This can cause difficulties in the filtering process as well decrease robustness of the converter connected to different networks (i.e. different frequency variation).

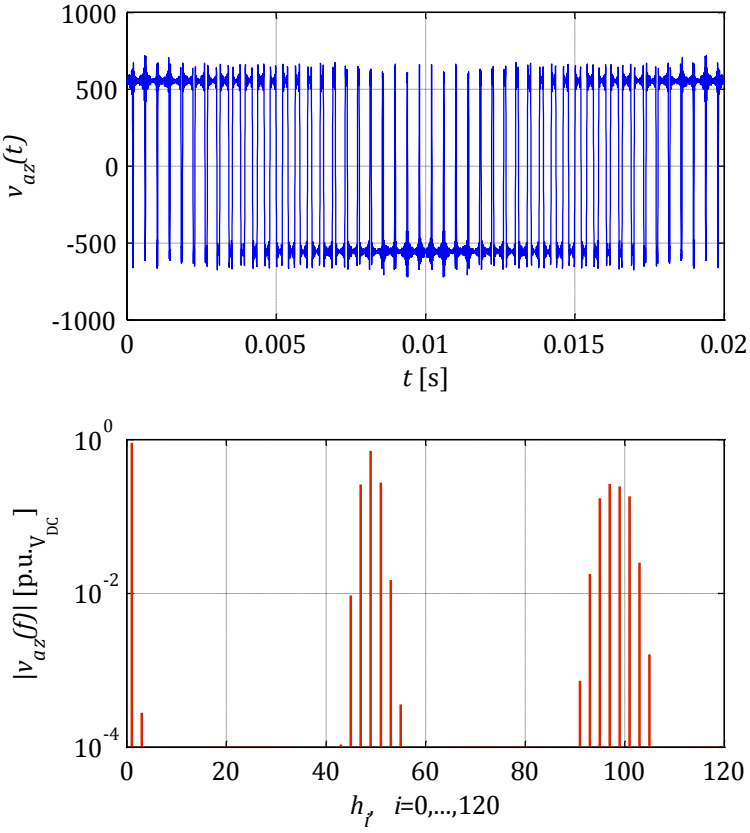

Figure 5.46 Theoretical waveform and spectrum obtained for double-edge asymmetrically sampled pulse-width modulation ($M = 0.9, m_f = 49$).

In comparison to naturally sampled pulse-width modulation, asymmetrically regular sampled pulse-width modulation exhibits a certain asymmetry in magnitudes of corresponding harmonic components pairs around carrier fundamental and its integer multiples. Also additional baseband harmonic component are present as it can be seen in Figure 5.46.

Based on modulation index variation in measurements it was observed that the third harmonic is injected in the reference signal in order to extend linear dependency between the modulation index and the fundamental component magnitude. The complex Fourier coefficient of asymmetrically regular sampled pulse-width modulation is given by

$$A_{mn}+jB_{mn}$$
$$=\frac{2V_{DC}}{q\pi}\left\{\begin{array}{l} J_0\left(q\frac{\pi}{2}M\right)\sum_{l=1}^{\infty}J_l\left(q\frac{\pi}{2}M_3\right)\sin\left([m-l]\frac{\pi}{2}\right)\Big|_{n=-3l\,\cup\,n=3l} \\ +J_0\left(q\frac{\pi}{2}M_3\right)\sum_{k=1}^{\infty}J_k\left(q\frac{\pi}{2}M\right)\sin\left([m+k]\frac{\pi}{2}\right)\Big|_{n=-k\,\cup\,n=k} \\ +\sum_{k=1}^{\infty}\sum_{l=1}^{\infty}J_k\left(q\frac{\pi}{2}M\right)J_l\left(q\frac{\pi}{2}M_3\right)\sin\left([m+k-l]\frac{\pi}{2}\right)\Big|_{\substack{n=-(k+3l)\,\cup\,n=k+3l \\ n=-(k-3l)\,\cup\,n=k-3l}} \end{array}\right\} \quad 5.128$$

Due to the third-harmonic injection into the reference signal, magnitudes of the first and the second carrier group harmonic components are flattened and broadly distributed (i.e. harmonic energy from the first pair around the carrier harmonic component is distributed to outer sideband pairs). Please note that Eq. 5.97 and Eq. 5.128 do not differ so much between each other. If one would assume that $h=3$ and $\theta_h=\pi$ the Fourier coefficients are the same except the term q describing reference signal sampling. The term q is dependent on m as well as n indexes $q=m+n(\omega_o/\omega_c)$ therefore by changing the appropriate indexes it is possible to calculate baseband, sideband, and carrier harmonics from $\underline{C}_{mn}$. Also it is possible to analyze the effect of sampling in closed-form solutions derived based on naturally sampled pulse-width modulation by replacing m in the Bessel function of the first kind argument and in the scaling factor.

Taking onto consideration small power system frequency variation Δf_o, Eq. 5.128 can be expressed by substitution of $\omega_o=2\pi(f_o+\Delta f_o)$ in the following way

$$A_{mn}+jB_{mn}$$
$$=\frac{2V_{DC}}{\left[m+n\frac{\omega_o+\Delta\omega_o}{\omega_c}\right]\pi}\left\{\begin{array}{l} J_0\left(\left[m+n\frac{\omega_o+\Delta\omega_o}{\omega_c}\right]\frac{\pi}{2}M\right) \\ \times\sum_{l=1}^{\infty}J_l\left(\left[m+n\frac{\omega_o+\Delta\omega_o}{\omega_c}\right]\frac{\pi}{2}M_3\right)\sin\left([m-l]\frac{\pi}{2}\right)\Big|_{n=\pm3l} \\ J_0\left(\left[m+n\frac{\omega_o+\Delta\omega_o}{\omega_c}\right]\frac{\pi}{2}M_3\right) \\ +\times\sum_{k=1}^{\infty}J_k\left(\left[m+n\frac{\omega_o+\Delta\omega_o}{\omega_c}\right]\frac{\pi}{2}M\right)\sin\left([m+k]\frac{\pi}{2}\right)\Big|_{n=\pm k} \\ J_k\left(\left[m+n\frac{\omega_o+\Delta\omega_o}{\omega_c}\right]\frac{\pi}{2}M\right) \\ +\sum_{k=1}^{\infty}\sum_{l=1}^{\infty}\times J_l\left(\left[m+n\frac{\omega_o+\Delta\omega_o}{\omega_c}\right]\frac{\pi}{2}M_3\right) \\ \times\sin\left([m+k-l]\frac{\pi}{2}\right)\Big|_{\substack{n=\pm(k+3l) \\ n=\pm(k-3l)}} \end{array}\right\} \quad 5.129$$

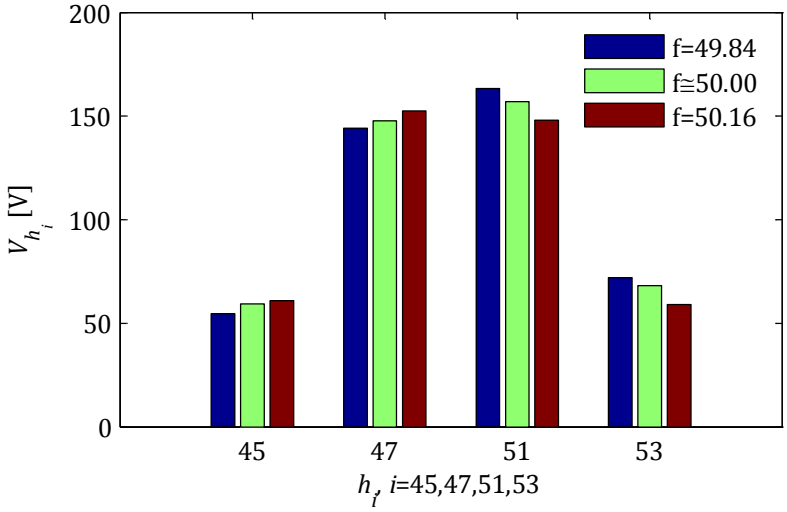

Figure 5.47 Magnitude dependence of sideband harmonic components in the first carrier group on power system frequency variation observed in measurements.

Due to fact that the power system frequency f_0 varies the amplitudes of sideband frequency components generated by asymmetrically regular sampled pulse-width modulation varies as well, as shown in Figure 5.47. Deterministic description of the power system to predict power system frequency changes is complex and requires taking many degrees of freedom into consideration. In this case probabilistic approach to describe harmonic generation can be useful.

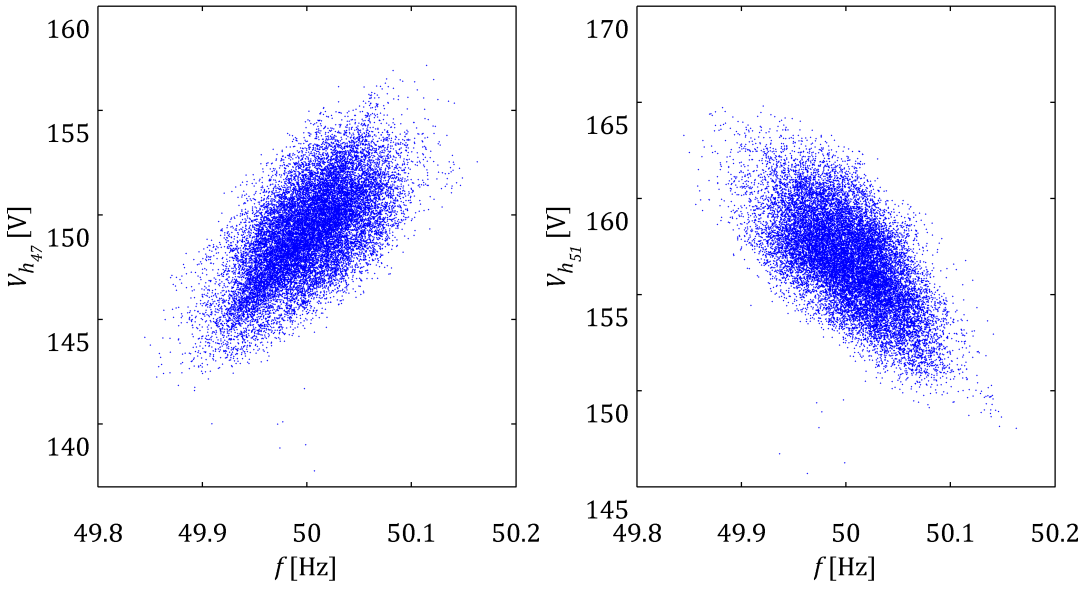

Figure 5.48 Magnitude dependence of sideband harmonic component on power system frequency variation observed in measurements.

In Figure 5.47 it is shown that all of sideband harmonics in the first carrier group are dependent on the power system frequency f_0. Also scatter plots from Figure 5.48 exhibit this phenomenon. From the same figures one can observe that there is a linear

tendency in sideband harmonics magnitude changes. It was possible to observe the effect of command signal sampling thanks to sophisticated statistical methods presented in the previous chapter. It was possible to separate unimodal distributions of sideband harmonic components and therefore their behaviour. Please note that uncertainties are caused by spectral leakage.

Presented spectrum estimation from measurements in Figure 5.49 of voltage waveform measurements, acquired at the AC terminals of the grid-side converter, show that the pulse width modulation technique is used in order to generate smooth sine waveform after the shunt filter. Phase-to-phase voltage waveform exhibits two-level voltage source converter. The switching frequency is 2450 Hz and around this frequency one can clearly see sideband harmonics. Sideband harmonics are skewed due to asymmetrically regular sampled pulse-width modulation.

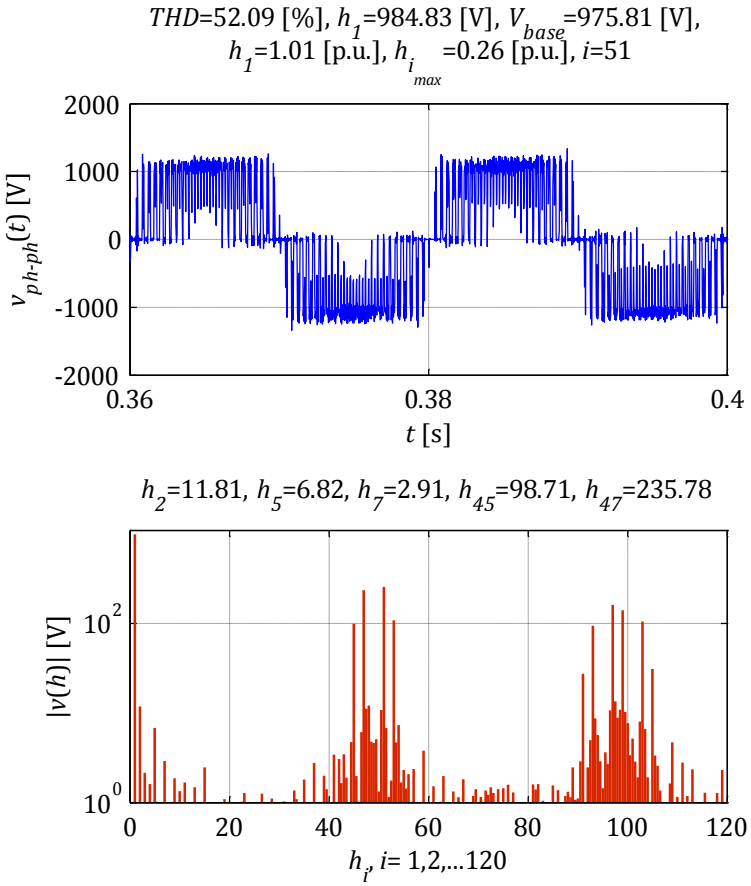

Figure 5.49 Grid-side converter voltage phase-to-phase waveform and its estimated spectrum from measurements during full production.

From Figure 5.49 it can be also seen that the frequency ratio $m_f = f_c/f_m = 49$. If the carrier signal frequency f_c in carrier-based pulse-width modulation technique is not a multiple integer of the fundamental power frequency f_o, the frequency ratio is not an integer as well. This affects generation of carrier group harmonic components which are not integer multiple of the fundamental frequency. Such situation appears

very often existing in real-life wind turbines with constant carrier frequency because the power system frequency independently varies.

One also can observed that the modulation index M of analyzed grid-side converter is higher than 1 and the converter always operates in range of linear control of the output fundamental component. Therefore no additional baseband distortions are produced. The range can be extended by introduction of zero-sequence third-harmonic component to asymmetrical regular sampled pulse-width modulation as it is done in the analysed turbine.

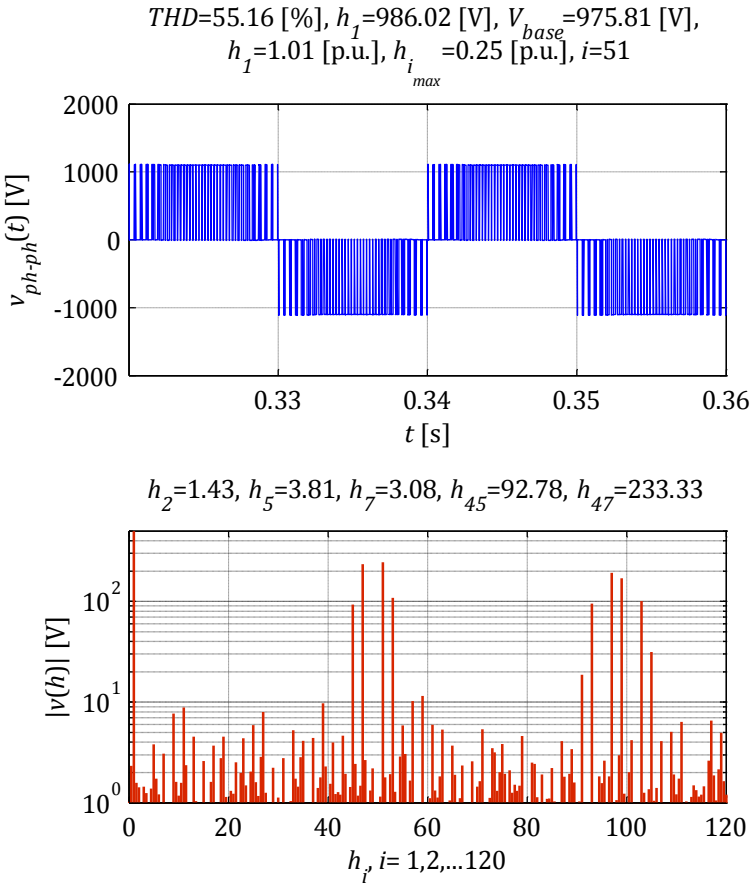

Figure 5.50 Grid-side converter voltage phase-to-phase waveform and its estimated spectrum from numerical simulations during full production.

Figure 5.50 presents results from numerical simulations. As it was mentioned before asymmetrically regular sampled pulse-width modulation was used with third-harmonic injection. As can be observed, based on the plot above almost the whole spectrum of generated voltage can be successfully compared with measurements from Figure 5.49. This indicated good agreement between theoretical assumptions and practical implementation of the wind turbine.

Figure 5.51 shows theoretical grid-side converter voltage and theoretical spectrum of the voltage obtained based on analytical closed-form solution. In case of the numerical simulation the amplitude of injected third-harmonic component

$M_h = 0.136$ while in case of analytical solution the amplitude $M_h = 0.135$. The modulation index is equal 1.025 and 1.03 for the analytical solution and numerical simulation respectively.

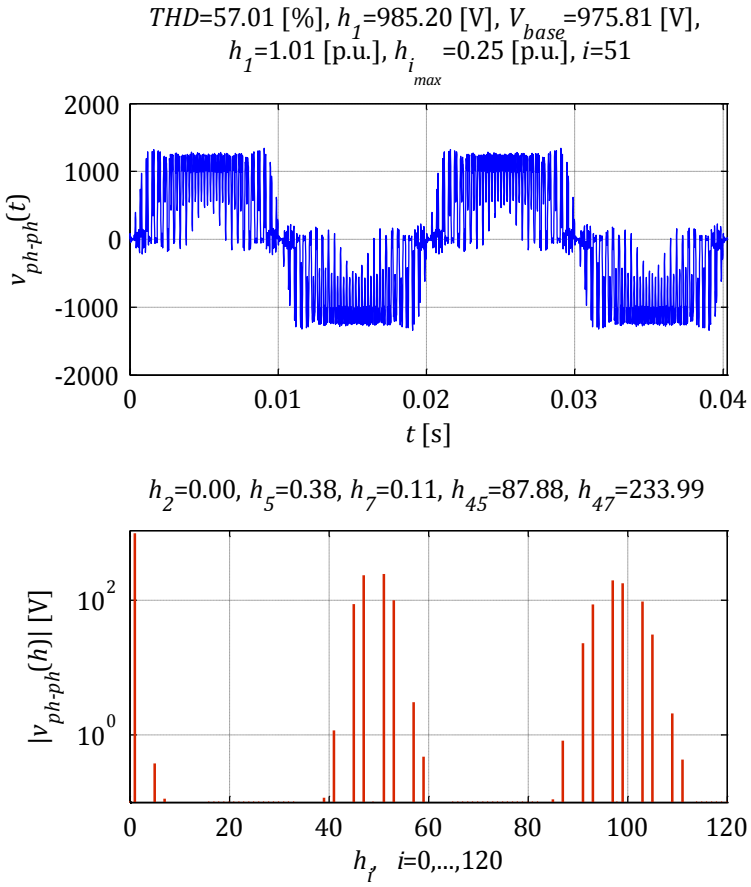

Figure 5.51 Grid-side converter theoretical phase-to-phase voltage and its theoretical spectrum from analytical description.

Analysis in time domain takes both amplitude and angles of harmonic components into consideration. Another huge advantage of validation results in time domain is that it is free of possible spectral leakage. Therefore validation using in both time and frequency domain gives more complete overview about obtained results. Additional time series analysis techniques such as autocorrelation of residuals can be successfully used. In order to separate frequency components of interest filtering by using digital filters can be successfully applied to every kind of analysed signal. This means that different signals (i.e. measurement data, simulation results) can be repeatedly analysed. Signal processing errors are minimized within filter passband. In contrast signal filtering based on fast Fourier transform is strongly affected by the nature of analysed signal (i.e. periodicity, stationarity) and such phenomena as spectral leakage can significantly disturb analysis and validation process. That is why both in time domain as well as frequency domain simulation results and measurements are analysed and compared.

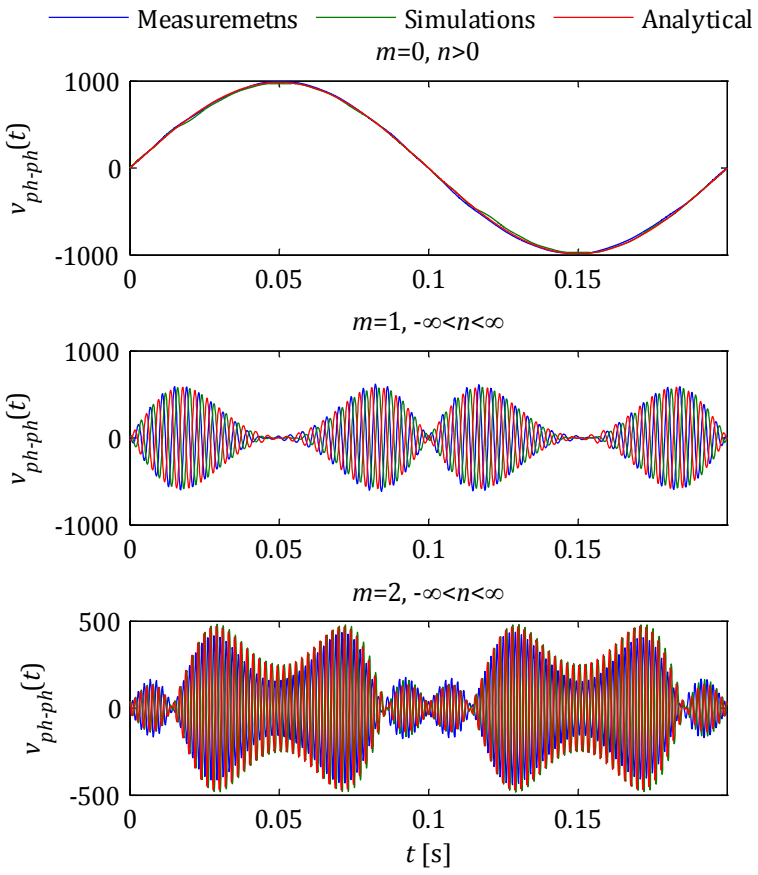

Figure 5.52 Filtered baseband harmonics and harmonic carrier group presented in time domain.

Figure 5.52 presents measurements filtered using digital filters with a bandwidth within the frequency range of interest. Baseband, first carrier group, and second carrier groups' frequency components are separated. This procedure allows comparing and analysing separately different frequencies which nature and origin is different. From Figure 5.52 one can see that the shape of waveforms and amplitude are closed to each other for all results (i.e. measurements, simulations, analytical calculations). This shape (envelope) is characteristic for asymmetrically regular sampled pulse-width modulation with third-harmonic injection. Please note that the phase angle of carrier group harmonics is different. However earlier it was shown that it can be easily determined. The difference is caused by the quite random nature of the carrier signal phase angle when the wind turbine is turned on.

In order to present separately baseband harmonics with the fundamental one, the first carrier harmonic group as well as the second carrier harmonic group, band-pass filters are used. Applied infinite impulse response (IIR) digital filters with zero-phase shift characterizes flat passband, narrow transition band and sufficient attenuation within stopband (-40 dB). In order to filter appropriate frequency components zero-phase shift inverse Chebyshev IIR filter is used. The filter is also known as type II Chebyshev filter which is characterized by no ripple in the passband. It also does not roll off as fast as type I [5.45], which is not so crucial especially if adjacent carrier group harmonics

are situated sufficiently far from each other. The considered converter has frequency ratio $m_f = f_c/f_0 = 49$ which easily allows to separate carrier harmonic groups by application of notch filters. The cut-off frequency for the low-pass filter $f_c = 1600$ Hz as well as lower and upper cut-off frequencies of band-pass filters, $f_L = 1800$ Hz and $f_H = 3800$ Hz for band-pass filter of the first carrier group, $f_L = 4000$ Hz and $f_H = 6000$ Hz for the second carrier group. Please note that zero-phase filters are non-casual filters and can only be used in off-line data processing [5.46].

Any kind of modelling brings always some limitations. Regardless of how detailed is the model, it always will be an approximation of real-life existing systems. The analytical model which is based on double Fourier series approach is affected by Gibbs phenomenon [5.47]. It is the peculiar manner in which the Fourier series of a piecewise continuously differentiable periodic function (i.e. switching function of the converter) overshoots at a jump discontinuity. Additionally the Fourier series representation does not take into consideration different aspects of practical implementation, thus theoretical spectrum does not contain even baseband harmonic components.

5.2.2 HARMONIC CONTROL SCENARIOS

Nowadays in wind turbines full-size back-to-back converter configuration is commonly considered. This allows separating (decoupling) from harmonic perspective the wind turbine generator with the generator-side converter from one side and the grid with the grid-side converter from the other side. The grid-side converter takes care of the wind turbine interaction with the utility grid and thus possible harmonic emission and compensation. The grid-side controller normally regulates the DC-link voltage in order to maintain the power flow balance between the generator-side converter and the grid-side converter. Additionally it is capable to take care of the quality of the generated power by controlling the output current. Robust synchronization (i.e. independent on frequency variation, harmonic distortion and transients) with the grid voltage and grid (voltage and frequency) monitoring are also crucial tasks in a proper operation of the controller. Since in the considered back-to-back topology, the output power is completely decoupled from the input power by a DC-link circuit, the grid side converter is mainly responsible for power quality improvements and fault tolerance.

Different control structures are possible in modern wind turbine converters [5.48]. The implementation of the control strategy can be achieved in different reference frames such as rotating reference frame (dq), stationary ($\alpha\beta$), and natural (abc) reference frames. Each of them has its advantages and drawbacks. Based on measurements and literature studies [5.11], [5.49] it was decided to implement the model of the grid-side converter controlled by proportional-integral (PI) current controllers in rotating reference frame (dq) which is synchronized with the power system frequency. The rotating reference frame is defined as synchronous if it rotates

with angular frequency ω which is defined as $\omega = 2\pi f$ where f is the grid frequency. Rotating reference frame of the main current control (i.e. fundamental frequency control) will be also called synchronous reference frame.

The dq control structure is using the $abc \rightarrow dq$ transformation module to transform the control variables from their natural abc frame to a frame that synchronously rotates with the frequency of the grid voltage. As a consequence, the control variables are becoming DC signals. Specific to this control structure is the necessity of information about the phase angle of utility voltage in order to perform the transformation. This can be achieved by application of phase-locked loop (PLL). A typical transfer function of continuous (i.e. s-domain) PI controllers used in the control is given by

$$G_{PI}(s) = K_p + \frac{K_i}{s} \tag{5.1}$$

where K_p is the proportional and K_i is the integral gain of the controller. The control structure of the positive sequence current involving cross coupling and grid voltage feedforward in rotating reference frame is presented in Figure 5.53.

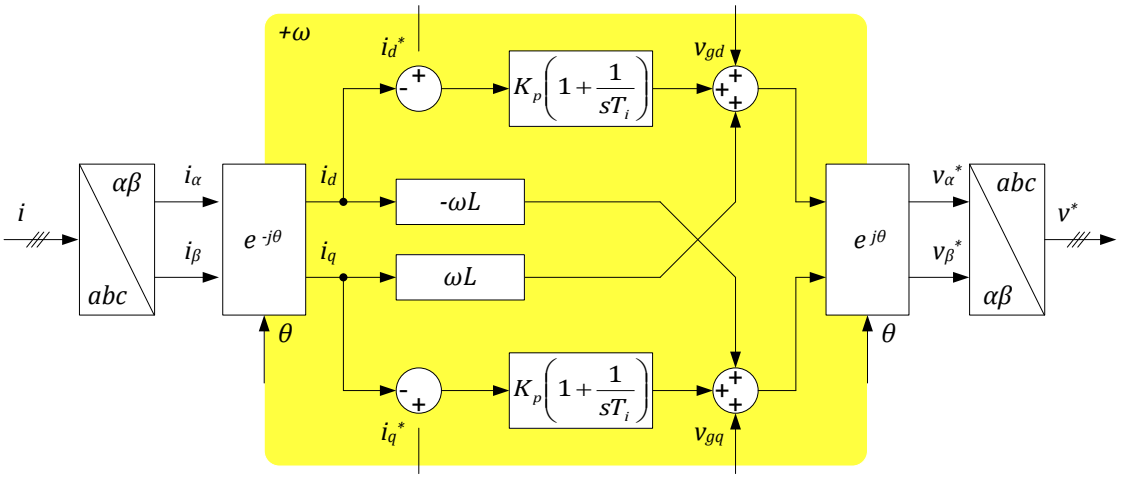

Figure 5.53 Basic current control for three-phase systems based on rotating reference frame.

$$G_{PI}^{dq}(s) = \begin{bmatrix} K_p + \frac{K_i}{s} & 0 \\ 0 & K_p + \frac{K_i}{s} \end{bmatrix} \tag{5.2}$$

$$G_{PI}^{\alpha\beta}(s) = \begin{bmatrix} K_p + \frac{K_i s}{s^2 + \omega_o^2} & \frac{K_i \omega_0}{s^2 + \omega_o^2} \\ -\frac{K_i \omega_0}{s^2 + \omega_o^2} & K_p + \frac{K_i s}{s^2 + \omega_o^2} \end{bmatrix} \tag{5.3}$$

The feedforward of the grid voltage directly in the dq frame affects the improvement of the controller dynamics during grid voltage fluctuations. Every deviation in the grid voltage amplitude will be almost instantaneously reflected in the control reference

signal leading to the fast response of the control system. On the other hand this approach has a drawback considering possible harmonic compensation [5.50]. The capability of the controller's harmonic compensation can be limited because of distorted voltage feedforward as well as errors in the phase detection of distorted grid voltage. These aspects are described more broadly later based on particular harmonic compensation scenarios in [5.50].

Considering grid-side converter control scenarios it is more and more popular to control both positive and negative sequence fundamental components. Such control structure is used to deal with converter operation under grid faults when negative sequence control is required. Figure 5.54 presents converter control of positive and negative sequence components in rotating reference frame (i.e. double synchronous reference frame) [5.51].

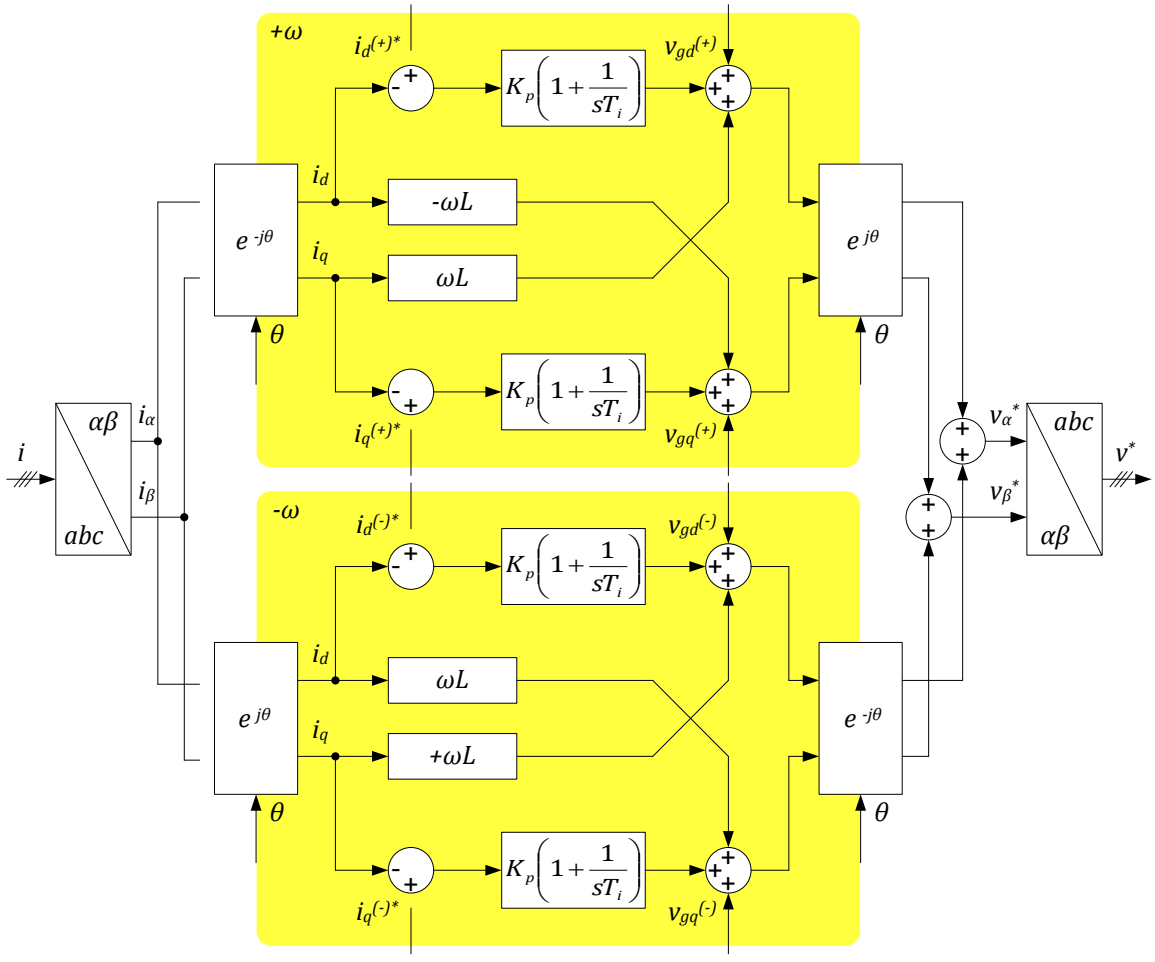

Figure 5.54 Fundamental frequency current control for three-phase systems based on rotating reference frame for both positive and negative sequence components.

Considering control of positive and negative sequence components in synchronous reference frame the PI controllers transfer functions in dq and $\alpha\beta$ can be expressed in the following way [5.52]

$$G_{PI}^{dq(+)}(s) = G_{PI}^{dq(-)}(s) = \begin{bmatrix} K_p + \frac{K_i}{s} & 0 \\ 0 & K_p + \frac{K_i}{s} \end{bmatrix} \tag{5.4}$$

$$G_{PI}^{\alpha\beta(+)} = \begin{bmatrix} K_p + \frac{K_i s}{s^2 + \omega_o^2} & \frac{K_i \omega_0}{s^2 + \omega_o^2} \\ -\frac{K_i \omega_0}{s^2 + \omega_o^2} & K_p + \frac{K_i s}{s^2 + \omega_o^2} \end{bmatrix} \tag{5.5}$$

$$G_{PI}^{\alpha\beta(-)} = \begin{bmatrix} K_p + \frac{K_i s}{s^2 + \omega_o^2} & -\frac{K_i \omega_0}{s^2 + \omega_o^2} \\ \frac{K_i \omega_0}{s^2 + \omega_o^2} & K_p + \frac{K_i s}{s^2 + \omega_o^2} \end{bmatrix} \tag{5.6}$$

Please note that joint operation of the positive and negative synchronous reference frames is equal to operation of controllers in stationary reference frame, as can be seen below. Such feature can be successfully used in case of harmonic components control which will be shown later.

$$\begin{aligned} G_{PI}^{\alpha\beta}(s) &= G_{PI}^{\alpha\beta(+)} + G_{PI}^{\alpha\beta(-)} \\ &= 2\begin{bmatrix} K_p + \frac{K_i s}{s^2 + \omega_o^2} & 0 \\ 0 & K_p + \frac{K_i s}{s^2 + \omega_o^2} \end{bmatrix} \end{aligned} \tag{5.7}$$

Please note that cross-coupling exists between dq signals in both synchronous reference frames. Due to the coupling 2^{nd} harmonic oscillations ($2\omega_o$) can be observed in both frames. Such oscillations cannot be completely attenuated by PI controllers and therefore causes the steady-state errors. In order to improve control performance these oscillations should be cancelled to achieve full control of measured positive and negative sequence currents under unbalanced conditions. This can be obtained by application of notch filters only to attenuate the unwanted 2^{nd} harmonic component [5.53]. This solution can cause some stability issues which will be shown later.

5.2.2.1 HARMONIC COMPENSATION

As described above the control method based on PI control in rotating reference frame with grid voltage feed-forward [5.54] is applied in the grid-side converter analysis, but this solution exhibits an instability of the PI controller to track a sinusoidal reference without steady-state error and poor disturbance rejection capability. This poor performance of the integral action can cause some problems in harmonic compensation.

Double harmonic current control

The voltage in real-life existing wind power systems is distorted and contains mainly low-order harmonics. To compensate unwanted harmonic current flow additional

harmonic current control loops are combined with the basic current control. Figure 5.53 shows basic control structure of the current controller in rotating reference frame. Harmonic compensation can be applied by implementation of additional control to the basic one, that can provide appropriate reference signal for each harmonic of interest.

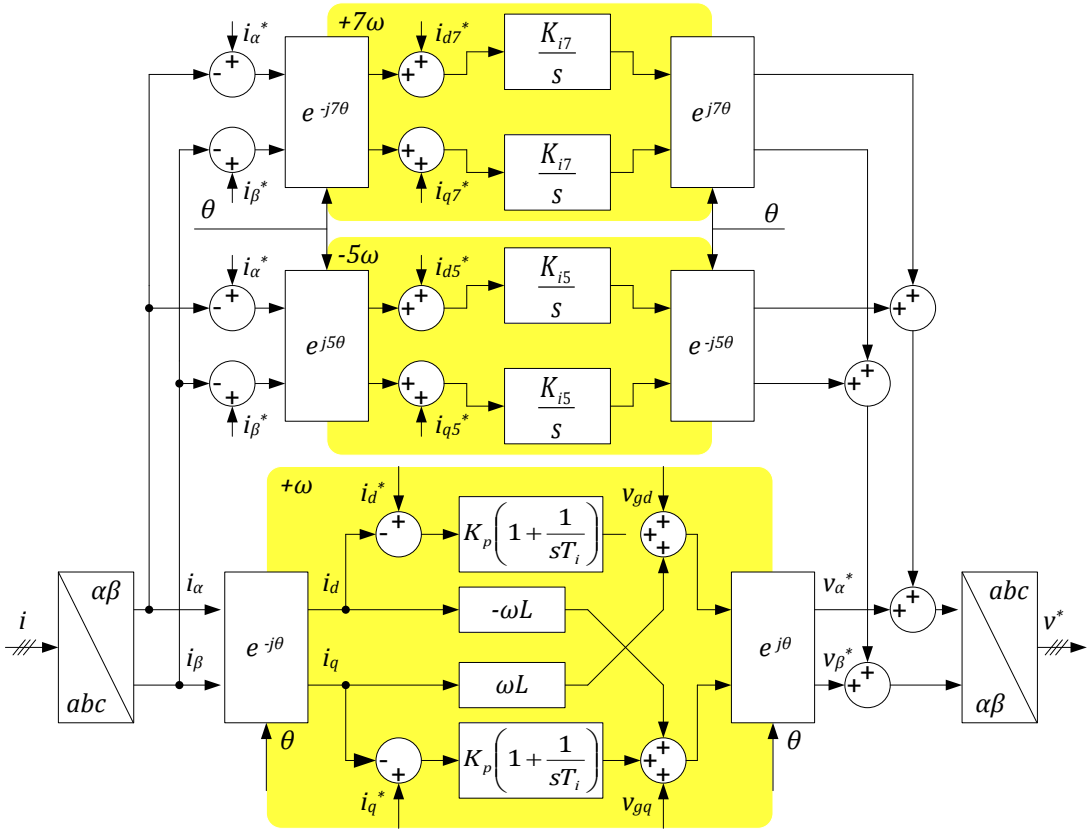

Figure 5.55 Double harmonic current control in two separated rotating frames.

In order to control harmonic current there is a need to implement a controller for each harmonic of interest. Therefore if one would like to control typically observed in the network harmonics, such as 5^{th} and 7^{th}, two controllers should be implemented in two frames rotating at -5ω and 7ω respectively. Of course it is assumed that the 5^{th} is a negative sequence harmonic and the 7^{th} is a positive sequence harmonic. This simply means that harmonic compensation using this method will effectively work in case of balanced harmonics. Normally there is no intention to have any harmonics in the system so the control is basically tuned to completely eliminate controlled harmonics (i.e. $i_{d7}^* = 0$, $i_{q7}^* = 0$, $i_{d5}^* = 0$, and $i_{q5}^* = 0$). From this perspective the converter impedance within the control bandwidth and affected by the control scenario is expected to by ideally equal to infinity for these selected harmonics.

Transforming measured currents into the 5^{th} and 7^{th} harmonic reference frame, the respective harmonic components can be easily extracted. The reference values are set to zero and controlled using integral controller. Normally proportional controller is not needed in this case because sudden changes in harmonic currents

are not expected and even if would happen it does not affect significantly the overall control behaviour. In other words fast response of harmonic controllers is not of special concern. Additionally a low-pass filter can be introduced with cut-off frequency around 10 Hz which limits disturbances affected by other harmonics [5.55].

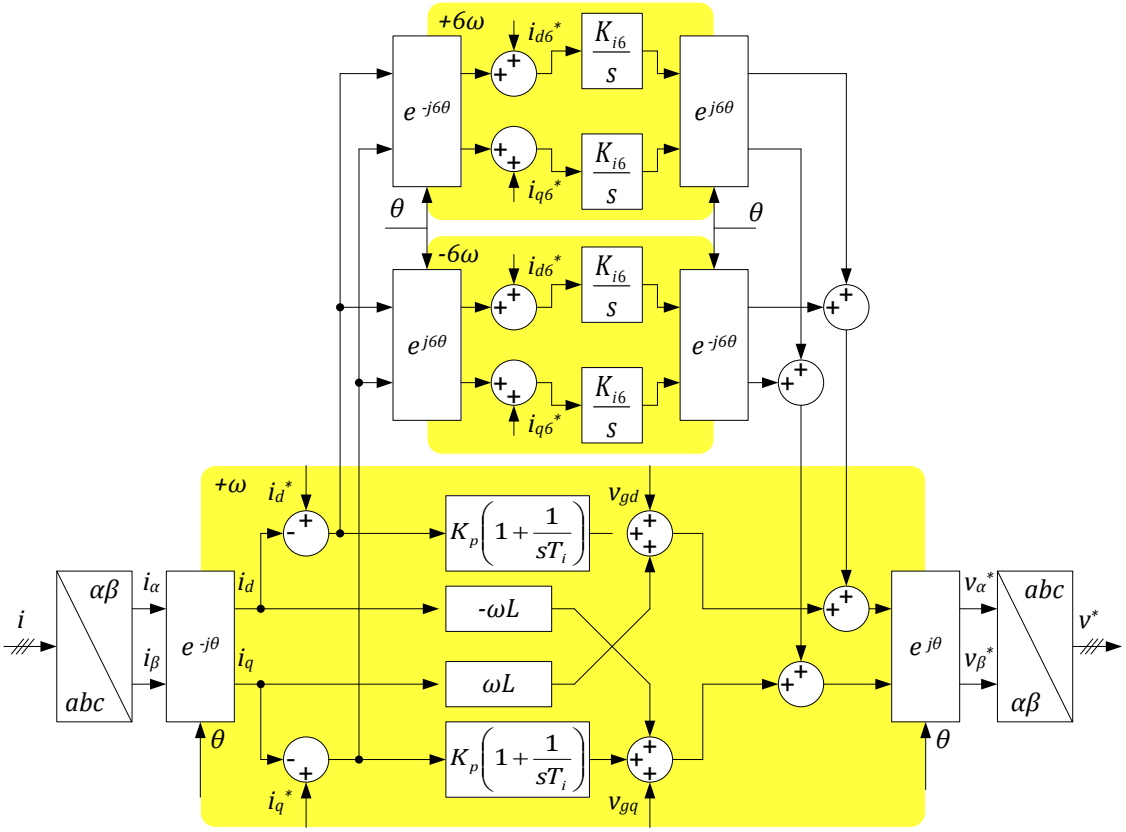

Figure 5.56 Double harmonic current control in two nested rotating frames.

Another possibility of implementing an equivalent solution in terms of implementation and computation burden is to introduce harmonic compensation directly in the main current controller synchronous reference frame [5.50]. It should be emphasized that it is not possible to use only one controller to compensate the 5^{th} and the 7^{th} harmonics because in synchronous reference frame of the fundamental controller even if both are 6^{th}-order harmonics, but in different sequences. The 5^{th} is the negative sequence 6^{th} harmonic (-6ω) in the synchronous reference frame and the 7^{th} is the positive sequence 6^{th} harmonic (6ω) in the synchronous reference frame. Double harmonic current control in two nested rotating frames is shown in Figure 5.56.

As an example, Figure 5.57 shows grid voltage $v_g(t)$, grid current $i_g(t)$ and grid-side converter voltage $v_c(t)$ within baseband harmonic frequency range during harmonic current compensation. The harmonic compensation is based on nested in synchronous reference frame, integral controllers for both positive and negative sequence 6^{th} harmonic component.

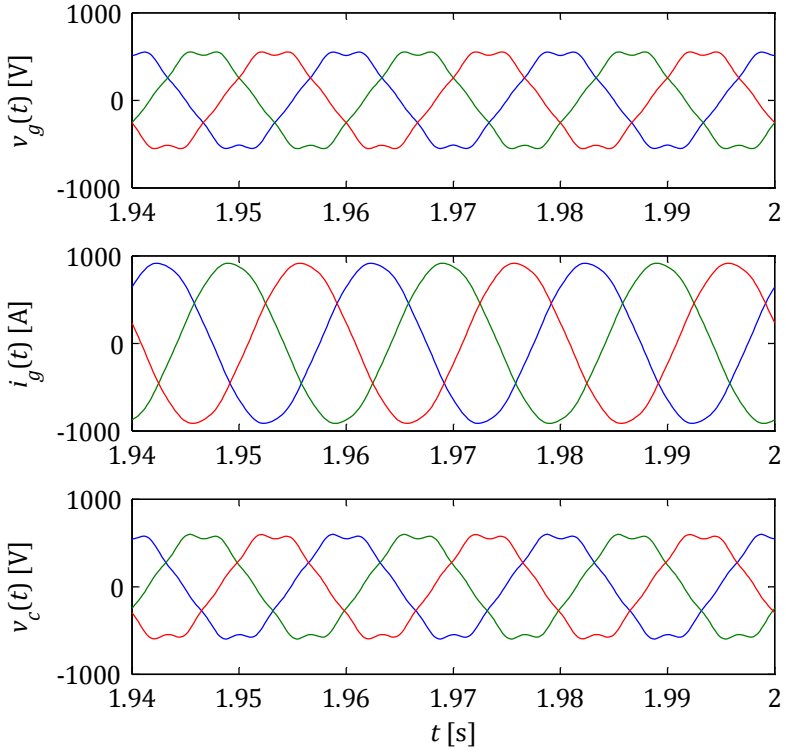

Figure 5.57 Grid voltage, grid current and grid-side converter voltage during harmonic current compensation.

During simulations it was decided to introduce external network distortions at high level. Both negative sequence 5^{th} harmonic and positive sequence 7^{th} harmonic voltages were considered. Significant harmonic distortions were applied in order to observe clearly the performance of harmonic controllers. Namely the 5^{th} harmonic distortion was $5\,\%$ of the fundamental component level and the 7^{th} was $4\,\%$ of the fundamental. Significant background distortion can be seen in Figure 5.57 ($v_g(t)$).

Figure 5.58 presents the 5^{th} harmonic current peak value before the harmonic compensation was activated and after the activation. Before the harmonic current was controlled by nested integral controllers in reference frames rotating with angular frequency of $\pm 6\omega_o$ significant distortion can be observed. In this case the current flow is mainly affected by external network voltage distortions. However when the harmonic compensation is turned on significant improvement can be seen in the 5^{th} harmonic current flow as well as current total harmonic distortions. Please note that except the 5^{th} harmonic also the 7^{th} is included in the background distortions. Of course one cannot change background distortions locally at the wind turbine level, therefore, in order to improve current harmonics additional voltage distortions at the AC terminals of the grid-side converter should be applied.

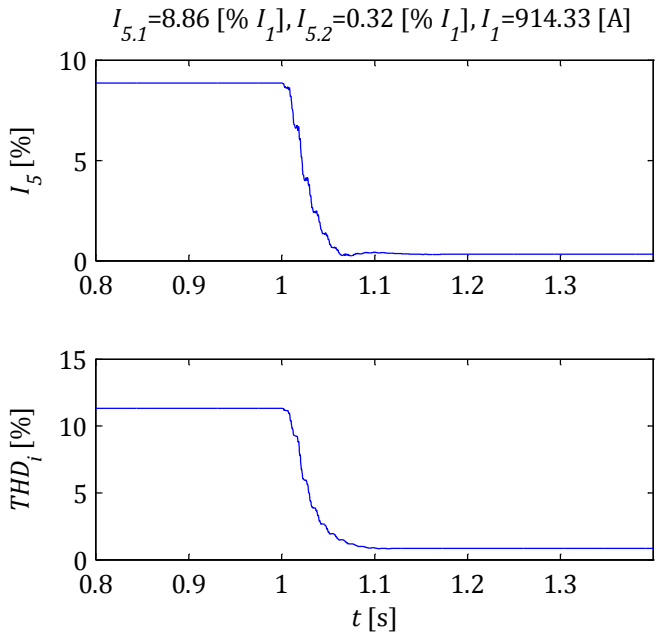

Figure 5.58 Harmonic current distortions before and after activation of harmonic compensation.

Thus obviously an increment of harmonic voltage distortion is present after the harmonic control is enabled as presented in Figure 5.59. The converter selective harmonic controller tracks changes in harmonic current and tries to keep the error as close as possible to zero. It is assumed that harmonic current reference is equal to zero as well.

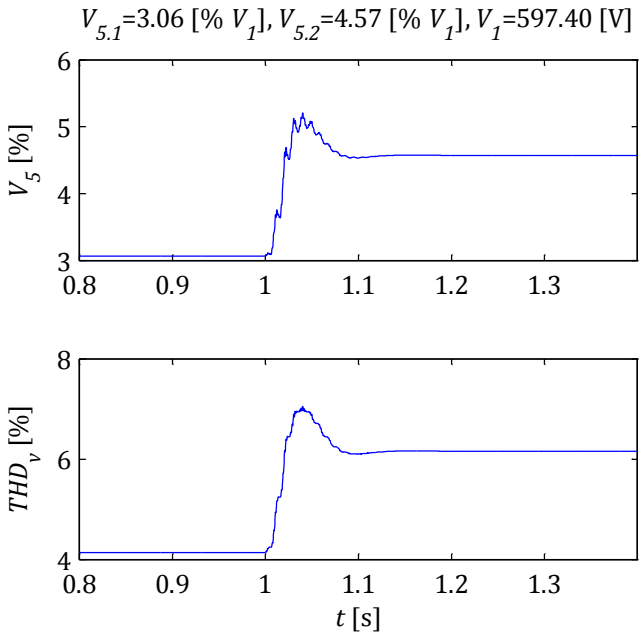

Figure 5.59 Harmonic voltage distortions before and after activation of harmonic compensation.

Based on waveforms presented in Figure 5.57 it can be seen that no harmonic current flow is present between converter terminals and the grid. From this perspective it can be said that the converter impedance is infinity (i.e. open circuit) for controlled

harmonic frequencies. This also will be presented later based on converter control frequency response which included harmonic compensation.

It was observed also based on computer simulations that the performance of different harmonic compensations provides the same results. An example of nested structure is put forward. Due to also this fact later in stability investigation all described harmonic compensation structures will be expressed in the same way in stationary reference frame. Also there was no significant difference if voltage feedforward of the converter was either enabled or not. However, some studies show how voltage feedforward and grid synchronization could affect harmonic compensation [5.50].

In the simulation voltage feed-forward component was taken into consideration in the controller which was measured at the LV side of the wind turbine transformer and afterwards filtered using low-order low-pass filters. In order to improve transient response of the controller, feedback decoupling was used and the controlled system (plant) inductance was needed to be assessed [5.11]. Specific to this control structure there was a necessity to detect the phase angle of the grid voltage by application of PLL in order to perform the transformation to synchronous reference frame. PLL was implemented using second-order generalized integrator quadrature signal generation (SOGI-QSG) and estimated frequency is also filtered [5.56]. It was shown that unfiltered phase signal θ used for orientation of the synchronous reference frame can also affect harmonic behaviour of the converter [5.50].

Resonant selective controller

In order to successfully compensate harmonics caused by the external network a resonant controller can be used. The resonant controller is a controller that achieves an infinite gain at a certain tuned frequency of interest (also called resonance frequency). Due to its selectivity it is characterized by almost no attenuation outside the tuned frequency. Thus, it can be used as a notch filter in order to compensate the harmonics in a very selective way. This technique has been successfully used in both single-phase grid-side converter and three-phase grid converter as reported in [5.54] and [5.50], where closed-loop harmonic control is introduced.

Instead of using two separated harmonic controllers in rotating (-5ω and 7ω) reference frame, or nested frames rotating at 6ω and -6ω in the main synchronous frame one resonant controller can be used as presented in Figure 5.60. One of the most important features of a resonant controller is that it is capable to track AC currents of different frequencies (i.e. resonant frequencies) of interest and sufficiently eliminate steady-state error of controlled variables [5.57]. The open-loop transfer function in s-domain of the controller presented in Figure 5.60 can be expressed in the following way

$$G_{OL}(s) = K_p + \frac{K_i}{s} + K_{th}\frac{s}{s^2 + (h\omega)^2} \qquad 5.8$$

where K_p is the proportional gain, K_i is the integral gain, K_{th} is the resonant gain for the h^{th} harmonic controller, and $h\omega$ is the angular resonant frequency of the h^{th} harmonic. The simplified transfer function from Eq. 5.8 is without taking into account such things as voltage feedforward, decoupling, elaboration delay of the computation device, pulse-width modulation delay due to asymmetrically regular sampled modulation, and additional filtering.

The use of resonant controllers changes the frequency response of the basic current controller by additional gain peaks at the harmonic frequencies. What is interesting to note that the dynamics of the controller in terms of bandwidth and stability margin these remains almost unaltered (i.e. in theory selective harmonic compensator bandwidth is very narrow) which will be shown later. However in real-life applications application of various notch filters can cause some stability problems.

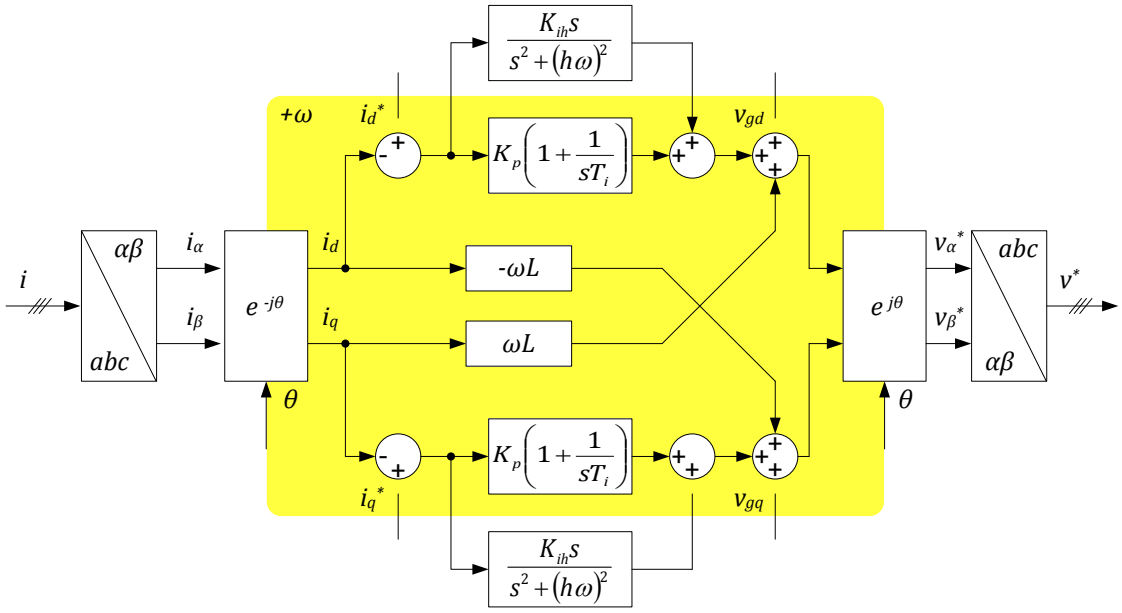

Figure 5.60 Harmonic compensation based on resonant controller in synchronous reference frame.

Considering that analysed controllers have no cross-coupling between d and q components, the double harmonic current control in two nested rotating frames can be expressed in stationary reference frame according to the following equation derived in [5.58]

$$G_{\alpha\beta}(s) = \frac{1}{2}\begin{bmatrix} G_{dq}(s+j\omega_o)+G_{dq}(s-j\omega_o) & jG_{dq}(s+j\omega_o)-jG_{dq}(s-j\omega_o) \\ -jG_{dq}(s+j\omega_o)+jG_{dq}(s-j\omega_o) & G_{dq}(s+j\omega_o)+G_{dq}(s-j\omega_o) \end{bmatrix} \quad 5.9$$

In this case (i.e. no cross-coupling) only diagonal components of Eq. 5.10 will not be equal to 0 in stationary reference frame. The integral controller in nested rotating reference frame can be expressed in stationary reference frame as follows

$$
\begin{aligned}
G_{\alpha\beta}(s) &= \frac{1}{2}\left[G_{dq}(s+jh\omega_o) + G_{dq}(s-jh\omega_o)\right] \\
&= \frac{1}{2}\left[\frac{K_{ih}}{s+jh\omega_o} + \frac{K_{ih}}{s-jh\omega_o}\right] \\
&= \frac{1}{2}\left[\frac{K_{ih}(s-jh\omega_o) + K_{ih}(s+jh\omega_o)}{(s+jh\omega_o)(s-jh\omega_o)}\right] \\
&= \frac{K_{ih}s}{s^2 + (h\omega_o)^2}
\end{aligned}
\qquad 5.10
$$

Knowing that nested rotating reference frame is with angular frequency equal to $6\omega_o$ [5.50]

$$
G_{\alpha\beta}(s) = \frac{K_{ih}s}{s^2 + (6\omega_o)^2} \qquad 5.11
$$

It means that theoretically harmonic compensation in both rotating and stationary reference frames are equal. Of course in rotating reference frame it is possible to observe additional oscillations affected by presence of other harmonic components. Therefore additional filtering is needed to improve compensation performance [5.55]. Typically low-pass filters with cut-off frequency around 10 Hz are used in practical applications for 5^{th} and 7^{th} harmonic compensation. Assuming that resonant controllers have sufficiently narrow bandwidth such additional filtering is not needed.

It is commonly accepted that power quality from harmonic perspective is investigated during steady-state operation. That is also why harmonic compensators are mainly based on integral control in rotating reference frame and resonant control in stationary reference frame. Harmonic controller dynamics and response are not the most crucial features. Such things as decoupling inductance in rotating reference frame for higher frequencies is not taken into consideration because of difficulties in estimation of the value (i.e. plant frequency response can change especially in large offshore wind farms) and there is no need of fast controller response. Even in IEC 61400-21 it is mentioned that harmonics are considered harmless as long as the duration is limited to a short period of time. Hence, the standard does not require specification of short-duration harmonics caused by wind turbine start-up or other switching operations.

5.2.3 WIND FARM STABILITY EVALUATION

Since, as it was shown, different wind farms exhibit different frequency characteristics as well as different control methods can behave in various ways there is a need to investigate more broadly stability for particular study cases. A typical control of the grid-side converter is shown in Figure 5.53. As it was described above that different modification in the control (e.g. voltage feedforward, decoupling, harmonic compensation) can affect changes in the frequency response of the converter and its interaction with the wind farm to which is connected [5.11].

In general such a controller is implemented digitally and in steady state the reference (i_d^*, i_q^*) and the feedback (i_d, i_q) signals are DC quantities which are controlled by the PI controller in order to achieve the steady-state error equal to zero. Such control scenario also includes a voltage feedforward which is typically in wind turbines taken from the LV side of the wind turbine transformer and contributes in the modulator output voltage.

Normally the control method described above is successfully applied in the industry. Please note that in case of large offshore wind farms many resonance scenarios are possible. They are mainly caused due to widespread internal cable collector systems and other capacitances introduced by capacitor banks or long HVAC export cables. This provides significant gain for higher frequencies of the plant due to possible series resonances.

Earlier it was also shown that even small changes in wind farm internal structure due to varying number of wind turbines in operation can significantly affect possible resonance frequencies and their gains. That is why it is crucial not only to investigate stability for different wind farms but even variation in their internal structures.

5.2.3.1 STABILITY INDICES

Consider a single-loop system with unity feedback gain and forward transfer function $D(s)G(s)$ as shown in Figure 5.61.

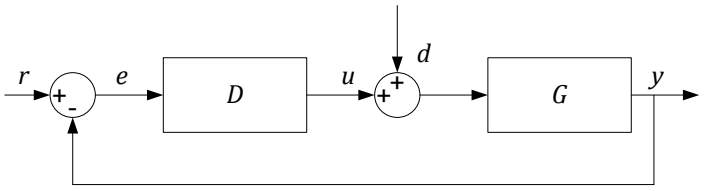

Figure 5.61 Unity feedback system.

Gain and phase margins

The Nyquist plot shows the number of encirclements and thus the stability of the closed-loop system. Gain and phase margins are defined to provide a two-point measure of how close the Nyquist plot is to encircling the -1 point. The gain margin (GM) is the factor by which the gain can be increased before causing the system to be unstable, and is the inverse of the magnitude of $D(s)G(s)$ when its phase is 180°. The phase margin (PM) is the difference between -180° and the phase of $D(s)G(s)$ when its amplitude is 1. The PM is a measure of how much additional phase lag or time delay can be tolerated in the loop before instability results [5.59], [5.60], [5.61].

Vector gain margin

The gain and phase margins give useful information about the relative stability of nominal systems but can be misleading as guides to the design of realistic control

problems [5.59]. A more accurate margin can be given in terms of the sensitivity function. For the unity feedback system drawn in Figure 5.61 the error is given by

$$E(j\omega) = \frac{1}{1+DG} R \triangleq S(j\omega)R \tag{5.12}$$

where the sensitivity function S is defined [5.62]. In addition to being a factor of the system error, the sensitivity function is also the reciprocal of the distance of the Nyquist curve of DG from the critical point -1 which can be directly used for stability assessment purposes. A large value for S indicates a Nyquist plot that comes close to the point of instability. The maximum value of $|S|$ is often a more accurate measure of stability margin than either gain or phase margin alone.

It can be also seen that the maximum value of the sensitivity function can be associated with different frequency than indicated by either gain margin or phase margin (see Figure 5.62). This becomes a crucial issue in tuning the control of grid-side converter as well as in the analysis of possible resonances in the external network. Knowing that the frequency response of the plant can also be strongly affected by wind farm internal cable network and export cable, this analysis approach can be also used at the wind farm design stage.

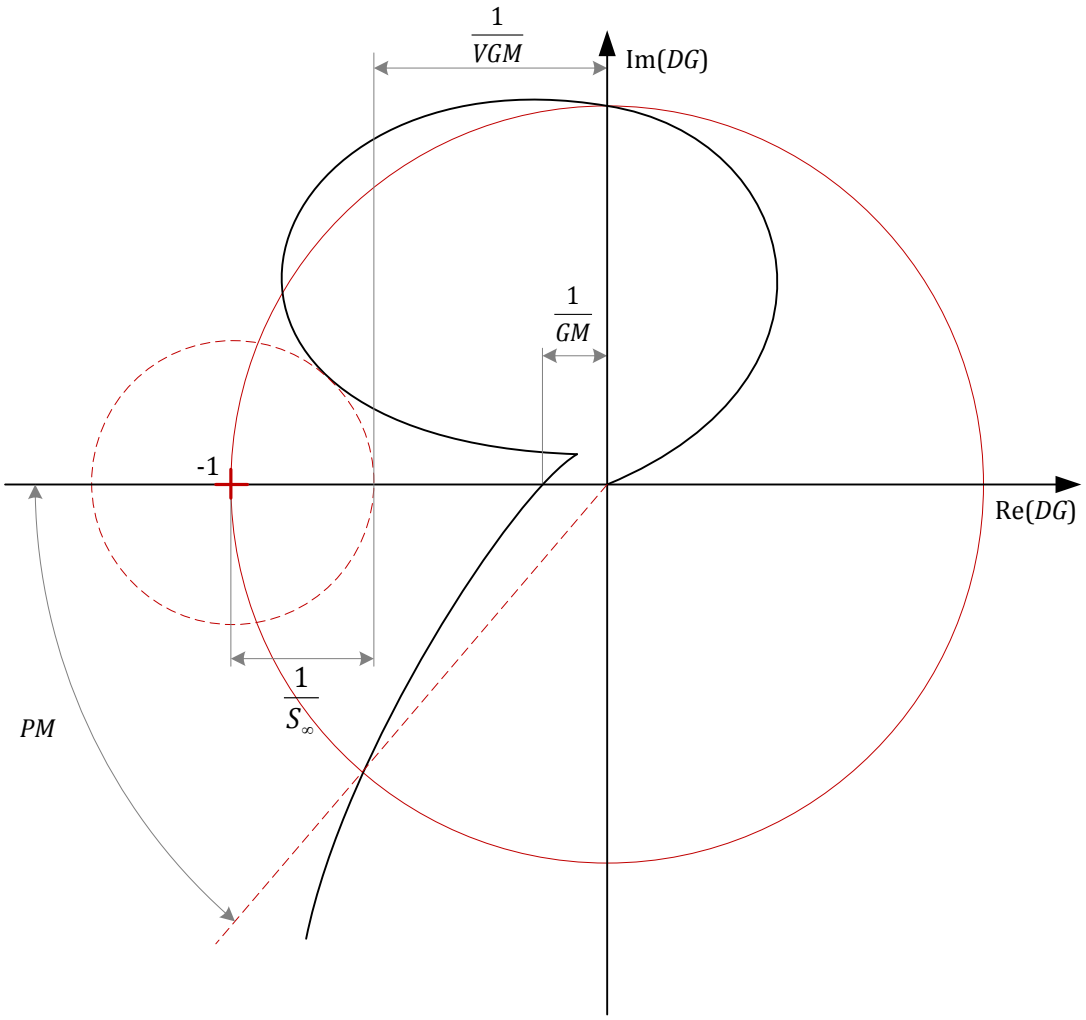

Figure 5.62 Nyquist plot showing stability margins.

In Figure 5.62 a Nyquist plot is sketched and it can be easily seen that the system is actually much closer to instability than either gain or phase margin would indicate. The vector gain margin (VGM) [5.59] is defined as the gain margin in the direction of the worst possible phase and can provide better overview about system stability. It can be said that the vector gain margin is a good supplement of commonly used gain margin because if the Nyquist plot comes closest to -1 on the negative real axis, then the vector gain margin is the same as the standard gain margin. The VGM is defined to provide a one-point measure of how close the Nyquist plot is to encircling the -1 (i.e. the system is on stability boundary) point and is a very good supplement for stability analysis based on PM and GM.

The vector gain margin can be easily derived from geometrical relations. The distance of the closest point on the Nyquist curve from -1 is

$$\frac{1}{S_\infty} = 1 + DG$$

where $S_\infty = \max_\omega |S|$. According to geometric relations presented in Figure 5.62 the vector gain margin can be expressed in the following way

$$\frac{1}{VGM} + \frac{1}{S_\infty} = 1$$

therefore

$$VGM = \frac{1}{1 - \frac{1}{S_\infty}} = \frac{S_\infty}{S_\infty - 1} \qquad 5.13$$

5.2.3.2 GRID CONVERTER FREQUENCY DOMAIN MODEL

In order to investigate stability in continuous frequency domain (i.e. s-domain) there is a necessity to precisely represent both the converter current control as well as electrical system in frequency domain.

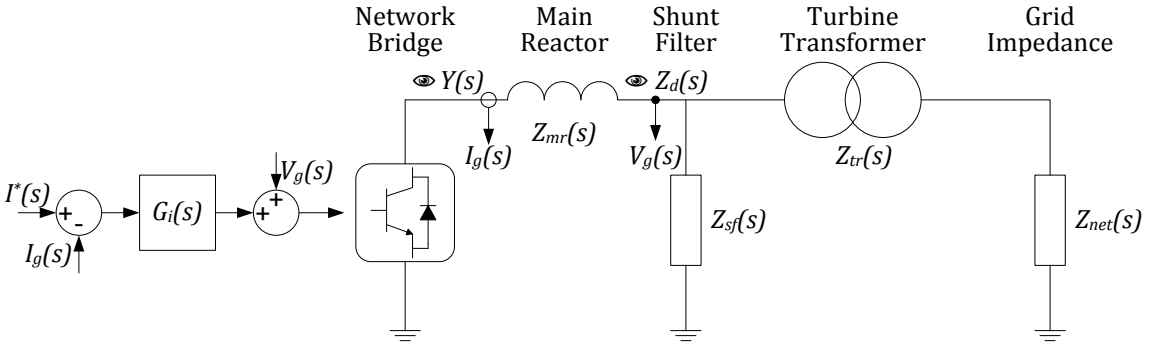

Figure 5.63 Single line diagram showing the admittance seen from AC terminals and the impedance seen from voltage measurement point as well as simplification of the control method.

Disturbance rejection

Feedforward control is always used along with feedback control because a feedback control system is required to track setpoint changes and to suppress disturbances that are always present [5.63]. Combined voltage feedforward control plus current feedback control can significantly improve performance over simple current feedback control whenever there is a major disturbance (i.e. sudden grid voltage changes) that can be measured before it affects the current flowing in the plant. A sudden increase or decrease in the grid voltage will directly and proportionally change the voltage reference signal provided to the modulator.

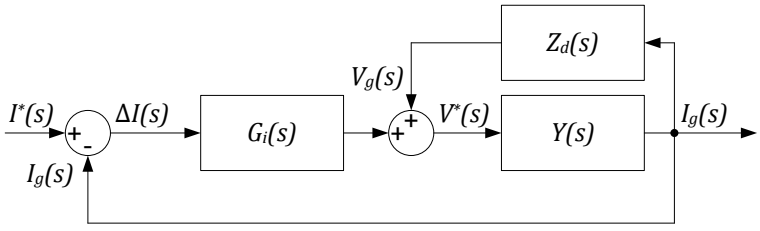

Figure 5.64 Grid-side converter current control with disturbance rejection.

Any deviation of the line voltage waveform from the ideal sine waveform can be considered as a disturbance d acting on process as shown in Figure 5.61 [5.64]. For the particular grid-side converter presented in Figure 5.63 the control of the wind farm (i.e. plant) taking into consideration voltage feedforward is presented in Figure 5.64. It can be seen that the overall open loop transfer function of the system can be expressed in the following way

$$G_{ol}(s) = G_i(s)\frac{Y(s)}{1 - Y(s)Z_d(s)} \tag{5.14}$$

where G_i is the transfer function of the whole current control including possible harmonic compensation, filtering, and decoupling. Y and Z_d are defined as follows

$$Z_d(s) = \big(Z_{tr}(s) + Z_{net}(s)\big)\big\|Z_{sf}(s) \tag{5.15}$$

$$Y(s) = \frac{1}{Z_{mr}(s) + Z_d(s)} \tag{5.16}$$

In this particular case the impedance Z_{net} also contains wind farm internal cable network, park transformer, HV cable, possible capacitor banks and shunt reactors as well as external network impedance. Based on Karnice Wind Farm this impedance was derived earlier.

Feedback decoupling

In the synchronous reference frame there is a cross-coupling of the plant between d and q components. In order to improve tracing performance of the PI current controller additional decoupling in the control frame has to be introduced as in Figure 5.53. Different studies regarding this issue were performed in different application of industrial power electronics [5.38], [5.39].

Please note that decoupling does not affect the frequency response of the controller in stationary reference frame. It was assumed that the description in frequency domain of the controller and the plant will be in stationary reference frame. As long as there is no coupling in the control method the transfer function of the system in stationary reference frame is the same as in natural reference frame and can be calculated from rotating reference frame according to Eq. 5.20.

It was observed in [5.65] that the feedback method shows somehow better performance regarding the oscillation, since there are no current oscillations in this method, which is not the case with the feedforward method. In order to successfully apply decoupling in synchronous reference frame there is a need to evaluate the inductance L of the plant.

Of course in many cases exact calculation of L can be troublesome due to the fact that it is not exactly known at the design stage to which system the wind turbine will be connected. This becomes even more problematic in case of large offshore wind farms which can introduce resonance at low frequencies. That is also why stability assessment

for a particular study case can show some limitations in the control method and allow tuning the system (i.e. either the wind farm structure or the controller parameters).

Other factors

In real-life existing grid-side converters control structure will operate in a discontinuous environment. To change measured signals (i.e. currents and voltages) into digital form an analog to digital converter (A/D) is used and the conversion always takes non-zero time. Therefore there is a necessity to take into account sampling period T_s and this is done by usage of sample and hold (S/H). Additionally the statistical delay of pulse-width modulation $T_{PWM} = 0.5T_s$ should be taken into consideration. The block diagram of the analysed converter including sampling and pulse-width modulation delay is presented in Figure 5.65.

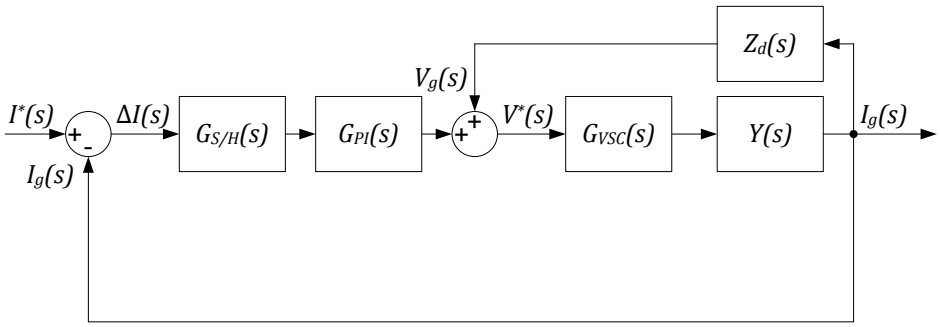

Figure 5.65 Block diagram of the grid-side converter taking into consideration the most important factors affecting frequency response of the system.

The A/D converter can be approximated by the simplest Padé first-order approximation (i.e. first-order transfer function) [5.59]. It is worth emphasizing that the delay associated with the hold has a major impact in the digital implementation. In general a delay in any feedback system degrades the stability and damping of the system. The same approach is taken in case of pulse-width modulation delay of the voltage source converter. Additionally, considering non-ideal switches, the dead-time of the converter can be included.

$$G_{S/H}(s) = \frac{1}{sT_s + 1} \tag{5.17}$$

$$G_{VSC}(s) = \frac{K_c e^{-s\tau_0}}{sT_{PWM} + 1} \tag{5.18}$$

where K_c is the converter gain, T_s is the sampling period of the analog to digital converter, T_{PWM} is the delay associated with pulse-width modulation and τ_0 is the dead-time [5.38].

Sometimes both delays (i.e. T_s and T_{PWM}) can be gathered together and expressed as one first-order transfer function. This can be done if one would consider steady state operation without any disturbances from the network. Considering wind farms stability the approach from Figure 5.65 is closer to reality.

The whole analysed system open-loop transfer function can be expressed in the following way

$$G_{ol}(s) = G_{S/H}G_{PI}\frac{G_{VSC}Y}{1-G_{VSC}YZ_d}\left(\frac{1-G_{VSC}YZ_d}{1-G_{VSC}YZ_d}\right)^{-1} = \frac{G_{S/H}G_{PI}G_{VSC}Y}{1-G_{VSC}YZ_d} \quad 5.19$$

Stationary frame representation

Many grid-side converter regulators analysed in this chapter, use dq reference frame transformations to convert three-phase electrical network AC quantities into DC quantities. The dq transformation essentially performs frequency shifts of the system signals. [5.58], [5.66]. This frequency shift can provide misleading interpretation of the controller in the rotating reference frame and its interaction with the external system harmonic impedance.

That is why it is better to express the regulator either in natural reference frame or stationary reference frame. Of course it has to be emphasized that the analysis considers linear time-invariant transformations between abc and dq reference frames as well as balanced natural reference frame (i.e. line currents and phase voltages sum to zero).

Assuming that the controller transfer function in the rotating reference frame is $G_{DC}(s)$ it is possible to express the controller in synchronous reference frame according to [5.58] in the following way

$$G_{AC}(s) = \frac{1}{2}[G_{DC}(s+j\omega) + G_{DC}(s-j\omega)] \quad 5.20$$

Earlier it was shown how to calculate stationary reference frame representation of PI controller operating in synchronous reference frame. It was shown that, in theory, PI controller operating in rotating reference frame is equal to PR controller operating in stationary reference frame. Of course except the controller the grid-side converter frequency domain model contains different filters (e.g. notch filters, low-pass filter) which also should be represented in stationary reference frame. Delays such as network bridge delay, sample and hold delay are already in stationary reference frame.

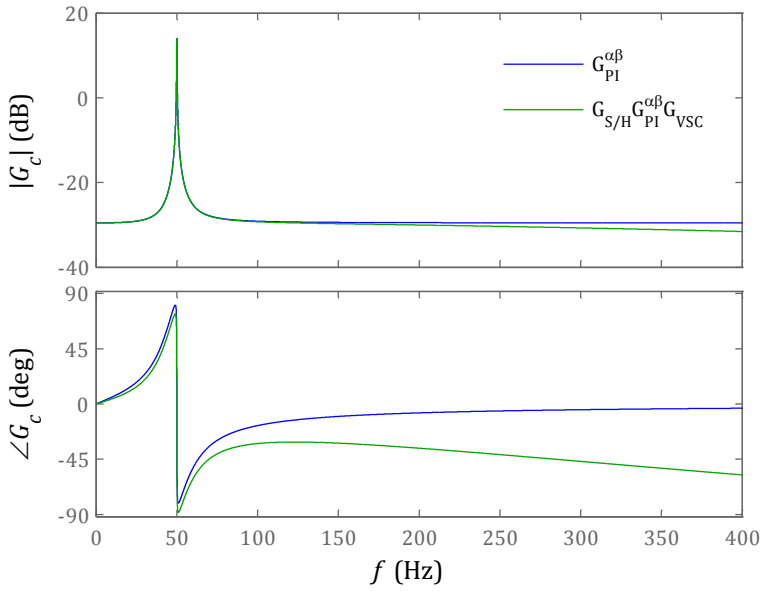

Figure 5.66 Proportional-integral controller frequency characteristic represented in stationary reference frame.

Figure 5.66 shows how additional delays in the control chain caused by sample and hold as well as voltage-source converter delays. Please note that the proportional-integral controller in the Bode plot is already represented in stationary reference frame. This shows that the theoretical infinity gain is associated with the fundamental frequency f_o instead of DC value, which is in synchronous reference frame.

In order to represent the whole frequency domain model in stationary reference frame all additional transfer functions also have to be transformed by application of Eq. 5.20. The simple delay which characterize both sample and hold and voltage source converter delays is already expressed in the stationary reference frame. However, different filters can be applied in the rotating reference frame in order to attenuate oscillations caused by other harmonic components. This can be a notch filter tuned for the 2^{nd} harmonic to attenuate negative sequence fundamental component in the positive sequence synchronous reference frame and vice versa. Also additional low-pass filters are used in case of selective harmonic compensation carried out in rotating reference frame with angular frequency equal to harmonic of interest.

A typical notch filter can be represented in the following way

$$G_N(s) = \frac{s^2 + \frac{\omega_N}{Q_n}s + \omega_N^2}{s^2 + \frac{\omega_N}{Q_d}s + \omega_N^2} \qquad 5.21$$

where ω_N is the tuned angular frequency in [rad/s] and parameters Q_n, Q_d can be adjusted depending on application. Please note that in case of the notch filters used in double synchronous reference frame the tuned frequency ω_N is equal to $2\omega_o$.

It is worth to emphasize that the notch filter affects the direct chain in the control loop which can affect stability constraints. Appropriate adjustment of Q_n and Q_d parameters can make the notch filter either more selective or more band-stop. For selective notch filters the angular frequency ω_N should be adaptive depending on power system frequency changes while wide stopband would affect the settling time of the system [5.51].

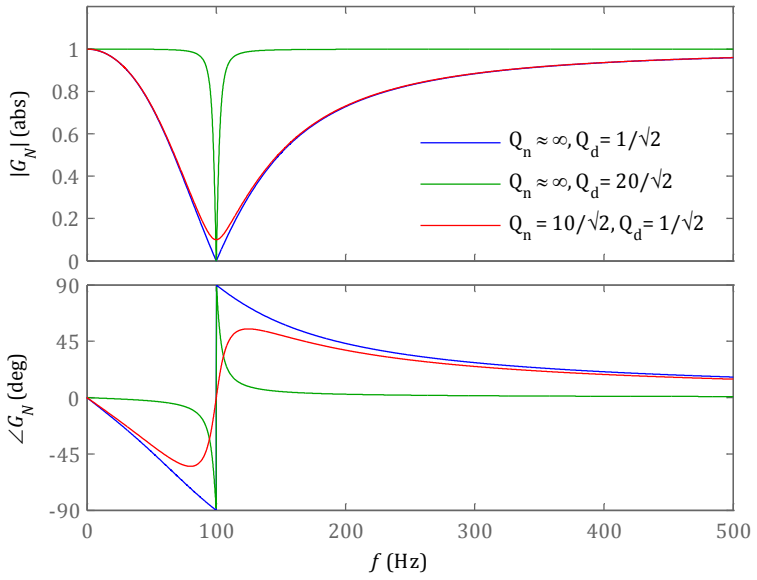

Figure 5.67 Different notch filters depending on parameters Q_n and Q_d ($\omega_N = 2\omega_o$).

Such notch filter in stationary reference frame can be expressed by using Eq. 5.20

$$G_N^{\alpha\beta}(s) = Q_d \begin{bmatrix} s^4 Q_n Q_d + s^3(Q_n + Q_d)\omega_N \\ +s^2(2Q_n Q_d \omega_o^2 + 2Q_n Q_d \omega_N^2 + \omega_N^2) \\ +s\left((Q_n + Q_d)\omega_o^2 \omega_N + (Q_n + Q_d)\omega_N^3\right) \\ +(Q_n Q_d \omega_o^4 + Q_n Q_d \omega_N^4 + \omega_o^2 \omega_N^2 - 2Q_n Q_d \omega_o^2 \omega_N^2) \end{bmatrix} \times Q_n \begin{bmatrix} s^4 Q_d^2 + s^3 2Q_d \omega_N \\ +s^2(2Q_d^2 \omega_o^2 + 2Q_d^2 \omega_N^2 + \omega_N^2) \\ +s(2Q_d \omega_o^2 \omega_N + 2Q_d \omega_N^3) \\ +(Q_d^2 \omega_o^4 + Q_d^2 \omega_N^4 + \omega_o^2 \omega_N^2 - 2Q_d^2 \omega_o^2 \omega_N^2) \end{bmatrix}^{-1} \quad 5.22$$

And knowing that in case of double synchronous reference frame $\omega_N = 2\omega_o$

$$G_N^{\alpha\beta}(s) = Q_d \begin{bmatrix} s^4 Q_n Q_d + s^3 2(Q_n + Q_d)\omega_o \\ +s^2(2Q_n Q_d \omega_o^2 + 8Q_n Q_d \omega_o^2 + 4\omega_o^2) \\ +s(2(Q_n + Q_d)\omega_o^3 + 8(Q_n + Q_d)\omega_o^3) \\ +(Q_n Q_d \omega_o^4 + 16Q_n Q_d \omega_o^4 + 4\omega_o^4 - 8Q_n Q_d \omega_o^4) \end{bmatrix} \times Q_n \begin{bmatrix} s^4 Q_d^2 + s^3 4Q_d \omega_o \\ +s^2(2Q_d^2 \omega_o^2 + 8Q_d^2 \omega_o^2 + 4\omega_o^2) \\ +s(4Q_d \omega_o^3 + 16Q_d \omega_o^3) \\ +(Q_d^2 \omega_o^4 + 16Q_d^2 \omega_o^4 + 4\omega_o^4 - 8Q_d^2 \omega_o^4) \end{bmatrix}^{-1} \quad 5.23$$

Figure 5.69 shows how the frequency response of current controller represented in stationary reference frame can be affected by a notch filter which is used in synchronous reference frame. Please note that the filter was also represented in stationary reference frame. Representation in stationary (or natural) reference frame of the grid-side converter control is convenient if analysed plant frequency response exhibits significant variation within relatively low and narrow frequency range.

First order ($b_i = 0$) and second order low-pass filters [5.67] used in rotating reference frame

$$G_{LP}(s) = \frac{A_0}{1 + a_i s + b_i s^2} \quad 5.24$$

can be expressed in stationary reference frame in the following way (assuming unity gain $A_0 = 1$)

$$\begin{aligned} G_{LP}^{\alpha\beta}(s) &= \frac{1}{2}\left[G_{LP}^{dq}(s + j\omega_o) + G_{LP}^{dq}(s - j\omega_o)\right] \\ &= \frac{1}{2}\left[\frac{1}{b_i(s + j\omega_o)^2 + a_i(s + j\omega_o) + 1} + \frac{1}{b_i(s - j\omega_o)^2 + a_i(s - j\omega_o) + 1}\right] \\ &= \left(1 + a_i s + b_i(s^2 - \omega_o^2)\right) \times \begin{pmatrix} s^4 b_i^2 + 2s^3 a_i b_i \\ +s^2(a_i^2 + 2b_i^2 \omega_o^2 + 2b_i) + \\ s(2a_i b_i \omega_o^2 + 2a_i) \\ -2b_i \omega_o^2 + a_i^2 \omega_o^2 + b_i^2 \omega_o^4 + 1 \end{pmatrix}^{-1} \end{aligned} \quad 5.25$$

Assuming that $b_i = 0$ the first-order low-pass filter can be expressed in stationary reference frame as

$$
\begin{aligned}
G_{LP}^{\alpha\beta}(s)\Big|_{b_i=0} &= \frac{1}{2}\left[G_{LP}^{dq}(s+j\omega_o)+G_{LP}^{dq}(s-j\omega_o)\right]\Big|_{b_i=0} \\
&= \frac{1}{2}\left[\frac{1}{a_i(s+j\omega_o)+1}+\frac{1}{a_i(s-j\omega_o)+1}\right] \\
&= \frac{a_i s+1}{a_i^2(s^2+\omega_o^2)+2a_i s+1}
\end{aligned}
\qquad 5.26
$$

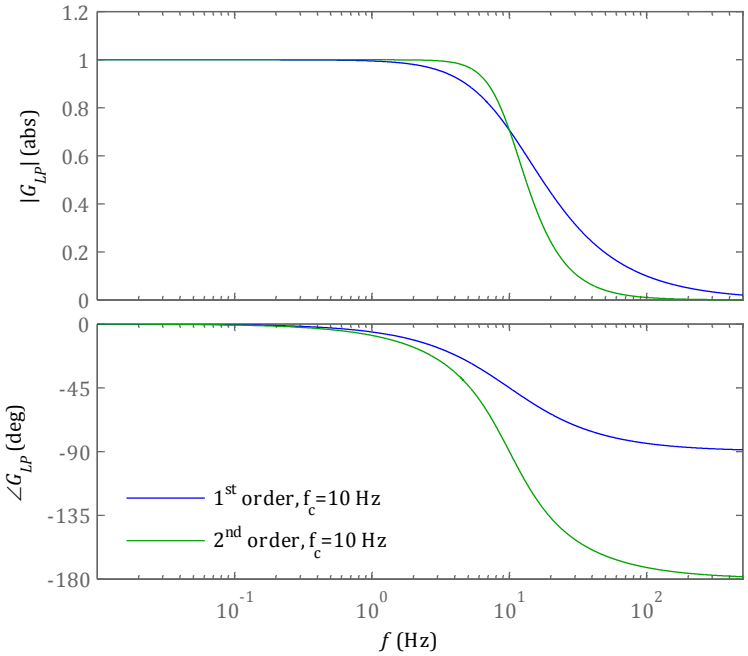

Figure 5.68 Typical low-pass filters to attenuate oscillations during harmonic compensation in rotating reference frame.

Different harmonic compensation scenarios were shown earlier. Both based on resonant controllers and integral controllers were presented and briefly explained. It was presented earlier that resonant controller with natural angular frequency equal to $6\omega_o$ operating in synchronous reference frame is equal to nested integral controller in rotating reference frame with angular frequency $\pm 6\omega_o$. It was also explained that such harmonic control scenarios are also theoretically equal to harmonic compensation from stationary reference frame using integral controllers operating in rotating reference frames with angular frequencies $-5\omega_o$ and $7\omega_o$.

It is worth emphasizing that integral controllers performance can be affected by additional oscillations in rotating reference frame. It was mentioned and also considered in [5.55] that possible low-pass filter (typical low-pass filter Bode plot is shown in Figure 5.68) application can solve this problem. However, this affects the grid-side converter frequency response which also might be important to take into consideration is stability studies.

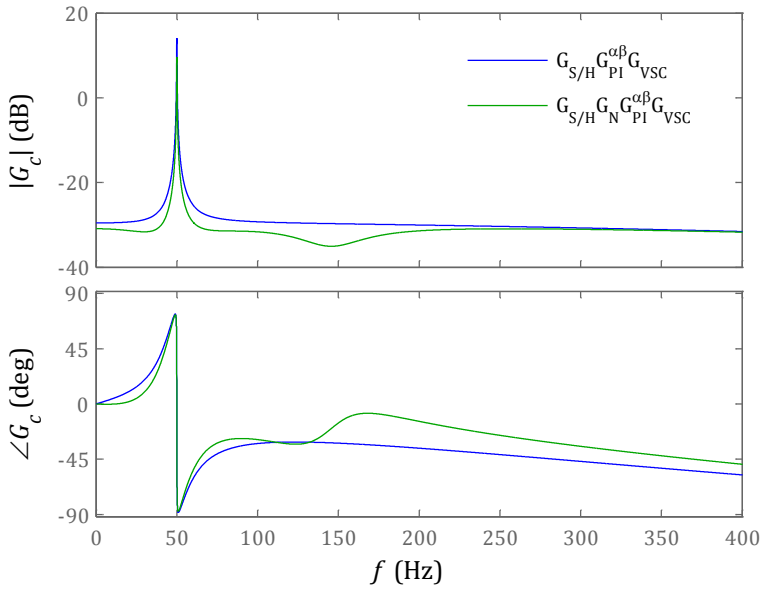

Figure 5.69 Current controller frequency response affected by application of a non-ideal notch filter.

It was described earlier that both nested controllers used in rotating reference frame with frequency of $6\omega_o$ and resonant controllers used in synchronous reference frame are in theory identically described in synchronous reference frame. Both controllers in synchronous reference frame can be described as in Eq. 5.11. In order to represent this harmonic controller in stationary reference frame Eq. 5.9 can be used. As mentioned previously Eq. 5.9 can be simplified to Eq. 5.20 with assumption that there is no cross-coupling in the control structure.

The harmonic compensator in stationary reference frame is derived in the following way

$$\begin{aligned} G_{PR}^{\alpha\beta}(s) &= \frac{1}{2}\left[G_{PR}^{dq}(s+j\omega_o)+G_{PR}^{dq}(s-j\omega_o)\right]\Big|_{b_i=0} \\ &= \frac{1}{2}\left[\frac{K_{ih}(s+j\omega_o)}{(s+j\omega_o)^2+{\omega_h}^2}+\frac{K_{ih}(s-j\omega_o)}{(s-j\omega_o)^2+{\omega_h}^2}\right] \\ &= K_{ih}\frac{s^3+s(\omega_h^2+\omega_o^2)}{s^4+2s^2(\omega_h^2+\omega_o^2)-2\omega_h^2\omega_o^2+\omega_h^4} \end{aligned} \tag{5.27}$$

Knowing that in this particular case $\omega_h = 6\omega_o$

$$G_{PR}^{\alpha\beta}(s) = K_{ih}\frac{s^3+37\omega_o^2}{s^4+74s^2\omega_o^2+1225\omega_o^4} \tag{5.28}$$

It is worth emphasizing that in real-life applications a non-ideal integrator can be used, as presented in [5.52]. The transfer function of such non-ideal integral controller used in rotating reference frame with angular frequency ω is as follows [5.68]

$$G_I^{dq}(s) = \frac{K_i}{1 + \frac{s}{\omega_c}} \tag{5.29}$$

where K_i is the controller gain and $\omega_c \ll \omega$ is the controller cut-off frequency. Based on Eq. 5.20 the controller can be expressed in stationary reference frame

$$G_I^{\alpha\beta}(s) = K_i \frac{s\omega_s + \omega_c^2}{s^2 + 2\omega_c s + \omega_c^2 + \omega} \tag{5.30}$$

Figure 5.70 shows how the grid-side converter controller frequency response is changed if selective harmonic compensation is added. It can be seen that the 5^{th} and the 7^{th} harmonic current is controlled. It should be emphasized that for non-ideal current controllers (either integral or resonant) it is not possible to obtain infinite gain for the controlled frequency. In that case the gain K_i starts to play a significant role. Unfortunately the non-ideal controllers do not roll-off as fast as ideal and therefore some stability problems may occur for relatively high gains. In that case there will be always a trade-off between high gain and good noise (harmonic) rejection. In Figure 5.70, due to the notch filter of $2\omega_o$ frequency in the main control chain, the noise rejection is much more important. The resonance peaks for the notch filter ($2\omega_o$) applied in synchronous reference frame (ω_o) and represented in stationary reference frame are equal to $2\omega_o \pm \omega_o$. And therefore it is not surprising to see the third harmonic component in the controller step response. Attenuation of such oscillations can be done at the cost of the gain of fundamental frequency controller.

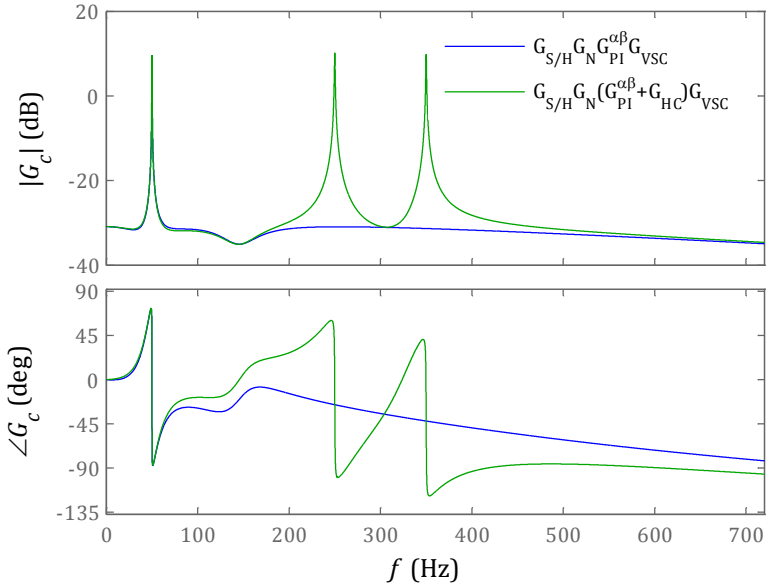

Figure 5.70 Frequency response of current controller including non-ideal notch filter and non-ideal harmonic compensators.

5.2.3.3 STABILITY ASSESSMENT

As it was presented, grid-side converter control tuning is not straight forward task and even if all design criteria (e.g. overshoot, settling time) are met, it is still not sure that this particular control can be successfully applied in any system [5.69].

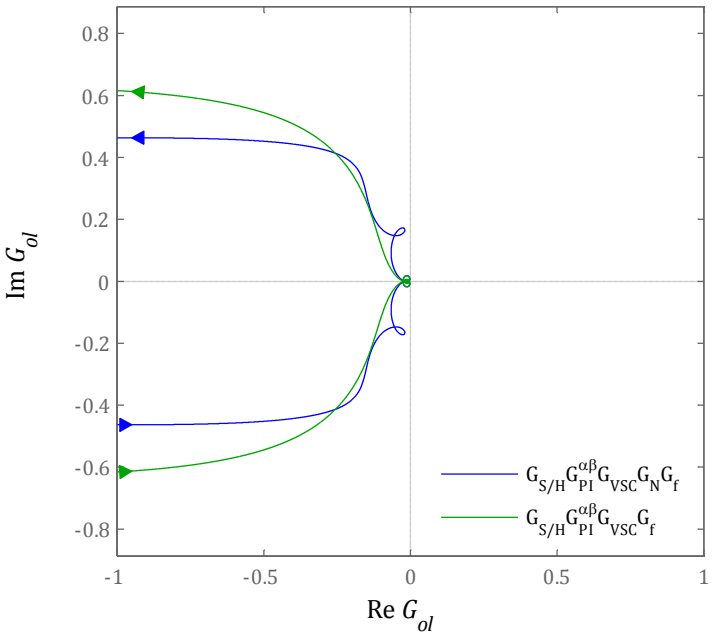

Figure 5.71 Nyquist plot of open loop system with and without notch filter in the main control chain.

Figure 5.71 presents how the notch filter affects the overall stability of the system in the Nyquist plot. Please note that the notch filter used in both positive and negative sequence synchronous reference frame is tuned for low frequencies. Thus only low frequency part of the Nyquist plot is changed.

It is also common practice to use different types of notch filters in the main control chain [5.69], [5.11] in order to improve noise (harmonic) rejection of the control system for higher frequencies. One of the good examples is to attenuate the effect of converter filter resonance [5.69]. The resonance poles of the filter can be compensated by application of appropriately tuned notch filter. Another practice of using notch filters is the compensation of resonant poles of the plant caused by significant capacitance in the system (e.g. capacitor banks, long HVAC cables) [5.11].

The effect of notch filter in the main control chain as well as low-frequency resonances in the plant will be investigated based on real-life existing systems. Once again Karnice onshore wind farm and Horns Rev II offshore wind farm are taken closely into consideration. Earlier it was presented how different modelling (i.e. passive components models, aggregation techniques) can affect the frequency domain representation of the system. Now it will be shown how control techniques can interact with real-life systems.

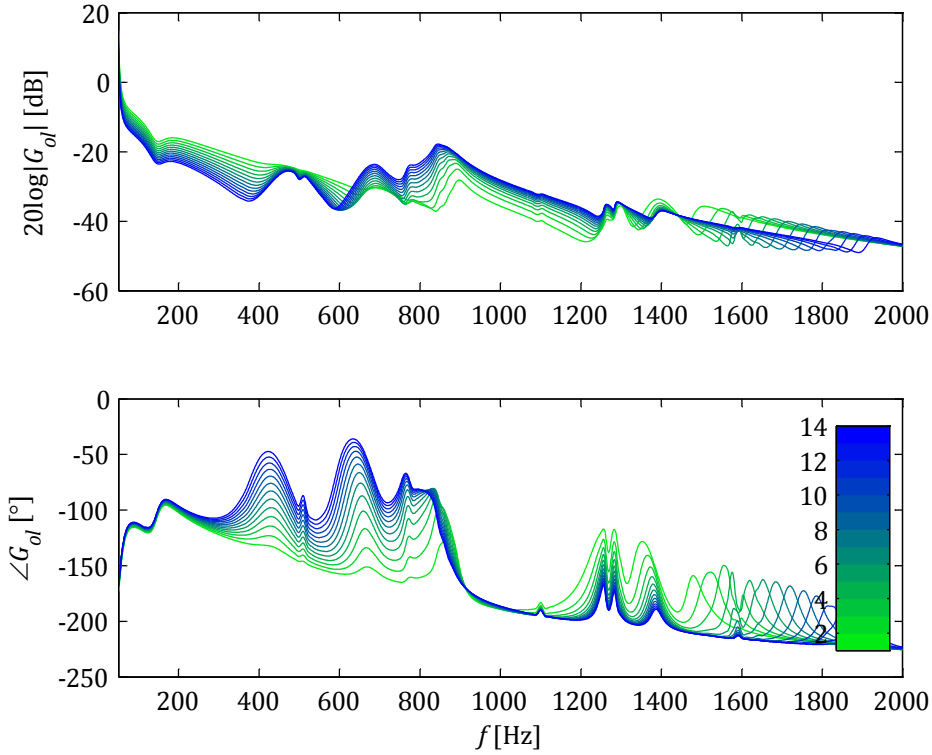

Figure 5.72 Open loop system frequency response where Karnice is the plant.

It was presented how the frequency response of current controller can change depending of different factors (e.g. filters, harmonic compensation). It was also presented how to represent the controller in stationary reference frame (equal to natural reference frame [5.58]). Based on the results it is now possible to analyse how both the grid-side converter (i.e. compensator) and the wind farm (i.e. plant) can interact. In order to investigate the system within the wide range of frequency Bode and Nyquist plots are used.

Figure 5.72 represents Bode plot of the open loop system for frequencies higher than the fundamental and lower than around Nyquist frequency of the command signal. In this particular system the plant is the Karnice wind farm. The plot shows how the frequency response can change depending on number of wind turbines connected in the wind farm. Please note that Karnice contains 13 wind turbines connected together by relatively small MV network and relatively short cable to the distribution system

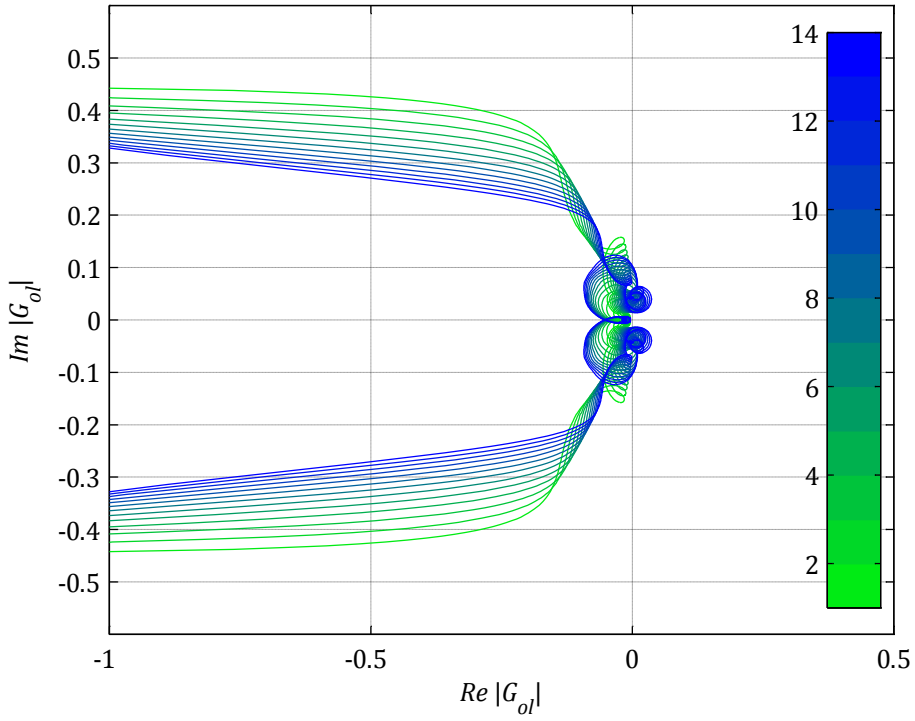

Figure 5.73 Nyquist plot of the open loop system where Karnice is the plant.

The Nyquist plot of open loop system comprising designed control and aggregated Karnice wind farm is shown in Figure 5.73. As it can be seen from the figure, the system is stable for all analysed cases. Calculated stability margins (i.e. gain margin, phase margin, and vector gain margin) dependent on number of wind turbines in operation are presented in Figure 5.74. It can be seen that all margins indicate the system robustness. It is interesting to emphasize that actually the gain margin and the vector gain margin significantly differs between each other. The vector gain margin is much smaller. Please note that gain margin and vector gain margin are supplementary, i.e. when the system is on the stability boundary both margins are equal to 0 dB.

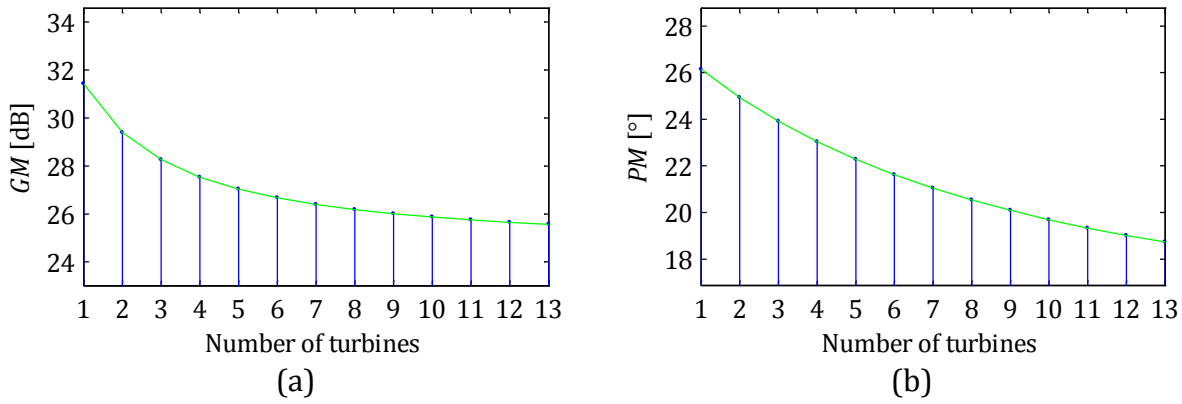

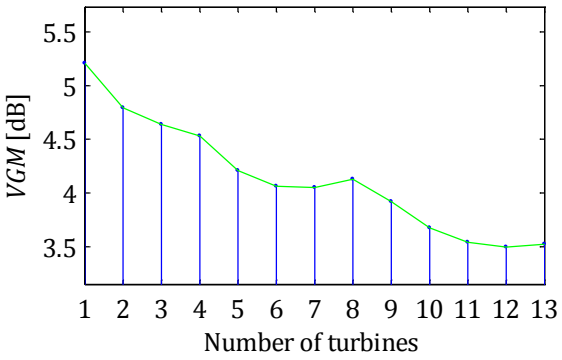

(c)

Figure 5.74 Gain margin, phase margin, and vector gain margin calculated for different number of wind turbines in operation of Karnice wind farm.

The vector gain margin presented in Figure 5.74(c) is much smaller from the gain margin in Figure 5.74(a) because of the notch filter tuned for $2\omega_0$ in synchronous reference frame. The notch filter affects the Nyquist characteristic when closer to the -1 point but does not affect any crossover points and therefore this change in the open loop characteristic cannot be observed by the gain margin.

In order to compare different wind farm system also Horns Rev II offshore wind farm was considered. The Bode plot of open loop system is presented in Figure 5.75. Please note that the same current controller is used in case of both wind farms (i.e. Karnice and Horns Rev II). It is assumed that both wind farms are equipped with the same wind turbines with the same control strategy. Even if in real-life they are the same wind turbines it is not difficult to adjust the control strategy for particular systems of interest. It was presented that for different wind farms, especially large offshore wind farms with complex structure, the frequency dependent characteristic of the plant can significantly change. Therefore robustness assumption stated by different wind turbine manufacturers can be violated. It might not be unusual that wind turbines control should be changed depending on application (i.e. internal wind farm structure and the grid to which the wind farm is connected).

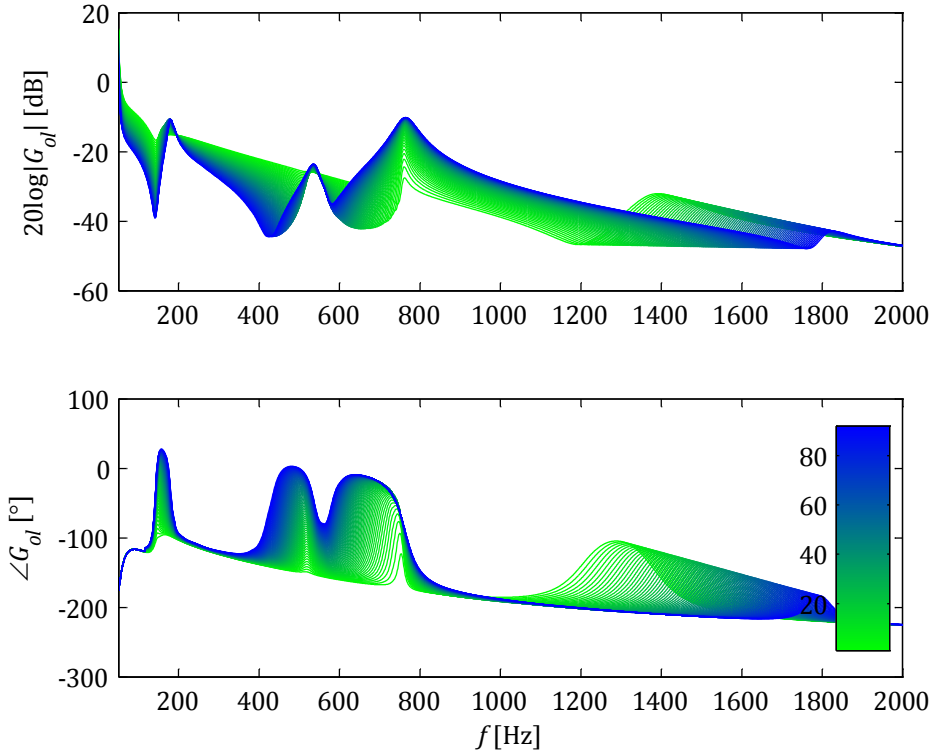

Figure 5.75 Open loop system frequency response where Horns Rev 2 is the plant.

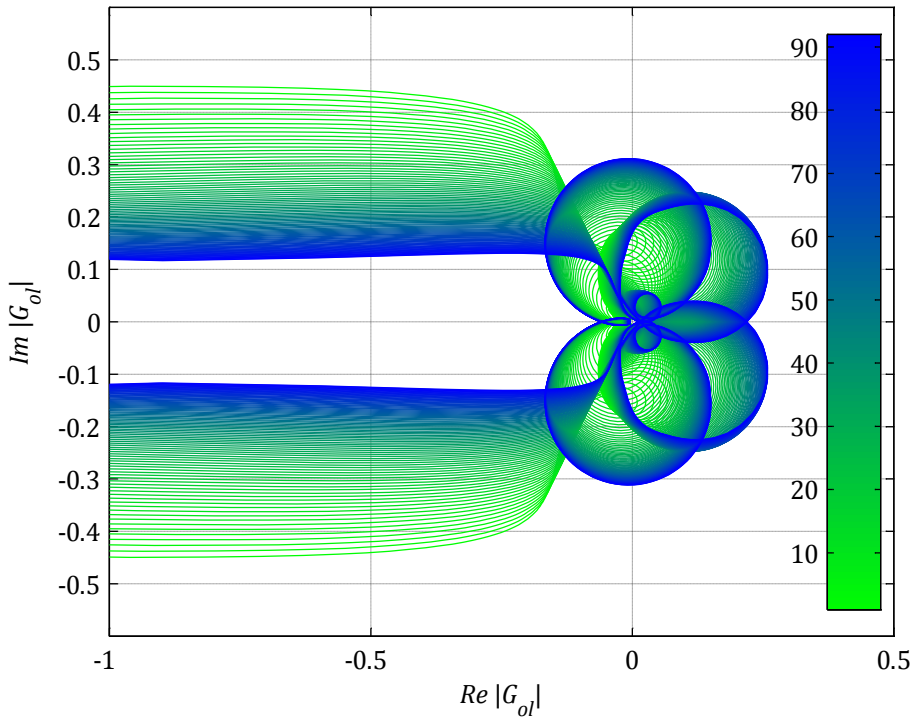

Figure 5.76 Nyquist plot of the open loop system where Horns Rev 2 is the plant.

Figure 5.75 and Figure 5.76 show how the open loop system can vary depending on number of wind turbines in operation. In case of Horns Rev II the changes are even more significant because the wind farm comprise of 91 wind turbines connected together by a widespread MV cable network. In Figure 5.75 one can see quite significant resonance peak around 200 Hz. This is caused by a series resonance between the park transformer inductance and the long HVAC cable capacitance. Such phenomenon cannot be seen in case of Karnice and shown in Figure 5.72 because there are no such long cables. This indicates that the overall system stability may be of concern, especially in large offshore wind farms.

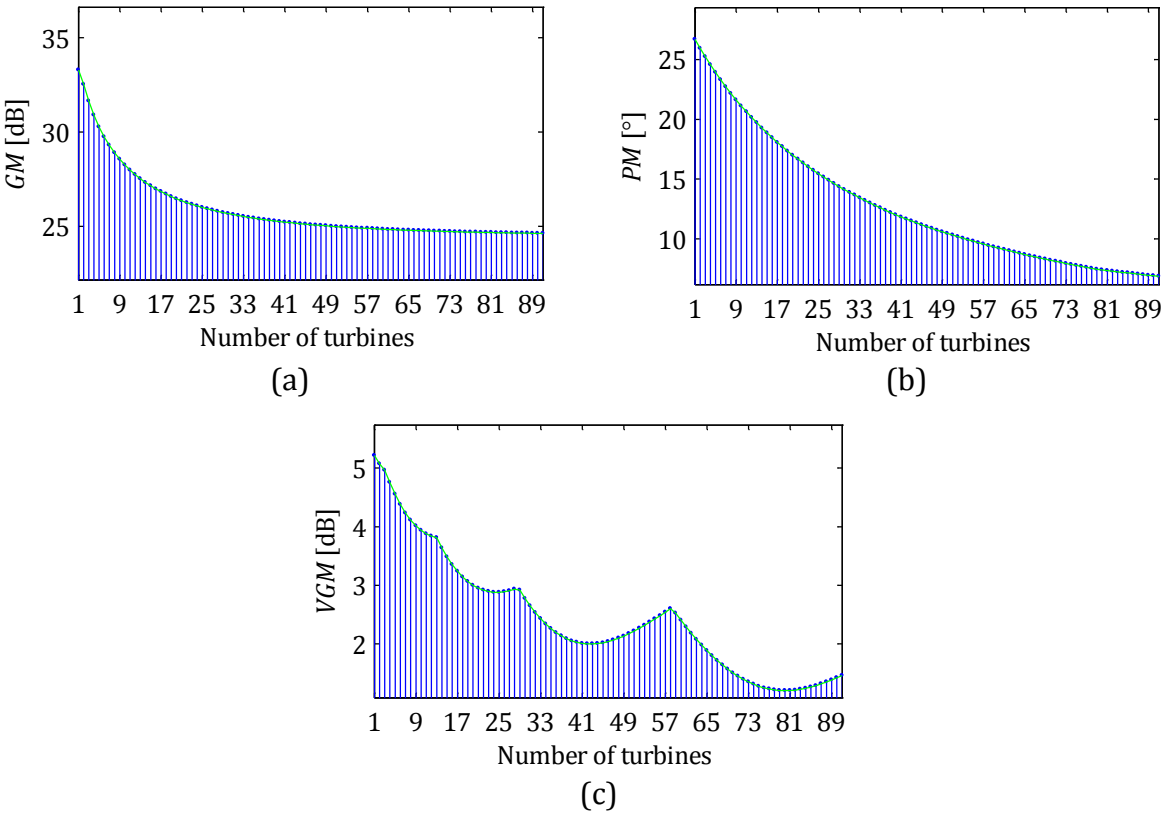

Figure 5.77 Gain margin, phase margin, and vector gain margin calculated for different number of wind turbines in operation of Horns Rev II wind farm.

Also based on stability margins from Figure 5.77 it can be seen that the vector gain margin is significantly lower when almost all wind turbines are connected. It was observed that the notch filter can significantly affect the vector gain margin in Karnice while the gain margin was high (around 26 dB). In case of Horns Rev II also the series resonance easily seen in the Bode plot additionally affects the system overall stability. Comparing Figure 5.75 and Figure 5.77(c) one can see that the vector gain margin is more affected by the notch filter for lower number of wind turbines in operation and more affected by the series resonance for higher number of wind turbines in operation.

5.2.4 SUMMARY OF WIND TURBINE MODELLING

Nowadays wind turbines are complex devices equipped with the latest technologies. Therefore, harmonic analysis of such devices is not a straightforward task. Due to the complexity of wind turbine structure, harmonic studies can be divided into several parts such as control strategy, modulation technique, converter build, or hardware implementation. Thus, wind turbine modelling and models application in this chapter were divided taking those aspects into consideration.

At the beginning, it must be emphasized that the behaviour of harmonics in wind turbines significantly varies depending on their origin and nature. As a good example are sideband harmonics in which the frequency is dependent on both the power system frequency and the carrier frequency. Fortunately, an analytical approach based on the double Fourier series allows understanding the deterministic nature and behaviour of harmonics generated by voltage source converters.

Different aspects of harmonic behaviour were theoretically explained in this chapter. It was analytically explained how the additional harmonic content in the reference signal and the DC-link circuit can affect harmonics in the ac network. Derived generic closed-form solutions were helpful in understanding these phenomena. The analytical approach was compared with numerical simulations and agreement was found. Also the impact of reference signal sampling was explained theoretically and observed in real-life measurements.

Except for modulation technique analytical description and modelling, also the wind turbine control structure from harmonic perspective was investigated. Please note that the control of the grid-side converter determines the shape (including harmonic components) of the reference signal. It was analytically explained how the distorted reference signal affects the harmonic generation and also how the control structure affects the reference signal.

Various control strategies were taken into consideration, and their impact on possible harmonic emission and overall system stability. The analysis was performed mainly in the frequency domain. One analysed how particular components (e.g. filters, controllers, etc.) can affect the control and its harmonic rejection capability. The influence of control strategies on overall wind farm stability was deeply investigated. The vector gain margin was suggested as a supplementary index to evaluate overall system stability in the frequency domain.

5.3 SUMMARY

Carefully modelled and aggregate large wind farms in the frequency domain together with wind turbines' frequency response can provide a good overview about large offshore wind farms' behaviour. Such approach can be successfully used in wind farm

studies with wind turbines from various manufacturers as well as even wind turbines from the same manufacturer, but with different control solutions.

It was observed that additional and necessary application of notch filters in positive and negative rotating reference frames can affect the overall system stability. Additionally, it was observed that significant low-frequency series resonances can intensify this negative impact. Therefore, the suggested stability indices occurred to be very useful in the analysis of large offshore wind farms.

Based on the presented studies in this chapter, one can see that large offshore wind farms, in comparison to typical onshore wind farms, can affect more unwanted resonance scenarios. Unwanted resonances can affect the overall wind farm stability and performance (e.g. unwanted harmonic excitation and amplification). Therefore, it is of great importance to carefully analyse wind farms, especially large offshore wind farms, also from a harmonic perspective.

5.4 REFERENCES

[5.1] M. Garcia-Gracia, M. Paz Comech, J. Sallan, and A. Llombart, "Modelling wind farms for grid disturbance studies," *Renewable energy*, vol. 33, no. 9, pp. 2109-2121, 2008.

[5.2] L. M. Fernandez, C. A. Garcia, J. R. Saenz, and F. Jurado, "Equivalent models of wind farms by using aggregated wind turbines and equivalent winds," *Energy conversion and management*, vol. 50, no. 3, pp. 691-704, 2009.

[5.3] Ł. H. Kocewiak, J. Hjerrild, and C. Leth Bak, "Wind Farm Structures' Impact on Harmonic Emission and Grid Interaction," in *European Wind Energy Conference*, Warsaw, 2010, pp. 1-8.

[5.4] N. R. Watson and J. Arrillaga, *Power System Harmonics*. Wiley and Sons, 2003.

[5.5] W. Wiechowski, "Harmonics in Transmission Power Systems," PhD Thesis, Aalborg University, Aalborg, 2006.

[5.6] U. S. Gudmundsdottir, "Modelling of long High Voltage AC cables in Transmission Systems," PhD Thesis, Departament of Energy Technology, Aalborg University, Aalborg, 2011.

[5.7] U. S. Gudmundsdottir, C. L. Bak, and W. T. Wiechowski, "Measurements for validation of high voltage underground cable modelling," in *International Conference on Power Systems Transients*, Kyoto, 2009, pp. 1-7.

[5.8] C. H. Chien and R. W. G. Bucknall, "Theoretical Aspects of the Harmonic Performance of Subsea AC Transmission Systems for Offshore Power Generation Schemes," in *Proc. Generation Transmission and Distribution*, 2006, pp. 599-609.

[5.9] S. Ramo, J. R. Whinnery, and T. van Duzer, *Fields and Waves in Communication Electronics*, 3rd ed. United States of America: John Wiley & Sons, 1994.

[5.10] W. D. Stevenson, *Elements of Power System Analysis*, F. E. Terman, Ed. New York, United States of America: McGraw-Hill, 1955.

[5.11] P. Brogan, "The stability of multiple, high power, active front end voltage sourced converters when connected to wind farm collector systems," in *EPE Wind Energy Chapter Seminar*, Stafford, 2010, pp. 1-6.

[5.12] V. Akhmatov, "Experience with voltage control from large offshore windfarms: the Danish case," *Wind Energy*, vol. 12, no. 7, pp. 692-711, 2009.

[5.13] W. Wiechowski and P. B. Eriksen, "Selected studies on offshore wind farm cable connections – challenges and experience of the Danish TSO," in *Proc. Power and Energy Society General Meeting – Conversion and Delivery of Electrical Energy in the 21st Century*, July 2008, pp. 1-8.

[5.14] F. Blaabjerg and Z. Chen, *Power Electronics for Modern Wind Turbines*, 1st ed. Morgan & Claypool, 2006.

[5.15] SEMIKRON, "Parallel Operation of 'GB'-type SKiiP Systems," Application Notes, 2004.

[5.16] N. Pluschke, "High Power Density Design for Windmill Converter," in *China WInd Power*, Beijing, 2009, pp. 1-6.

[5.17] C. Saniter, "Frequency-domain modelling of voltage source converters and doubly-fed induction machines facing distorted ac power networks," PhD Thesis, Technischen Universität Berlin, Berlin, 2006.

[5.18] J. Verboomen, R. L. Hendriks, Y. Lu, and R. Voelzk, "Summation of Non-Characteristic Harmonics in Wind Parks," in *Proc. Nordic Wind Power Conference*, Bornholm, 2009.

[5.19] R. Jones, R. V. Fulcher, and E. A. Lewis, "Control Methods for Pulse Width Modulation (PWM)," Patent US 2008/00622728 A1, Mar. 13, 2008.

[5.20] C. L. DeVito, *Harmonics Analysis: A Gentle Introduction*. United States of America: Jones and Bartlett Publishers, 2007.

[5.21] M. Abramowitz and I. A. Stegun, *Handbook of Mathematical Functions with Formulas, Graphs, and Mathematical Tables*, 10th ed. Washington: Department of Commerce, 1972.

[5.22] A. Vretblad, *Fourier Analysis and Its Applications*. New York: Springer-Verlag, 2003.

[5.23] D. G. Holmes, "A general analytical method for determining the theoretical harmonic components of carrier based PWM strategies," in *Industry Applications Conference*, St. Louis, 1998, pp. 1207-1214.

[5.24] M. Odavic, M. Sumner, P. Zanchetta, and J. C. Clare, "A Theoretical Analysis of the Harmonic Content of PWM Waveforms for Multiple-Frequency Modulators," *IEEE Transactions on Power Electronics*, vol. 25, no. 1, pp. 131-141, Jan. 2010.

[5.25] B. P. McGrath, D. G. Holmes, M. Manjrekar, and T. A. Lipo, "An improved modulation strategy for a hybrid multilevel inverter," in *Industry Applications Conference*, Rome, 2000, pp. 2086-2093.

[5.26] L. Mathe, H. Cornean, D. Sera, P. O. Rasmussen, and J. K. Pedersen, "Unified analytical equation for theoretical determination of the harmonic components of modern PWM strategies," in *Industrial Electronics*, Melbourne, 2011, pp. 1-6.

[5.27] A. M. Razali and Z. Salam, "Analysis Of Natural Sampled PWM Switching Strategy For A Cascaded Multilevel Inverter Using Double Integral Fourier Method," in *Power Electronics and Drives Systems*, Kuala Lumpur, 2005, pp. 1468-1473.

[5.28] S. R. Bowes and B. M. Bird, "Novel approach to the analysis and synthesis of modulation processes in power convertors," *Proceedings of the Institution of Electrical Engineers*, vol. 122, no. 5, pp. 507-513, May 1975.

[5.29] J. W. Kimball and M. Zawodniok, "Reducing Common-Mode Voltage in Three-Phase Sine-Triangle PWM With Interleaved Carriers," *IEEE Transactions on Power Electronics*, vol. 26, no. 8, pp. 2229-2236, Aug. 2011.

[5.30] D. G. Holmes and T. A. Lipo, *Pulse Width Modulation for Power Converters: Principles and Practice*. IEEE Press, 2003.

[5.31] A. Yazdani and R. Iravani, *Voltage-Sourced Converters in Power Systems: Modeling, Control, and Applications*. New Jersey, United States of America: John Wiley & Sons, 2010.

[5.32] N. Benaifa, H. Bierk, A. H. M. Rahim, and E. Nowicki, "Analysis of Harmonic Reduction for Synchronized Phase-shifted Parallel PWM Inverters with Current

Sharing Reactors," in *Electrical Power Conference*, Montreal, 2007, pp. 134-139.

[5.33] J. I. Llorente Gonzales, B. Andersen, and J. Birk, "Methods for Operation of a Converter System," U.S. Patent 0 073 445 A1, Mar. 29, 2007.

[5.34] T. Beechner and J. Sun, "Harmonic cancellation under interleaved PWM with harmonic injection," in *Power Electronics Specialists Conference*, Rhodes, 2008, pp. 1515-1521.

[5.35] R. Jones, R. V. Fulcher, and H. Stiesdal, "Control methods for the synchronization and phase shift of the pulse width modulation (PWM) strategy of power converters.," Patent US 2008/0284252 A1, Nov. 20, 2008.

[5.36] Y.-M. Park, H.-S. Yoo, H.-W. Lee, M.-G. Jung, S.-H. Lee, C.-D. Lee, S.-B. Lee, and J.-Y. Yoo, "A Simple and Reliable PWM Synchronization & Phase-Shift Method for Cascaded H-Bridge Multilevel Inverters based on a Standard Serial Communication Protocol," in *Industry Applications Conference*, Tampa, 2006, pp. 988-994.

[5.37] J. Birk and B. Andresen, "Parallel-connected converters for optimum reliability and grid performance in the Gamesa G10X 4.5 MW wind turbine," in *European Wind Energy Conference*, Brussels, 2008.

[5.38] M. Jasiński, "Direct Power and Torque Control od AC-DC-AC Converter-Fed Induction Motor Drives," PhD Thesis, Warsaw University of Technology, Warsaw, 2005.

[5.39] M. Malinowski, "Sensorless Control Strategies for Three-Phase PWM Rectifiers," PhD Thesis, Warsaw University of Technology, Warsaw, 2001.

[5.40] G. N. Watson, *A Treatise on the Theory of Bessel Functions*. London: Cambridge University Press, 1922.

[5.41] N. Mohan, T. M. Undeland, and W. P. Robbins, *Power electronics: Converters, Applications, and Design*, 3rd ed. New York: Wiley and Sons, 2003.

[5.42] M. H. Rashid, *Power Electronics Handbook*, 2nd ed. San Diego, California, United States of America: Elsevier, 2007.

[5.43] F. Bowman, *Introduction to Bessel Functions*. United States of America: Dover Publications, 1958.

[5.44] S. R. Bowes, "New Sinusoidal Pulse Width Modulated Inverter," *IEEE Proceedings*, vol. 122, no. 11, pp. 1279-1285, Nov. 1975.

[5.45] S. W. Smith, *The Scientist and Engineer's Guide to Digital Signal Processing*, 2nd ed. San Diego, California: California Technical Publishing, 1999.

[5.46] J. O. Smith, *Introduction to Digital Filters with Audio Applications*. W3K Publishing, 2007.

[5.47] C. Gasquet and P. Witomski, *Fourier analysis and applications: filtering, numerical computation, wavelets*, 1st ed. New York: Springer-Verlag, 1999.

[5.48] A. Timbus, M. Liserre, R. Teodorescu, P. Rodriguez, and F. Blaabjerg, "Evaluation of Current Controllers for Distributed Power Generation Systems," *IEEE Transactions on Power Electronics*, vol. 24, no. 3, pp. 654-664, Mar. 2009.

[5.49] R. Jones, P. B. Brogan, E. Grondahl, and H. Stiesdal, "Power Converters," U.S. Patent 7 372 174 B2, May 13, 2008.

[5.50] M. Lieserre, R. Teodorescu, and F. Blaabjerg, "Multiple Harmonics Control for Three-Phase Grid Converter Systems with the Use of PI-RES Current Controller in a Rotating Frame," *IEEE Transactions on Power Electronics*, vol. 21, no. 3, pp. 836-841, May 2006.

[5.51] R. Teodorescu, M. Liserre, and P. Rodríguez, *Grid Converters for Photovoltaic and Wind Power Systems*. New Delhi: John Wiley and Sons, 2011.

[5.52] R. Teodorescu, F. Blaabjerg, M. Liserre, and P. C. Loh, "Proportional-resonant controllers and filters for grid-connected voltage-source converters," *IEE Proceedings - Electric Power Applications*, vol. 153, no. 5, pp. 750-762, Sep. 2006.

[5.53] H.-S. Song and K. Nam, "Dual current control scheme for PWM converter under unbalanced input voltage conditions," *IEEE Transactions on Industrial Electronics*, vol. 46, no. 5, pp. 953-959, Oct. 1999.

[5.54] R. Teodorescu, F. Blaabjerg, U. Borup, and M. Liserre, "A new control structure for grid-connected LCL PV inverters with zero steady-state error and selective harmonic compensation," in *Applied Power Electronics Conference and Exposition*, Anaheim, 2004, pp. 580-586.

[5.55] J.-I. Jang and D.-C. Lee, "High Performance Control of Three-Phase PWM Converters under Nonideal Source Voltage," in *International Conference on Industrial Technology*, Mumbai, 2006, pp. 2791-2796.

[5.56] P. Rodriguez, A. Luna, M. Ciobotaru, R. Teodorescu, and F. Blaabjerg, "Advanced Grid Synchronization System for Power Converters under Unbalanced and Distorted Operating Conditions," in *32nd IEEE Annual Conference on Industrial*

Electronics, Paris, 2006, pp. 5173-5178.

[5.57] V.-T. Phan, H.-H. Lee, and T.-W. Chun, "An Improved Control Strategy Using a PI-Resonant Controller for an Unbalanced Stand-Alone Doubly-Fed Induction Generator," *Journal of Power Electronics*, vol. 10, no. 2, pp. 194-202, Mar. 2010.

[5.58] D. N. Zmood, D. G. Holmes, and G. Bode, "Frequency-Domain Analysis of Three-Phase Linear Current Regulators," *Transactions on Industry Applications*, vol. 37, no. 2, pp. 601-610, Mar. 2001.

[5.59] G. F. Franklin, J. D. Powell, and M. L. Workman, *Digital control of dynamic systems*, 3rd ed. Prentice-Hall, 2006.

[5.60] G. Franklin, J. D. Powell, and A. Emami-Naeini, *Feedback Control of Dynamic Systems*, 4th ed. Prentice-Hall, 2002.

[5.61] K. Ogata, *Modern Control Engineering*, Third Edition ed. United States of America: Prentice-Hall, 1997.

[5.62] O. J. M. Smith, "A Controller to Overcome Dead Time," *ISA Journal*, vol. 6, no. 2, pp. 28-33, 1959.

[5.63] M. A. Johnson and M. H. Moradi, *PID Control: New Identification and Design Methods*. London: Springer-Verlag, 2005.

[5.64] R. Pöllänen, "Converter-flux-based current control of voltage source PWM rectifiers - analysis and implementation," PhD Thesis, Lappeenranta University of Technology, Lappeenranta, 2003.

[5.65] M. Milosevic, G. Andersson, and S. Grabic, "Decoupling Current Control and Maximum Power Point Control in Small Power Network with Photovoltaic Source," in *Power Systems Conference and Exposition*, Atlanta, 2006, pp. 1005-1011.

[5.66] A. Kulka, T. Undeland, S. Vazquez, and L. G. Franquelo, "Stationary Frame Voltage Harmonic Controller for Standalone Power Generation," in *European Conference on Power Electronics and Applications*, Aalborg, 2007, pp. 1-10.

[5.67] T. Kugelstadt, "Active Filter Design Techniques," in *Op Amps for Everyone*. United States of America: Elsvier, 2009, ch. 20, pp. 376-285.

[5.68] R. Stata, "Operational Integrators," Analog Devices Application Note.

[5.69] M. Liserre, R. Teodorescu, and F. Blaabjerg, "Stability of Photovoltaic and Wind Turbine Grid-Connected Inverters for a Large Set of Grid Impedance Values,"

IEEE Transactions on Power Electronics, vol. 21, no. 1, pp. 263-272, Jan. 2006.

[5.70] B. Boulet, *Fundamentals of Signals & Systems*, 1st ed. Charles River Media, 2005.

Chapter 6
SUMMARY

The most interesting and significant findings of the project are summarized in the final chapter. It constitutes an essence of previous chapters. Of course, there are still many things to develop in future which are also mentioned in this chapter. Except for conclusions, also several interesting aspects observed during project development regarding harmonic analyses are discussed.

6.1 CONCLUSIONS

The project hypothesis was specified at the beginning of the project in order to clearly specify the scope of the project. Based on the hypothesis, the project was focused on development of various analysis methods and tools which can be successfully used in the development of future commercial wind farm projects. Additionally, extensive knowledge regarding harmonic phenomenon in wind farms was required and gained in the company.

During the research, the project development framework was shaped. The framework emphasizes that measurements, data processing and analysis, model development and application, and validation are equally important in harmonic studies and crucial in appropriate harmonic evaluation.

Harmonic measurements require well-developed measurements systems comprising carefully adjusted and designed hardware and software layers. Optimization from an electromagnetic compatibility perspective is especially important in wind turbines with high power density switching converters.

In data processing it is of great importance to choose the appropriate processing method. It was observed that:

- Discrete Fourier transform is useful in the processing of large datasets, but spectral leakage might be an issue if data are not well-prepared.

- In order to avoid spectral leakage, resampling based on spline interpolation gives the best results taking into consideration the processing errors and calculation burden.
- Baseband harmonics are dependent only on the power system's fundamental frequency and resampling significantly reduces spectral leakage.
- Sideband harmonics are dependent on both the power system's fundamental frequency and the carrier signal fundamental frequency and thus not resampled signal processing giving satisfactory results.
- Commercial power quality meters adjust sample rate according to the power system frequency variation and therefore can only correctly estimate baseband harmonics.
- The time-frequency analysis allows distinguishing if harmonics are generated by the wind turbine or affected by the external network.

The statistical analysis of measurement data analysis gives a better understanding of the harmonic origin, nature, and propagation. It was observed that:

- A calculation of statistics such as mean, variance, kurtosis gives more information about harmonics than only a single bar (bin) from the discrete Fourier transform.
- There are few types of harmonics in wind turbines and wind farms depending on their origin and nature, and a different approach and analysis and modelling are required.
- Sideband harmonics are not affected by the network, because the short circuit impedance seen by the grid-side converter does not vary significantly, and the harmonic background within this frequency range is limited.
- Baseband harmonics purely generated by the converter are also not common in the grid, and therefore it is easy to analyse them.
- Baseband harmonics in the grid can significantly affect current distortions in the wind turbine and interrupt wind turbine power quality assessment.
- It is difficult to analyse baseband harmonics present in the grid, because they vary frequently due to changes in the short circuit impedance and non-linear loads.
- Harmonics are averaged during processing according to standards, and therefore they are expected to be normally distributed according to the central limit theorem.
- Harmonics are not directly dependent on power production. Harmonics generated by voltage source converters are dependent on the output fundamental voltage.
- Harmonic distortions seen by wind turbines are more significant in wind farms connected to the distribution system instead of the transmission system.

- Internal resonances in large offshore wind farms are the main contributors of harmonic problems, because wind turbines can meet the most demanding power quality requirements and do not generate significant harmonics.
- Wind turbines are the main sources of harmonics in wind farms. Harmonics generated by wind turbines are at low levels, but possible resonances change it and thus resonance studies are of great importance.

Wind farm description in the frequency domain allows studying possible resonances and their impact on the overall system behaviour. It was observed that:

- The short circuit impedance seen from the grid-side converter terminals is mainly affected by the wind turbine's main power circuit.
- However, possible resonances in large offshore wind farms connected via long HVAC cables can be significant and affect the impedance seen by the converter.
- Various wind farm collection grid aggregation techniques do not affect significantly overall short circuit impedance.
- The wind farm aggregated impedance can vary depending on the number of wind turbines in operation and other changes in its configuration; therefore careful analysis is crucial during the design stages.

Harmonic generation by wind turbines is affected by many factors such as control strategy, modulation technique, and network bridge build. It was observed that:

- Based on the Fourier series, the decomposition frequency components generated by the modulator even for non-integer frequency rations are still harmonics.
- It is possible to analytically describe the voltage source converter switching function depending on various harmonic conditions.
- Harmonics generated by the modulator of grid-connected converter in wind turbines are affected by the harmonic content in the DC-link circuit, harmonic content in the reference signal, modulation index, and command signal sampling.
- Harmonic components magnitude varies in asymmetrically regular sampled pulse-width modulation with fixed carrier frequency while the power system fundamental frequency changes.
- It is possible to control deterministically sideband harmonics phase angles in order to cancel carrier group harmonics in parallel connected wind turbines.
- The command signal is affected by various control techniques, and the wind turbine's current control plays a crucial role in the mitigation of harmonic distortions.
- Control in stationary reference frame is expected to be characterized by better harmonic rejection in comparison to control in rotating reference frame.
- Additional filters in the control structure can affect the overall robustness of the converter controller.

- Even robust wind turbines can introduce some stability problems in large offshore wind farms, because wind farm structures can have a negative influence on the controller behaviour.
- It is sometimes not enough in large offshore wind farms to tune the controller, considering only the wind turbine's main power circuit as a plant.
- Each large offshore wind farm should be analysed separately from a stability perspective for frequencies within the wind turbine controller bandwidth, and possible adjustment in the control strategy may be required.
- Vector gain margin is a good supplementary index in the stability assessment and can provide a better overview of the overall system stability.

6.2 DISCUSSION

6.2.1 PROJECT INITIALIZATION AND DEVELOPMENT

Recently, the wind power sector is rapidly developing. This creates new challenges to the industry, and therefore more and more research projects, including harmonic analysis especially focused on wind power applications, are constructed, which is why the project was initiated and successfully developed. Also experience from the past regarding offshore projects developed in the company, and various harmonic aspects caused a need to carry out extensive harmonic research.

Even if the major part of harmonic studies is nowadays state-of-the-art, there were still many issues at the beginning of the project to investigate and improve regarding harmonics. It was especially associated with the application of harmonic analyses in wind turbines and large offshore wind farms.

The research project was initiated by the industry and carried out in cooperation with the academia. In order to organize the project development process, the research development framework was suggested based on rationalistic tradition approach in order to provide knowledge and a better understanding of the different aspects (e.g. measurements, data processing, data analysis, modelling, models application) in harmonic studies. Some issues related with knowledge sharing in order to better utilize the project findings were also mentioned.

A strong advantage of the PhD project was that the project was industry-oriented. This created a unique opportunity to carry out research gathering benefits from the industry (measurements, real-life study cases, etc.) as well as the academia (strong theoretical background, the newest trends in research, etc.).

The advantage of industry-oriented research was associated with dealing with real-life existing electrical systems, such as wind turbines, onshore as well as offshore wind farms. This created a unique opportunity of applying the developed knowledge and technology directly in commercial projects. On the other hand, it helped solving real-life problems based on academic knowledge. It is obvious that during academic

research, some aspects which simply occur in real existing systems might not be taken into consideration. Therefore this industrial PhD had this unique opportunity to create the link between the industry and the academia.

Within the confines of this industry-oriented project, measurements constituted an extremely important part. Therefore, it was of great importance to develop appropriate measurement systems for specific applications and carry out well planned measurement campaigns. Based on such well-performed measurements, further data processing, data analysis, and modelling were possible.

6.2.2 MEASUREMENTS IN INDUSTRY-ORIENTED RESEARCH

It was shown that measurements constitute a core part in industry-oriented research. The project due to this fact owes its uniqueness. It was proven that an analysis of such systems as large offshore wind farms considers many aspects related to extended and accurate models, complex measurement campaigns and of course appropriate and more suitable data processing methods. Before any of the above aspects could be seriously taken into consideration, a reliable and robust measurement system was needed. This was achieved by careful designing of the hardware and the software layers of the measurement system.

Appropriate understanding of harmonics behaviour in wind farms required extended measurement campaigns carried out in rough offshore environments. In places where access was limited due to weather conditions and significant operational costs, robust and reliable measurement systems were especially important. Therefore, acquiring sufficient amount of data for harmonic studies was difficult but possible.

6.2.3 IMPORTANCE OF DATA PROCESSING

Within the harmonic studies carried out in the report various data processing techniques were applied. The application of methods was dependent on the nature of analysed signals. It was observed that data processing plays a crucial role in overall harmonic emission evaluation.

It was presented that it is of great importance to know the nature of generated harmonics in large offshore wind farms in order to apply the most suitable data processing technique. A wavelet analysis was used in order to perform time-frequency domain analysis helpful to distinguish harmonic origin and observe short-term variation. Non-parametric spectrum estimation was made on interpolated signals adjusted according to the varying power system frequency.

It was mentioned that according to IEC standards, it is recommended to adjust the sample rate of the power quality meters according to the variation of the power system frequency. Therefore, based on measurement results, sideband harmonic components were inappropriately estimated by commercial power quality meters. One can simply conclude that for research purposes, it is better not to use commercial power quality

meters and develop dedicated measurements systems instead, as it was done within the project.

Different data processing techniques were presented and applied depending on the signal (i.e. stationary or non-stationary) or harmonic nature (i.e. spline resampling or direct spectrum estimation). It was observed that certain harmonic components generated by the grid-side converter in the wind turbine are not only linked with the power system's fundamental frequency, but also with the carrier signal's fundamental frequency. Therefore, harmonic assessment by major part of commercial power quality meters is inappropriate and affects misleading measurement interpretation.

6.2.4 DATA ANALYSIS IN MODEL DEVELOPMENT

Processed data were analysed by the application of sophisticated statistical methods. Observations and conclusions from data analyses contributed to better understanding the nature and origin of various harmonic components as well as constituted a solid basis in further model development.

A comprehensive comparison of voltage and current harmonics based on probability distribution estimation, and an appropriate statistics calculation (mean, variance, probability density function, etc.) was presented. Such an approach provides a better overview of harmonic components variation and occurrence frequency. The results were clearly compared using solid statistical techniques.

Different statistical tools were used in order to analyse the origin and nature of various harmonic components. It was observed that one can distinguish few different types of harmonics in measurements, i.e. DC-link harmonic content, sideband harmonic, baseband harmonic not affected by the grid, and baseband harmonic strongly affected by the grid.

DC-link harmonics in measurements were affected by slightly unbalanced voltages (1^{st} harmonic) and by the nature of the network bridge (6^{th} harmonic). Sideband harmonics were negligibly dependent on the external network (i.e. short circuit impedance variation and background distortions) and contained a sufficient number of periods within the analysed window. Baseband harmonics not affected by the grid (i.e. purely generated by the converter), the same as sideband harmonics, were easy to analyse. However, baseband harmonics strongly affected by the grid are in general difficult to analyse, because the external network is usually of great uncertainty.

Baseband harmonics present in the background distortions can significantly affect the harmonic current flowing in the wind turbine. This current is of the main concern in wind turbine power quality measurements and assessments based on IEC standards. Therefore, modelling based on IEC test reports can be significantly inappropriate. It was also observed that actual power quality assessment of wind turbines should be adapted

depending on the assumed control strategy (e.g. with and without harmonic compensation).

On the other hand, it was observed that in large offshore wind farms harmonic distortions in the grid do not significantly affect the harmonic current flow at the wind turbine level. This emphasizes that modelling of wind turbines in large offshore wind farms cannot be performed only based on current measurements of a wind turbine connected to the distribution network. Needless to say, an appropriate and trustful harmonic study of wind farms connected to the grid requires cooperation with distribution and transmission system operators.

It was observed that nowadays sideband harmonic components are not emphasized enough. Baseband harmonic are mainly of interest based on traditional power system harmonic studies. However, more and more grid-connected power electronic equipment is installed in modern power systems. They are mainly generating harmonics due to pulse-width modulation. Such harmonic components are affected by two driven frequencies (i.e. power system fundamental frequency and carrier signal fundamental frequency). Please note that wind turbines provided by different manufacturers can introduce different modulation techniques and thus different harmonic spectrum. Such diversity can affect different harmonic phenomena at higher frequency levels.

In order to find a good match between academic findings and their successful application in the industry, appropriate validation methods should be applied. This is always strongly associated with extensive field measurements. In order to get a good overview of harmonic phenomena in large offshore wind farms, long-term measurements need to be carried out. It is known that harmonic components can vary in time depending on the different states of the system. Therefore, it is not a straightforward task to obtain trustful information about analysed system behaviour from measurements. And here statistical tools can really be helpful to describe measured datasets and to compare different datasets (i.e. measured harmonic components) between each other (e.g. different harmonic components, different measurement points, different wind farms).

A probabilistic approach of harmonic analysis in wind farms gives supplementary information in relation to harmonic assessment recommended in standards. Except one average value within certain power production levels, stochastic modelling also provides information about probability of occurrence certain harmonic amplitudes and angles. In the standard about power quality measurements and assessment in wind turbines it is specified to measure and evaluate different harmonic levels depending on active power production.

It was shown that wind turbine modelling as a harmonic current source according to measurements provided based on IEC standard about wind turbine power quality assessment and measurements can provide misleading understanding about wind

turbines' harmonic behaviour. Since most nowadays wind turbines are equipped with voltage source converters, it is better to think about converters as a harmonic voltage source. Please note that if harmonic compensation is included in the wind turbine control (i.e. theoretically infinite gain at the frequency of interest) it is worth thinking about the grid-side converter as a harmonic current source for such particular controlled frequencies.

Unfortunately, harmonic voltage measured at the LV side of the wind turbine transformer is a consequence of current flowing from the grid into the wind turbine (in case of control focused on voltage quality at the grid-side converter AC terminals). Therefore, harmonic models of wind turbines should be provided by manufacturers having extensive knowledge about their grid-side converter build (e.g. control method, modulation, possible harmonic compensation), or at least harmonic should be developed based on measurement at the ac side of the wind turbine network bridge.

6.2.5 WIND FARM MODELLING

Calculation of equivalent impedance is relatively straightforward and can be applied to any wind farm system. Different aggregation techniques provide different results, but it was observed that the differences do not significantly affect an overall system description in the frequency domain.

It is of great importance to know how the frequency characteristics of any aggregated wind farm are going to be used. It was presented that different calculation approaches must be used if one would like to aggregate wind turbines into one equivalent wind turbine and an electrical system to which is connected. It was also described that another calculation approach is needed if one would like to investigate how one wind turbine can behave when it is connected to the whole system with a varying number of wind turbines in operation. Please note that the converter impedance was not taken into consideration. This can be easily done by taking the controller transfer function. It was mentioned that in theory the converter control should not affect higher frequencies (if not intended), and therefore the impedance can sometimes simply be omitted.

It was observed that large offshore wind farms can introduce additional unwanted resonances within a low frequency range. This can significantly affect the overall system stability. Therefore, analysis and design optimization of large offshore wind farms are more complex than smaller onshore wind farms. In the case of the Horns Rev 2 analysis, it was observed that the capacitance of a long HVAC export cable and series inductance of the wind farm transformer create unwanted and significant series resonance. Such a situation is of concern in most erected large offshore wind farms.

6.2.6 WIND TURBINE MODELLING

Nowadays wind turbines are complex devices equipped with the newest technologies. Therefore, the harmonic analysis of such devices is not a straightforward task. Harmonic studies, due to the complexity of wind turbine structure, can be focused on several parts such as control strategy, modulation technique, converter build, and hardware implementation.

At the beginning it was emphasized that the behaviour of harmonics in wind turbines significantly varies depending on harmonic origin and nature. As a good example are sideband harmonics which frequency is dependent on both power system frequency and carrier frequency. Fortunately, the analytical approach based on the double Fourier series allows understanding deterministic nature and behaviour of harmonics generated by voltage source converters.

Except modulator modelling also the wind turbine control structure from a harmonic perspective was investigated. Please note that the control of the grid-side converter determines the shape (including harmonic components) of the reference signal. It was analytically explained how the distorted reference signal affects harmonic generation and also how the control structure affects the reference signal.

Various control strategies were taken into consideration as well as their impact on possible harmonic emission and overall system stability. An analysis was conducted mainly in the frequency domain. One analysed how particular components in the control structure (e.g. filters, controllers, etc.) can affect the control and its harmonic rejection capability. The influence of control strategies on overall wind farm stability was deeply investigated. The vector gain margin was suggested as a supplementary index to evaluate overall system stability in the frequency domain.

Carefully modelled and aggregate large wind farms in the frequency domain together with wind turbines' frequency response can provide a good overview of large offshore wind farm behaviour for different frequencies. Such an approach can be successfully used in wind farm studies with wind turbines from various manufacturers as well as even wind turbines from the same manufacturer, but with different control solutions.

It was observed that additional and necessary application of notch filters in positive and negative rotating reference frames can affect the overall system stability. Additionally, it was observed that significant low-frequency series resonances can intensify this negative impact. Therefore, the suggested stability indices turned out to be very useful in the analysis of large offshore wind farms.

Based on the presented studies, one can see that large offshore wind farms, in comparison to typical onshore wind farms, can affect more unwanted resonance scenarios. Unwanted resonances can affect the overall wind farm stability and performance (e.g. unwanted harmonic excitation and amplification). Therefore, it is of

great importance to carefully analyse wind farms, especially large offshore wind farms, also from a harmonic perspective.

Since harmonics in wind turbines and wind farms are characterized by different origin and nature comparison of them may be problematic. Therefore, sometimes selective validation of particular frequency components is more suitable. It was observed that comparison of results in the frequency domain and time domain as well as application of statistical methods is the core part of understanding the results.

6.3 FUTURE WORK

It was observed during the project development that appropriate modelling of the external network (e.g. short circuit impedance, harmonic voltage source) is crucial in appropriate harmonic evaluation, especially at the point of common coupling. Due to lack of sufficient data, it was decided to focus more on wind turbine harmonic behaviour as well as internal wind farm structures. There are still many things to improve regarding wind farm interaction with the external network. Therefore, further cooperation with both distribution and transmission system operator is required.

In the research only wind farms connected via AC export cables to the grid were considered. Nowadays, also the HVDC technology becomes more and more popular in large offshore projects. Probably in the next few years most of the large-scale offshore investments will be seen with HVDC link. Therefore, it is a natural way to analyse such system also from a harmonic analysis perspective (e.g. resonance scenarios, converter control solutions, stability assessment, converter topology, possible modulation strategies).

It was emphasized based on the project's outcome that wind turbine harmonic current can be significantly affected by the distorted grid voltage. This would probably look slightly different in large offshore wind farms with HVDC transmissions. In that case, harmonic background distortions should be insignificant. Such configuration could imply slightly different control solutions (e.g. harmonic compensation not needed). Furthermore, such closed networks with many grid-connected converters could create some challenges to the industry also from a harmonic point of view (e.g. behaviour of sideband harmonic component affected by various modulation techniques).

In the project it was observed, based on measurements and theoretical investigations, that the DC-link circuit in back-to-back converter of wind turbines can be considered as harmonic decoupling between the generator and the grid. It is not certain that in case of HVDC converter this is the case. For sure harmonic ripples in the DC-link are expected to be more significant than in wind turbines (e.g. lower switching frequency to reduce the losses, small DC-link reactor also to reduce the losses).

Based on the premises of possible future trends in the wind project development as well as experience from previous projects regarding harmonics, it was decided to initiate another research project. This time it will be focused on harmonic aspects of wind farms connected via VSC-HVDC to the grid taking into consideration also the grid aspect more deeply. The new project is expected to significantly gain from this PhD project's findings (e.g. methods, tools, models) and experience (e.g. measurements, development).

LIST OF PUBLICATIONS

[1] Ł. H. Kocewiak, C. L. Bak, and J. Hjerrild, "Harmonic Aspects of Offshore Wind Farms," in *Danish PhD Seminar on Detailed Modelling and Validation of Electrical Components and Systems*, Fredericia, 2010, pp. 40-45. (Published)

[2] Ł. H. Kocewiak, J. Hjerrild, and C. Leth Bak, "Wind Farm Structures' Impact on Harmonic Emission and Grid Interaction," in *European Wind Energy Conference*, Warsaw, 2010, pp. 1-8. (Published)

[3] Ł. Kocewiak, J. Hjerrild, and C. L. Bak, "Harmonic models of a back-to-back converter in large offshore wind farms compared with measurement data," in *Proc. Nordic Wind Power Conference*, Bornholm, 2009. (Published)

[4] Ł. H. Kocewiak, I. Arana Aristi, J. Holbøll, C. L. Bak, and J. Hjerrild, "Development and Design of a Flexible Measurement System for Offshore Wind Farm Applications," in *10th International Workshop on Large-Scale Integration of Wind Power into Power Systems as well as on Transmission Networks for Offshore Wind Power Plants*, Aarhus, 2011. (Published)

[5] Ł. H. Kocewiak, C. L. Bak, and J. Hjerrild, "Harmonic Generation and Mitingation by Full-Scale Converter Wind Turbines: Measurements and Simulation," in *International Workshop on Large-Scale Integration of Wind Power and on Transmission Networks for Offshore Wind Power Plants*, Aarhus, 2011, pp. 136-143. (Published)

[6] C. F. Jensen, C. L. Bak, Ł. Kocewiak, J. Hjerrild, and K. K. Berthelsen, "Probabilistic Aspects of Harmonic Emission of Large Offshore Wind Farms," in *International Workshop on Large-Scale Integration of Wind Power into Power Systems as well as on Transmission Networks for Offshore Wind Power Plants*, Aarhus, 2011, pp. 699-703. (Published, Co-author)

[7] I. Arana, L. Kocewiak, J. Holbøll, C. L. Bak, A. H. Nielsen, A. Jensen, J. Hjerrild, and T. Sørensen, "How to improve the design of the electrical system in future wind power plants," in *Nordic Wind Power Conference*, Rønne, 2009, pp. 1-7. (Published, Co-author)

[8] Ł. H. Kocewiak, C. L. Bak, and J. Hjerrild, "Statistical Analysis And Comparison Of Harmonics Measured In Offshore Wind Farms," in *OFFSHORE 2011*, Amsterdam, 2011, pp. 1-10. (Published)

[9] Ł. H. Kocewiak, C. L. Bak, and J. Hjerrild, "Software Development for Harmonic and Transient Measurements in Wind Farms," *IEEE Transactions on Instrumentation and Measurement*, 2011. (Submitted)

[10] Ł. H. Kocewiak, J. Hjerrild, and C. L. Bak, "Wind turbine control impact on stability of wind farms based on real-life systems," in *EWEC 2012*, Copenhagen, 2012. (Submitted)

[11] Ł. H. Kocewiak, J. Hjerrild, and C. Leth Bak, "The Impact of Harmonics Calculation Methods on Power Quality Assessment in Wind Farms," in *International Conference on Harmonics and Quality of Power*, Bergamo, 2010, pp. 1-9. (Published)

[12] Ł. Kocewiak, J. Hjerrild, and C. L. Bak, "Harmonic analysis of offshore wind farms with full converter wind turbines," in *Proc. 7th International Workshop on Large Scale Integration of Wind Power and on Transmission Networks for Offshore Wind Farms*, 2009, pp. 539-544. (Published)

[13] Ł. H. Kocewiak, I. A. Arana, J. Hejrrild, T. S. Sørensen, C. L. Bak, and J. Holbøll, "EMC Challenges During Harmonic and Transient Measurements in Offshore Wind Farms," in *Deep Sea Offshore Wind R&D Seminar*, Trondheim, 2012. (Accepted)

[14] Ł. H. Kocewiak, I. A. Arana, J. Hejrrild, T. S. Sørensen, C. L. Bak, and J. Holbøll, "GPS Synchronisation of Harmonic and Transient Measurements in Offshore Wind Farms," in *Deep Sea Offshore Wind R&D Seminar*, Trondheim, 2012. (Accepted)